Fakultät für Chemie

Einzelpartikel-Massenspektrometrie zur Analyse von Silbernanopartikeln in Umweltproben – Eintragsrouten und Schicksal von Silbernanopartikeln in der aquatischen Umwelt

Andreas Wimmer

Vollständiger Abdruck der von der

Fakultät für Chemie

der Technischen Universität München zur Erlangung des akademischen Grades eines

Doktors der Naturwissenschaften (Dr. rer. nat.)

genehmigten Dissertation.

Vorsitzender: Prof. Dr. Klaus Köhler

Prüfende der Dissertation:

1. Prof. Dr. Michael Schuster

2. Prof. Dr. Martin Elsner

3. Prof. Dr. Alfred V. Hirner

Die Dissertation wurde am 18.05.2021 bei der Technischen Universität München eingereicht und durch die Fakultät für Chemie am 25.11.2021 angenommen.

Die vorliegende Arbeit entstand in der Zeit von November 2015 bis März 2019 unter Anleitung von Herrn Prof. Dr. Michael Schuster in der Fachgruppe Analytische Chemie an der Fakultät für Chemie der Technischen Universität München.

Danksagung

Mein größter Dank gebührt meinem Doktorvater,

Herrn Professor Dr. Michael Schuster,

für die freundliche Aufnahme in den Arbeitskreis Analytische Chemie und die überaus interessante Themenstellung. Vielen Dank für das mir entgegengebrachte Vertrauen, die forscherische Freiheit und die Möglichkeit, dass ich den Arbeitskreis bei so vielen Konferenzen und Tagungen vertreten durfte. Herzlichen Dank für Ihre intensive Betreuung und die anregenden Diskussionen innerhalb und außerhalb der Chemie!

Außerdem möchte ich mich bedanken bei ...

... meinem Mentor, Herrn Hon-Prof. Dr. Richard Fischer, für die vielen Ratschläge rund um die Promotion und die interessanten Einblicke in die chemische Industrie.

... meinen AK-Kollegen Isabelle Dolique, Dr. Jasmin Haberl, Christine Hettenkofer, Stephan Fromm, Dr. Dominik Huber und Florian Weigl. Danke für Eure stete Hilfsbereitschaft, den Spaß und die schöne, unvergessene gemeinsame Zeit im Labor. Ein ganz besonderer Dank gilt meinem Kollegen Dr. Alexander Urstöger, meinem Mitstreiter im Bereich des Nanosilbers. Danke für Deine Unterstützung und die vielen wertvollen Diskussionen! Euch allen außerdem vielen Dank für die Unterstützung bei manch einer Probenahme an schönen, aber auch weniger schönen Tagen an und auf bayerischen Gewässern.

... unseren Azubis Maxi, Isi, Karo und Michael für die Unterstützung bei den unzähligen Probenvorbereitungen und Messungen.

... meinen Vorgängern im Bereich des Nanosilbers, Dr. Georg Hartmann, Dr. Monika Stoiber und Dr. Anna Kalinnik. Danke für Eure herausragende Vorarbeit, die das Gelingen der Folgeprojekte zum Nanosilber entscheidend beeinflusst hat.

« **Nothing in life is to be feared,**

it is only to be understood.

Now is the time to understand more,

so that we may fear less. »

Marie Skłodowska Curie, 1867 – 1934

1903 Nobelpreis für Physik - 1911 Nobelpreis für Chemie

Kurzfassung

Die vorliegende Studie befasst sich mit der Bestimmung von silberbasierten Nanopartikeln (Ag-b-NPs) in Umweltproben, wie z. B. Leitungswasser, Abwasser, natürlichen Gewässern und Seesedimenten. Bislang stellte die Bestimmung von Ag-b-NP in solchen Proben mit den gängigen Analysetechniken eine Herausforderung dar, da die Partikel nur geringe Konzentrationen im ng L^{-1}-Bereich aufweisen und gleichzeitig große Mengen an gelösten Ag(I)-Spezies und anderen natürlich vorkommenden Probenbestandteilen vorhanden sind.

Die Einzelpartikel-Massenspektrometrie mit induktiv gekoppeltem Plasma (sp-ICP-MS) ist eine vielversprechende Technik, die in der Lage ist, gleichzeitig die Konzentration und die Partikelgrößen von nanopartikulären Analyten wie Ag-b-NP selbst bei Konzentrationen von nur einigen ng L^{-1} zu bestimmen. Allerdings bereiten gleichzeitig vorhandene gelöste Analytspezies der sp-ICP-MS Probleme, da diese hohe Hintergrundsignale verursachen. Diese Hintergrundsignale überdecken einen Großteil der von den nanopartikulären Analyten stammenden Signale und begrenzen daher die Größendetektionsgrenze (*engl.* size detection limit, SDL), d.h. die kleinste detektierbare Partikelgröße. Ag-b-NP in Umweltproben weisen in der Regel Durchmesser < 20 nm auf. Leider können aktuelle sp-ICP-MS-Ansätze solche niedrigen SDL-Werte kaum erreichen.

In dieser Studie wurde daher die sp-ICP-MS mit einer tensidbasierten Probenvorbehandlung, der sogenannten Cloud-Point-Extraktion (CPE), kombiniert, die eine selektive Extraktion und Anreicherung von Ag-b-NP aus Umweltproben ermöglicht. Dabei werden Ag-b-NP quantitativ von gelösten Silberspezies getrennt. Durch diese spezifische Probenvorbehandlung werden die Hintergrundsignale bei sp-ICP-MS-Messungen auf ein absolutes Minimum reduziert, was den Weg zur Quantifizierung und Bestimmung von Partikelgrößenverteilungen von Ag-b-NP in Umweltproben mit einer Größe < 20 nm ebnet. Die Cloud-Point-Extraktion wurde darüber hinaus mit der Elektronenmikroskopie gekoppelt, um die Bildgebung von Ag-b-NP in Umweltproben zu ermöglichen.

Diese Technik wurde erfolgreich auf verschiedene Umweltproben angewendet. So wurden z. B. ng L^{-1} Spuren von Ag-b-NP in Flusswasser bestimmt, wobei das Vorkommen dieser Partikel hauptsächlich auf Abwässer von Kläranlagen zurückzuführen ist. Darüber hinaus konnte gezeigt werden, dass Ag-b-NP aus metallischen Leitungswasserrohren in Leitungswasser freigesetzt, aber auch in Seen auf natürliche Weise gebildet werden können. Sobald Ag-b-NPs ins Seewasser gelangen, werden sie im Wesentlichen aufgelöst.

Abstract

The present study focuses on the determination of silver-based nanoparticles (Ag-b-NPs) in environmental samples, such as tap water, wastewater, natural waters and lake sediments. Hitherto, determination of Ag-b-NPs in such samples has been challenging with current analytical techniques, owing to the particles' low concentrations in the ng L^{-1} range and the co-existence of high amounts of dissolved Ag(I) species and other naturally occurring samples constituents.

Single-particle inductively coupled plasma mass spectrometry (sp-ICP-MS) is a promising technique able to simultaneously determine the concentration and particle sizes of nanoparticulate analytes such as Ag-b-NPs even at concentrations of only several ng L^{-1}. However, sp-ICP-MS suffers from the coexistence of dissolved analyte species causing high background signals. These background signals cover a majority of signals deriving from the nanoparticulate analytes and therefore limit the size detection limit (SDL), i.e. the minimum particle size detectable. Ag-b-NPs in environmental samples usually size diameters < 20 nm. Unfortunately, current sp-ICP-MS approaches can barely reach such low SDL values.

In this study, sp-ICP-MS has, thus, been combined with a surfactant-mediated sample pre-treatment, the so-called Cloud Point Extraction (CPE), which allows for the selective extraction and enrichment of Ag-b-NPs from environmental samples. Thereby, Ag-b-NPs are quantitatively separated from dissolved silver species. Due to this specific sample pretreatment, background signals during sp-ICP-MS measurements are reduced to an absolute minimum, paving the way to quantification and determination of particle size distributions of Ag-b-NPs in environmental samples sizing < 20 nm. Cloud Point Extraktion has also been coupled to electron microscopy to allow for picturing Ag-b-NPs in environmental samples.

This technique has been successfully applied to different environmental samples. For instance, ng L^{-1} traces of Ag-b-NPs in river water have been determined whereas the occurrence of these particles is mainly attributed to wastewater treatment plant effluents. Moreover, it could have been shown that Ag-b-NPs can be released from metallic tap water tubes into tap water but can also be formed naturally in lakes. Once Ag-b-NPs reach sea water, they are substantially dissolved.

Abkürzungsverzeichnis

AF^4	Asymmetrische-Fluss-Feldflussfraktionierung
Ag-NP	Silbernanopartikel
Ag-b-NP	silberbasierte Nanopartikel
CA	Citrat
cmc	critical micelle concentration (*engl.* kritische Mizellbildungskonzentration)
CPE	Cloud-Point-Extraktion
DIC	dissolved inorganic carbon (*engl.* gelöster organischer Kohlenstoff)
DLS	dynamische Lichtstreuung
EDTA	Ethylendiammintetraacetat
EDX	energiedispersive Röntgenspektroskopie
ENP	engineered nanoparticle (*engl.* technisch hergestellter Nanopartikel)
ET-AAS	elektrothermale Atomabsorptionsspektrometrie
FFF	Feld-Fluss-Fraktionierung
GPC	Gel-Permeations-Chromatographie
HKL	Hohlkathodenlampe
iCPE	improved CPE (*engl.* verbesserte CPE)
ICP-MS	inductively coupled plasma mass spectrometry (*engl.* Massenspektrometrie mit induktiv gekoppeltem Plasma)
LC$_{50}$	mittlere letale Konzentration
m/z	Masse-zu-Ladungs-Verhältnis
NOM	natural organic matter (*engl.* natürliches organisches Material)
NP	Nanopartikel
NWG	Nachweisgrenze
PEC	predicted environmental concentration (*engl.* prognostizierte Umweltkonzentration)
pH	negativer dekadischer Logarithmus der Protonenkonzentration
PNEC	predicted non effect concentration (*engl.* prognostizierten Konzentration ohne negative Umwelteffekte)
REM	Rasterelektronenmikroskopie

rCPE	repetitive iCPE
RQ	Risikoquotient
SDL	size detection limit (*engl.* Größenbestimmungsgrenze)
sp	single particle (*engl.* Einzelpartikel)
T$_{CP}$	Cloud-Point-Temperatur
TC	total carbon (*engl.* gesamter Kohlenstoff)
TEM	Transmissionselektronenmikroskopie
TIC	total inorganic carbon (*engl.* gesamter anorganischer Kohlenstoff)
TOC	total organic carbon (*engl.* gesamter organischer Kohlenstoff)
TOF	time of flight (*engl.* Flugzeit)
TX-114	Triton X-114
UPW	ultra pure water (*engl.* ultrareines Wasser)
UV/Vis	ultraviolette/sichtbare Strahlung
WHO	World Health Organization (*engl.* Weltgesundheitsorganisation)

Inhaltsverzeichnis

1 Einleitung, Zielsetzung und Motivation

« In the year 2000, when they look back at this age, they will wonder why it was not until the

year 1960 that anybody began seriously to move in this direction. » [1]

« Wenn man im Jahr 2000 auf heute zurückblickt, wird man sich fragen, warum erst im Jahr 1960 jemand

ernsthaft begann, in diese Richtung zu forschen. » [2]

So stellt sich *Richard Feynman*, Physiker und Nobelpreisträger, bei seiner zukunftsweisenden Rede „There's Plenty of Room at the Bottom" (zu Deutsch: „Viel Spielraum nach unten" [2]) im Rahmen der Jahresversammlung der Amerikanischen Physikalischen Gesellschaft am California Institute of Technology unseren heutigen Blick auf die Anfänge der Nanotechnologie vor.

« But I am not afraid to consider the final question as to whether, ultimately—in the great

future—we can arrange the atoms the way we want; the very atoms, all the way down! What

would happen if we could arrange the atoms one by one the way we want them (within

reason, of course; you can't put them so that they are chemically unstable, for example)? Up

to now, […] we must always accept some atomic arrangement that nature gives us. » [1]

« Dennoch scheue ich mich nicht, in letzter Konsequenz über die Frage nachzudenken, ob wir zu guter Letzt —

in ferner Zukunft — die Atome so anordnen können, wie wir es wollen. Die bloßen Atome, bis ins Kleinste! Was

würde geschehen, wenn wir die Atome so anordnen können, wie wir wollen (natürlich in gewissen Grenzen,

man kann sie zum Beispiel nicht so platzieren, dass sie chemisch instabil sind)? Bisher […] müssen wir immer

eine gewisse Atomordnung akzeptieren, die uns die Natur vorgibt. » [2]

Er schilderte damals seine Visionen von einer Technologie, die es erlaubt, Atome beliebig anzuordnen, um schließlich miniaturisierte Computer und Maschinen auf atomarer Ebene herzustellen und zu betreiben. Tatsächlich begründeten viele seiner Ideen das erst sehr viel später als Nanotechnologie bezeichnete Forschungsgebiet.

So war es der Japaner *Norio Taniguchi*, der 1974 als erster den Terminus „Nanotechnologie" benutzte. Unabhängig von *Taniguchi* verwendete ab 1986 *Eric Drexler* diesen Begriff in vielen,

meist populärwissenschaftlichen Berichten, die letztlich *Richard E. Smalley* zur Entwicklung und Untersuchung der Fullerene inspiriert haben sollen. Fullerene sind kugelförmige, nanoskalige Käfigstrukturen aus meist 60 Kohlenstoffatomen oder mehr und werden zu Ehren des Architekten und Kuppelbauers *Richard Buckminster Fuller* auch Buckminster-Fullerene genannt. *Smalley* erhielt zusammen mit *Robert F. Curl* und *Harold Kroto* 1996 für die Entdeckung der Fullerene den Nobelpreis für Chemie.[3]

Feynman nennt in seiner damaligen Rede jedoch auch die Limitierungen, die eine Entwicklung der von ihm erträumten Systeme bisher noch nicht möglich gemacht haben. Insbesondere beklagt er die in den 1960er Jahren noch unzureichende Entwicklung der Bildgebungstechnologie auf atomarer Ebene.[1]

Erst in den 1980er Jahren öffneten die Physiker *Gerd Binning*, *Ernst Ruska* und *Heinrich Rohrer* durch die Entwicklung der Rastertunnelmikroskopie als bildgebendes Verfahren auf atomarer Ebene die Tore zur „Nano-Welt". Alle drei wurden 1986 dafür mit dem Nobelpreis für Physik ausgezeichnet. Seither überschlagen sich die Ereignisse und machen die Nanotechnologie zu einem der am stärksten wachsenden Technologiezweige unserer Zeit.[3]

Die von *Feynman* angesprochenen Nanomaschinen bzw. molekularen Maschinen – also supramolekulare Verbindungen, die mechanische Bewegungen ausführen können – konnten beispielsweise erst viele Jahre später durch *Jean-Pierre Sauvage*, *Sir J. Fraser Stoddart* und *Bernard L. Feringa* realisiert werden, die dafür 2016 mit dem Nobelpreis für Chemie ausgezeichnet wurden.[3]

Die Nanotechnologie umfasst mittlerweile zahlreiche Felder, wie Nanopartikel, nanostrukturierte Oberflächen oder molekulare Maschinen. Diese Arbeit ist insbesondere auf Nanopartikel (NP) gerichtet, die gemäß IUPAC als partikelförmige Gebilde mit einer Größe im Bereich von 1 bis 100 nm definiert sind.[4]

NP sind jedoch keine Erfindung des 21. Jahrhunderts – ganz im Gegenteil. Deren dokumentierte Verwendung, wenngleich unbewusst, reicht sogar bis in die Antike zurück. Bereits die Römer nutzten kolloidales Gold zum Färben von Glas, wobei Farben von Violett bis Rot erreicht werden konnten.[3] NP werden heute in extrem vielfältiger Weise angewandt und

haben Einzug in viele Bereiche des Alltags gefunden: So enthält Sonnencreme zur Absorption von hautschädlicher UV-Strahlung nanoskaliges TiO_2.[3] TiO_2-NP werden auch in Wandfarbe suspendiert und sind aufgrund ihrer photokatalytischen Eigenschaften in der Lage, Moleküle zu zersetzten, die für schlechte Gerüche in Räumen verantwortlich sind.[5] Außerdem werden NP-basierte Produkte zur Oberflächenveredelung eingesetzt, um in Anlehnung an den Lotus-Effekt nanostrukturierte, selbstreinigende Oberflächen zu schaffen.[6] NP werden auch in Spezialanwendungen eingesetzt, wie der heterogenen Katalyse,[7-9] der Sensortechnik,[10] in medizinischen Anwendungen zur Diagnose sowie zur Aufklärung des Wirkstofftransports [11] oder als optische Anwendung in Form von Quantum-Dots [12]. Außerdem spielen NP (z.B. TiO_2) bei der Herstellung neuartiger Fluide, die beim Hydraulic-Fracturing eingesetzt werden, eine Rolle.[13] In der Analytik sind Lanthanoid-dotierte $NaYF_4$-NP in der Lage, molekulare Fluorophore für Bioapplikationen zu ersetzten.[14] Magnetische Nanopartikel können zur Anreicherung und Reinigung von Analyten verwendet werden.[15-17] In der Umwelttechnik werden Fe-NP zur Reinigung von mit chlorierten Lösungsmitteln belastetem Boden und Wasser verwendet.[18, 19]

Eine der bedeutendsten Vertreter der NP sind Silber-Nanopartikel (Ag-NP). Aufgrund ihrer antimikrobiellen Eigenschaften werden Ag-NP mittlerweile in einer Vielzahl von Artikeln des täglichen Lebens eingesetzt, beispielsweise als Zusätze zu Kosmetika oder bei antimikrobiellen Beschichtungen und Textilien.[20] Aufgrund der außerordentlichen Relevanz von Ag-NP ist der Verwendung dieser Partikel ein eigenes Kapitel (siehe Kapitel 2.2.2) gewidmet.

Werden Ag-NP-haltige Produkte verwendet, so kommt es unweigerlich zu einer Freisetzung der Ag-NP in die Umwelt – sei es bei Herstellung, Verwendung oder Entsorgung dieser Produkte. Die Eintragsrouten von Ag-NP in natürliche Gewässer verlaufen meist über Haushalts- und Industrieabwässer.[21] Ag-NP können aufgrund ihrer antimikrobiellen Eigenschaften auf viele Organismen toxisch wirken und stellen somit eine potentielle Gefahr für den Mensch und die Umwelt dar. Das Risiko und die Umweltrelevanz der Ag-NP wird in den Kapiteln 2.2.3 und 2.2.4 ausführlich diskutiert.

Die vorliegende Arbeit stellt sich insbesondere die Frage, wie Ag-NP in die Umwelt eingetragen werden können, in welchen Mengen sie dort verbleiben und welchem Schicksal sie

unterliegen. Da die Reaktivität und Mobilität von Ag-NP in natürlichen Systemen ganz entscheidend von der Partikelgröße abhängen, ist auch die Größenverteilung von Ag-NP in der Umwelt von großem Interesse.[22] Die Literatur liefert bis heute dazu noch keine zufriedenstellende Antwort. Ursache dafür ist das Fehlen geeigneter Analyseverfahren, um Ag-NP in Umweltmatrices selbst bei geringen Konzentrationen im ng L^{-1} Bereich selektiv nachweisen zu können.

Im Rahmen dieser Arbeit wurde deshalb ein analytisches Verfahren zur Quantifizierung und Bestimmung der Partikelgrößenverteilung von Ag-NP in Umweltmatrices entwickelt. Im Bereich der Instrumentellen Analytischen Chemie etablierte Systeme, wie die Atomabsorptionsspektrometrie oder Plasma-Massenspektrometrie, sind zwar in der Lage, Silberspuren in Umweltmatrices zu quantifizieren, können aber nicht zwischen gelösten und nanopartikulären Analyten unterscheiden. Das Fundament der im Rahmen dieser Arbeit eingesetzten Analytik ist deshalb die Einzelpartikel-Massenspektrometrie – eine neuartige Entwicklung im Bereich der Plasma-Massenspektrometrie, die es erlaubt, nicht nur nanopartikuläre Analyten zu quantifizieren, sondern simultan deren Partikelgröße zu bestimmen. Die Größenbestimmung wird jedoch von einem durch gelöste Analytspezies hervorgerufenes Untergrundrauschen stark eingeschränkt. Da Ag-NP in Umweltproben fast ausschließlich zusammen mit gelösten Silberspezies existieren, war es deshalb notwendig, die Einzelpartikel-Massenspektrometrie mit einem Verfahren zur Trennung von Ag-NP und gelösten Ag-Spezies zu koppeln.

Dazu kam eine in einem vorherigen Projekt entwickelte Methode zur speziesselektiven Anreicherung von Ag-NP aus Umweltproben zum Einsatz, die sogenannte Cloud-Point-Extraktion.[23-25] Diese Technik erlaubt es, Ag-NP in Gegenwart gelöster, ionischer Silberspezies selektiv in einer Tensidphase anzureichern. Hierbei war jedoch stets eine gewisse, wenn auch geringe, Koextraktion von gelöstem Silber in die Tensidphase zu verzeichnen. Die außerordentliche Empfindlichkeit der Einzelpartikel-Massenspektrometrie gegenüber gelösten Ag-Spezies machte es deshalb notwendig, diese Koextraktion durch Einsatz ausgewählter Komplexbildner für gelöste Ag-Spezies während der Extraktion auf ein absolutes Minimum zu reduzieren.

Die hier entwickelte Methode wurde anschließend auf ihre Anwendbarkeit als routinefähiges Messsystem für ein effizientes Umweltmonitoring getestet und unter anderem zur Analytik von Ag-NP in Trinkwasser, Klärwerksströmen, Flüssen, Binnengewässern und Seesedimenten angewendet. Es wurde darüber hinaus untersucht, ob Ag-NP auch auf natürliche Weise gebildet werden und somit nicht ausschließlich anthropogener Natur sind. Ferner konnte geklärt werden, ob Ag-NP in Meerwasser noch stabil sind, sobald sie über Flüsse dorthin gelangen.

Abschließend sei angemerkt, dass Ag-NP technisch unterschiedlich oberflächenbehandelt sind und in der Umwelt einer Vielzahl von Transformationen unterliegen (siehe Kapitel 2.2.4). Um der Existenz von verschiedenen Beschichtungen sowie unterschiedlicher chemischer Zusammensetzungen (Silber, Silberhalogenid, Silbersulfid u.v.m.) Rechnung zu tragen, wird nachfolgend der Sammelbegriff „silberbasierte Nanopartikel" (Ag-b-NP) in Bezug auf die Gesamtheit des Nanosilbers verwendet.

2   Nanomaterialien

2.1   Definition und bedeutende Vertreter

Die Klassifizierung „Nano" (*altgr.* nànos, Zwerg) ist strengen Definitionen unterworfen: Nanomaterialien zeichnen sich dadurch aus, dass mindestens die Hälfte der Oberflächenstrukturen 1 bis 100 nm messen.[4] Erstrecken sich diese Abmessungen in alle drei Raumrichtungen, so liegen Nanopartikel (NP) vor. Sind solche Abmessungen nur in zwei bzw. einer Dimension vorhanden, so spricht man von Nanofasern bzw. Nanoplättchen.[4] NP können natürlichen Ursprungs sein, wie z.B. Viren, Proteine oder auch Staubpartikel nach Waldbränden oder Vulkanausbrüchen. Zur Abgrenzung gegenüber anthropogenen Nanomaterialien hat sich für letztere der Begriff ENPs (*engl.* engineered nanoparticles, technisch hergestellte Nanopartikel) etabliert. ENPs werden gezielt hergestellt und meist als Beimischung zu Produkten verwendet, um spezielle technische Effekte zu erzielen. Die Einsatzgebiete von Nanopartikeln sind extrem breit gefächert, weshalb die Nanotechnologie zurecht als Schlüsseltechnologie des 21. Jahrhunderts bezeichnet werden kann.

Sun et al. zählen nanoskaliges TiO_2, ZnO sowie Ag zu den industriell bedeutendsten Metall(oxid)-Nanopartikeln. TiO_2- sowie ZnO-NP weisen sehr hohe Produktionsvolumina auf, beispielsweise 10.200 t bzw. 1.580 t in der EU für das Jahr 2012. Ag-NP werden zwar in geringeren Mengen produziert (32,4 t in der EU für das Jahr 2012), stellen jedoch diejenigen NP dar, die in den meisten Produktkategorien eingesetzt sind.[26, 27] Tatsächlich werden in einem Drittel aller NP-enthaltenden Produkte Ag-NP verwendet.[28]

Anatas-TiO_2 wird insbesondere in Sonnencreme und dabei ausschließlich in nanoskaliger Form als UV-Absorbens eingesetzt.[29] Der Einsatz von nanoskaligem TiO_2 in Sonnencreme hat unter anderem den Vorteil, dass die Creme nach Auftragung auf die Haut transparent ist und dennoch vor schädlicher UV-Strahlung schützt. Aufgrund besonderer photokatalytischer Eigenschaften werden Anatas-TiO_2-NP in selbstreinigender Wandfarbe im Außenbereich verwendet. Eine Bandlücke von 3.2 eV in Anatas macht eine Anregung über UV-Licht (ca. 380 nm Wellenlänge) unter Bildung eines Elektronen-Loch-Paares möglich. Durch Wechselwirkung der angeregten TiO_2-NP mit Luftsauerstoff oder Luftfeuchtigkeit entstehen radikalische Moleküle, die organische Substanzen auf der NP-Oberfläche, wie beispielsweise Schmutzpartikel oder geruchsbildende Substanzen, zersetzen. Durch Dotierung der TiO_2-NP

mit Fremdmetallen kann die Bandlücke so verändert werden, dass auch eine Anregung mit Strahlung außerhalb des UV-Bereichs erfolgen kann. So ist ein Einsatz der selbstreinigenden Wandfarbe selbst im Innenbereich möglich, wo aufgrund der UV-Absorption durch Fensterglas kaum UV-Strahlung auftritt.[30] Auch ZnO-NP sind im sichtbaren Bereich des Lichtspektrums transparent, absorbieren jedoch UV-Strahlung und werden deshalb als physikalischer UV-Filter in Sonnenschutzmitteln eingesetzt. Da diese NP zusätzlich antimikrobielle Eigenschaften haben, werden sie auch in Textilien, Holz sowie Kunstoffen verwendet.[31] Bei Produkten mit Ag-b-NP wird vor allem deren antimikrobielle Wirkung ausgenutzt.[28] Da der Einsatz von Ag-b-NP, wie nachfolgend dargelegt, extrem vielseitig ist, geht damit eine erhöhte Umweltrelevanz einher. Die vorliegende Arbeit adressiert deshalb insbesondere den Bereich von silberbasierten Nanopartikeln.

2.2 Silbernanopartikel

2.2.1 Herstellung, Stabilisierung und Charakterisierung

Die folgenden Ausführungen betreffen Ag-b-NP, sind jedoch in den Grundzügen auf praktisch alle Metall(oxid)-NP anzuwenden.

Grundsätzlich können Ag-b-NP in einem bottom-up oder einem top-down Verfahren hergestellt werden.[32] Beim bottom-up Verfahren werden die Ag-b-NP ausgehend von gelöstem Ag(I) hergestellt, indem das gelöste Ag(I) mit geeigneten Reduktionsmitteln, wie beispielsweise Natriumborhydrid, Hydrazin oder Citrat, zu Ag(0) reduziert wird. Aus dem entstehenden elementaren Silber, das in Lösung gewissermaßen stark dispergiert vorliegt, bildet sich an Nukleationskeimen partikuläres Silber.[33] Da die NP-Bildung und deren Wachstum stark von der Anzahl der Nukleationskeime abhängt, ist die Reaktion kinetisch gesteuert und daher nur schwer in Morphologie und Partikelgrößenverteilung reproduzierbar.[32, 34] Im Gegensatz dazu bietet das top-down Verfahren die Möglichkeit, Ag-b-NP mit engerer Partikelgrößenverteilung herzustellen, weshalb dieses Verfahren insbesondere großtechnisch relevant ist. Dabei werden makroskopische Festkörper (z.B. elementares Silber), mechanisch in nanoskalige Teilchen umgewandelt. Die Umwandlung kann durch Zermahlen, Ultraschallzerkleinerung oder Laserablation erfolgen. Da sich die Festkörper dabei meist in einem wässrigen Medium befinden, wird eine NP-Dispersion erhalten. Bei Ag-b-NP ist die Laserablation die Methode der Wahl. Dabei werden

hochenergetische Laserpulse auf den Festkörper gerichtet, was eine NP-Abgabe in das den Festkörper umgebende Medium induziert. Es ist ferner vorteilhaft, dass beim top-down Verfahren reine Ag-b-NP-Dispersionen ohne jegliche Verunreinigungen erhalten werden – im Gegensatz zum bottom-up Verfahren, bei dem die Ag-b-NP in Gegenwart von umgesetztem und nicht umgesetztem Reduktionsmittel vorliegen.[35]

Ag-b-NP sind aufgrund ihrer extrem hohen intrinsischen Oberfläche äußerst reaktiv, aggregieren jedoch sehr leicht zu einer thermodynamisch günstigeren Form. Da dies mit einem Verlust an Reaktivität einhergeht, wird eine Aggregation durch Zusatz von an die Partikeloberfläche adsorbierenden Stabilisierungsmitteln unterbunden. Insgesamt gibt es drei Stabilisierungskonzepte: bei der elektrostatischen Stabilisierung mit beispielsweise Citrat weisen die Partikel eine negativ geladene Citrat-Hülle auf und stoßen sich aufgrund gleichnamiger Ladung untereinander ab. Polyvinylpyrrolidon (PVP) ist ein Polymer, das zur sterischen Stabilisierung von NP eingesetzt werden kann. Eine sterisch anspruchsvolle Ligandensphäre reduziert eine interpartikuläre Wechselwirkung und damit die Wahrscheinlichkeit einer Aggregation. Zusätzlich ist auch eine Kombination beider Stabilisierungskonzepte denkbar, die sogenannte elektrosterische Stabilisierung. Langkettige Carbonsäuren können beispielsweise eingesetzt werden, um Partikel gleichzeitig sterisch und elektrostatisch zu stabilisieren.[32]

Industriell hergestellte Ag-NP werden insbesondere im Hinblick auf deren chemische Zusammensetzung, Morphologie und Partikelgrößenverteilung charakterisiert. Meistens kommen dabei bildgebende Verfahren der Elektronenmikroskopie oder laserbasierte Verfahren zum Einsatz. Den analytischen Methoden der Nanotechnologie ist nachfolgend das Kapitel 3 gewidmet.

2.2.2 Eigenschaften und Verwendung

Die vielfältigen Einsatzmöglichkeiten von Ag-b-NP sind insbesondere den folgenden vier Eigenschaften geschuldet:

Industriell besonders bedeutend ist die **antimikrobielle** Eigenschaft von Ag-b-NP. Eine biozide Wirkung gegen multiresistente Bakterien, Hefen, Pilze und Viren ist bekannt.[36] Ag-b-NP kommen deshalb zur Infektionsprophylaxe und im medizinischen Bereich in Form

von Wundauflagen, Verbandsmaterialien und Wandfarbe zum Einsatz.[37-39] Zudem sind mit Ag-b-NP versetzte Textilien auf dem Markt, die insbesondere im Sportbereich verwendet werden, um bakterienbedingte Geruchsbildung zu hemmen.[40-45] Im Zuge der SARS-Cov-2-Pandemie im Jahr 2020/2021 wurde außerdem die viruzide Eigenschaft von Ag-b-NP gegen das neuartige Corona-Virus mehrfach bestätigt.[46-49] *Balagna* et al. berichten beispielsweise von mit Ag-b-NP behandelten Atemschutzmasken, die die Viruslast der eingeatmeten Luft deutlich herabsetzen.[46]

Neben den antimikrobiellen Eigenschaften ist auch die **elektrische und thermische Leitfähigkeit** von Ag-b-NP herausragend. Silber als das Element mit der höchsten elektrischen und thermischen Leitfähigkeit wird in nanopartikulärer Form deshalb auch in der Elektronik in Form von transparenten, leitfähigen Folien eingesetzt.[36, 50]

Ag-b-NP zeichnen sich weiterhin durch einen optischen Effekt, der sogenannten **Plasmonenresonanz**, aus. Plasmonen sind Schwingungen von freien Elektronen in Metallen, die sich gegenüber ihren Ionenrümpfen bewegen. Treten diese an der Oberfläche eines Metalls auf, spricht man von Oberflächenplasmonen. Da solche Oberflächenplasmonen durch sichtbares Licht einer spezifischen Wellenlänge angeregt werden können, weisen Ag-b-NP eine spezifische Absorptionsbande im Wellenlängenbereich zwischen 300 und 400 nm auf.[51] Der Absorptionsprozess von Strahlung durch Nanopartikel wird als Oberflächenplasmonenresonanz bezeichnet. Da die Stärke dieser Resonanz von der Morphologie und Partikelgröße der Ag-b-NP abhängt, ist es möglich, die durchschnittliche Partikelgröße von Ag-b-NP anhand der Lage der Absorptionsbande der Oberflächenresonanz zu bestimmen.[52] Aufgrund dieser besonderen optischen Eigenschaften werden Ag-b-NP ferner im Bereich der Sensortechnik und Spektroskopie eingesetzt.[53] Ein Beispiel ist der Einsatz von Ag-b-NP oder anderen metallischen NP mit geeigneter Oberflächenplasmonenresonanz in der oberflächenverstärkten Ramanspektroskopie (SERS, *engl.* Surface Enhanced Raman Spectroscopy). Durch den Zusatz von NP zu den zu untersuchenden Proben kann das Raman-Signal deutlich verstärkt werden.[54]

Die **katalytische** Eigenschaft von Silber wird durch die intrinsisch hohe Oberfläche intensiviert. In der Literatur wird beispielweise berichtet, dass die auf ein Trägermaterial

immobilisierten Ag-b-NP die CO- oder Benzol-Oxidation oder auch eine reduktive Darstellung von 4-Aminophenol aus 4-Nitrophenol katalysieren können.[55, 56]

2.2.3   Silbernanopartikel – Chancen und Risiken

Wie im vorangehenden Kapitel dargestellt, haben Ag-b-NP insbesondere aufgrund ihrer antimikrobiellen Eigenschaften Einzug in viele Bereiche des täglichen Lebens gefunden. Die Nanotechnologie bereichert zweifelsohne unsere Zeit – stößt jedoch auch auf Kritik und Bedenken in der Bevölkerung und der Wissenschaftsgemeinde.[57] In diesem Zusammenhang wird meist eine mögliche Toxizität von Ag-b-NP auf Mensch und Natur diskutiert – besonders wenn diese Nanopartikel in die aquatische Umwelt freigesetzt werden.

Ein Werkzeug zur Risikoabschätzung von Ag-b-NP in der Umwelt ist im Anhang 1 der REACH-Verordnung zu finden.[58] Demnach ist das Risiko einer bestimmten Substanz von deren Exposition und Toxizität abhängig. Ein Risikoquotient RQ lässt sich dazu aus der prognostizierten Umweltkonzentration PEC (*engl.* predicted environmental concentration) und der prognostizierten Konzentration ohne negative Umwelteffekte $PNEC$ (*engl.* predicted non effect concentration) nach folgender Gleichung (2.1) berechnen:

$$RQ = \frac{PEC}{PNEC} \tag{2.1}$$

Für $RQ \ll 1$ sind vernachlässigbare Risiken zu erwarten, für $RQ > 1$ besteht eine signifikante Umweltgefahr. Eine Gefahr geht somit nur von Substanzen aus, bei denen $PEC > PNEC$ ist. Stark exponierte Substanzen weisen beispielsweise bei geringer Toxizität ein geringes Risiko auf. Umgekehrt können Substanzen aufgrund einer hohen Toxizität bereits bei geringen Umweltkonzentrationen ein Risiko darstellen. Für Ag-b-NP gilt also, dass das Risiko von deren Toxizität sowie der Umweltexposition abhängt.

Der folgende Abschnitt soll einen kursorischen Einblick in Studien zur Toxizität von Ag-b-NP, insbesondere in aquatischen Matrices, geben.

Allein die Tatsache, dass Ag-b-NP antimikrobiell wirken, impliziert eine gewisse Toxizität von Silber. Die Frage, ob von Silber in gelöster Form eine stärkere toxische Wirkung ausgeht als

von Ag-b-NP, konnte bis heute nicht zweifelsfrei geklärt werden. Studien zeigen zum Teil, dass Ag-b-NP toxischer wirken als die gleiche Menge Silber in ausschließlich gelöster Form. So wurden beispielsweise unterschiedliche Organismen mit Ag-b-NP und Ionen behandelt. Dabei wurde festgestellt, dass bei Behandlung mit NP die Expression stressassoziierter Proteine häufiger auftritt als bei Behandlung mit Ionen.[59, 60] Andere Studien mit Zebrafisch-Embryonen kommen aber zum Schluss, dass NP und Ionen gleichermaßen toxisch wirken.[61] Es ist jedoch anzumerken, dass viele Toxizitätsstudien von Ag-b-NP, aber auch von anderen untersuchten NP, nur sehr schwer vergleichbar sind, da bei den Studien unterschiedliche Organismen, Matrices und Konzentrationen der aktiven Spezies betrachtet werden.[62]

Die toxische Wirkung von Ag-b-NP beruht auf aus den Partikeln freigesetzten Silberionen und entspricht damit der der ionischen Spezies. Durch langsame Oxidation mit in Wasser gelöstem Luftsauerstoff setzt Silber in wässrigen Matrices Silberionen frei. Dies gilt insbesondere für Ag-b-NP, denn im Gegensatz zu Bulk-Silber ist die Freisetzung von Ionen aus Ag-b-NP aufgrund der extrem höheren intrinsischen Oberfläche deutlich verstärkt.[63]. Ag-NP sind im Körper sehr mobil und bioverfügbar. Es liegen Hinweise vor, dass sie Zellmembranen durchdringen [64-66] und sogar die Blut-Hirn-Schranke passieren können [67].

Neben rein qualitativen wurden auch quantitative Untersuchungen zur Toxizität von Ag-b-NP durchgeführt, die zu sehr unterschiedlichen Ergebnissen geführt haben, aber die Abschätzung einer Größenordnung für die toxische Konzentration möglich machen. Mitunter wurden negative Effekte von Ag-b-NP bereits bei Konzentrationen im Bereich des Grenzwerts von Silber für Trinkwasser von 100 µg L^{-1} (WHO) bzw. 10 µg L^{-1} (deutsche Trinkwasserverordnung) [64, 68, 69] festgestellt. Der LC_{50}-Wert, also die Konzentration, bei der 50% der mit einer Substanz behandelten Individuen sterben, wird in der Literatur mit 40 µg L^{-1} angegeben, weshalb Ag-b-NP für aquatische Organismen als toxisch eingestuft werden. Ag-b-NP wirken auf Daphnien und Forellen nachweislich ab einer Konzentration von 40 µg L^{-1} bzw. 30-170 µg L^{-1} toxisch.[70, 71]

Aus den vorangehenden Ausführungen wird deutlich, dass von Ag-b-NP eine gewisse Toxizität ausgeht. Um abschließend das Risiko von Ag-b-NP abschätzen zu können, bedarf es jedoch noch Untersuchungen zur tatsächlichen Exposition von Ag-b-NP in der Umwelt (siehe

Gleichung 2.1). Die Frage, ob die oben genannten toxischen Konzentrationen von Ag-b-NP in natürlichen Gewässern wie Flüssen und Seen erreicht werden, soll im Rahmen dieser Arbeit geklärt werden.

2.2.4   Umweltrelevanz - Exposition und Transformation

Wie oben bereits dargelegt, ist die Textilindustrie ein Haupteinsatzgebiet der Ag-b-NP. Beim Waschen dieser Textilien werden Ag-b-NP aus den Fasern freigesetzt und über das Abwassersystem in die Umwelt eingetragen. Nach vier Waschgängen gelangen nahezu 100 % der in Textilien eingesetzten Ag-b-NP ins Abwasser.[42-44] Die so aus den Textilien freigesetzten Ag-b-NP bleiben intakt oder werden lediglich leicht modifiziert.[45, 72] Auch Ag-b-NP, die in Kosmetika eingesetzt werden, gelangen beispielsweise beim Duschen über das Abwasser ebenfalls in die Umwelt.[72]

Freigesetzte Ag-b-NP schlagen dann zunächst in den Klärwerken auf. *Li* et al. haben gezeigt, dass ein Großteil der Ag-b-NP gebunden an Schwebstoffe im Klärschlamm verbleibt, wohingegen nurmehr ein geringer Teil der Ag-b-NP über den Klärwerksablauf in Flüsse abgegeben wird.[21] Klärwerke sind also grundsätzlich die entscheidende Barriere für Ag-b-NP vor dem Eintrag in natürliche Gewässer. Der Klärschlamm wird mittlerweile meist thermisch verwertet, in geringerem Ausmaß jedoch als Dünger für Felder verwendet. Aufgrund des im Schlamm enthaltenen hohen Anteils von Ag-b-NP (neben weiteren Schwermetallen) stellt die Klärschlammdüngung jedoch ein gewisses Risiko für die Böden dar.[57, 73]. *Blaser* et al. gehen davon aus, dass 15 % des Silbers im gesamten Süßwasserökosystem der EU von der Anwendung von belastetem Klärschlamm in der Landwirtschaft stammen.[74] Die Belastung des Klärschlamms mit Ag-b-NP hat sogar zu einer Zunahme an silberresistenten Bakterien im Klärschlamm geführt.[75, 76]

Eine Gefahr, die von Ag-b-NP in natürlichen Gewässern ausgeht, ist deren Persistenz. Nanopartikuläres Silber reichert sich besonders in marinem Phytoplankton oder an Schwebstoffen, meist unlöslichem organischen Material im Wasser, in zunächst schwer abbaubarer Form an. Änderungen der Umweltbedingungen, wie Temperatur oder pH-Wert, können allerdings eine plötzliche Remobilisierung einleiten. Resultat ist ein in hohen lokalen Konzentrationen bioverfügbares Silber im Wasser.[77] Im Biosystem akkumulierte Ag-b-NP dienen also sozusagen als Depot für toxische Silberionen.[64]

Nicht alle Ag-b-NP in der Umwelt sind anthropogener Natur – ganz im Gegenteil können sie sich auch auf natürliche Weise bilden. In der Natur sind potentielle Reduktionsmittel wie Huminsäuren vorhanden, die in Gewässern vorhandene Silberionen zu Nanopartikeln reduzieren können. *Hartmann* et al. konnten in ersten Versuchen eine Bildung von Ag-NP aus Ionen durch NOM (*engl.* natural organic matter, natürliches organisches Material) zeigen.[23] Publikation 9 greift diese Thematik nochmals auf und untersucht die Grundprinzipien der natürlichen Bildung von Ag-b-NP aus gelösten Ag-Spezies in natürlichen Gewässern sowie vergleichend im Labormaßstab.

Abschließend soll das Schicksal von Ag-b-NP in der Umwelt kurz skizziert werden. Sobald sich Ag-b-NP in der Umwelt befinden, liegen sie zusammen mit einer Vielzahl an Substanzen vor, die mit den NP aufgrund ihrer großen Oberfläche leicht interagieren können und NP-Transformationen initiieren.[72, 78] Dabei können sich sowohl die chemische Zusammensetzung der Partikel also auch die Ligandensphäre, also die Partikelbeschichtung, ändern.[78]

Die teils hohe Umweltkonzentration von Halogeniden X (X = Cl, Br, I) in Gewässern zusammen mit der Schwerlöslichkeit von Silberhalogeniden sind die Ursache dafür, dass Ag-b-NP leicht in AgX-NP umgewandelt werden können.[78]

Wesentlich bedeutender ist aber die Tatsache, dass Silber, wie alle Edelmetalle, sehr oxidationsbeständig ist, aber eine hohe Thiophilie aufweist. Silbersulfid ist mit einem Löslichkeitsprodukt von $5.5 \cdot 10^{-51}$ das schwerlöslichste Silbersalz und eines der schwerlöslichsten Salze überhaupt. Die Transformationen in der Umwelt sind also insbesondere von der hohen Thiophilie des Silbers bestimmt.[78]

Es ist bisher detailliert untersucht worden, welchen Transformationen Ag-b-NP in Klärwerksmatrices, die einen hohen Anteil an Sulfid aufweisen, unterliegen. Basierend auf physikochemischen Berechnungen kann davon ausgegangen werden, dass alle ins Klärwerk eingetragenen Ag-b-NP als thermodynamisch begünstigtes Silbersulfid vorliegen oder damit beschichtet sind.[79] Die Reaktion von Ag-b-NP mit umweltrelevanten Sulfid-Konzentrationen ist rein kinetisch gesteuert und wird deshalb nicht durch die Sulfid-Konzentration limitiert.[80] Die Bildung von Silbersulfid kann weder durch

Oberflächenfunktionalisierungen und Coatings noch die chemische Zusammensatzung des Nanosilbers verhindert werden. Silbersulfide – im Gegensatz zu Sulfiden des Kupfers oder Zinks – bleiben sogar bei Kompostierung des Klärschlamms bestehen.[81] Aufgrund der extremen Schwerlöslichkeit von Silbersulfid senkt die Sulfidierung in Klärwerksmatrices die Toxizität der Ag-b-NP enorm.[82] Der Großteil der in die Klärwerke eingetragenen Ag-b-NP verbleibt gebunden an Schlammflocken im Klärschlamm.[83] *Bojeong* et al. konnten mittels elektronenmikroskopischer Untersuchungen gekoppelt mit energiedispersiver Röntgenfluoreszenzanalyse nachweisen, dass Nanosilber im Klärschlamm in Form von 5-20 nm großen α-Ag_2S-NP vorliegt, wobei überschüssiger Schwefel an der Oberfläche der Partikel gebunden ist.[84]

Mechanistisch gesehen reagieren entweder Ag-b-NP in einer Fest-Flüssig-Reaktion direkt mit gelöstem Sulfid oder Ag-b-NP werden zunächst mit gelöstem O_2 zum Oxid umgesetzt. Da Silberoxid besser wasserlöslich als Silber ist, werden nach der Oxidation deutlich mehr Silberionen freigesetzt, die in einem nachfolgenden Reaktionsschritt mit gelösten Sulfiden Ag_2S-NP bilden. Der alternative Reaktionsweg der oxidativen Auflösung und anschließender Sulfidierung betrifft insbesondere sehr kleine Partikel.[79] Sowohl die Bildung vollständiger Ag_2S-NP als auch die Ausbildung einer Ag_2S-Phase um einen mehr oder weniger großen Ag^0-Kern werden diskutiert.[85, 86]

Der Ligandenaustausch bei in die Umwelt freigesetzten Ag-b-NP ist weniger ausführlich untersucht. In Umweltmatrices existieren eine Vielzahl potentieller Liganden, besonders (Makro)Moleküle, wie z. B. schwefelhaltige Proteine, Huminsäuren und Tannine. Insbesondere diejenigen in die Umwelt eingetragenen Ag-b-NP, die mit schwach bindenden und sterisch wenig anspruchsvollen Liganden wie Citrat beschichtet sind, durchlaufen einen sehr schnellen Ligandenaustausch. Sind erst einmal schwefelhaltige Liganden auf der Oberfläche der Ag-Partikel adsorbiert, ist die Umwandlung zum Silbersulfid nicht mehr weit.[87, 88]

3 Nanopartikelanalytik: Standardverfahren und aktuelle Entwicklungen

Die Nanopartikelanalytik zeichnet sich insbesondere durch zwei Gruppen analytischer Verfahren aus: bildgebende und quantitative Verfahren. Erstere sind in der Lage, die Partikelgröße, Morphologie und gegebenenfalls chemische Zusammensetzung der Partikel zu bestimmen, während letztere auf die Bestimmung der Konzentration von nanopartikulären Analyten in meist wässrigen Proben gerichtet ist.

Wichtige Vertreter der bildgebenden Techniken sind **mikroskopische Verfahren**. Da die Auflösung einfacher Lichtmikroskopie nicht für den Nano-Bereich ausreicht, kommen elektronenmikroskopische Verfahren, wie die Rasterelektronenmikroskopie (REM) oder die Transmissionselektronenmikroskopie (TEM) zum Einsatz, die Auflösungen bis in den sub-nano Bereich ermöglichen. Neben Partikelgröße und Morphologie kann durch Kopplung mit energiedispersiver Röntgenfluoreszenzanalyse (EDX) die Elementzusammensetzung des untersuchten Nanomaterials ortsaufgelöst untersucht werden. Bildgebende Verfahren liefern einzigartige Informationen zu Nanopartikeln, die so nur sehr schwer mit anderen instrumentellen analytischen Methoden zugänglich sind, sind aber gleichzeitig sehr kosten- und zeitintensiv und bilden nur einen kleinen Anteilteil der Gesamtheit der Analytpartikel einer Probe ab. Um nicht nur Größe, Morphologie und chemische Zusammensetzungen der Partikel zu untersuchen, sondern auch eine repräsentative Abschätzung der Partikelkonzentration in der Probe vornehmen zu können, müssen deshalb viele Messungen durchgeführt werden. Um statistisch valide Aussagen zu treffen, sollte dabei die Partikelkonzentration mehr als 100 Partikel pro mL Probe betragen. Solch hohe Konzentrationen sind für Umweltproben nicht gegeben. Weitere Nachteile elektronenmikroskopischer Verfahren sind der hohe apparative Aufwand verbunden mit hohen Kosten je Messung.[89, 90] Publikation 4 beschreibt ein im Rahmen dieser Arbeit neu entwickeltes Verfahren zur Anreicherung von Ag-b-NP auf einem TEM-Probenträger, das eine elektronenmikroskopische Untersuchung von Ag-b-NP-Spuren in Umweltproben möglich macht. Doch auch dabei ist eine quantitative Aussage nicht möglich.

Quantitative Verfahren zur Bestimmung von NP, insbesondere im Spuren- und Ultraspurenbereich sind bisher rar. Konventionelle quantitative Analysetechniken, wie die

Atomabsorptionsspektrometrie oder die Massenspektrometrie, sind in den meisten Fällen nicht in der Lage, zwischen gelösten und nanopartikulären Analyten zu unterscheiden.

Neuste Entwicklungen im Bereich der **elektrothermalen Atomabsorptionsspektrometrie** (ET-AAS) ermöglichen jedoch, eine solche Unterscheidung zu treffen und sogar die Größe der untersuchten NP zu bestimmen. Diese Technologie, die von *Leopold* et al. entwickelt wurde, nutzt den Effekt aus, dass ionische Analytspezies in der ET-AAS zu einem geringfügig anderen Zeitpunkt atomisiert werden als nanopartikuläre Analyten und dass bei Letzteren sogar eine Abhängigkeit des Atomisierungszeitpunkts von der Partikelgröße besteht.[91-94]

Die **Einzelpartikel-Massenspektrometrie** (*engl.* Single Particle Inductively Coupled Plasma Mass Spectrometry, sp-ICP-MS) ist ein neuartiges massenspektrometrisches Verfahren zur größenselektiven Quantifizierung von NP bei geringen Konzentrationen. Details dazu sind in Kapitel 4.3.3 aufgeführt. Obwohl die Massenspektrometrie grundsätzlich eine Multielementanalyse ist, ist die Einzelpartikel-Massenspektrometrie bei Einsatz eines Quadrupolmassenselektors – was den häufigsten Fall darstellt – nicht in der Lage, mehrere Elemente in einem NP zu quantifizieren.[95] *Günther* et al. haben jedoch ein Messverfahren entwickelt, bei dem mit Hilfe eines Flugzeit-Massenspektrometers anstelle eines Quadrupol-Massenspektrometers mehrere Elemente gleichzeitig detektiert werden können. Dadurch können neben der Größe und Konzentration der NP auch Informationen über die Elementzusammensetzung der Partikel und damit über mögliche NP-Beschichtungen erhalten werden.[96]

Einige quantitative Verfahren in der Nanopartikelanalytik werden auch mit Maßnahmen zum Abtrennen nanopartikulärer Analyten kombiniert. Die in dieser Arbeit eingesetzte **mizellare Extraktion** ist nur ein Beispiel dafür. Auch mittels mechanischer Trennverfahren wie der **Ultra- und Nanofiltration** ist es möglich, NP der Größe von 100 bis 10 nm bzw. 10 bis 1 nm im Filtrat zurückzuhalten. Filtrationstechniken sind jedoch hauptsächlich als Aufreinigungsschritt nach Synthesen von Nanopartikeln zu finden, da der Einsatz von Membranen zur Abtrennung von NP aus spurenanalytischen Proben zu hohen Analyt-Verlusten führen würde. Aufgrund der hohen intrinsischen Oberfläche der NP adsorbieren diese nämlich stark an die Oberfläche der Membranen und werden so im Filter zurückgehalten. Ein Analytrückhalt im Filter ist insbesondere beim Einsatz von Membranen

zur Abtrennung von NP aus Umweltproben zu beobachten, da NP vorwiegend an in der wässrigen Probe vorhandenen Schwebstoffen adsorbiert vorliegen und so noch leichter im Filter verbleiben. Ein Einsatz von Filtrationstechniken zur Abtrennung von NP aus Realproben ist also nicht möglich.[97]

Um Messverfahren, die per se nicht zwischen NP-Größen unterscheiden können, zur größenaufgelösten Nanopartikelanalytik einsetzen zu können, stehen verschiedene Techniken zur Größenfraktionierung zur Verfügung, die den Messverfahren vorangestellt werden können.

Die **Elektrophorese** ist eine solche Größenfraktionierungstechnik und basiert auf einer Wanderung geladener Teilchen in einem elektrischen Feld. Die sogenannte elektrophoretische Mobilität hängt dabei von der Größe der Partikel und deren Ladung ab, sodass eine Auftrennung nach Partikelgrößen möglich ist.[98] Dieses Verfahren stammt zwar aus der Biochemie, kann aber auch für metallische NP verwendet werden.[99] Da nur Partikel getrennt werden können, die eine Ladung tragen, können ungeladene oder nur schwach geladene Partikel durch Modifikation mit geeigneten Liganden so modifiziert werden, dass sie eine elektrophoretische Mobilität aufweisen.[100] In Umweltproben stören Oberflächenmodifikationen der NP, die durch natürlich vorkommende Liganden hervorgerufen werden, die elektrophoretische Mobilität, weshalb ein Einsatz im Bereich der vorliegenden Arbeit nicht möglich ist. *Mozhayeva* et al. setzen Kapillarelektrophorese gekoppelt mit Einzelpartikel-Massenspektrometrie ein, um Ag-b-NP in Modellsystemen in Abhängigkeit von deren Größe sowie Oberflächenbeschichtung aufzutrennen.[101]

Auch die **Gelpermeationschromatographie** (GPC) ermöglicht die Größenfraktionierung von NP. Zum Einsatz kommt dabei eine Säule, die mit einer mobilen Phase laminar durchströmt wird. Partikel mit kleinem hydrodynamischem Radius passieren diese Säule langsamer als diejenigen mit großem Radius, da kleine Partikel leichter in die Hohlräume des Säulenmaterials diffundieren können und damit einen längeren Weg zurücklegen als größere Partikel. Damit werden große Partikel vor den kleineren Partikeln eluiert.[102] Auch diese Methode ist für den Einsatz in der Umweltanalytik von NP nur schlecht geeignet, da die natürlich vorkommenden Schwebstoffe die Lebensdauer der Säulen und die Trennleistung stark beeinträchtigen würden. Der unvermeidbare Analytverlust in den hochporösen GPC

Säulen ist darüber hinaus nicht mit den geringen Konzentrationen von NP in Umweltproben vereinbar.

Ein weiteres Beispiel für eine Technik zur Größenfraktionierung ist die **Feld-Fluss-Fraktionierung** (FFF). Die Methode basiert auf einer Flusszelle, die laminar durchströmt wird, wobei innerhalb der Zelle ein parabolisches Strömungsprofil ausgebildet wird. Bei der Asymmetrischen Fluss-FFF (AF4) wird ein zur Strömungsrichtung der Zelle senkrecht stehender zweiter Fluss eingesetzt (Cross Flow). Wie in untenstehender Abbildung dargestellt, bestimmt sich die Position von in der Flusszelle befindlichen NP durch ein Gleichgewicht zwischen der Diffusion in die Mitte der Zelle und der durch den cross-flow entgegengerichteten Kraft zum Rand der Zelle. Kleine Partikel befinden sich aufgrund des höheren Diffusionskoeffizienten weiter in der Mitte der Zelle und passieren diese aufgrund des parabolischen Strömungsprofils des Elutionsflusses schneller als große Partikel. Das AF4-System ist zur Detektion mit einem ICP-MS, einem UV/Vis- oder einem Lichtstreudetektor gekoppelt.[103-105] Vorteil eines AF4 Systems ist, dass Partikel durch Fokussierung in der Zelle vor der Fraktionierung angereichert werden können. Nachteile sind jedoch die hohen Anschaffungskosten, die geringen Wiederfindungen und der hohe Zeitaufwand einer Messung.[106-108] Ferner schränken natürlich vorkommende Schwebstoffe in Umweltmatrices die Lebenszeit der verwendeten Flusszellen deutlich ein. AF4-Systeme können neben metallischen NP auch Mikro- und Nanoplastik auftrennen. *Schwaferts* et al. beispielsweise verwenden die AF4 gekoppelt mit Ramanmikroskopie zur Separation und chemischen Charakterisierung von Nanoplastik in Wasserproben.[109]
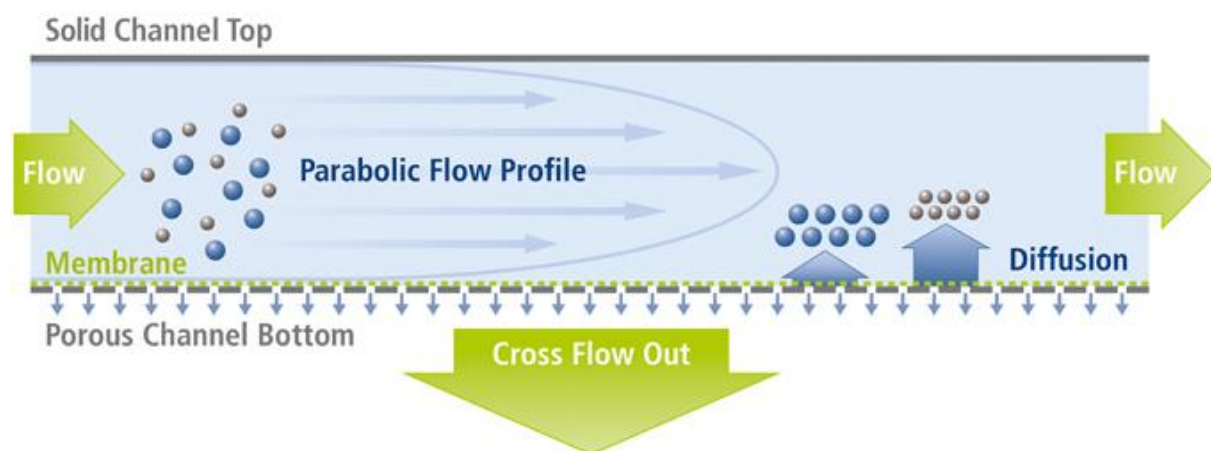
Abbildung 1: Schematische Darstellung der Größenfraktionierung bei der AF4. Durch ein Wechselspiel aus Diffusion und durch den Cross Flow entgegengerichteter Kraft verlassen kleinere Partikel die Flusszelle schneller als größere.[105]

Li et al. verwenden eine **Festphasenextraktion** zur Extraktion und Anreicherung von NP auf einer Säule, die mit alkylfunktionalisiertem Kieselgel gefüllt ist.[110] Zudem existieren Arbeiten über den Einsatz von **Ionenaustauscherharzen**, die Kationen oder Anionen zurückhalten. NP, die aufgrund ihrer Oberflächenfunktionalisierung Ladungen aufweisen, können so aus verschiedenen Umweltproben extrahiert werden.[111]

Aufgrund der Plasmonenresonanz metallischer NP, können diese auch mit Strahlung wechselwirken. Deshalb ist eine Konzentrationsbestimmung mittels **UV/Vis-Spektrometrie** möglich. Bei diesem spektrophotometrischen Verfahren wird die Extinktion bei einer spezifischen Wellenlänge bestimmt und damit über das *Lambert-Beer'sche* Gesetz die Konzentration der unbekannten Probe berechnet. Da die plasmonenbasierte Lichtabsorption von der Partikelgröße abhängt, kann durch Bestimmung der Lage der Absorptionsbande auch auf die Partikelgröße rückgeschlossen werden.[112] Da die Selektivität dieses Verfahrens aber sehr gering ist und andere photoaktive Stoffe in der Probe die Messung des Nanomaterials stören können, ist eine Verwendung in der Umweltanalytik nur schwer möglich.

Mittels Lichtstreuung an den Partikeln kann der hydrodynamische Radius der NP in Suspension bestimmt werden. Der hydrodynamische Radius wird definiert als der Radius einer hypothetischen festen Kugel, die in einem spezifischen Lösungsmittel die gleichen Diffusionseigenschaften aufweist wie der durch den hydrodynamischen Radius beschriebene Nanopartikel. Es ist dabei zu beachten, dass der hydrodynamische Radius stark vom eigentlichen Radius der Partikel abweichen kann. Eine Bestimmung des hydrodynamischen Radius erfolgt mittels **Dynamischer Lichtstreuung** (DLS), einer Standardtechnik für Kolloidsysteme. Dabei wird Laserlicht auf die in einer wässrigen Matrix suspendierten Nanopartikel geleitet, wobei die auftreffende Strahlung an den NP als Streuzentren gestreut wird und das an verschiedenen Streuzentren entstehende Streulicht miteinander interferiert. Da sich die Streuzentren aufgrund der *Brown'schen* Molekularbewegung ständig relativ zueinander bewegen, fluktuiert die Stärke der Interferenz und damit die Intensität des Streulichts. Aus diesen Fluktuationen lässt sich die Bewegungsgeschwindigkeit und damit der Diffusionskoeffizient der NP ableiten. Gemäß der *Stokes-Einstein*-Beziehung ist der hydrodynamische Radius direkt proportional zum Diffusionskoeffizient der NP und lässt sich letztlich daraus berechnen. Im Gegensatz zu elektronenmikroskopischen Verfahren sind DLS-Messungen sehr gut automatisierbar und beruhen auf einer Analyse einer Vielzahl an

streuenden NP. Ein Nachteil dieses Verfahrens ist die bereits angesprochene Abweichung zwischen hydrodynamischem und realem Radius der NP. Außerdem können bimodale Größenverteilungen sehr schlecht gemessen werden, da große Partikel die Streuintensitäten der kleinen Partikel so stark überdecken, dass diese nicht mehr sichtbar sind. Eine verlässliche DLS Messung setzt neben hohen Konzentrationen die Abwesenheit weiterer streuender partikulärer Substanzen voraus. Da dies für Umweltproben nicht gegeben ist, scheidet DLS als Analyseverfahren für Umweltproben aus.[113]

Abschließend sei noch ein entscheidendes Werkzeug zur Aufreinigung von NP erwähnt. Insbesondere bei langer Lagerung von Nanopartikeldispersionen können NP trotz Stabilisierung (z.B. Citrat oder Polyvinylpyrrolidon bei Ag-NP) geringe Mengen an Ionen freisetzen. Diese Ionen können mittels **Dialyse** von den NP abgetrennt werden. Neben der Lagerung kommt die Dialyse auch nach der NP-Synthese zum Einsatz. Im Fall der Bottom-Up-Synthese beispielsweise werden nicht umgesetzte Reaktanden von den gebildeten NP mittels Dialyse abgetrennt. Im Allgemeinen wird die zu reinigende Suspension in eine schlauchförmige Dialysemembran, die eine bestimmte Porengröße aufweist und Moleküle und Partikel bis zu einer bestimmten Größe sowie Ionen passieren lässt, gefüllt und darin verschlossen. Der befüllte Dialyseschlauch wird für mehrere Stunden (meist für mindestens einen Tag) in einem Behälter mit Reinstwasser gegeben. Der Transport der unerwünschten Stoffe in das den Dialyseschlauch umgebende Wasser erfolgt diffusionsgetrieben durch die Dialysemembran, wobei die Partikel zurückgehalten werden. Die Trennleistung wird verbessert, wenn das Reinstwasser nach einiger Zeit ausgetauscht wird.[114]

4   Verwendete analytische Methoden

4.1   Cloud-Point-Extraktion (CPE)

4.1.1   Grundprinzip sowie Anwendung in der Analytischen Chemie

Um Ag-NP in komplexen Umweltmatrices bei extrem niedrigen Konzentrationen im einstelligen ng L^{-1} Bereich größenaufgelöst mittels sp-ICP-MS zu quantifizieren und dabei einen minimalen SDL-Wert zu gewährleisten, ist es essentiell, die Analyt-NP von gelösten Analytbestandteilen und möglichst dem Großteil der Matrix zu separieren und gleichzeitig anzureichern. Dazu wird in der vorliegenden Arbeit die Cloud-Point-Extraktion (CPE) (vgl. *engl.* Cloud Point = Trübungspunkt) eingesetzt, die es erlaubt, Ag-b-NP von der

Probenmatrix abzutrennen. Da das Volumen des Extrakts sehr viel kleiner ist als das der Probe, wird außerdem ein hoher Anreicherungsfaktor erreicht.

Die CPE ist eine ursprünglich aus der Biochemie stammende Methode zur Proteinaufreinigung und basiert auf einer Phasenseparierung von nicht-ionischen Tensiden, die in einer wässrigen Lösung dispergiert vorliegen. Tenside sind grenzflächenaktive Stoffe, die aufgrund ihres amphiphilen Aufbaus hydrophile und hydrophobe Teile aufweisen. Bei der Phasenseparierung entstehen hydrophobe Kompartimente in der wässrigen Lösung (sogenannte Mizellen), die die zu extrahierende Substanz, wie beispielsweise Proteine, enthalten und abgetrennt werden können.[115, 116]

Eine wässrige Dispersion, die das Tensid oberhalb der kritischen Mizellbildungskonzentration (*engl.* critical micelle concentration, cmc) enthält, wird nach Überschreiten der Cloud Point Temperatur (*engl.* Trübungstemperatur, T_{CP}) in ein Zweiphasensystem überführt. Da sich neben der wässrigen Phase eine tensidreiche Phase, die die Mizellen umfasst, bildet, trübt sich die Dispersion bei einer Temperatur über der T_{CP}. Die Mizellen sind hochdynamische, reversible Systeme kugel-, diskus- oder zylinderförmiger Assoziate aus 40 bis 400 Tensidmolekülen. Wie in **Abbildung 2** gezeigt ist, schafft die Orientierung der hydrophoben Tensid-Anteile in das Innere der Mizellen innerhalb der wässrigen Phase einen lipophilen Raum, in den während des Extraktionsvorgangs lipophile Ziel-Substanzen eingeschlossen werden können.[117]
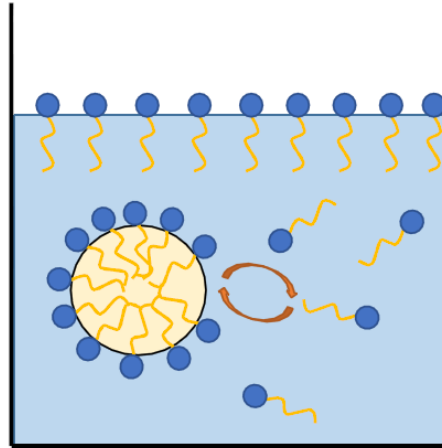
Abbildung 2: Dynamisches Gleichgewicht zwischen Mizellen und freien Tensiden im Lösungsmittel Wasser. Die Wasseroberfläche ist von Tensidmolekülen besetzt. Wasser (hellblau), Luft (weiß), hydrophile Gruppe (dunkelblau), hydrophober Rest (orange).

Durch das ständige Aufbrechen und Neubilden der Mizellen, wird die zu extrahierende Substanz in der Tensidphase angereichert. Die Mizellbildung ist dabei entropiegetrieben: Wassermoleküle, die zuvor an freie Tenside koordiniert waren, werden frei.[117] Durch diese Entsolvatisierung der Tensidmoleküle wird Entropie frei. Durch Zentrifugation der Proben wird die Phasentrennung verbessert und nach Entfernen der wässrigen Phase verbleibt eine Tensidphase mit der zu extrahierenden Substanz. Durch Verwendung einer sehr geringen Menge Tensid wird zusätzlich eine Anreicherung erzielt.[24]

Bei Anwendung der CPE in der Analytischen Chemie ist die zu extrahierende Substanz der Analyt. So können geringste Mengen Analyt messbar gemacht werden, selbst wenn diese Spurenbestandteile einer komplexen Matrix sind. Im Fall von ionischen (und damit hydrophilen) Analyten (z.B. Metallionen) müssen diese zunächst in eine hydrophobere Form überführt werden, um ein Einschließen in den hydrophoben Mizellen zu ermöglichen. Für eine Vielzahl von Metallen existieren dafür unterschiedliche hydrophobe Komplexbildner, die der CPE-Mischung zugesetzt werden. Die dann gebildeten hydrophoben Metallkomplexe können schließlich mizellar extrahiert und angereichert werden. Bei Quantifizierung des angereicherten Analyts mittels spektrometrischer Techniken werden dann sehr niedrige Nachweisgrenzen erreicht.[118]

4.1.2 CPE in der Nanopartikelanalytik

Sind Nanopartikel in Umweltmatrices Gegenstand der analytischen Untersuchung, hindern oftmals die die NP umgebende Matrix mit ihren Bestandteilen sowie die geringe Menge an Analytpartikeln in der Probe eine valide Analytik. CPE kann auch erfolgreich zur Abtrennung von NP von Umweltmatrices sowie zur Anreicherung der NP eingesetzt werden. Im Gegensatz zu ionischen Analyten weisen NP in den meisten Fällen eine sehr geringe Oberflächenladung auf und sind damit ausreichend hydrophob, um ohne den Einsatz hydrophobisierender Liganden in den Mizellen eingeschlossen zu werden.[23-25, 119]

4.1.2.1 Exkurs: Zeta-Potential von Nanopartikeln [32, 113]

Die Oberflächenladung von NP wird durch deren Zeta-Potential charakterisiert und beruht unter anderem auf einer unvollständigen Koordination der Oberflächenatome, auf Protonierung und Deprotonierung von funktionellen Gruppen (z.B. Silanol-Gruppen bei Silica-Partikeln) und insbesondere auf Adsorption von Anionen und Kationen an der Partikeloberfläche. Letztere führt zur Ausbildung einer elektrochemischen Doppelschicht um einen Partikel in wässriger Phase (siehe **Abbildung 3**).

Aufgrund von *Van-der-Waals*-Anziehungskräften adsorbieren unabhängig vom *Nernst*-Potential Ψ_0, der Oberflächenladung des reinen Partikels, stets zunächst Anionen an die Partikeloberfläche, was zur Ausbildung der inneren *Helmholtz*-Schicht mit dem Potential Ψ_i führt. Innerhalb der äußeren *Helmholtz*-Schicht adsorbieren im Fall eines negativen Ψ_0 solvatisierte Kationen. Das an dieser Stelle auftretende Potential wird als *Stern*-Potential Ψ_a bezeichnet. Die beiden *Helmholtz*-Schichten bilden zusammen die *Stern*-Schicht, an die eine diffuse Schicht aus solvatisierten Kationen und Anionen anschließt. Aufgrund der Ladungskompensation durch Anionen und Kationen nimmt das Potential ab diesem Punkt mit zunehmendem Abstand zum Partikel ab. In der diffusen Schicht des Partikels befindet sich eine Grenze, innerhalb derer sich bei Bewegung des Partikels alle Ionen mit dem Partikel in die gleiche Richtung bewegen und außerhalb derer keine Bewegung der Ionen stattfindet. Das Potential, das an dieser Scherebene d_S auftritt, ist das Zeta-Potential. Als elektrochemische Doppelschicht werden beide Schichten, die *Stern*-Schicht und die diffuse Schicht, bis zu der angesprochenen Scherebene bezeichnet.
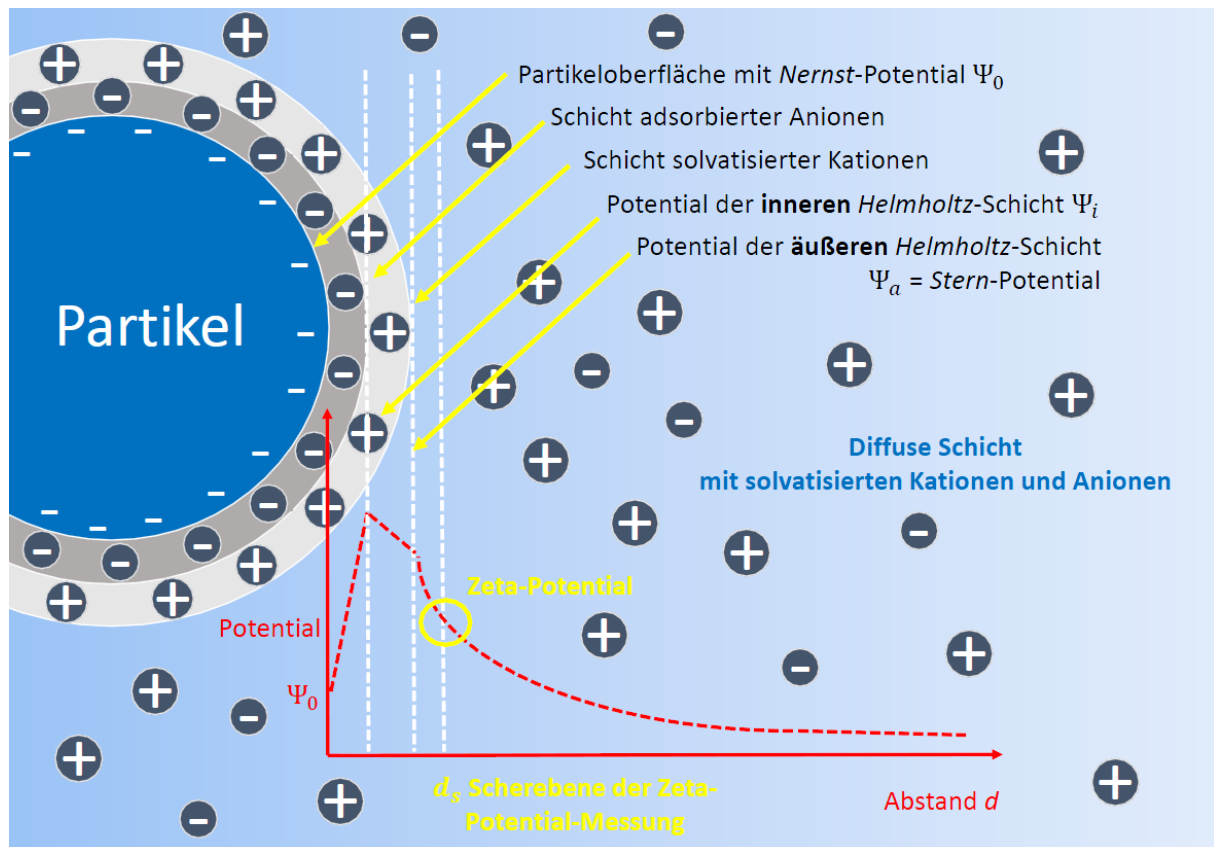
Abbildung 3: Elektrochemische Doppelschicht (dunkelgrau, hellgrau) an einem Partikel (dunkelblau) mit negativem *Nernst*-Potential in wässrigem System (hellblau). Der Verlauf des Potentials mit zunehmendem Abstand d zum Partikel ist in rot dargestellt, wobei das Zeta-Potential einschließlich der Scherebene d_S gelb markiert ist.

Die Oberflächenladung eines Partikels Ψ_0 selbst ist nicht direkt messbar, sondern nur indirekt über die Messung des Zeta-Potentials. Dieses Potential gibt Aufschluss über die Stabilität des kolloidalen Systems. Partikel mit einem Potential, das größer als 30 mV und kleiner als -30 mV ist, gelten als stabil. Die elektrostatische Abstoßung einzelner Partikel verhindert dabei eine Agglomeration.

Zur Bestimmung des Zeta-Potentials werden elektrokinetische Effekte ausgenutzt. Wenn in einer Flüssigkeit suspendierte Partikel einem elektrischen Feld ausgesetzt werden, bewegen sich diese relativ zur flüssigen Phase entlang des elektrischen Feldes. Die Bewegungsgeschwindigkeit ist dabei proportional zum Zeta-Potential der Partikel.

Das Zeta-Potential kann deshalb durch Untersuchung der Bewegung von suspendierten NP in einem elektrischen Feld, der sogenannten elektrophoretischen Mobilität, bestimmt werden.

Dies erfolgt in einer Laser-Doppler-Geschwindigkeitsmessung. Die NP haltige Probe wird dabei in eine Probenzelle gegeben, die mit zwei Elektroden ausgestattet ist. Nach Anlegen eines elektrischen Feldes setzen sich die NP in Richtung der Elektrode in Bewegung, die eine den NP entgegengesetzte Ladung aufweist (siehe **Abbildung 4**).
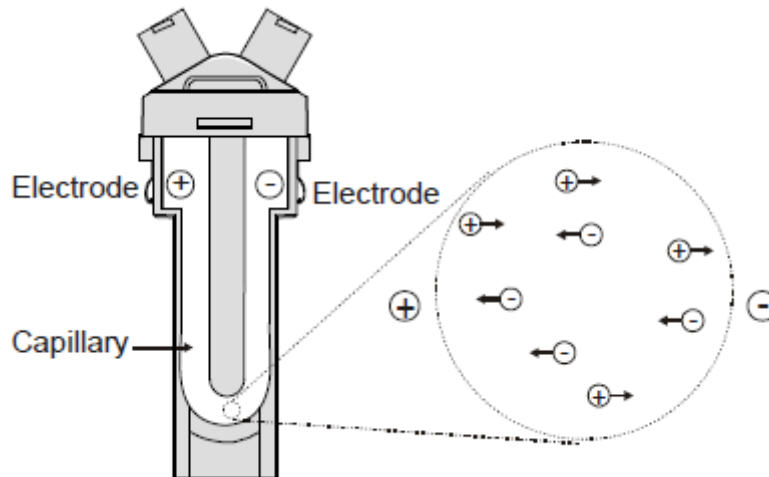
Abbildung 4: Probenzelle in der Laser-Doppler-Geschwindigkeitsmessung zur Bestimmung der elektrophoretischen Mobilität von suspendierten Partikeln.[113]

Während der Messung wird Laserlicht auf die Kapillare fokussiert und die Streulichtintensität bei einem bestimmten Beobachtungswinkel (z.B. 17°) aufgezeichnet (siehe **Abbildung 5**). Aufgrund der elektrophoretischen Bewegung der Partikel wird am Strahlungsdetektor eine mit der Zeit fluktuierende Streulichtintensität aufgezeichnet. Die Rate der Fluktuation ist dabei direkt proportional zur Bewegungsgeschwindigkeit der Partikel. Daraus lässt sich die Elektrophoretische Mobilität und schlussendlich das Zeta-Potential ableiten. Der apparative Aufbau zur Messung des Zeta-Potentials ähnelt dem der DLS-Messung.

Abschließend sei angemerkt, dass der pH-Wert der NP-Suspension einen großen Einfluss auf das Zeta-Potential ausübt. Insbesondere Oberflächenfunktionalitäten und adsorbierte Ionen werden durch den pH-Wert stark beeinflusst. In **Abbildung 5** ist der typische Verlauf des Zeta-Potentials eines negativ geladenen Partikels in Abhängigkeit vom pH-Wert dargestellt. Mit abnehmendem pH-Wert steigt das Zeta-Potential von einem ursprünglich negativen Wert auf einen positiven. Dabei wird der Isoelektrische Punkt durchlaufen, an dem das Zeta-Potential

0 ist. Die Stabilität einer Partikelsuspension beim pH-Wert des Isoelektrischen Punktes erreicht dabei ihr Minimum.
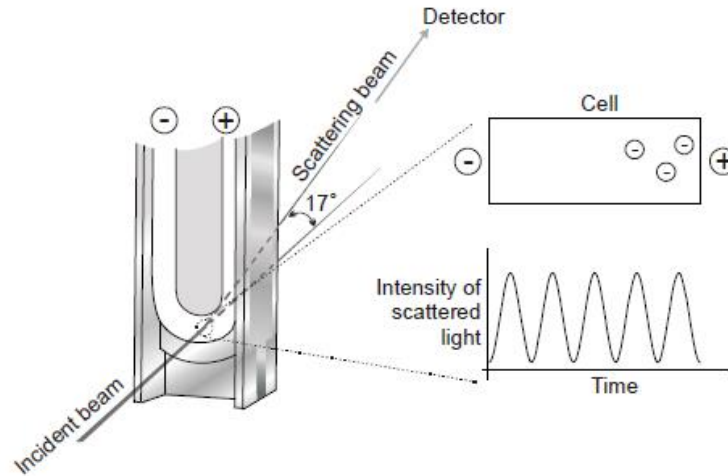
Abbildung 5: Laser-Doppler-Geschwindigkeitsmessung mit gestreutem Licht. Die Partikel bewegen sich in der Zelle zu den Elektroden entgegengesetzter Ladung. Durch die Bewegung der Partikel wird eine mit der Zeit fluktuierende Streulichtintensität aufgezeichnet.[113]
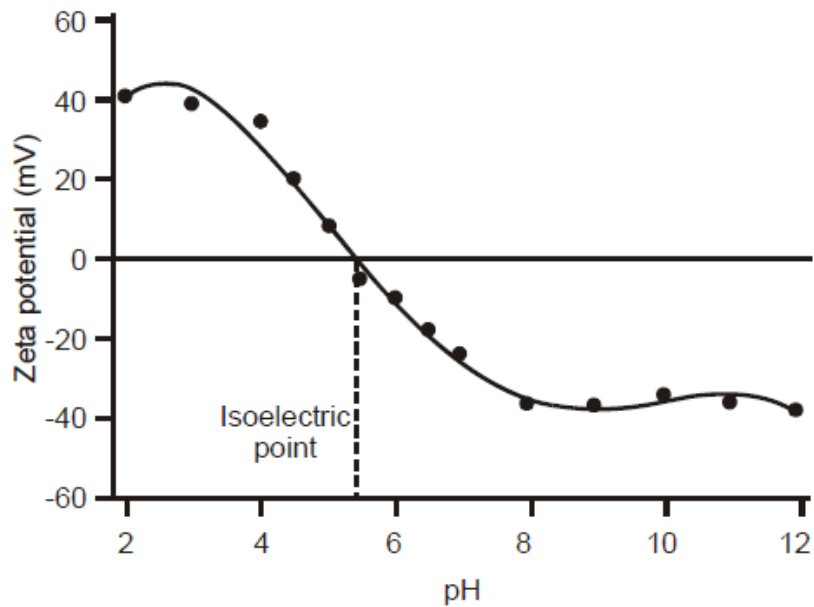
Abbildung 6: Abhängigkeit des Zeta-Potentials vom pH-Wert der flüssigen Phase. Am isoelektrischen Punkt wird ein Zeta-Potential von 0 erreicht.[113]

4.1.2.2 Cloud-Point-Extraktion von Nanopartikeln

Liu et al. haben 2009 zum ersten Mal ein Verfahren zur mizellar unterstützen NP-Extraktion beschrieben. Durch Kopplung der Extraktionsmethode mit einem Massenspektrometer konnte eine Nachweisgrenze (NWG) von 6 ng L^{-1} erzielt werden.[119] Die in dieser Arbeit verwendete Methode zur Extraktion und Anreicherung von Nanosilber durch die CPE geht auf *Hartmann* et al. zurück und erreichte bisher bei der Messung mittels ET-AAS eine NWG unter 1 ng L^{-1}.[24]

Die CPE für Ag-b-NP basiert auf dem nicht-ionischen Tensid Triton-X 114 (TX-114) aus der Klasse der Octylphenolethoxylate (siehe **Abbildung 7**). TX-114 besitzt eine T_{CP} von 23 °C und eine cmc von 0,23 mM. Die Mizellen sind durchschnittlich aus etwa 80 Molekülen aufgebaut.[120]
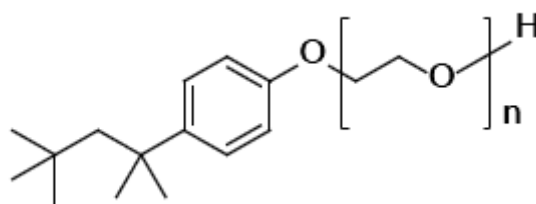
Abbildung 7: Strukturformel von TX-114, wobei n = 7, 8.

Der pH Wert ist für die Oberflächenladung der Ag-b-NP und damit deren Extraktionseffizienz entscheidend, weshalb dieser mittels Essigsäure-Acetat-Puffer auf einen Wert ≥ 5 eingestellt wird.[24]

Grundsätzlich verbleiben gelöste Ag-Spezies aufgrund ihrer Ladung zum größten Teil in der wässrigen Phase. Koextrahierte gelöste Ag-Spezies sind unerwünscht, weshalb die Speziesselektivität weiter verbessert werden soll. Dazu werden stark hydrophile Liganden eingesetzt, die gelöste Ag-Spezies binden, deren Hydrophilie stark erhöhen und somit das Verteilungsgleichgewicht des gelösten Silbers zwischen wässriger und tensidreicher Phase stark in Richtung wässrige Phase verschieben. Die bereits für Ag-b-NP entwickelte CPE sieht den Einsatz nur eines Chelators, des hexdentaten Liganden Ethylendiamintetraacetat (EDTA, siehe **Abbildung 8**) in Form eines Dinatriumsalzes, vor.[24] Zur Optimierung der Speziesselektivität im Rahmen dieser Arbeit kommt ein zusätzlicher Ligand, D-Penicillamin

(D-PA, siehe **Abbildung** 8), zum Einsatz. Die Entwicklung der optimalen Zusammensetzung der CPE-Mischung ist nachfolgend in Publikation 3 gezeigt. Diese Publikation enthält auch Informationen über die Strukturen der Ag(I)-EDTA und Ag(I)-D-PA Komplexe.
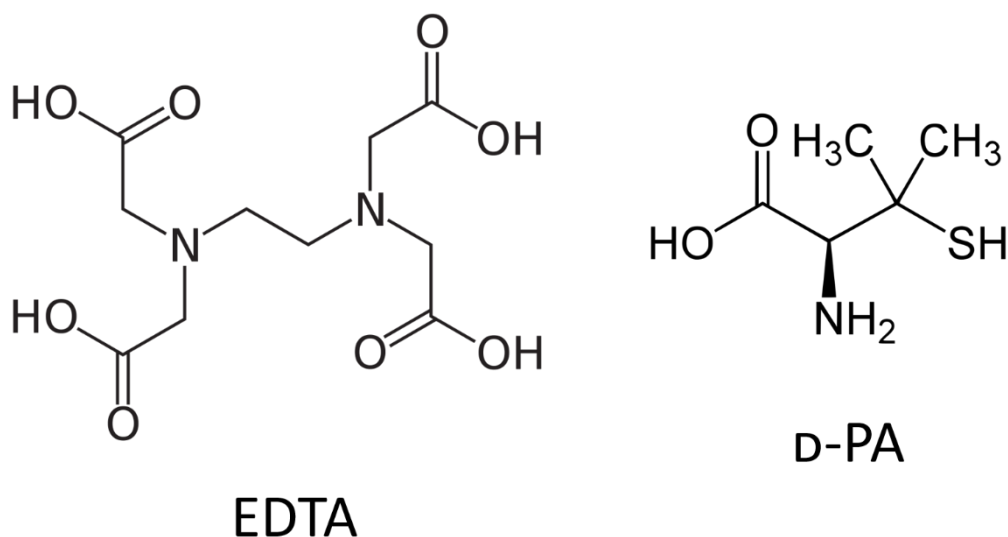
Abbildung 8: Strukturformeln der in dieser Arbeit eingesetzten Liganden EDTA und D-PA.

Penicillamin ist eine nicht-proteinogene α-Aminosäure und insbesondere in der Medizin als starker Chelatbildner bekannt. So wird es unter anderem bei der als Morbus Wilson bekannten Kupferspeicherkrankheit eingesetzt. Morbus Wilson ist eine krankhafte Störung des Kupferstoffwechsels, der zu unerwünschten Einlagerungen von Kupfer in beispielsweise der Leber, den Augen und dem zentralen Nervensystem führt. Daher rührt auch das für diese Krankheit typische Symptom, der *Kayser-Fleischer*-Kornealring, ein kupferfarbiger Ring auf der Hornhaut um die Iris des Auges. D-PA bindet aufgrund der hohen Thiophilie das krankhaft überschüssige Kupfer, das so über den Urin den Körper verlässt.[121, 122] D-PA findet aufgrund der starken Komplexbildung mit anderen Metallen auch bei Schwermetallvergiftungen Verwendung.[123] Diese hohe Tendenz zur Bildung von (Schwer)Metallkomplexen mit D-PA wird auch in der CPE der vorliegenden Arbeit zur Bindung und Hydrophilisierung von gelösten Ag-Spezies ausgenutzt.

Die Extraktion von Ag-b-NP aus Umweltproben umfasst dabei mehrere Schritte (siehe **Abbildung** 9): Zunächst werden 40 mL der NP-haltigen wässrigen Probe mit dem Puffer aus Natriumacetat und Essigsäure, den Liganden EDTA und D-PA sowie dem Tensid TX-114

versetzt und vermischt. Die genaue Zusammensetzung des bereits etablierten sowie des in dieser Arbeit optimierten CPE-Ansatzes mit verbesserter Speziesselektivität ist in nachfolgender Tabelle zusammengestellt und in Publikation 3 im Detail beschrieben. Die CPE-Mischung wird dann für etwa 30 min bei 40 °C temperiert. Die Mischung trübt sich dabei unter Ausbildung der Mizellen. Durch anschließende Zentrifugation der Proben wird die Phasentrennung verbessert und nach Entfernen der an Ag-b-NP abgereicherten wässrigen Phase verbleibt eine Ag-b-NP enthaltende Tensidphase. Durch Verwendung einer sehr geringen Menge Tensidlösung wird zusätzlich eine hohe Anreicherung erzielt.
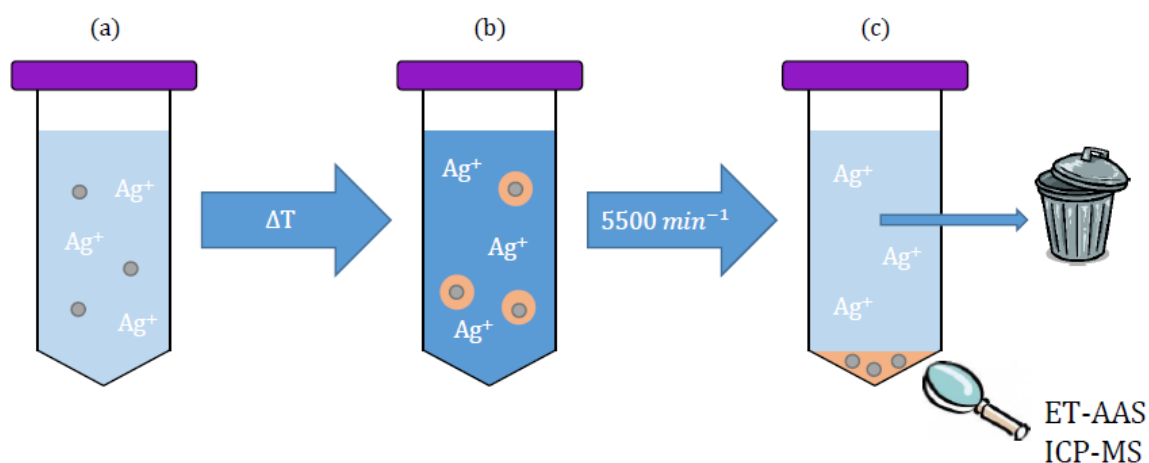
Abbildung 9: Schematischer Ablauf der Cloud-Point-Extraktion: Das Gemisch (a) aus Probe mit Ag-Ionen und Ag-NP (grau) wird nach Zugabe der CPE-Reagenzien über T_{CP} erwärmt. Die Mischung (b) trübt sich und die NP werden in den gebildeten Mizellen (orange) eingeschlossen. Nach Zentrifugation (c) wird die wässrige Phase verworfen und die Tensidphase (orange) weiter untersucht, z.B. mit ET-AAS oder (sp)-ICP-MS.

Tabelle 1: Zusammensetzung der verwendeten CPE-Mischungen. UPW bezeichnet Reinstwasser (*engl.* Ultra Pure Water). Die verbesserte CPE wird nachfolgend auch als iCPE (improved CPE, *engl.* verbesserte CPE) bezeichnet.

Reagenz	etablierte CPE[24]	verbesserte CPE
TX-114 (Lösung in UPW, 10 % (w/w))	1 mL	1 mL
Essigsäure (1.25 M in UPW)	1 mL	1 mL
Natriumacetat (1 M in UPW)	400 µL	400 µL
EDTA (gesättige Lösung von Na₂EDTA in UPW)	1 mL	3 mL
D-PA (ges. Lösung in UPW)	---	1 mL

Ein großer Vorteil der CPE ist die Tatsache, dass nur wenig Extraktionsmittel (Tensid) eingesetzt werden muss und deshalb sehr hohe Anreicherungsfaktoren erzielt werden können. Dies ist der niedrigen cmc von TX-114 geschuldet und der Tatsache, dass Durchmischungseffekte klassischer Flüssig-Flüssig-Extraktionen nicht auftreten. Nach Zugabe der Reagenzien zur Probe liegt zunächst ein homogenes System vor, wobei die Phasentrennung erst nach Überschreiten der T_{CP} einsetzt. Die niedrige T_{CP} schont zudem den Analyten vor thermischer Belastung. Ein Einfluss der CPE-Bedingungen auf die zu extrahierenden Ag-b-NP (z. B. Größenänderungen) konnte nicht festgestellt werden.[24] Zusätzlich anzumerken ist die kurze Analysezeit (ca. 1 h), die aufgrund der schnellen Equilibrierung des Systems und der durch die Zentrifugation beschleunigten Phasentrennung erreicht werden kann. Ferner ist das eingesetzte Tensid nicht toxisch und kaum umweltschädlich und führt im Gegensatz zu manchen organischen Lösungsmitteln nicht zur Denaturierung empfindlicher Analyten wie Proteine oder Nanopartikel.

Problematisch ist die weitere Untersuchung der Tensidphase: Diese stellt eine anspruchsvolle Matrix dar und kann nur mit dazu kompatiblen Analyseverfahren weiterbearbeitet werden. Aufgrund des Siedepunkts > 200 ˚C kann das Extraktionsmittel nicht durch einfaches Verdampfen entfernt werden. Die Tenside sind außerdem nicht selektiv auf Silber ausgerichtet, sondern koextrahieren auch andere hydrophobe Substanzen, weshalb eine selektive, nachgeschaltete Analysentechnik von größter Bedeutung ist. Bei einer Untersuchung des Tensidextrakts mittels Atomabsorptionsspektroskopie oder Massenspektrometrie ist dies gegeben – wie in Publikation 3 ausführlich dargestellt.[124]

4.2 Elektrothermale Atomabsorptionsspektrometrie [125-128]

Die Elektrothermale Atomabsorptionsspektrometrie (ET-AAS) ist ein etabliertes Verfahren zur Quantifizierung meist gelöster Analyten und basiert auf der Absorption elektromagnetischer Strahlung durch den Analyten. Grundsätzlich wird die Probe in einem ersten Schritt in einem Graphitrohr so stark erhitzt, dass die Matrix verdampft bzw. eliminiert wird und eine Atomisierung des Analyten zu einer Atomwolke eintritt. Wird nun Licht durch die Atomwolke im Graphitrohr geleitet, folgt eine Absorption von Strahlung bei einer spezifischen Wellenlänge λ_0, der sogenannten Resonanzlinie. Diese Absorption ist elementspezifisch, hängt also vom zu messenden Analyten ab, und entspricht der

Energiedifferenz eines Übergangs vom elektronischen Grundzustand in einen angeregten Zustand. Die Verringerung der Strahlungsintensität (Extinktion) des eingestrahlten Lichts bei dieser elementcharakteristischen Wellenlänge λ_0 wird mittels eines Detektors gemessen und hängt von der Konzentration des Analyten in der Probe. Die gemessene Extinktion kann deshalb zur Bestimmung der Analytkonzentration verwendet werden.

Die durch die Strahlungsabsorption angeregten Atome in der Atomwolke emittieren die absorbierte Strahlungsenergie wieder bei der gleichen Wellenlänge λ_0 (Fluoreszenz). Dass dennoch eine Absorption detektiert werden kann, liegt daran, dass die Fluoreszenzemission als Kugelwelle emittiert wird und nur ein marginaler Anteil der Fluoreszenzstrahlung durch den Austrittsspalt den Detektor erreicht.

Das *Lambert-Beer'sche*-Gesetz beschreibt den Zusammenhang zwischen Verringerung der Lichtintensität und Anzahl der absorbierenden Teilchen wie folgt:

$$E = -lgT = lg\left(\frac{I_0}{I}\right) = \epsilon_{\lambda_0} \cdot c \cdot l \qquad (4.1)$$

mit E Extinktion

        T Transmission

        I Intensität des transmittierten Lichts

        I_0 Intensität des eingestrahlten Lichts

        ϵ_{λ_0} molarer, dekadischer Extinktionskoeffizient bei Wellenlänge λ_0 [L mol⁻¹ cm⁻¹]

        c Konzentration des Analyten [mol L⁻¹]

        l Weglänge des Lichts durch die Probe [cm]

Bei ϵ_{λ_0} handelt es sich folglich um das Maß, wieviel elektromagnetische Strahlung der Wellenlänge λ_0 eine 1 M Lösung des Analyten bei einer Weglänge von 1 cm durch den Analyten absorbiert.

Die Absorptionsprozesse im Fall einer Atomwolke der ET-AAS können aber nur unzureichend mit Gleichung (4.1) beschrieben werden. Da eine genaue Definition der Weglänge des Lichts

(Strahlengang durch die absorbierende Atomwolke im Graphitrohr) in der ET-AAS nicht möglich ist, wird diese zusammen mit dem Extinktionskoeffizienten in einer gerätespezifischen Konstante A zusammengefasst.

$$E = A \cdot c'$$ (4.2)

A enthält neben der Geometrie des Strahlengangs unter anderem die Atomisierungsrate des zu bestimmenden Elements in Abhängigkeit von den Messbedingungen. Da für die Atomwolke der ET-AAS auch keine klassische Konzentrationsangabe in mol L^{-1} sinnvoll ist, stellt c' hier auf den Anteil des Analyten in der Atomwolke im Graphitrohr ab. c' ist aber weiterhin proportional zu c.

Aufgrund des linearen Zusammengangs zwischen Extinktion und Konzentration c' bzw. c, kann A durch Kalibrierung bei Messung von Proben bekannter Konzentration bestimmt werden. Im nächsten Schritt kann dann aus der gemessenen Extinktion von Proben unbekannter Konzentration deren Konzentration berechnet werden.

Voraussetzung für einen linearen Zusammenhang obigen Gesetzes sind eine niedrige Analytkonzentration, eine vollständige Atomisierung der Probe und eine homogene Verteilung der absorbierenden Analytatome in der Atomwolke im Strahlengang. Durch ein auf die Probe angepasstes Temperaturprogramm des Graphitrohrs und speziell aufgebaute Graphitrohre wird eine vollständige Atomisierung und Homogenität im Strahlengang sichergestellt.

Der grundlegende Aufbau eines ET-AAS – auch Graphitrohrofen-AAS genannt – ist in folgender Abbildung dargestellt.

Eine Hohlkathodenlampe (HKL) dient dabei als Strahlungsquelle und emittiert elementspezifisches Licht verschiedener Wellenlängen (Emissionsspektrum). Das Licht passiert nach Umlenkung über die Spiegel M1 und M2 die beheizbare Atomisierungseinheit (Graphitofen), in dem der Absorptionsprozess stattfindet. M3-M5 sind weitere Spiegel, die den Strahlengang leiten. Ein Gitter-Monochromator isoliert die für die Messung relevante

Resonanzlinie λ_0 aus dem Emissionsspektrum der HKL. Die isolierte und durch Absorption durch den Analyten geschwächte Strahlung der Wellenlänge λ_0 trifft anschließend auf einen Detektor zur Bestimmung der Lichtintensität, wobei beispielsweise Photomultiplier oder Photodioden eingesetzt werden. Moderne ET-AAS-Geräte enthalten ferner eine Einheit zur Untergrundkorrektur (nicht gezeigt).
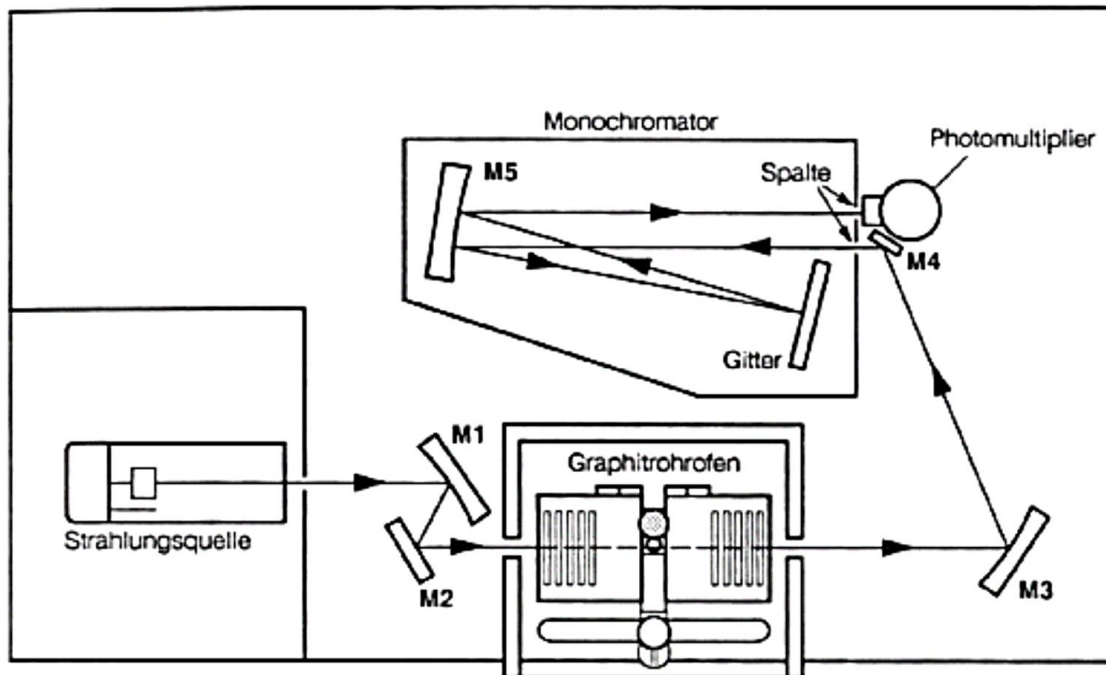
Abbildung 10: Schematischer Aufbau eines Graphitrohrofen-Atomabsorptionsspektrometers.[129]

Für die Bestimmung eines jeden Elements muss eine spezifische HKL verwendet werden. Grundsätzlich absorbiert ein nicht angeregtes Atom eines bestimmten Elements den von einem angeregten Atom desselben Elements emittierten Lichtquant. Die HKL (siehe **Abbildung 11**) umfasst deshalb eine zylinderförmige Kathode, die entweder aus dem zu bestimmenden Element besteht oder mit diesem beschichtet ist. Die dazugehörige Anode ist ein Wolfram- oder Nickel-Draht. Zwischen Kathode und Anode wird in einem mit Argon gefüllten Glaszylinder eine Spannung von mehreren hundert Volt angelegt. Die so induzierte Glimmentladung führt zu positiv geladenen Argon-Ionen, die auf die Katode beschleunigt werden und beim Auftreffen angeregte Atome des zu bestimmenden Elements herausschlagen. Diese kehren unter Emission der elementspezifischen Strahlung wieder in den Grundzustand zurück. Wie oben ausgeführt, umfasst das Emissionsspektrum unter

anderem Lichtquanten der Resonanzlinie λ_0, welche von den nicht angeregten Analytatomen in der Atomisierungseinheit absorbiert werden (Resonanzabsorption).
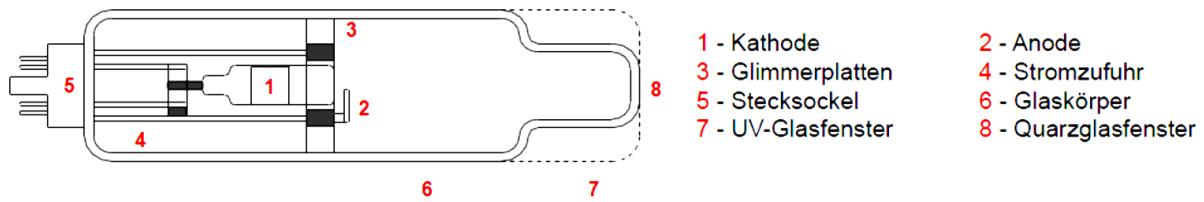
Abbildung 11: Schematischer Aufbau einer Hohlkathodenlampe.[130]

Namensgebend für die ET-AAS ist die elektrothermale Atomisierung mittels Graphitofen (oder auch Graphitrohr genannt), einem Hohlzylinder aus Graphit (siehe **Abbildung 12**). Graphit ist anisotrop leitend und ermöglicht ein Temperieren des Ofens nach dem Prinzip der Widerstandsheizung auf unterschiedliche Temperaturen bis etwa 3000 K. Über zwei gekühlte Graphitkontakte werden hohe Stromstärken (bis zu 500 A) bei geringen Spannungen (ca. 10 V) angelegt. Die Stromstärke ist dabei maßgeblich für den Temperaturanstieg des Graphitrohrs. Um die Oxidation des Rohrs bei derart hohen Temperaturen zu verhindern, wird das Rohr mit Schutzgas (meist Argon) umspült. Die in Lösungsmittel gelöste oder dispergierte Probe wird über eine kleine Öffnung mit Hilfe von Präzisionspipetten in den Graphitofen eingebracht.
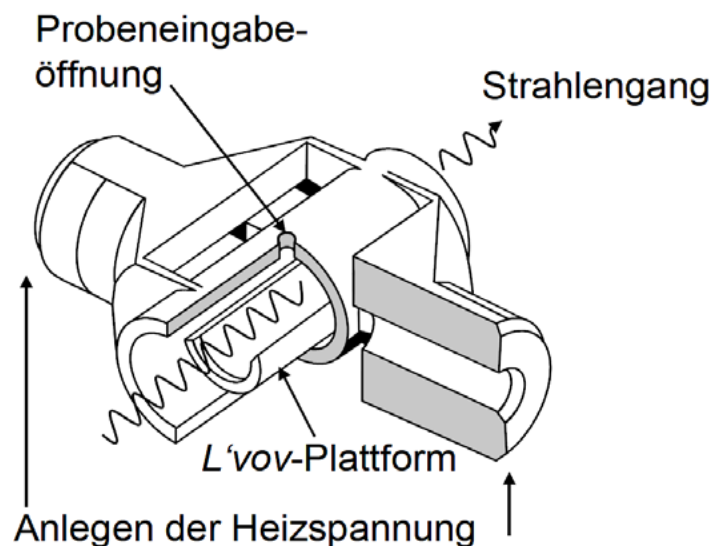
Abbildung 12: Aufbau eines Graphitrohrofens.[130]

Die Probe durchläuft während der Analyse ein individuell einstellbares Temperaturprogramm, bestehend aus der Trocknungsphase zur langsamen Verdampfung des Lösungsmittels, gefolgt von der Pyrolyse, bei der bei erhöhten Temperaturen Matrixbestandteile verascht und über den Gasstrom entfernt werden. In der darauffolgenden Atomisierungs- und Messphase wird der Analyt, der als Ion oder als Bestandteil einer chemischen Verbindung vorliegen kann, bei hohen Temperaturen atomisiert. Die Aufheizzeit zur Atomisierungstemperatur sollte nur etwa 0.1 s umfassen, da so die maximale Atomwolkendichte im Graphitrohr erreicht wird. Damit die so entstehende Atomwolke für die Messung ausreichend lange im Graphitofen verbleibt, wird der Argon-Gasstrom durch den Graphitofen während der Messung abgeschaltet. Zur Messung wird die durch Resonanzabsorption reduzierte Lichtintensität der HKL-emittierten Strahlung detektiert. Nach Messung sorgt der wieder eingeschaltete Argon-Gasstrom für ein Entfernen der Atomwolke aus dem Strahlengang. Das Programm wird mit einem Reinigungsschritt komplettiert, bei dem der Ofen bei maximaler Temperatur kurz ausgeheizt wird. Auf diese Weise werden Rückstände der Probe entfernt, sodass die nächste Messung mit einem rückstandsfreien Ofen gestartet werden kann.

Graphitöfen existieren in verschiedenen Ausführungsformen: Einfache System verwenden Öfen in Form eines Hohlzylinders, der longitudinal, also durch Anlegen einer Spannung an beiden Enden temperiert wird. Der so entstehende Temperaturgradient über die Länge des Rohres bedingt jedoch eine ungleichmäßige Atomisierung des in den Ofen eingebrachten Analyten. Moderne ET-AAS-Systeme verwenden deshalb ein wie in **Abbildung 12** gezeigtes, transversal beheiztes Graphitrohr, bei dem die Spannung senkrecht zum Strahlengang durch den Ofen angelegt wird. Da kein Temperaturgradient in Längsrichtung ausgebildet wird, ist eine homogene Atomisierung garantiert. Es wird so außerdem verhindert, dass der Analyt an bestimmten Stellen im Rohr wieder kondensiert. Um die Lebensdauer der Graphitöfen zu steigern, sind die Öfen mit pyrolytischem Graphit beschichtet, einer besonders harten und gasundurchlässigen Graphitform. Insbesondere wird damit auch ein destabilisierend wirkendes Einlagern von Analytatomen und -molekülen in den Graphit verhindert. Um die Atomisierung noch gleichmäßiger zu gestalten, sind moderne Graphitöfen zusätzlich mit einer *L'vov*-Plattform als Probenträger ausgestattet. Da diese Plattform minimalen Kontakt zum Graphitofen hat, wird sie hauptsächlich durch Wärmestrahlung der heißen Rohrwand erwärmt. Die Atomisierungstemperatur wird verzögert erreicht, nämlich erst nach Einstellung

eines thermischen Gleichgewichts zwischen der Plattform und der Gastemperatur im Ofen. Dadurch wird die Reproduzierbarkeit der Messergebnisse verbessert.

Wie oben bereits erwähnt, handelt es sich bei HKLs um Linienstrahler, die kein kontinuierliches Spektrum sondern mehrere elementspezifische Spektrallinien des Kathodenelements emittieren. Damit im Anschluss an die Atomisierungseinheit die Detektion einer spezifischen Resonanzlinie λ_0 möglich ist, ist vor dem Detektor ein Monochromator zwischengeschaltet. Dieser isoliert als Wellenlängenselektor die Resonanzlinie. Moderne Geräte arbeiten mit kompakten Gittermonochromatoren in *Czerny-Turner*-Anordnung, deren Wellenlängenselektion auf wellenlängenabhängigen Beugungswinkeln an optischen Gittern und beweglichen Ein- und Austrittsspalten beruht.

Um die Resonanzabsorption analysieren zu können, werden Detektoren verwendet, die die geschwächte Strahlung nach der Atomisierungs- und Messeinheit registrieren und in ein elektrisches Signal umwandeln. In den meisten Fällen wird eine Photomultiplier-Röhre als Detektor eingesetzt, siehe **Abbildung 13**. Dabei treffen die Photonen nach Verlassen des Graphitofens und Passieren des Monochromators auf eine Photokathode, wodurch Photoelektronen aus der Kathode in die Detektorröhre freigesetzt werden. In der Röhre befinden sich Dynoden, an denen eine Beschleunigungsspannung angelegt ist und die beim Eintreffen eines Elektrons eine konstante Zahl an Sekundärelektronen freisetzen. Eine spezielle Anordnung der Dynoden führt dazu, dass das anfängliche Photoelektron kaskadenartig vervielfältigt wird und ein messbarer Sekundärelektronenstrom generiert wird. Da die Stromstärke des Sekundärelektronenstroms proportional zur Anzahl der einfallenden Photonen und damit auch zur Anzahl absorbierender Analytatome im Graphitrohr ist, ergibt sich ein direkter Zusammenhang zwischen Stromsignal und Analytkonzentration. Durch Kalibrierung mit Proben bekannter Analytkonzentration kann so die Analytkonzentration unbekannter Proben anhand des gemessenen Sekundärelektronenstroms berechnet werden.

Alternativ werden CCD-Detektoren eingesetzt, die Halbleiterdioden (sogenannte Photodioden) umfassen. Trifft Licht auf diese Dioden, werden aufgrund des inneren photoelektrischen Effekts des Halbleitermaterials Elektronen-Loch-Paare induziert. Das dabei messbare elektrische Signal ist abhängig von der Intensität des eintreffenden Lichts.
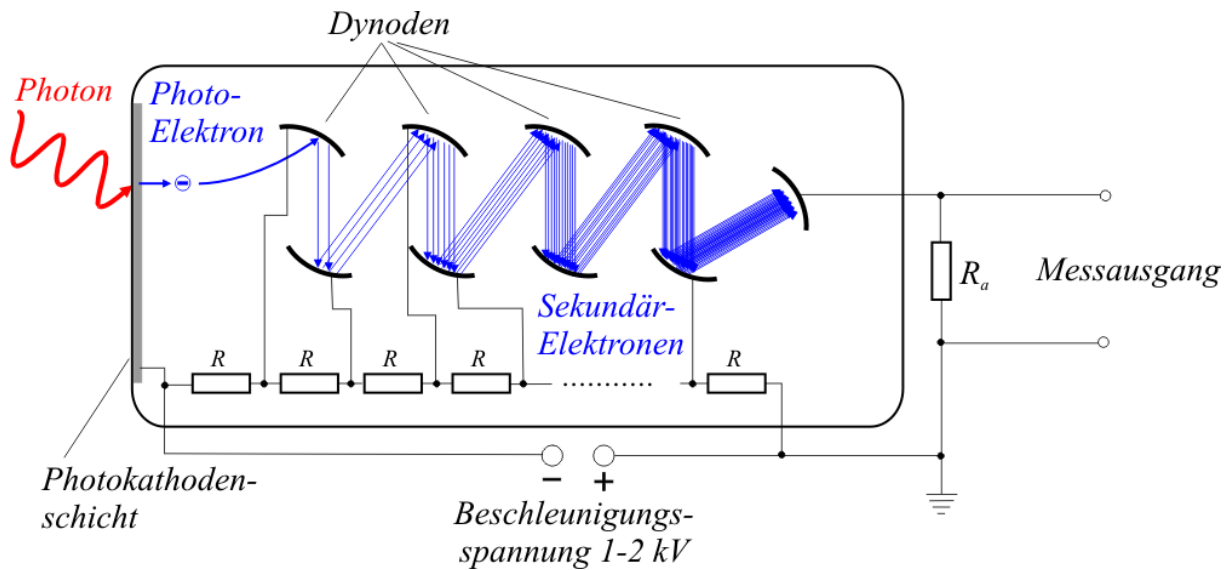
Abbildung 13: Schematischer Aufbau eines Photomultipliers.[131]

Neben der gewünschten Absorption durch den atomisierten Analyten treten in der ET-AAS auch unerwünschte Prozesse der Strahlungsmodulation auf. Diese sogenannten Interferenzen können die Strahlungsintensität der Resonanzlinie verstärken oder verringern und führen zu einem Über- oder Minderbefund des Analyten, sofern sie nicht kompensiert werden. Man unterscheidet hierbei spektrale und nicht spektrale Interferenzen.

Zu den spektralen Interferenzen zählen vor allem Schwarzkörperstrahlung des glühenden Graphitrohrs, Absorption durch Matrixbestandteile auf der Resonanzlinie oder Lichtstreuung.

Spektrale Interferenzen, insbesondere die unspezifische Absorption durch die Probenmatrix, können jedoch technisch mittels des *Zeeman*-Effekts korrigiert werden. *Peter Zeeman* zeigte 1897, dass der Einfluss eines starken Magnetfelds zur Aufhebung der Entartung der elektronischen Zustände in den Atomen führt. Damit gehen unterschiedliche Anregungswellenlängen einher und die Resonanzlinie wird in drei Linien aufgespalten (siehe **Abbildung 14**). Die π-Komponente ist die Linie des ursprünglichen elektronischen Übergangs der Resonanz (ν_0). Daneben existieren die σ-Komponenten der Linie, die jeweils um einen gleichen Betrag zu höheren und niedrigeren Wellenlängen verschoben (ν_1, ν_2) und senkrecht zur π-Komponente polarisiert sind. Die Größe der Aufspaltung ist dabei proportional zur angelegten magnetischen Feldstärke.
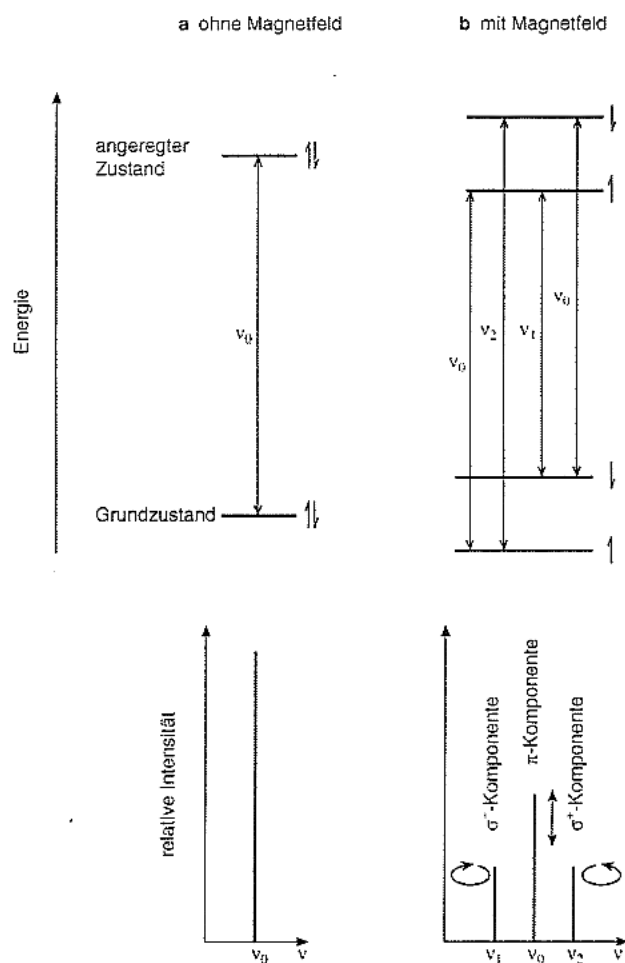
Abbildung 14: Aufspaltung der elektronischen Zustände eines Atoms beim Zeeman-Effekt nach Anlegen eines Magnetfeldes (b).[127]

Dieser Aufspaltungseffekt kann zur Untergrundkorrektur ausgenutzt werden: Wird das Magnetfeld so installiert, dass dessen Feld parallel zum Lichtweg durch den Ofen orientiert ist, so setzt nach Einschalten des Magnetfelds zunächst die Aufspaltung der Resonanzlinie und die Polarisierung ein. Die π-Komponente weist die falsche elektromagnetische Polarisation auf, um das Licht, dass sich parallel zum Magnetfeld bewegt, zu absorbieren. Nutzt man nun ein starkes, pulsierendes Magnetfeld während der Messung, wird bei ausgeschaltetem Feld die Absorption von Probe und Untergrund und bei eingeschaltetem Feld nur der Untergrund gemessen, indem in diesem Fall die Probenabsorption gewissermaßen ausgeblendet wird. Die Differenz der beiden Signale liefert schließlich nur die von der Probe ausgehende Absorption.

Nicht spektrale Interferenzen sind chemische Interferenzen, die beim Atomisierungsvorgang entstehen. Elemente wie Wolfram oder Bor bilden beispielsweise mit dem Ofenmaterial

stabile Carbide, die nicht mehr atomisiert werden können. Ferner können bestimmte Matrixbestandteile (z.B. Sulfate) mit einzelnen Analytelementen schwer verdampfbare Verbindungen bilden. Alkalimetalle sind mittels Graphitrohr zwar grundsätzlich messbar, reduzieren aber die Haltbarkeit der Rohre, da diese Elemente bei den hohen Temperaturen des Atomisierungsvorgang in den Graphit interkalieren können.

Grundsätzlich ist die ET-AAS eine Methode der Einzelelementanalyse, da für jedes zu bestimmende Element eine bestimmte HKL verwendet und eine spezielle Resonanzlinie beobachtet werden muss. Es existieren jedoch Ansätze zur simultanen Mehrelementanalyse. Beispielsweise kann Licht mehrerer HKLs durch die Atomisierungs- und Messeinheit geleitet und danach wieder aufgetrennt werden. Ähnlich funktionieren High-Resolution-Continuum-Source Geräte, bei denen einen Xenon-Lampe ein kontinuierliches Spektrum, das Resonanzlinien einer Vielzahl von Elementen umfasst, emittiert. Da aber trotzdem nur eine Atomisierungseinheit vorhanden ist, können dabei nur diejenigen Elemente analysiert werden, die in einem ähnlichen Temperaturbereich atomisieren. Eine Analyse von Elementen mit stark abweichenden Atomisierungstemperaturen ist deshalb nur in einer sequentiellen Multielementanalyse möglich, bei der die Probe mehrmals hintereinander bei unterschiedlichen Temperaturen atomisiert wird.[132]

4.3   Massenspektrometrie mit induktiv gekoppeltem Plasma

Die Massenspektrometrie ist eine analytische Methode, die auf der Detektion von Massen ionisierter Analyten beruht. Die zu untersuchende Probe wird in einer Ionenquelle ionisiert, dann wird der ionisierte Analyt in einem elektrischen Feld beschleunigt und nach seinem spezifischen Masse-zu-Ladungs-Verhältnis (m/z-Verhältnis) von den restlichen ionisierten Probenbestandteilen in einem Massenselektor getrennt. Da die Analytionen in den meisten Fällen einfach geladen sind, entspricht das m/z-Verhältnis der Masse des Analytelements – was dazu geführt hat, dass sich der - wenn auch streng genommen falsche - Begriff der „Masse" im Zusammenhang mit der Detektion etabliert hat. Nach Auftreffen des ionisierten Analyten auf einem Detektor kann unter Zuhilfenahme einer Kalibrierung die Konzentration des Analyten in der Probe bestimmt werden. Generell passieren die Ionen im Massenspektrometer ein Vakuum, um Stoßprozesse zu vermeiden, die die Natur der freien Ionen und Elektronen ansonsten beeinträchtigen würden.

Die Massenspektrometrie mit induktiv gekoppeltem Plasma hat sich in den letzten Jahrzehnten zu einer Standardmethode der Elementanalytik entwickelt und zeichnet sich durch extrem niedrige Nachweisgrenzen für viele Elemente (unterer ng L^{-1} Bereich), hohe Linearität, eindeutig und leicht interpretierbare Spektren (im Vergleich zu optischen Emissionsspektren) sowie die Möglichkeit der Bestimmung von Isotopenverhältnissen aus. Nachteilig sind jedoch die hohen Anschaffungskosten für ein Massenspektrometer, ein hoher Gerätedrift (bis zu 10 % pro Stunde) und die Beeinträchtigung durch Störungen (siehe Kapitel 4.3.3).[133]

4.3.1   konventionelle Massenspektrometrie [133-140]

Ein konventionelles Massenspektrometer ist grundsätzlich aus einer Probenzufuhr mit Ionenquelle, einem Massenselektor sowie einem Detektor aufgebaut.

Die Molekül-Massenspektrometrie kommt insbesondere bei der Strukturaufklärung zum Einsatz (qualitative Analyse).   Essentiell ist dabei die Verwendung schwacher Ionisationsmethoden, die zur Bildung geladener, aber intakter Moleküle oder Molekülfragmente führen. Die Analyse des Fragmentierungsmusters erlaubt es, auf die Struktur des Analyt-Moleküls rückzuschließen. Üblicherweise werden hierbei die Elektronenstoß- oder die Elektronenspray-Ionisation eingesetzt.

Bei der Elektronenstoß-Ionisation wird die Probe verdampft und in eine Vakuumkammer überführt, in der die Analyt-Moleküle neben weiteren Probenbestandteilen mit einem Strahl aus beschleunigten Elektronen wechselwirken. Dadurch werden aus den Molekülen Elektronen herausgeschlagen. Die so entstehenden positiv geladenen Radikalionen können weiter zerfallen und ionisierte Molekülfragmente bilden. Ein elektrisches Feld beschleunigt die ionisierten Moleküle und Molekülfragmente anschließend und leitet diese an den Massenselektor weiter. Wegen der hohen Fragmentierungsrate zählt die Elektronenstoß-Ionisation zu den harten Ionisationstechniken.

Bei der Elektronenspray-Ionisation wird die Probe durch eine Metallkapillare geleitet, an der eine Spannung angelegt ist. Beim Austritt der Probe aus der Spitze der Kapillare werden die Analyt-Moleküle und die weiteren Probenbestandteile in eine Vakuumkammer versprüht und ionisiert. Diese Art der Ionisierung zählt zu den weichen Ionisationstechniken und ist

wesentlich sanfter als die Elektronenstoß-Ionisation. Aufgrund der geringeren Fragmentierungsrate eignet sich die Elektronenspray-Ionisation besonders für empfindliche Analyten, wie z.B. komplexe Biopolymere (Proteine).

Die vorliegende Arbeit beschränkt sich auf die quantitative Massenspektrometrie in der Elementanalytik. In diesem Bereich kommt meist die Massenspektrometrie mit induktiv gekoppeltem Plasma (*engl.* inductively coupled plasma mass spectrometry, ICP-MS) zum Einsatz. In **Abbildung 15** ist der grundlegende Aufbau eines ICP-MS gezeigt.
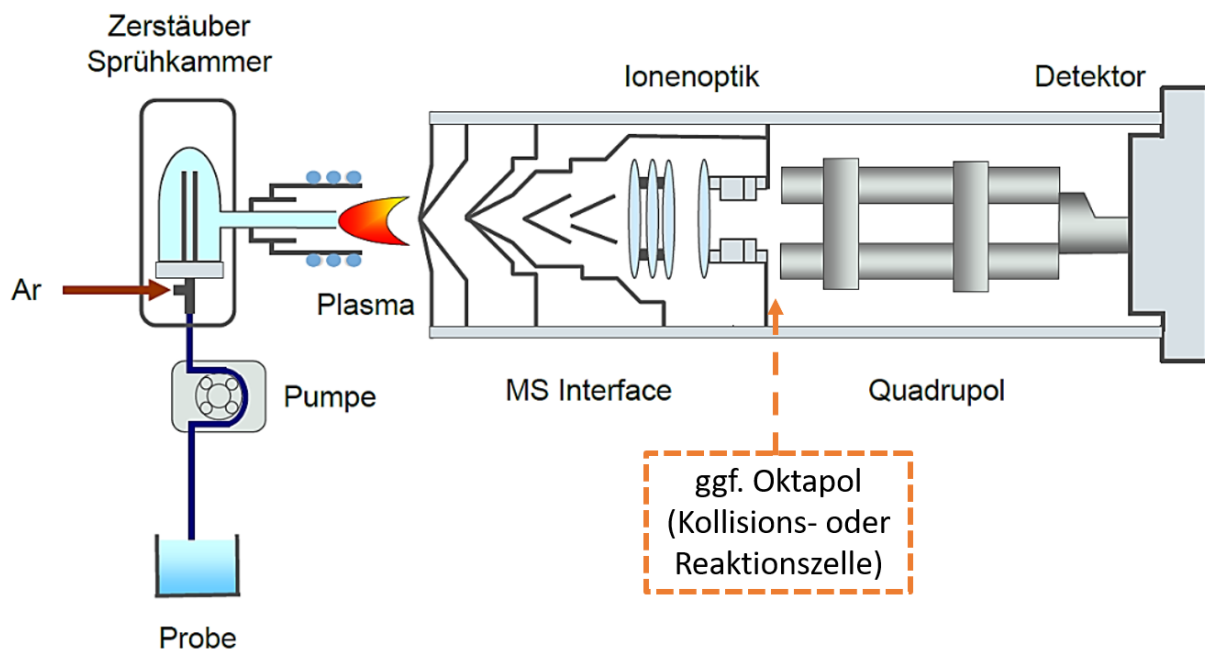
Abbildung 15: Schematischer Aufbau eines Massenspektrometers mit induktiv gekoppeltem Plasma.[130]

Der Analyt wird über das induktiv gekoppelte Plasma ionisiert. Ein Plasma ist ein hochenergetischer Zustand von Materie, die als Mischung von Elektronen, positiv und negativ geladenen Ionen, neutralen Atomen, positiv und negativ geladenen sowie neutralen Molekülen bestehen kann und deshalb freie Ladungsträger enthält. Ein Plasma ist üblicherweise quasineutral, also in einem Gleichgewichtszustand positiv und negativ geladener Teilchen. Durch Reibung der Ladungsträger können mitunter extrem hohe Temperaturen von mehreren 10.000 °C erreicht werden. In der Ionenquelle des Massenspektrometers wird das Plasma durch Ionisierung von Plasmagas, meist Argon, nach

Durchströmen einer Plasmafackel erzeugt. Die Plasmafackel ist von einer Induktionsspule umgeben, die das Plasma durch Anlegen eines starken Hochfrequenzfeldes kontinuierlich mit Energie versorgt und damit aufrechterhält. Da neutrales Plasmagas jedoch nicht mit dem Hochfrequenzfeld wechselwirkt, wird durch eine Entladung an einer Teslaspule zunächst eine Ionisationsspur im Plasmagas erzeugt. Erst dann ist eine Energieeinstrahlung durch das Hochfrequenzfeld möglich. Das Plasmagas passiert die Plasmafackel über drei konzentrisch angeordnete Hohlzylinder aus Quarz. Plasmagas, das über den äußeren Zylinder zugeführt wird, dient zur Kühlung der Fackelwand, während Plasmagas, das über den zweiten Zylinder zugeführt wird, das Plasma positioniert und stabilisiert. Plasmagas, das den innersten Zylinder durchströmt, wird zum Plasma ionisiert und dient als Zufuhrmedium der Probe. Die Probe wird in einer, der Plasmafackel vorgeschalteten, peltier-gekühlten Zerstäuberkammer fein zerstäubt, dem Zufuhrmedium beigefügt und in das Plasma ans Ende der Plasmafackel transportiert. Dort wird das Analyt-Aeorosol getrocknet, verdampft und bei ca. 5.000 bis 10.000 °C ionisiert. Ein Großteil der Probenmatrix wird dabei eliminiert und der Analyt in einfach positiv geladene Ionen umgewandelt. Nur die so erzeugten positiv geladenen Analyt-Ionen werden im ICP-MS detektiert und machen damit die Quantifizierung von Elementen möglich. Es sei hier bereits angemerkt, dass bei so hohen Plasmatemperaturen auch mehrfach geladene Ionen entstehen können, die als meist unerwünschte Interferenz die Messung stören (siehe Kapitel 4.3.2).

Um das Plasma aufrechterhalten zu können, ist ein hoher Volumenstrom an Plasmagas durch die Plasmafackel notwendig. Nach dem Plasma müssen die Analyt-Ionen jedoch in ein Hochvakuum überführt werden, um die Massenselektion nach einem bestimmten m/z-Verhältnisses durchlaufen zu können. Dieser Übergang von Atmosphärendruck in das Hochvakuum wird durch das MS-Interface realisiert. Mit Hilfe von mehreren (meist zwei) hintereinander geschalteten, wassergekühlten Nickel- oder Platin-Konen mit immer kleiner werdenden, konzentrisch angeordneten Löchern wird stufenweise ein Hochvakuum angelegt (10^{-4} – 10^{-6} Pa). Durch die Löcher werden die Analyt-Ionen vom Plasma in das Hochvakuum der Ionenoptik transportiert.

Im Hochvakuum angekommen werden die positiv geladenen Analyt-Ionen in einem negativen elektrischen Feld beschleunigt, sodass alle Analyt-Ionen die gleiche kinetische Energie aufweisen. Ebenfalls ins Vakuum eintretende Elektronen können das elektrische

Beschleunigungsfeld nicht passieren und werden dadurch bereits beim Eintritt ins Vakuum abgetrennt.

Die im Anschluss in die Ionenoptik eintretende diffuse Wolke aus positiv geladenen Analyt-Ionen wird beim Passieren positiv geladener Ringelektroden (sogenannte elektronische Linsen) durch elektrostatische Abstoßung gebündelt. Durch versetzte Anordnung der elektronischen Linsen (*off-axis*-Anordnung) beschreiben die Analyt-Ionen eine S-Kurve beim Passieren des MS-Interface. Ebenfalls in die Ionenoptik eintretende Photonen und Neutralteilchen aus dem Plasma treffen ohne Ablenkung auf die Innenwände des MS-Interface und können somit nicht den Massenselektor und Detektor erreichen. So kann das Untergrundrauschen verringert werden.

Der Massenselektor ist das Herzstück eines jeden Massenspektrometers. Nur Analyt-Ionen eines spezifischen m/z-Verhältnisses können den Massenselektor passieren und im Anschluss detektiert werden. Zusätzliche Ionen, die beispielsweise aus der Probenmatrix stammen, werden abgetrennt - vorausgesetzt, sie weisen ein zum Analyt unterschiedliches m/z-Verhältnis auf.

Das in dieser Arbeit verwendete ICP-MS ist mit einem Quadrupolmassenselektor ausgestattet (siehe **Abbildung 15**). Ein solcher Massenselektor ist der mit Abstand am häufigsten eingesetzte Massenselektor in der Elementanalytik. Dieser Massenselektortyp ist sehr kompakt und robust und erreicht hohe Scan-Geschwindigkeiten, sodass ein vollständiges Massenspektrum in weniger als 100 ms gemessen werden kann.[141] Der Quadrupol besteht aus vier parallel und symmetrisch ausgerichteten Stäben aus Metall oder metallbeschichteter Keramik, die als Elektroden dienen. An jedem Stab wird eine Gleichspannung angelegt, wodurch vier, sich in der Mitte des Quadrupols überschneidende konzentrische Magnetfelder um die einzelnen Stäbe ausgebildet werden. Ionen, die dem Quadrupol zugeführt werden, werden so innerhalb des Quadrupols fokussiert. Die Massenselektion eines Ions eines bestimmten m/z-Verhältnisses wird dadurch erreicht, dass nur dieses bestimmte Ion aufgrund eines Zusammenspiels der an den Stäben angelegten Gleich- und Wechselspannungen eine stabile Ionentrajektorie beim Passieren des Quadrupols beschreibt. Ionen anderer m/z-Verhältnisse werden abgelenkt, schlagen in die Stäbe und/oder das

Gehäuse des Quadrupols ein oder werden von der Vakuumpumpe abgesaugt und erreichen damit nicht das Ende des Quadrupols und den anschließenden Detektor.
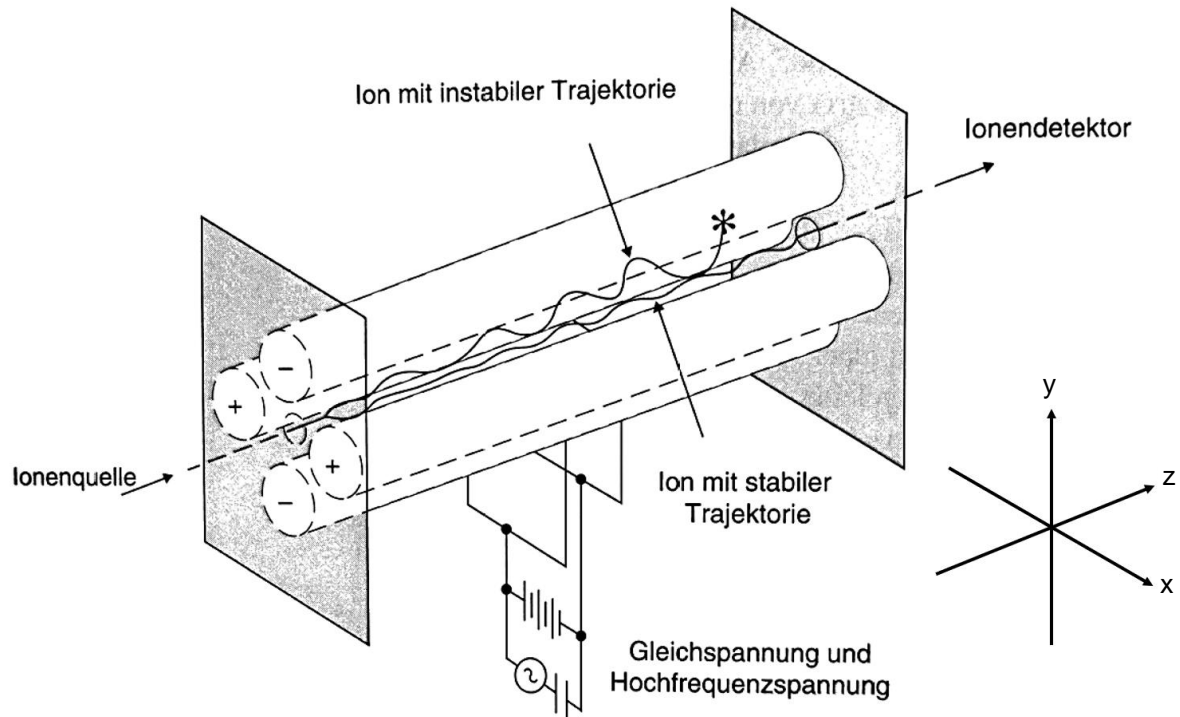
Abbildung 16: Schematischer Aufbau eines Quadrupolmassenselektors. Nur die Ionen eines bestimmten m/z-Verhältnisses können eine stabile Flugbahn durch den Massenselektor beschreiben, während Ionen anderer m/z-Verhältnisse abgelenkt werden. [133]

Die Ionentrajektorie wird beeinflusst, indem an den zwei gegenüberliegenden Stäben, die sich in der xz-Ebene befinden, eine positive Gleichspannung angelegt ist, die von einem Wechselstromsignal überlagert ist (siehe **Abbildung 16**). Die positiv geladenen Ionen bewegen sich deshalb in z-Richtung, werden jedoch durch den Einfluss der Wechselspannung abgelenkt. Nach den Gesetzen der *Newton'schen* Mechanik sind Impulse von Ionen gleicher kinetischer Energie direkt proportional zur Wurzel ihrer Masse. In anderen Worten reagieren leichtere Ionen leichter auf die Wechselspannung als schwerere Ionen. Das Stäbe-Paar der xz-Ebene bildet deshalb einen Hochpass-Massenfilter, den nur Ionen passieren können, die schwer genug sind – leichtere Ionen werden in Folge der Wechselspannung abgelenkt und damit entfernt. Das Stäbe-Paar der zy-Ebene hingegeben bildet einen gegensätzlichen Massenfilter. Hier wird eine negative Gleichspannung von einem Wechselfeld überlagert. Die Gleichspannung würde dazu führen, dass alle Ionen in Richtung der Stäbe gezogen würden. Diese Ionenbewegung wird jedoch durch eine durch die Wechselspannung begründete

Auslenkung kompensiert. Leichtere Ionen können einfacher ausgelenkt werden als schwere Ionen, denn letztere bleiben von der Wechselspannung nahezu unberührt und kollidieren mit den Stäben. Somit wird in der zy-Ebene ein Tiefpass-Massenfilter geschaffen, den nur Ionen passieren können, die leicht genug sind. Folglich muss ein Ion, das den Quadrupol insgesamt ohne Ablenkung passieren soll, schwer genug sein, um den Hochpass-Massenfilter in der xz-Ebene passieren zu können, jedoch gleichzeitig leicht genug sein, um den Tiefpass-Massenfilter in der zy-Ebene passieren zu können. Nur Ionen, die einen sehr engen Bereich des m/z-Verhältnisses erfüllen, beschreiben also eine stabile Ionentrajektorie durch den Quadrupolmassenselektor. Durch Variation der Gleich- und Wechselspannungen kann die Lage des m/z-Verhältnisses mit stabiler Ionentrajektorie angepasst werden. Moderne Geräte ermöglichen eine problemlose Separation von Ionen, die sich nur mehr um eine Masseneinheit unterscheiden. Um eine höhere Massenauflösung zu erreichen, können anstelle des Quadrupols doppelfokussierende Analysatoren eingesetzt werden, die einen elektrostatischen Analysator und einen magnetischen Sektorfeldanalysator umfassen.[142]

In diesem Zusammenhang sei angemerkt, dass bestimmte Geräte eine Zelle aus acht stabförmigen Elektroden (sogenannter Oktapol) vor dem Quadrupolmassenselektor verwenden (siehe **Abbildung 15**). Dieser Oktapol dient als Kollisions- bzw. Reaktionszelle zur Verringerung von Interferenzen. Details zu Interferenzen in der ICP-MS sowie Vorgänge in der Kollisions- bzw. Reaktionszelle sind im nachfolgenden Kapitel aufgeführt.

Ein alternativer Massenselektor, wenn auch nicht so verbreitet, ist der Flugzeit-Massenselektor (*engl.* time of flight, TOF). Die Ionen werden dabei nach ihrer auf dem m/z-Verhältnis basierenden Flugzeit aufgetrennt. Die Ionen werden zunächst über ein elektrisches Feld beschleunigt und erfahren dabei unabhängig von ihrer Masse dieselbe kinetische Energie. Sobald die beschleunigten Ionen anschließend in einen feldfreien Raum eintreten, bewegen sich Ionen mit einem höheren m/z-Verhältnis langsamer als diejenigen mit einem niedrigeren m/z-Verhältnis. Die Flugzeit bis zum Detektor ist also vom m/z-Verhältnis abhängig, weshalb eine Detektion von Ionen eines oder mehrerer gewünschter m/z-Verhältnisse möglich ist. Im Gegensatz zum Quadrupol ist bei einem TOF-Massenspektrometer also eine simultane Messung mehrerer Isotope möglich.[143] Quadrupol-Geräte sind jedoch sehr viel kompakter aufgebaut und außerdem kostengünstiger.

Die abgetrennten Analyt-Ionen werden schlussendlich mit Hilfe eines Detektors registriert. Üblicherweise handelt es sich dabei um einen Diskreten Dynoden Detektor, der in analoger Weise zum Photomultiplier in der ET-AAS funktioniert. Im Gegensatz zu Photonen treffen bei der ICP-MS Analyt-Ionen auf eine erste Dynode, wodurch Elektronen aus der Dynode herausgeschlagen werden. Die weitere kaskadenartige Erzeugung von Sekundärelektronen erfolgt analog zu der im Photomultiplier der ET-AAS. Sekundärelektronenvervielfacher, die 20 Dynoden umfassen, erreichen üblicherweise einen Verstärkungsfaktor von 10^7. Der am Ende der Dynodenkaskade gemessene Stromfluss korreliert mit der Anzahl der anfangs eingetroffenen Analyt-Ionen. Moderne Geräte erreichen dabei Ansprechzeiten im Nanosekundenbereich. Durch Kalibrierung mit Lösungen bekannten Analyt-Gehalts ist eine Konvertierung des Stromflusses in die ursprüngliche Analyt-Konzentration der Probe möglich.

4.3.2 Limitierungen der Massenspektrometrie [133, 144-146]

Auch wenn die ICP-MS mittlerweile eine Standardmethode in der Elementspurenanalytik für eine Vielzahl von verschiedenen Elementen darstellt, ist auch diese analytische Methode von Limitierungen durch spektrometrische und nicht spektrometrische Interferenzen betroffen. Diese Interferenzen führen zu unerwünschten Signalintensitäten der beobachteten Analytmasse.

Nicht spektrometrische Interferenzen beruhen in den meisten Fällen auf simplen Matrixablagerungen an Bauteilen des Massenspektrometers, wie der Probenzuführung, dem Zerstäuber oder den Konen. Diese Ablagerungen können einen Signaldrift verursachen oder die Zerstäubung und Ionisierung stark beeinträchtigen. Sobald sich diese Ablagerung lösen und damit analytenthaltende Verunreinigungen in das Plasma eingetragen werden, steigt das Analytsignal kurzfristig signifikant an – eine Überbestimmung ist die Folge (Memoryeffekt). Bestimmte Elemente, die neben dem Analytelement in der Probe koexistieren, können weitere Interferenzen hervorrufen. *Hieftje* et al. haben den sogenannten Raum-Ladung-Effekt beobachtet und gezeigt, dass Ionen leichter Massen und damit geringeren Durchmessers von Ionen schwererer Massen aus dem Ionenstrahl verdrängt werden können.[147] *Olivares* und *Houk* weisen darauf hin, dass leicht ionisierbare Elemente (z.B. Alkalimetalle) das Ionisationsgleichgewicht stören, indem sie die zur Verfügung stehende Ionisierungsenergie zuerst verbrauchen, ehe Elemente mit höheren Ionisationspotential ionisiert werden.

Alkalimetalle, die in starkem Überschuss vorliegen, bewirken also eine Signalsupression eines etwaigen Analytelements mit höherem Ionisationspotential.[148] Nicht spektrometrische Matrixeffekte können meist durch Kalibrierung kompensiert werden, indem die Zusammensetzung der Kalibrierlösungen an die der Probenlösung angepasst wird. Wenn dies bei besonders komplexen Matrices nicht möglich ist, schafft das Standardadditionsverfahren Abhilfe.

Spektrometrische Interferenzen stellen im Vergleich zu den nicht spektrometrischen Interferenzen eine bedeutendere Limitierung der ICP-MS dar. Sie treten dann auf, wenn ein im Plasma erzeugtes Ion dasselbe m/z-Verhältnis wie ein Analyt-Ion aufweist. Ersteres Ion wird dann als vermeintliches Analytion im Detektor registriert. Die Folge ist eine Überbestimmung des Analyten. Bei den spektralen Interferenzen unterscheidet man zwischen isobaren Interferenzen, Interferenz durch doppelte geladene Ionen und polyatomare Störungen.

4.3.2.1 Isobare Störungen

Isobare Störungen treten auf, wenn Atome mit näherungsweise gleicher Massenzahl aber unterschiedlicher Ordnungszahl im Plasma ionisiert werden. Problematisch sind Massenunterschiede um weniger als eine Masseneinheit. Hochauflösende Spektrometer (beispielsweise Sektorfeldgeräte) können dagegen geringere Massendifferenzen noch auflösen.[142]

Beispielsweise überlagert ^{40}Ar, das als Plasmagas bei der ICP-MS ubiquitär vorhanden ist, Signale des häufigsten Calciumisotops ^{40}Ca (97 % Isotopenhäufigkeit). Deshalb kann nur ^{44}Ca (2,1 % Isotopenhäufigkeit) zur Messung herangezogen werden. Der Wechsel von ^{40}Ca auf ^{44}Ca geht aufgrund der geringeren Isotopenhäufigkeit jedoch mit einem Verlust von Nachweisstärke einher. Ein weiteres Beispiel ist ^{204}Hg, das die Messung von ^{204}Pb stört.

Diese Störungen können überwunden werden, wenn ein anderes Analytisotop zur Messung ausgewählt wird, dessen Masse nicht mit der eines Isotops eines anderen Elements überlappt oder die Koexistenz dieses störenden Elements ausgeschlossen werden kann. Wenn ein anderes Isotop des Analytelements aber nur eine sehr geringe Häufigkeit aufweist oder das Analytelement sogar ein Reinelement ist, ist ein Wechsel auf ein störungsfreies Analytisotop

nicht möglich. In diesem Fall kann eine isobare Störung auch mathematisch korrigiert werden. Voraussetzung dafür ist, dass ein Isotop des isobar störenden Elements vorhanden ist, welches wiederum selbst störungsfrei gemessen werden kann. Das Ausmaß der isobaren Störung ergibt sich dann aus dem Verhältnis der Isotopenhäufigkeiten des isobar störenden Elements. Nachfolgendes Beispiel illustriert eine mathematische Korrektur der Störung von ^{204}Pb durch ^{204}Hg.[149] Da ^{200}Hg störungsfrei messbar ist, ist eine mathematische Korrektur der ^{204}Hg-Störung möglich, wie in den Gleichungen 4.3-4.5 dargestellt ist. I stellt dabei die Signalintensität dar.

$$I_{gesamt} = I(^{204}Pb) + I(^{204}Hg) \tag{4.3}$$

$$I(^{204}Hg) = I(^{200}Hg) \cdot \frac{Isotopenh\ddot{a}ufigkeit\ ^{204}Hg}{Isotopenh\ddot{a}ufigkeit\ ^{200}Hg} \tag{4.4}$$

$$I(^{204}Pb) = I_{gesamt} - I(^{200}Hg) \cdot \frac{Isotopenh\ddot{a}ufigkeit\ ^{204}Hg}{Isotopenh\ddot{a}ufigkeit\ ^{200}Hg} \tag{4.5}$$

Die Störung von ^{204}Hg^{+}-Ionen kann alternativ durch das Einleiten von NH$_3$ in eine Reaktionszelle verringert werden (siehe Kapitel 4.3.2.5).

4.3.2.2   Störung durch doppelt geladene Ionen

Neben einfach geladenen Ionen können auch doppelt geladene Ionen im Plasma generiert werden. Solche Ionen überlagern Signale der einfach geladenen Ionen mit halber Elementmasse. Eine doppelte Ionisierung tritt vermehrt bei Elementen mit einer geringen zweiten Ionisierungsenergie auf, welche insbesondere geringer als die zweite Ionisierungsenergie des Argons (15 eV) ist. Beispiele sind schwerere Erdalkali- und Seltenerdelemente. Enthält eine Probe beispielsweise hohe Sr Gehalte bei gleichzeitiger Messung von Ca, so kann ^{88}Sr^{2+} zu einer Störung der ^{44}Ca^{+} Messung führen und eine Überbestimmung durch Signalüberlagerung verursachen.

4.3.2.3   Polyatomare Störungen

Die komplexeste Störungsklasse in der ICP-MS stellen jedoch polyatomare Störungen dar.[150] Insbesondere an den gekühlten Konen oder später im MS-Interface können sich

einfach positiv geladene Molekülionen bilden, die ein m/z-Verhältnis aufweisen, das dem des Analytelements näherungsweise entspricht.[151] Besonders störend sind Molekülionen, die sich aus den Hauptbestandteilen des Plasmas (Ar) und der Matrix (H_2O, HNO_3 etc.) bilden. Von polyatomaren Störungen sind insbesondere Analyten mit einem m/z-Verhältnis < 82 betroffen.[133] Beispielsweise kann sich aus dem Plasmagas Argon zusammen mit Spuren Sauerstoff, ein $^{40}Ar^{16}O^+$ Molekülion bilden, das mit dem m/z-Verhältnis von $^{56}Fe^+$ überlappt und zu einer Überbestimmung des Eisens führen würde. Neben Oxiden sind auch Interferenzen durch Bildung von Hydriden besonders relevant. Um polyatomare Interferenzen zu vermeiden, kann das zu messende Isotop des Analytelements variiert werden. Dies ist jedoch nur dann praktikabel, wenn ein weiteres Isotop, welches nicht von polyatomaren (oder isobaren) Störungen betroffen ist, auch eine ausreichend hohe Häufigkeit aufweist, um gute Nachweisgrenzen zu gewährleisten. Ist ein Wechsel des zu messenden Isotops nicht möglich, schafft eine Kollisions- oder Reaktionszelle Abhilfe, die sich zwischen den Konen des Massenspektrometers und dem Quadrupolmassenselektor (siehe **Abbildung 15**) befindet. Polyatome werden dabei in einem Multipol durch Kollision oder Reaktion mit eingeleiteten Gasen reduziert. Ein Multipol ist eine Zelle aus mehreren stabförmigen Elektroden, wobei meistens ein Oktapol aus acht Stabelektroden verwendet wird. Der Vorteil eines Oktapols gegenüber einem Quadrupol ist beispielsweise die kleinere Abmessung.

4.3.2.4 Kollisionszelle

Bei Verwendung des Multipols als Kollisionszelle werden der ionisierten Probe geringste Mengen eines inerten Gases (beispielweise Helium) zugesetzt. Da die störenden Molekülionen größer sind als das ionisierte Analytelement, besteht für die Molekülionen eine höhere Wahrscheinlichkeit, mit den zugesetzten Helium-Atomen zu kollidieren. Die Kollision führt zu einem deutlichen Verlust an kinetischer Energie. Aufgrund einer spezifischen Zellspannung am Multipol können diesen nur Ionen mit ausreichender kinetischer Energie passieren (kinetische Energiediskriminierung). Kollidierte Ionen weisen nicht mehr genug kinetische Energie auf und werden vor Erreichen des Quadrupolmassenselektors abgetrennt. Im Mittel wird die kinetische Energie eines deutlich höheren Anteils von Molekülionen als von ionisierten Analytatomen aufgrund der unterschiedlichen Kollisionswahrscheinlichkeit reduziert. Von den störenden Molekülionen erreicht nur ein geringer Anteil den Quadrupolmassenselektor, während die Menge der ionisierten Analytatome, die die Kollisionzelle in Richtung des Quadrupols passiert, kaum verringert wird. Somit werden die

polyatomaren Interferenzen auf ein Minimum reduziert. Bei Einsatz der kinetischen Energiediskriminierung ist jedoch zu beachten, dass auch die Signalintensität des Analytelements geringfügig sinkt und deshalb die Nachweisgrenze steigen kann.

Die bereits erwähnte Störung von $^{56}Fe^+$ durch das Polyatom $^{40}Ar^{16}O^+$ kann mit Hilfe einer Kollisionszelle und Helium als Kollisionsgas eliminiert werden.[152, 153]. Alternativ ist eine Unterscheidung von $^{56}Fe^+$ mit einer Masse von 55,935 atomaren Einheiten und $^{40}Ar^{16}O^+$ mit einer Masse von 55,957 atomaren Einheiten mit hochauflösenden Sektorfeldgeräten [142] möglich, ohne dass eine Kollisions- oder Reaktionszelle notwendig ist.

4.3.2.5 Reaktionszelle

Bei Verwendung des Multipols als Reaktionszelle wird reaktives Gas anstelle von Kollisionsgas zugeführt. *Rowan* und *Houk* zeigten bereits 1989, dass durch gezielte Auswahl des Reaktionsgases polyatomare Störungen reduziert werden können.[154] Die Reaktion der störenden Molekülionen mit dem Reaktionsgas hat entweder die Dissoziierung der Molekülionen zur Folge oder führt zur Addition weiterer Atome an die Molekülionen. In beiden Fällen wird das m/z-Verhältnis der störenden Molekülionen verschoben und die polyatomare Störung beseitigt.

Beispielsweise kann die $^{38}Ar^1H^+$ Störung bei der Messung von $^{39}K^+$ mittels Reaktionszelle und H_2 als Reaktionsgas behoben werden. Nur $^{38}Ar^1H^+$ reagiert mit $^1H_2$ unter der Bildung von $^1H_3^+$ und ^{38}Ar, während $^{39}K^+$ nicht reagiert.[155]

Zudem besteht auch die Möglichkeit, den Analyten selbst zur Reaktion zu bringen und damit dessen m/z-Verhältnis auf ein nicht von Störungen betroffenes Verhältnis zu erhöhen. Beispielsweise ist das Schwefel-Hautpisotop $^{32}S^+$ stark durch $^{16}O_2^+$ gestört. Aufgrund geringer Isotopenhäufigkeiten ist ein Ausweichen auf ein Schwefel-Nebenisotop nicht zielführend. Mittels O_2-Reaktionszelle wird $^{32}S^+$ in $^{32}S^{16}O^+$ umgewandelt, dessen m/z-Verhältnis von 48 ohne störende Interferenz messbar ist.[156] Neben Sauerstoff kommen auch reaktive Gase wie Ammoniak zum Einsatz.

Reaktionszellen finden auch bei Störungen durch isobare oder doppelt geladene Ionen Verwendung: Das isobar störende Isotop ^{204}Hg für die Messung von ^{204}Pb kann mittels

Reaktionszelle entfernt werden. $^{204}Hg^+$ reagiert mit NH_3 als Reaktionsgas in einer Ladungstransfer-Reaktion zu ^{204}Hg und NH_3^+. $^{204}Pb^+$ reagiert dabei nicht. Das Isotop ^{204}Hg wird durch die Neutralisierung nicht mehr detektiert. Die Störung auf ^{204}Pb ist somit aufgehoben.[149]

Die Quantifizierung von Titan erfolgt anhand des häufigsten Isotops $^{48}Ti^+$, welches jedoch durch $^{48}Ca^+$ oder $^{96}Zr^{2+}$ gestört wird. $^{48}Ti^+$ bildet in einer NH_3-Reaktionszelle Addukte wie $^{48}Ti^{14}N^1H^+$, die störungsfrei messbar sind.[157]

4.3.2.6   Triple-Quad-Geräte

Es existieren auch Geräte, die vor der Kollisions- oder Reaktionszelle einen zusätzlichen Quadrupol verwenden, um bereits vor Kollision bzw. Reaktion eine Massenselektion durchzuführen (sogenannte Triple-Quad-Geräte). Damit werden Ionenstrahlen mit enger m/z-Verteilung in die Reaktionszelle geleitet, wodurch die Effizienz der Störungsbeseitigung durch kontrollierte Reaktionen sowie die Massenauflösung erhöht wird. Beispielsweise kann verhindert werden, dass das Reaktionsgas bei breitem m/z-Bereich neue Interferenzen schafft.

4.3.2.7   Störungen in Bezug auf Silber

Die vorliegende Arbeit beschränkt sich auf die Quantifizierung von Ag mittels ICP-MS. Von Ag existieren die beiden Isotope ^{107}Ag und ^{109}Ag mit einer vergleichbaren Isotopenhäufigkeit von 51,5 % bzw. 48,2 %. Beide Isotope sind frei von isobaren Störungen. Potentiell störende Polyatome beruhen auf Zr, nämlich $^{91}Zr^{16}O^+$ für ^{107}Ag und $^{92}Zr^{16}O^1H^+$ für ^{109}Ag.[150] Für die beschriebenen Messungen sind diese polyatomaren Störungen jedoch irrelevant, da die untersuchten Proben keine relevanten Mengen an Zr enthalten und die Isotope ^{91}Zr und ^{92}Zr im Gegensatz zum Hauptisotop ^{90}Zr (Isotopenhäufigkeit 51,45 %) nur geringe Häufigkeiten von 11,22 % bzw. 17,15 % aufweisen. Als reine Vorsichtsmaßnahme werden in den vorliegenden Messungen jedoch stets beide Ag Isotope für die Messung herangezogen und diese zudem mit und ohne Helium-Kollisionszelle gemessen. Es sei bereits angemerkt, dass zwischen den Messungen mit und ohne Kollisionszelle sowie der beiden Isotope nie relevante Abweichungen festgestellt werden konnten. Eine störungsfreie Messung von Ag mittels ICP-MS in den hier betrachteten Proben ist also sichergestellt.

4.3.3 Einzelpartikel-Massenspektrometrie und ihre Limitierungen [95, 158-162]

Die oben beschriebene, konventionelle Plasma-Massenspektrometrie erlaubt die Quantifizierung von Elementspuren bis in den niedrigen ng L^{-1} Bereich, jedoch ohne Informationen über einen potentiellen partikulären Zustand des Analyten. Die Einzelpartikel-Massenspektrometrie (*engl.* single particle inductively coupled mass spectrometry, sp-ICP-MS) ist eine Variante der ICP-MS, die eine größenselektive Quantifizierung von Nanopartikeln in Lösung ausschließlich durch besondere Datenverarbeitung ermöglicht. Entscheidend für die Entwicklung der sp-ICP-MS war es, sehr kurze Messzeiten am Detektor, die sogenannten dwell times, im Bereich von wenigen ms oder µs zu realisieren. Dabei wird ausgenutzt, dass bei Atomisierung eines Nanopartikels im Plasma eine große Anzahl an Ionen entsteht, die als „Ionenwolke" nahezu gleichzeitig auf den Detektor auftreffen (siehe **Abbildung 17**). Gelöster Analyt hingegen erzeugt konstant Ionen, die den Detektor gleichmäßig erreichen. Dadurch erzeugen die gelösten Analyten ein gleichmäßiges Hintergrundsignal (siehe „ionischer Hintergrund" in **Abbildung 17**), während das Auftreffen der nanopartikelbedingten Ionenwolken auf den Detektor zu einer kurzzeitigen signifikanten Erhöhung des Signals führen und in Form von Intensitätsspitzen (siehe transiente „Partikelsignale" in **Abbildung 17**) sichtbar werden. Durch die extrem kurzen Messzeiten in der sp-ICP-MS können diese transienten Partikelsignale aufgezeichnet werden. Die Messzeiten, die in der konventionellen Plasma-Massenspektrometrie üblich sind, sind sehr viel länger als die durchschnittliche Lebensdauer einer Ionenwolke [95] und deshalb nicht im Stande, Partikelsignale aufzulösen.

Die Anzahl der Partikelsignale korreliert mit der Anzahl der Nanopartikel in der Probe sowie die Fläche unter den Partikelsignalen mit der Masse und damit Größe der Nanopartikel. Es können nur diejenigen Partikel identifiziert werden, die so groß sind, dass deren Signal das des Hintergrunds übersteigt. Man spricht hier vom sogenannten Size Detection Limit (*engl.* Größenbestimmungsgrenze, SDL).
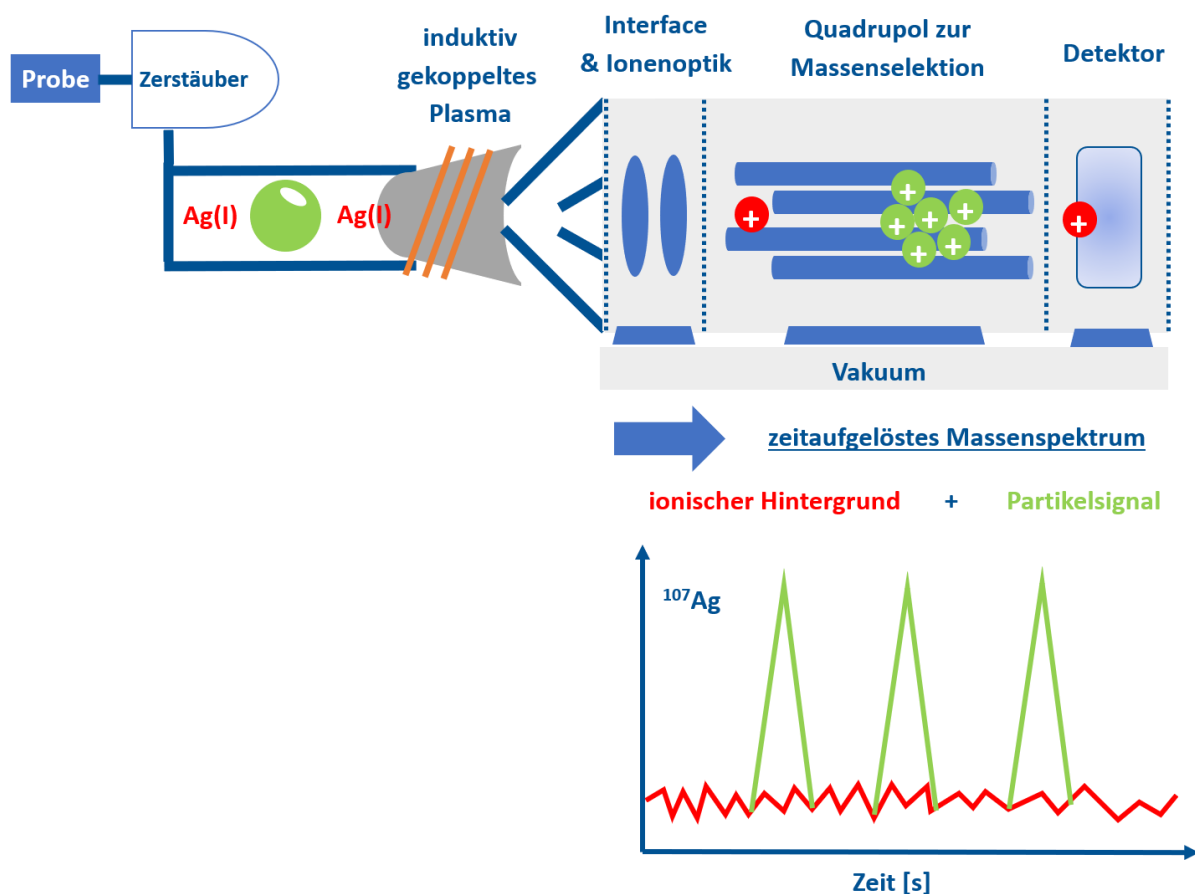
Abbildung 17: Schema der Signalerzeugung und -verarbeitung der Einzelpartikelmassenspektrometrie. Grün: nanopartikuläres Silber; Rot: gelöstes Silber.

Neben der Messzeit wird jedes sp-ICP-MS-System zusätzlich durch eine Stabilisierungszeit charakterisiert, jener Zeit, in der zwischen den Messintervallen keine Ioneneinschläge vom Detektor registriert werden können. **Abbildung 18** zeigt, dass eine optimale Abstimmung von Mess- und Stabilisierungszeit für eine erfolgreiche sp-ICP-MS-Messung entscheidend ist. Die Messzeit darf nicht zu lang sein (a), denn dann werden mehrere Ionenwolken gleichzeitig registriert und fälschlicherweise als ein großer Partikel ausgewertet. Ist die Stabilisierungszeit zu lang (c – d) verschieben sich die Messzeiten, sodass Partikel teilweise (b, c) oder gar nicht (d) detektiert werden können. Im optimalen Fall (b) liegt eine Partikelwolke innerhalb einer Messzeit.
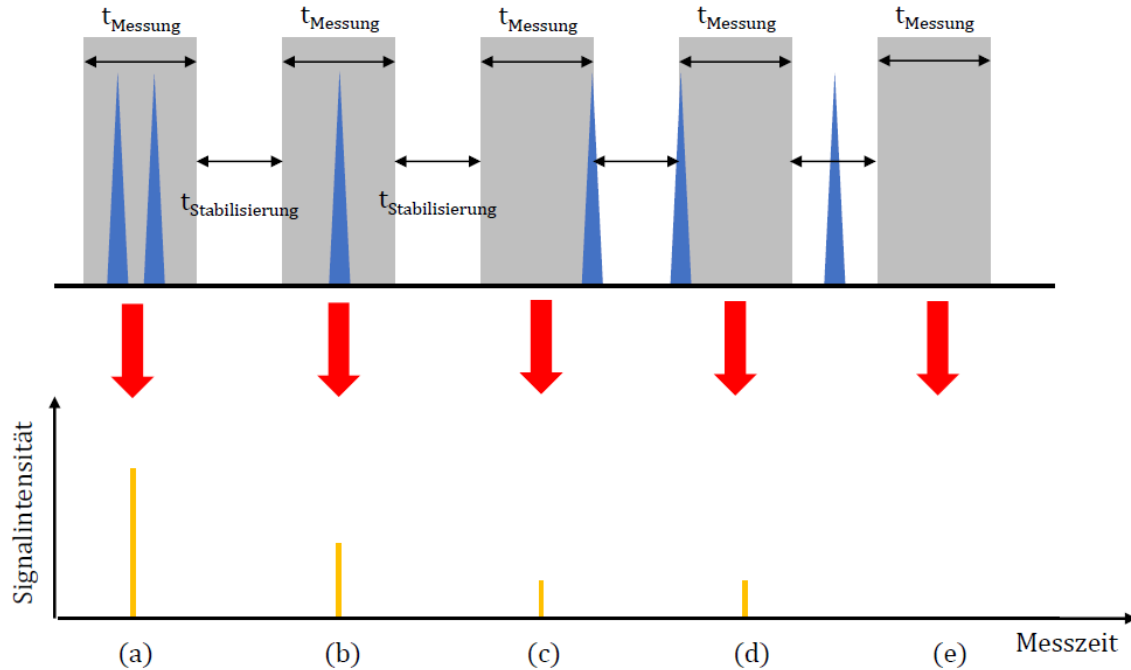
Abbildung 18: Zusammengang von Messzeit und Stabilisierungszeit auf die Detektion der Partikel im sp-ICP-MS-Modus; nach [158].

Moderne Geräte lassen sp-ICP-MS Messungen bei extrem kurzen Messzeiten ohne signifikante Stabilisierungszeiten zu, sodass eine Ionenwolke innerhalb mehrerer Messzeiten durchgängig aufgezeichnet werden kann (siehe **Abbildung 19**). Nachdem Anfang und Ende des transienten Signals softwarebasiert bestimmt ist, kann die Gesamtintensität eines transienten Partikelsignals durch Integration über mehrere Messzeiten berechnet werden. Eine Messzeit von 100 µs bis 10 ms gilt als optimal, wobei die Verdünnung der Probe so stark sein sollte, dass in maximal 10 % aller Messzeiten ein Partikel detektiert wird. Es ist deshalb vorteilhaft, Proben mit einer Konzentration des nanopartikulären Analyten im ng L^{-1} Bereich zu messen.
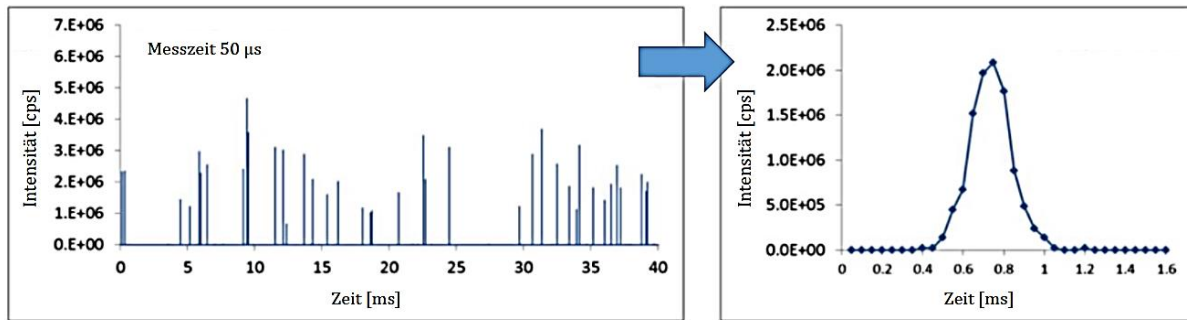
Abbildung 19: Erfassung eines Partikelsignals innerhalb mehrerer Messzeiten ohne signifikante Stabilisierungszeit. Links: Signalverteilung einer sp-ICP-MS-Messung. Rechts: Vergrößerung eines Partikelsignals. nach [158]

Obwohl die ICP-MS grundsätzlich eine Multielementmethode ist, ist bei der sp-ICP-MS während einer Messung die Bestimmung von nur einer Analytmasse möglich. Aufgrund der hohen Zeitauflösung der Messung ist es nicht möglich, während der Messung auf eine andere Masse umzuschalten. Bei einem Isotopenwechsel würde eine relativ hohe Stabilisierungszeit notwendig sein, innerhalb derer keine Detektion möglich ist. Außerdem kann eine Ionenwolke nach Massenwechsel teilweise in die Messzeit eines anderen Isotops reichen und nicht vollständig detektiert werden. Es existieren aber bereits Ansätze zur Multielementbestimmung in der Einzelpartikelmassenspektrometrie mittels sp-ICP-TOF-MS, womit Partikelzusammensetzungen und Beschichtungen messbar werden.[96]

Die Umwandlung von Rohdaten der sp-ICP-MS-Messungen in Partikelgrößenverteilungen setzt folgende Annahmen voraus:

a) Die Form der Partikel wird als sphärisch und nicht hohl definiert.
b) Die Elementzusammensetzung der Partikel muss bekannt sein oder angenommen werden, damit eine definierte Dichte zur Berechnung herangezogen werden kann. Die Dichte des Materials der NP entspricht der des entsprechenden Bulk-Materials.
c) Matrixeffekte müssen ausgeschlossen werden und bezüglich des zu untersuchenden Elements treten keine Interferenzen auf oder mögliche Interferenzen können beseitigt werden.

Zur Auswertung der Rohdaten wird herangezogen, dass zum einen die Anzahl der Signale proportional zur Anzahl der Partikel in der Probe und damit deren Konzentration ist. Die

Transporteffizienz η gibt an, welcher Anteil der Partikel von der Probe über den Zerstäuber das Plasma erreicht. Zum anderen ist die Intensität des Signals ein Maß für die Masse des Partikels und damit nach Kenntnis der Dichte und der Annahme einer sphärischen Partikelgeometrie ein Maß für den Partikeldurchmesser. Im Folgenden soll der Gang der Berechnung der Partikelgrößenverteilung und Konzentration anhand der verwendeten Formeln und Zusammenhänge zusammen mit der durchgeführten Kalibrierung erläutert werden.[163] Diese Berechnung setzt zudem voraus, dass die Messzeit ausreichend lang gewählt ist und dass eine Partikelwolke vollständig innerhalb einer Messzeit detektiert wird. Wie bereits erwähnt setzen moderne Geräte und Auswertungssoftware das Partikelsignal aus den Signalen mehrere Messzeiten zusammen.

Zur Bestimmung der Transporteffizienz wird eine Kalibrierung mit einer Au-NP-Suspension durchgeführt. Au-NP werden insbesondere deshalb eingesetzt, weil sie mit sehr hoher Reproduzierbarkeit der Partikelgröße synthetisiert und sehr gut stabilisiert werden können. Die Transporteffizienz ist in erster Näherung gerätespezifisch und kann direkt auf andere NP (hier Ag-NP) übertragen werden. Die Partikelkonzentration der Au-NP in der Probe c_p^{Au} [mL^{-1}] hängt wie folgt von der gegebenen Massenkonzentration der Suspension c_m^{Au} [g mL^{-1}] und der Partikelmasse eines Au-NP m_p^{Au} [g] ab:

$$c_p^{Au} = \frac{c_m^{Au}}{m_p^{Au}} \tag{4.6}$$

60 nm große Au-NP beispielsweise besitzen bei der Annahme einer sphärischen Partikelform und der Dichte von Gold ρ_{Au} von 19.32 g cm^{-3} eine Partikelmasse m_p^{Au} von 2.2·10^{-15} g. Der Partikelfluss q_p [s^{-1}] in das Plasma ergibt sich aus dem Quotienten der Anzahl der Signale N_s in der gesamten Messzeit t_m [s] durch die Messzeit nach:

$$q_p = \frac{N_s}{t_m} \tag{4.7}$$

Zusammen mit der Partikelkonzentration lässt sich daraus die Transporteffizienz η [%] berechnen, wobei der gerätespezifische Probenfluss v [mL min^{-1}] bekannt sein muss. Der Faktor 60 in Gleichung 4.8 ergibt sich aus der Umrechnung auf gleiche Einheiten.

$$\eta = \frac{60 \cdot q_p}{c_p^{Au} \cdot v} \cdot 100\ \%$$

(4.8)

Die Transporteffizienz macht schlussendlich eine Berechnung der Partikelkonzentration c_p [L^{-1}] der gemessenen Probe möglich. In nachfolgender Gleichung beschreibt N_p [min^{-1}] die Anzahl der bei der Messung der Probe detektierten Partikel pro Messzeit.

$$c_p = \frac{N_p}{\eta} \cdot \frac{1000}{v}$$

(4.9)

Für die weiteren Berechnungen ist eine zweite Kalibrierung notwendig. Eine ionische Lösung des zu bestimmenden Elements (hier Ag$^+$-Lösung) bekannter Konzentration c_{Ag^+} [µg L^{-1}] wird im selben sp-Modus gemessen, wie die Proben, die Ag-NP enthalten. Die Elementsensitivität ES_{ion} [cps L µg^{-1}] ergibt sich dabei aus dem Mittelwert aller je Messintervall gemessenen Signalintensitäten $\bar{I}_{mess}$ [cps] nach folgender Gleichung:

$$ES_{ion} = \frac{\bar{I}_{mess}}{c_{Ag^+}}$$

(4.10)

Die Masse jedes einzelnen Partikels m_p [ng] hängt wie folgt von der Signalintensität dieses Partikels I_p [cps], der Messzeit t_d [ms], der Elementsensitivität ES_{ion}, der Transporteffizienz η, dem Probenfluss v und den Molaren Massen des Nanopartikels M_p [g mol^{-1}] und des in der Messung beobachteten Elements M_e [g mol^{-1}] ab:

$$m_p = \frac{I_p}{ES_{ion}} \cdot t_d \cdot v \cdot \frac{\eta}{60} \cdot \frac{M_p}{M_e}$$

(4.11)

$t_d \cdot v$ entspricht dabei dem Probenvolumen, in dem ein Partikel detektiert werden kann. Sind die Einzelmassen aller Partikel m_{p_i} [ng] berechnet, ist die Berechnung der

Massenkonzentration des Analyten β [ng L^{-1}] nach Gleichung 4.12 bei Kenntnis der Gesamtmessdauer (Summe aller Messintervalle) t_{ges} [min] möglich:

$$\beta = \frac{\sum_i m_{p_i}}{\eta \cdot \nu \cdot 1000 \cdot t_{ges}} \tag{4.12}$$

Die berechnete Massenkonzentration muss im Anschluss nach Korrektur um alle Verdünnungsschritte und dem Anreicherungsfaktor der CPE in die Konzentration der Probe umgerechnet werden. Unter Berücksichtigung der Dichte ρ_p [g mL^{-1}] der NP ist eine Berechnung des Partikeldurchmessers d_p [nm] eines jeden detektierten Partikels aus der Masse über das Partikelvolumen möglich, sofern angenommen wird, dass die Partikel in der Probe von sphärischer Gestalt sind.

$$d_p = \sqrt[3]{\frac{6 \cdot m_p}{\pi \cdot \rho_p}} \cdot 10^4 \tag{4.13}$$

Zusätzlich ist es essentiell, die Signalintensitätsgrenze festzulegen, ab der Signale Partikeln zugeordnet werden und nicht mehr von Ionen stammen (SDL). Dazu existieren verschiedene Methoden. Eine in der Literatur vielfach verwendete Methode ist nachfolgend in Zusammenhang mit Publikation 3 aufgeführt. Die in dieser Arbeit verwendete Probenvorbereitung mittels CPE vor den sp-ICP-MS Messungen ist jedoch in der Lage das Hintergrundsignal und damit den SDL-Wert auf ein Minimum zu reduzieren (siehe Publikation 3).

4.4 Total-Organic-Carbon-Messungen [164]

Der Begriff „gesamter organischer Kohlenstoff" (*engl.* Total Organic Carbon, TOC) umfasst die Menge des Kohlenstoffs, der in gelösten oder suspendierten Substanzen im Wasser gebunden ist, sowie Cyanate, Isocanate und Thiocyanate. Letztgenannte Verbindungen gehören eigentlich dem anorganischen Kohlenstoff an, sind bei Messungen des TOC aber nicht abgrenzbar.

Der „gesamte Kohlenstoff" (*engl.* Total Carbon, TC) schließt den anorganisch und organisch gebundenen Kohlenstoff sowie elementaren Kohlenstoff ein.

Der „gesamte anorganisch gebundene Kohlenstoff" (*engl.* Total Inorganic Carbon, TIC) umfasst Kohlenstoff anorganischer Verbindungen, partikulären und suspendierten elementaren Kohlenstoff, gelöstes Kohlenstoffdioxid, Cyanide, Cyanate, Isocyanate und Thiocyanate.

Unter „gelöstem organisch gebundenem Kohlenstoff" (*engl.* Dissolved Organic Carbon, DOC) wird der Anteil des TOC verstanden, der erfasst wird, wenn die Proben vor der Messung einen Membranfilter mit einer Porenweite von 0.45 µm passieren. Außerdem sind Cyanide, Cyanate, Isocyanate und Thiocyanate enthalten.

Grundsätzlich werden zur Bestimmung des TOC-Gehalts wässriger Proben kohlenstoffhaltige Verbindungen vollständig oxidiert und das so entstandene CO_2 anschließend quantifiziert. Dabei unterscheidet man eine Direkt- und eine Differenzmethode:

Bei der Direktmethode wird der anorganisch gebundene Kohlenstoff (TIC) nach Ansäuern mit Hilfe eines Gasstroms (z.B. Stickstoff, synthetische Luft) ausgetrieben. Der übrig gebliebene Kohlenstoff wird oxidiert und quantifiziert. Der TOC-Gehalt wird jedoch in geringem Maße überbestimmt, da durch Ansäuern nur ein Teil des TIC (insbesondere Carbonate, gelöstes CO_2) entfernt wird.

Bei der Differenzmethode wird vor dem Ansäuern der Probe zunächst der TC-Gehalt durch vollständige Oxidation aller in der Probe erhaltenen Kohlenstoffverbindungen und des elementaren Kohlenstoffs mit anschließender Quantifizierung des dabei entstandenen Kohlenstoffdioxids bestimmt. Der TIC ergibt sich aus der Wiederholung der erwähnten Schritte nach dem Ansäuern. Der TOC ist dann die Differenz von TC und TIC. Da hier während der TIC-Bestimmung wieder nur Carbonate und gelöstes CO_2 erfasst werden, resultiert die Messung insgesamt wieder in einem Überbefund an TOC.

Die Oxidation selbst erfolgt entweder nasschemisch mittels Natriumperoxodisulfat, mit Hilfe von UV-Licht oder im Hochtemperaturofen unter Sauerstoffzufuhr und Zuhilfenahme von

Katalysatoren wie Platin, Kupferoxid oder Kobaltoxid. CO_2 wird mit speziellen Detektoren infrarotspektrometrisch, coulometrisch oder konduktometrisch bestimmt oder nach Reduktion zu Methan anhand der Wärmeleitfähigkeit oder in Flammenionisationsdetektoren quantifiziert. Moderne Geräte ermöglichen eine Messung des TOC im Bereich von 0.1 mg L^{-1} bis 1000 mg L^{-1}.

5 Zusammenfassung der Publikationen

Nachfolgend sind die im Rahmen dieser Arbeit entstandenen Publikationen zusammengefasst. Es sei darauf hingewiesen, dass die Reihenfolge der Publikationen dabei nicht dem Erscheinungszeitpunkt entspricht. Sie folgen vielmehr dem Entwicklungsprozess im Rahmen dieser Studie. Publikation 1 umfasst die ersten Messungen von Ag-b-NP in Flusswasser. Publikation 2 ist ein Feature-Paper, das einen Überblick über das Potential der Cloud-Point-Extraktion im Umweltmonitoring von Nanomaterialien geben soll. Die Publikationen 3 und 4 sind analytisch-methodischer Natur und beschreiben die Entwicklung der Kombination der Cloud-Point-Exktraktion mit der Einzelpartikelmassenspektrometrie (Publikation 3) sowie der Elektronenmikroskopie (Publikation 4). Publikationen 5 bis 9 sind auf Anwendungsbeispiele des entwickelten Analytischen Verfahrens gerichtet, nämlich die Messung von Ag-b-NP in Flusswasser (Publikationen 5 und 6), in Leitungswasser (Publikation 7) und in Meerwasser (Publikation 8). Publikation 9 zeigt schließlich, dass Ag-b-NP nicht nur anthropogener Natur sind, sondern auch natürlich gebildet werden können.

5.1 PUBLIKATION 1: To What Extent Can Full-Scale Wastewater Treatment Plant Effluent Influence the Occurrence of Silver-Based Nanoparticles in Surface Waters?

in Environmental Science and Technology

Diese Studie stellt sich die Frage, in welchem Ausmaß Klärwerksabflüsse den Ag-b-NP Gehalt in Oberflächengewässern beeinflussen. Experimentelle Details sowie die Abhängigkeit der Rückhalteeffizienz der Ag-b-NP von verschiedenen Prozessschritten im Klärwerk und den Jahreszeiten sind der Publikation zu entnehmen. Die Konzentrationsbestimmung von Ag-b-NP erfolgte mittels CPE-ET-AAS. Größenverteilungen von Ag-b-NPs in Klärwerk-Abflussproben wurden mittels CPE-sp-ICP-MS bestimmt. Die CPE basierte zum Zeitpunkt dieser Publikation noch auf dem Verfahren nach *Hartmann* et al..[24]

Es konnte gezeigt werden, dass Klärwerke mehr als 96,4 % der Ag-b-NP zurückhalten, auch wenn der Klärwerkszulauf mehrere Hundert ng L^{-1} Ag-b-NP enthalten hat. Dies resultierte in Ablaufkonzentrationen von 0,7 bis 11,1 ng L^{-1} an nanopartikulärem Silber. Die durchschnittlichen Partikelgrößen der Ag-b-NP in KW-Abfluss lagen zwischen 15 und 20 nm. Allein auf Klärwerksabflüsse bezogen werden hochgerechnet auf Deutschland pro Jahr ca. 33 kg Ag-b-NP in die Umwelt freigesetzt.

Im Rahmen dieser Studie wurde außerdem der reale Beitrag von KW zum Ag-b-NP Gehalt in der Isar untersucht. Die Isar ist ein mehr als 290 km langer Fluss in Süddeutschland, der in Österreich im Karwendelgebirge entspringt und zunächst ländliche Gebiete des Alpenvorlands passiert, ehe Städte wie Lenggries und Bad Tölz und schließlich die Metropolregion Münchens erreicht werden. Die Isar fließt weiterhin durch Freising, Moosburg, Landshut, Dingolfing, Landau an der Isar und Plattling, bevor sie südlich von Deggendorf in die Donau mündet. Die Isar wurde stromaufwärts vielfach beprobt und die Konzentration an Ag-b-NP wurde mittels CPE-ET-AAS gemessen. Die Isar enthielt 0,9 bis 2,3 ng L^{-1} nanopartikuläres Silber, wobei die Konzentration mit steigender Anzahl passierter Städte und nahegelegener Klärwerke zunahm. Nahe den Klärwerken wurden Belastungsspitzen von 2,0 bis 8,6 ng L^{-1} Ag-b-NP gemessen, was den anthropogenen Eintrag der Ag-b-NP in die Isar zweifelsfrei abbildet. Neben der Isar wurde eine Vielzahl bayerischer

Seen auf Ag-b-NP untersucht. Dabei enthielten sowohl Seen, die über deren Zuflüsse Klärwerkseinträge erhalten, als auch Seen ohne Klärwerkseintrag Ag-b-NP in Konzentrationsbereichen unter 1 ng L^{-1}. Ob ein gewisser geogener Untergrund an Nanosilber vorliegt oder sich Partikel natürlich bilden, wurde im Rahmen der unten angeführten Publikation 9 weiter beleuchtet.

Eigener Beitrag:
- *Durchführung und Auswertung von CPE-sp-ICP-MS Messungen von Klärwerk-Abflussproben*
- *Beprobung der Isar*
- *Durchführung und Auswertung von CPE-sp-ICP-MS Messungen von Wasserproben der Isar*
- *Anmerkung: Vorarbeiten zur Messung von Ag-b-NP in der Isar waren Teil meiner Masterarbeit. Die Messungen wurden zum Teil noch im Rahmen der Masterarbeit durchgeführt. Eine detaillierte Auswertung und Interpretation der Ergebnisse im Rahmen dieser Publikation erfolgte zum Zeitpunkt meiner Dissertation.*

Wesentliche Beiträge Dritter:
- *L. Li und M. Stoiber: Detaillierte Untersuchungen der Ag-b-NP-Gehalte in Klärwerksproben*
- *L. Li: Verfassen der Publikation*

5.2   PUBLIKATION 2: Can cloud point-based enrichment, preservation, and detection methods help to bridge gaps in aquatic nanometrology?

<div align="right">in Analytical and Bioanalytical Chemistry</div>

Diese Publikation ist ein im Rahmen eines Forschungsverbunds entstandenes Feature-Paper, das das Potential der CPE für das Umweltmonitoring von Nanomaterialien zusammenfassen und bewerten soll.

Die Publikation stellt sich insbesondere die Frage, ob die CPE zukünftig ein Routinewerkzeug zur Extraktion von Nanomaterialien aus Umweltproben darstellen und gleichzeitig dazu dienen kann, die Nanomaterialien in dem Zustand, in dem sie in den Umweltproben vorliegen, zu konservieren.

Es wird eine Übersicht über CPE-Ansätze für unterschiedliche metallische Nanopartikel sowie Kopplungsmöglichkeiten der CPE mit verschiedenen analytischen Techniken gegeben. Die Darstellung der Präparationsschritte während der CPE wird zudem mit einer Modellierung der Vorgänge während der CPE kombiniert.

Eigener Beitrag:
- *Verfassen des Kapitels „Applications and uncertainties in enrichment and sample preservation"*

5.3 PUBLIKATION 3: Separating Dissolved Silver from Nanoparticulate Silver is the Key: Improved Cloud-Point-Extraction Hyphenated to Single Particle ICP-MS for Comprehensive Analysis of Silver-Based Nanoparticles in Real Environmental Samples Down to Single-Digit nm Particle Sizes

in Analytica Chimica Acta

Da die Umwelttoxizität sowie Persistenz der Ag-b-NP deutlich von der Partikelgröße abhängen, ist es essenziell, neben der Konzentration von Ag-b-NP in Umweltproben auch deren Partikelgröße zu bestimmen.

Grundsätzlich existiert eine Vielzahl an Techniken zur Bestimmung der Partikelgröße, wie Elektronenmikroskopie oder Dynamische Lichtstreuung. Eine Analyse von Ag-b-NP in Umweltproben mit diesen Techniken ist jedoch aufgrund der geringen Analytkonzentration sowie der herausfordernden Matrix nicht möglich.

Die sp-ICP-MS, ein neuartiger Teilbereich der Plasma-Massenspektrometrie, ist im Gegensatz zu oben genannten Techniken in der Lage, neben der Konzentration die Größenverteilung partikulärer Analyten selbst bei geringen Konzentrationen im ng L^{-1} Bereich zu bestimmen. Werden nanopartikuläre Analyten, wie z.B. Ag-b-NP, im Plasma ionisiert, entsteht eine Ionenwolke, deren ionische Bestandteile den Detektor des Massenspektrometers nahezu zeitgleich erreichen. Bei zeitaufgelöster Detektion der Ioneneinschläge in den Detektor wird im Falle von nanopartikulären Analyten ein transientes Signal detektiert. Die Anzahl dieser Signale lässt Rückschlüsse auf die Partikelkonzentration zu, während die Höhe respektive Fläche dieser Signale von der Partikelmasse und damit inhärent dem Durchmesser abhängen. Sind in der Probe jedoch zusätzlich signifikante Anteile ionischer Analyten vorhanden, wird neben den transienten Signalen ein konstantes Untergrundsignal detektiert, das bei entsprechender Menge ionischer Analyten die transienten Signale, insbesondere der kleinen Analyt-Partikel, überdeckt und eine Analyse letzterer unmöglich macht. Der SDL-Wert steigt entsprechend an.

Gemäß dem aktuellen Stand der Technik wird der SDL-Wert von Ag-b-NP bei sp-ICP-MS-Analysen auf etwa 20 nm geschätzt.[165] Dieser Wert ist aufgrund der Tatsache, dass Ag-b-NP in Umweltproben selten über 20 nm messen,[84] unzureichend. Ziel der vorliegenden Studie war es deshalb, den SDL-Wert auf wenige nm zu senken, um eine Analyse von Ag-b-NP in Umweltmatrices möglich zu machen.

Um Ag-b-NP aus Umweltproben anzureichern und von störenden Matrixbestandteilen und insbesondere ionischen Ag-Spezies zu separieren, wurde zur Probenvorbereitung deshalb die CPE eingesetzt. Da der bisherige Extraktionsansatz [24] eine zu hohe Koextraktion ionischer Ag-Spezies in den organischen Extrakt zulässt, wurde die CPE unter Verwendung einer neuen Ligandenzusammensetzung aus EDTA und D-Penicillamin verbessert (iCPE, improved CPE, *engl.* verbesserte CPE). Die iCPE wurde zunächst anhand von Ag-b-NP enthaltenden Modelllösungen entwickelt und anschließend auf Realproben übertragen. Es hat sich herausgestellt, dass die iCPE der CPE bzgl. der Speziesselektivität um Größenordnungen überlegen ist. Die iCPE war nämlich in der Lage, die Koextraktion ionischer Ag-Spezies so stark zu senken, dass bei einer anschließenden sp-ICP-MS-Analyse der SDL-Wert auf 4.5 nm reduziert werden konnte.

In der Studie wurde außerdem die Kopplung von iCPE und sp-ICP-MS intensiv untersucht und dabei insbesondere auf die Herausforderungen einer Zufuhr von viskosen, organischen iCPE-Extrakten in ein zerstäuberbasiertes Messsystem des Massenspektrometers abgestellt. In diesem Zusammenhang wurden die Zerstäubereffizienz sowie der Einfluss der dwell time auf die Richtigkeit der Partikelgrößenverteilung eingehend analysiert. Es hat sich als vorteilhaft herausgestellt, nicht die niedrigste dwell time zu wählen, die möglich ist, sondern eine dwell time im Bereich von 100 bis 500 µs zu wählen, um Verzerrungen der Partikelgrößenverteilungen vorzubeugen.

Abschließend wurde die neu entwickelte iCPE-sp-ICP-MS-Kopplung mit dem etablierten CPE-ET-AAS-System verglichen und der Einfluss unterschiedlicher Kalibriertechniken auf das Messergebnis untersucht. Die mittels iCPE-sp-ICP-MS gemessenen Konzentrationswerte stimmten mit denen der CPE-ET-AAS hervorragend überein. Darüber hinaus lässt sich mit der iCPE-sp-ICP-MS auch die Partikelgrößenverteilung ermitteln.

Der Ansatz der Kopplung von iCPE mit sp-ICP-MS stellt also eine vielversprechende Technik für die Bestimmung von Ag-b-NP in Umweltproben im Routinemaßstab dar.

Eigener Beitrag:
- *Entwicklung des Versuchskonzepts*
- *Entwicklung, Optimierung und Validierung der iCPE*
- *Entwicklung und Durchführung von Studien zur Kopplung von iCPE mit sp-ICP-MS*
- *Analyse und Bestimmung des SDL-Werts*
- *Auswertung, Visualisierung und Interpretation der Messergebnisse*
- *Schreiben der Publikation (ausgenommen Beiträge von A. Urstoeger, s. u.)*

Wesentliche Beiträge Dritter:
- *A. Urstoeger: Durchführung der Studien zur Kopplung von iCPE mit sp-ICP-MS sowie Analyse und Auswertung der entsprechenden Daten*
- *A. Urstoeger: Schreiben der Publikation (Kapitel 2.2.4 sowie Kapitel 3.8)*

5.4 PUBLIKATION 4: Looking at Silver-Based Nanoparticles in Environmental Water Samples: Repetitive Cloud Point Extraction Bridges Gaps in Electron Microscopy for Naturally Occurring Nanoparticles

in Environmental Science and Technology

Diese Publikation basiert auf einer Kollaboration des Arbeitskreises Analytische Chemie der TUM mit Dr. Ralf Kaegi der Eawag (Forschungsanstalt der ETH in Zürich). Diese Zusammenarbeit verfolgte das Ziel, Ag-b-NP in natürlichen Wasserproben so stark anzureichern, dass diese im TEM sichtbar gemacht werden können und mittels EDX die chemische Zusammensetzung der Partikel bestimmt werden kann.

Da die Umwelttoxizität von Ag-b-NP deutlich von deren Größe, Morphologie und chemischen Zusammensetzung abhängt, stellt eine TEM-EDX-Analyse von natürlichen Ag-b-NP das letzte und entscheidende Puzzleteil in der Analyse von Ag-b-NP in Realproben dar.

Bislang waren solche Proben der Elektronenmikroskopie aufgrund der extrem niedrigen Analytkonzentration sowie dem Überschuss an störenden Matrixbestandteile nicht zugänglich. Eine TEM-Analyse von Ag-b-NP bei Konzentrationen von wenigen ng L^{-1} in Wasserproben glich deshalb bislang einer „Suche nach der Nadel im Heuhaufen", die aufgrund des extrem hohen Arbeitsaufwands nicht zielführend war.

Die iCPE ist in diesem Zusammenhang in zweierlei Hinsicht von großem Vorteil: Einerseits werden Ag-b-NP stark angereichert und andererseits zusätzlich von störenden Matrixbestandteilen separiert. Um den Anreicherungsfaktor weiter zu erhöhen, wurde eine repetitive iCPE (rCPE) durchgeführt, also eine mehrmalige Extraktion ein und derselben Probe mit der gleichen Tensidphase.

Die im rCPE-Extrakt angereicherten und von der Probenmatrix separierten Ag-b-NP wurden im Anschluss unter Verwendung einer Zentrifugationstechnik nahezu vollständig auf einem TEM-Probenträger abgeschieden.

Tensidrückstände des Extrakts führen beim Trocknen des TEM-Probenträgers zu Filmbildung, die die Bildgebung deutlich stört und erschwert. Entscheidend für die Probenpräparation war deshalb die Entwicklung einer speziellen Waschprozedur der TEM-Probenträger. Ein sechsmaliges Waschen mit Ethanol hat sich als am vielversprechendsten zur Entfernung letzter Tensidreste von dem präparierten TEM-Grid herausgestellt.

Das Bildgebungsverfahren umfasste also

      (i)   Durchführung der rCPE mit Ag-b-NP enthaltenden wässrigen Proben;

      (ii)   Zentrifugation der im Extrakt angereicherten Ag-b-NP auf den TEM-Probenträger;

      (iii)   sechsmaliges Waschen der TEM-Probenträger mit EtOH; und

      (iv)   TEM-EDX-Analyse der so präparierten Proben.

Die Studie betrifft ferner Versuche zur Extraktion und TEM-EDX-Analyse von Ag-NP und Ag_2S-NP in Reinstwasser und Flusswasser. Selbst bei nur 5 ng L^{-1} anfänglicher Analytkonzentration konnten Ag-b-NP mittels des entwickelten Bildgebungsverfahrens zuverlässig im TEM nachgewiesen und mittels EDX charakterisiert werden.

Eigener Beitrag:
- *Organisation der Kollaboration der TEM mit der Eawag*
- *Mitentwicklung des Versuchskonzepts*
- *Optimierung der Zentrifugationstechnik und des Waschverfahrens für die TEM-Probenträger*
- *Verfassen von Teilen der Publikation (Optimierung der Zentrifugationstechnik und des Waschverfahrens, theoretische Überlegungen zur Partikelanzahl auf dem TEM-Probenträger)*

Wesentliche Beiträge Dritter:
- *R. Kaegi: Entwicklung der Zentrifugationstechnik und Durchführung und Auswertung der TEM Messungen*
- *A. Urstoeger: Entwurf und Ausarbeitung des Versuchskonzeptes; Synthese der Ag-b-NP; Entwicklung und Optimierung der rCPE; Realwasserprobenahme und Charakterisierung; Auswertung und Interpretation der Ergebnisse*
- *A. Urstoeger: Verfassen der Publikation (ausgenommen Beiträge von A. Wimmer, s. o.)*

5.5 PUBLIKATION 5: Sampling and pre-treatment effects on the quantification of (nano)silver and selected trace elements in surface water – Application in a Dutch case study

in Science of the Total Environment

Diese Publikation entstammt einer Zusammenarbeit des Arbeitskreises Analytische Chemie der TUM mit zwei Laboratorien in den Niederlanden, Stichting Waterproef in Edam und TNO in Utrecht. Dabei war das Ziel, die aus den Untersuchungen von Ag und Ag-b-NP in Oberflächenwasserproben der Isar gewonnen Erkenntnisse auch auf Proben aus den Niederlanden zu übertragen. Messungen von Ag und einer Vielzahl von (Erd)alkali- und Übergangsmetallen in den Wasserproben wurden vergleichend in allen partizipierenden Laboratorien durchgeführt. Die Probenahme erfolgte durch Stichting Waterproef, die die Proben den anderen Laboratorien zur Verfügung gestellt haben.

In der Studie wurde der Kanal *Goyersgracht* (gracht, *niederl.* Kanal), der sich etwa 40 km südöstlich von Amsterdam befindet, beprobt. Die erste Probe wurde nahe einer Einleitstelle eines Klärwerks, die zweite im weiteren Kanalverlauf und die dritte an einer Schleuse vor der Mündung des Kanals in einen See genommen. Ein möglicher Ag-b-NPs Eintrag über das Klärwerk und dessen Verdünnung im weiteren Kanalverlauf war dabei von besonderem Interesse. Noch am Ort der Probenahme wurde eine Teilprobe filtriert, eine weitere filtriert und angesäuert (HNO_3) und eine dritte nicht vorbehandelt. Letztgenannte Teilprobe war für die Ag-b-NP-Analyse vorgesehen, da Ag-b-NP in Säure gelöst und im Filter zurückgehalten werden können.

Die Messung in den drei Laboratorien erfolgte immer mittels ICP-MS. Anfordernisse an die weitere Probenvorbereitung vor der Messung wurden den einzelnen Laboratorien nicht gesetzt. So sollte ein realistisches Szenario abgebildet werden, in dem unterschiedliche Laboratorien mit gleichen Messverfahren aber unterschiedlich entwickelten Protokollen zur Probenvorbereitung arbeiten. Die partizipierenden Laboratorien sind unterschiedlichen etablierten Messprotokollen oder zertifizierten Messmethoden gefolgt, weshalb sich zusätzliche Unterschiede in der Probenvorbereitung ergaben, z. B. in Form von weiterem

Säurezusatz (HNO₃ oder *aqua regia*) oder Druckaufschluss der Proben. Die Ag-b-NP Bestimmung wurde nur an der TUM mittels iCPE-(sp)-ICP-MS durchgeführt.

Die gemessenen Konzentrationen von Ag und den weiteren Spurenelementen war über die Laboratoriumsgrenzen hinaus sehr vergleichbar. Erwartungsgemäß führte der Druckaufschluss der Proben zu den höchsten messbaren Ag-Konzentrationen, da mittels Aufschluss unter anderem partikuläres, kolloidales oder sedimentär gebundenes Ag mobilisiert und in der Probe homogenisiert wird, das sich ohne Aufschluss der Messung entzogen hat. Durch Filtration der Wasserproben mit Spritzenfiltern aus Polyethersulfon (Porengröße 0,45 µm) wurde die messbare Ag-Konzentration hingegen reduziert. Es liegt nahe, dass Ag, das z. B. an Partikel oder Schwebstoffe in den Wasserproben gebunden ist, im Spritzenfilter zurückgehalten wird.

In Übereinstimmung mit den Ergebnissen der Messung von Ag und Ag-b-NP im Verlauf der Isar,[166] nahm auch im Verlauf des *Goyersgracht* die Konzentration von Ag und Ag-b-NP nach einer Ladungsspitze nahe des Klärwerks bis hin zur Mündung in den See ab. Das Klärwerk trägt als anthropogene Quelle Ag-b-NP lokal in den Kanal ein, die im weiteren Verlauf dann verdünnt werden. Die Ag-b-NP wiesen die üblichen Größen im Bereich von 8-20 nm auf.

Interessanterweise konnte bei der Messung der weiteren Spurenelemente *(nicht an der TUM durchgeführt)* festgestellt werden, dass nur ein Teil der untersuchten Elemente, nämlich Cr, Cu, Fe, Pb und Zn, Schwankungen der messbaren Konzentration in Abhängigkeit von der Probenvorbereitung, wie z. B. der Filtration, zeigten. Dies legt nahe, dass insbesondere diese Elemente in den Wasserproben partikulär oder an Sediment gebunden vorlagen und die restlichen untersuchten Elemente (vorwiegend (Erd)alkalielemente) viel stärker homogenisiert/dispergiert waren. Dies bedarf natürlich weitergehender Untersuchungen, die im Rahmen der Studie noch nicht durchgeführt werden konnten. Ein Screening mittels sp-ICP-MS auf partikuläre Analyten ist aufgrund des hohen Aufwands der Erstellung eines verlässlichen Messprogramms für jedes einzelne Element nicht schnell realisierbar.

Eigener Beitrag:

- *Messung von Ag mittels ICP-MS sowie Ag-b-NP mittels iCPE-sp-ICP-MS in den Wasserproben inkl. Bestimmung weiterer relevanter Parameter wie dem TOC-Gehalt*
- *Auswertung, grafische Darstellung und Interpretation aller Messergebnisse*
- *Verfassen von Teilen der Publikation*

Wesentliche Beiträge Dritter

- *R. Ritsema: Probenahme*
- *P. Krystek und R. Ritsema: elementanalytische Untersuchungen der Wasserproben; Auswertung und Interpretation aller Messergebnisse; Verfassen von Teilen der Publikation*

5.6 PUBLIKATION 6: Silver Nanoparticle Levels in River Water: Real Environmental Measurements and Modeling Approaches – A comparative Study

in Environmental Science & Technology Letters

Diese Publikation entstammt einer Zusammenarbeit des Arbeitskreises Analytische Chemie der TUM mit Deltares, einem Forschungsinstitut aus Delft, den Niederlanden, das sich unter anderem mit Nanopartikeln in Gewässern beschäftigt.

Ziel dieser Studie war es, reale Messungen von Ag-b-NP und Gesamt-Ag in Wasserproben der Isar mit Modellrechnungen zum Eintrag und Verbleib von Ag-b-NP in die Isar zu vergleichen. Die Isar wurde an denselben Stellen wie in Publikation 1 von der Quelle bis zur Mündung beprobt, wobei das Augenmerk wieder besonders auf den Einleitstellen der Klärwerke in die Isar lag.

Die Messung von Gesamt-Ag erfolgte durch ICP-MS aus den unfiltrierten und lediglich angesäuerten Wasserproben. Da sich zum Zeitpunkt der Probenahme die Entwicklung der iCPE-sp-ICP noch in einem frühen Stadium befand, wurde die Ag-b-NP Konzentration aus den unbehandelten Wasserproben nach Extraktion der Ag-b-NP mittels iCPE-ET-AAS bestimmt.

Analog zu den Erkenntnissen aus Publikationen 1 und 5 konnte auch in dieser Studie festgestellt werden, dass die Klärwerke zu Ag-b-NP Beladungsspitzen in der Isar führen, wobei diese lokalen Konzentrationen schnell verdünnt werden. Dennoch war ein langsam ansteigendes Niveau von Ag-b-NP in der Isar bis hin zur Mündung in die Donau zu verzeichnen. Die Konzentrationen lagen im Mittel zwischen 1 und 2 ng L^{-1} Ag-b-NP.

Das verwendete Modell ist ein eindimensionales Modell, bei dem die Klärwerke als Punktquellen in das Flusssystem angesehen werden. Auf der Basis der Kapazitätsdaten der einleitenden Klärwerke, dem durchschnittlichen Wasserverbrauch pro Kopf sowie einer auf Marktanalyse beruhenden Schätzung über den pro-Kopf-Eintrag von Nanosilber in Fließgewässer, die die Verwendung von Ag-b-NP enthaltenen Produkten berücksichtigt,[167] konnte der Eintrag von Ag-b-NP in die Isar an jedem Klärwerk bestimmt werden. Im weiteren

Verlauf der Isar unterscheidet das Modell insbesondere - unter Berücksichtigung der Fließgeschwindigkeit sowie des Gehalts an Schwebstoffen - zwischen an Sediment adsorbierte Ag-b-NP und nicht-adsorbierte.

Aufgrund des hohen Gehalts an Schwebstoffen erfolgte die Adsorption gemäß dem Modell sehr schnell. Eine Sedimentation von Ag-b-NP selbst war aufgrund der hohen Fließgeschwindigkeit aber sehr unwahrscheinlich und wurde deshalb im Modell ignoriert.

Durch den Vergleich der bei den Klärwerken gemessenen Beladungsspitzen und dem hochgerechneten Eintrag von Ag-b-NP an diesen Stellen gemäß dem Modell konnte der Rückhalt von Ag-b-NP im Klärschlamm zu etwa 97 % bestimmt werden.

Insgesamt zeigte sich eine gute Übereinstimmung zwischen den gemessenen Gesamt-Ag und Ag-b-NP Konzentrationen im Verlauf der Isar mit den Modellrechnungen. Der graduelle Anstieg der Ag-b-NP Konzentration konnte im Modell sehr gut reproduziert werden. Einzig die lokalen Beladungsspitzen in der Isar nahe den Klärwerks-Einleitungen konnte das Modell nicht erfassen.

Eigener Beitrag:
- *Entwicklung des Versuchskonzepts*
- *Planung und Durchführung der Probenahme*
- *Durchführung und Auswertung aller analytischen Messungen der Wasserproben*
- *Zusammenstellung der hydrogeologischen Parameter der Isar*
- *Auswertung, grafische Darstellung und Interpretation aller Messergebnisse und Ergebnisse der Modellrechnung*
- *Verfassen der Publikation (ausgenommen den Beträgen von A. Markus, s.u.)*

Wesentliche Beiträge Dritter:
- *A. Markus: Berechnungen und Auswertungen im Rahmen des Modells*
- *A. Markus: Verfassen von Teilen Publikation („Modeling Method", „Waste Loads from WWTPs", Beschreibung der Ergebnisse des Modells in „Concentration of Ag-b-NPs and Total Ag along River Isar: Measurement and Model", „Transverse mixing downstream of the WWTPs" (SI), „Detailed Information on the modeling approach" (SI))*

5.7 PUBLIKATION 7: Copper Drinking Water Pipes as a Previously Undocumented Source of Silver-Based Nanoparticles

in Environmental Science & Technology

Diese Publikation betrifft eine Studie zur Freisetzung von Ag-b-NP aus Ag-Spuren im Rohrmaterial von Kupferwasserleitungen.

Trinkwasserleitungen mehrerer Gebäude unterschiedlichen Baujahrs, die jedoch alle Trinkwasserleitungen aus Kupfer verbaut haben, wurden beprobt. Dazu wurde der entsprechende Wasserhahn zunächst für einige Tage geschlossen gehalten. Die Probenahme des Trinkwassers erfolgte je Wasserhahn in mehreren aufeinanderfolgenden Proben geringen Volumens.

In den Trinkwasserproben wurde Gesamt-Ag mittels ICP-MS sowie die Konzentration an Ag-b-NP mit Hilfe von iCPE-ET-AAS und iCPE-sp-ICP-MS bestimmt. Die Ag-Messungen wurden durch ICP-MS-Bestimmung der Konzentration einer Vielzahl von Übergangsmetallen im Trinkwasser ergänzt.

In einem Teil der untersuchten Bauwerke konnten im Trinkwasser geringe Ag-Spuren detektiert werden, wobei 30 % des gesamten Silbers in Form von Ag-b-NP vorlagen. Im Durchschnitt waren 83 ng Gesamt-Ag und 25 ng Ag-b-NP pro Liter Trinkwasser nachweisbar. Die Partikel wiesen eine Partikelgröße von etwa 10 bis 36 nm auf. Ag-b-NP waren ausschließlich in den ersten Probenvolumina je Wasserhahn zu finden, was nahelegt, dass sich Ag-b-NP im Trinkwasser anreichern, wenn dieses mehrere Tage in der Wasserleitung steht. Sobald das vormals stehende Wasser abgelaufen war, war kein Ag mehr nachweisbar. Erst nachdem der Wasserhahn für mehrere Tage nicht mehr geöffnet wurde, waren wieder Ag-b-NP im Trinkwasser vorhanden.

Die Studie wollte zudem klären, woher Ag-b-NP im Trinkwasser stammen. Um etwaige Ag-Spuren im Rohrleitungsmaterial nachzuweisen, wurde ein Stück des Trinkwasserrohrs in HNO_3 aufgeschlossen. Nach ET-AAS Messung der so erhaltenen Lösung, die vorwiegend aus Cu bestand, konnten Ag-Spuren im Rohrleitungsmaterial zu 0,0027 Gew.-% Ag bezogen auf

die Masse des Trinkwasserrohrs quantifiziert werden. Es ist sehr wahrscheinlich, dass diese Ag-Spuren für einen Eintrag von Ag-b-NP in das Trinkwasser verantwortlich sind.

Dies gilt insbesondere, da die gemessene Cu-Konzentration im Trinkwasserlauf nahezu perfekt mit der Konzentration von Ag-b-NP und Gesamt-Ag korrelierte. Eine Korrelation mit Elementen, die typischerweise aus den Sanitärarmaturen stammen, wie z.B. Zn, Ni und Fe, war im Gegensatz dazu nicht zu beobachten.

Somit liegt die Vermutung nahe, dass Ag zusammen mit Cu aus dem Rohrleitungsmaterial in nanopartikulärer Form freigesetzt wird und nicht aus verbauten Armaturen oder Rohrverbindungsstücken, die nicht aus Kupfer bestehen, stammt.

Die vorliegende Studie konnte eine bisher unbeachtete Quelle von Ag-b-NP im Trinkwasser, das zum Großteil die Klärwerke und damit Fließgewässer erreicht, identifizieren und dessen Wirkung abschätzen.

Basierend auf den Messergebnissen der Studie konnte abschließend eine grobe Schätzung über den Eintrag von Ag-b-NP in die Natur über das Trinkwasser gemacht werden. Basierend auf der Einwohnerzahl Deutschlands, dem Anteil von Cu in Trinkwassersystemen und dem durchschnittlichen Wasserverbrauch pro Kopf ergab sich eine Freisetzung von 3 kg Ag, die pro Jahr über Trinkwasser in Deutschland in die Umwelt freigesetzt werden. Unter Berücksichtigung des gemessenen Anteils von Ag-b-NP am Gesamt-Ag im Trinkwasser ergibt sich somit eine jährliche Pro-Kopf-Freisetzung von 37 µg Ag-b-NP.

Eigener Beitrag:
- *Entwicklung des Versuchskonzepts*
- *Planung und Durchführung der Probenahme und aller analytischen Messungen*
- *Auswertung, grafische Darstellung und Interpretation aller Messergebnisse*
- *Verfassen der Publikation*

5.8 PUBLIKATION 8: What happens to silver-based nanoparticles if they meet seawater?

in Water Research

Bisher wurde der Weg der Ag-b-NP aus dem Abwasser über die Klärwerke in natürliche Fließgewässer und Seen untersucht. Konsequenterweise stellt sich nun die Frage, welches Schicksal Ag-b-NP erleiden, wenn sie in Fließgewässern bis hin zum Meer transportiert werden.

Es ist bisher bekannt, dass Ag-b-NP im Meerwasser zwei gegenläufigen Prozessen unterliegen: Aggregation und Auflösen. Aufgrund der hohen Ionenstärke im Meerwasser aggregieren Ag-b-NP dort verstärkt und werden kaum weitertransportiert.[168, 169] Demgegenüber steht eine Beobachtung von Liu et al., dass sich Ag-b-NP in einem kooperativen Oxidationsprozess in Gegenwart von gelöstem Sauerstoff unter Bildung löslicher Ag(I)-Spezies auflösen.[170] In Gegenwart hoher Konzentrationen an Chlorid im Meerwasser liegt es ferner nahe, dass sich wasserlösliche Silber-Chloro-Komplexe $AgCl_x^{1-x}$ (x > 1) aus den Ag(I)-Spezies bilden.

Die in der Literatur verfügbaren Studien betreffen jedoch lediglich hohe Mengen an Ag-b-NP im µg bis mg L^{-1} Bereich [171-173] und sind damit Größenordnungen von realitätsnahen Betrachtungen von ng L^{-1} Spuren von Ag-b-NP [174] entfernt. Der Mangel an solchen realitätsnahen Studien rührt daher, dass eine Analytik von Ag-b-NP im ng L^{-1} Bereich bisher aufgrund dieser niedrigen Konzentration in Verbindung mit einem extremen Chloridüberschuss in der Matrix nicht möglich war. Da die Proben verdünnt werden müssen, um die Chloridkonzentration auf ein für die instrumentellen analytischen Methoden praktikables Niveau zu senken, sinkt die Nachweisgrenze für Nanosilber weiter rapide.

Die iCPE bietet hier einen einzigartigen Lösungsansatz: Ag-b-NP können von gelösten Silberanteilen und von der Chloridmatrix abgetrennt und gleichzeitig angereichert werden und damit problemlos mittels (sp)-ICP-MS größenaufgelöst quantifiziert werden. Die Versuche wurden außerdem durch elektronenmikroskopische Untersuchungen ergänzt, um auch aufzuklären, ob sich die Zusammensetzung der Partikel im Meerwasser ändert.

In der vorliegenden Studie wurden 50 ng L^{-1} Ag-b-NP unterschiedlicher Beschichtung (Citrat, Sulfat, Chlorid) und Größe in künstlichen Meerwasser-Matrices steigender Salinität sowie in realem Meerwasser bei unterschiedlichen Temperaturen und bis zu drei Tage inkubiert. Alle eingesetzten Ag-b-NP Varianten haben sich nahezu unabhängig von der Beschichtung aufgelöst. Die Löslichkeit stieg dabei mit steigender Salinität und abnehmender Partikelgröße. Nach drei Tagen Inkubation waren alle Ag-b-NP Varianten nahezu vollständig aufgelöst. Die höchsten Auflösungsraten konnten bei Ag-b-NP in echtem Meerwasser beobachtet werden. sp-ICP-MS Messungen konnten die Abnahme der durchschnittlichen Partikelgröße der Ag-b-NP während des Auflösens im Meerwasser verfolgen. TEM/EDX-Messungen haben außerdem gezeigt, dass sich insbesondere bei Ag_2S-NP eine schwefelreiche Schicht um die sich auflösenden Partikel bildet. Silber wird also gewissermaßen aus dem Ag_2S-Verbund herausgelöst.

Das oben beschriebene Auflösen von Ag-b-NP in hochsalinen Matrices konnte auch bei real existierenden Ag-b-NP in Klärwerksabfluss festgestellt werden. Zur Imitierung eines Freisetzungsszenarios von Klärwerksabfluss in Meerwasser wurde dabei eine Probe des Klärwerksabflusses mit der Menge an Natriumchlorid versetzt, die der von Meerwasser entspricht.

Insgesamt scheinen Ag-b-NP in Meerwasser bei Langzeitbetrachtung somit nicht existent zu sein. Dies ist für eine zukünftige Risikobewertung von Ag-b-NP in natürlichen Gewässern unbedingt zu berücksichtigen.

Eigener Beitrag:
- *Entwicklung des Versuchskonzepts*
- *Durchführung aller Inkubationsmessungen*
- *Auswertung, grafische Darstellung und Interpretation aller Messergebnisse*
- *Verfassen der Publikation (ausgenommen Beiträge von A. Urstoeger, s. u.)*

Wesentliche Beiträger Dritter:
- *A. Urstoeger: Synthese und Charakterisierung der eingesetzten Ag-b-NP sowie Auswertung der elektronenmikroskopischen Aufnahmen*
- *A. Urstoeger: Verfassen von Teilen der Publikation (Einleitung Absätze 1-3, 6-9; Kapitel 2.2. Absatz 3, Kapitel 3.1., Kapitel 3.2. letzter Absatz)*
- *M. Doeblinger: Durchführung der elektronenmikroskopischen Untersuchungen*

5.9 PUBLIKATION 9: New Insights into the formation of silver-based nanoparticles under natural and semi-natural conditions

in Water Research

Erste Messung von Seewasser verschiedener Oberbayerischer Voralpenseen, die nur teilweise von Klärwerken über ihre Zuflüsse belastet waren, haben gezeigt, dass Spuren von Ag-b-NP (ca. 0.5 ng L^{-1}) in allen Seen zu finden waren, unabhängig von einer etwaigen Klärwerksbelastung [175].

Daher lag die Vermutung nahe, dass ein geogener Untergrund an Ag-b-NP in natürlichen Gewässern existieren könnte. Dazu wurde zum einen der Königssee beprobt, ein Beispiel eines oligotrophen Sees (1.5 mg L^{-1} TOC) ohne Klärwerkseinflüsse, und zum anderen der Waginger See, der trotz Ringkanalisation und keinen Zuflüssen, die Klärwerksabläufe empfangen, vergleichsweise eutroph ist (5 mg L^{-1} TOC). Die Wasserproben wurden je Probenahmestelle tiefengestaffelt genommen. Der Waginger See wurde bis zum Grund bei etwa 23 m Wassertiefe beprobt. Da die Maximaltiefe des Königssee von etwa 190 m [176] mit den verfügbaren Probenahmegeräten bei weitem nicht erreicht werden konnte, erfolgte hier die Probenahme bis 10 m Tiefe.

Gesamtsilber im Seewasser wurde mittels ICP-MS bestimmt. Die Ag-b-NP Analyse erfolgte mittels iCPE-ET-AAS und iCPE-(sp)-ICP-MS.

In beiden Seen konnte eine vergleichbare Menge Gesamtsilber gemessen werden (ca. 1 – 5 ng L^{-1}), wobei im Oberflächenwasser beider Seen die höchsten Konzentrationen gemessen wurden, gefolgt von einer Abnahme mit zunehmender Tiefe. Ag-b-NP waren nur im Waginger See detektierbar. Das Silber im Oberflächenwasser des Waginger See bestand zu 40 % aus partikulärem Silber. Insgesamt scheinen lichtempfindliche Mikroorganismen gelöste Silberspuren zu akkumulieren und an die Oberfläche zu transportieren, während die Ag-b-NP von diesem Transportmechanismus nicht beeinflusst werden.

Interessanterweise stieg die Ag-Konzentration im Waginger See nahe des Grundes wieder. Dies kann daher rühren, dass Ag-Spuren aus dem Sediment freigesetzt werden können. Da

Sedimente im Rahmen dieser Studie noch nicht untersucht werden konnten, wurden ergänzende Untersuchungen durchgeführt (siehe nachfolgende Messungen),

Da der Waginger See den TOC-Gehalt des Königssees um den Faktor 5 überstieg, lag die Vermutung nahe, dass sich Ag-b-NP aus gelöstem Ag über eine NOM-induzierte Reduktion bilden könnten.

Dass ein Zusammenhang zwischen der Bildung von Ag-b-NP aus gelösten Silberspezies und dem Gehalt an TOC (als quantitatives Maß für NOM) besteht, konnte in Laborexperimenten nachgewiesen werden. Dazu wurden 50 ng L^{-1} gelöstes Silber mit naturnahen NOM Konzentrationen bis zu 5 mg L^{-1} TOC versetzt und die Bildung von Ag-b-NP unter verschiedenen Reaktionsbedingungen mittels iCPE-sp-ICP-MS studiert. Diese Versuche haben gezeigt, dass – entgegen der vorherrschenden Literaturmeinung – Ag-b-NP sogar bevorzugt im Dunkeln gebildet werden. Mit zunehmender Reaktionszeit steigt die Partikelgröße der neugebildeten Ag-b-NP, was deutlich macht, dass selbst bei so geringen Konzentrationen noch eine Ostwaldreifung stattfinden kann. Im Beisein umweltrelevanter Mengen an Sulfid bildeten sich mehr Ag-b-NP, die zusätzlich eine engere Partikelgrößenverteilung aufwiesen.

Insgesamt konnte also gezeigt werden, dass Ag-b-NP in der Umwelt nicht nur anthropogener Natur sind, sondern auch natürlich aus dem Zusammenspiel geogener Silberspuren und NOM gebildet werden können. Diese Tatsache ist bei zukünftiger Risikobewertung von Ag-b-NP in Umweltproben zu berücksichtigen.

Eigener Beitrag:
- *Entwicklung des Versuchskonzepts (zusammen mit A. Kalinnik in Bezug auf die Ag-b-NP-Bildung unter Laborbedingungen)*
- *Planung und Durchführung der Probenahme*
- *Durchführung aller analytischen Messungen der Wasserproben*
- *Durchführung aller Versuche zur Bildung von Ag-b-NP unter Laborbedingungen*
- *Interpretation und grafische Darstellung der Messergebnisse*
- *Verfassen der Publikation*

Ergänzende Untersuchungen zu Publikation 9:

Diese Studie wurde um Untersuchungen zu Ag-b-NP in Seesedimenten ergänzt. Die Untersuchungen selbst sind nicht in der Publikation veröffentlicht und deshalb nachfolgend zusammengefasst:

Wie oben dargestellt haben Messungen des Waginger Sees gezeigt, dass die Konzentration an Silber an der Oberfläche am höchsten war und mit zunehmender Wassertiefe absank bis wieder ein sprunghafter Anstieg kurz vor Erreichen des Seegrundes zu verzeichnen war. Silber scheint sich demnach in den Sedimenten anzureichern, weshalb in einer weiteren Messkampagne zwei Stellen des Waginger Sees (A: 47°56'26.0"N 12°46'34.6"E, maximale Tiefe 24 m; B: 47°56'31.4"N 12°45'51.7"E, maximale Tiefe 26 m, siehe **Abbildung 20**) weiter untersucht wurden.

Abbildung 20: Probenahmestellen zur Sedimentbeprobung am Waginger See. Maximale Tiefe 24 m (A) bzw. 26 m (B). 1/2 entspricht dabei den einzelnen Teilproben je Sedimentkern. (Bildquelle: Google Maps, Waginger See, aufgerufen am 20.08.2020)

An diesen Stellen wurde je ein Sedimentkern entnommen, wobei an Stelle A eine Beprobung bis 24 cm Sedimenttiefe und an Stelle B bis 20 cm Sedimenttiefe möglich war. Der Sedimentkern wurde in je zwei Segmente (A1: 0-20 cm Sedimenttiefe, A2: 20- 24 cm Sedimenttiefe, B1: 0-16 cm Sedimenttiefe, B2: 16-20 cm Sedimenttiefe) aufgeteilt. Die einzelnen Teilproben wurden daraufhin homogenisiert. Über eine Trocknungswaage konnte der Trockenanteil in jeder Sedimentprobe bestimmt werden (Tabelle 2). Der Trockenanteil betrug dabei 28 % bis 59 %. Die Elution der Ag-b-NP aus dem Sediment kann nur aus nicht getrocknetem Sediment erfolgen, da ansonsten die Gefahr besteht, dass sich die Partikel beim Trocknungsprozess verändern. Deshalb ist es notwendig, die Ergebnisse erst im Anschluss an die Messung auf die Trockenmasse zu beziehen.

Da für die Bestimmung des Gesamtsilbergehalts der Sedimente ein Aufschluss in Salz- und Salpetersäure mit anschließender ICP-MS aufgrund zu hoher Nachweisgrenzen nicht zielführend war, wurde das trockene Sediment ohne Aufschluss mit einer definierten Menge Reinstwasser aufgeschlämmt und mit einer Standardadditionsmethode zur Matrixkorrektur mittels ET-AAS gemessen. Die ET-AAS war die Methode der Wahl, da nur sie eine so komplexe Matrix (Sedimentdispersion) toleriert.

Die Ergebnisse sind Tabelle 2 zu entnehmen. Beide Sedimentkerne enthielten Spuren an Silber, wobei im Fall A die Menge von 81,0 auf 214,6 µg Silber pro kg trockenem Sediment mit der Sedimenttiefe zunahm. Im Fall B fiel die Menge von 124,6 auf 108,1 µg Silber pro kg trockenem Sediment ab.

Für die Elution des partikulären Silbers aus dem Sediment wurden ca. 5 g feuchtes Sediment mit 50 mL Reinstwasser unter Schütteln eluiert, wobei jeweils 10 g Quarzsand zugesetzt wurden, um die Elution mechanisch zu unterstützen. Zur Messung des gesamten, eluierbaren Silbers wurde je Probe ein Teileluat mit Säure stabilisiert und mittels ICP-MS gemessen. Daneben wurde die Konzentration und die Partikelgrößenverteilung der eluierbaren Ag-b-NP mit Hilfe von iCPE-(sp)-ICP-MS untersucht.

Silber war aus allen Sedimentproben eluierbar, nämlich 181,9 (A1), 44,3 (A2), 89,0 (B1) und 37,9 (B2) ng Gesamtsilber pro kg trockenem Sediment (Tabelle 2). Die Menge an eluierbarem Silber lag damit eine Größenordnung unter dem Gesamtsilber im Sediment und nahm mit

zunehmender Sedimenttiefe ab. Da der Gesamtgehalt an Silber aber teilweise mit zunehmender Tiefe sogar zunahm, scheint Silber in den oberen Sedimentschichten leichter mobilisierbar zu sein – unabhängig vom Gesamtgehalt. Die eluierbaren Ag-b-NP, also der Anteil partikulären Silbers am gesamten eluierten Silber, folgen diesem Trend. Damit waren 30 bis 92 % des eluierbaren Silbers partikulär (siehe Tabelle 2). Für A2 waren mehr Ag-b-NP im Eluat als Gesamtsilber zu messen (196 %), was nur auf Messungenauigkeiten beruhen kann. Trotzdem zeigen die Versuche deutlich, dass Silber in den Sedimenten angereichert wird und daraus an umgebendes Wasser, teilweise sogar in partikulärer Form, abgegeben werden kann.

Tabelle 2: Zusammenstellung der Ergebnisse der Untersuchungen der Sedimentproben des Waginger Sees. Die gemessenen Mengen an Gesamtsilber und Ag-b-NP beziehen sich immer auf ein kg trockenes Sediment.

Sedimentprobe	Trockenanteil [%]	Gesamtsilber [µg/kg]	eluierbares Silber insgesamt [ng/kg]	eluierbare Ag-b-NP [ng/kg]	Anteil Ag-b-NP [%]
A1	28	81,0 ± 15,0	181,9 ± 46,6	167,1 ± 17,8	92
A2	59	214,6 ± 17,9	44,3 ± 6,1	86,7 ± 7,9	196
B1	46	124,6 ± 27,6	89,0 ± 32,7	38,3 ± 14,3	43
B2	37	108,1 ± 16,6	37,9 ± 1,8	11,3 ± 10,0	30

Die sp-ICP-MS Messungen führten außerdem zu vergleichbaren Partikelgrößenverteilungen für Ag-b-NP in allen Teilproben des Sediments bzw. den Eluaten. Die Partikelgrößen waren im Bereich von 8 bis 20 nm allesamt sehr eng verteilt (siehe **Abbildung 21**). Dies stimmt gut überein mit den Partikelgrößen der Ag-b-NP, die im Seewasser, den Flüssen und den Klärwerksströmen gefunden wurden. **Abbildung 21** zeigt beispielhaft die Partikelgrößenverteilung der Ag-b-NP des Eluats von A1.
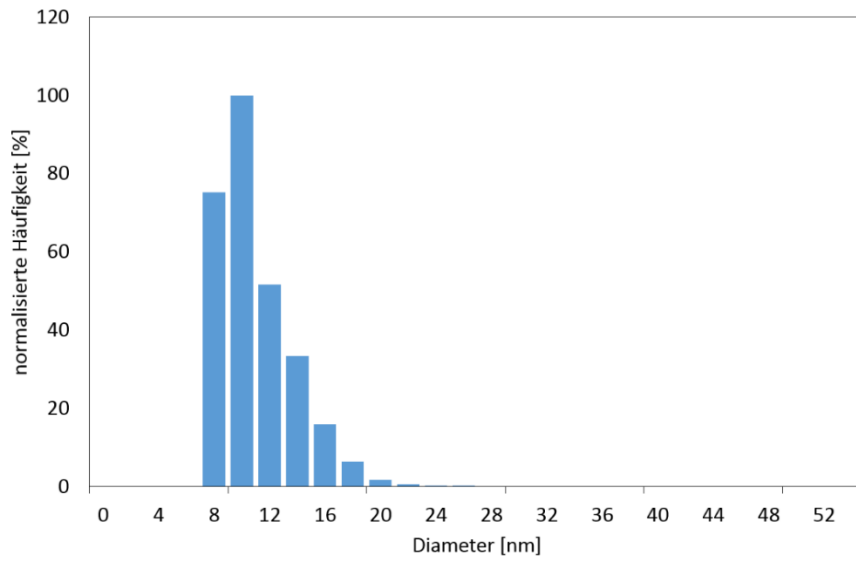
Abbildung 21: Partikelgrößenverteilung der Ag-b-NP in Eluat von Sedimentteilprobe A1.

6   Schlussfolgerungen und Ausblick

Um den Eintrag und das Schicksal von Ag-b-NP in der aquatischen Umwelt umfassend aufklären zu können, sind nachweisstarke Analyseverfahren unabdingbar. Nachdem Umweltpersistenz und -toxizität maßgeblich von der Partikelgröße der Ag-b-NP beeinflusst werden, sollten solche Analyseverfahren außerdem in der Lage sein, neben Konzentrationen im ng L^{-1} Bereich auch die Größenverteilungen der Ag-b-NP zu bestimmen.

Ein vielversprechender Ansatz hierfür ist die Einzelpartikel-Massenspektrometrie, die die Quantifizierung von ng L^{-1} Spuren nanopartikulärer Analyten bei gleichzeitiger Bestimmung der Partikelgrößenverteilungen erlaubt. Allerdings ist die minimal bestimmbare Partikelgröße durch koexistierende gelöste Analytspezies limitiert, die während der Messung ein störendes Signalrauschen erzeugen. Es ist deshalb essentiell, vor der eigentlichen Messung die nanopartikulären von den gelösten Analytspezies zu separieren.

Die Limitierungen der Einzelpartikel-Massenspektrometrie konnten durch die im Rahmen dieser Arbeit entwickelte Extraktionsmethode iCPE überwunden werden. Dieses Verfahren erlaubt eine selektive Extraktion und Anreicherung von Ag-b-NP aus verschiedenen Umweltproben (z. B. Fluss-, See-, Meerwasser, Klärwerksströme sowie Seesedimente), wobei gelöste Silberspezies effizient abgetrennt werden konnten. Durch den den sp-ICP-MS Messungen vorgeschalteten Einsatz der iCPE konnte das durch gelöste Analytspezies hervorgerufene Signalrauschen auf ein Minimum reduziert werden. Hierdurch konnten geringe Spuren von Ag-b-NP mit Durchmessern bis in den einstelligen Nanometerbereich sicher quantifiziert werden. Ferner konnten Ag-b-NP mit Hilfe der Elektronenmikroskopie in den iCPE-Extrakten sichtbar gemacht werden und mittels Röntgenfluoreszenz auf ihre chemische Zusammensetzung untersucht werden, was Rückschlüsse auf die Zusammensetzung und Beschichtung der NP möglich macht.

Die iCPE hat außerdem die Vorteile, dass sie leicht erlernbar ist und sehr reproduzierbare Ergebnisse liefert. Diese Extraktion ist deshalb in Kombination mit der ET-AAS, (sp-)ICP-MS oder der Elektronenmikroskopie für den Routineeinsatz zur Gewässerüberwachung sehr gut geeignet.

Mit Hilfe des entwickelten Analyseverfahrens konnten mehrere Eintragsrouten von Ag-b-NPs in die Umwelt identifiziert werden.

So wurden Ag-b-NP Spuren im einstelligen ng L^{-1} Bereich in mehreren Flüssen detektiert, wobei die Herkunft der Partikel eindeutig auf Klärwerkseinleitungen in die Flüsse zurückzuführen war. Modellrechnungen zur Verteilung von Ag-b-NP in der Isar sowie reale Messungen führten dabei zu vergleichbaren Ergebnissen.

Es wurde ferner festgestellt, dass Trinkwasserleitungen aus Kupfer, die geringe Mengen Silber enthalten, eine nicht unwesentliche Eintragsquelle von Ag-b-NP in Trinkwasser und damit in die Umwelt darstellen können.

Ag-b-NP in der aquatischen Umwelt sind jedoch nicht ausschließlich anthropogener Natur: Mit Hilfe des entwickelten Analyseverfahrens konnte nachgewiesen werden, dass sich Ag-b-NP aus gelösten Ag-Spezies in Gegenwart organischer Verbindungen bilden können. Entgegen der vorherrschenden Literaturmeinung findet die Bildung der Ag-b-NP sogar bevorzugt im Dunkeln statt. Dieser natürliche Bildungsmechanismus erklärt die gemessenen, signifikanten Konzentrationen an Ag-b-NP in Seen, die kaum anthropogen belastet sind, also beispielsweise keine Zuflüsse mit Klärwerkseinleitungen aufweisen. Da die höchsten Konzentrationen an Ag-b-NP im Oberflächengewässer der Seen zu finden waren und die Konzentrationen mit zunehmender Tiefe abgenommen haben, liegt es nahe, dass Mikroorganismen wie Phytoplankton an der Verteilung der Ag-b-NP innerhalb der Seen maßgeblich beteiligt sind.

Ag-b-NP, die in die Umwelt eingetragen werden, enden in den meisten Fällen entweder im Sediment von Flüssen und Seen oder werden über die Flüsse ins Meer transportiert. Der Anteil von Ag-b-NP, der dann das Meer erreicht, wird dort innerhalb von wenigen Tagen nahezu vollständig aufgelöst. Eine Umwelttoxizität von Nanosilber in Meeren sollte deshalb kaum gegeben sein.

Insgesamt kann unter Berücksichtigung der tatsächlich gemessenen Konzentrationen von Ag-b-NP in natürlichen Gewässern von wenigen ng L^{-1} im Moment nicht davon ausgegangen werden, dass Ag-b-NP eine Gefahr für Mensch und Umwelt darstellen.[62]

Insbesondere die Tatsache, dass Silberspuren in Trinkwasserleitungen aus Kupfer zum Auftreten von Ag-b-NP in Trinkwasser führen können, lässt Berechnungen und Bilanzierungen der Eintragswege von Ag-b-NP in unsere Abwassersysteme jedoch in einem neuen Licht erscheinen und sollte unbedingt bei der zukünftigen Risikobewertung berücksichtigt werden. Insgesamt sollte der steigenden Verwendung von Ag-b-NP in verschiedenen Produkten des täglichen Lebens Rechnung getragen werden, indem die Konzentration von Ag-b-NP in der Umwelt in der Zukunft regelmäßig überwacht wird.

Die (Umwelt-)Toxizität von Ag-b-NP hängt ganz entscheidend davon ab, wie leicht diese NP reaktive, ionische Ag-Spezies freisetzen können. Oberflächenmodifikationen, wie die in der Natur häufig auftretende Sulfidierung zu Ag_2S, verringern das Ausmaß der Ionenfreisetzung und damit die Toxizität. Zukünfte Studien zu Ag-b-NP in der Umwelt sollten deshalb neben Konzentration und Partikelgröße auch die chemische Zusammensetzung der Partikel adressieren.

Dazu hat die vorliegende Arbeit eine analytische Grundlage geschaffen.

7 Abdruckgenehmigungen

7.1 Publikation 1

ACS Publications
Most Trusted. Most Cited. Most Read.

To What Extent Can Full-Scale Wastewater Treatment Plant Effluent Influence the Occurrence of Silver-Based Nanoparticles in Surface Waters?

Author: Lingxiangyu Li, Monika Stoiber, Andreas Wimmer, et al

Publication: Environmental Science & Technology

Publisher: American Chemical Society

Date: Jun 1, 2016

Copyright © 2016, American Chemical Society

Quick Price Estimate

This service provides permission for reuse only. If you do not have a copy of the portion you are using, you may copy and paste the content and reuse according to the terms of your agreement. Please be advised that obtaining the content you license is a separate transaction not involving RightsLink.

⚐ Permission for this particular request is granted for print and electronic formats, and translations, at no charge. Figures and tables may be modified. Appropriate credit should be given. Please print this page for your records and provide a copy to your publisher. Requests for up to 4 figures require only this record. Five or more figures will generate a printout of additional terms and conditions. Appropriate credit should read: "Reprinted with permission from {COMPLETE REFERENCE CITATION}. Copyright {YEAR} American Chemical Society." Insert appropriate information in place of the capitalized words.

I would like to... ⑦	reuse in a Thesis/Dissertation	Will you be translating? ⑦	No
Requestor Type ⑦	Author (original work)	Select your currency	EUR - €
Portion ⑦	Full article	Quick Price	Click Quick Price
Format ⑦	Print		

QUICK PRICE **CONTINUE**

To request permission for a type of use not listed, please contact the publisher directly.

ACS Publications
Most Trusted. Most Cited. Most Read.

To What Extent Can Full-Scale Wastewater Treatment Plant Effluent Influence the Occurrence of Silver-Based Nanoparticles in Surface Waters?

Author: Lingxiangyu Li, Monika Stoiber, Andreas Wimmer, et al

Publication: Environmental Science & Technology

Publisher: American Chemical Society

Date: Jun 1, 2016

Copyright © 2016, American Chemical Society

PERMISSION/LICENSE IS GRANTED FOR YOUR ORDER AT NO CHARGE

This type of permission/license, instead of the standard Terms & Conditions, is sent to you because no fee is being charged for your order. Please note the following:

- Permission is granted for your request in both print and electronic formats, and translations.
- If figures and/or tables were requested, they may be adapted or used in part.
- Please print this page for your records and send a copy of it to your publisher/graduate school.
- Appropriate credit for the requested material should be given as follows: "Reprinted (adapted) with permission from (COMPLETE REFERENCE CITATION). Copyright (YEAR) American Chemical Society." Insert appropriate information in place of the capitalized words.
- One-time permission is granted only for the use specified in your request. No additional uses are granted (such as derivative works or other editions). For any other uses, please submit a new request.

BACK **CLOSE WINDOW**

7.2 Publikation 2

Bei dieser Publikation handelt es sich um ein frei verfügbares „Open-Access"-Dokument. Wie nachfolgend ersichtlich, ist keine Berechtigung zur Verwendung dieses Artikel notwendig.

SPRINGER NATURE

Can cloud point-based enrichment, preservation, and detection methods help to bridge gaps in aquatic nanometrology?

Author: Lars Duester et al

Publication: Analytical and Bioanalytical Chemistry

Publisher: Springer Nature

Date: Aug 24, 2016

Copyright © 2016, The Author(s)

7.3   Publikation 3

Separating dissolved silver from nanoparticulate silver is the key: Improved cloud-point-extraction hyphenated to single particle ICP-MS for comprehensive analysis of silver-based nanoparticles in real environmental samples down to single-digit nm particle sizes

Author: Andreas Wimmer,Alexander Urstoeger,Tobias Hinke,Margit Aust,Philipp J. Altmann,Michael Schuster

Publication: Analytica Chimica Acta

Publisher: Elsevier

Date: 15 March 2021

© 2021 Elsevier B.V. All rights reserved.

Quick Price Estimate

This service provides permission for reuse only. If you do not have a copy of the content, you may be able to purchase a copy using RightsLink as an additional transaction. Simply select 'I would like to….. 'Purchase this content'.

Unclear about who you are?

I would like to... ⑦	reuse in a thesis/dissertation	I am the author of this Elsevier article... ⑦	Yes
I would like to use... ⑦	full article	I will be translating... ⑦	No
Circulation	11	My currency is...	EUR - €
My format is... ⑦	both print and electronic	Quick Price	Click Quick Price

QUICK PRICE   CONTINUE

To request permission for a type of use not listed, please contact Elsevier Global Rights Department.

Are you the author of this Elsevier journal article?

Separating dissolved silver from nanoparticulate silver is the key: Improved cloud-point-extraction hyphenated to single particle ICP-MS for comprehensive analysis of silver-based nanoparticles in real environmental samples down to single-digit nm particle sizes

Author: Andreas Wimmer,Alexander Urstoeger,Tobias Hinke,Margit Aust,Philipp J. Altmann,Michael Schuster

Publication: Analytica Chimica Acta

Publisher: Elsevier

Date: 15 March 2021

© 2021 Elsevier B.V. All rights reserved.

Journal Author Rights

Please note that, as the author of this Elsevier article, you retain the right to include it in a thesis or dissertation, provided it is not published commercially. Permission is not required, but please ensure that you reference the journal as the original source. For more information on this and on your other retained rights, please visit: https://www.elsevier.com/about/our-business/policies/copyright#Author-rights

BACK   CLOSE WINDOW

7.4   Publikation 4

Looking at Silver-Based Nanoparticles in Environmental Water Samples: Repetitive Cloud Point Extraction Bridges Gaps in Electron Microscopy for Naturally Occurring Nanoparticles

Author: Alexander Urstoeger, Andreas Wimmer, Ralf Kaegi, et al

Publication: Environmental Science & Technology

Publisher: American Chemical Society

Date: Oct 1, 2020

Copyright © 2020, American Chemical Society

Quick Price Estimate

This service provides permission for reuse only. If you do not have a copy of the portion you are using, you may copy and paste the content and reuse according to the terms of your agreement. Please be advised that obtaining the content you license is a separate transaction not involving RightsLink.

⚑ Permission for this particular request is granted for print and electronic formats, and translations, at no charge. Figures and tables may be modified. Appropriate credit should be given. Please print this page for your records and provide a copy to your publisher. Requests for up to 4 figures require only this record. Five or more figures will generate a printout of additional terms and conditions. Appropriate credit should read: "Reprinted with permission from {COMPLETE REFERENCE CITATION}. Copyright {YEAR} American Chemical Society." Insert appropriate information in place of the capitalized words.

I would like to... ⑦	reuse in a Thesis/Dissertation ⌄	Will you be translating? ⑦	No ⌄
Requestor Type ⑦	Author (original work) ⌄	Select your currency	EUR - € ⌄
Portion ⑦	Full article ⌄	Quick Price	Click Quick Price
Format ⑦	Print ⌄		

QUICK PRICE   **CONTINUE**

To request permission for a type of use not listed, please contact the publisher directly.

Looking at Silver-Based Nanoparticles in Environmental Water Samples: Repetitive Cloud Point Extraction Bridges Gaps in Electron Microscopy for Naturally Occurring Nanoparticles

Author: Alexander Urstoeger, Andreas Wimmer, Ralf Kaegi, et al

Publication: Environmental Science & Technology

Publisher: American Chemical Society

Date: Oct 1, 2020

Copyright © 2020, American Chemical Society

PERMISSION/LICENSE IS GRANTED FOR YOUR ORDER AT NO CHARGE

This type of permission/license, instead of the standard Terms & Conditions, is sent to you because no fee is being charged for your order. Please note the following:

- Permission is granted for your request in both print and electronic formats, and translations.
- If figures and/or tables were requested, they may be adapted or used in part.
- Please print this page for your records and send a copy of it to your publisher/graduate school.
- Appropriate credit for the requested material should be given as follows: "Reprinted (adapted) with permission from (COMPLETE REFERENCE CITATION). Copyright (YEAR) American Chemical Society." Insert appropriate information in place of the capitalized words.
- One-time permission is granted only for the use specified in your request. No additional uses are granted (such as derivative works or other editions). For any other uses, please submit a new request.

BACK   **CLOSE WINDOW**

7.5 Publikation 5

Sampling and pre-treatment effects on the quantification of (nano)silver and selected trace elements in surface water - Application in a Dutch case study

Author: Andreas Wimmer,Rob Ritsema,Michael Schuster,Petra Krystek

Publication: Science of The Total Environment

Publisher: Elsevier

Date: 1 May 2019

Quick Price Estimate

This service provides permission for reuse only. If you do not have a copy of the content, you may be able to purchase a copy using RightsLink as an additional transaction. Simply select 'I would like to..... 'Purchase this content'.

Unclear about who you are?

I would like to... ⑦	reuse in a thesis/dissertation	I am the author of this Elsevier article... ⑦	Yes
I would like to use... ⑦	full article	I will be translating... ⑦	No
Circulation	11	My currency is...	EUR - €
My format is... ⑦	both print and electronic	Quick Price	Click Quick Price

QUICK PRICE **CONTINUE**

To request permission for a type of use not listed, please contact Elsevier Global Rights Department.

Are you the author of this Elsevier journal article?

Sampling and pre-treatment effects on the quantification of (nano)silver and selected trace elements in surface water - Application in a Dutch case study

Author: Andreas Wimmer,Rob Ritsema,Michael Schuster,Petra Krystek

Publication: Science of The Total Environment

Publisher: Elsevier

Date: 1 May 2019

Journal Author Rights

BACK **CLOSE WINDOW**

7.6 Publikation 6

Silver Nanoparticle Levels in River Water: Real Environmental Measurements and Modeling Approaches—A Comparative Study

Author: Andreas Wimmer, Adriaan A. Markus, Michael Schuster
Publication: Environmental Science & Technology Letters
Publisher: American Chemical Society
Date: Jun 1, 2019

Copyright © 2019, American Chemical Society

Quick Price Estimate

This service provides permission for reuse only. If you do not have a copy of the portion you are using, you may copy and paste the content and reuse according to the terms of your agreement. Please be advised that obtaining the content you license is a separate transaction not involving RightsLink.

⚑ Permission for this particular request is granted for print and electronic formats, and translations, at no charge. Figures and tables may be modified. Appropriate credit should be given. Please print this page for your records and provide a copy to your publisher. Requests for up to 4 figures require only this record. Five or more figures will generate a printout of additional terms and conditions. Appropriate credit should read: "Reprinted with permission from {COMPLETE REFERENCE CITATION}. Copyright {YEAR} American Chemical Society." Insert appropriate information in place of the capitalized words.

I would like to... ⑦	reuse in a Thesis/Dissertation ⌄	Will you be translating? ⑦	No ⌄
Requestor Type ⑦	Author (original work) ⌄	Select your currency	EUR - € ⌄
Portion ⑦	Full article ⌄	Quick Price	Click Quick Price
Format ⑦	Print ⌄		

QUICK PRICE **CONTINUE**

To request permission for a type of use not listed, please contact the publisher directly.

Silver Nanoparticle Levels in River Water: Real Environmental Measurements and Modeling Approaches—A Comparative Study

Author: Andreas Wimmer, Adriaan A. Markus, Michael Schuster
Publication: Environmental Science & Technology Letters
Publisher: American Chemical Society
Date: Jun 1, 2019

Copyright © 2019, American Chemical Society

PERMISSION/LICENSE IS GRANTED FOR YOUR ORDER AT NO CHARGE

This type of permission/license, instead of the standard Terms & Conditions, is sent to you because no fee is being charged for your order. Please note the following:

- Permission is granted for your request in both print and electronic formats, and translations.
- If figures and/or tables were requested, they may be adapted or used in part.
- Please print this page for your records and send a copy of it to your publisher/graduate school.
- Appropriate credit for the requested material should be given as follows: "Reprinted (adapted) with permission from (COMPLETE REFERENCE CITATION). Copyright (YEAR) American Chemical Society." Insert appropriate information in place of the capitalized words.
- One-time permission is granted only for the use specified in your request. No additional uses are granted (such as derivative works or other editions). For any other uses, please submit a new request.

BACK **CLOSE WINDOW**

7.7 Publikation 7

Copper Drinking Water Pipes as a Previously Undocumented Source of Silver-Based Nanoparticles

Author: Andreas Wimmer, Jessica Beyerl, Michael Schuster
Publication: Environmental Science & Technology
Publisher: American Chemical Society
Date: Nov 1, 2019

Copyright © 2019, American Chemical Society

Quick Price Estimate

This service provides permission for reuse only. If you do not have a copy of the portion you are using, you may copy and paste the content and reuse according to the terms of your agreement. Please be advised that obtaining the content you license is a separate transaction not involving RightsLink.

⚑ Permission for this particular request is granted for print and electronic formats, and translations, at no charge. Figures and tables may be modified. Appropriate credit should be given. Please print this page for your records and provide a copy to your publisher. Requests for up to 4 figures require only this record. Five or more figures will generate a printout of additional terms and conditions. Appropriate credit should read: "Reprinted with permission from {COMPLETE REFERENCE CITATION}. Copyright {YEAR} American Chemical Society." Insert appropriate information in place of the capitalized words.

I would like to... ⑦	reuse in a Thesis/Dissertation ⌄	Will you be translating? ⑦	No ⌄
Requestor Type ⑦	Author (original work) ⌄	Select your currency	EUR - € ⌄
Portion ⑦	Full article ⌄	Quick Price	Click Quick Price
Format ⑦	Print ⌄		

QUICK PRICE   CONTINUE

To request permission for a type of use not listed, please contact the publisher directly.

Copper Drinking Water Pipes as a Previously Undocumented Source of Silver-Based Nanoparticles

Author: Andreas Wimmer, Jessica Beyerl, Michael Schuster
Publication: Environmental Science & Technology
Publisher: American Chemical Society
Date: Nov 1, 2019

Copyright © 2019, American Chemical Society

PERMISSION/LICENSE IS GRANTED FOR YOUR ORDER AT NO CHARGE

This type of permission/license, instead of the standard Terms & Conditions, is sent to you because no fee is being charged for your order. Please note the following:

- Permission is granted for your request in both print and electronic formats, and translations.
- If figures and/or tables were requested, they may be adapted or used in part.
- Please print this page for your records and send a copy of it to your publisher/graduate school.
- Appropriate credit for the requested material should be given as follows: "Reprinted (adapted) with permission from (COMPLETE REFERENCE CITATION). Copyright (YEAR) American Chemical Society." Insert appropriate information in place of the capitalized words.
- One-time permission is granted only for the use specified in your request. No additional uses are granted (such as derivative works or other editions). For any other uses, please submit a new request.

BACK   CLOSE WINDOW

7.8   Publikation 8

What happens to silver-based nanoparticles if they meet seawater?

Author: Andreas Wimmer,Alexander Urstoeger,Nils Christoph Funck,Franziska Petra Adler,Leonhard Lenz,Markus Doeblinger,Michael Schuster
Publication: Water Research
Publisher: Elsevier
Date: 15 March 2020

Quick Price Estimate

This service provides permission for reuse only. If you do not have a copy of the content, you may be able to purchase a copy using RightsLink as an additional transaction. Simply select 'I would like to..... 'Purchase this content'.

Unclear about who you are?

I would like to... ⑦	reuse in a thesis/dissertation	I am the author of this Elsevier article... ⑦	Yes
I would like to use... ⑦	full article	I will be translating... ⑦	No
Circulation	11	My currency is...	EUR - €
My format is... ⑦	both print and electronic	Quick Price	Click Quick Price

QUICK PRICE   **CONTINUE**

To request permission for a type of use not listed, please contact Elsevier Global Rights Department.

Are you the author of this Elsevier journal article?

What happens to silver-based nanoparticles if they meet seawater?

Author: Andreas Wimmer,Alexander Urstoeger,Nils Christoph Funck,Franziska Petra Adler,Leonhard Lenz,Markus Doeblinger,Michael Schuster
Publication: Water Research
Publisher: Elsevier
Date: 15 March 2020

Journal Author Rights

Please note that, as the author of this Elsevier article, you retain the right to include it in a thesis or dissertation, provided it is not published commercially. Permission is not required, but please ensure that you reference the journal as the original source. For more information on this and on your other retained rights, please visit: https://www.elsevier.com/about/our-business/policies/copyright#Author-rights

BACK   **CLOSE WINDOW**

7.9 Publikation 9

New insights into the formation of silver-based nanoparticles under natural and semi-natural conditions

Author: Andreas Wimmer,Anna Kalinnik,Michael Schuster
Publication: Water Research
Publisher: Elsevier
Date: 15 September 2018

Quick Price Estimate

This service provides permission for reuse only. If you do not have a copy of the content, you may be able to purchase a copy using RightsLink as an additional transaction. Simply select 'I would like to….. 'Purchase this content'.

Unclear about who you are?

I would like to... ⓘ	reuse in a thesis/dissertation	I am the author of this Elsevier article... ⓘ	Yes
I would like to use... ⓘ	full article	I will be translating... ⓘ	No
Circulation	11	My currency is...	EUR - €
My format is... ⓘ	both print and electronic	Quick Price	Click Quick Price

QUICK PRICE   CONTINUE

To request permission for a type of use not listed, please contact Elsevier Global Rights Department.

Are you the author of this Elsevier journal article?

New insights into the formation of silver-based nanoparticles under natural and semi-natural conditions

Author: Andreas Wimmer,Anna Kalinnik,Michael Schuster
Publication: Water Research
Publisher: Elsevier
Date: 15 September 2018

Journal Author Rights

Please note that, as the author of this Elsevier article, you retain the right to include it in a thesis or dissertation, provided it is not published commercially. Permission is not required, but please ensure that you reference the journal as the original source. For more information on this and on your other retained rights, please visit: https://www.elsevier.com/about/our-business/policies/copyright#Author-rights

BACK

CLOSE WINDOW

8 Bibliographische Angaben, Abdruck der Publikationen

8.1 PUBLIKATION 1

To What Extent Can Full-Scale Wastewater Treatment Plant Effluent Influence the Occurrence of Silver-Based Nanoparticles in Surface Waters?

Lingxiangyu Li, Monika Stoiber, Andreas Wimmer, Zhenlan Xu, Claus Lindenblatt, Brigitte Helmreich, and Michael Schuster

To What Extent Can Full-Scale Wastewater Treatment Plant Effluent Influence the Occurrence of Silver-Based Nanoparticles in Surface Waters?

Lingxiangyu Li,[†] Monika Stoiber,[†] Andreas Wimmer,[†] Zhenlan Xu,[‡] Claus Lindenblatt,[§] Brigitte Helmreich,*,[§] and Michael Schuster*,[†]

[†]Division of Analytical Chemistry, Department of Chemistry, Technical University of Munich, Garching 85748, Germany
[‡]Institute of Quality and Standard of Agro-Products, Zhejiang Academy of Agricultural Sciences, Hangzhou 310021, China
[§]Chair of Urban Water Systems Engineering, Technical University of Munich, Garching 85748, Germany

S *Supporting Information*

ABSTRACT: Silver-based nanoparticles (Ag-*b*-NPs) emitted by wastewater treatment plants (WWTPs) are considered to be widely present in the natural environment. However, there is much that is unknown about the effect of WWTP effluent on the occurrence of Ag-*b*-NPs in surface waters. On the basis of field analysis of representative WWTPs in Germany, we demonstrate that more than 96.4% of Ag-*b*-NPs from wastewater influent are removed through WWTPs, even though influent contains Ag-*b*-NP concentrations of tens to hundreds ng L^{-1}, resulting in effluent Ag-*b*-NP concentrations of 0.7−11.1 ng L^{-1} over the seasons. The estimated flux of Ag-*b*-NPs associated with WWTPs effluent discharge is ∼33 kg y^{-1} in Germany. WWTPs effluent increases Ag-*b*-NP levels of the River Isar to 2.0−8.6 ng L^{-1}, while remarkable decreases are observed at sites ∼1.5 km downstream of each discharge point, and Ag-*b*-NP levels then keep stable (0.9−2.3 ng L^{-1}) until the next discharge point, showing subtle differences in Ag-*b*-NP levels between the river and reference lakes without industrial sources and WWTPs effluent discharge. Our results demonstrate that WWTPs effluent can exert a clear influence on the occurrence of Ag-*b*-NPs in surface waters.

INTRODUCTION

Silver nanoparticles (AgNPs) are widely applied in personal care products,[1] functional textiles,[2,3] house appliances,[4] and food storage materials,[5] resulting in the inevitable release of AgNPs during usage and disposal of these commercial products.[6−9] AgNPs involve a confusing diversity of particles with different sizes, morphologies, and surface coatings. Uncoated metallic AgNPs do not exist in real environments, and even in AgNP fabrication, coating reagents are used to enhance dispersibility and to reduce aggregation of particles. Dissolved silver species, e.g., Ag$^+$ and Ag(I) complex compounds, are also expected to form AgNPs with different compositions, depending on the surrounding chemical environment.[10,11] Reducing conditions and the presence of chloride or sulfide lead to the formation of nanoparticulate AgCl or Ag$_2$S, a transformation which happens to both dissolved silver species and AgNPs. In sewer systems, the majority of anthropogenic silver from different sources is believed to end up as a vast variety of silver-based nanoparticles (Ag-*b*-NPs) such as Ag$_2$S, AgCl, and AgNPs with numerous coatings due to the complex matrix containing a variety of compounds which can bind to AgNPs.[12−15] As it is not possible to specify all these particles, we designate them as Ag-*b*-NPs in this study.

A number of laboratory studies investigated the transformations[16−18] and fate[19−21] of spiked (∼mg L^{-1}) AgNPs in pilot-simulated wetlands or bioreactors. These showed that the particles are partially removed through the treatment process, with tens to hundreds µg L^{-1} of silver-based particles remaining in the effluent. On the basis of these data, it was proclaimed that effluent of sewage treatment systems may exert a considerable effect on the occurrence of AgNPs in surface waters. However, there are fundamental differences between pilot bioreactors and field-scale WWTPs which usually treat more complex matrices with seasonal fluctuating temperatures, higher sewage loadings, and much lower concentrations (µg to ng L^{-1}) of Ag-*b*-NPs instead of AgNPs.[22] For that reason, we cannot rule out the possibility that the removal efficiency of Ag-*b*-NPs in field-scale WWTPs may be completely different compared to that of pilot sewage treatment systems. Considering potential exposure of aquatic organisms to Ag-*b*-NPs in surface waters receiving WWTP effluent, it is very

important to know the real Ag-*b*-NP levels of field-scale WWTP effluent. More importantly, to what extent can field-scale WWTP effluent influence the occurrence of Ag-*b*-NPs in surface waters? Accordingly, what is the true level of Ag-*b*-NPs in surface waters? There are no systematic data available on these issues, which is definitely hindering comprehensive risk assessment of Ag-*b*-NPs to human and environmental health.

Here, we investigate the way of Ag-*b*-NPs through representative municipal WWTPs with different treatment techniques and sewage loadings to surface waters by using a robust analytical method developed in our group (Materials and Methods). We further investigate the true level of Ag-*b*-NPs along the River Isar (∼295 km) receiving WWTP effluent and in surrounding reference lakes without industrial pollution and effluent inputs. The results of this work clearly present the influence of WWTP effluent discharge on the occurrence of Ag-*b*-NPs in surface waters, paving a way to a more comprehensive understanding of the risk Ag-*b*-NPs may pose to aquatic organisms in natural environments.

■ MATERIALS AND METHODS

Water Samples Collection. In the present study, two representative full-scale municipal WWTPs, operating at 8 °C in winter and 18 °C in summer, were chosen for their different biological treatment techniques, being an activated sludge unit (pre-anoxic denitrification and aerobic carbon degradation with sludge age of 8 days) combined with a trickling filter (nitrification) at WWTP 1 and two-step activated sludge units at WWTP 2 (anoxic denitrification and aerobic carbon degradation in one activated sludge unit with sludge age of 2 days and nitrification in a second activated sludge unit with sludge age of 8−10 days). WWTP 1 is connected to a separated sewer system, receiving wastewater mainly from households, and WWTP 2 is connected to a combined sewer system, receiving wastewater from households and industry. Sampling sites along the wastewater treatment process are shown in Figure S1. Four sampling periods were performed at both WWTPs from July 2013 to May 2014 (Table S1). Each sampling day, aqueous samples were collected every 2 h over a day period at each sampling point in the WWTPs, and the 12 samples were pooled into one 24 h composite sample. All wastewater samples were collected in polyethylene (PE) containers (1 L).

Surface water samples (basic characteristics are shown in Table S2) from the River Isar and pre-alpine lakes in Southern Germany were collected in April 2014 (22, 24, 25) and September 2014 (14−16) under dry weather conditions (after 3 continuous sunny days). Sampling sites are shown in Figure S2 and Table S3. Flow rates of the River Isar are listed in Table S4. In addition to sampling of surface water, samples were also collected at different depths (0, 2, 4, 6, 8, and 10 m) of the largest lake (Chiemsee, Figure S2), with an area of 80 km², an average depth of 26 m (max depth 73 m), and a total volume of 2.05 × 10⁹ m³. Three locations (namely, sites 5, 6, and 7 in Figure 3c; Figure S2) near the estuaries of the inflowing rivers Tiroler Achen and Prien and the only outlet to the River Alz chosen in this lake. Samples were taken with a LIMNOS water sampler (Hydro-Bios, Kiel, Germany). Chiemsee, like most of the pre-alpine lakes, is a dimictic mesotrophic lake (TP: 10 μg L^{-1}). From September 1 to September 17, 2014, the average daily maximum temperature was 19.7 °C, so the lake was most likely in the summer stratification phase. It should also be noted that the lakes were chosen because they are located around the

River Isar, and more importantly, with two exceptions, no WWTP effluents flow into these lakes. All surface water samples were collected in polyvinyl chloride (PVC) containers (0.5 L), and all containers were rinsed three-fold with the sample before they were filled up to volume.

Water Samples Pretreatment and Ag-*b*-NPs Concentration Analysis. The extraction of Ag-*b*-NPs was based on the method of our previous publications.[23,24] In brief, 40 mL of aqueous sample without filtration was mixed with 1.0 mL of saturated ethylenediaminetetraacetic acid disodium salt (EDTA) solution, 400 μL of 1 mol L^{-1} sodium acetate, 100 μL of 1.25 mol L^{-1} acetic acid, and 1 mL of 10% (w/w) TX-114 in a 50 mL tapered polypropylene sample tube. The mixture was incubated at 40 °C for 30 min and then centrifuged for 12 min at 5000 rpm (4472 g) to enhance phase separation. Afterward, the sample was cooled in an ice bath for 3 min. The aqueous supernatant was then decanted. The remaining surfactant-rich phase containing the enriched Ag-*b*-NPs was dissolved in 100 μL of ethanol and measured with electrothermal atomic absorption spectrometry (ET-AAS). The concentration of Ag-*b*-NPs was determined using an Analyst800 GFAAS spectrometer (PerkinElmer, Ueberlingen, Germany), equipped with a Zeeman background correction, a transversally heated graphite atomizer, and an AS-800 autosampler. Here, the limit of detection (LOD) of this method is improved further to 0.2 ng L^{-1} (Supporting Information and Figure S3). Calibration was performed using AgNP solutions of known concentrations that were subjected to the complete extraction procedure and measured the same way as the environmental samples.

Ag-*b*-NP Removal Efficiency Calculation. To show the contribution of each treatment unit to the Ag-*b*-NP removal through WWTP, the removal efficiency of Ag-*b*-NPs was calculated by using the following equation: efficiency (%) = $(C_{input} − C_{output})/C_{influent} \times 100\%$. Here, $C_{influent}$ is the Ag-*b*-NPs concentration of influent (ng L^{-1}), C_{input} is the Ag-*b*-NPs concentration of wastewater obtained before treatment (ng L^{-1}), and C_{output} is the Ag-*b*-NPs concentration of wastewater obtained after treatment (ng L^{-1}).

sp-ICP-MS Analysis. The size distribution of Ag-*b*-NPs was determined with an Agilent 7700x ICP-MS instrument (Waldbronn, Germany) equipped with an autosampler ASX-520. The autosampler was kept in a laminar flow-box (Mac Petek, LFB-457 MP610E) to avoid sample contamination. Dwell time was set to 3.0 ms and acquisition time to 1 min, resulting in 20,000 data points. The pump rate of the peristaltic pump was determined as 325 μL min^{-1}, and an m/z ratio 107 u/e for Ag was observed. Transport efficiency (TE), i.e., the number of particles which finally reach the detector, was determined with a gold nanoparticle (AuNP) dispersion (30 nm, 55 ng L^{-1}). AuNPs instead of AgNPs were used because they can be prepared with narrower size distribution and higher chemical stability of the particles. Since TE is virtually identical for Au and Ag, a calibration with Au is also possible because the intensity of the signals is mainly correlated to the particle size. Due to the fact that the signal intensity is element specific, a further calibration with Ag (Ag⁺ standard 1 μg L^{-1}, in nitric acid) was used to determine element sensitivity. Software based on the calculations of the National Institute of Food Safety in The Netherlands (RI-KILT) was used to generate the information on particle size, size distribution, and analyte concentration. In general, it is assumed that ∼20 nm is the smallest particle size measurable with single particle inductively

coupled plasma mass spectrometry (sp-ICP-MS).[25,26] In this work, however, by coupling cloud point extraction (CPE) with sp-ICP-MS, LOD and s/n ratio could be significantly improved, leading to a LOD of 2 ng L^{-1} (Supporting Information) for particles with sizes down to 14 nm. This is due to selective particle enrichment and separation of particles from dissolved silver species. For coupling of CPE to sp-ICP-MS, we diluted the surfactant with 500 μL of ethanol and 9 mL of ultrapure water. The solution was gently shaken and then subjected to measurement.

■ RESULTS

Characterization of Ag-b-NPs in WWTP Waters. The concentration of Ag-b-NPs was analyzed through both WWTPs (Figure S1), showing significant decreases in Ag-b-NP concentrations along the wastewater treatment process (Figure S4). Ag-b-NPs are mainly (63.5 $\pm$ 19.8% at WWTP 2; 94.8 $\pm$ 5.4% at WWTP 1) removed by activated sludge denitrification/carbon degradation units (Figure 1; Figures S1, S4). It appears that the activated sludge denitrification/carbon degradation unit of WWTP 1 is much more efficient compared to WWTP 2, which is mainly attributed to the lack of primary sedimentation
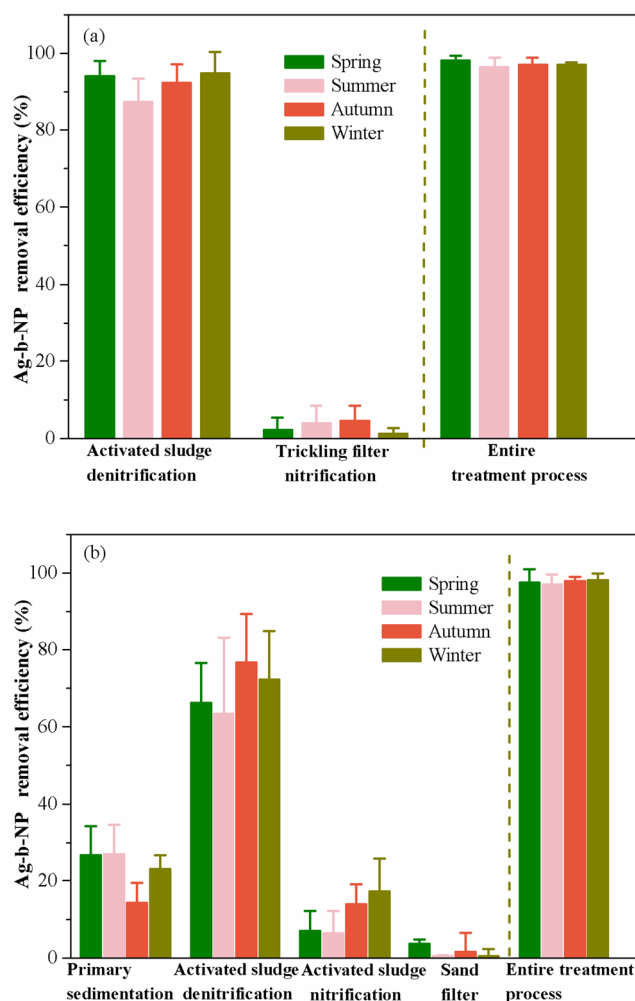
Figure 1. Season-independent removal efficiency of Ag-b-NPs in aqueous matrices through representative full-scale municipal WWTPs: (a) WWTP 1 with average flow rate of 5300 m^3/d and (b) WWTP 2 with average flow rate of 160,000 m^3/d.

in WWTP 1. As shown in Figure 1, the primary sedimentation already removed ∼30% of the Ag-b-NPs in WWTP 2. In the second biological step, a slight (2.3 $\pm$ 1.4% to 17.4 $\pm$ 8.4%) reduction through the (trickling filter or activated sludge) nitrification unit (Figure 1, Figures S1, S4) occurs, resulting in total removal efficiencies higher than 96.4% (Figure 1). The Ag-b-NP concentrations of the wastewater influent span an order of magnitude over the seasons, with a maximum concentration of 357 ng L^{-1} in winter and a minimum concentration of 10.1 ng L^{-1} in summer with rainstorms (Figure S4, Table S1). Despite the notable contribution of activated sludge to Ag-b-NPs removal, the denitrification/carbon degradation rather than nitrification unit plays a remarkable role (Figure 1, Figure S4). Furthermore, compared with biofilm (trickling filter in WWTP 1), activated sludge as a second biological step is much more efficient in Ag-b-NPs removal (Figure 1).

Effluent Ag-b-NP concentrations are lower than 11.1 ng L^{-1} for both WWTPs (Figure 2a), showing subtle fluctuation over the seasons; the lowest Ag-b-NP concentrations (down to 0.7 ng L^{-1}) were measured in summer (Figure 2a). Furthermore, our analysis based on CPE coupling with sp-ICP-MS shows for the first time that a slight variation ($p = 0.0006 < 0.001$) in size distribution of Ag-b-NPs through WWTP occurs, with average sizes of 20.4 $\pm$ 3.1 and 15.3 $\pm$ 3.6 nm in influent and effluent, respectively (Figure 2b, c), while a high efficiency for Ag-b-NP removal was observed. In addition, the concentration of Ag-b-NPs in WWTP effluent is correlated with that of TOC (r = 0.61, $p < 0.05$) (Figure 2d).

Along with a significant reduction of Ag-b-NP levels through the wastewater treatment process, levels of total organic carbon (TOC), total nitrogen (TN), ammonia nitrogen (NH$_4$−N), and total phosphorus (TP) also show remarkable decreases with removal efficiencies of 85.0% to 95.1%, 51.3% to 78.4%, 94.1% to 99.9%, and 72.1% to 90.1% for TOC, TN, NH$_4$−N, and TP, respectively.

Effects of WWTP Effluent on the Occurrence of Ag-b-NPs in Surface Waters. Daily Ag-b-NP fluxes associated with effluent discharge are estimated in the range from 5.7 to 48.2 mg d^{-1} for WWTP 1 and 110 to 1588 mg d^{-1} for WWTP 2 (Figure S5a), of which the mean fluxes are 22.7 $\pm$ 11.3 and 397.2 $\pm$ 275.9 mg d^{-1}, accounting for 3.7 $\pm$ 2.0% and 2.4 $\pm$ 1.0% of Ag-b-NPs in wastewater influent, respectively. Ag-b-NP fluxes of 7.7 and 123 g y^{-1} are further estimated for WWTPs 1 and 2, respectively (Figure S5b). Ag-b-NPs were not detected in the upstream (sites 1−9 in Figure S2) of the River Isar (Figure 3a, b), while Ag-b-NPs with a concentration of ∼1.9 ng L^{-1} were determined in water taken at site 10 (Figure 3a, b; Figure S2), where the above-mentioned WWTPs 1 and 2 discharge their effluents (Figure S2). There are other five effluent discharge points either in the middle and lower reaches or in the channel of the River Isar (Figure S2). At each point where the corresponding WWTP discharges effluent into the river, Ag-b-NP peaks can be easily observed (Figure 3b), with 2.0−8.6 ng L^{-1}.

However, remarkable decreases in Ag-b-NP levels were observed at sites 1.5 km downstream of each effluent discharge point (Figure 3b), and Ag-b-NP levels then keep stable (0.9−2.3 ng L^{-1}) until the following discharge point along the river (Figure 3b). As a result, a gradual progressive increase in the Ag-b-NP level from the middle reaches of the River Isar to its confluence with the River Danube was observed with a final Ag-b-NP concentration of ∼1.7 ng L^{-1}.
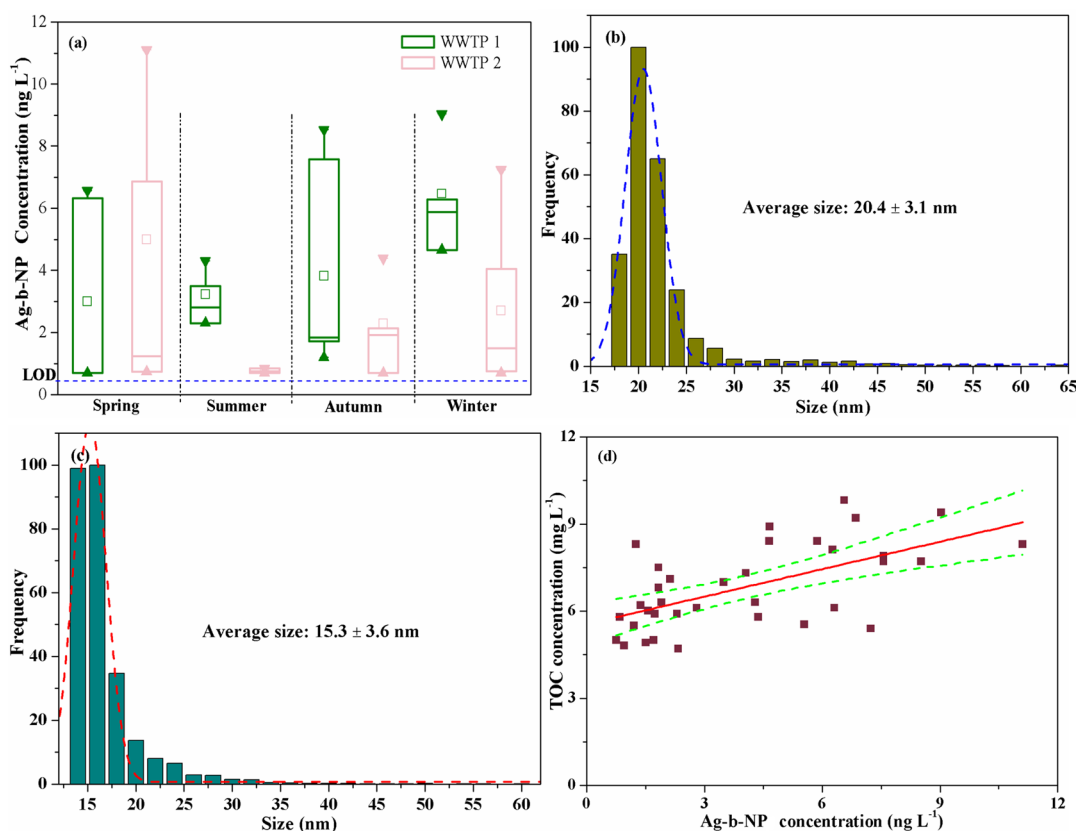
Figure 2. Characterization of Ag-*b*-NPs in WWTP effluent: (a) Ag-*b*-NP concentrations in effluent of WWTP 1 and WWTP 2 over the seasons. (b and c) Size distribution of Ag-*b*-NPs in wastewater influent (b) and effluent (c) measured by sp-ICP-MS. It should be noted that the data are obtained from samples in WWTP 2. (d) Correlation between Ag-*b*-NP and TOC concentrations in WWTP effluent ($r = 0.61$, $p < 0.05$).

Most of the lakes also show measurable Ag-*b*-NP concentrations, with levels ranging from 0.5 to 1.3 ng L^{-1} (Figure 3a, b), while some lakes receiving WWTP effluent show Ag-*b*-NP concentrations of 0.3−0.7 ng L^{-1} (Figure 3b), with negligible changes of the Ag-*b*-NP level within a depth of 0 to 10 m (Figure 3c).

■ DISCUSSION

The data presented here demonstrate that the removal efficiency of Ag-*b*-NPs through full-scale WWTPs is as high as values reported from laboratory research using pilot bioreactors.[20,21,27,28] This indicates that field-scale WWTPs are very efficient in Ag-*b*-NP removal. Furthermore, seasonal variations in total removal efficiency are negligible, indicating that fluctuations of ambient temperature and influent flow rates (Table S1) do not significantly influence Ag-*b*-NP removal through full-scale WWTPs. The lowest concentrations of Ag-*b*-NPs in wastewater influent were observed in summer (Figure S4), mainly due to the dilution from the high flow rate of influent (Table S1). Due to the small differences in total removal efficiency over the seasons and the lowest Ag-*b*-NP concentrations of influent in summer, WWTPs effluent also shows the lowest concentration of Ag-*b*-NPs during this season (Figure 2a).

To date only modeling studies based on material flow analysis of engineered silver nanoparticles (EAgNPs) rather than real measurements in environmental compartments are known.[29,30] Most recent predictions[29] for EAgNP concentrations in WWTP effluent and surface waters (most frequent value) are 0.17 and 0.66 ng L^{-1} respectively. The corresponding lower and upper percentiles (Q0.15 and Q0.85) are 0.06 and 16 ng L^{-1} for WWTP effluent and 0.51 and 0.94 ng L^{-1} for surface waters. In the present work, Ag-*b*-NPs rather than EAgNPs were measured which prevents a direct comparison with the data obtained by the cited material flow analyses. Taking into account that Ag-*b*-NP concentrations are most probably higher than those of EAgNPs, the forecast made by material flow analysis is close to the values measured in the present work.

The effect of WWTP effluent on the occurrence of Ag-*b*-NPs in surface waters depends on the magnitude of Ag-*b*-NP flux and the chemical and physical stability of Ag-*b*-NPs in surface waters. In Germany, a total of 10 billion m^3 of wastewater was treated in WWTPs in 2010, almost exclusively (99.9%) through biological treatment systems as shown in this study,[31] so the amount of Ag-*b*-NPs associated with effluent discharge is estimated to ∼33 kg y^{-1}, accounting only for ∼0.4% of the silver consumption in Germany. Given the fact that Ag-*b*-NPs were not detected in the River Isar until it receives WWTP effluent, we believe that Ag-*b*-NPs determined in the middle and lower reaches of the River Isar originate from WWTP effluent. Due to the large differences in the flow rate between the River Isar (Table S4) and WWTP effluent, Ag-*b*-NP peaks are quickly diluted in the direction of flow. According to the German DIN 38 402 T15, 2012, substances discharged into running waters are homogenized within ∼1 km.[32] Therefore, it is anticipated that Ag-*b*-NPs originating from WWTP effluent are homogenized in the river within ∼1.5 km downstream of discharge points. The gradual increase in Ag-*b*-NP levels from the middle reaches of the River Isar to its confluence with the River Danube over a distance of approximately 150 km and a
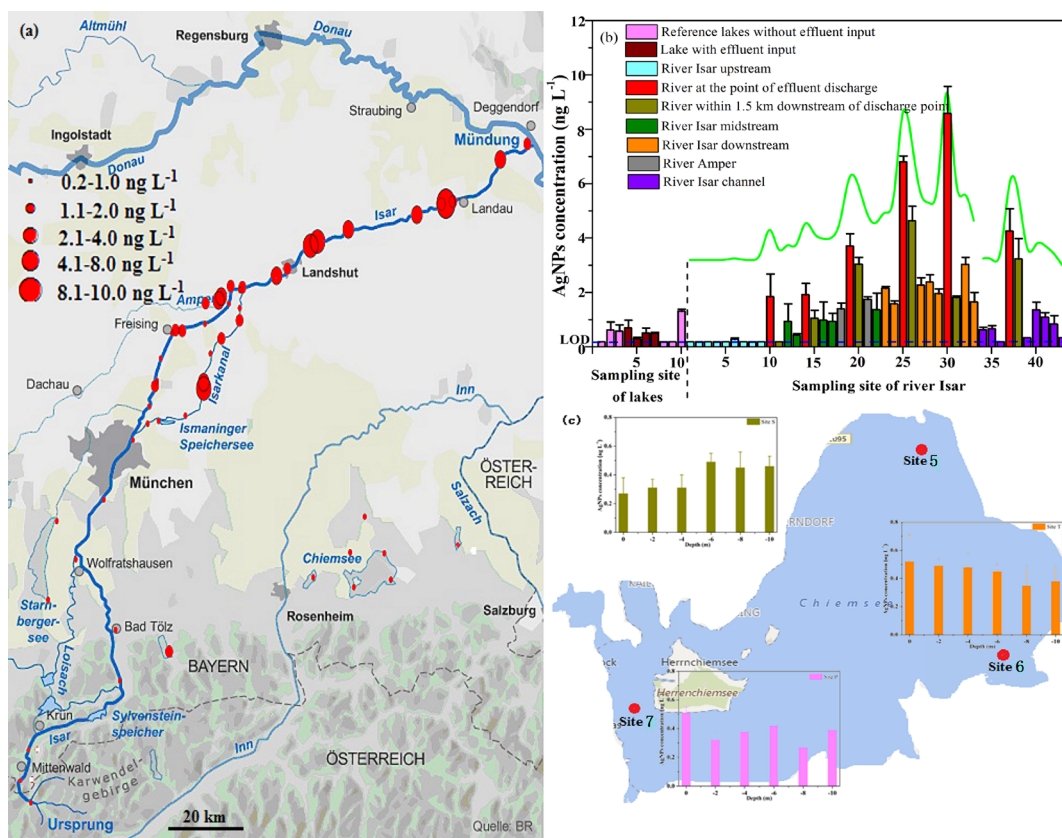
Figure 3. Occurrence of Ag-*b*-NPs in surface waters in South Germany. Source of map is Bayerischer Rundfunk (http://www.br.de/themen/bayern/isar-dossier-karte104.html). (a) Ag-*b*-NP levels of surface waters; image is obtained through ArcGIS 9. (b) Effect of WWTP effluent on the Ag-*b*-NP levels of surface waters. (c) Depth independent level of Ag-*b*-NPs in the Lake Chiemsee.

final Ag-*b*-NP level of ∼1.7 ng L^{-1} indicates that Ag-*b*-NPs from effluent may possess remarkable stability and will be suspended in natural water for a long time or delivered far distances. This may be related to the weak basic pH (7.6−8.6) of the River Isar since previous studies have reported that AgNPs remain stable in solutions with basic pH (pH > 7).[33,34] In general, pH is an important factor influencing the stability of Ag-*b*-NPs; dissolution of the particles can be accelerated in acidic solutions.[34,35] NOM occurring in the aquatic environment, usually at concentrations far higher than that of Ag-*b*-NPs, is also known to entangle and stabilize NPs.[36−38] Here, measurable levels (TOC: 0.9−2.1 mg L^{-1}) of NOM are observed along the river after receiving effluent. Evidently, these findings reveal that WWTP effluent is responsible for the increase in the Ag-*b*-NP concentration in the River Isar. In comparison, negligible differences in Ag-*b*-NP levels between the reference lakes and the lakes receiving WWTP effluent are observed (Figure 3a, b). In the case of the Lake Chiemsee (Figure S2), ∼68% of water input comes from the River Tiroler Achen with effluent input from WWTPs (145,000 inhabitant equivalents, approximately 28,000 m^3 d^{-1}). Water exchange of the lake takes place within 1.26 y, so we propose that the lake is a reservoir for Ag-*b*-NPs submitted by the River Tiroler Achen. This is likely to be the main explanation for the uniform distribution of Ag-*b*-NPs over the lake (Figure 3c) and the negligible differences in Ag-*b*-NP levels observed within a depth of 0 to 10 m (Figure 3c).

The occurrence of Ag-*b*-NPs in the reference lakes (Figure 3a, b) is most likely attributable to the natural formation of Ag-*b*-NPs in the aquatic environment with NOM, even though we

cannot distinguish and identify whether the Ag-*b*-NPs are of natural or anthropogenic origin. This inference is supported by the good correlation between Ag-*b*-NPs and NOM levels measured as total organic carbon (TOC) in the reference lakes. Ag-*b*-NPs were not detected in reference lakes with low NOM concentrations, but 1.3 and 0.7 ng L^{-1} of Ag-*b*-NPs were measured in lakes with 3.3 and 5.0 mg L^{-1} NOM, respectively (Table S5). The most likely explanation for this observation is that NOM promotes the formation of Ag-*b*-NPs from soluble Ag species and also leads to a stabilization and improved dispersion of Ag-*b*-NPs in natural waters.[39,40] Previous studies have already demonstrated the natural formation of Ag-*b*-NPs in surface waters in the presence of NOM under light conditions.[41−43] Herein, we believe that the occurrence of Ag-*b*-NPs in the reference lakes is likely a result of natural formation.

The techniques for wastewater treatment described in this work are currently very typical and widely used in the European Union (EU). The inevitable consequence of high removal efficiency for Ag-*b*-NPs through wastewater treatment processes is a considerable enrichment of the latter in excess sludge, having the potential to impose risks on terrestrial organisms because excess sludge is widely applied as an agricultural fertilizer. Indeed, high silver concentrations up to 856 mg kg^{-1} were observed in excess sludge from WWTPs in EU and United States.[44,45] Even on the assumption that anthropogenic silver is completely transferred to Ag$_2$S-NPs in excess sludge,[13] the impacts on organisms still cannot be ignored because of the fact that phytotoxicity of Ag$_2$S-NPs has been reported in a recent study.[46]

Here, we conclude that WWTP effluent can exert influences on the occurrence of Ag-b-NPs in surface waters since the trace level of Ag-b-NPs in the River Isar is clearly attributed to the effluent discharge from full-scale WWTPs along the river. The crucial question, do ng L^{-1} levels of Ag-b-NPs in surface waters impact the health of living organisms in the aquatic environment, cannot be answered sufficiently at the moment. It was reported that concentrations of AgNPs as low as a few ng L^{-1} can indeed affect invertebrates, prokaryotes, and fish,[47] even though it was observed that chronic exposure to AgNPs in the ng L^{-1} range did not induce a cytotoxic response.[48] Obviously, more research is needed to evaluate the real influence of trace levels of Ag-b-NPs on aquatic organisms in surface waters. This also includes Ag-b-NPs which might be formed naturally. We consider that the Ag-b-NPs determined in the reference lakes are likely formed naturally because there are no anthropogenic inputs like industrial pollution and WWTP effluent discharge. Also, additional research is necessary to determine the chemical composition of Ag-b-NPs and to differentiate whether Ag-b-NPs in natural waters are of natural or anthropogenic origin.

■ ASSOCIATED CONTENT

Ⓢ Supporting Information

The Supporting Information is available free of charge on the ACS Publications website at DOI: 10.1021/acs.est.6b00694.

> Schematic diagrams of the investigated full-scale WWTPs (Figure S1). Sampling sites along the River Isar and surrounding lakes (Figure S2). Typical function for a CPE ET-AAS calibration with 0.2, 0.5, 1.0, and 3.0 ng L^{-1} AgNPs (Figure S3). Ag-b-NP concentrations (ng L^{-1}) in samples collected from different treatment units of two representative full-scale municipal WWTPs (Figure S4). Estimated Ag-b-NP fluxes associated with WWTP effluent (Figure S5). Seasonal and weather influences on the influent flow rate of the investigated municipal WWTPs (Table S1). Basic characteristics of water samples from the River Isar with total length of 295 km (Table S2). Location of sampling sites (Table S3). Flow rates of the River Isar at different sampling sites (Table S4). Basic characteristics of water samples from lakes (Table S5). (PDF)

■ AUTHOR INFORMATION

Corresponding Authors

*B. Helmreich. E-Mail: b.helmreich@tum.de. Tel: +49 (0)89 289 13719. Fax: +49 (0)89 289 13718.
*M. Schuster. E-Mail: michael.schuster@tum.de. Tel: +49 (0) 89 289 13763. Fax: +49 (0)89 289 14513.

Notes

The authors declare no competing financial interest.

■ ACKNOWLEDGMENTS

■ REFERENCES

(1) Kessler, R. Engineered nanoparticles in consumer products: understanding a new ingredient. *Environ. Health Perspect.* **2011**, *119*, 120−125.

(2) Geranio, L.; Heuberger, M.; Nowack, B. The behavior of silver nanotextiles during washing. *Environ. Sci. Technol.* **2009**, *43*, 8113−8118.

(3) Benn, T.; Cavanagh, B.; Hristovski, K.; Posner, J. D.; Westerhoff, P. The release of nanosilver from consumer products used in the home. *J. Environ. Qual.* **2010**, *39*, 1875−1882.

(4) Jiang, D.; Chen, L.; Xie, J.; Chen, M. Ag$_2$S/g-C$_3$N$_4$ composite photocatalysts for efficient Pt-free hydrogen production. The co-catalyst function of Ag/Ag$_2$S formed by simultaneous photodeposition. *Dalton Trans.* **2014**, *43*, 4878−4885.

(5) Richter, A. P.; Brown, J. S.; Bharti, B.; Wang, A.; Gangwal, S.; Houck, K.; Cohen Hubal, E. A.; Paunov, V. N.; Stoyanov, S. D.; Velev, O. D. An environmentally benign antimicrobial nanoparticle based on a silver-infused lignin core. *Nat. Nanotechnol.* **2015**, *10*, 817−823.

(6) Glover, R. D.; Miller, J. M.; Hutchison, J. E. Generation of metal nanoparticles from silver and copper objects: nanoparticle dynamics on surfaces and potential sources of nanoparticles in the environment. *ACS Nano* **2011**, *5*, 8950−8957.

(7) Benn, T. M.; Westerhoff, P. Nanoparticle silver released into water from commercially available sock fabrics. *Environ. Sci. Technol.* **2008**, *42*, 4133−4139.

(8) Kaegi, R.; Sinnet, B.; Zuleeg, S.; Hagendorfer, H.; Mueller, E.; Vonbank, R.; Boller, M.; Burkhardt, M. Release of silver nanoparticles from outdoor facades. *Environ. Pollut.* **2010**, *158*, 2900−2905.

(9) Hedberg, J.; Skoglund, S.; Karlsson, M.; Wold, S.; Wallinder, I. O.; Hedberg, Y. Sequential studies of silver released from silver nanoparticles in aqueous media simulating sweat, laundry detergent solutions and surface water. *Environ. Sci. Technol.* **2014**, *48*, 7314−7322.

(10) Adegboyega, N. F.; Sharma, V. K.; Siskova, K. M.; Vecerova, R.; Kolar, M.; Zboril, R.; Gardea-Torresdey, J. L. Enhanced formation of silver nanoparticles in Ag$^+$-NOM-iron (II, III) systems and antibacterial activity studies. *Environ. Sci. Technol.* **2014**, *48*, 3228−3235.

(11) Akaighe, N.; MacCuspie, R. I.; Navarro, D. A.; Aga, D. S.; Banerjee, S.; Sohn, M.; Sharma, V. K. Humic acid-induced silver nanoparticle formation under environmentally relevant conditions. *Environ. Sci. Technol.* **2011**, *45*, 3895−3901.

(12) Kent, R. D.; Oser, J. G.; Vikesland, P. J. Controlled evaluation of silver nanoparticle sulfidation in a full-scale wastewater treatment plant. *Environ. Sci. Technol.* **2014**, *48*, 8564−8572.

(13) Kim, B.; Park, C.; Murayama, M.; Hochella, M. F. Discovery and characterization of silver sulfide nanoparticles in final sewage sludge products. *Environ. Sci. Technol.* **2010**, *44*, 7509−7514.

(14) Thalmann, B.; Voegelin, A.; Sinnet, B.; Morgenroth, E.; Kaegi, R. Sulfidation kinetics of silver nanoparticles reacted with metal sulfides. *Environ. Sci. Technol.* **2014**, *48*, 4885−4892.

(15) Nowack, B. Nanosilver revisited downstream. *Science* **2010**, *330*, 1054−1055.

(16) Lowry, G. V.; Espinasse, B. P.; Badireddy, A. R.; Richardson, C. J.; Reinsch, B. C.; Bryant, L. D.; Bone, A. J.; Deonarine, A.; Chae, S.; Therezien, M.; Colman, B. P.; Hsu-Kim, H.; Bernhardt, E. S.; Matson, C. W.; Wiesner, M. R. Long-term transformation and fate of manufactured Ag nanoparticles in a simulated large scale freshwater emergent wetland. *Environ. Sci. Technol.* **2012**, *46*, 7027−7036.

(17) Colman, B. P.; Espinasse, B.; Richardson, C. J.; Matson, C. W.; Lowry, G. V.; Hunt, D. E.; Wiesner, M. R.; Bernhardt, E. S. Emerging contaminant or an old toxin in disguise? silver nanoparticle impacts on ecosystems. *Environ. Sci. Technol.* **2014**, *48*, 5229−5236.

(18) Levard, C.; Hotze, M.; Lowry, G. V.; Brown, G. E. Environmental transformations of silver nanoparticles: impact on stability and toxicity. *Environ. Sci. Technol.* **2012**, *46*, 6900−6914.

(19) Brunetti, G.; Donner, E.; Laera, G.; Sekine, R.; Scheckel, K. G.; Khaksar, M.; Vasilev, K.; De Mastro, G.; Lombi, E. Fate of zinc and

silver engineered nanoparticles in sewerage networks. *Water Res.* **2015**, *77*, 72−84.

(20) Kaegi, R.; Voegelin, A.; Sinnet, B.; Zuleeg, S.; Hagendorfer, H.; Burkhardt, M.; Siegrist, H. Behavior of metallic silver nanoparticles in a pilot wastewater treatment plant. *Environ. Sci. Technol.* **2011**, *45*, 3902−3908.

(21) Ma, R.; Levard, C.; Judy, J. D.; Unrine, J. M.; Durenkamp, M.; Martin, B.; Jefferson, B.; Lowry, G. V. Fate of zinc oxide and silver nanoparticles in a pilot wastewater treatment plant and in processed biosolids. *Environ. Sci. Technol.* **2014**, *48*, 104−112.

(22) Li, L.; Hartmann, G.; Döblinger, M.; Schuster, M. Quantification of nanoscale silver nanoparticles removal and release from municipal wastewater treatment plants in Germany. *Environ. Sci. Technol.* **2013**, *47*, 7317−7323.

(23) Hartmann, G.; Hutterer, C.; Schuster, M. Ultra-trace determination of silver nanoparticles in water samples using cloud point extraction and ETAAS. *J. Anal. At. Spectrom.* **2013**, *28*, 567−572.

(24) Hartmann, G.; Baumgartner, T.; Schuster, M. Influence of particle coating and matrix constituents on the cloud point extraction efficiency of silver nanoparticles (Ag-NPs) and application for monitoring the formation of Ag-NPs from Ag⁺. *Anal. Chem.* **2014**, *86*, 790−796.

(25) Wilbur, S.; Yamanaka, M.; Sannac, S.*Characterization of nanoparticles in aqueous samples by ICP-MS*; White Paper 5991-5516EN; Agilent Technologies, 2015

(26) Lee, S.; Bi, X.; Reed, R.; Ranville, J. F.; Herckes, P.; Westerhoff, P. Nanoparticle size detection limts by single particle ICP-MS for 40 elements. *Environ. Sci. Technol.* **2014**, *48*, 10291−10300.

(27) Kiser, M. A.; Ryu, H.; Jang, H.; Hristovski, K.; Westerhoff, P. Biosorption of nanoparticles to heterotrophic wastewater biomass. *Water Res.* **2010**, *44*, 4105−4114.

(28) Gomez-Rivera, F.; Field, J. A.; Brown, D.; Sierra-Alvarez, R. Fate of cerium dioxide (Ce₂O) nanoparticles in municipal wastewater during activated sludge treatment. *Bioresour. Technol.* **2012**, *108*, 300−304.

(29) Sun, T. Y.; Gottschalk, F.; Hungerbühler, K.; Nowack, B. Comprehensive probabilistic modelling of environmental emissions of engineered nanomaterials. *Environ. Pollut.* **2014**, *185*, 69−76.

(30) Gottschalk, F.; Sun, T. Y.; Nowack, B. Environmental concentrations of engineered nanomaterials: review of modeling and analytical studies. *Environ. Pollut.* **2013**, *181*, 287−300.

(31) *Water Management in Germany Water Supply − Waste Water Disposal*; Federal Ministry for the Environment, Nature Conservation, Building and Nuclear Safety: Berlin, April 2014.

(32) Deutsche Einheitsverfahren zur Wasser-, Abwasser- und Schlammuntersuchung − Probenahme aus Fließgewässern, German DIN 38 402 T15, 2012.

(33) Csapo, E.; Patakfalvi, R.; Hornok, V.; Toth, L. T.; Sipos, A.; Szalai, A.; Csete, M.; Dekany, I. Effect of pH on stability and plasmonic properties of cysteine-functionalized silver nanoparticle dispersion. *Colloids Surf., B* **2012**, *98*, 43−49.

(34) El Badawy, A. M.; Luxton, T. P.; Silva, R. G.; Scheckel, K. G.; Suidan, M. T.; Tolaymat, T. M. Impact of environmental conditions (pH, ionic strength, and electrolyte type) on the surface charge and aggregation of silver nanoparticles suspensions. *Environ. Sci. Technol.* **2010**, *44*, 1260−1266.

(35) Axson, J. L.; Stark, D. I.; Bondy, A. L.; Capracotta, S. S.; Maynard, A. D.; Philbert, M. A.; Bergin, I. L.; Ault, A. P. Rapid kinetics of size and pH-dependent dissolution and aggregation of silver nanoparticles in simulated gastric fluid. *J. Phys. Chem. C* **2015**, *119*, 20632−20641.

(36) Gunsolus, I. L.; Mousavi, M. P. S.; Hussein, K.; Bühlmann, P.; Haynes, C. Effects of humic and fulvic acids on silver nanoparticle stability, dissolution, and toxicity. *Environ. Sci. Technol.* **2015**, *49*, 8078−8086.

(37) Yang, X.; Jiang, C.; Hsu-Kim, H.; Badireddy, A. R.; Dykstra, M.; Wiesner, M.; Hinton, D. E.; Meyer, J. N. Silver nanoparticle behavior, uptake, and toxicity in Caenorhabditis elegans: effects of natural organic matter. *Environ. Sci. Technol.* **2014**, *48*, 3486−3495.

(38) Yin, Y.; Shen, M.; Tan, Z.; Yu, S.; Liu, J.; Jiang, G. Particle coating-dependent interaction of molecular weight fractionated natural organic matter: impacts on the aggregation of silver nanoparticles. *Environ. Sci. Technol.* **2015**, *49*, 6581−6589.

(39) Sharma, V. K.; Filip, J.; Zboril, R.; Varma, R. S. Natural inorganic nanoparticles - formation, fate, and toxicity in the environment. *Chem. Soc. Rev.* **2015**, *44*, 8410−8423.

(40) Akaighe, N.; MacCuspie, R. I.; Navarro, D. A.; Aga, D. S.; Banerjee, S.; Sohn, M.; Sharma, V. K. Humic acid-induced silver nanoparticle formation under environmentally relevant conditions. *Environ. Sci. Technol.* **2011**, *45*, 3895−3901.

(41) Yin, Y.; Liu, J.; Jiang, G. Sunlight-induced reduction of ionic Ag and Au to metallic nanoparticles by dissolved organic matter. *ACS Nano* **2012**, *6*, 7910−7919.

(42) Yin, Y.; Shen, M.; Zhou, X.; Yu, S.; Chao, J.; Liu, J.; Jiang, G. Photoreduction and stabilization capability of molecular weight fractionated natural organic matter in transformation of silver ion to metallic nanoparticle. *Environ. Sci. Technol.* **2014**, *48*, 9366−9373.

(43) Adegboyega, N. F.; Sharma, V. K.; Siskova, K. M.; Vecerova, R.; Kolar, M.; Zboril, R.; Gardea-Torresdey, J. L. Enhanced formation of silver nanoparticles in Ag⁺-NOM-Iron (II, III) systems and antibacterial activity studies. *Environ. Sci. Technol.* **2014**, *48*, 3228−3235.

(44) Blaser, S. A.; Scheringer, M.; MacLeod, M.; Hungerbühler, K. Estimation of cumulative aquatic exposure and risk due to silver: contribution of nano-functionalized plastics and textiles. *Sci. Total Environ.* **2008**, *390*, 396−409.

(45) Kim, B.; Murayama, M.; Colman, B. P., Jr.; Hochella, M. F. Characterization and environmental implications of nano- and larger TiO2 particles in sewage sludge, and soils amended with sewage sludge. *J. Environ. Monit.* **2012**, *14*, 1128−1136.

(46) Wang, P.; Menzies, N. W.; Lombi, E.; Sekine, R.; Blamey, P. C.; Hernandez-Soriano, M. C.; Cheng, M.; Kappen, P.; Peijnenburg, W. J. G. M.; Tang, C.; Kopittke, P. M. Silver sulfide nanoparticles (Ag₂S-NPs) are taken up by plants and are phytotoxic. *Nanotoxicology* **2015**, *9*, 1041−1049.

(47) Fabrega, J.; Luoma, S. N.; Tyler, C. R.; Galloway, T. S.; Lead, J. R. Silver nanoparticles: behaviour and effects in the aquatic environment. *Environ. Int.* **2011**, *37*, 517−531.

(48) Comfort, K. K.; Braydich-Stolle, L. K.; Maurer, E. I.; Hussain, S. M. Less is more: long-term in vitro exposure to low levels of silver nanoparticles provides new insights for nanomaterial evaluation. *ACS Nano* **2014**, *8*, 3260−3271.

Supporting Information

To what extent can full-scale wastewater treatment plant effluent influence the occurrence of silver based nanoparticles in surface waters?

Lingxiangyu Li[a], Monika Stoiber[a], Andreas Wimmer[a], Zhenlan Xu[b], Claus Lindenblatt[c], Brigitte Helmreich[c, *], and Michael Schuster[a, *]

[a] Division of Analytical Chemistry, Department of Chemistry, Technical University of Munich, Garching 85748, Germany

[b] Institute of Quality and Standard of Agro-Products, Zhejiang Academy of Agricultural Sciences, Hangzhou 310021, China

[c] Chair of Urban Water Systems Engineering, Technical University of Munich, Garching 85748, Germany

Total pages: 14 pages

5 Figures

5 Tables

Chemicals and materials

All reagents were of analytical grade and used as received without further purification. Nitric acid, hydrochloric acid, acetic acid, sodium acetate, ethylenediaminetetraacetic acid, disodium salt, dihydrate (EDTA), Triton X-114 (TX-114) and ethanol were purchased from VWR International (Leuven, Belgium).

Determination of LOD for CPE ET-AAS measurement

In comparison to our former measurements, the LOD in this study could be improved from 0.7 ng L^{-1} to about 0.2 ng L^{-1} by using peak height instead of peak area in data processing. A further increase could be achieved by using less surfactant (10 % (w/w) TX-114, 750 µL) to achieve a higher enrichment factor for Ag-b-NPs. Additionally, the use of multiple pipetting and pyrolysis steps before the final ET-AAS atomization step improved the LOD. The latter was calculated from the calibration function according to German DIN 32 645[1]. A typical calibration function from 0.2 ng L^{-1} to 3 ng L^{-1} is given in Fig S3. For higher Ag-b-NP concentrations, e.g. WWTP effluent a calibration from 3 ng L^{-1} to 20 ng L^{-1} was used with a LOD of 1.1 ng L^{-1}.

Determination of LOD for CPE sp-ICP-MS measurement

In contrast to CPE ET-AAS, measurement LOD of CPE sp-ICP-MS cannot be calculated from calibration functions. Instead we used an algorithm described by *Peters et al*[2] based on the 3-σ-method. A ten-fold measurement of blank values (ultra-pure water containing all chemicals for CPE sp-ICP-MS except Ag-b-NPs) was used for the calculation of LOD, which could be determined to 2 ng L^{-1}.

Water quality analysis

47

48   In WWTP samples pH, TOC, TN, NH_4-N and TP were measured, and in samples of the River

49   Isar and the pre-alpine lakes, pH and TOC were determined. The pH was measured using an Qph 70

50   pH-meter (VWR, Darmstadt, Germany). TOC was measured with an Elementar High TOC

51   Analyzer (Elementar, Hanau, Germany). After removal of inorganic carbon with hydrochloric acid,

52   TN, NH_4-N and TP were measured according to the EPA methods.

53

Statistical analysis

54

55   Statistical analysis and correlations were performed using SPSS for Windows version 16.0

56   (Chicago, IL, USA). Statistical significance was defined as $p < 0.05$.

57

References

58

59   1.   German DIN 32 645, Chemische Analytik - Nachweis-, Erfassungs- und Bestimmungsgrenze

60   unter Wiederholbedingungen - Begriffe, Verfahren, Auswertung, 2008

61   2. Peters, R. J. B., Rivera, Z. H., van Bemmel, G, Marvin, H. J. P., Weigel, S., Bouwmeester, H.

62   *Anal. Bioanal. Chem.* 2014, 406, 3875-3885.

63

64

65

66

67

68

69
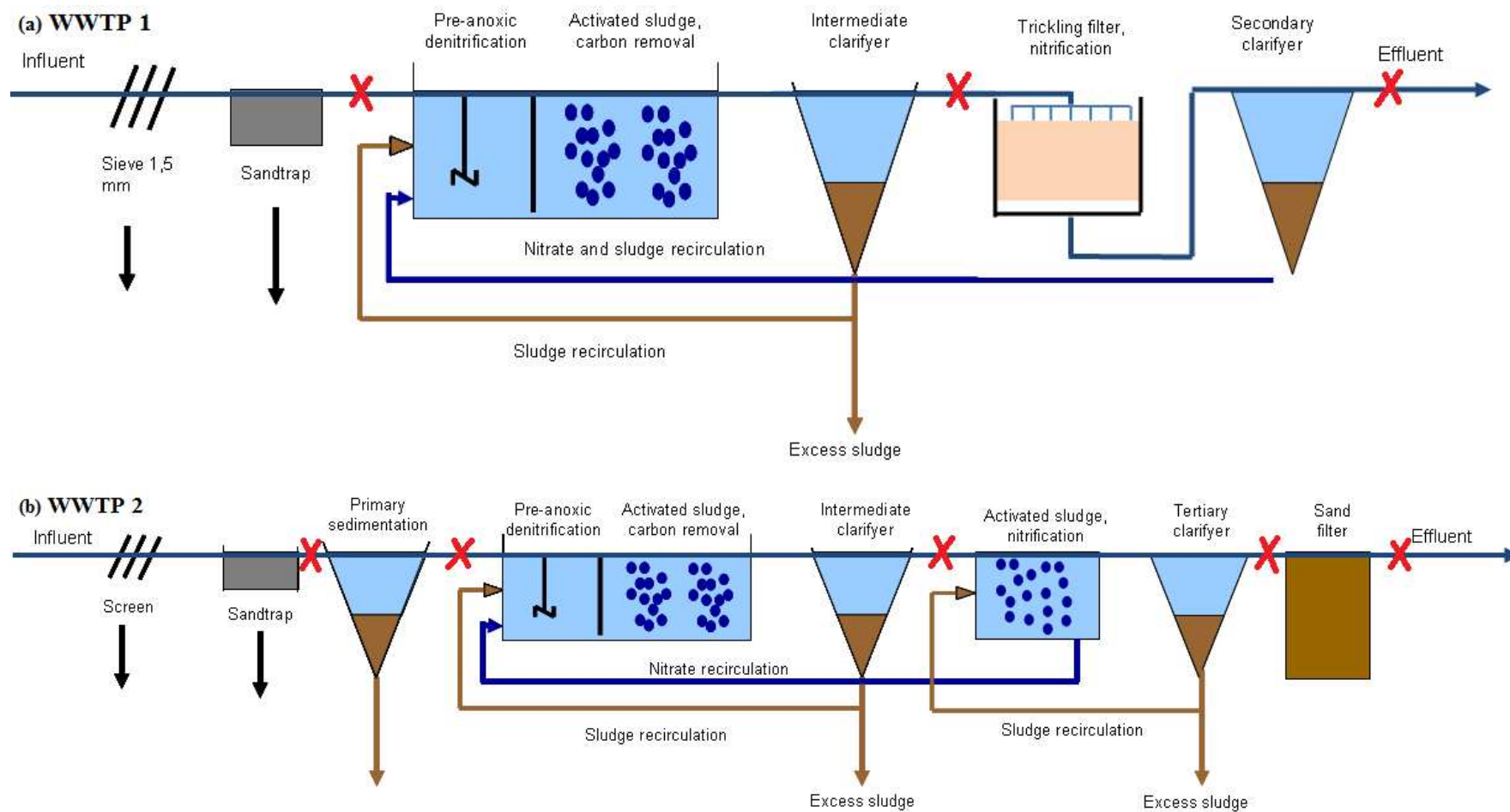
70

71

72 **Fig S1.** Schematic diagrams of the investigated full-scale WWTPs. The crossings in red present sampling sites along the wastewater treatment process. (a) WWTP 1 with

73 average flow rate of 5,300 m^3/d (population served ～26,000). (b) WWTP 2 with an average flow rate of 160,000 m^3/d (population served ～850,000) .
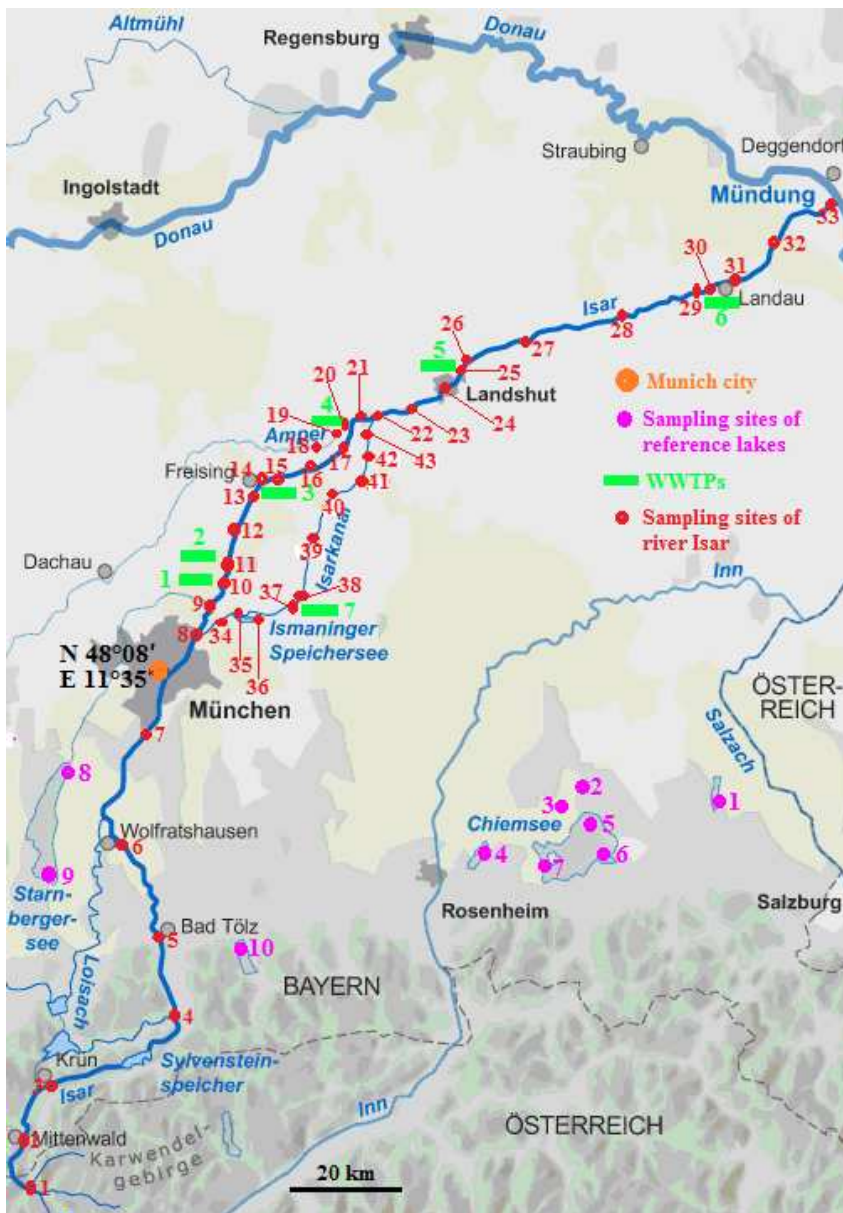
Fig. S2 Sampling sites along the River Isar and the pre-alpine lakes.
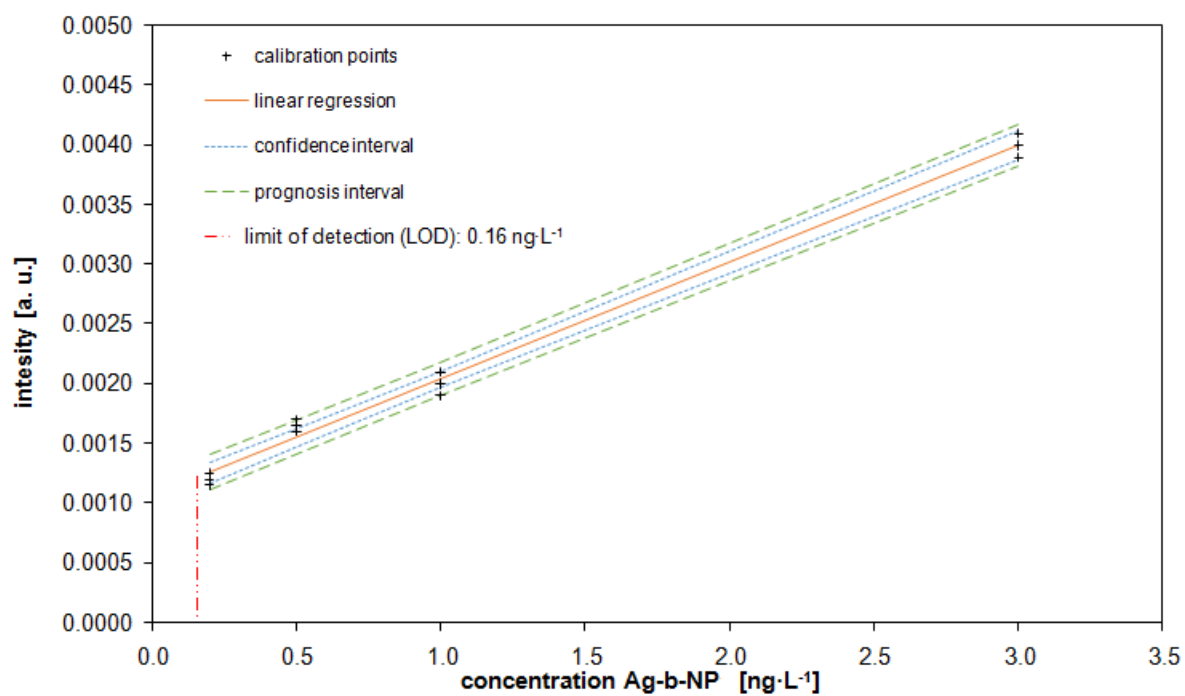
Fig. S3 Typical function for a CPE ET-AAS calibration with 0.2, 0.5, 1.0 and 3.0 ng L^{-1} AgNPs. The calculated LOD is 0.16 ng L^{-1}.
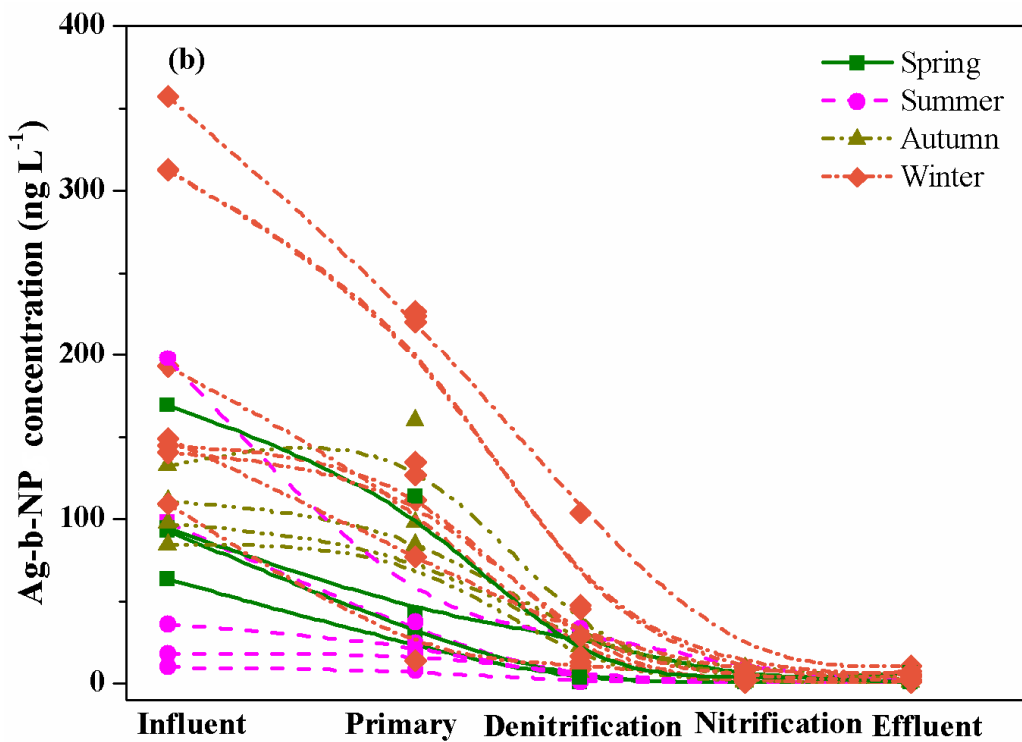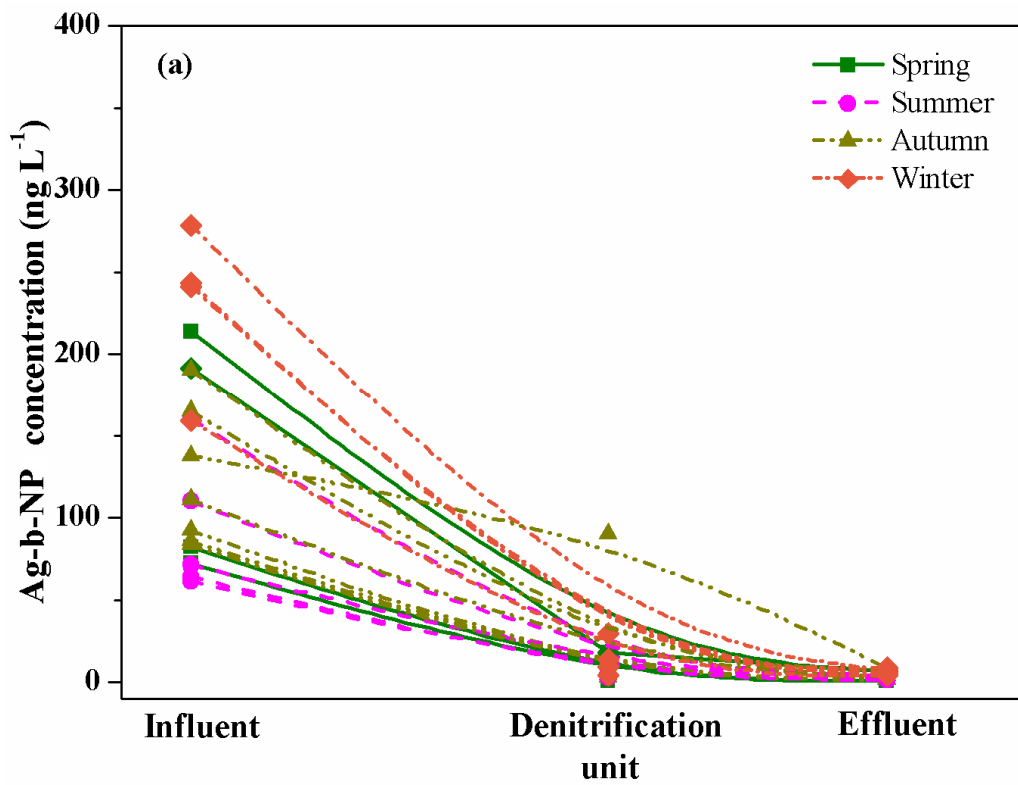
Fig. S4 Ag-b-NP concentrations (ng L^{-1}) in samples collected from different treatment units of two representative full-scale municipal WWTPs. (a) WWTP 1. (b) WWTP 2.
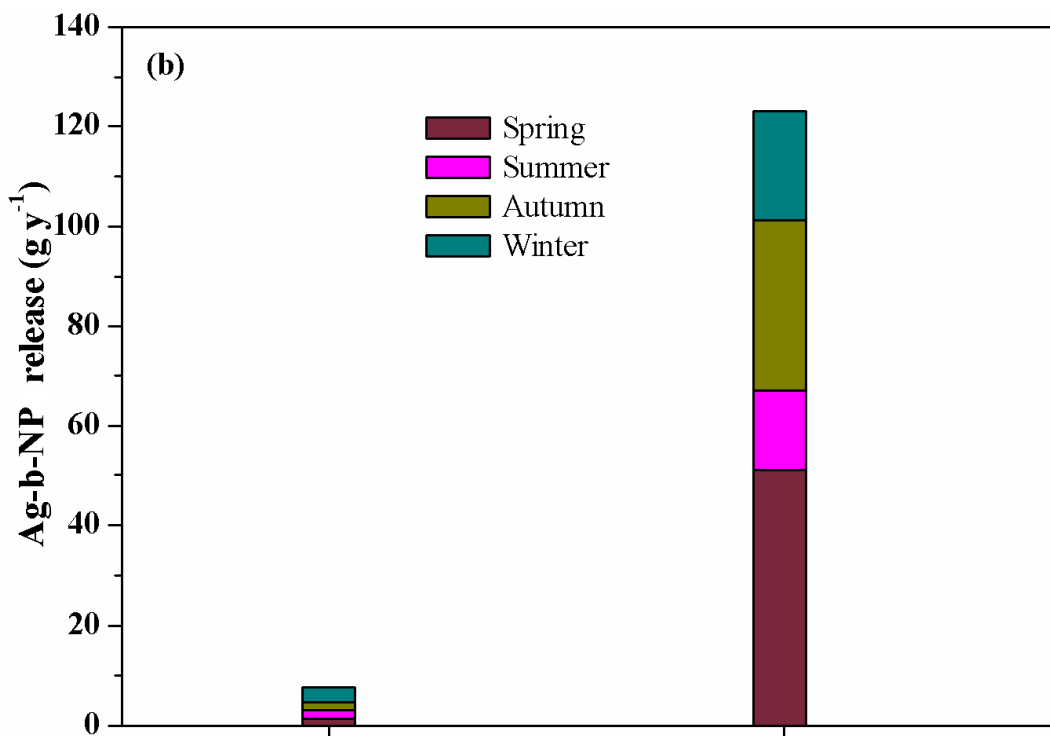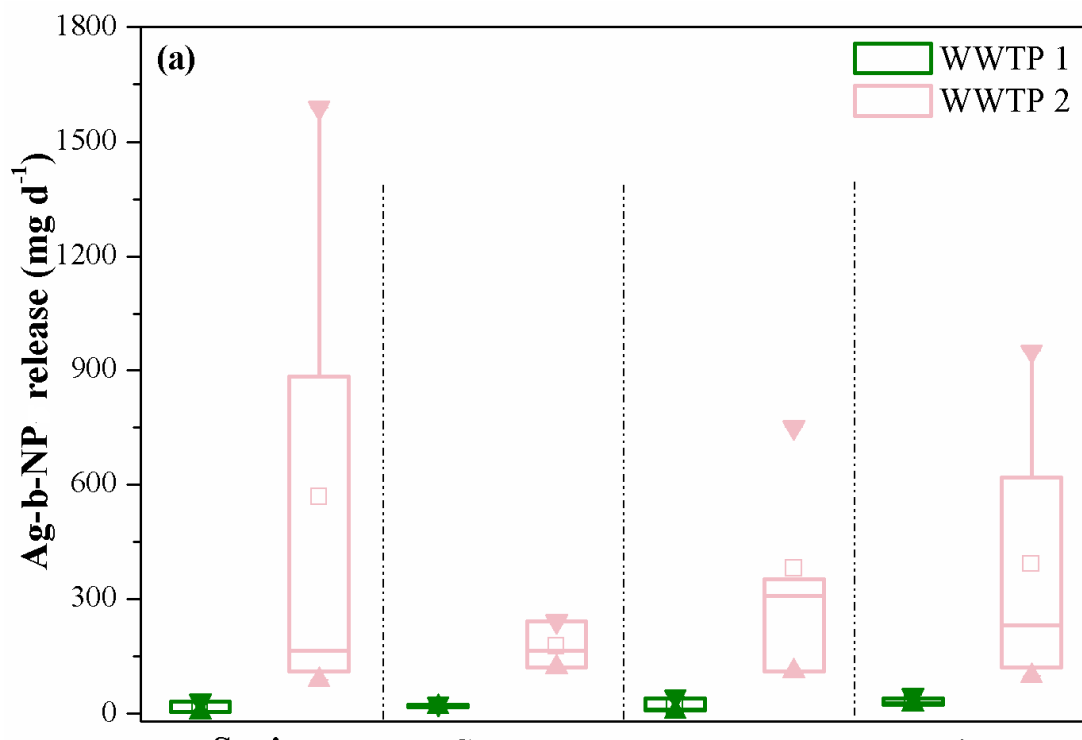
Fig. S5 Estimated Ag-b-NP fluxes associated with WWTP effluent. (a) daily and (b) annual Ag-b-NP fluxes to the

River Isar.

Table S1. Seasonal and weather influences on the influent flow rate of the investigated municipal WWTPs

		Date	Weather	Rainfall (mm/d)	flow rate of influent (m³/d)
WWTP 1	Spring	2014-5-5	cloudy	0.0	4,865
		2014-5-6	cloudy	0.0	4,820
		2014-5-7	rainy	13.1	5,219
		2014-5-8	rainy	0.6	4,930
		2014-5-9	rainy	3.3	4,852
	Summer	2013-7-16	sunny	0.0	5,487
		2013-7-17	sunny	0.0	5,523
		2013-7-18	sunny	0.0	5,640
		2013-7-22	sunny	0.0	5,302
	Autumn	2013-10-16	rainy	5.9	6,516
		2013-10-23	rainy	1.9	5,339
		2013-10-24	cloudy	0.01	5,247
		2013-10-25	sunny	0.0	4,976
		2013-10-29	cloudy	0.0	5,315
		2013-10-30	cloudy	0.0	5,207
	Winter	2013-11-5	rainy	1.9	5,250
		2013-11-6	rainy	6.3	5,433
		2013-11-7	cloudy	0.0	5,247
		2013-11-8	cloudy	0.0	5,006
WWTP 2	Spring	2014-5-2	rainy	1.3	180,300
		2014-5-6	cloudy	0.0	129,500
		2014-5-7	rainy	11.8	180,500
		2014-5-8	rainy	0.3	129,500
		2014-5-9	rainy	3.9	160,500
	Summer	2013-7-17	sunny	0.0	180,100
		2013-7-18	sunny	0.0	168,500
		2013-7-22	rainstorm	7.3	258,300
		2013-7-23	sunny	0.0	179,500
	Autumn	2013-10-21	cloudy	0.6	141,600
		2013-10-26	cloudy	0.1	147,000
		2013-10-27	rainy	0.7	155,300
		2013-10-28	cloudy	0.0	148,000
		2013-12-3	cloudy	0.0	136,000
		2013-12-4	cloudy	0.0	152,300
		2013-12-5	cloudy	0.02	151,400
		2013-12-10	cloudy	0.0	126,500
	Winter	2013-12-11	cloudy	0.0	144,600
		2013-12-12	cloudy	0.0	144,000
		2013-12-17	cloudy	0.0	139,200
		2013-12-18	cloudy	0.0	131,000
		2013-12-19	cloudy	0.0	140,100

Table S2. Basic characteristics of water samples from the River Isar. Total length of the river is 295 km

	Sampling site	pH	TOC (mg/L)	EC (mS/cm)
Upstream	1	8.2	n.d.	n.d.
	2	8.4	n.d.	n.d.
	3	8.4	n.d.	n.d.
	4	8.2	n.d.	n.d.
	5	8.2	n.d.	n.d.
	7	8.4	n.d.	n.d.
	8	8.4	2.13	0.45
	9	8.0	n.d.	0.49
Midstream	12	8.6	n.d.	0.49
	13	8.2	n.d.	0.50
	16	8.2	0.96	0.58
	17	8.3	0.85	0.57
	21	8.3	n.d.	0.58
Downstream	23	8.2	n.d.	0.52
	27	8.2	n.d.	0.54
	28	7.6	n.d.	0.61
	29	8.0	n.d.	0.54
	32	8.1	n.d.	0.54
	33	8.2	n.d.	0.55
Channel	34	8.4	n.d.	0.31
	35	8.3	n.d.	0.34
	36	8.4	n.d.	0.36
	39	7.8	n.d.	0.62
	40	8.3	n.d.	0.53
	41	7.8	n.d.	0.46
	42	8.1	n.d.	0.49
	43	7.9	n.d.	0.51

n.d.: not detected

Table S3. Location of sampling sites

	Number	Latitude	Longitude
	1	47.38916	11.264634
	2	47.43856	11.268847
	3	47.50343	11.286528
	4	47.65107	11.571643
	5	47.7604	11.557014
	6	47.9120	11.419208
	7	48.04057	11.516108
	8	48.16791	11.615542
	9	48.24129	11.673736
	10	48.28426	11.692419
	11	48.29526	11.698813
	12	48.34322	11.712873
	13	48.39745	11.751185
	14	48.40357	11.762644
	15	48.40234	11.786462
	16	48.41788	11.864825
River Isar	17	48.46112	11.946815
	18	48.46167	11.866348
	19	48.46754	11.911023
	20	48.47592	11.920593
	21	48.49849	11.953037
	22	48.49596	11.993609
	23	48.52051	12.110597
	24	48.53622	12.148319
	25	48.58510	12.228561
	26	48.59412	12.252687
	27	48.62035	12.35843
	28	48.65186	12.594808
	29	48.67491	12.678691
	30	48.67619	12.69457
	31	48.68025	12.719418
	32	48.77070	12.882153
	33	48.80385	12.975408
	34	48.20345	11.667402
	35	48.20927	11.705356
	36	48.22091	11.797495
	37	48.27871	11.860345
Channel Isar	38	48.29265	11.859776
	39	48.35386	11.88368
	40	48.38591	11.921017
	41	48.42460	11.983587
	42	48.45125	11.984617
	43	48.49028	11.985089

	1	47.92991	12.790161
	2	48.00348	12.41516
	3	47.92682	12.365035
	4	47.87324	12.237834
Lakes	5	47.92492	12.482623
	6	47.86818	12.505605
	7	47.85217	12.378232
	8	47.99446	11.353585
	9	47.82515	11.324231
	10	47.71369	11.741025

Table S4. Flow rates of River Isar at different sampling sites

Sampling site	Flow rates $(m^3\ sec^{-1})$	Mean flow rates over the year $(m^3\ sec^{-1})$
7	45	63.8
14	27	24.5
22	62	no data
24	138	162
30	140	168
32	150	174

Table S5. Basic characteristics of water samples from the pre-alpine lakes

Sampling site	TOC (mg/L)	pH	EC (mS/cm)
1	0.62	8.2	0.48
2	5.51	8.3	0.39
3	1.89	8.2	0.31
4	5.00	8.3	0.36
5	0.53	7.8	0.37
6	1.44	7.8	0.40
8	2.50	8.3	0.31
9	n.d.	8.2	0.32
10	3.34	8.3	0.40

n.d.: not detected

8.2 PUBLIKATION 2

Can cloud point-based enrichment, preservation, and detection methods help to bridge gaps in aquatic nanometrology?

Lars Duester, Anne-Lena Fabricius, Sven Jakobtorweihen, Allan Philippe, Florian Weigl, Andreas Wimmer, Michael Schuster, and Muhammad Faizan Nazar

Abdruck des Artikels mit allgemeiner Genehmigung (siehe Kapitel 7.2) aus Analytical and Bioanalytical Chemistry 2016, 408, 7551−7557.

CrossMark

FEATURE ARTICLE

Can cloud point-based enrichment, preservation, and detection methods help to bridge gaps in aquatic nanometrology?

Lars Duester[1] · Anne-Lena Fabricius[1] · Sven Jakobtorweihen[2] · Allan Philippe[3] ·
Florian Weigl[4] · Andreas Wimmer[4] · Michael Schuster[4] · Muhammad Faizan Nazar[5]

Abstract Coacervate-based techniques are intensively used in environmental analytical chemistry to enrich and extract different kinds of analytes. Most methods focus on the total content or the speciation of inorganic and organic substances. Size fractionation is less commonly addressed. Within coacervate-based techniques, cloud point extraction (CPE) is characterized by a phase separation of non-ionic surfactants dispersed in an aqueous solution when the respective cloud point temperature is exceeded. In this context, the feature article raises the following question: May CPE in future studies serve as a key tool (i) to enrich and extract nanoparticles (NPs) from complex environmental matrices prior to analyses and (ii) to preserve the colloidal status of unstable environmental samples? With respect to engineered NPs, a significant gap between environmental concentrations and size- and element-specific analytical capabilities is still visible. CPE may support efforts to overcome this "concentration gap" via the analyte enrichment. In addition, most environmental colloidal systems are known to be unstable, dynamic, and sensitive to changes of the environmental conditions during sampling and sample preparation. This delivers a so far unsolved "sample preparation dilemma" in the analytical process. The authors are of the opinion that CPE-based methods have the potential to preserve the colloidal status of these instable samples. Focusing on NPs, this feature article aims to support the discussion on the creation of a convention called the "CPE extractable fraction" by connecting current knowledge on CPE mechanisms and on available applications, via the uncertainties visible and modeling approaches available, with potential future benefits from CPE protocols.

Keywords Nanoparticles · Cloud point extraction · Colloids · Coacervate-based techniques · Enrichment · Sample preservation

Introduction

Coacervate-based techniques are intensively used in environmental analytical chemistry to enrich and extract different kinds of analytes. Most methods, also presented in several reviews (e.g., [1]), focus on the total content or the speciation of inorganic and organic substances. Size fractionation is less commonly addressed. Within coacervate-based techniques, the cloud point extraction (CPE) is characterized by a phase separation of non-ionic surfactants dispersed in an aqueous solution when the respective cloud point temperature (T_c) is exceeded. In the 1970s, Watanabe and co-workers presented a first series of studies describing methods capable to enrich metals from different matrices (e.g., [2]), and in 2009 Liu and co-workers published the first articles focusing on the extraction and pre-concentration of engineered nanomaterials by CPE [3].

✉ Lars Duester
duester@bafg.de

1 Department G2—Aquatic Chemistry, Federal Institute of Hydrology, Am Mainzer Tor 1, 56068 Koblenz, Germany

2 Thermal and Separation Processes, Hamburg University of Technology, Eißendorfer Straße 38, 21073 Hamburg, Germany

3 Environmental Chemistry, University of Koblenz-Landau, Fortstraße 7, 76829 Landau, Germany

4 Department of Chemistry, Technical University of Munich, Lichtenbergstraße 4, 85747 Garching, Germany

5 Department of Chemistry, University of Gujrat, Gujrat 50700, Pakistan

Springer

In this context, this feature article raises the question: May CPE in future studies serve as a key tool to (i) enrich and extract nanoparticles (NPs) from complex environmental matrices prior to analyses and to (ii) preserve the colloidal status of unstable environmental samples? With respect to engineered NPs, a significant gap between environmental concentrations (ng/L) and size- and element-specific analytical capabilities is still visible (µg/L or mg/L) [4]. CPE may support efforts to overcome this "concentration gap." Most colloidal environmental systems known (e.g., waste water, sediment pore water, or surface water) are unstable, dynamic, and prone to changes of the environmental conditions during sampling and sample preparation (e.g., impacted by the oxygen concentration). Even if samples are transported to the laboratory and analyzed as fast as possible, it remains questionable if the state "zero" (representing the in situ) status can be captured. This "sample preparation dilemma" in environmental nanometrology is often, in the absence of an adequate convention, ignored. An example for the impact of such a sample preparation convention is the operationally defined 0.45-µm filtration cut-off for the "dissolved fraction" in combination with an acidification of the samples to preserve the total metal content. When this convention was defined in the 1930s (with a focus on bacteria and the membranes available), it was already known that the term "dissolved" is wrong, since the cut-off allows colloids to pass the membrane. Nevertheless, creating this convention enabled the comparability of data worldwide. The authors are of the opinion that an operationally defined convention for size fractionation is also needed for NPs/colloids in unstable environmental or ecotoxicity test matrices. Such a convention could be supported by CPE-based methods. Focusing on NPs, this feature article sparks the discussion on the creation of a convention called the "CPE extractable fraction" by connecting (i) current knowledge on CPE mechanisms and on available applications, via (ii) the uncertainties visible and modeling approaches, with (iii) potential future benefits from CPE protocols.

Cloud point extraction

Phase separation and CPE theory

Referring to Nazar et al. 2011, the aqueous solutions of non-ionic surfactant micelles exhibit thermoreversible phase separation phenomena on heating/cooling through a T_c. As explained by the authors, T_c can be considered to be the upper stability temperature for the diluted dispersed micellar phase. By approaching T_c from lower temperatures, intermicellar interactions increase and clouding becomes visible. The previously transparent micellar dispersions scatters now light efficiently. As explained by the authors, above T_c micelle attractions dominate, and this generates a macroscopic separation in the diluted and the concentrated surfactant phases [5]. Furthermore, the authors describe that the phase behavior of certain non-ionic surfactants in aqueous solutions can readily yield a surfactant-rich phase with a reduced volumes above T_c and that from an economic and environmental point of view, the process is simple, cheap, highly efficient, and less environmentally hazardous compared to approaches containing organic solvents [5].

Several authors proposed mechanisms based on the phase separation phenomenon. It was suggested that above the T_c, a temperature-induced dehydration process occurs in the external layer of the micelles of the non-ionic surfactants. This is due to a decrease in the dielectric constant of water with an increase in temperature that reduces the interaction between the hydrophilic portion of surfactant and water [6]. By breaking hydrogen bonds between water molecules and hydrophilic chains of the surfactant with rising temperature, surfactant micelles become more hydrophobic and phase separation starts (Fig. 1).

Mechanisms

As previously published in several studies, it is proposed that for non-ionic surfactants the core is surrounded by a mantle of aqueous hydrophilic chains, and solubilization may occur in

Fig. 1 Schematic representation of the surfactant-mediated phase separation process

$T < T_c$ $T > T_c$ $T > T_c$

$T \uparrow$ Centrifugation

Transparent   Clouding   Phase separation

⬤ = NP   ⩶ = Surfactant (hydrophobic/hydrophilic part)   ✳ = Micelle
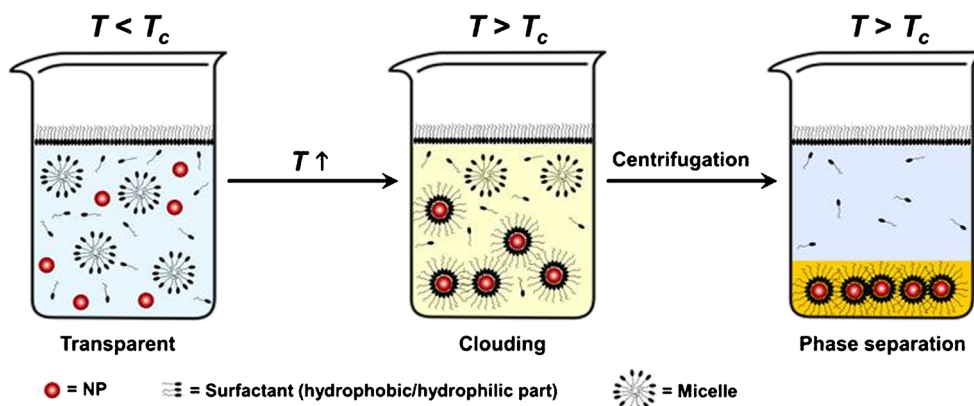
both (core and mantle), e.g., [7, 8]. As detailed by Purkait et al. 2004: The relative amount of solubilization in these two regions of non-ionic micelles depends on the ionic character of the solubilizate, and the non-ionic surfactants appear relatively to be more hydrophobic at higher temperatures due to an equilibrium shift that favors dehydration of the ether-groups. As T_c is approached, the solubilization of non-polar solubilizates increases. For polar solubilizates, solubilization decreases caused by dehydration of the nonpolar chains accompanied by increased coiling. In contrast, it is described by the authors that nonpolar compounds are solubilized in the core of micelles, while polar solubilizates are located on the mantle. The authors state that both of the mentioned temperature effects are also consistent with considerations on variations of the space available for the solubilized molecules in the micelles [8].

CPE and fractionation

Applications and uncertainties in enrichment and sample preservation

As mentioned before, Liu et al. were the first to apply CPE to concentrate and separate a variety of nanomaterials, like CdSe/ZnS quantum dots, Fe_3O_4, TiO_2, Ag and Au NPs, C_{60} fullerenes, and single-walled carbon nanotubes in aqueous samples [3]. Based on these early findings, CPE methods were worldwide designed to enrich and detect metal-containing NPs in complex matrices. Due to the variety of materials (including also core-shell particles), matrices, and CPE-protocols, a thorough validation for each specific application is inevitable to implement adequate procedures and to identify preparation steps and factors that influence and (potentially) bias the results. To support a better understanding on the current scientific status, in this section, a brief selection of methods, sorted by the target analyte and focusing on metal-containing NPs, is presented.

In different publications, Hartmann et al. optimized the CPE procedure for an enrichment of AuNPs and different AgNPs (including several particle coatings) from aqueous samples in the presence of the respective dissolved fractions [9, 10]. Using Triton X-114 as surfactant, an enrichment factor of 80 from an initial 40-mL sample volume was achieved. Besides different coatings and NP concentrations, the influence of matrix constituents on the extraction was examined. It was shown that the CPE protocols were capable to address different concentrations and a variety of coatings also in the presence of high contents of inorganic salts, colloids, or organic matter. Moreover, the particle size distribution determined using transmission electron microscopy (TEM) was constant for several hours. However, the results also showed that the extraction efficiency can be dependent on the particle size (e.g., 101 % for 2 nm and 52 % for 150 nm AuNPs) as well as that the coating (e.g., bovine serum albumin) possibly lowers the extraction efficiency. To increase traceability, an exemplary protocol to enrich Ag NPs developed by Hartmann et al. [10] is presented: 40 mL of a Ag NPs containing aqueous sample was mixed with 1.0 mL of saturated ethylenediaminetetraacetic acid disodium salt solution, 400 μL of 1 M sodium acetate, 100 μL of 1.25 M acetic acid, and 1 mL of 10 % (w/w) Triton X-114. The mixture was incubated at 40 °C for 30 min and centrifuged for 12 min at 4427 g to enhance phase separation. Afterwards, the samples were cooled in an ice bath for 5 min to increase phase separation. The aqueous supernatant was removed by decanting. The remaining surfactant-rich phase containing the enriched Ag NPs was dissolved in 100 μL ethanol and subjected to electrothermal atomic absorption spectrometry (ET-AAS) measurement.

Comparably, CPE procedures were established for CuO NPs and ZnO with enrichment factors of 100 and 220 and extraction efficiencies of almost 90 and 64–123 %, respectively [11, 12]. In the case of ZnO NPs, TEM and UV/Vis measurements revealed that particle size and shape were stable over 2 months of storage. By investigating the potential impact of several parameters (e.g., of natural organic matter (NOM)) on the extraction efficiency of CuO NPs, Majedi et al. demonstrated that an interfering effect of adsorbed NOM can be lowered by adding H_2O_2 [13]. To simultaneously address Ag, Au, and Fe_3O_4 NPs in a single CPE protocol, Tsogas et al. applied a sequential back-extraction and dissolution method of the extracted NPs with recoveries between 74 and 114 % [14]. The method was adapted to complex environmental matrices considering the challenges of co-extracted dissolved species.

Although some of the studies mentioned above addressed the effect of particle size on the extraction efficiency during CPE, it is of utmost importance to increase our understanding on size-resolved extraction efficiencies in order to define precisely the upper and lower particle size cut-off and to properly describe the "CPE extractable size fraction." So far, the storing capabilities of some CPE protocols are very promising (e.g., [12]). However, to increase the reliability, further investigations concerning size preservation capabilities of CPE for mid- and long-term storing purposes have to be undertaken for other engineered NPs and colloids. To gain a better understanding on the natural occurring processes, the relevant environmental concentration levels for engineered NPs (ng/L range) together with a high colloidal and particle background (mg/L range) should be addressed in the future.

Detectors and combination with size-specific methods

Together with the colloids and particles, various other substances (e.g., NOM) are known to be present in the

extracted phase [15]. Hence, like for almost any other method, the use of selective and sensitive determination techniques is essential for quantitative and qualitative NP analysis due to a limited species selectivity of CPE. ET-AAS is a quantitative, sensitive, and robust element-specific direct detection method for metal-containing NPs. The ET-AAS provides a good matrix tolerance by gradual temperature programs and an effective background correction option. Plasma-based mass spectrometer systems provide a sensitive multi detection opportunity in combination with CPE. However, in contrast to ET-AAS, the samples have to be diluted or digested prior to analyses, unless an ET oven is coupled to the spectrometer [16]. Even though size determination of NPs in environmental relevant concentrations (sub-ng/L up to µg/L) is still challenging, several options are available as a size-specific method after enriching the NPs by CPE: Microscopy-based methods, like TEM, are common tools to determine the size distributions of (nano)particles [9]. Advantages of the methods are the high resolution and a direct data evaluation. Drawbacks are limitations with respect to the particle concentration and the time required for data processing. CPEs enriching capabilities, prior to microscopy-based analyses, have the potential to improve the data reliability and the overall costs.

Size-specific separation techniques in combination with CPE and inductively coupled plasma-mass spectrometry (ICP-MS) are also promising tools. An advantage of the combination with CPE is, to a certain extent, a consistent matrix influence on the analysis. Examples for separation techniques are field-flow fractionation systems (e.g., asymmetric flow field-flow fractionation). However, in this context, the previously mentioned "concentration gap" between environmental concentration and laboratory methods becomes visible, and the CPE extraction and enrichment capabilities display also in this case a potential solution to overcome this gap. The single particle mode of ICP-MS (spICP-MS) appears to be another option to combine a high selectivity and good sensitivities with satisfying analyses times. Via species separation and fractionation, CPE can help to lower or even eliminate the background signal from dissolved species. Multi-element analysis is not sufficiently supported by currently available spICP-MS systems. New developments on time of flight analyzers in combination with spICP-MS allow simultaneous size determination of various elements and isotopes [17], and again future fractionation and NP enrichment multi-element methods may benefit from CPE.

Taken together, CPE can serve as a powerful enrichment and preservation tool for (engineered) NPs in complex environmental matrices in combination with different element- and size-specific detectors.

Applications and uncertainties in colloidal/dissolved species separation

As mentioned before, usually CPE protocols are designed to extract and pre-concentrate ionic species, organic substances, or NPs in the surfactant-rich phase. The aqueous phase is usually removed and (if at all) only analyzed to validate the CPE procedure. However, to examine the environmental fate and toxicity of engineered NPs, the information on dissolved fractions should also be taken into account. In some cases, the latter is simply calculated as the difference between the particulate and the total concentration. To the best of the authors' knowledge, only one publication analyzes the aqueous phase to determine the dissolved fraction obtained by application of the CPE [18]. Therefore, additional efforts and method development are needed to further optimize and validate CPE fractionation approaches for determining mass balances.

Regarding natural colloids, no optimized CPE protocol is available, yet. Natural organic colloids (e.g., humic substances) are so far addressed solely with regard to their influence on the extraction efficiency of engineered NPs [13].

Modeling

Due to their complex phase behavior, colloidal systems are difficult to model. Therefore, most of the models were based on correlations only. In quantitative structure–property relationship (QSPR) models, the target property is correlated with the compounds' properties and structures, where a training data set is needed to determine the parameters. As a result, the applicability is often limited to molecules similar to those in the training set. Furthermore, no information on the underlying atomistic phenomena is provided. Nevertheless, QSPR models for surfactants have been introduced for example for critical micelle concentrations, cloud point temperatures, surface tensions, biodegradation potentials, etc. [19]. For CPE, the T_c is a key property that is a priori unpredictable by any thermodynamic model yet. Even the molecular structures at the cloud point and in the micellar phase are not finally resolved. There is some controversy whether the structure is composed of giant micelles or of small aggregated micelles. However, this discrepancy may have been solved, as branched micelles were found near the cloud point [20]. If co-acervate systems are used for the enrichment of compounds, the partition behavior of these compounds between the aggregates (e.g., micelles) and the aqueous phase are another key property. Often, octanol/water partition coefficients are used to approximate partition coefficients in micellar systems. To predict partition behavior in such anisotropic systems, an extension of the thermodynamic model COSMO-RS, named COSMOmic, was introduced [21] and successfully applied to predict micelle/water partition coefficients [22]. Unfortunately, this model cannot take into account structural changes of micelles due to the insertion of

solutes and, hence, cannot be applied to NPs that alter the microstructures in the micellar phase. Due to the size of NPs, it is important to understand their interactions with surfactants and the microstructures formed with respect to these interactions. To predict suspension microstructures and phase behavior of micelle-NP systems, a statistical mechanical model was introduced that was found to be in agreement with experimental results of dilute suspensions and could be used to analyze colloidal interactions of polymer-like micelles [23]. Another option to investigate molecular structures is the application of molecular dynamics (MD) simulations. For example, with the aid of these simulations, aqueous systems containing cationic surfactants were recently studied. It was shown that the surfactants form a bilayer around NPs with negatively charged surfaces and monolayers around hydrophobic NPs [24].

In the future, it will be particularly important to understand the microstructures formed in coacervate systems. The T_c, as one of the key properties, can probably only be modeled on a physically sound basis, if the structures at the cloud point and in the colloidal phase are known. Furthermore, the microstructures formed between NPs and surfactants are of high interest. As these particles can have different morphologies, sizes, and coatings, a diverse variety of structures, especially after surface transformations in complex (environmental) matrices, are given. In addition, the large varieties of surfactants and surfactant-like natural compounds have different influences. Moreover, complex mixtures will influence the microstructures and therefore T_c and extraction efficiencies. To obtain a better understanding of these structures, MD simulations and experimental techniques should be used. As in other fields, a combination of both could help to overcome the limitations of a single method. MD simulations can give a detailed atomistic picture at the cost of computationally demanding simulations. Especially, NP systems can be demanding due to the large size (compared to molecules) of the particles. Although atomistic detail is preferable, the simulations could be speed-up by using coarse-grained models at the expense of losing atomistic details. Once the microstructures are understood, general conclusions may be drawn about the formation of these structures and the influencing factors. With this knowledge, it is then probably possible to introduce a thermodynamic model to predict T_c and partition behavior of NPs.

Future perspective: by convention—the CPE extractable fraction

Besides its usefulness to recover and re-use high-value engineered NPs or to remove NPs from industrial waste water, a large number of different CPE protocols applied to numerous scientific questions of different working areas (e.g., the extraction and/or pre-concentration of metal ions, NPs, or organic substances or the speciation of metals and metalloids [1]) make CPE today a powerful tool in environmental analytical chemistry.

Against this background, it is remarkable that the chance to combine state of the art multi-element analyses by means of ICP-MS with CPE is still fairly unexploited. As detailed in the mechanisms and the modeling sections, a lack of understanding of basic mechanisms of the fractionation process is still apparent. It should be further clarified, which compounds, in dependence of the protocol applied, are exactly included in the two phases. This is a challenge with respect to the experimental as well as the analytical settings, but is urgently needed to better understand and characterize the size fractionation principles. Prospectively, the development of more universal, but still easily implementable, routine-suitable procedures is desirable to increase the efficiency, reproducibility, and comparability of CPE applications. Automatization of the preparative steps and an on-line coupling to the detectors might become a solution. If future studies can address the mentioned uncertainties, CPE may become a key enrichment and, even more important, preservation method in environmental nanometrology and colloid sciences. To foster the potential of cost-efficient and simple CPE methods, (i) a better understanding on the basic CPE mechanisms, (ii) an open access data base with varying CPE protocols in complex matrices, and, finally, (iii) models on the micelle formation in complex systems are needed to create a convention on the "CPE extractable fraction." Even if the previous points appear challenging, the earning would be not less than an international common basis for coordinated environmental monitoring efforts on NPs and colloids. As a surplus, via a common convention to fix the status of dynamic colloidal systems, a higher reliability in environmental nanometrology can be achieved for spectroscopy, mass spectrometry, or microscopy-based analyses.

Compliance with ethical standards

Conflict of interest The authors declare that they have no conflict of interest.

References

1. Melnyk A, Namiesnik J, Wolska L. Theory and recent applications of coacervate-based extraction techniques. TrAC, Trends Anal Chem. 2015;71:282–92.

2. Watanabe H, Tanaka H. A non-ionic surfactant as a New solvent for liquid-liquid extraction of zinc(Ii) With1-(2-pyridylazo)-2-naph-thol. Talanta. 1978;25:585–9.

3. Liu J, Chao J, Liu R, Tan Z, Yin Y, Wu Y, et al. Cloud point extraction as an advantageous preconcentration approach for analysis of trace silver nanoparticles in environmental waters. Anal Chem. 2009;81(15):6496–502.

4. Duester L, Burkhardt M, Gutleb AC, Kaegi R, Macken A, Meermann B, et al. Toward a comprehensive and realistic risk evaluation of engineered nanomaterials in the urban water system. Front Chem. 2014;2:39.

5. Nazar MF, Shah SS, Eastoe J, Khan AM, Shah A. Separation and recycling of nanoparticles using cloud point extraction with non-ionic surfactant mixtures. J Colloid Interface Sci. 2011;363(2):490–6.

6. Nilsson PG, Wennerstroem H, Lindman B. Structure of micellar solutions of nonionic surfactants. Nuclear magnetic resonance self-diffusion and proton relaxation studies of poly(ethylene oxide) alkyl ethers. J Phys Chem. 1983;87(8):1377–85.

7. Hiemenz PC, Rajagopalan R. Principles of colloid and surface chemistry. 3rd ed. New York: CRC Press; 1997.

8. Purkait MK, Vijay SS, DasGupta S, De S. Separation of Congo Red by surfactant mediated cloud point extraction. Dyes Pigments. 2004;63(2):151–9.

9. Hartmann G, Schuster M. Species selective preconcentration and quantification of gold nanoparticles using cloud point extraction and electrothermal atomic absorption spectrometry. Anal Chim Acta. 2013;761:27–33.

10. Li L, Hartmann G, Döblinger M, Schuster M. Quantification of nanoscale silver particles removal and release from municipal wastewater treatment plants in Germany. Environ Sci Technol. 2013;47(13):7317–23.

11. Liu JF, Sun J, Jiang GB. Use of cloud point extraction for removal of nanosized copper oxide from wastewater. Chin Sci Bull. 2010;55(4–5):346–9.

12. Majedi SM, Lee HK, Kelly BC. Chemometric analytical approach for the cloud point extraction and inductively coupled plasma mass spectrometric determination of zinc oxide nanoparticles in water samples. Anal Chem. 2012;84(15):6546–52.

13. Majedi SM, Kelly BC, Lee HK. Evaluation of a cloud point extraction approach for the preconcentration and quantification of trace CuO nanoparticles in environmental waters. Anal Chim Acta. 2014;814:39–48.

14. Tsogas GZ, Giokas DL, Vlessidis AG. Ultratrace determination of silver, gold, and iron oxide nanoparticles by micelle mediated preconcentration/selective back-extraction coupled with flow injection Chemiluminescence detection. Anal Chem. 2014;86(7):3484–92.

15. Hartmann G, Baumgartner T, Schuster M. Influence of particle coating and matrix constituents on the cloud point extraction efficiency of silver nanoparticles (Ag-NPs) and application for monitoring the formation of Ag-NPs from Ag$^+$. Anal Chem. 2014;86(1):790–6.

16. Duester L, Rakcheev D, Bayer JV, Abraham PM, Dabrunz A, Schulz R, et al. A robust, particle size independent, method for quantifying metal(Loid Oxide) nanoparticles and their agglomerates in complex environmental matrices by electrothermal vaporisation coupled to ICP-MS. J Anal At Spectrom. doi:10.1039/C0JA00149J.

17. Borovinskaya O, Hattendorf B, Tanner M, Gschwind S, Guenther D. A prototype of a new inductively coupled plasma time-of-flight mass spectrometer providing temporally resolved, multi-element detection of short signals generated by single particles and droplets. J Anal At Spectrom. 2013;28(2):226–33.

18. Fabricius A-L, Duester L, Meermann B, Ternes TA. ICP-MS-based characterization of inorganic nanoparticles-sample preparation and off- line fractionation strategies. Anal Bioanal Chem. 2014;406(2):467–79.

19. Hu J, Zhang X, Wang Z. A review on progress in QSPR studies for surfactants. Int J Mol Sci. 2010;11(3):1020–47.

20. Dong R, Hao J. Complex fluids of poly(oxyethylene) monoalkyl ether nonionic surfactants. Chem Rev. 2010;110(9):4978–5022.

21. Klamt A, Huniar U, Spycher S, Keldenich J. Cosmomic: a mechanistic approach to the calculation of membrane-water partition coefficients and internal distributions within membranes and micelles. J Phys Chem B. 2008;112(38):12148–57.

22. Ritter E, Yordanova D, Gerlach T, Smirnova I, Jakobtorweihen S. Molecular dynamics simulations of various micelles to predict micelle water partition equilibria with cosmomic: influence of micelle size and structure. Fluid Phase Equilib. 2016;422:43–55.

23. Helgeson ME, Wagner NJ. Colloidal interactions mediated by end-adsorbing polymer-like micelles. J Chem Phys. 2011;135(8):084901.

24. Sarnbasivam A, Sangwai AV, Sureshkumar R. Self-assembly of nanoparticle-surfactant complexes with rodlike micelles: a molecular dynamics study. Langmuir. 2016;32(5):1214–9.

Lars Duester is an environmental scientist and obtained his PhD in environmental analytical chemistry at the University of Duisburg-Essen, Germany. In 2010, he joined the Department for Aquatic Chemistry at the Federal Institute of Hydrology. His current research interests are the fate of metal(loid)s in surface waters, soils, and sediments.

Anne-Lena Fabricius is a PhD student at the Department of Aquatic Chemistry of the Federal Institute of Hydrology. After her master degree in biology, within her PhD thesis, she focuses on methodological questions concerning the analyses (including size fractionation) of nanoparticle suspensions as well as on the fate metal(loid) containing natural colloids at sediment water interfaces.

Sven Jakobtorweihen is a group leader for molecular methods at the Institute of Thermal Separation Processes, Hamburg University of Technology. His research focuses on the application of molecular simulations in engineering and life sciences with the aim of a better atomistic understanding to enable molecular design. His studies encompass systems such as biological membranes, micellar systems, nanoporous materials, and complex formation. He also works on new algorithms, computer code, and force field parameters for molecular dynamics and Monte Carlo simulations.

Andreas Wimmer received his master's degree in chemistry at Technical University of Munich in 2015. His master's thesis dealt with the size selective determination of silver nanoparticles in river water or sewage sludge. Currently, he is doing his PhD program at the working group for analytical chemistry at Technical University of Munich examining the combination of separation and enrichment procedures for nanoparticles in environmental samples with several analytical techniques, e.g., sp-ICP-MS.

Allan Philippe has completed his PhD in 2015 at the Institute of Environmental Chemistry at Koblenz-Landau University on the interactions of natural organic matters and engineered nanoparticles and on the development of HDC-ICP-MS for environmental samples. He is currently working at the University Koblenz-Landau on the further development of analytical techniques and methods development for characterizing colloids in environmental matrices. His research interests also encompass the fate of nanomaterials in water, sediment, and soil compartments.

Michael Schuster is Professor and Head of the Working Group Analytical Chemistry at the Technical University of Munich, Germany. His research interests are within trace and ultra-trace analysis of elements and element species in complex matrices.

Florian Weigl achieved his master's degree in chemistry at Technical University of Munich (TUM) in 2015. In the same year, he started his PhD at the working group for analytical chemistry on the development of enrichment and characterization techniques for nanoparticles in environmental samples. His main focus is the coupling of those procedures to ICP-MS and other detection techniques.

Muhammad Faizan Nazar is specialized in colloids and surfactants. He obtained his Ph.D. in physical chemistry from Quaid-i-Azam University Islamabad, Pakistan, in 2011. He is currently working as Assistant Professor at the University of Gujrat, Pakistan. His research interests include colloidal self-assembly fluids and their applications in pharmaceuticals and nanoparticles technology.

8.3   PUBLIKATION 3

Separating Dissolved Silver from Nanoparticulate Silver is the Key: Improved Cloud-Point-Extraction Hyphenated to Single Particle ICP-MS for Comprehensive Analysis of Silver-Based Nanoparticles in Real Environmental Samples Down to Single-Digit nm Particle Sizes

Andreas Wimmer, Alexander Urstoeger, Tobias Hinke, Margit Aust, Philipp J. Altmann, and Michael Schuster
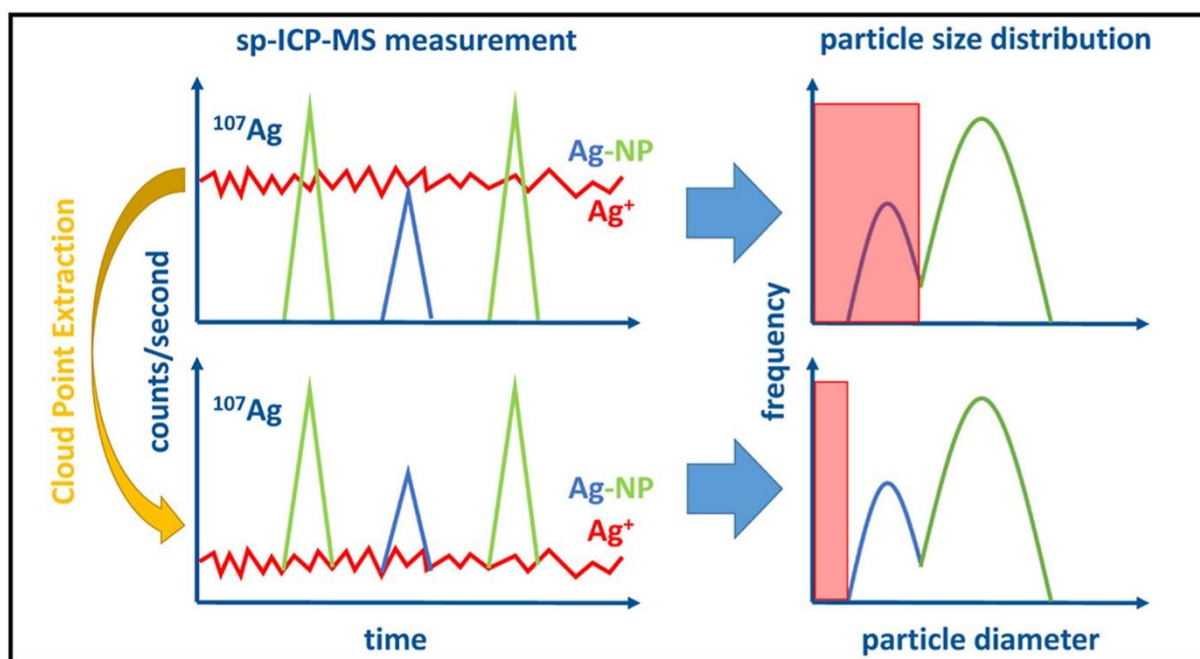
Separating dissolved silver from nanoparticulate silver is the key: Improved cloud-point-extraction hyphenated to single particle ICP-MS for comprehensive analysis of silver-based nanoparticles in real environmental samples down to single-digit nm particle sizes

Andreas Wimmer [a, 1], Alexander Urstoeger [a, 1], Tobias Hinke [a], Margit Aust [a], Philipp J. Altmann [b], Michael Schuster [a, *]

[a] Division of Analytical Chemistry, Department of Chemistry, Technical University of Munich, Garching, 85748, Germany
[b] Catalysis Research Center, Technical University of Munich, Garching, 85748, Germany

GRAPHICAL ABSTRACT
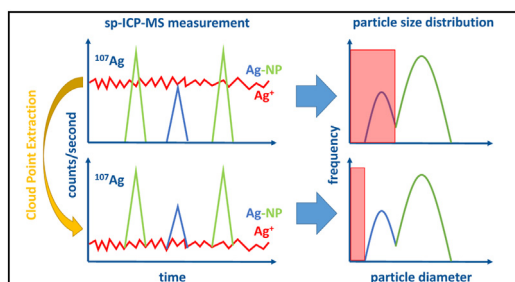
ARTICLE INFO

ABSTRACT

Investigating silver-based nanoparticles (Ag-b-NPs) in environmental samples is challenging with current analytical techniques, owing to their low concentrations (ng L^{-1}) in the presence of high quantities of dissolved Ag(I) species. sp-ICP-MS is a promising technique able to simultaneously determine the concentration and particle sizes of Ag-b-NPs even at concentrations of several ng L^{-1}. However, sp-ICP-MS suffers from the coexistence of dissolved analyte species causing high background signals. These background signals cover particle signals and therefore limit the size detection limit (SDL) in sp-ICP-MS. Ag-b-NPs in environmental samples exhibit diameters of < 20 nm, whereas the current sp-ICP-MS approaches barely reach an SDL as low as 20 nm. Using a surfactant-mediated sample pre-treatment (improved cloud point extraction, iCPE), we were able to separate Ag-b-NPs in aqueous samples from dissolved Ag(I) species and enrich the NPs in the extract. By hyphenating iCPE to sp-ICP-MS, we were able to reach SDL values as low as 4.5 nm, thus paving the way for the successful monitoring of Ag-b-NPs in the environment.

---

* Corresponding author.
   E-mail address: michael.schuster@tum.de (M. Schuster).
[1] These authors contributed equally to the present study.

1. Introduction

Silver-based nanoparticles (Ag-b-NPs) are being widely applied due to their antimicrobial properties, such as in consumer products, fabrics, and surgery products [1–9]. However, concerns are being raised about the threats NPs might present to the environment. During usage of such products or their disposal, Ag-b-NPs may be released into (waste)water streams, pass wastewater treatment plants [10,11], and finally reach natural water bodies [12,13]. Moreover, it has recently been shown that Ag-b-NPs even occur for natural reasons to a very slight extent in lakes due to a reduction of dissolved Ag(I) species [14].

Despite benefits of Ag-b-NPs, emerging technologies should always go hand-in-hand with a balanced risk assessment. In general, the risk of Ag-b-NPs in the environment is derived from three main features: the elemental composition, the concentration and the size distribution. Since Ag^+ deriving from Ag-b-NPs is assumed to be the relevant toxic agent in the environment, Ag species having a lower solubility, such as Ag_2S, exhibit a limited environmental impact [15]. Furthermore, smaller particles have a higher intrinsic surface and therefore exhibit an enhanced release of Ag^+ eventually increasing the NPs' environmental impact [16].

Literature reports toxicity of Ag-b-NPs and Ag(I) to human and environmental health in the $\mu g\ L^{-1}$ range and above [1]. To the best of the authors knowledge, no toxic effects of $ng\ L^{-1}$ traces of Ag-b-NPs and Ag(I) have been reported so far. However, Ag-b-NP and Ag(I) traces are prone to accumulation in the environment and may eventually represent a potential threat to human and environmental health.

Therefore, establishing an analytical approach that is able to simultaneously determine the concentration and size distribution of Ag-b-NPs is regarded essential. Electron microscopy, for instance, enables the determination of particle size distributions. However, such measurements are time-consuming and require extensive sample pretreatment and instrumental effort, resulting in distributions based on only several hundred NPs. In contrast, single particle inductively coupled plasma mass spectrometry (sp-ICP-MS) allows for a fast and simultaneous determination of concentration and particle size distribution. This approach leads to results within minutes, with distributions being based on large numbers of particles. Consequently, size distributions measured by sp-ICP-MS are much more reliable and practicable than those acquired by electron microscopy.

In sp-ICP-MS, the analyte mass is recorded in a time-resolved manner. Instrument noise and dissolved ionic analyte species lead to a continuous signal in the mass spectra representing a background signal. As to the particulate analytes, they are atomized to an ion cloud in the plasma, whereas ions derived from one single particle reach the detector of the mass spectrometer more or less simultaneously. Since sp-ICP-MS detectors record signal intensity consecutively and with very short detection times (the so-called dwell time), NP atomization events in the plasma are recorded as time-resolved transient peaks. Once separated from the background signal, these peaks are eventually converted into particle size distributions and mass concentration of the nanoparticulate analyte [17,18].

However, sp-ICP-MS suffers from some limitations − especially regarding environmental samples. The size detection limit (SDL) in sp-ICP-MS represents the minimum particle size detectable at a reasonable confidence level. The peak signal area is proportional to the size of the corresponding particle ionized in the plasma. Smaller particles cause signals that are not distinguishable from the background signal anymore. Therefore, high background signals lead to an increase of the SDL. Environmental samples containing Ag-b-NPs regularly also contain significant traces of dissolved Ag(I)

species resulting in high background signals overlapping the NP peaks. Ag(I) concentration, thus, correlates with the size detection limit (SDL) of Ag-b-NPs [19]. The current literature regards 20 nm as the minimum SDL for Ag-b-NPs [19]. This is insufficient for environmental analysis because Ag-b-NPs in environmental samples are assumed to be smaller than this 20 nm limit. In fact, Kim et al. have reported on Ag-b-NPs in sewage sludge at the 5−20 nm size [20]. The literature suggests diluting the sample in order to decrease the background signal, which is, however, counterproductive to analysis sensitivity, especially in view of the low analyte concentration [17,19,21−23]. In fact, Ag-b-NPs in natural water bodies are present at the level of several $ng\ L^{-1}$ [11,12,24], which is far beyond the limit of detection (LOD) in current sp-ICP-MS approaches. Finally, additional environmental constituents in real water samples have to be separated prior to measurement in order to avoid cone clogging of the ICP instrument. Therefore, in order to achieve environmental applicability of sp-ICP-MS, it is essential to both enrich Ag-b-NPs and to separate them from the matrix constituents and dissolved Ag(I) species so as to obtain proper LODs in the low $ng\ L^{-1}$ range and an SDL < 20 nm.

In order to separate the NP signal in sp-ICP-MS from the background signal, various approaches have been suggested, mainly based on mathematical models. Mozhyeva et al., for instance, presented a data deconvolution approach for the extraction of such peaks in the presence of high background signals using microsecond time resolved signals [25]. In order to achieve SDL values sufficient for environmental analysis, we sought to physically separate dissolved Ag(I) species from NPs prior to the measurement, without the need of mathematical discrimination techniques. Therefore, we hyphen a new coacervate-based technique, namely cloud point extraction (CPE), to (sp)-ICP-MS in order to overcome the aforementioned limitations by enriching and separating Ag-b-NPs from aqueous media. Recently, Torrent et al. applied CPE hyphenated to sp-ICP-MS for detection of Ag-b-NPs in soil leachates. A limited background elimination, however, resulted in SDL values of 40 nm, which is insufficient for environmental water samples of the present study [26].

CPE is a sample pretreatment method able to species-selectively enrich and extract Ag-b-NPs from aqueous (environmental) samples. In the 1970s, Watanabe et al. were the first to describe CPE for the extraction of metals from aqueous samples [27] and, thereafter, Liu et al. applied this technique to the extraction of NPs [28]. The samples are mixed with non-ionic surfactants at concentrations exceeding their critical micellar concentration and heated above the respective cloud point temperature. This results in the formation of micells and, thus, a two-phase system comprising aqueous and surfactant rich phase. Ag-b-NPs are "trapped" in the micelles and separated together with the surfactant rich phase. Owing to the volume reduction during extraction in the surfactant rich phase, high enrichment rates can be achieved (approximately factor of 80 considering a 500 μL surfactant rich extract from an initial aqueous phase of 40 mL) [29−32]. The use of CPE for Ag-b-NPs has been thoroughly investigated and validated by our group, whereas quantification of the extracted Ag-b-NPs was achieved by hyphenation to electro thermal atomic spectrometry (ET-AAS), which is a solely quantitative technique [11,29−32]. However, this approach lacks information about the size distribution of Ag-b-NPs.

Therefore, we are in this study (i) presenting an improved version of CPE (hereinafter called iCPE) which exhibits improved species selectivity. In order to obtain size information of nanoparticulate analytes, (ii) iCPE extracts are measured using sp-ICP-MS. Owing to the significantly reduced co-extraction of dissolved Ag(I) species into the surfactant rich phase, (iii) we also studied improvements regarding the SDL of sp-ICP-MS measurements. We further (iv) examined iCPE-sp-ICP-MS with regard to particle size

distribution and parameters influencing the size results, with a special focus on the dwell-time. We finally (v) compared the quantitative results of iCPE-(sp)-ICP-MS hyphenation to the previously validated and established CPE-ET-AAS approach [30,32].

2. Experimental section

2.1. Materials

This study was conducted using citrate-stabilized silver (CA@AgNPs) and gold nanoparticles (CA@AuNPs) of different size. Experiments including dissolved Ag(I) species applied a dissolved Ag(I) ICP-standard (AgNO$_3$ in 3% HNO$_3$). Main reagents for iCPE are acetic acid and sodium acetate anhydrous and the complexing agents ethylenediaminetetraacetate disodium salt dihydrate (Na$_2$EDTA·2H$_2$O; C$_{10}$H$_{14}$N$_2$Na$_2$O$_8$·2H$_2$O) and D-penicillamine (PA, C$_5$H$_{11}$NO$_2$S). All chemicals were of at least analytical grade and ultra pure water (UPW) was used as diluent. For details regarding used materials, please see the Appendix.

The natural water was sampled in Garching, Germany, from the "*Wiesäckerbach*" stream in June 2016. According to the conventional ICP-MS quantification of Ag in the stream water, the samples contained no Ag beyond the limit of detection (0.15 ng L^{-1}). The water samples were thus used as blank matrix for the further experiments.

2.2. Instrumentation

In essence, the Ag quantification in this study was performed using two different measurement approaches: (i) ET-AAS and (ii) ICP-MS. The latter can be run in conventional ICP-MS mode for the Ag quantification, and in single-particle mode (sp-ICP-MS) for the simultaneous determination of particle size distribution and concentration of nanoparticulate Ag.

2.2.1. ET-AAS

Ag quantification was conducted with a Zeeman-corrected ET-AAS instrument (AAnalyst 800, PerkinElmer, Waltham, MA, USA) equipped with a transversally heated THGA 800 graphite tube atomizer and an AS-72 autosampler. Highly pure Argon 4.8 (Westfalen, Münster, Germany) served as the inert gas during measurements. A silver hollow cathode lamp (Photron, Victoria, Australia) was operated at the recommended current of 10 mA, and the silver quantification was based on the absorption line at λ = 328.1 nm at an integration time of 5 s. The temperature program of the graphite furnace for the quantification Ag in organic extracts of iCPE followed an approach previously developed in our working group [32].

2.2.2. (sp)-ICP-MS

(sp)-ICP-MS measurements were performed on a quadrupole mass spectrometer 7900 ICP-MS (Agilent, Santa Clara, CA, USA) equipped with a SPS4 autosampler (Agilent) and a MicroMist nebulizer (Glass Expansion, Melbourne, Australia). Argon 4.8 (Westfalen, Münster, Germany) was used as the plasma gas.

Regarding ICP-MS, the Ag quantification was performed by targeting [107]Ag (no isobaric interferences) in He collision cell (CCT) mode in order to reduce polyatomic interferences via kinetically energy discrimination. [115]In was used as the internal standard.

In sp mode, the dwell time was set to a value ranging from 100 μs to 1000 μs for an acquisition time of 60–90 s. [107]Ag was chosen as the target mass, and the pump rate was gravimetrically determined as 0.310 mL min^{-1}. The transport efficiency η describes the proportion of initial particles in the sample finally reaching the detector. CA@Au-NP dispersions (RM 8012, 8013) were used for

determining η, following a previously approved procedure [17,33]. Elemental sensitivity was calibrated using a 1 μg L^{-1} Ag(I) standard solution to compensate for an element-specific signal intensity. Particle size distributions were evaluated using Agilent's Mass-Hunter Workstation 4.4 (version C.01.04, build 544.3) software equipped with the Single Nanoparticle Application Module. sp-ICP-MS analysis relies on certain approximations: the investigated CA@Ag-NPs are assumed to be of a spherical shape exhibiting the density of the bulk material Ag (ρ = 10.49 g cm^{-3}). See Table A.1 for further instrumental details on sp-ICP-MS measurements.

2.2.3. Total organic carbon (TOC) measurements

The TOC of real water samples was determined using a TOC-L CSH/CSN analyzer (Shimadzu, Kyoto, Japan). All samples were measured in undiluted form without filtration and mixed thoroughly seconds before starting the TOC analysis. For calibration, standard solutions containing 10–100 mg L^{-1} TOC in UPW were prepared from potassium hydrogen phthalate solutions.

2.2.4. Electron microscopy

Transmission Electron Microscopy (TEM) was applied as a supplementary technique for particle size determination. TEM measurements were conducted using a TEM Jeol 1400 plus instrument equipped with a LaB$_6$ filament at an operating voltage of 120 kV along with a CCD-camera. (JEOL, Freising, Germany). Samples were measured on a copper grid covered with a continuous carbon film (Micro to Nano, Haarlem, the Netherlands).

2.2.5. X-ray diffractometry

Regarding the crystal structure analysis, the X-ray intensity data were measured on a Bruker (Billerica, MA, USA) D8 Venture Duo IMS system equipped with a Helios optic monochromator and a Mo IMS microsource (λ = 0.71073 Å). CCDC 2006750 contains the supplementary crystallographic data for this paper. These data can be obtained free of charge from The Cambridge Crystallographic Data Centre. Please see the Appendix for further crystallographic details.

2.3. Cloud point extraction (CPE)

This study seeks to further improve CPE, i.e. maximally reduce the co-extraction of dissolved Ag species without affecting the extraction efficiency (EE) of Ag-b-NPs [30–32]. In brief, 40 mL of an aqueous sample containing Ag-b-NPs was mixed with 400 μL of 1 M sodium acetate solution, 1 mL of 1.25 M acetic acid, and 1 mL of 10% TX-114 (w/w) [9–31]. In addition to the established CPE approach, a mixture of the multidental ligands EDTA and PA was applied in iCPE. Like EDTA, PA is able to complex Ag(I) and form highly hydrophilic complexes. For method development, 1–5 mL of saturated EDTA and 1–3 mL of 0.1 M aqueous PA solution were added to the aforementioned CPE mixture (best results were achieved for 3 mL of saturated EDTA solution and 1 mL of 0.1 M PA; see results below). The iCPE mixture was thoroughly mixed and incubated at 40 °C for 30 min. Afterwards, phase separation was accelerated by means of centrifugation (4500 g, 12 min), and both phases were separated by decanting the aqueous phase. The remaining Ag-b-NP-containing organic phase was mixed with 100 μL of EtOH in case the extract was forwarded to ET-AAS measurement or mixed with 500 μL of EtOH and UPW to reach a final volume of 10 mL in case the extract was forwarded to conventional ICP-MS and sp-ICP-MS techniques.

2.4. Hyphenation of iCPE to quantitative analytical techniques

As presented above, the iCPE extract was investigated by means

of ET-AAS and ICP-MS. Since the extract consisted mainly of the surfactant and was highly viscous, the sample introduction was challenging.

2.4.1. iCPE-ET-AAS

ET-AAS tolerates high concentrations of organic matrix constituents. The organic extract was mixed with only 100 µL of EtOH (to reduce sample viscosity) and transferred via a low-volume pipette (20 µL) into the graphite furnace of the ET-AAS instrument. Considering an initial sample volume of 40 mL and 500 µL of resulting extract, an enrichment factor of 80 was achieved.

2.4.2. iCPE-ICP-MS and iCPE-sp-ICP-MS

ICP-MS instruments are more sensitive to highly viscous samples. Therefore, the iCPE extracts were mixed with 500 µL of EtOH and gravimetrically filled with UPW to a total volume of 10 mL. The samples intended for sp-ICP-MS analysis were forwarded to measurement without further treatment. Samples intended for conventional ICP-MS analysis further contained 3.25% HNO_3 (v/v) in order to dissolve NPs and increase sample homogeneity. An enrichment factor of approximately 4 was achieved.

2.5. iCPE method development

ET-AAS and ICP-MS are not able to distinguish between particulate and dissolved Ag, and sp-ICP-MS results are distorted by dissolved Ag traces in the sample. Thus, species selectivity during iCPE is crucial. Therefore, we focused on (i) minimizing the co-extraction of dissolved Ag(I) into the organic phase, (ii) improving size selective EE for Ag-b-NPs, and (iii) reducing the influence of the natural water matrix on the iCPE outcome.

2.5.1. Co-extraction of dissolved Ag(I)

Several solutions containing ng L^{-1} amounts of Ag(I) in 40 mL UPW were prepared. iCPE was applied to all of the samples, whereas the amount of EDTA and PA was varied. As comparison, CPE without ligand addition was carried out (hereinafter referred to as CPE^0). The iCPE and CPE^0 extracts were measured by means of ET-AAS. The signal intensities measured relate to the co-extraction of dissolved Ag(I) species into the organic phase.

2.5.2. Size dependency of the extraction efficiency (EE)

Calibration of iCPE-ET-AAS or iCPE-ICP-MS can be performed using calibration samples containing Ag-b-NPs of known concentration forwarded to the same extraction procedure as the unknown samples. It is intended that the system can be calibrated using Ag-b-NPs of arbitrary size (within a broad range of 10 to 100 nm diameter). This is only valid if there is no size dependent EE. To investigate potential size effects, 40 mL of UPW were mixed with CA@AgNPs of varying size (10, 20, 40, 60, 80, 100, 200 nm) and forwarded to iCPE. To mimic the case of 100% EE, the same type and amount of NPs were added to the organic extracts <u>after</u> iCPE of UPW-only samples (reference). The extracts were measured by means of ET-AAS. The EE can be calculated by dividing the signal intensities measured for the NP-containing extracts by the signal intensities measured for the reference.

2.5.3. Influence of the natural water matrix

Freshly sampled river water (TOC 2.5 mg L^{-1}; initial β_{Ag} < 0.15 ng L^{-1}) was spiked with specific amounts of dissolved Ag(I) standard, yielding in final concentrations of 5, 10 and 50 ng L^{-1} Ag(I). Further, a non-spiked blank river water sample was also subjected to iCPE as basis for evaluation. Moreover, the same amount of Ag(I) as used in the spiked samples was added to the organic extracts after iCPE of blank river water, thus mimicking the

case of 100% co-extraction. Spiked samples and samples mimicking 100 % co-extraction were measured by ET-AAS and signal intensities were divided by the signal intensities measured for blank samples to gain the factor for signal increase compared to the blank sample.

2.6. Calibration approaches

As relative quantification techniques, ET-AAS and (sp)-ICP-MS require calibration samples of known analyte concentration. If calibration samples are not pre-treated similar to unknown samples, potential enrichment factors occurring during the sample pretreatment must be considered for data evaluation. sp-ICP-MS requires a calibration approach which significantly differs from the conventional techniques [17].

2.6.1. iCPE-ET-AAS/AgNPs as the calibrant

All experiments were related to iCPE-ET-AAS, a hyphenation which has already been thoroughly developed and validated in our working group [30–32]. It is noted, that no influence of using the iCPE approach instead of the CPE approach could be observed for (i) CPE-ET-AAS (data not shown). The calibration samples containing 60 nm CA@AgNPs of known concentration in the range of β_{Ag} = 5–30 ng L^{-1} were subjected to iCPE together with the unknown samples. This offered the advantage that both the calibration and the unknown samples undergo the same enrichment and are present in the same matrix. The iCPE extracts were diluted as described above in section 2.4.1 and forwarded to ET-AAS.

2.6.2. iCPE-ICP-MS/AgNPs as the calibrant

Calibration samples of iCPE-ICP-MS/AgNP were identical to those for iCPE-ET-AAS/AgNP. The iCPE extracts were diluted as described above in section 2.4.2 and forwarded to ICP-MS. Nebulization in the ICP-MS process was highly dependent on the viscosity of the sample. Given that both the calibration and the unknown samples were present in the same matrix, the nebulization required no correction.

2.6.3. iCPE-ICP-MS/Ag(I) as the calibrant

Here, solutions of dissolved Ag(I) (5–150 ng L^{-1}) served as the calibrant instead of NPs. Since these solutions underwent no iCPE, they were prepared in a UPW matrix (acidified to 3.25% (v/v) HNO_3) including 5% (v/v) of 10% TX-114 (w/w) and 5% (v/v) ethanol to mimic iCPE extract matrix. Samples of 40 mL resulted in a 10 mL diluted iCPE extract forwarded to measurement. Since the calibration solutions were not subjected to the iCPE enrichment, this enrichment factor must be considered in the data evaluation (division by a factor of 4).

2.6.4. iCPE-sp-ICP-MS/AuNPs + Ag(I) as the calibrant

According to Peters et al. [17], all calculations were based on the pump rate, which has been gravimetrically determined as 0.310 mL min^{-1}. The nebulization efficiency η was calculated on the basis of a dispersion containing CA@Au-NPs (RM 8012 and 8013) [17,33]. The elemental sensitivity was calibrated using a 1 µg L^{-1} Ag(I) solution. All calibration samples used were prepared in a matrix consisting of 5% (v/v) TX-114 (10% (w/w)) and 5% (v/v) ethanol. This ensured that both the calibration and the unknown samples were of the same matrix and behaved similarly during nebulization and atomization in the plasma. We investigated the influence of different dwell times (100–1000 µs). We also investigated the consistency of η and how it is influenced by surfactant content. Therefore, η was determined on the basis of several independently prepared CA@AuNP calibration samples containing various quantities of TX-114 and EtOH ranging from 0.5% (v/v) to

1.0% (v/v) (TX-114 10% (w/w)) and 5% (v/v) to 10% (v/v) (EtOH), respectively.

2.7. Determining the SDL of iCPE-sp-ICP-MS

As explained above, the SDL of sp-ICP-MS is highly dependent on the constant background signal overlapping with the transient particle signals. In order to determine the SDL, we mixed UPW with increasing amounts of dissolved Ag(I) (0, 10, 50, 100, 500 ng L^{-1}), carried out sp-ICP-MS measurements with and without iCPE prior to measurement and compared the received single particle mass spectra. The Ag(I) concentrations were chosen so as to represent environmentally-relevant levels (~0–100 ng L^{-1}) [11,12] and a concentration exceeding environmental scenarios (500 ng L^{-1}).

2.8. Error calculations

Three independent aliquots were treated and measured individually in all of the measurements conducted. Each sample was measured using three replicates (U, n = 3). The uncertainty U was calculated via Gaussian error propagation in consideration of pipetting uncertainties and standard deviations of the independently measured aliquots. Blank samples were used to correct Ag concentrations in all incubation experiments.

3. Results and discussion

3.1. Crystal structure of $C_{10}H_{14}Ag_2N_2O_8$

During iCPE, the dissolved Ag(I) species were complexed both by EDTA and PA. The crystal structure of Ag(I)-PA complexes is well known in the literature [34] and is described as eight Ag(I)-PA monomers connected with a nearly linear AgS$_2$-coordination. Two intertwined polymeric strands in a double helix assembly are formed as a result [34]. As,- to the best of the authors' knowledge- no structure for Ag(I)-EDTA complexes has yet been published, we investigated the corresponding crystal structure. This is especially interesting because complexation of the d^{10} metal species Ag(I) in the octaedric coordination sphere of EDTA may be challenging. The preparation of the crystallized Ag-EDTA complex is presented in the Appendix. The elemental analysis revealed a sum formula of $C_{10}H_{14}Ag_2N_2O_8$, indicating that the Ag(I)-EDTA complex comprises two Ag(I) ions for each EDTA molecule. The Ag(I)-EDTA complex crystallizes in spacegroup C2/c from UPW. The Ag(I) ions are coordinated by three oxygen atoms of adjacent carboxylate groups in a distorted trigonal fashion (Ag1–O1 2.178(2) Å, Ag1–O4 2.220(2) Å, Ag1–O4' 2.506(2) Å). Two silver ions form handles which are held together by argentophilic interactions [35] at an Ag–Ag distance of 3.2005(6) Å, which is well below the sum of their van der Waals radii (3.44 Å). Both amine groups of the EDTA ligand are protonated, so they do not participate in metal coordination. The *N*-bound protons form intramolecular H-bonds to the non-coordinating oxygen atoms of the spatially closest carboxyl group. These properties result in an overall three dimensional polymeric structure, as shown in Fig. A.1.

3.2. Reducing the co-extraction rates of Ag(I) by means of iCPE

The previously developed CPE approach indeed exhibits good species selectivity for Ag-b-NPs [30,32]. However, coupling CPE to ICP-MS, and especially sp-ICP-MS places even greater demands on species selectivity. We developed iCPE to reduce the co-extraction of dissolved Ag(I) species into the organic extract to an absolute minimum by applying a mixture of EDTA and PA during the iCPE process. To investigate the optimum amount and ratio of both

ligands, co-extraction for solutions initially containing 500 and 1000 ng L^{-1} Ag(I), respectively, underwent iCPE using a varying amount of EDTA and PA (see section 2.5.1). The Ag(I) concentrations were chosen to represent the upper limit of environmentally-relevant Ag traces [11,12]. If co-extraction is minimized for such relatively high values, then the approach is even more suitable for environmentally-relevant Ag traces in the low ng L^{-1} range.

The Ag signal measured in an iCPE extract (intensity I_{iCPE}) was related to the (higher) signal intensity measured for the same initial sample, which, however, underwent a CPE approach without added ligands (hereinafter referred to as CPE^0; intensity I_{CPE^0}). The latter represents the worst case of maximized co-extraction. Fig. 1 shows the remaining Ag signal (in percent), which equals to $\frac{I_{iCPE}}{I_{CPE^0}} \cdot 100\%$.

Increasing the amount of EDTA added during iCPE from 2 to 3 mL led to a reduction of the co-extraction. A further increase to 4 mL no longer affected the co-extraction rates (data not shown). Therefore, it appears that co-extraction can be minimized only to a certain extent by applying solely EDTA during iCPE. It is very likely that the Ag(I)-EDTA system is running into a state of equilibrium at this stage. However, it was surprisingly found that 500 and 1000 μL of 0.01 M PA in addition to 3 mL of EDTA caused a further significant reduction of co-extraction. Using 2000 μL of PA did not further reduce the co-extraction, possibly again due to an equilibrium situation due to the PA-Ag(I) system or a partition equilibrium of the Ag(I) complexes between the aqueous and organic phases. In sum, using a combination of 3 mL of saturated EDTA solution and 1 mL of 0.01 M PA solution in iCPE is optimal for further reducing the co-extraction, namely to only 1.6% (3.1%) for aqueous samples initially containing 500 ng L^{-1} (1000 ng L^{-1}) of dissolved Ag(I). Combining EDTA and PA during iCPE is a powerful tool to significantly reduce the co-extraction of dissolved Ag(I) species. However, we do not recommend completely replacing EDTA with PA since PA is much more expensive than EDTA. Furthermore, EDTA readily complexes dissolved species of alkaline earth metals which are usually present in natural water samples, and, therefore, serves as kind of a wideband complexing agent.

3.3. The influence of incubation time during iCPE on Ag-b-NP EE and Ag(I) co-extraction rates

Similar to the already established CPE approach [32], 30 min incubation time is the optimum for iCPE. For more details, please see the Appendix.

3.4. The influence of iCPE on the Ag-b-NPs being extracted

Particles to be extracted were not affected by iCPE. For more details, please see the Appendix.

3.5. The influence of particle size on the EE of Ag-b-NPs during iCPE

We also investigated whether the EE depends on the size of the Ag-b-NPs (see section 2.5.2). This outcome is crucial with regard to NP-based calibration approaches. If the EE was size-dependent, then the calibration particles should have the same size as the sample particles. However, the particle size of sample particles is the object of the analysis itself and, thus, unknown. Fig. A.2 summarizes the EEs for CA@AgNPs during iCPE at increasing CA@AgNP concentrations (A: 5, B: 50, C: 300 ng L^{-1} nanoparticulate Ag) as a function of the particle size. Overall, particles at sizes from 10 nm to 100 nm were equally well extracted – i.e., within a range from approximately 80–110% EE. Lowest EE of approximately 80% could be observed for 40 nm NPs at 50 ng L^{-1}, 60 nm NPs at 300 ng L^{-1} and 100 nm NPs at all investigated concentrations. As to the 100 nm
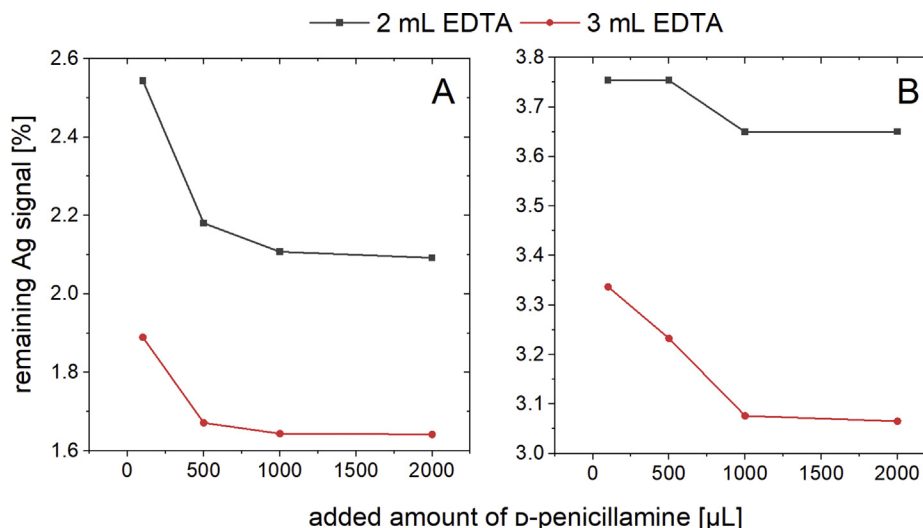
Fig. 1. Reduction of the Ag signal measured for iCPE extracts of samples initially containing 500 (A) and 1000 (B) ng L^{-1} Ag(I) with increasing amounts of EDTA and PA added during iCPE. The calculations are related to CPE^0.

NPs, we thus assume that EE is reduced due to an increasing particle size which inhibits proper arrangement of the NPs in the iCPE-induced micelles. This, however, differs from the observations made for 40 nm and 60 nm NPs. Lower EE values were only observable for some of the investigated concentrations, which is probably caused by inconsistencies in the experimentation. In particular, samples initially containing 5 ng L^{-1} (50 ng L^{-1}, resp. 300 ng L^{-1}) CA@AgNPs resulted in an EE ranging from approximately 91−112% (81−109%, resp. 77−109%). Consequently, particles which are by definition nanoparticles [36] (i.e., exhibiting diameters from 1 to 100 nm), are almost quantitatively extracted. In this context, it should be noted that CPE is feasible for the purpose of nanoparticle enrichment regardless of their chemical composition and coating [30]. Therefore, the aforementioned high EE can be applied to a wide variety of Ag-b-NP compositions and coatings. In contrast to the foregoing, significantly lower EE levels were obtained for particle sizes of 200 nm, in particular 33% (5 ng L^{-1}), 39% (50 ng L^{-1}), and 24% (300 ng L^{-1}). The decrease in EE for particles of >100 nm particle size corresponds to earlier observations made by our working group [31] and continues the trend started for 100 nm particles as noted above. This may possibly occur due to improper NP inclusion in the micelles and limitations of the partition equilibrium between the two phases. However, this decrease in EE for particles exceeding 100 nm is acceptable since, according to the IUPAC, particles > 100 nm are not considered to be nanoparticles given that their properties no longer differ from the corresponding bulk material to any significant degree [36]. However, it should be noted that currently there is no consensus on this boundary between nano and non-nano. Nevertheless, the proposed iCPE approach is able to reproducibly and quantitatively extract Ag-b-NPs of a certain range of particle size, whereas the extraction gives satisfactory results up to a size of 100 nm with EE of 80−110%.

3.6. Comparing CPE to iCPE

Further, we compared the extent of reduced co-extraction of dissolved Ag(I) species in iCPE extracts to CPE extracts. Therefore, aqueous samples containing 100 ng L^{-1} 60 nm CA@AgNPs and increasing amounts of dissolved Ag(I) (1000, 2000, and 4000 ng L^{-1}) were subjected to CPE^0 (i.e., without added ligands), CPE (i.e., 1 mL EDTA) [30−32], and iCPE (i.e., 3 mL EDTA, 1 mL PA). Samples were supplemented by reference samples only containing

Ag-b-NPs (i.e. 0 ng L^{-1} Ag(I)) to mimic the case in which no Ag(I) co-extraction into the organic phase occurs. ET-AAS measurements of CPE^0, CPE and iCPE extracts resulted in measured intensities I_{CPE^0}, I_{CPE} and I_{iCPE}, respectively. Further it is to be noted that ET-AAS measurements of CPE and iCPE extracts of the reference samples resulted in comparable signal intensities $I_{reference}$. Fig. 2 depicts the factor of ET-AAS signal increase, which equals to $\frac{I_{CPE0}}{I_{reference}}$, $\frac{I_{CPE}}{I_{reference}}$ or $\frac{I_{iCPE}}{I_{reference}}$, respectively. The red dotted line represents the case without signal increase, i.e. the optimum case without any co-extraction of Ag(I) species into the extract at all (i.e. signal increase factor of 1.0). The presence of 1000 ng L^{-1} Ag(I) species led to an undesirable increase of the measured signal intensity by factors of 1.05 (iCPE), 1.12 (CPE), and 1.27 (CPE^0). These findings indicate a distinct co-extraction effect of dissolved species into the organic phase. In case 2000 ng L^{-1} dissolved Ag(I) species were added to the aqueous sample prior to extraction, the signal intensity increased by factors of 1.11 (iCPE), 1.35 (CPE), and 1.34 (CPE^0). Very interestingly, iCPE was able to significantly reduce co-extraction even for 2000 or 4000 ng L^{-1} Ag(I), whereas CPE did not show any advantageous effect as compared to CPE^0. Although co-extraction was visible for iCPE, the measured signal was only increased by a factor of 1.50. Since a concentration of 4000 ng L^{-1} Ag(I) is far from any environmentally relevant scenario, the co-extraction measured was not considered to be problematic. In sum, it was shown that only iCPE was capable of reducing the co-extraction of dissolved silver traces for samples containing 1000 and 2000 ng L^{-1} Ag(I) to a marginally remaining value, which is due to an increased amount of chelating agents compared to CPE.

3.7. The applicability of iCPE to real environmental samples

As already shown in section 3.6, iCPE worked well in model systems. However, the next step was applying the method to real environmental systems. River water contains considerable amounts of natural organic matter in either dissolved or dispersed form. Conceivably, dissolved Ag(I) species may adsorb thereto and form potentially poorly hydrophilic species. Therefore, these species may have the tendency to be undesirably co-extracted into the organic iCPE extract. In order to evaluate potential limitations regarding the applicability of iCPE to environmental samples, river
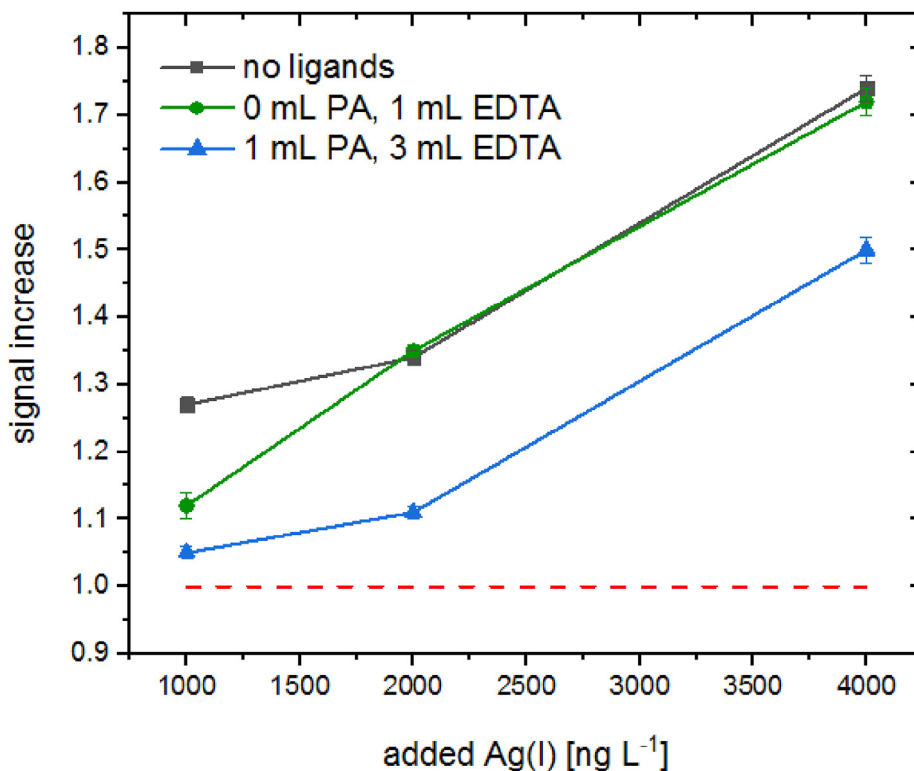
Fig. 2. Factor by which the measured signal intensity increased for samples initially containing 100 ng L^{-1} Ag-b-NPs mixed with 1000, 2000, and 4000 ng L^{-1} dissolved Ag(I) species, related to reference samples only containing 100 ng L^{-1} Ag-b-NPs. Ideal case with no signal increase is represented by the red dotted line. Prior to the measurements, the samples underwent iCPE (▲), CPE (●) and CPE^0 (■).
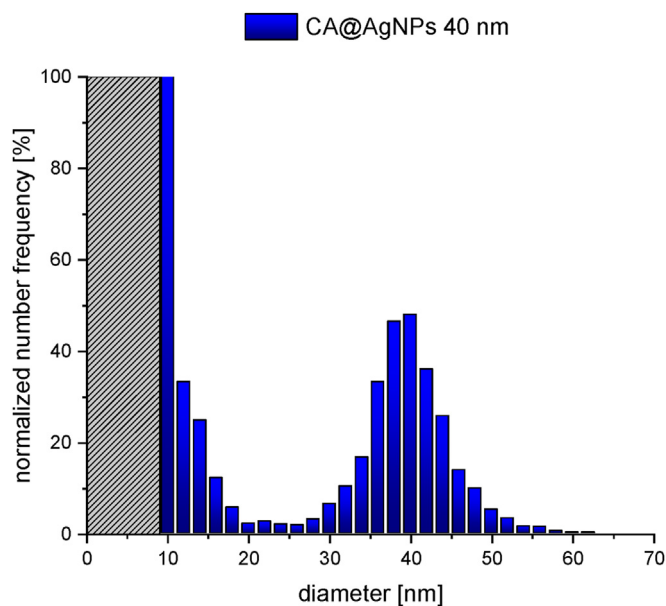
Fig. 3. Particle size distribution of Ag-b-NPs with a medium diameter of 40 nm measured at a dwell time of 100 μs. The grey dashed bar in the particle size distribution indicates the SDL, i.e., the cutoff at which NPs can no longer be identified as NPs. For reasons of comparison, we chose an SDL similar to that applied for measurements with a dwell time of 500 μs.

water (TOC 2.5 mg L^{-1}; initial $\beta_{Ag} < 0.15$ ng L^{-1}) was spiked with 5, 10, and 50 ng L^{-1} dissolved Ag(I) species, and the co-extraction during iCPE was examined (see also section 2.5.3).

As presented in Fig. A.3, iCPE significantly reduced the amount

of co-extracted Ag(I) species into the organic phase to negligible levels. Whereas a 100% co-extraction would lead to an increase of the blank signal by a factor of 2 (5 ng L^{-1} Ag(I)), 4 (10 ng L^{-1}Ag(I)), and 17 (50 ng L^{-1} Ag(I)), almost no signal increase was observed for samples that underwent iCPE. Only co-extraction rates as low as 3% (5, 10 ng L^{-1} Ag(I)) or 5% (50 ng L^{-1} Ag(I)) were calculated.

Comparable experiments using river water spiked with 60 nm CA@Ag-NPs resulted in EEs of 97% (5 ng L^{-1} CA@Ag-NP), 96% (10 ng L^{-1} CA@Ag-NP) and 98% (50 ng L^{-1} CA@Ag-NP). Thus, iCPE is perfectly suited for selectively separating dissolved Ag(I) species from their nanoparticulate counterparts in real environmental matrices, whereas Ag-b-NPs were extracted with a high EE.

3.8. iCPE-sp-ICP-MS

3.8.1. η consistency and the influence of surfactant content

We further intended to measure iCPE extracts with sp-ICP-MS. Even though the extracts were diluted as described above, they were highly viscous. Therefore, sample introduction and measurement using a conventional ICP-MS system might be challenging. In sp-ICP-MS, especially η is crucial for data evaluation and is supposed to be strongly influenced by the sample's viscosity. However, our results showed a good consistency for η over several measurements. Neither the dwell time nor the size of the particles used for the determination of η showed an influence on η itself (see Table A.3). The samples containing surfactant resulted in a higher η of ~0.08 than those prepared in UPW with a η of ~0.06.

3.8.2. Influences on particle size distribution: sample matrix

The overall particle number concentration in the measured sample (sp-ICP-MS) showed no influence on particle size distribution (Fig. A.4 A). This presumes a number of particles being not so

low as to give enough particle signals for being sufficiently informative (< 2000 particles mL^{-1}) or so high that particle signal coincidence occurred, which broadens the particle size distribution ($> 1.600.000$ particles mL^{-1}) (see Fig. A.4).

The particle size distribution was slightly shifted to higher diameters for samples prepared in a surfactant matrix instead of UPW (see Fig. A.5). This shift increased with the size of the particles. While no shift was observable for small particles (see Fig. A.6 A), one was apparent for larger particles (see Fig. A.6 B). However, this discrepancy between smaller and larger particles might be a consequence of reaching the SDL for the smaller particles, thus veiling this shift to some extent. A comparison with TEM measurement shows that the particle size distribution obtained from sp-ICP-MS measurement in surfactant matrix matched that obtained from TEM measurement (see Fig. A.7). This observation indicates that the nebulization efficiency calculated in an UPW matrix is somewhat underestimated.

3.8.3. Influences on particle size distribution: dwell time

Commercially available instruments allow for dwell times in the microsecond to millisecond range [18]. In particular, high dwell times may result in unwanted situations, e.g., particle coincidence (two or more particles recorded within one single dwell time, thus resulting in one bigger NP instead of two or more smaller NPs) [18]. To overcome this limitation, modern instruments use very short dwell times (in the µs range). However, we report that it is not recommended to use the lowest dwell time allowed by the instrument and respective vendor software, but rather to consider each measurement and the specific requirements thereof. We sought to elucidate the correct choice of appropriate dwell times adjusted to a certain measurement situation.

Once a nanoparticle is atomized and ionized in the plasma, an ion cloud is generated exhibiting an average duration in the order of a few hundreds of microseconds [18]. Using dwell times shorter than this ion cloud event results in the observation of the particle event as transient signal comprising several data points. It is noted that on the one hand, it is theoretically favorable to use dwell times as short as possible to improve the resolution of the investigated transient signal [37−39]. On the other hand, however, we observed for dwell times as short as 100 µs that current data evaluation approaches struggle with the differentiation between noise and actual particle signal. (Just for the sake of completeness, it is noted that samples have not been spiked with ionic species in these experiments.) In particular, we found that a "virtual" fragmentation occurs for a dwell time of 100 µs. First and last portions of a certain transient signal are difficult to be sufficiently recognized as signal boundaries and, thus, ascribed to the whole transient signal (see Fig. A.8). Consequently, the nanoparticle size is underestimated and respective first and last signal portions are considered as separate, small particles. This resulted in a false particle size distribution and, consequently, a too small medium particle diameter. As can be seen in Fig. 3, a large quantity of very small particles occurred for CA@Ag-NPs, which should measure about 40 nm in diameter. Such small particles could not be found in the particle size distribution obtained from the TEM measurement. This indicates that these signals derived from heavy particle fragmentation, a potential result of incorrect data processing by the data evaluation approach. The grey dashed bar in Fig. 3 indicates the diameter, whereas below particles were identified as a background signal in the sp-ICP-MS measurement. Thus, these signals could thus no longer be identified as particles (SDL). Particle fragmentation even occurred at dwell times of 500 µs and 800 µs (Fig. A.9 A). However, if the particle number frequency is converted into mass distribution, the high number of small particles only negligibly contributed to the distribution (Fig. A.9 B). Further examples are shown in Fig. A.10.

Therefore, no generally applicable dwell time can be defined for samples having unknown particle diameters, i.e., natural samples. It is necessary to measure these samples with various dwell times and to then choose the most suitable dwell time on the basis of a comparison of the particle size distributions obtained. If a broad particle size distribution is obtained, it may even be possible to consider various dwell times and compare the particle size distributions to each other for an ideal characterization of the sample.

Of course, this software issue can be overcome by using proper data evaluation tools and software settings. However, users of sp-ICP-MS should always consider and double-check this issue with their instrument and software − especially for dwell times as short as 100 µs. Given our data evaluation approach, we did not apply such short dwell times since heavy particle fragmentation did occur.

3.9. Determining the SDL of iCPE-sp-ICP-MS

It is well known that Ag-b-NPs in the aquatic environment usually size 20 nm or less [20]. Current state of the art sp-ICP-MS approaches are not applicable to such samples as they only reach a size detection limit (SDL) above 20 nm, mainly due to coexisting dissolved Ag(I) causing high background signals [19]. Thus, it is crucial to lower the SDL accordingly. We used iCPE prior to analysis in order to quantitatively separate the dissolved Ag(I) fraction from Ag-b-NPs. As a result, the background signal was significantly reduced and the SDL massively improved. The SDL was then only affected by instrument noise, and not by the interferences caused by dissolved Ag(I) species.

According to literature, SDL can be calculated as follows [19,40] (see the Appendix for more information on the development of the following equation), with the median of all the signal intensities throughout an entire measurement I_{median} [cps], the dwell time t_d [µs], the pump rate ν [ml min^{-1}] of the nebulizer, the nebulizing efficiency η, the ratio of molar masses of the whole nanoparticle and the analyte element $\frac{M_{NP}}{M_e}$ (which is 1 for AgNPs), and the elemental sensitivity ES_{ion} [cps/(µg/L)] and the density ρ [g cm^{-3}] of the material the NPs are composed of:

$$SDL = \sqrt[3]{\frac{18}{\pi \cdot \rho} \cdot \frac{I_{median} \cdot t_d \cdot \nu \cdot \eta}{ES_{ion}} \cdot \frac{M_{NP}}{M_e}}$$

Fig. 4 A-E depicts mass spectra acquired by sp-ICP-MS (t_d=100 µs) of aqueous samples with initial amounts of dissolved Ag(I) with and without iCPE prior to the measurement. It clearly shows that the background signal was massively increased at an increasing Ag(I) content. However, this increase can be significantly reduced after performing iCPE prior to sp-ICP-MS.

Using iCPE, the corresponding SDL was in a range from 4.8 nm to 5.2 nm for samples initially containing 0−100 ng L^{-1} Ag(I) (Fig. 4 F). Increasing this concentration up to 500 ng L^{-1} resulted in an SDL of 8.0 nm. Although it is obvious that slight traces of Ag(I) were co-extracted by iCPE, the SDL remained at very low values. In contrast, measurements without iCPE prior sp-ICP-MS showed SDL values of up to 23.1 nm. Since I_{median} is directly proportional to the Ag(I) concentration and further, $SDL \sim \sqrt[3]{I_{median}}$ is derived from the equation given above, SDL should be a cubic root function of the Ag(I) concentration. This is perfectly displayed in the measurement itself (Fig. 4 F, Fig. A.11 F).

Obviously, initial Ag(I) concentrations in the aqueous samples influence the amount of co-extracted Ag(I) and, thus, SDL. Therefore, it is not possible to present a universally valid SDL. However, in the case of environmentally relevant dissolved Ag(I) concentrations (typically up to 100 ng L^{-1}) [11,12] coexisting in the aqueous
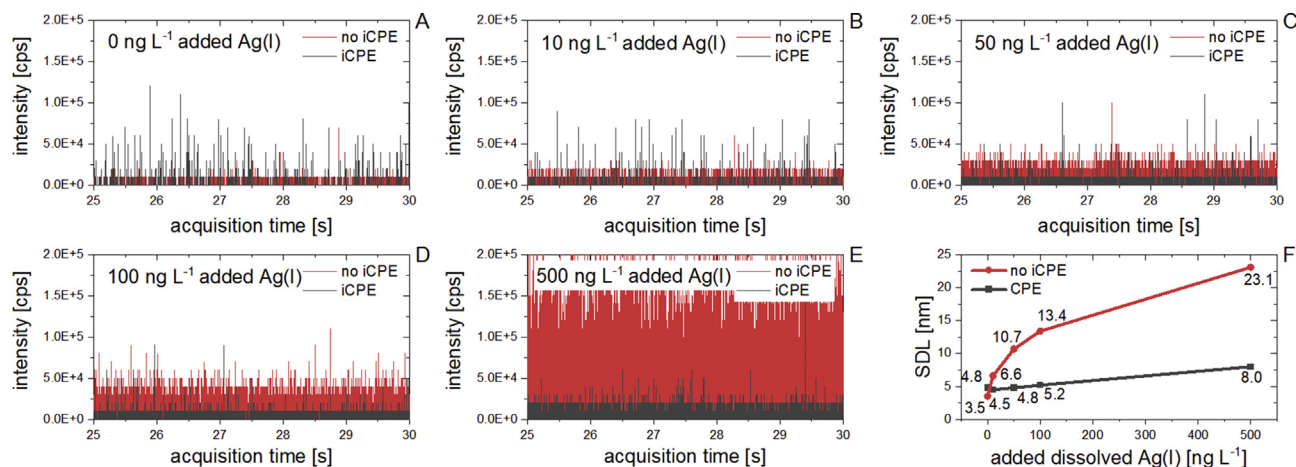
Fig. 4. Mass spectra obtained by sp-ICP-MS ($t_d = 100$ µs) in presence of increasing amounts of dissolved Ag(I) with and without iCPE prior to measurement (A−E). SDL as a function of Ag(I) added to samples (F).

sample, a SDL ranging from 4.8 to 5.2 nm can be assumed.

The measurements were repeated with $t_d = 500$ µs. According to above given equation, SDL should be increased by a factor of $\sqrt[3]{500/100} \approx 1.7$ compared to experiments with $t_d = 100$ µs. As shown in Fig. A.11, this factor was fairly accurately depicted in the experiments. In the case of initial Ag(I) concentrations of 0−100 ng L^{-1}, the SDL was determined as 5.9−23.5 nm without iCPE and 4.8−8.5 nm with iCPE prior to sp-ICP-MS measurement. For 500 ng L^{-1} Ag(I), SDL was increased to 39.6 nm (without iCPE) and 13.8 nm (with iCPE), respectively. It should be noted that the aforementioned advantages of higher dwell times should be assessed in consideration of slightly higher SDLs. Nonetheless, an SDL of 8.5 nm for $t_d = 500$ µs is still sufficient for environmental analysis when assuming a maximum dissolved Ag(I) concentration of 100 ng L^{-1}, which is typical for environmental samples [11,12].

Of course, the exact concentrations of coexisting dissolved Ag(I) species in the sample are not accessible prior to analysis. Therefore, a more conservative but more reliable SDL of approximately 5.2 nm ($t_d = 100$ µs) and 8.5 nm ($t_d = 500$ µs) has to be assumed instead of the lowest SDL values representing the ideal case with no coexisting Ag(I).

Owing to the influence on SDL by the concentration of coexisting Ag(I), it is simply not possible to present a universally valid SDL value.

3.10. Determination of the concentration of nanoparticulate Ag using all investigated measurement approaches

After optimizing the iCPE and successfully transferring this technique to ICP-MS and sp-ICP-MS, the final step was the quantification of unknown samples by means of (sp)-ICP-MS and relating these values to the previously established approach based on ET-AAS as reference [30−32]. The calibration differed significantly among the approaches and was performed as presented above in section 2.6.

Determined concentrations of nanoparticulate Ag were in good agreement with one another, independent of the utilized approach (see Table 1). Deviations from the reference values determined by ET-AAS were randomly distributed. According to the mean recovery rates, all approaches were excellently suitable for reproducing the reference results. As for the ICP-MS measurements, it should be noted that the calibration using dissolved Ag(I) species was much less time-consuming and therefore preferable over calibration using CA@AgNPs. Moreover, it is favourable that the analyte homogeneity was much higher for dissolved Ag(I) species, and Ag(I) species can be handled and diluted much more easily than CA@AgNPs (for instance, no sonication step for Ag(I)).

The excellent consistency among all of the three above methods was surprising but very pleasing given that the methods are based on entirely different physical and mathematical principles: ET-AAS

Table 1
Compilation of measured concentrations (incl. corresponding standard deviations) of nanoparticulate Ag in aqueous samples initially containing approximately 25 ng L^{-1} 40/60 nm CA@Ag-NPs using iCPE followed by quantification via ET-AAS, ICP-MS and sp-ICP-MS. All results are related to the validated ET-AAS approach [30−32]. rr represents the calculated recovery rate based on the concentrations measured by ET-AAS as reference. The calibration was performed using either aqueous dispersions of CA@AgNP of known concentrations or aqueous solutions of dissolved Ag(I) of known concentrations. The dwell time for sp-ICP-MS measurement was set to 500 µs. All measurements were performed in triplicate (n = 3).

Measurement approach	ET-AAS (reference)	ICP-MS		ICP-MS		sp-ICP-MS	
Calibrant	AgNP	Ag(I)		AgNP		AuNP/Ag(I)	
LOD [ng L^{-1}]	0.20[a]	0.15[b]		0.15[c]		0.25[d]	
Diameter [nm]	conc.	conc.	rr [%]	conc.	rr [%]	conc.	rr [%]
40	**25.95 ± 3.63**	24.8 ± 2.01	95	22.96 ± 2.26	88	27.49 ± 1.96	106
40	**26.05 ± 2.31**	23.5 ± 2.34	90	22.93 ± 2.18	88	23.77 ± 2.03	91
60	**24.32 ± 2.47**	25.5 ± 0.63	105	25.5 ± 5.27	105	25.35 ± 1.45	104
60	**22.51 ± 2.00**	24.9 ± 3.54	111	24.92 ± 3.54	111	26.74 ± 1.56	119
Mean recovery rate relative to reference [%]		**100**		**98**		**105**	

[a, b, c] calculated from the calibration curve [32].

[d] completely different calibration approach; approximated LOD is derived from blank measurements (blank-limited LOD).

measures light absorption, whereas in ICP-MS, masses of ions formed in the plasma are detected. Furthermore, sp-ICP-MS does not at first glance measure the concentration but measures the masses of each single particle by mathematically transferring the acquired data in a separate data evaluation step into concentration values based on certain assumptions as presented above. Fortunately, the LODs for all the approaches were very low and were therefore well-suited for the purpose of quantifying Ag-b-NPs in real environmental samples. The LOD for iCPE-sp-ICP-MS was, rather, a blank-limited approximation. iCPE-sp-ICP-MS measurements within the magnitude of the LOD should therefore be supplemented by iCPE-ICP-MS measurements exhibiting a more reliable LOD. However, such supplementary measurements are not particularly disadvantageous since both approaches can be performed subsequently on the same instrument using the same sample within acceptable measurement times.

4. Conclusion

We presented an improved CPE approach applying highly argentophilic complexing agents able to species-selectively extract and enrich Ag-b-NPs from aqueous samples. The method was developed using model systems of dissolved and nanoparticulate Ag species in UPW and was successfully applied to real environmental samples. Species selectivity allows hyphenation of iCPE to ICP-MS and even sp-ICP-MS, the latter being very sensitive to traces of dissolved Ag(I) species causing undesired background signals. Reducing this background by iCPE is a key in sp-ICP-MS in order to achieve a SDL as low as 4.5 nm, instead of the > 20 nm as discussed in the literature [19]. However, a single-digit SDL is essential for environmental samples, because Ag-b-NPs in natural waters usually measure < 20 nm. Finally, we were able to demonstrate perfect accordance between the quantitative results obtained by iCPE-(sp)-ICP-MS and a previously established hyphenation of CPE to ET-AAS. iCPE-(sp)-ICP-MS is a fast, cheap and easy applicable approach to nanoparticle analysis. Once established in a lab, this approach is capable of running hundreds of samples per day and can be performed by lab technicians after moderate training. Therefore, iCPE-(sp)-ICP-MS represents a key technique for the routine environmental monitoring of transport and fate of Ag-b-NPs in the aquatic environment. Application examples are presented in a parallel study of our working group addressing the fate of Ag-b-NPs in seawater by iCPE-(sp)-ICP-MS [41].

CRediT authorship contribution statement

Andreas Wimmer: Conceptualization, Methodology, Validation, Formal analysis, Investigation, Writing - original draft, Writing - review & editing, Visualization. **Alexander Urstoeger:** Methodology, Validation, Formal analysis, Investigation, Writing - original draft, Writing - review & editing, Visualization. **Tobias Hinke:** Investigation. **Margit Aust:** Investigation. **Philipp J. Altmann:** Validation, Formal analysis, Investigation, Writing - original draft, Visualization. **Michael Schuster:** Supervision, Project administration, Funding acquisition.

Declaration of competing interest

The authors declare that they have no known competing financial interests or personal relationships that could have appeared to influence the work reported in this paper.

Appendix A. Supplementary data

Supplementary data to this article can be found online at https://doi.org/10.1016/j.aca.2021.01.001.

References

[1] H.F. Krug, Nanosafety research—are we on the right track? Angew. Chem. Int. Ed. 53 (46) (2014) 12304—12319.

[2] P. Krystek, A. Ulrich, C.C. Garcia, S. Manohar, R. Ritsema, Application of plasma spectrometry for the analysis of engineered nanoparticles in suspensions and products, J. Anal. At. Spectrom. 26 (9) (2011) 1701—1721.

[3] R. Kessler, Engineered nanoparticles in consumer products: understanding a new ingredient, Environ. Health Perspect. 119 (3) (2011) A120—A125.

[4] T.M. Benn, P. Westerhoff, Nanoparticle silver released into water from commercially available sock fabrics, Environ. Sci. Technol. 42 (11) (2008) 4133—4139.

[5] L. Geranio, M. Heuberger, B. Nowack, The behavior of silver nanotextiles during washing, Environ. Sci. Technol. 43 (21) (2009) 8113—8118.

[6] D.M. Mitrano, P. Limpiteeprakan, S. Babel, B. Nowack, Durability of nano-enhanced textiles through the life cycle: releases from landfilling after washing, Environ. Sci.: Nano 3 (2) (2016) 375—387.

[7] D.M. Mitrano, E. Rimmele, A. Wichser, R. Erni, M. Height, B. Nowack, Presence of nanoparticles in wash water from conventional silver and nano-silver textiles, ACS Nano 8 (7) (2014) 7208—7219.

[8] D. Jiang, L. Chen, J. Xie, M. Chen, Ag2S/g-C3N4 composite photocatalysts for efficient Pt-free hydrogen production. The co-catalyst function of Ag/Ag2S formed by simultaneous photodeposition, Dalton Trans. 43 (12) (2014) 4878—4885.

[9] A.P. Richter, J.S. Brown, B. Bharti, A. Wang, S. Gangwal, K. Houck, E.A. Cohen Hubal, V.N. Paunov, S.D. Stoyanov, O.D. Velev, An environmentally benign antimicrobial nanoparticle based on a silver-infused lignin core, Nat. Nanotechnol. 10 (2015) 817.

[10] L. Li, G. Hartmann, M. Döblinger, M. Schuster, Quantification of nanoscale silver particles removal and release from municipal wastewater treatment plants in Germany, Environ. Sci. Technol. 47 (13) (2013) 7317—7323.

[11] L. Li, M. Stoiber, A. Wimmer, Z. Xu, C. Lindenblatt, B. Helmreich, M. Schuster, To what extent can full-scale wastewater treatment plant effluent influence the occurrence of silver-based nanoparticles in surface waters? Environ. Sci. Technol. 50 (12) (2016) 6327—6333.

[12] T.Y. Sun, N.A. Bornhöft, K. Hungerbühler, B. Nowack, Dynamic probabilistic modeling of environmental emissions of engineered nanomaterials, Environ. Sci. Technol. 50 (9) (2016) 4701—4711.

[13] M. Troester, H.-J. Brauch, T. Hofmann, Vulnerability of drinking water supplies to engineered nanoparticles, Water Res. 96 (2016) 255—279.

[14] A. Wimmer, A. Kalinnik, M. Schuster, New insights into the formation of silver-based nanoparticles under natural and semi-natural conditions, Water Res. 141 (2018) 227—234.

[15] C. Levard, E.M. Hotze, G.V. Lowry, G.E. Brown, Environmental transformations of silver nanoparticles: impact on stability and toxicity, Environ. Sci. Technol. 46 (13) (2012) 6900—6914.

[16] Y.-M. Cho, Y. Mizuta, J.-i. Akagi, T. Toyoda, M. Sone, K. Ogawa, Size-dependent acute toxicity of silver nanoparticles in mice, J. Toxicol. Pathol. 31 (1) (2018) 73—80.

[17] R.J.B. Peters, Z.H. Rivera, G. van Bemmel, H.J.P. Marvin, S. Weigel, H. Bouwmeester, Development and validation of single particle ICP-MS for sizing and quantitative determination of nano-silver in chicken meat, Anal. Bioanal. Chem. 406 (16) (2014) 3875—3885.

[18] D. Mozhayeva, C. Engelhard, A critical review of single particle inductively coupled plasma mass spectrometry — a step towards an ideal method for nanomaterial characterization, J. Anal. At. Spectrom. 35 (2020) 1740—1783.

[19] S. Lee, X. Bi, R.B. Reed, J.F. Ranville, P. Herckes, P. Westerhoff, Nanoparticle size detection limits by single particle ICP-MS for 40 elements, Environ. Sci. Technol. 48 (17) (2014) 10291—10300.

[20] B. Kim, C.-S. Park, M. Murayama, M.F. Hochella, Discovery and characterization of silver sulfide nanoparticles in final sewage sludge products, Environ. Sci. Technol. 44 (19) (2010) 7509—7514.

[21] C. Degueldre, P.Y. Favarger, Colloid analysis by single particle inductively coupled plasma-mass spectroscopy: a feasibility study, Colloid. Surface. Physicochem. Eng. Aspect. 217 (1—3) (2003) 137—142.

[22] F. Laborda, E. Bolea, G. Cepriá, M.T. Gómez, M.S. Jiménez, J. Pérez-Arantegui, J.R. Castillo, Detection, characterization and quantification of inorganic engineered nanomaterials: a review of techniques and methodological approaches for the analysis of complex samples, Anal. Chim. Acta 904 (2016) 10—32.

[23] M.D. Montano, H.R. Badiei, S. Bazargan, J.F. Ranville, Improvements in the detection and characterization of engineered nanoparticles using spICP-MS with microsecond dwell times, Environ. Sci.: Nano 1 (4) (2014) 338—346.

[24] R. Vogt, D. Mozhayeva, B. Steinhoff, A. Schardt, B.T.F. Spelz, A. Philippe,

S. Kurtz, G.E. Schaumann, C. Engelhard, H. Schönherr, D.K. Lamatsch, J. Wanzenböck, Spatiotemporal distribution of silver and silver-containing nanoparticles in a prealpine lake in relation to the discharge from a wastewater treatment plant, Sci. Total Environ. 696 (2019) 134034.

[25] D. Mozhayeva, C. Engelhard, A quantitative nanoparticle extraction method for microsecond time resolved single-particle ICP-MS data in the presence of a high background, J. Anal. At. Spectrom. 34 (8) (2019) 1571−1580.

[26] L. Torrent, F. Laborda, E. Marguí, M. Hidalgo, M. Iglesias, Combination of cloud point extraction with single particle inductively coupled plasma mass spectrometry to characterize silver nanoparticles in soil leachates, Anal. Bioanal. Chem. 411 (20) (2019) 5317−5329.

[27] H. Watanabe, H. Tanaka, A non-ionic surfactant as a new solvent for liquid-—liquid extraction of zinc(II) with 1-(2-pyridylazo)-2-naphthol, Talanta 25 (10) (1978) 585−589.

[28] J.-f. Liu, R. Liu, Y.-g. Yin, G.-b. Jiang, Triton X-114 based cloud point extraction: a thermoreversible approach for separation/concentration and dispersion of nanomaterials in the aqueous phase, Chem. Commun. (12) (2009) 1514−1516.

[29] L. Duester, A.-L. Fabricius, S. Jakobtorweihen, A. Philippe, F. Weigl, A. Wimmer, M. Schuster, M.F. Nazar, Can cloud point-based enrichment, preservation, and detection methods help to bridge gaps in aquatic nanometrology? Anal. Bioanal. Chem. 408 (27) (2016) 7551−7557.

[30] G. Hartmann, T. Baumgartner, M. Schuster, Influence of particle coating and matrix constituents on the cloud point extraction efficiency of silver nanoparticles (Ag-NPs) and application for monitoring the formation of Ag-NPs from Ag+, Anal. Chem. 86 (1) (2014) 790−796.

[31] G. Hartmann, M. Schuster, Species selective preconcentration and quantification of gold nanoparticles using cloud point extraction and electrothermal atomic absorption spectrometry, Anal. Chim. Acta 761 (2013) 27−33.

[32] G. Hartmann, C. Hutterer, M. Schuster, Ultra-trace determination of silver nanoparticles in water samples using cloud point extraction and ETAAS, J. Anal. At. Spectrom. 28 (4) (2013) 567−572.

[33] M.D. Montano, J.W. Olesik, A.G. Barber, K. Challis, J.F. Ranville, Single Particle ICP-MS: advances toward routine analysis of nanomaterials, Anal. Bioanal. Chem. 408 (19) (2016) 5053−5074.

[34] B.O. Leung, F. Jalilehvand, V. Mah, M. Parvez, Q. Wu, Silver(I) complex formation with cysteine, penicillamine, and glutathione, Inorg. Chem. 52 (8) (2013) 4593−4602.

[35] H. Schmidbaur, A. Schier, Argentophilic interactions, Angew. Chem. Int. Ed. 54 (3) (2015) 746−784.

[36] J.H. Duffus, M. Nordberg, D.M. Templeton, Glossary of Terms Used in Toxicology, 2nd Edition (IUPAC Recommendations 2007), vol. 79, 2007, p. 1153, 7.

[37] R. Aznar, F. Barahona, O. Geiss, J. Ponti, T. José Luis, J. Barrero-Moreno, Quantification and size characterisation of silver nanoparticles in environmental aqueous samples and consumer products by single particle-ICPMS, Talanta 175 (2017) 200−208.

[38] D. Mozhayeva, I. Strenge, C. Engelhard, Implementation of online preconcentration and microsecond time resolution to capillary electrophoresis single particle inductively coupled plasma mass spectrometry (CE-SP-ICP-MS) and its application in silver nanoparticle analysis, Anal. Chem. 89 (13) (2017) 7152−7159.

[39] I. Strenge, C. Engelhard, Single particle inductively coupled plasma mass spectrometry: investigating nonlinear response observed in pulse counting mode and extending the linear dynamic range by compensating for dead time related count losses on a microsecond timescale, J. Anal. At. Spectrom. 35 (1) (2020) 84−99.

[40] H.E. Pace, N.J. Rogers, C. Jarolimek, V.A. Coleman, E.P. Gray, C.P. Higgins, J.F. Ranville, Single particle inductively coupled plasma-mass spectrometry: a performance evaluation and method comparison in the determination of nanoparticle size, Environ. Sci. Technol. 46 (22) (2012) 12272−12280.

[41] A. Wimmer, A. Urstoeger, N.C. Funck, F.P. Adler, L. Lenz, M. Doeblinger, M. Schuster, What happens to silver-based nanoparticles if they meet seawater? Water Res. 171 (2020) 115399.

Appendix A

Separating Dissolved Silver from Nanoparticulate Silver is the Key: Improved Cloud-Point-Extraction Hyphenated to Single Particle ICP-MS for Comprehensive Analysis of Silver-Based Nanoparticles in Real Environmental Samples Down to Single-Digit nm Particle Sizes

Andreas Wimmer [1,#], Alexander Urstoeger [1,#], Tobias Hinke [1], Margit Aust [1], Philipp J. Altmann[2], Michael Schuster [1,*]

[1] Division of Analytical Chemistry, Department of Chemistry, Technical University of Munich, Garching 85748, Germany
[2] Catalysis Research Center, Technical University of Munich, Garching, 85748, Germany
[#] These Authors contributed equally to the present study.

22	pages
11	figures
5	tables

Author contribution:

M.S. supervised the study. A.W. designed the study and its experimental set-up. A.W. carried out the iCPE development assisted by T.H. and M.A.. A.W. synthesized the Ag(I)-EDTA complex assisted by T.H.. P.A. carried out the X-ray diffractometry and evaluated the crystal structure. A.U. and A.W. carried out the CPE-sp-ICP-MS hyphenation. A.W. determined the SDL of sp-ICP-MS and carried out comparative measurements of all investigated measurement approaches. The manuscript was written through the contributions of all authors. All authors have given approval to the final version of the manuscript.

Detailed information on the materials used in this study:

The dissolved Ag(I) ICP-standard (AgNO$_3$ in 3% HNO$_3$, β_{Ag} = 1000 mg L^{-1}) and dissolved In(III) ICP-standard (In(NO$_3$)$_3$ in 2-3% HNO$_3$, β_{In} = 1000 mg L^{-1}) used as an internal standard were obtained from Merck (Darmstadt, Germany). AgNO$_3$ was obtained from Merck. Dispersions of citrate-stabilized silver nanoparticles (CA@AgNPs) sizing 10, 20, 40, 60, 80, 100 and 200 nm (mass concentration β_{Ag} ~ 20 mg L^{-1}) were purchased from Sigma-Aldrich (St. Louis, MO, USA). Gold nanoparticle (CA@AuNP) dispersions (reference material RM 8012, 8013, 28 nm, 58 nm, β_{Au} ~ 50 mg L^{-1}, citrate stabilized) and silver nanoparticle (PVP@AgNP) dispersions (reference material RM 8017, 75 nm, pressed powder) were supplied by the National Institute of Science and Technology (NIST) (Gaithersburg, MD, USA). iCPE reagents, e.g., acetic acid (glacial), ethanol (Emsure®), ethylenediaminetetraacetate disodium salt dihydrate (Na$_2$EDTA·2H$_2$O; C$_{10}$H$_{14}$N$_2$Na$_2$O$_8$·2H$_2$O), sodium acetate anhydrous (C$_2$H$_3$NaO$_2$), and nitric acid (HNO$_3$, 65%, suprapure) were purchased from Merck. Triton X-114 ((C$_2$H$_4$O)$_n$C$_{14}$H$_{22}$O, n = 7 or 8) was obtained from AppliChem (Darmstadt, Germany). D-Penicillamine (PA, C$_5$H$_{11}$NO$_2$S) was purchased from Sigma Aldrich. Potassium hydrogen phthalate used as a calibrant for TOC measurements was obtained from Naclai Tesque Inc. (Kyoto, Japan). All chemicals were of at least analytical grade and were checked for contamination via ICP-mass spectrometry (ICP-MS) analysis prior to use. Ultrapure water (UPW, resistivity of 18.2 MΩ cm^{-1}) was obtained using a Milli-Q-Gradient-System (Millipore GmbH, Schwalbach, Germany). All solutions and dilutions were prepared in UPW unless otherwise indicated.

CA@Ag-NP dispersions were freed from impurities of dissolved Ag by dialysis (3.5 kDa regenerated cellulose membrane by ZelluTrans, Carl Roth, Karlsruhe, Germany) prior to use. Aliquots of the purified NP dispersions were dissolved in 3.25% (v/v) HNO$_3$ to ensure sample homogeneity and subjected to Ag quantification by ICP-MS. Before usage and each dilution step, CA@AgNP dispersions were ultrasonicated for 1 min in an ultrasonic bath (Ulsonix Proclean 3.0DSP; Ulsonix, Berlin, Germany) to prevent particle aggregation.

All glass vessels were rinsed three times with 6.5% HNO$_3$ (w/w), steamed with HNO$_3$ vapor for at least 4 h, rinsed three times with UPW, and then stored in a particle-free environment until use.

Table A.1. Compilation of instrumental details of the sp-ICP-MS measurements.

acquisition time	60 s
dwell time	100 - 1000 µs
analyte mass	^{107}Ag
RF power	1550 W
RF matching	1.80 V
sample depth	8.0 mm
nebulizer gas	1.05 L min^{-1}
S/C temperature	2 °C

Preparation of crystalline Ag(I)-EDTA

To prepare crystalline Ag(I)-EDTA, we mixed 2 mL of an aqueous Na_2EDTA ($C_{10}H_{14}N_2Na_2O_8$) solution (8 g $Na_2EDTA \cdot 2H_2O$ in 100 mL UPW) dropwise with 3 mL of an aqueous $AgNO_3$ solution (15 g $AgNO_3$ in 100 mL UPW) at room temperature within a time period of 1 h. After stirring for another 1 h at room temperature, a colorless, flaked solid was formed. After separation from the reaction mixture by filtration, the solid was washed carefully with EtOH and dried in the vacuum. The colorless crystalline solid was forwarded to CHN analysis supplemented by Ag and Na elemental analysis and X-ray crystallographic analysis. A clear colorless plate-like specimen of the Ag(I)-EDTA complex, approximate dimensions 0.047 mm x 0.070 mm x 0.116 mm, was used for the X-ray crystallographic analysis.
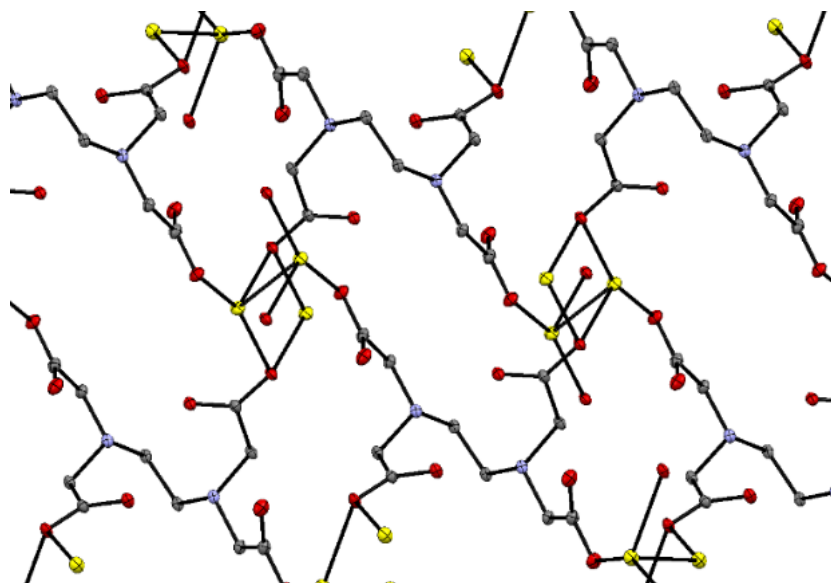
Figure A.1. Detail of the ORTEP representation of the Ag(I)-EDTA complex ($C_{10}H_{14}Ag_2N_2O_8$). Ellipsoids are shown at 70% probability. Color code: C = grey, N = blue, O = red, Ag = yellow.

For more details, please see Crystallographic Details attached to the end of Appendix A.

iCPE development

The influence of incubation time during iCPE on Ag-b-NP EE and Ag(I) co-extraction rates. Similar to the already established CPE approach[3], 30 min incubation time is the optimum for iCPE. We further examined whether the EE of Ag-b-NPs and the co-extraction of Ag(I) are influenced when the incubation time exceeds the suggested 30 min at 40 °C.[3] Therefore, solutions containing either 50 ng L^{-1} 60 nm CA@AgNP or 50 ng L^{-1} dissolved Ag(I) in UPW were subjected to iCPE, whereas the incubation time was set to 10, 20, 30, 60, and 90 min at 40 °C. The EE for Ag-b-NPs was determined as described in sections 2.5.2 in conjunction with 3.5 and the co-extraction of dissolved Ag(I) species determined as described in sections 2.5.1 in conjunction with 3.2. The maximum EE was reached after 30 min of incubation and was not further affected by increasing the incubation time, even by up to 90 min (see Table A.2). This is in line with the findings of our former CPE study.[3] However, the co-extraction rates were consistently low for incubation times of 10, 20, and 30 min, but they were increased in an unreproducible manner for incubation times of 60 and 90 min. This increase was possibly due to the formation of Ag-b-NPs from dissolved Ag(I) species after long incubation times, which has already been proven for naturally-occurring Ag(I).[4] These Ag-b-NPs were then transferred into the organic phase during iCPE. Therefore, in order to achieve the maximum EE along with maximally reduced co-extraction of dissolved Ag(I) species, it must be ensured that incubation times of exactly 30 min are adhered to.

Table A.2. Effect of iCPE incubation time on extraction efficiency (EE) of Ag-b-NPs and the remaining Ag signal as a measure of co-extraction rates of Ag(I)

incubation time	10 min	20 min	30 min	60 min	90 min
EE (Ag-b-NPs)	57 %	78 %	95 %	89 %	93 %
remaining Ag signal (Ag(I))	0.9%	0.9%	1.2%	4.7%	3.4%

The influence of iCPE on the Ag-b-NPs being extracted. Particles to be extracted were not affected by iCPE. It has already been shown that CPE applying 1 mL EDTA and no PA has no influence on the particle size of Ag-b-NPs during the extraction procedure.[3] This is an essential prerequisite for the use of CPE in environmental nanoparticle analysis, because it is possible to 'freeze' the particles in environmental samples in their current state. Samples containing 100 ng L^{-1} of 60 nm CA@AgNP were subjected to iCPE in order to investigate whether iCPE

also has no effect on particle sizes. Similar samples were analyzed by sp-ICP-MS without conducting iCPE. The corresponding particle size distributions were determined by means of sp-ICP-MS. Measured particle sizes were marginally reduced from 60.16 nm before CPE to 59.9 nm after CPE, indicating that the particle sizes were not affected by iCPE.
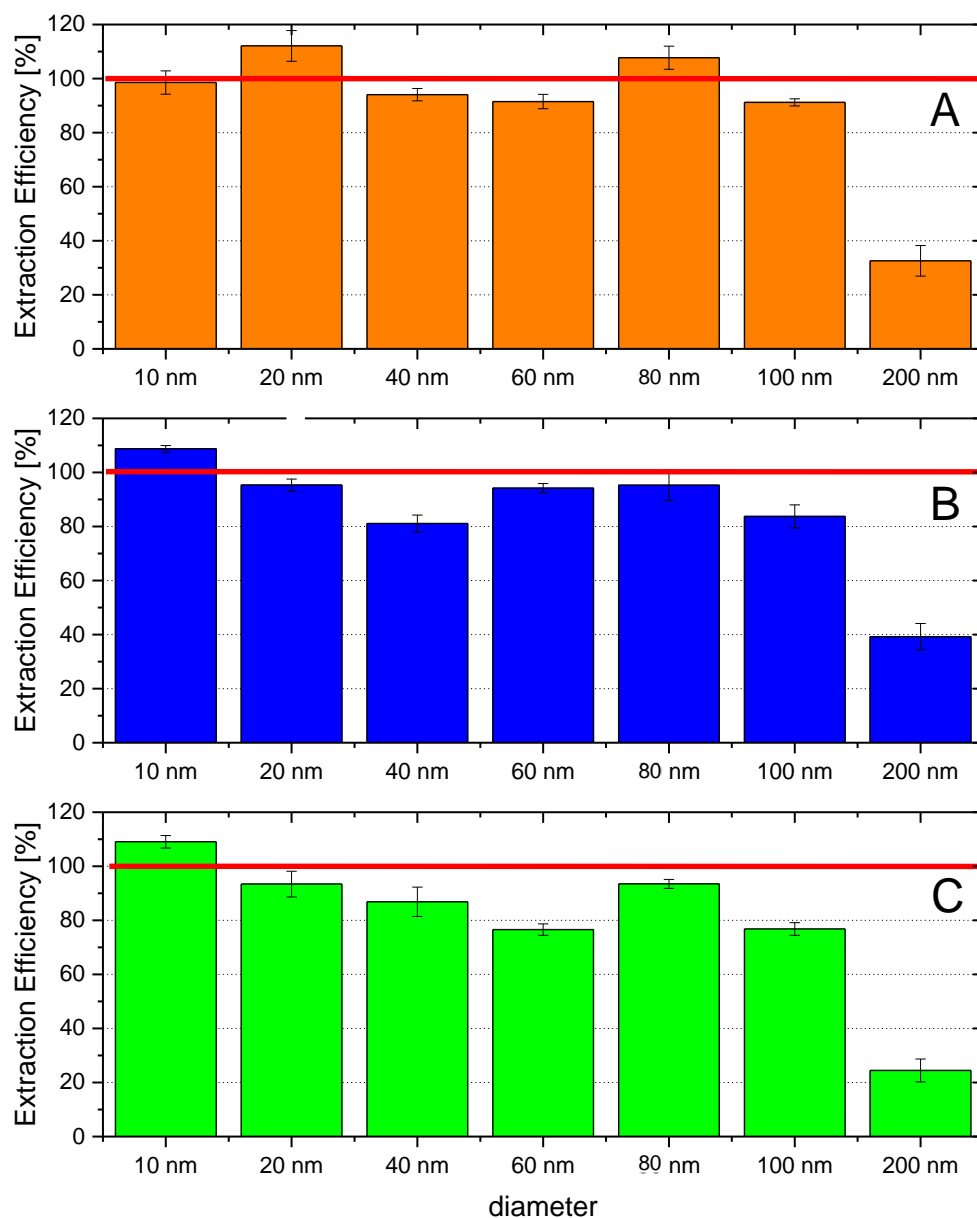
Figure A.1: EE for CA@AgNPs dependent of their mean particle size for samples initially containing 5 (A), 50 (B), and 300 ng L^{-1} (C) nanoparticulate Ag prior to iCPE.
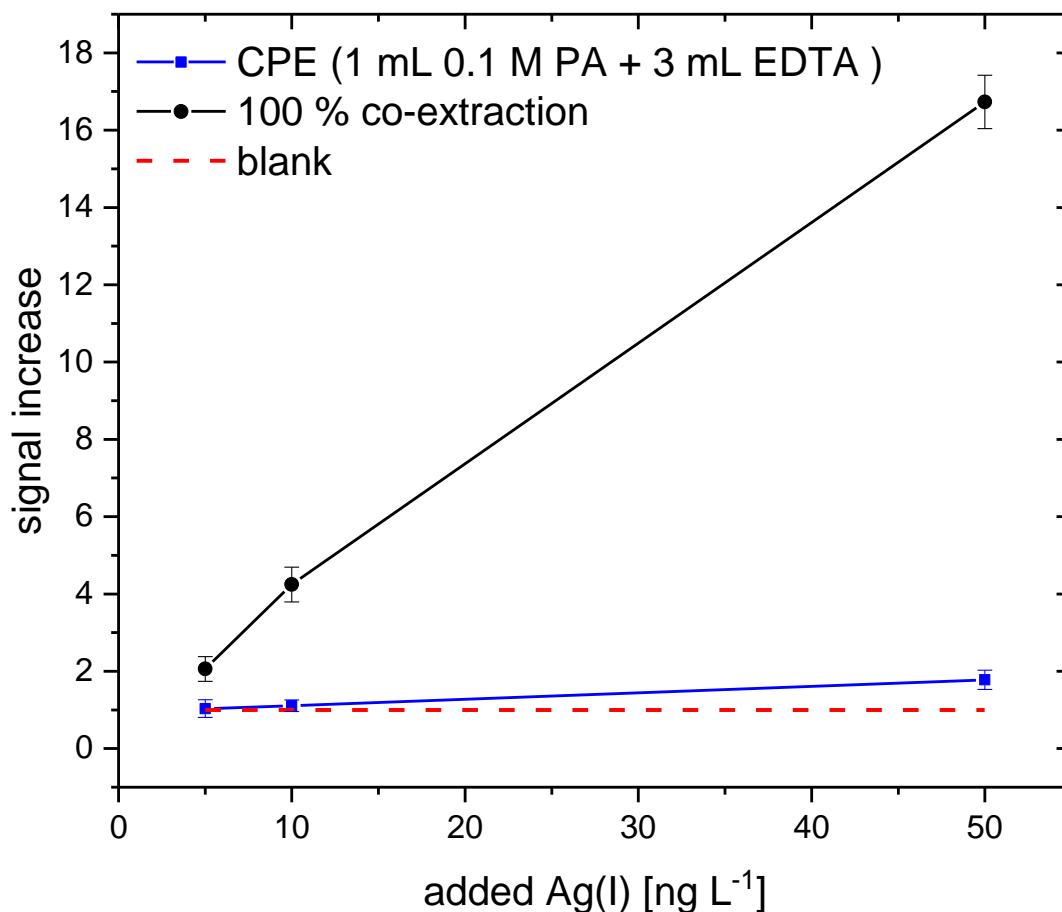
Figure A.3: Factor by which the measured signal intensity increased for river water samples initially containing 5, 10, and 50 ng L^{-1} dissolved Ag(I) mimicking 100% co-extraction (●) and after performing iCPE (■) compared to the blank measurement (i.e. a iCPE extract of river water containing no Ag at all). Assuming the ideal case of no Ag(I) co-extraction into the iCPE extract, the signal increase factor should be 1.0 (red dotted line).

Table A.3. Nebulization efficiencies at different dwell times in UPW and surfactant matrix determined with RM 8012 and RM 8013.

RM	η	Matrix	Dwell time
8012	0.064 ± 0.006	UPW	100 µs
8012	0.075 ± 0.000	surfactant	100 µs
8012	0.068 ± 0.004	UPW	500 µs
8012	0.080 ± 0.004	surfactant	500 µs
8013	0.060 ± 0.004	UPW	100 µs
8013	0.058 ± 0.002	UPW	500 µs
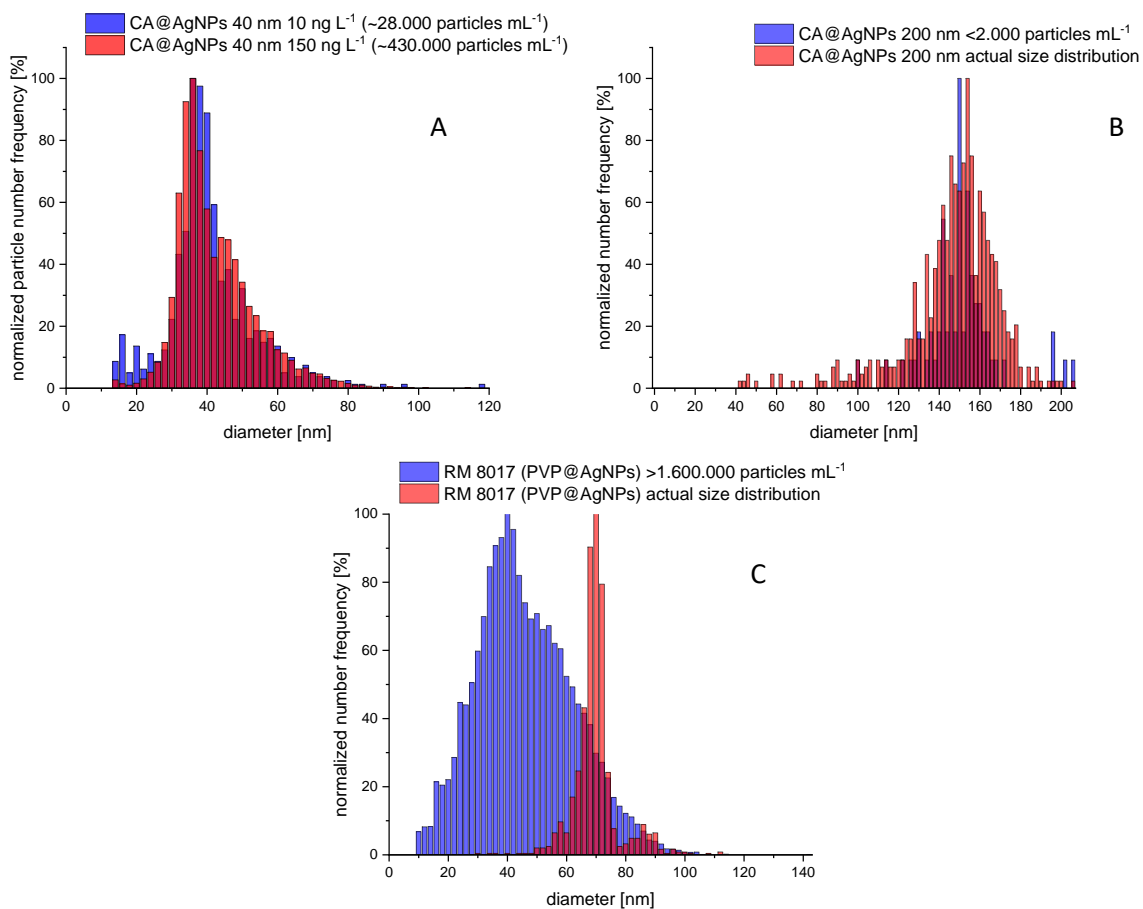
Figure A.4. Stability of particle size distributions over concentration range (A) and particle size distribution at a too low (B) and too high particle number concentration (C) in comparison to the actual size distributions.
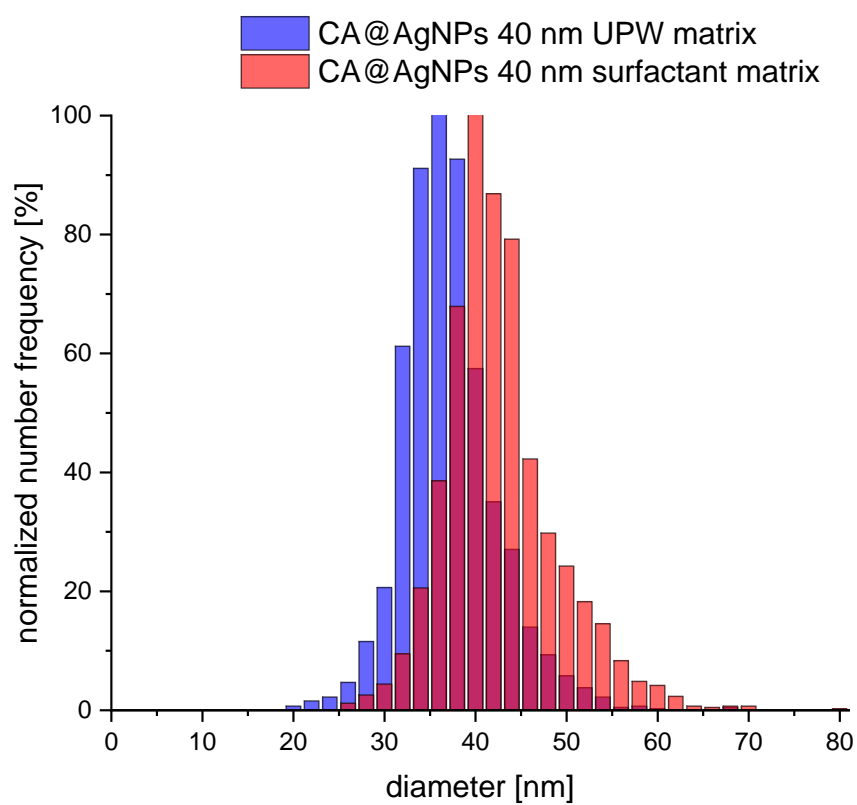
Figure A.5. Comparison of the particle size distribution obtained from sp-ICP-MS measurement in UPW and surfactant matrix.
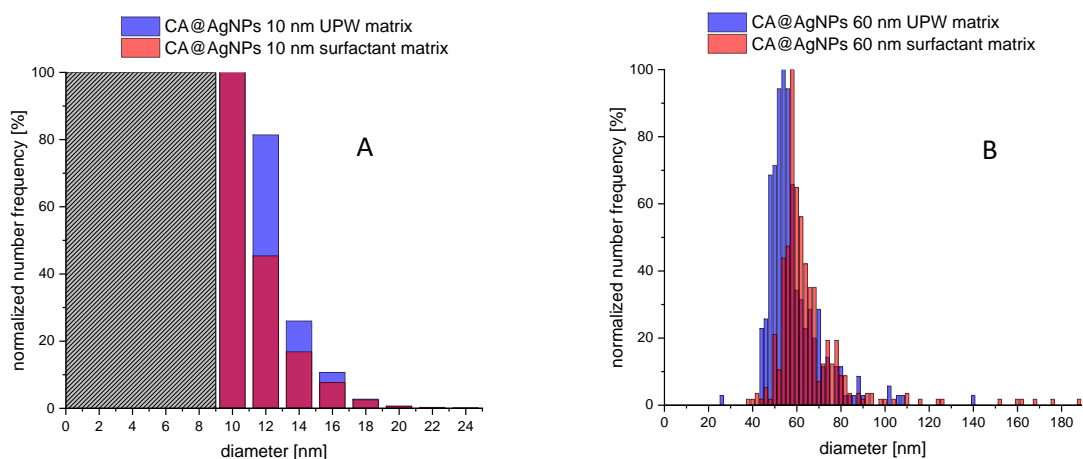
Figure A.6. Comparison of the particle size distributions obtained from sp-ICP-MS measurement of CA@Ag-NP dispersions prepared in UPW and surfactant matrix (A, B). In sp-ICP-MS measurement, t_d was set 100 µs for CA@AgNPs 10 nm (A) and 500 µs for CA@AgNPs 60 nm (B). The grey dashed bar in the particle size distribution A indicates the SDL, i.e. the cutoff, where NPs cannot be identified as NPs anymore. For reasons of comparison, we chose similar SDL values for both dwell times.
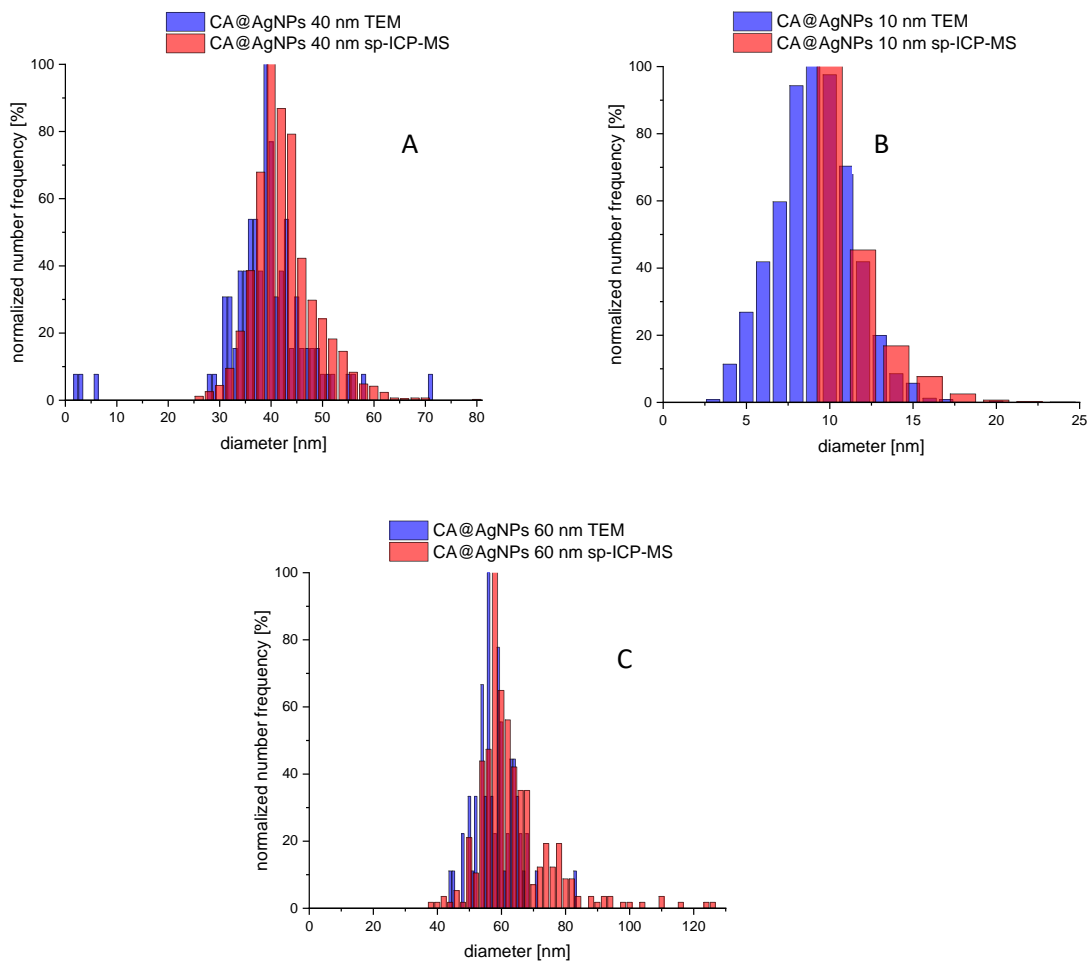
Figure A.7. Comparison of the particle size distributions obtained from sp-ICP-MS measurement in surfactant matrix and TEM measurement of CA@AgNP 40 nm (A), CA@AgNP 10 nm (B) and CA@AgNP 60 nm (C) dispersions.
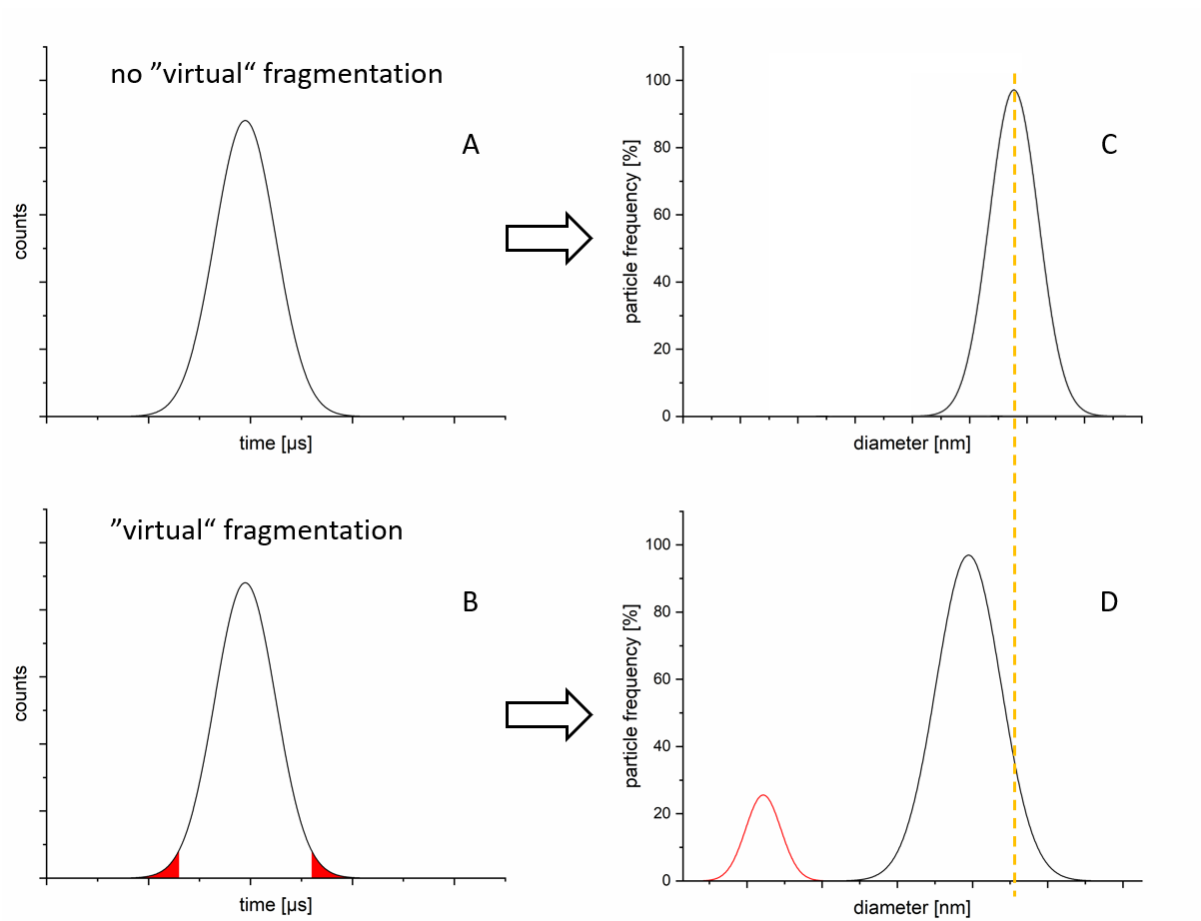
Figure A.8. Data processing struggling with correct evaluation of boundaries of the transient NP signal leading to ideal situation with correct particle boundary evaluation (A, C) and virtual particle fragmentation (B, D).
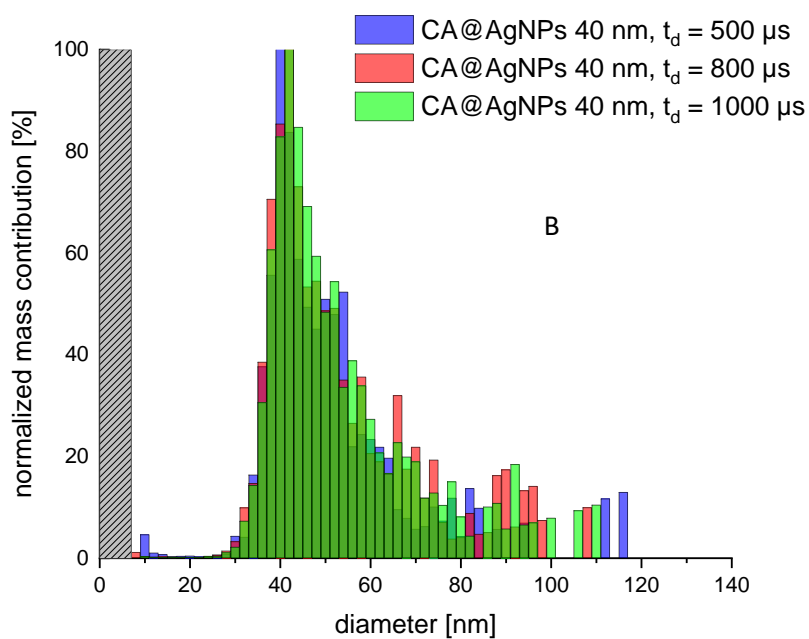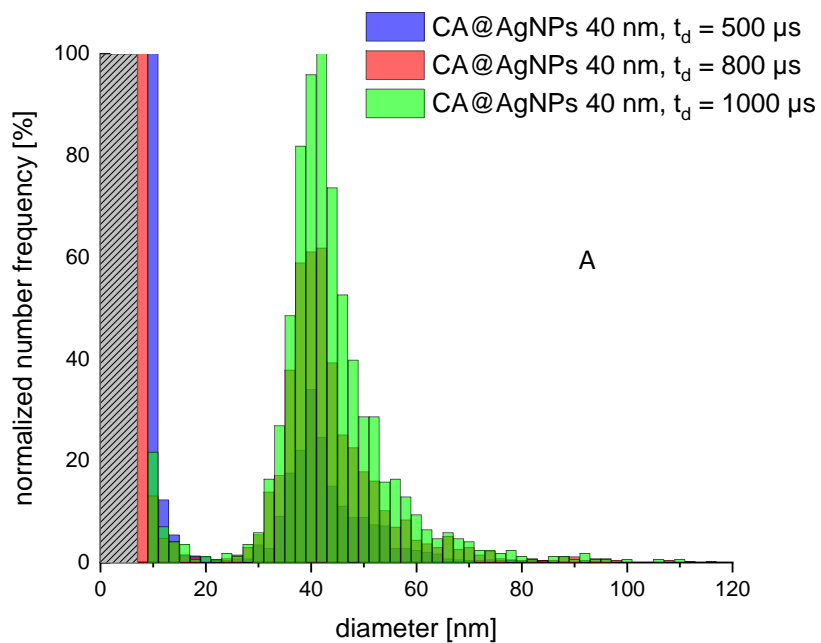
Figure A.9. Particle size distribution on a number frequency basis (A) and a mass contribution basis (B) of 40 nm CA@AgNPs measured by sp-ICP-MS applying different dwell times (t_d). The grey dashed bar in the particle size distributions indicates the SDL.
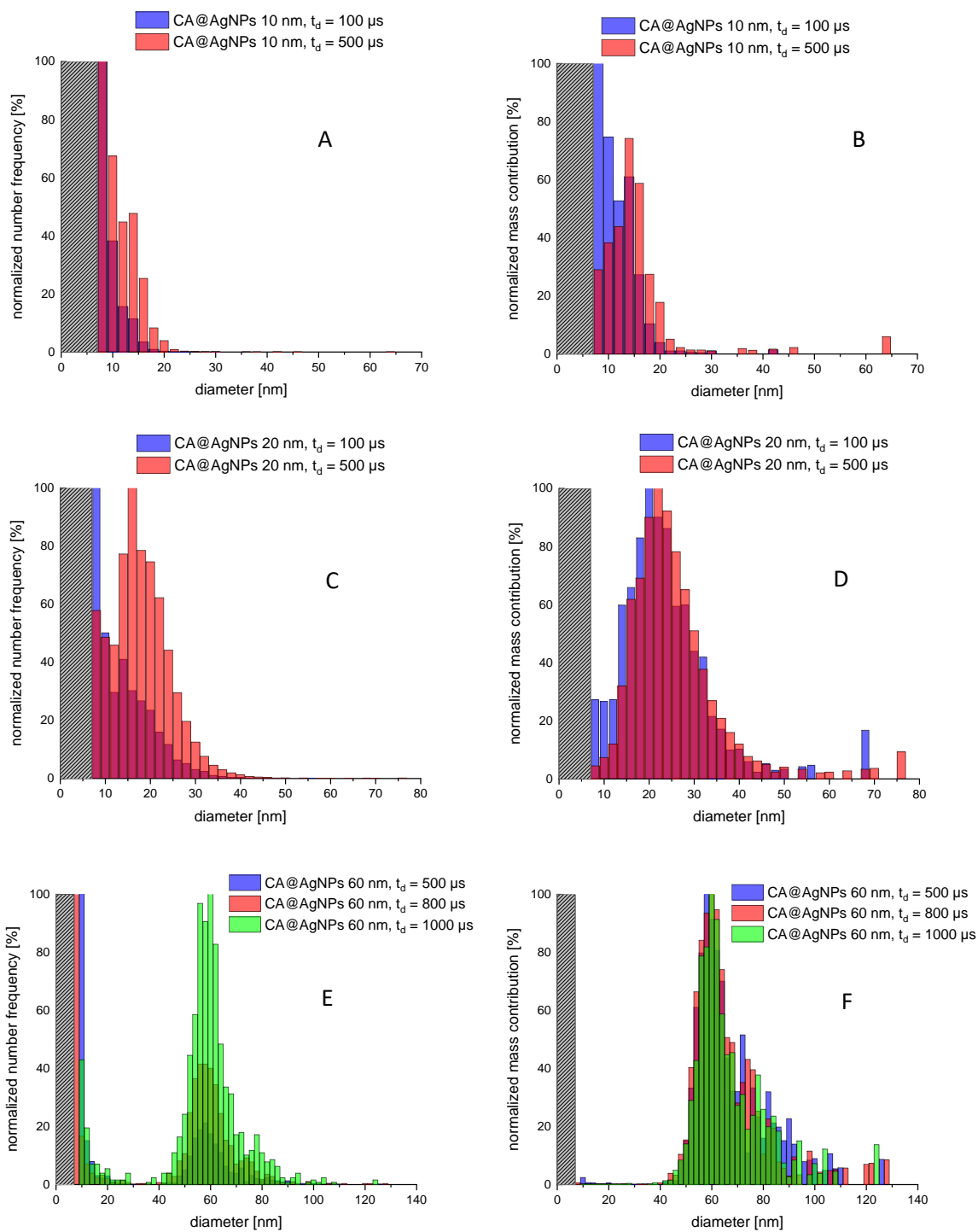
Figure A.10. Comparison of particle size distributions depicted as number frequency and mass contribution for CA@AgNP with a medium diameter of 10 nm (A, B), 20 nm (C, D) and 60 nm (E, F) at different dwell times (t_d). The grey dashed bar in the particle size distributions indicates the SDL, i.e. the cutoff, where NPs cannot be identified as NPs anymore. For reasons of comparison, we chose similar SDL values for both dwell times.

Determination of the size detection limit (SDL) in sp-ICP-MS:

In sp-ICP-MS, peak signals can be transformed into information on masses of each single nanoparticle causing the corresponding peak in the mass spectra. Following the calculations of Pace at al., the mass m_{NP} of a nanoparticle is calculated as follows from the signal intensity I_{NP} [cps] of the corresponding peak, the dwell time t_d [µs], the pump rate v [ml min^{-1}] of the nebulizer, the nebulizing efficiency η, the ratio of molar masses of the whole nanoparticle and the analyte element $\frac{M_{NP}}{M_e}$ (which is 1 for AgNPs), and the elemental sensitivity ES_{ion} [cps/(µg/L)] correlating a signal intensity to a certain analyte concentration:[5]

$$m_{NP} = \frac{I_{NP} \cdot t_d \cdot v \cdot \eta}{ES_{ion}} \cdot \frac{M_{NP}}{M_e} \qquad \text{(Equation 1)}$$

Given the assumptions of a spherical shape of the particles and a homogeneous particle density ρ of the corresponding bulk element, the particle size d_{NP} can be derived from Equation 2 as follows:

$$d_{NP} = \sqrt[3]{\frac{6}{\pi \cdot \rho} \cdot \frac{I_{NP} \cdot t_d \cdot v \cdot \eta}{ES_{ion}} \cdot \frac{M_{NP}}{M_e}} \qquad \text{(Equation 2)}$$

Since I_{NP} must be clearly distinguishable from the background signal, SDL is dependent on the limit of detection (LOD) of I_{NP}. The corresponding LOD signal intensity I_{LOD} was therefore defined as $3 \cdot I_{median}$,[6] whereas I_{median} represents the median of all the signal intensities throughout an entire measurement. I_{median} is in particular influenced by the signals derived from dissolved Ag(I) species and instrument noise. Therefore, SDL can be calculated as follows:

$$SDL = \sqrt[3]{\frac{18}{\pi \cdot \rho} \cdot \frac{I_{median} \cdot t_d \cdot v \cdot \eta}{ES_{ion}} \cdot \frac{M_{NP}}{M_e}} \qquad \text{(Equation 3)}$$
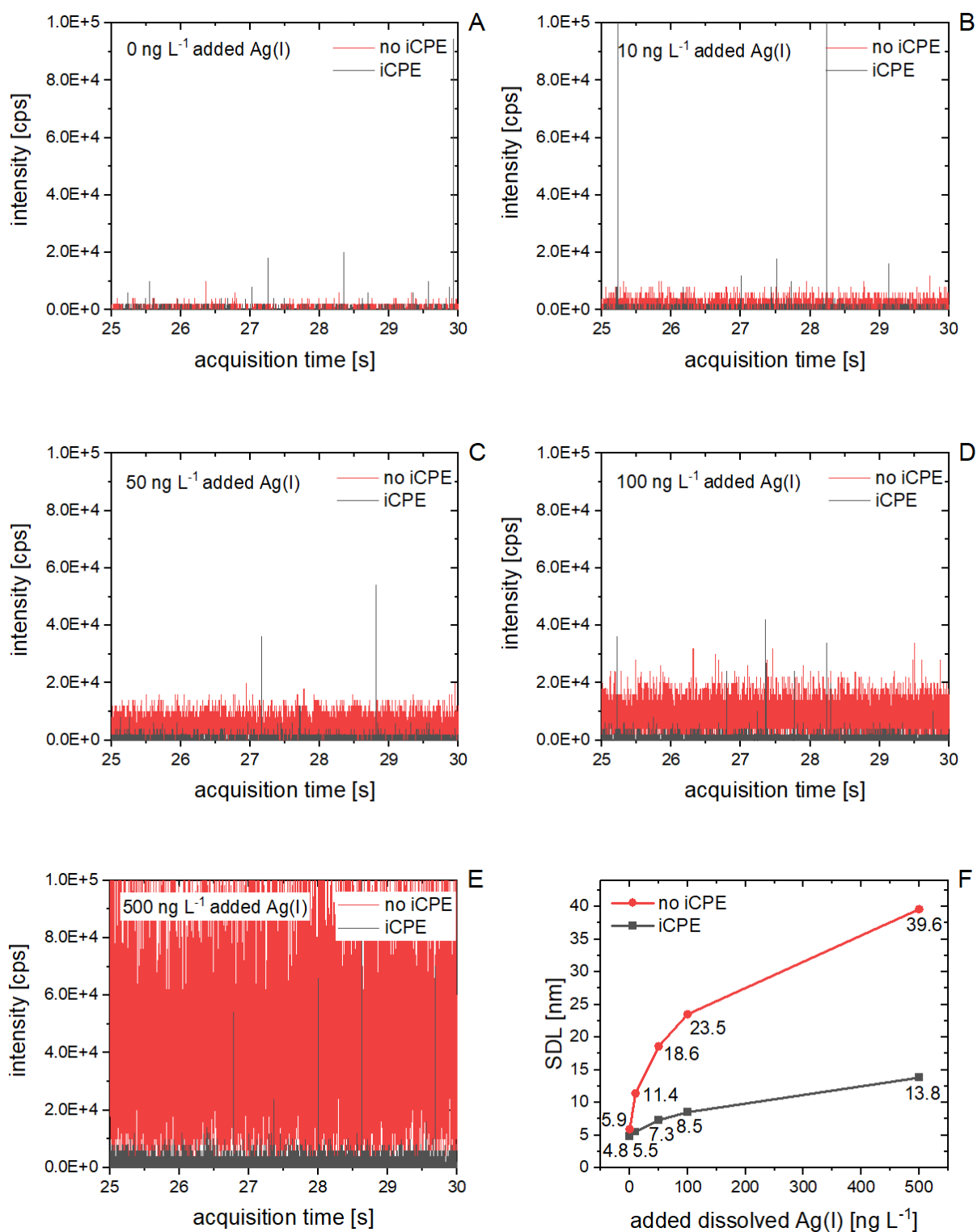
Figure A.11. Mass spectra obtained by sp-ICP-MS (t_d = 500 µs) in presence of increasing amounts of dissolved Ag(I) with and without CPE prior to measurement (A-E). SDL as function of Ag(I) added to samples (F).

References

1. Leung, B. O.; Jalilehvand, F.; Mah, V.; Parvez, M.; Wu, Q., Silver(I) Complex Formation with Cysteine, Penicillamine, and Glutathione. *Inorganic Chemistry* **2013,** *52* (8), 4593-4602.

2. Schmidbaur, H.; Schier, A., Argentophilic Interactions. *Angewandte Chemie International Edition* **2015,** *54* (3), 746-784.

3. Hartmann, G.; Hutterer, C.; Schuster, M., Ultra-trace determination of silver nanoparticles in water samples using cloud point extraction and ETAAS. *Journal of Analytical Atomic Spectrometry* **2013,** *28* (4), 567-572.

4. Wimmer, A.; Kalinnik, A.; Schuster, M., New insights into the formation of silver-based nanoparticles under natural and semi-natural conditions. *Water Research* **2018,** *141*, 227-234.

5. Pace, H. E.; Rogers, N. J.; Jarolimek, C.; Coleman, V. A.; Gray, E. P.; Higgins, C. P.; Ranville, J. F., Single Particle Inductively Coupled Plasma-Mass Spectrometry: A Performance Evaluation and Method Comparison in the Determination of Nanoparticle Size. *Environmental Science & Technology* **2012,** *46* (22), 12272-12280.

6. Lee, S.; Bi, X.; Reed, R. B.; Ranville, J. F.; Herckes, P.; Westerhoff, P., Nanoparticle Size Detection Limits by Single Particle ICP-MS for 40 Elements. *Environmental Science & Technology* **2014,** *48* (17), 10291-10300.

Crystallographic details

a) General information

The X-ray intensity data were collected on an X-ray single crystal diffractometer equipped with a CMOS detector (Bruker Photon-100), an IMS microsource with MoK_α radiation ($\lambda = 0.71073$ Å) and a Helios mirror optic by using the APEX III software package.[S1] The measurement was performed on single crystals coated with perfluorinated ether. The crystal was fixed on the top of a microsampler, transferred to the diffractometer and frozen under a stream of cold nitrogen. A matrix scan was used to determine the initial lattice parameters. Reflections were merged and corrected for Lorenz and polarization effects, scan speed, and background using SAINT.[S2] Absorption corrections, including odd and even ordered spherical harmonics were performed using SADABS.[S2] Space group assignments were based upon systematic absences, E statistics, and successful refinement of the structures. Structures were solved by direct methods with the aid of successive difference Fourier maps, and were refined against all data using the APEX III software[S1] in conjunction with SHELXL-2014[S3] and SHELXLE[S4]. Methyl hydrogen atoms were refined as part of rigid rotating groups, with a C–H distance of 0.98 Å and $U_{iso(H)} = 1.5 \cdot U_{eq(C)}$. Other H atoms were placed in calculated positions and refined using a riding model, with methylene and aromatic C–H distances of 0.99 and 0.95 Å, respectively, and $U_{iso(H)} = 1.2 \cdot U_{eq(C)}$. If not mentioned otherwise, non-hydrogen atoms were refined with anisotropic displacement parameters. Full-matrix least-squares refinements were carried out by minimizing $\Delta w(F_o^2 - F_c^2)^2$ with SHELXL-97[S5] weighting scheme. Neutral atom scattering factors for all atoms and anomalous dispersion corrections for the non-hydrogen atoms were taken from International Tables for Crystallography.[S6] Images of the crystal structures were generated by Mercury.[S7-10]

b) Details for Ag(I)-EDTA

A clear colorless fragment-like specimen of $C_{10}H_{14}Ag_2N_2O_8$ that was crystallized from an aqueous solution, approximate dimensions 0.047 mm x 0.070 mm x 0.116 mm, was used for the X-ray crystallographic analysis.

A total of 1194 frames were collected. The total exposure time was 9.95 hours. The frames were integrated with the Bruker SAINT software package[S2] using a narrow-frame algorithm. The integration of the data using a monoclinic unit cell yielded a total of 11556 reflections to a

maximum θ angle of 25.02° (0.84 Å resolution), of which 1160 were independent (average redundancy 9.962, completeness = 100.0%, R_{int} = 4.18%, R_{sig} = 1.91%) and 995 (85.78%) were greater than $2\sigma(F^2)$. The final cell constants of <u>a</u> = 15.967(3) Å, <u>b</u> = 5.5779(8) Å, <u>c</u> = 15.342(3) Å, β = 106.428(7)°, volume = 1310.6(4) Å^3, are based upon the refinement of the XYZ-centroids of 128 reflections above 20 σ(I) with 5.262° < 2θ < 51.35°. Data were corrected for absorption effects using the multi-scan method (SADABS).[S4] The ratio of minimum to maximum apparent transmission was 0.885. The calculated minimum and maximum transmission coefficients (based on crystal size) are 0.7200 and 0.8710.

The final anisotropic full-matrix least-squares refinement on F^2 with 105 variables converged at R1 = 2.07%, for the observed data and wR2 = 4.53% for all data. The goodness-of-fit was 1.061. The largest peak in the final difference electron density synthesis was 0.511 e$^-$/Å^3 and the largest hole was -0.453 e$^-$/Å^3 with an RMS deviation of 0.102 e$^-$/Å^3. On the basis of the final model, the calculated density was 2.564 g/cm^3 and F(000), 984 e$^-$.

Table A.4: Sample and crystal data for **Ag(I)-EDTA**.

Identification code	WimAn1
Chemical formula	$C_{10}H_{14}Ag_2N_2O_8$
Formula weight	505.97
Temperature	100(2) K
Wavelength	0.71073 Å
Crystal size	0.047 mm x 0.070 mm x 0.116 mm
Crystal habit	clear colorless fragment
Crystal system	monoclinic
Space group	C 2/*c*
Unit cell dimensions	a = 15.967(3) Å $\qquad$ α = 90°
	b = 5.5779(8) Å $\qquad$ β = 106.428(7)°
	c = 15.342(3) Å $\qquad$ γ = 90°
Volume	1310.6(4) Å^3
Z	4
Density (calculated)	2.564 g/cm^3
Absorption coefficient	3.035 mm^{-1}
F(000)	984

Table A.5: Data collection and structure refinement for **Ag(I)-EDTA**.

Diffractometer	Bruker D8 Venture Duo IMS
Radiation source	IMS microsource, Mo
Theta range for data collection	2.66 to 25.02°
Index ranges	-18<=h<=18, -6<=k<=6, -18<=l<=18
Reflections collected	11556
Independent reflections	1160 [R(int) = 0.0418]
Coverage of independent reflections	100.0%
Absorption correction	multi-scan
Max. and min. transmission	0.8710 and 0.7200
Refinement method	Full-matrix least-squares on F^2
Refinement program	SHELXL-2014/7 (Sheldrick, 2014)
Function minimized	$\Sigma\ w(F_o^2 - F_c^2)^2$
Data / restraints / parameters	1160 / 54 / 105
Goodness-of-fit on F^2	1.061
Δ/σ_{max}	0.002
Final R indices	995 data; I>2σ(I) R1 = 0.0207, wR2 = 0.0429
	all data R1 = 0.0284, wR2 = 0.0453
Weighting scheme	w=1/[$\sigma^2(F_o^2)$+(0.0159P)^2+8.6992P] where P=(F_o^2+2F_c^2)/3
Largest diff. peak and hole	0.511 and -0.453 eÅ^{-3}
R.M.S. deviation from mean	0.102 eÅ^{-3}

Supplementary References

[S1] *APEX suite of crystallographic software, APEX 3, version 2015.5-2,* Bruker AXS Inc., Madison, Wisconsin, USA (2015).

[S2] SAINT, Version 7.56a and SADABS Version 2008/1, Bruker AXS Inc., Madison, Wisconsin, USA (2008).

[S3] G. M. Sheldrick, "*SHELXL-2014*", University of Göttingen, Göttingen, Germany, (2014).

[S4] C. B. Huebschle, G. M. Sheldrick, B. Dittrich, *"SHELXLE", J. Appl. Cryst.* **2011,** *44,* 1281.

[S5] G. M. Sheldrick, *"SHELXL-97"*, University of Göttingen, Göttingen, Germany, (1998).

[S6] A. J. C. Wilson, *International Tables for Crystallography*, Vol. C, Tables 6.1.1.4 (pp. 500-502), 4.2.6.8 (pp. 219-222), and 4.2.4.2 (pp. 193-199); Kluwer Academic Publishers: Dordrecht, The Netherlands (1992).

[S7] C. F. Macrae, I. J. Bruno, J. A. Chisholm, P. R. Edgington, P. McCabe, E. Pidcock, L. Rodriguez-Monge, R. Taylor, J. van der Streek, P. A. Wood, *J. Appl. Crystallogr.* **2008,** *41,* 466-470.

[S8] C. F. Macrae, P. R. Edgington, P. McCabe, E. Pidcock, G. P. Shields, R. Taylor, M. Towler, J. van de Streek, *J. Appl. Crystallogr.* **2006,** *39,* 453-457.

[S9] I. J. Bruno, J. C. Cole, P. R. Edgington, M. K. Kessler, C. F. Macrae, P. McCabe, J. Pearson, R. Taylor, *Acta Cryst.* **2002,** *B58,* 389-397.

[S10] R. Taylor, C. F. Macrae, *Acta Cryst.* **2001,** *B57,* 815-827.

8.4 PUBLIKATION 4

Looking at Silver-Based Nanoparticles in Environmental Water Samples: Repetitive Cloud Point Extraction Bridges Gaps in Electron Microscopy for Naturally Occurring Nanoparticles

Alexander Urstoeger, Andreas Wimmer, Ralf Kaegi, Simon Reiter, and Michael Schuster

Abdruck des Artikels mit allgemeiner Genehmigung (siehe Kapitel 7.4) aus Environmental Science and Technology 2020, 54, 19, 12063−12071.

Article

Looking at Silver-Based Nanoparticles in Environmental Water Samples: Repetitive Cloud Point Extraction Bridges Gaps in Electron Microscopy for Naturally Occurring Nanoparticles

Alexander Urstoeger,[§] Andreas Wimmer,[§] Ralf Kaegi, Simon Reiter, and Michael Schuster*

ACCESS | Metrics & More | Article Recommendations | Supporting Information

ABSTRACT: The growing use of silver-based nanoparticles (Ag-b-NPs) in everyday products goes hand in hand with their release into the environment, resulting in ng L^{-1} traces in natural water bodies. In order to assess their fate, possible transformations and ecotoxicology—essential information to proper risk assessment—particle size, shape, and chemical composition have to be determined. Transmission electron microscopy coupled with energy dispersive X-ray spectroscopy (TEM-EDX) is a powerful tool for determining these particle characteristics, but it requires high particle concentrations in order to produce statistically reliable results. In this study, we will present the extraction of Ag-b-NPs at environmentally relevant concentrations down to 5 ng L^{-1} from artificial as well as environmental water samples via cloud point extraction on a repetitive basis. The combination with an on-grid centrifugation technique ensures an efficient concentration and deposition of the extracted particles onto the TEM grid for subsequent TEM-EDX measurements. Furthermore, electron microscopy investigations were supplemented by single particle inductively coupled plasma mass spectrometry (sp-ICP-MS) measurements. Ag-b-NPs were successfully visualized and characterized at environmentally relevant concentrations of 5 ng L^{-1} with TEM-EDX and sp-ICP-MS measurements. Their size, shape, and chemical composition were not affected by the sample preparation.
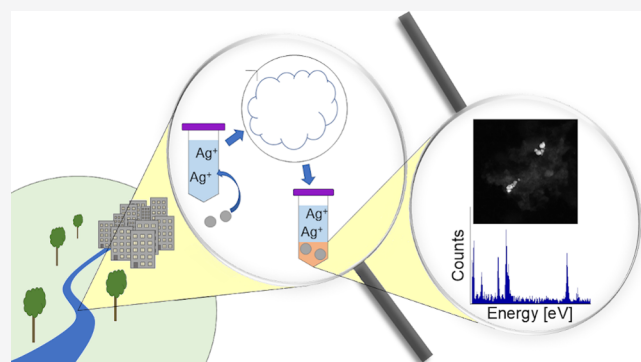
INTRODUCTION

The increasing use of silver nanoparticles (Ag-NPs) in everyday products like toiletries,[1,2] sportswear,[2] food packaging,[3,4] medical products,[4−7] cleaning products,[4] or even paint[8,9] leads to environmental exposure due to the washing, usage, and disposal of those goods.[2,8−11] Although wastewater treatment plants (WWTPs) are able to remove more than 90% of nanoparticulate silver material entering a WWTP, a small amount still reaches the environment via WWTP discharge, resulting in concentrations of 0.7−11.1 ng L^{-1} Ag in the effluent.[12,13] The major amount of nanoparticulate silver is retained in the sewage sludge and can also enter the environment via the sludge fertilization of fields.[12−15] In addition to discharges of Ag-NPs related to anthropogenic activities, Ag-NPs can also be formed via the reduction of dissolved silver by humic and fulvic acids in the environment.[7,16] Once in the environment, Ag-NPs are likely to interact with organisms and therefore pose a risk due to their biotoxicity.[7,15,17,18] Several studies have been carried out focusing on the toxicity of Ag-NPs on, e.g., freshwater invertebrates,[19] vertebrates,[20−22] bacteria,[23−25] algae, plants,[26,27] fungi,[26] and human cells.[28−30] A factor which greatly influences the toxicity of Ag-NPs is their size. It has been reported that smaller particles (<20 nm) are much more

toxic than bigger ones due to their large specific surface area. In one respect, this high intrinsic surface increases the chance of interacting with biomolecules and subsequently entering the cell and, in a second respect, the release of silver ions.[21,31,32] Besides size, it is important to evaluate the ecotoxicity of Ag-NPs on the basis of chemical composition. Levard et al. reported a large decrease in toxicity toward killifish and duckweed by the sulfidation of Ag-NPs.[33] A general decrease in toxicity was reported for all organisms in a wide range of exposure media if the partial sulfidation was larger than 0.073 S/Ag molar ratio. This effect can be explained by the low solubility of Ag_2S. Fewer silver ions are released if an Ag_2S layer is formed around the Ag-NPs.[34] When released into the environment, Ag-NPs readily undergo several transformations, including the adsorption onto organic materials present in the environment, oxidation, (partial) dissolution, and reactions with dissolved species, which result in particles or coatings of,

e.g., Ag_2S, the predominant species in the environment.[14,17,35−38] Also, Wimmer et al. found, that smaller Ag-*b*-NPs are dissolving much faster than bigger ones at environmentally relevant concentrations.[39] A factor, which also influences NP toxicity is their shape. Spherical particles enter cells much more likely than, e.g., nanotubes or fibers.[40] Also, the shape affects the size of NPs, therefore needing to be considered assessing nanoparticle toxicity. In order to address all kinds of silver nanoparticles, we will refer to them hereinafter as silver-based nanoparticles (Ag-*b*-NPs). As indicated above, their fate, possible transformations, and toxicological risks to the contaminated ecosystem predominantly depend on the size, shape, and chemical composition of Ag-*b*-NPs. Thus, these properties have to be investigated to allow for a comprehensive risk assessment. Transmission electron microscopy (TEM) equipped with energy-dispersive X-ray spectroscopy (EDX) is a powerful tool for determining these properties of Ag-*b*-NPs. However, particle-based TEM investigations require high particle concentrations which are well above the concentrations of environmentally occurring Ag-*b*-NPs. This limitation is actually intensified when looking at the conventional grid preparation of NP-containing samples. Only an aliquot of few μL of the whole sample is used for grid-preparation, further increasing detection limits. Screening the TEM grid for a disproportionate time range goes in hand with such high detection limits. Therefore, the present study follows the basic idea of concentrating the Ag-*b*-NPs in a sample of several mL onto a single TEM grid. As a result, detection limits are significantly reduced to environmentally relevant concentrations. One technique which greatly supports those efforts is cloud point extraction (CPE). CPE is capable of not only preconcentrating nanoparticles, but also separating them from dissolved and ionic species present in environmental samples without changing their size, shape, and composition. This technique was originally applied to the analysis of nonpolar organic substances and metal ions after complexation to nonpolar compounds in water.[41,42] Liu et al. were the first to use CPE for NP enrichment.[43,44] CPE for Ag-*b*-NP quantification has been thoroughly investigated and validated in our group.[13,45−47] However, preconcentration factors of CPE in view of environmentally relevant concentrations are not sufficient for subsequent TEM measurements. Thus, this study aims to present a novel method based on CPE in combination with a centrifugation technique for visualizing and characterizing silver nanoparticles in matrices comprising ultrapure water (UPW), as well as environmental water samples down to an environmental relevant concentration of 5 ng L^{-1} with TEM-EDX measurements. This approach covers (i) extracting and enriching Ag-*b*-NPs in environmental samples by CPE in a first step, followed by a second step of (ii) transferring the captured Ag-*b*-NPs onto a TEM grid. After extraction, Ag-*b*-NPs from an original 40 mL sample are present in some μL surfactant rich extract.

Further development of CPE was supported by inductively coupled plasma mass spectrometry (ICP-MS) measurements for Ag concentration analysis and single particle inductively coupled plasma mass spectrometry (sp-ICP-MS) measurements for particle number and size determination. sp-ICP-MS measurements were confirmed by TEM-EDX measurements.

■ MATERIALS AND METHODS

Materials. Acetic acid (glacial), Ag(I) ICP-standard ($AgNO_3$ in 3% HNO_3, β_{Ag} = 1000 mg L^{-1}), ethanol,

ethylenediaminetetraacetate (EDTA) disodium salt, nitric acid (suprapure, 65%), silver(I) nitrate, sodium acetate anhydrous, and sodium dodecyl sulfate were purchased from Merck (Darmstadt, Germany). Indium ICP-standard ($In(NO_3)_3$ in 2−3% HNO_3, β_{In} = 1000mg L^{-1}), dispersions of citrate stabilized silver nanoparticles (CA@Ag-NPs) (β_{Ag} = 20 mg L^{-1}), D-penicillamine, and sodium sulfide (Na_2S) were purchased from Sigma-Aldrich (St. Louis, MO, U.S.A.). According to the supplier, CA@Ag-NPs should have a size of 40 nm. As indicated in the Results and Discussion, the average diameter was 36 nm. The mean particle sizes indicated in this study represent the mean value based on particle number frequency. Since CA@Ag-NP, silver sulfide nanoparticle (Ag_2S-NP (type I and type II)) dispersions contain impurities of dissolved Ag, the stock dispersions were purified from dissolved Ag species by dialysis (3.5 kDa regenerated cellulose membrane by ZelluTrans, Carl Roth, Karslruhe, Germany) prior to use. A citrate stabilized gold nanoparticle dispersion (CA@Au-NPs, NIST reference material RM 8013, 56 nm, β_{Au} = 52 mg L^{-1}) was purchased from the National Institute of Standards and Technology (Gaithersburg, MD, U.S.A.). Poly-L-lysine solution was obtained from Boster Biological Technology (Pleasanton, CA, U.S.A.). Triton X-114 (TX-114) was purchased from AppliChem (Darmstadt, Germany). All chemicals were of at least analytical grade and were checked for Ag contaminations by ICP-MS measurements before use. UPW (resistivity of 18.2 MΩ cm^{-1}) was obtained by a Milli-Q-Gradient System (Millipore GmbH, Schwalbach, Germany).

Instrumentation. A quadrupole mass spectrometer 7900 ICP-MS (Agilent, Santa Clara, CA, U.S.A.) equipped with an autosampler SPS4 (Agilent) and a MicroMist nebulizer (Glass Expansion, Melbourne, Australia) was used for Ag concentration and particle size determination. Ar 4.8 (Westfalen, Münster, Germany) was used as plasma gas. For Ag quantification, the analyte target mass was ^{107}Ag, and ^{115}In for the internal standard. The measurement time was set to 1 s for the analyte and 0.1 s for the internal standard. Each sample was measured five times. Measurements were carried out in He CCT mode to avoid isobaric and polyatomic interferences. The detection limit (DL) was 0.56 ± 0.25 ng L^{-1} (0.14 ± 0.06 ng L^{-1} after conduction of single CPE and 0.03 ± 0.01 ng L^{-1} after $rCPE_5$). Corresponding enrichment factors were taken into account in calculating the detection limit after CPE ($rCPE_5$). Calibration was performed in the range of 1 ng L^{-1} to 200ng L^{-1}. The nebulizer gas pressure was 429 kPa.

In single particle mode, ^{107}Ag was chosen as the target mass as well, and the dwell time was set to 500 μs. The pump rate was determined to be 0.310 mL min^{-1}. A CA@Au-NP (RM 8013) dispersion at an Au concentration of β = 52 ng L^{-1} was used to determine the transport efficiency η, which is the proportion of initial particles in the sample which finally reach the detector. η was determined to be 8% according to a previously approved procedure.[48,49] To prevent particle aggregation, the nanoparticle suspensions were ultrasonicated for 1 min in an ultrasonic bath—Ulsonix Proclean 3.0DSP (Ulsonix, Berlin, Germany). To obtain an element specific signal intensity for the sp-ICP-MS measurements, the signal sensitivity was calibrated using an Ag(I) solution at a concentration of 1 μg L^{-1}. Agilent MassHunter Workstation 4.4 software (version C.01.04) equipped with the Single Nanoparticle Application Module was used to evaluate particle

size distributions. In sp-ICP-MS, transient, peak-like signals deriving from NP ionization events in the plasma are registered by the detector. The NP signal height and area are directly proportional to particle size. However, dissolved analyte species lead to a rather low yet constant signal. In sp-ICP-MS, it is essential to differentiate between the transient peak-like signals and the constant background. An excessive background covers small NP signals. In the event that no dissolved analyte species (β_{Ag} < DL) are present (such as after CPE), no background signal due to dissolved analyte species will be detected and, as a result, only the instrumental noise will limit the size detection limit (SDL). In our case, SDL was determined to be 8 nm.

A dedicated scanning transmission electron microscope (STEM, HD-2700-Cs, Hitachi, Japan) operated at an acceleration voltage of 200 kV was used for the TEM measurements. Images were recorded using either a secondary electron (SE) or a high angular annular dark field (HAADF) detector. Elemental analysis of individual particles was performed using an energy dispersive X-ray detector (EDAX, U.S.A.), and the spectra were recorded and processed using Digital Micrograph (v.1.85, Gatan Inc., U.S.A.).

The TOC content of river water samples was determined using a TOC-L analyzer (Shimadzu, Kyoto, Japan). Potassium hydrogen phthalate was used for calibration (Nacalai Tesque Inc., Kyoto, Japan).

Nanoparticle Synthesis and Characterization. Silver sulfide nanoparticles (Ag_2S-NPs) were synthesized according to a procedure previously published by Pettibone and Liu.[50] In brief, 0.16 mL of a 0.5 M Na_2S solution was added at once to 40 mL of a solution containing 2 mM $AgNO_3$. The mixture was stirred for 1 h in the dark at room temperature (RT). These nanoparticles are referred to as Ag_2S-NPs (type I) hereafter.

TEM-EDX measurements of the purified CA@Ag-NPs dialyzed in previously nonpurified dialysis membranes suggested that an Ag_2S layer formed around the silver core nanoparticles. The dialysis membranes probably contained small amounts of sulfide impurities and induced the sulfide formation for this reason. However, sulfidation might also have taken place during the storage or transport of the NPs. The molar ratio of Ag/S of the particles ranged from 3:1 to 5:1. These particles were used as Ag_2S-NPs (type II), suggesting a core−shell structure with an Ag core and an Ag_2S shell.

The CA@Ag-NP, Ag_2S-NP (type II), and synthesized Ag_2S-NP (type I) suspensions were dialyzed in the dark for 3 days. The water was changed twice a day. For CA@Ag-NPs, the dialysis membrane was put into UPW for several hours, whereas the water was changed twice to get rid of possible sulfide impurities before adding the NP suspension. Dialysis was carried out to separate the nanoparticles from the dissolved silver species and matrix constituents. After dialysis, the nanoparticle suspensions were stored in the dark at 5 °C and were stable for several weeks. The particle size, shape, and chemical composition were determined by TEM-EDX measurements. No sulfidation of CA@Ag-NPs could be detected.

Preconcentration and Separation of Ag-b-NPs from Aqueous Matrices. The UPW and river water samples were mixed with aqueous dispersions of CA@Ag-NPs, Ag_2S-NPs (type II), or synthesized Ag_2S-NPs (type I) to a total volume of 40 mL and a final Ag concentration of 5 ng L^{-1} and 50 ng L^{-1}, respectively. Afterward, CPE was conducted for the

selective enrichment of Ag-b-NPs and separation from dissolved silver species.[45,46,51] For this purpose, 40 mL of each sample were mixed with 100 μL of 1.25 M acetic acid, 400 μL of a 1 M sodium acetate solution, 3 mL of a saturated aqueous solution of ethylenediaminetetraacetic acid disodium salt (EDTA), 1 mL of a 0.1 M D-penicillamine (D-PA) solution, and 1 mL of an aqueous solution of the surfactant TX-114 (10% (w/w)).[16,39,45,46] The mixture was shaken vigorously to ensure thorough mixing and incubated for 30 min at 40 °C. Centrifugation for 12 min at 4500 g was then conducted to enhance phase separation before cooling the sample for 10 min in an ice bath to increase the viscosity of the surfactant rich phase at the bottom of the vial. The aqueous supernatant was removed by means of decantation. For the repetitive CPE, the residual surfactant phase was again mixed with 40 mL of nanoparticle-containing aqueous sample, and CPE reagents were added as described above. In order to compensate for the surfactant loss in the preceding CPE, which was determined gravimetrically, 140 μL of a solution of the surfactant TX-114 (10% (w/w)) was added. Again, the mixture was shaken vigorously and incubated for 30 min at 40 °C. After incubation, the separation of the surfactant phase was enhanced by centrifugation as described above. After cooling the phase-separated mixture in an ice bath, the aqueous supernatant was again removed by decanting. This procedure was repeated until a total of 5 CPEs in a row ($rCPE_5$) were conducted. For sp-ICP-MS measurement, the remaining surfactant droplet containing the extracted and enriched Ag-b-NPs was diluted with 500 μL of ethanol and filled up with UPW to a total volume of 10 mL. To determine the Ag concentration with ICP-MS measurement, the CPE extract was, after carrying out above-mentioned dilution, mixed with HNO_3 yielding 1.625% (v/v) HNO_3 to dissolve extracted Ag-b-NP, thereby increasing the analyte stability and homogeneity. Recovery rates were calculated by dividing the Ag concentration after $rCPE_5$ through the initial Ag concentration in the sample.

Development and Optimization of a Centrifugation Technique for Subsequent Visualization of Ag-b-NPs with TEM-EDX. In order to transfer the Ag-b-NPs in a sample onto a TEM grid for investigation of the particles via TEM-EDX, a direct on-grid centrifugation procedure was used.[52] Several dispersions of 500 ng L^{-1} CA@Ag-NP in UPW were subjected to single CPE as described above. Each CPE extract was applied to a poly-L-Lysin functionalized TEM grid (the preparation is described in the following) − either with or without prior mixing with 500 μL of ethanol. Copper TEM grids (Micro to Nano, Haarlem, Netherlands) were functionalized with poly-L-lysine solution to enhance nanoparticle attachment to the carbon coating of the TEM grid.[53] For this purpose, the TEM grids were put into a droplet of poly-L-Lysin solution for 10 min and then in UPW for another 10 min. This procedure was repeated three times. After each step, the remaining liquid was blotted away with a filter paper. The dry TEM grid was then positioned on an (custom-made) aluminum cone within a micro reaction tube (Eppendorf, Hamburg, Germany). The aluminum cone was covered in Parafilm (Bemis Company Inc., Oshkosh, WI, U.S.A.) prior to positioning the TEM grid to enhance adhesion of TEM grid on the aluminum cone. Figure 1 shows a schematic of the setup. The detailed procedure for the TEM grid preparation is also described in a video.[54] In the following, the NP containing CPE extract was added to this tube. After centrifugation of the whole assembly of extract, aluminum cone, and TEM grid in
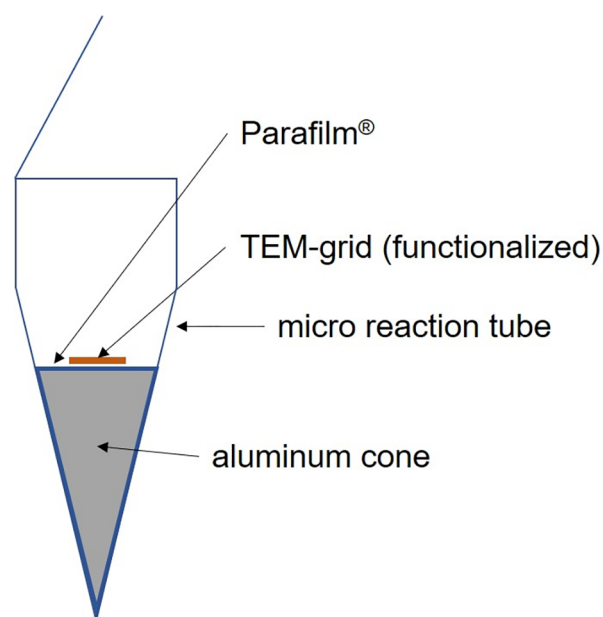
Figure 1. Poly-L-lysin functionalized TEM grid positioned onto an in Parafilm covered aluminum cone. The cone with adhered TEM grid is positioned into a micro reaction tube prior to addition of CPE extract for centrifugation.

the micro reaction tube at 10 000g for 30 min, the NPs from the original 40 mL sample were transferred onto the TEM grid. After centrifugation, the remaining surfactant rich phase was removed by pipetting. The fraction of particles deposited on the TEM grid corresponded to the volumetric fraction of the water column overlying the TEM grid compared to the total volume of suspension in the Eppendorf tube.

Several grid washing approaches using either ethanol or cyclohexane were evaluated to further reduce surfactant induced film formation during the grid preparation. Therefore, samples without added Ag-b-NP (to only observe the matrix effects) made from pure UPW or freshly sampled river water (without filtration) were subjected to a single CPE. As explained above, the extracts were mixed with 500 μL of ethanol in a first step and subsequently applied to the grid. After centrifugation was carried out and the residual surfactant rich phase was removed, the grids were covered with 500 μL of ethanol or cyclohexane. After incubation for 3 min, ethanol or cyclohexane, respectively, were carefully removed again via pipetting. This washing cycle was repeated six times in a row. After all six washing steps, the grid was dried in the reaction tube, gently removed from the aluminum cone, and stored in a TEM storage box until measurement.

In order to test the minimum detectable Ag-b-NP concentrations in environmental water samples, river water (without filtration) which did not contain any Ag traces above 0.56 $\pm$ 0.25 ng L^{-1} was mixed with 60 nm CA@Ag-NPs at concentrations ranging from 5 to 50 and to 500 ng L^{-1} nanoparticulate Ag. After performing CPE, all extracts were mixed with ethanol, and the grid was prepared as mentioned above, including the six washing steps with ethanol.

Investigation of Ag-b-NPs via TEM-EDX after Conduction of rCPE$_5$. For the TEM-EDX measurements, repetitive CPE was conducted 5-fold (rCPE$_5$), including experiments with six extractions in parallel (6 × rCPE$_5$) to lower the limit of detection for TEM measurements. The

rCPE$_5$ extract—diluted with 500 μL ethanol and treated for 5 min in an ultrasonic bath and afterward for 1 min in an ultrasonic device UP200 St coupled to a VialTweeter (Hielscher Ultrasonics GmbH, Teltow, Germany) at half power to prevent particle aggregation—was transferred to a micro reaction tube. Afterward, centrifugation was carried out for 30 min at 10 000 g, resulting in a quantitative deposition of the Ag-b-NPs on the aluminum cone and a corresponding fraction on the TEM grid. After centrifugation, the CPE extract was removed by pipetting. For the experiments with 6 × CPE$_5$, another CPE extract, which was diluted again with 500 μL ethanol and treated in an ultrasonic bath and in the ultrasonic device as described above, was added to the micro reaction tube with the aluminum cone with adhered TEM grid in it, and the aforementioned centrifugation procedure was carried out again. This was done for all six consecutive CPE extracts. After the last centrifugation step and the subsequent removal of the CPE extract via a pipette, the TEM grid was washed six times with ethanol in the micro reaction tube as described above.

River Water Sampling. Surface water samples were taken from the Isarkanal river in Garching, Germany in July 2019 under dry weather conditions. All samples were taken from the same spot and collected in polyvinyl chloride (PVC) containers (0.5 L). Every container was rinsed three times with the sample before being filled with it. Surface water sample characteristics such as pH, TOC, and O$_2$ content are shown in the Supporting Information (SI, Table S1). For the TOC measurements, equal amounts of all samples were mixed together and subjected to TOC measurement. The samples were then filtered with a syringe filter (0.45 μm, cellulose acetate, VWR, Ismaning, Germany) and, after filtration, checked for Ag-b-NP content by single CPE hyphenated to (sp-)ICP-MS measurements. The samples were spiked with Ag$_2$S-NPs (type I) to a final concentration of β_{Ag} = 5 ng L^{-1} before performing rCPE$_5$ to mimic naturally occurring Ag-b-NPs in an environmental surface water matrix. Ag$_2$S-NPs were selected because they represent the majority of naturally occurring Ag-b-NPs.[14,17,35−38] For the sp-ICP-MS measurement, aliquots of all subsamples were mixed together, spiked with Ag$_2$S-NPs (type I), and subjected to rCPE$_5$ as described above and, subsequently, to sp-ICP-MS measurement. For characterization by TEM-EDX measurements, rCPE$_5$ was conducted with each sample, and the remaining surfactant droplets were centrifuged onto a single TEM grid as described above.

Error Calculations. Three independent sample replicates were prepared and measured individually for all measurements. Each sample was measured with five measurement replicates. The uncertainty was calculated via Gaussian error propagation, including pipetting uncertainties and standard deviations of the independently measured sample replicates. The Ag concentrations were blank corrected via measurement of blank samples.

RESULTS AND DISCUSSION

Characterization of Ag-b-NPs. In order to gain information about the size, shape, and chemical composition of Ag-b-NPs in their pristine state, TEM and EDX as well as sp-ICP-MS measurements were carried out for dispersions of freshly synthesized and purified CA@Ag-NPs, Ag$_2$S-NPs (type II), and Ag$_2$S-NPs (type I). In the following, unless stated otherwise, the particle size distributions determined by sp-ICP-

MS measurements are presented on the basis of normalized particle number frequency.

CA@Ag-NPs showed a size range of approximately 16−74 nm (SI Figure S1) of nearly spherical particles (see the TEM image in SI Figure S2). The most frequent diameter of the particles determined by sp-ICP-MS measurement was 36 nm, while the average diameter was 35 nm. A TEM-SE image and the corresponding EDX spectrum of CA@Ag-NPs is shown in the SI, Figure S2.

TEM analyses revealed that the Ag_2S-NPs (type II) particles were spherical, with sizes between 20 and 80 nm (SI Figure S3). The most frequent diameter of the particles determined by sp-ICP-MS measurement was 44 nm, and the average diameter was 43 nm. EDX measurement revealed Ag to S ratios ranging from 3:1 to 5:1, suggesting the formation of an Ag_2S layer around an Ag core. A TEM-SE image of Ag_2S-NPs (type II) and the corresponding EDX spectrum is shown in the SI, Figure S4.

Ag_2S-NPs (type I) showed a size range of approximately 14−80 nm (SI Figure S5) of individual spherical particles, as well as particles which were possibly merged via Ag_2S nanobridges (see the TEM image in the SI Figure S6).[34] The most frequent diameter of the particles determined by sp-ICP-MS measurement was 16 nm, and the average diameter was 25 nm (SI Figure S5). EDX measurements revealed an Ag to S ratio of 2:1, which was consistent with the stoichiometry of acantite. A TEM-SE image of Ag_2S-NPs (type I) and corresponding EDX spectrum is shown in the SI, Figure S6.

Optimization of the Grid-Washing Procedure after the on-Grid Centrifugation for Subsequent TEM-EDX Measurement. In the development and optimization of the centrifugation technique for the subsequent visualization of Ag-*b*-NPs with TEM-EDX, dispersions of 500 ng L^{-1} CA@Ag-NP in UPW were subjected to CPE, and the extract was subsequently centrifuged onto a TEM grid, either with or without the addition of 500 μL of ethanol to the surfactant-rich extract prior centrifugation. As depicted in Figure S7, extracts mixed with ethanol resulted in less film formation, thus facilitating the identification of CA@Ag-NPs in the electron microscope.

TEM grids were washed after centrifugation with different washing reagents. Cyclohexane as a washing reagent led to an increased film formation both for samples made from UPW (Figure S8B) and river water (Figure S8D,F). Washing the prepared grids with ethanol resulted in less film formation (Figure S8A), even in the case of actual river water (Figure S8C,E). Therefore, grids were washed six times in a row using ethanol in all following experiments.

Considerations Regarding the Number of Nanoparticles on the Grid. After optimizing the grid preparation and the washing procedure for reducing film formation to an absolute minimum, the way was paved for the detection of traces of Ag-*b*-NPs in aqueous samples by means of TEM. We thus further investigated the lowest concentration of Ag-*b*-NPs in the samples prior to CPE, which were detectable with a reasonable effort. Theoretical considerations were factored into our experimental approaches. Assuming that the Ag-*b*-NPs exhibit a spherical shape and a density of 10.49 g cm^{-3} (such as the bulk material according to the GESTIS Substance Database, accessed in Mar. 2020 in the case of core Ag-NPs), it was possible to calculate the total number of particles present in a sample of a certain volume, e.g. a 40 mL aqueous sample. Ideally, all of these particles will be transferred onto

the aluminum cone (8 mm diameter). A certain proportion of these particles reach the TEM grid (3.05 mm diameter) positioned on the aluminum cone. The imaging unit exhibits a resolution of, for instance, 1024 × 1024 pixels. In our case, 5 pixels were required to map the entire diameter of one nanoparticle. Given a 60 nm Ag-*b*-NPs, 1 pixel represents 12 nm. Considering said resolution, the area of each image section can be calculated accordingly and, in the following, also the number of image sections per total grid area. The average number of Ag-*b*-NPs on each TEM image section can then be calculated (see Table 1). This illustrates the expected effort for "finding Ag-*b*-NPs" on the grid by microscopy.

Table 1. Calculation of Average Number of Particles Detectable on Each TEM Image, Depending on NP Size and Concentration

Ag-b-NP size (nm)	Ag-b-NP concentration (ng L^{-1})	number of particles each TEM image section
10	5	8
10	50	80
10	500	800
20	5	4
20	50	40
20	500	400
60	5	1
60	50	10
60	500	100

These calculations reveal that, even at concentrations as low as 5 ng L^{-1} of nanoparticulate Ag, it is likely that at least one particle will be detected in each TEM image. However, it must be taken into consideration that these calculations are based on an 100% extraction efficiency during the CPE process. Therefore, the minimum detectable concentrations were also tested via actual experiments.

As depicted in Figure 2, Ag-b-NPs were detected by TEM for all three analyte concentrations, whereas the 5 ng L^{-1}
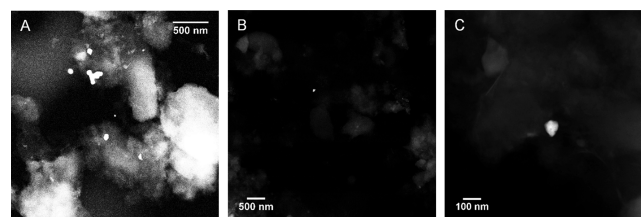
Figure 2. TEM-HAADF images of Ag-b-NPs after CPE of samples initially containing 500 ng L^{-1} (A), 50 ng L^{-1} (B), and 5 ng L^{-1} (C) nanoparticulate Ag from CA@Ag-NPs. Ag-b-NPs were detected in every sample and confirmed by EDX measurements (not shown).

analyte concentration required great effort to find Ag-b-NPs on the TEM grid. Therefore, it becomes necessary to further increase the enrichment factor during TEM grid preparation.

Repetitive Cloud Point Extraction in Ultrapure Water. In order to further improve the enrichment factor during CPE, CPE was performed as a repetitive CPE (rCPE), in this case CPE was repeated five times (rCPE$_5$). The recovery rates of rCPE$_5$ of CA@AgNPs, Ag_2S-NPs (type II), and Ag_2S-NPs (type I) at a final silver concentration of β_{Ag} = 5 ng L^{-1} and β_{Ag} = 50 ng L^{-1}, respectively, in ultrapure water (UPW) are presented in Table 2. Both nanoparticulate Ag concentrations

Table 2. Recovery Rates of Ag-b-NPs Conducting rCPE$_5$ at an Initial Concentration of β_{Ag} = 5 ng L^{-1} and 50 ng L^{-1}, Respectively

NPs	recovery rates (%)	
	β_{Ag} = 5 ng L^{-1}	β_{Ag} = 50 ng L^{-1}
CA@Ag-NPs	89 ± 4	100 ± 6
Ag$_2$S-NPs (type II)	83 ± 4	83 ± 4
Ag$_2$S-NPs (type I)	77 ± 2	73 ± 1

were extracted equally well. However, a higher degree of nanoparticle sulfidation showed slightly lower recovery rates than for core silver nanoparticles. The nanoparticle size and composition were not affected by the extraction method, as demonstrated by sp-ICP-MS and TEM-EDX measurements (Figures 3 and S9). The detailed procedure for the TEM grid preparation is described in a video[54] and in the Materials and Methods section (Development and optimization of a centrifugation technique for subsequent visualization of Ag-b-NPs with TEM-EDX). Particles of all sizes were extracted equally well. In order to achieve a further increase in the enrichment factors, which would be beneficial for visualizing Ag-b-NPs using TEM, rCPE$_5$ was run six times in parallel (6 × rCPE$_5$). However, the TEM measurements conducted on samples prepared after rCPE$_5$ and 6 × rCPE$_5$ (whereas all six extracts were centrifuged one after another onto a single TEM grid) were very comparable. Treating the grid several times with a CPE extract as described above may also lead to unproducible redispersion of Ag-b-NPs from the grid. This means that conducting only rCPE$_5$—without running it six times in parallel—ensures a preconcentration sufficient for

visualizing Ag-b-NPs down to an environmentally relevant concentration of β_{Ag} = 5 ng L^{-1} using TEM (-EDX) measurements and without a major search effort.

Repetitive Cloud Point Extraction in River Surface Water. In order to investigate the robustness and applicability of rCPE$_5$ using actual environmental water samples, rCPE$_5$ was conducted with river surface water samples. Surface water sample characteristics such as pH, TOC, and O$_2$ content are shown in the SI (Table S1). The water samples revealed Ag-b-NP concentrations of β_{Ag} = 0.34 ± 0.04 ng L^{-1} (LOD was 0.03 ± 0.01 ng L^{-1} after rCPE$_5$). However, sp-ICP-MS measurements showed no particle signals, indicating that no particles >8 nm were present in the samples. The river water was spiked with Ag$_2$S-NPs (type I) at a final concentration of β_{Ag} = 5 ng L^{-1}. Subsamples of the aforementioned river water were subjected to rCPE$_5$, and subsequent ICP-MS measurements showed recovery rates of 65 ± 15%, indicating that most particles of the original sample were successfully extracted. The particle size and composition were not affected by the extraction technique (Figures 4 and 5). As with the model-systems in ultrapure water, particles of each size were extracted equally well, which shows that the environmental water matrix does not influence the extraction efficiency (Figure 5). These findings show the huge potential of this method for particle size and composition determination in environmental samples with sp-ICP-MS and TEM-EDX measurements, because it is able to provide this information at environmentally relevant concentrations and in complex environmental matrices. The size, shape, and chemical composition of nanoparticles are the key parameters in determining their environmental fate,
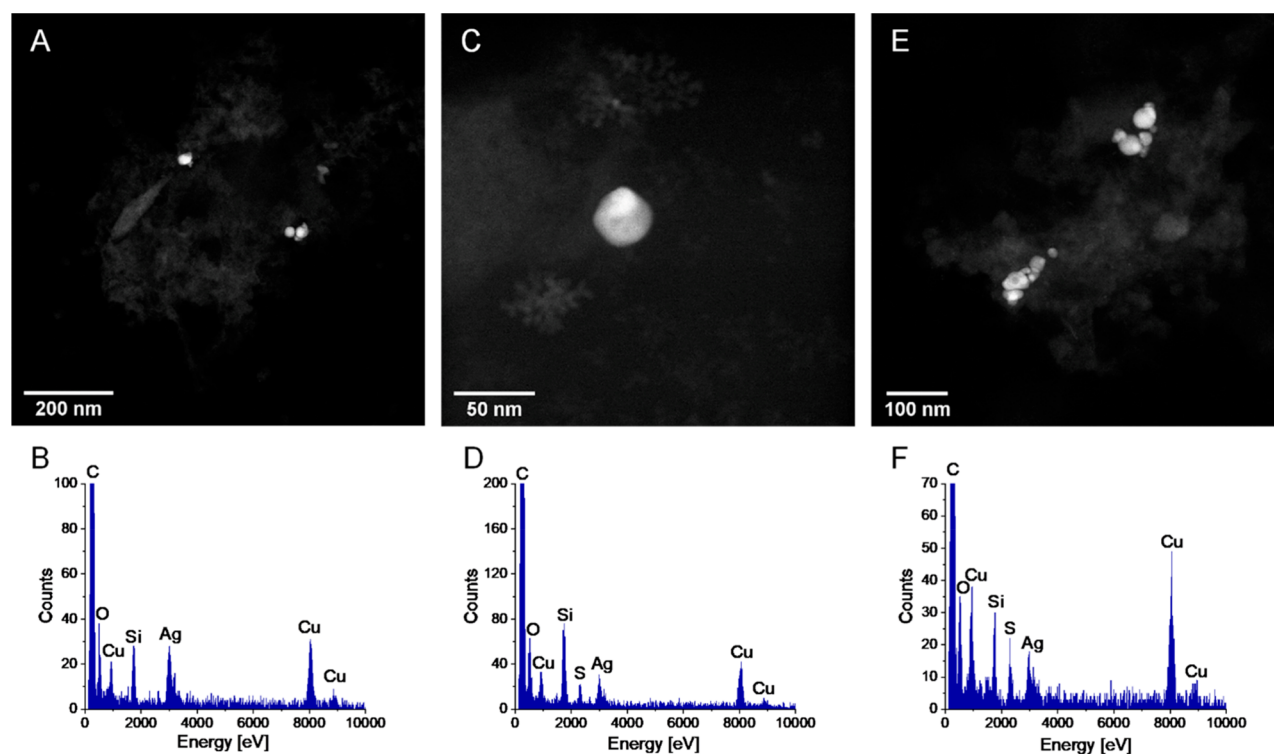
Figure 3. TEM-HAADF images and corresponding EDX spectra of CA@Ag-NPs (A, B), Ag$_2$S-NPs (type II) (C, D), and Ag$_2$S-NPs (type I) (E, F) at an environmental relevant silver concentration of β_{Ag} = 5 ng L^{-1} after rCPE$_5$ conducted in UPW. Additional C-, O-, Si-, and Cu-signals in the spectrum result from the sample carrier (copper grid with carbon film), and carbohydrate contamination during TEM measurement and residues from CPE chemicals.

Figure 5. Comparison of particle size distributions of Ag_2S-NPs (type I) spiked to a river water sample (Isarkanal river) after $rCPE_5$ at a concentration of $c(Ag) = 5$ ng L^{-1} and of Ag_2S-NPs (type I) before $rCPE_5$ (pristine state). The size distributions presented are based on normalized particle number frequencies obtained by sp-ICP-MS measurements.
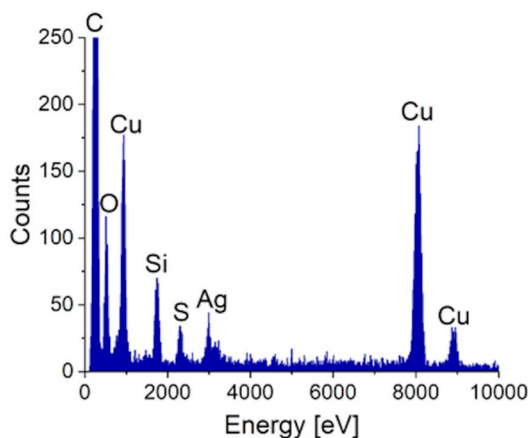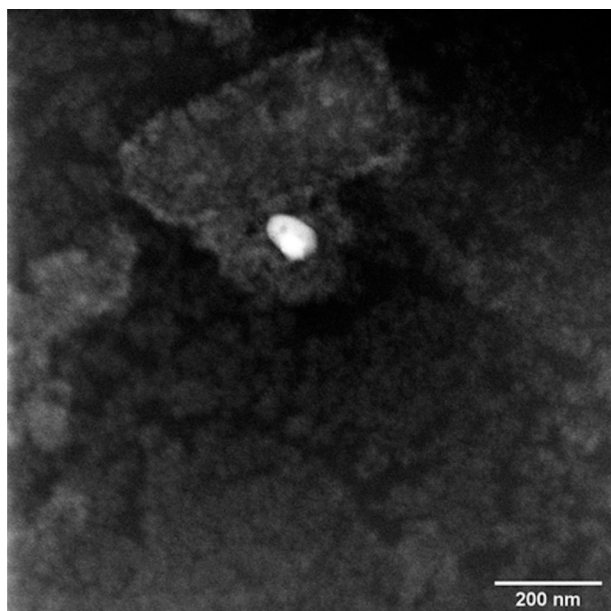
Figure 4. TEM-HAADF image and corresponding EDX spectrum of Ag_2S-NPs (type I) spiked to a river water sample (river Isarkanal) after $rCPE_5$ from samples originally containing 5 ng L^{-1} Ag. Additional C-, O-, Si-, and Cu-signals in the spectrum resulted from the sample carrier (copper grid with carbon film), carbohydrate contamination during illumination, residues from CPE chemicals and natural organic matter (NOM) residues from the environmental water sample.

possible transformations, and ecotoxicity, thus underlining the tremendous potential of the approach presented.

Environmental Impact. A proper risk assessment of the fate, transformations and ecotoxicity of NPs in the environment calls for essential information about particle size, shape, and chemical composition at environmentally relevant concentrations (ng L^{-1}) in complex environmental matrices. We hope that our presented approach can contribute to a comprehensive discussion on environmental concerns regarding the release, fate, possible transformations, and ecotoxicity of Ag-b-NPs in the environment. We hope the presented approach finds its way towards a standard procedure for the determination of nanoparticles in environmental samples, as it may also easily be adapted for the determination of other metal containing nanoparticles or even, e.g., micro- and nanoplastics.

ASSOCIATED CONTENT

Supporting Information

The Supporting Information is available free of charge at https://pubs.acs.org/doi/10.1021/acs.est.0c02878.

Particle size distributions, TEM images, and EDX spectra of Ag-b-NPs; TEM images of the development of the centrifugation approach; and environmental water sample characteristics (PDF)

AUTHOR INFORMATION

Corresponding Author

Michael Schuster − *Division of Analytical Chemistry, Department of Chemistry, Technical University of Munich, Garching 85748, Germany;* Phone: +49 (0)89 289 13763; Email: michael.schuster@tum.de; Fax: +49 (0)89 289 14513

Authors

Alexander Urstoeger − *Division of Analytical Chemistry, Department of Chemistry, Technical University of Munich, Garching 85748, Germany;* orcid.org/0000-0003-1911-5070

Andreas Wimmer − *Division of Analytical Chemistry, Department of Chemistry, Technical University of Munich, Garching 85748, Germany;* orcid.org/0000-0002-1746-8932

Ralf Kaegi − *Eawag, Swiss Federal Institute of Aquatic Science and Technology, Dübendorf 8600, Switzerland;* orcid.org/0000-0002-2430-4733

Simon Reiter − *Division of Analytical Chemistry, Department of Chemistry, Technical University of Munich, Garching 85748, Germany*

Complete contact information is available at:
https://pubs.acs.org/10.1021/acs.est.0c02878

Author Contributions

§These authors contributed equally to the present study. M. Schuster supervised the study. A. Urstoeger designed the study and its experimental setup. A. Urstoeger carried out the synthesis of the Ag-*b*-NPs, rCPE studies and river water sampling and all corresponding analytical measurements

■ REFERENCES

(1) Kessler, R. Engineered Nanoparticles in Consumer Products: Understanding a New Ingredient. *Environ. Health Perspect.* **2011**, *119*, A120−A125.

(2) Benn, T.; Cavanagh, B.; Hristovski, K.; Posner, J. D.; Westerhoff, P. The Release of Nanosilver from Consumer Products Used in the Home. *J. Environ. Qual.* **2010**, *39*, 1875−1882.

(3) Duncan, T. V. Applications of Nanotechnology in Food Packaging and Food Safety: Barrier Materials, Antimicrobials and Sensors. *J. Colloid Interface Sci.* **2011**, *363*, 1−24.

(4) Kim, B.; Park, C.-S.; Murayama, M.; Hochella, M. F. Discovery and Characterization of Silver Sulfide Nanoparticles in Final Sewage Sludge Products. *Environ. Sci. Technol.* **2010**, *44*, 7509−7514.

(5) Soenen, S. J.; Parak, W. J.; Rejman, J.; Manshian, B. (Intra)cellular Stability of Inorganic Nanoparticles: Effects on Cytotoxicity, Particle Functionality, and Biomedical Applications. *Chem. Rev.* **2015**, *115*, 2109−2135.

(6) Stark, W. J.; Stoessel, P. R.; Wohlleben, W.; Hafner, A. Industrial Applications of Nanoparticles. *Chem. Soc. Rev.* **2015**, *44*, 5793−5805.

(7) Sharma, V. K.; Filip, J.; Zboril, R.; Varma, R. S. Natural Inorganic Nanoparticles - Formation, Fate, and Toxicity in the Environment. *Chem. Soc. Rev.* **2015**, *44*, 8410−8423.

(8) Mueller, N. C.; Nowack, B. Exposure Modeling of Engineered Nanoparticles in the Environment. *Environ. Sci. Technol.* **2008**, *42*, 4447−4453.

(9) Kaegi, R.; Sinnet, B.; Zuleeg, S.; Hagendorfer, H.; Mueller, E.; Vonbank, R.; Boller, M.; Burkhardt, M. Release of Silver Nanoparticles from Outdoor Facades. *Environ. Pollut.* **2010**, *158*, 2900−2905.

(10) Benn, T. M.; Westerhoff, P. Nanoparticle Silver Released into Water from Commercially Available Sock Fabrics. *Environ. Sci. Technol.* **2008**, *42*, 4133−4139.

(11) Glover, R. D.; Miller, J. M.; Hutchison, J. E. Generation of Metal Nanoparticles from Silver and Copper Objects: Nanoparticle Dynamics on Surfaces and Potential Sources of Nanoparticles in the Environment. *ACS Nano* **2011**, *5*, 8950−8957.

(12) Tiede, K.; Boxall, A. B. A.; Wang, X.; Gore, D.; Tiede, D.; Baxter, M.; David, H.; Tear, S. P.; Lewis, J. Application of Hydrodynamic Chromatography-ICP-MS to Investigate the Fate of Silver Nanoparticles in Activated Sludge. *J. Anal. At. Spectrom.* **2010**, *25*, 1149−1154.

(13) Li, L.; Stoiber, M.; Wimmer, A.; Xu, Z.; Lindenblatt, C.; Helmreich, B.; Schuster, M. To What Extent Can Full-Scale Wastewater Treatment Plant Effluent Influence the Occurrence of Silver-Based Nanoparticles in Surface Waters? *Environ. Sci. Technol.* **2016**, *50*, 6327−6333.

(14) Kaegi, R.; Voegelin, A.; Ort, C.; Sinnet, B.; Thalmann, B.; Krismer, J.; Hagendorfer, H.; Elumelu, M.; Mueller, E. Fate and Transformation of Silver Nanoparticles in Urban Wastewater Systems. *Water Res.* **2013**, *47*, 3866−3877.

(15) Kampe, S.; Kaegi, R.; Schlich, K.; Wasmuth, C.; Hollert, H.; Schlechtriem, C. Silver Nanoparticles in Sewage Sludge: Bioavailability of Sulfidized Silver to the Terrestrial Isopod Porcellio Scaber. *Environ. Toxicol. Chem.* **2018**, *37*, 1606−1613.

(16) Wimmer, A.; Kalinnik, A.; Schuster, M. New Insights into the Formation of Silver-based Nanoparticles under Natural and Semi-Natural Conditions. *Water Res.* **2018**, *141*, 227−234.

(17) Levard, C.; Hotze, E. M.; Lowry, G. V.; Brown, G. E. Environmental Transformations of Silver Nanoparticles: Impact on Stability and Toxicity. *Environ. Sci. Technol.* **2012**, *46*, 6900−6914.

(18) Wijnhoven, S. W. P.; Peijnenburg, W. J. G. M.; Herberts, C. A.; Hagens, W. I.; Oomen, A. G.; Heugens, E. H. W.; Roszek, B.; Bisschops, J.; Gosens, I.; Van De Meent, D.; Dekkers, S.; De Jong, W. H.; van Zijverden, M.; Sips, A. J. A. M.; Geertsma, R. E. Nano-Silver - a Review of Available Data and Knowledge Gaps in Human and Environmental Risk Assessment. *Nanotoxicology* **2009**, *3*, 109−138.

(19) Lekamge, S.; Miranda, A. F.; Abraham, A.; Li, V.; Shukla, R.; Bansal, V.; Nugegoda, D. The Toxicity of Silver Nanoparticles (AgNPs) to Three Freshwater Invertebrates With Different Life Strategies: Hydra Vulgaris, Daphnia Carinata, and Paratya Australiensis. *Front. Environ. Sci.* **2018**, *6* DOI: 10.3389/fenvs.2018.00152.

(20) Asharani, P. V.; Lian Wu, Y.; Gong, Z.; Valiyaveettil, S. Toxicity of Silver Nanoparticles in Zebrafish Models. *Nanotechnology* **2008**, *19*, 255102.

(21) Cho, Y.-M.; Mizuta, Y.; Akagi, J.-I.; Toyoda, T.; Sone, M.; Ogawa, K. Size-Dependent Acute Toxicity of Silver Nanoparticles in Mice. *J. Toxicol. Pathol.* **2018**, *31*, 73−80.

(22) Kumar, V.; Sharma, N.; Maitra, S. S. In Vitro and In Vivo Toxicity Assessment of Nanoparticles. *Int. Nano Lett.* **2017**, *7*, 243−256.

(23) Hajipour, M. J.; Fromm, K. M.; Akbar Ashkarran, A.; Jimenez de Aberasturi, D.; de Larramendi, I. R.; Rojo, T.; Serpooshan, V.; Parak, W. J.; Mahmoudi, M. Antibacterial Properties of Nanoparticles. *Trends Biotechnol.* **2012**, *30*, 499−511.

(24) Pal, S.; Tak, Y. K.; Song, J. M. Does the Antibacterial Activity of Silver Nanoparticles Depend on the Shape of the Nanoparticle? A Study of the Gram-Negative Bacterium Escherichia Coli. *Appl. Environ. Microbiol.* **2007**, *73*, 1712−1720.

(25) Shrivastava, S.; Bera, T.; Roy, A.; Singh, G.; Ramachandrarao, P.; Dash, D. Characterization of Enhanced Antibacterial Effects of Novel Silver Nanoparticles. *Nanotechnology* **2007**, *18*, 225103.

(26) Navarro, E.; Baun, A.; Behra, R.; Hartmann, N. B.; Filser, J.; Miao, A. J.; Quigg, A.; Santschi, P. H.; Sigg, L. Environmental Behavior and Ecotoxicity of Engineered Nanoparticles to Algae, Plants, and Fungi. *Ecotoxicology* **2008**, *17*, 372−386.

(27) Yan, A.; Chen, Z. Impacts of Silver Nanoparticles on Plants: A Focus on the Phytotoxicity and Underlying Mechanism. *Int. J. Mol. Sci.* **2019**, *20*, 1003.

(28) Asharani, P. V.; Low Kah Mun, G.; Hande, M. P.; Valiyaveettil, S. Cytotoxicity and Genotoxicity of Silver Nanoparticles in Human Cells. *ACS Nano* **2009**, *3*, 279−290.

(29) Haase, A.; Tentschert, J.; Jungnickel, H.; Graf, P.; Mantion, A.; Draude, F.; Plendl, J.; Goetz, M. E.; Galla, S.; Mašić, A.; Thuenemann, A. F.; Taubert, A.; Arlinghaus, H. F.; Luch, A. Toxicity of Silver Nanoparticles in Human Macrophages: Uptake, Intracellular Distribution and Cellular Responses. *J. Phys.: Conf. Ser.* **2011**, *304*, 012030.

(30) Lu, W.; Senapati, D.; Wang, S.; Tovmachenko, O.; Singh, A. K.; Yu, H.; Ray, P. C. Effect of Surface Coating on the Toxicity of Silver Nanomaterials on Human Skin Keratinocytes. *Chem. Phys. Lett.* **2010**, *487*, 92−96.

(31) Park, M. V. D. Z.; Neigh, A. M.; Vermeulen, J. P.; de la Fonteyne, L. J. J.; Verharen, H. W.; Briedé, J. J.; van Loveren, H.; de

Jong, W. H. The Effect of Particle Size on the Cytotoxicity, Inflammation, Developmental Toxicity and Genotoxicity of Silver Nanoparticles. *Biomaterials* **2011**, *32*, 9810−9817.

(32) Sotiriou, G. A.; Pratsinis, S. E. Antibacterial Activity of Nanosilver Ions and Particles. *Environ. Sci. Technol.* **2010**, *44*, 5649−5654.

(33) Levard, C.; Hotze, E. M.; Colman, B. P.; Dale, A. L.; Truong, L.; Yang, X. Y.; Bone, A. J.; Brown, G. E., Jr.; Tanguay, R. L.; Di Giulio, R. T.; Bernhardt, E. S.; Meyer, J. N.; Wiesner, M. R.; Lowry, G. V. Sulfidation of Silver Nanoparticles: Natural Antidote to their Toxicity. *Environ. Sci. Technol.* **2013**, *47*, 13440−13448.

(34) Levard, C.; Reinsch, B. C.; Michel, F. M.; Oumahi, C.; Lowry, G. V.; Brown, G. E. Sulfidation Processes of PVP-coated Silver Nanoparticles in Aqueous Solution: Impact on Dissolution Rate. *Environ. Sci. Technol.* **2011**, *45*, 5260−5266.

(35) Kaegi, R.; Voegelin, A.; Sinnet, B.; Zuleeg, S.; Hagendorfer, H.; Burkhardt, M.; Siegrist, H. Behavior of Metallic Silver Nanoparticles in a Pilot Wastewater Treatment Plant. *Environ. Sci. Technol.* **2011**, *45*, 3902−3908.

(36) Kaegi, R.; Voegelin, A.; Sinnet, B.; Zuleeg, S.; Siegrist, H.; Burkhardt, M. Transformation of AgCl Nanoparticles in a Sewer System - A field study. *Sci. Total Environ.* **2015**, *535*, 20−27.

(37) Nowack, B. Nanosilver Revisited Downstream. *Science* **2010**, *330*, 1054−1055.

(38) Nowack, B.; Ranville, J. F.; Diamond, S.; Gallego-Urrea, J. A.; Metcalfe, C.; Rose, J.; Horne, N.; Koelmans, A. A.; Klaine, S. J. Potential Scenarios for Nanomaterial Release and Subsequent Alteration in the Environment. *Environ. Toxicol. Chem.* **2012**, *31*, 50−59.

(39) Wimmer, A.; Urstoeger, A.; Funck, N. C.; Adler, F. P.; Lenz, L.; Doeblinger, M.; Schuster, M. What Happens to Silver-based Nanoparticles if They Meet Seawater? *Water Res.* **2020**, *171*, 115399.

(40) Champion, J. A.; Mitragotri, S. Role of Target Geometry in Phagocytosis. *Proc. Natl. Acad. Sci. U. S. A.* **2006**, *103*, 4930−4934.

(41) Stalikas, C. D. Micelle-mediated Extraction as a Tool for Separation and Preconcentration in Metal Analysis. *TrAC, Trends Anal. Chem.* **2002**, *21*, 343−355.

(42) Quina, F. H.; Hinze, W. L. Surfactant-mediated Cloud Point Extractions: An Environmentally Benign Alternative Separation Approach. *Ind. Eng. Chem. Res.* **1999**, *38*, 4150−4168.

(43) Liu, J.-F.; Chao, J.-b.; Liu, R.; Tan, Z.-q.; Yin, Y.-g.; Wu, Y.; Jiang, G.-b. Cloud Point Extraction as an Advantageous Preconcentration Approach for Analysis of Trace Silver Nanoparticles in Environmental Waters. *Anal. Chem.* **2009**, *81*, 6496−6502.

(44) Chao, J. B.; Liu, J. F.; Yu, S. J.; Feng, Y. D.; Tan, Z. Q.; Liu, R.; Yin, Y. G. Speciation Analysis of Silver Nanoparticles and Silver Ions in Antibacterial Products and Environmental Waters via Cloud Point Extraction-based Separation. *Anal. Chem.* **2011**, *83*, 6875−6882.

(45) Hartmann, G.; Hutterer, C.; Schuster, M. Ultra-Trace Determination of Silver Nanoparticles in Water Samples Using Cloud Point Extraction and ETAAS. *J. Anal. At. Spectrom.* **2013**, *28*, 567−572.

(46) Hartmann, G.; Baumgartner, T.; Schuster, M. Influence of Particle Coating and Matrix Constituents on the Cloud Point Extraction Efficiency of Silver Nanoparticles (Ag-NPs) and Application for Monitoring the Formation of Ag-NPs from Ag⁺. *Anal. Chem.* **2014**, *86*, 790−796.

(47) Wimmer, A.; Ritsema, R.; Schuster, M.; Krystek, P. Sampling and Pre-Treatment Effects on the Quantification of (Nano)silver and Selected Trace Elements in Surface Water - Application in a Dutch Case Study. *Sci. Total Environ.* **2019**, *663*, 154−161.

(48) Peters, R. J.; Rivera, Z. H.; van Bemmel, G.; Marvin, H. J.; Weigel, S.; Bouwmeester, H. Development and Validation of Single Particle ICP-MS for Sizing and Quantitative Determination of Nano-Silver in Chicken Meat. *Anal. Bioanal. Chem.* **2014**, *406*, 3875−3885.

(49) Montaño, M. D.; Olesik, J. W.; Barber, A. G.; Challis, K.; Ranville, J. F. Single Particle ICP-MS: Advances Toward Routine Analysis of Nanomaterials. *Anal. Bioanal. Chem.* **2016**, *408*, 5053−5074.

(50) Pettibone, J. M.; Liu, J. In Situ Methods for Monitoring Silver Nanoparticle Sulfidation in Simulated Waters. *Environ. Sci. Technol.* **2016**, *50*, 11145−11153.

(51) Duester, L.; Fabricius, A. L.; Jakobtorweihen, S.; Philippe, A.; Weigl, F.; Wimmer, A.; Schuster, M.; Nazar, M. F. Can Cloud Point-based Enrichment, Preservation, and Detection Methods Help to Bridge Gaps in Aquatic Nanometrology? *Anal. Bioanal. Chem.* **2016**, *408*, 7551−7557.

(52) Mavrocordatos, D.; Perret, D. Non-artifacted Specimen Preparation for Transmission Electron Microscopy of Submicron Soil Particles. *Commun. Soil Sci. Plant Anal.* **1995**, *26*, 2593−2602.

(53) Prasad, A.; Lead, J. R.; Baalousha, M. An Electron Microscopy Based Method for the Detection and Quantification of Nanomaterial Number Concentration in Environmentally Relevant Media. *Sci. Total Environ.* **2015**, *537*, 479−486.

(54) How To Prepare a TEM Sample by Centrifugation. https:// www.youtube.com/watch?v=PplBlJ7zCCA (accessed 2020).

Supplementary Information

Looking at Silver-Based Nanoparticles in Environmental Water Samples: Repetitive Cloud Point Extraction Bridges Gaps in Electron Microscopy for Naturally Occurring Nanoparticles

Alexander Urstoeger,[†,§] *Andreas Wimmer,*[†,§] *Ralf Kaegi,*[‡] *Simon Reiter,*[†] *Michael Schuster*[*,†]

[†]Division of Analytical Chemistry, Department of Chemistry, Technical University of Munich, Lichtenbergstraße 4, Garching 85748, Germany

[‡]Eawag, Swiss Federal Institute of Aquatic Science and Technology, Überlandstrasse 133, Dübendorf 8600, Switzerland

[§]These authors contributed equally to the present study.

Corresponding author. *Tel: +49 (0)89 289 13763; fax: +49 (0)89 289 14513; email address: michael.schuster@tum.de

8 pages

9 figures

1 table

16
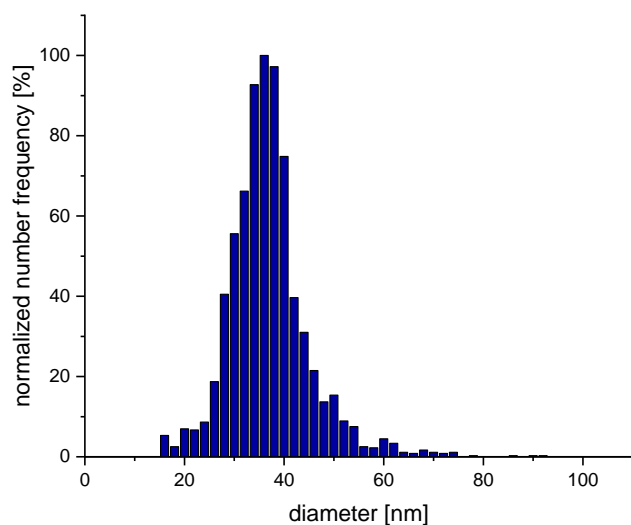
Figure S1. Particle size distribution of CA@Ag-NPs based on normalized particle number frequency obtained by sp-ICP-MS measurement. The most frequent diameter was 36 nm, and the average diameter was 35 nm.

20
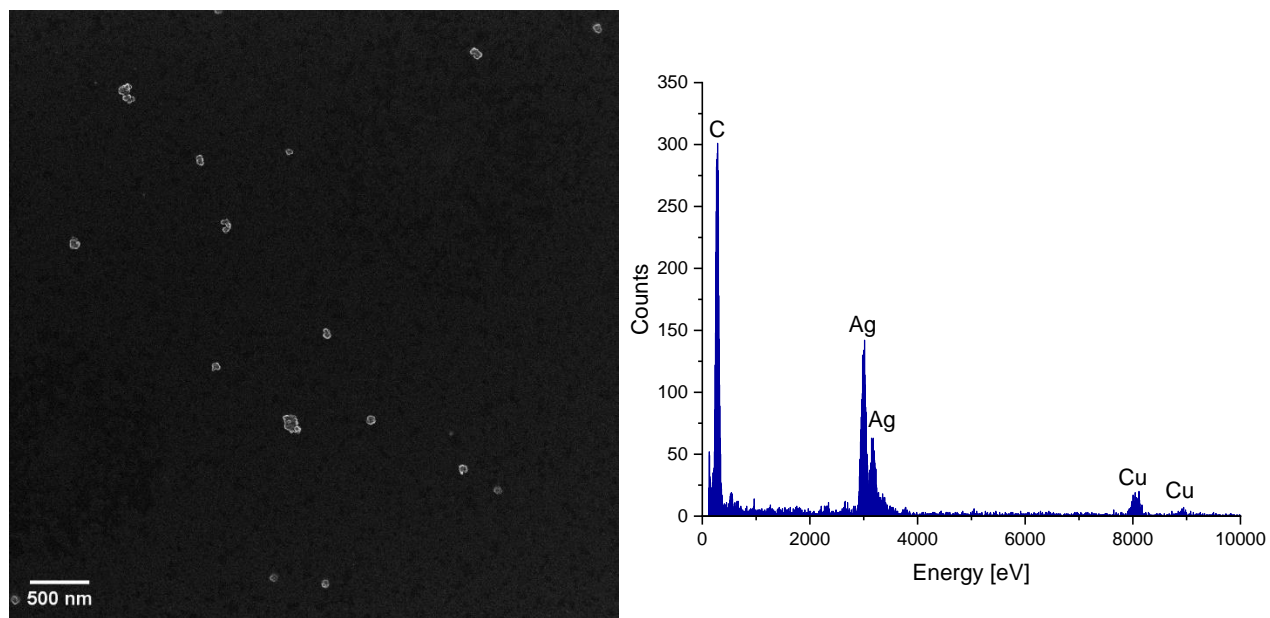
Figure S2. TEM-SE image of CA@Ag-NPs and the corresponding EDX spectrum. Additional C- and Cu-signals in the spectrum result from the sample carrier (copper grid with carbon film) and carbohydrate contamination during TEM measurements.

24

25
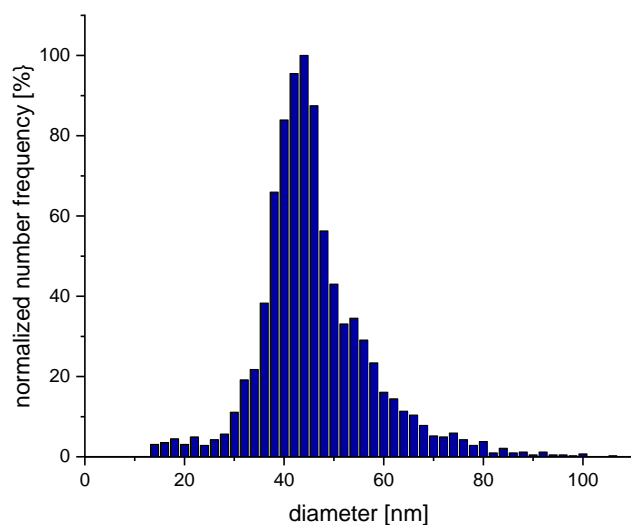
Figure S3. Particle size distribution of Ag2S-NPs (type II) based on normalized particle number frequency obtained by sp-ICP-MS measurement. The most frequent diameter was 44 nm, and the average diameter was 43 nm.

29
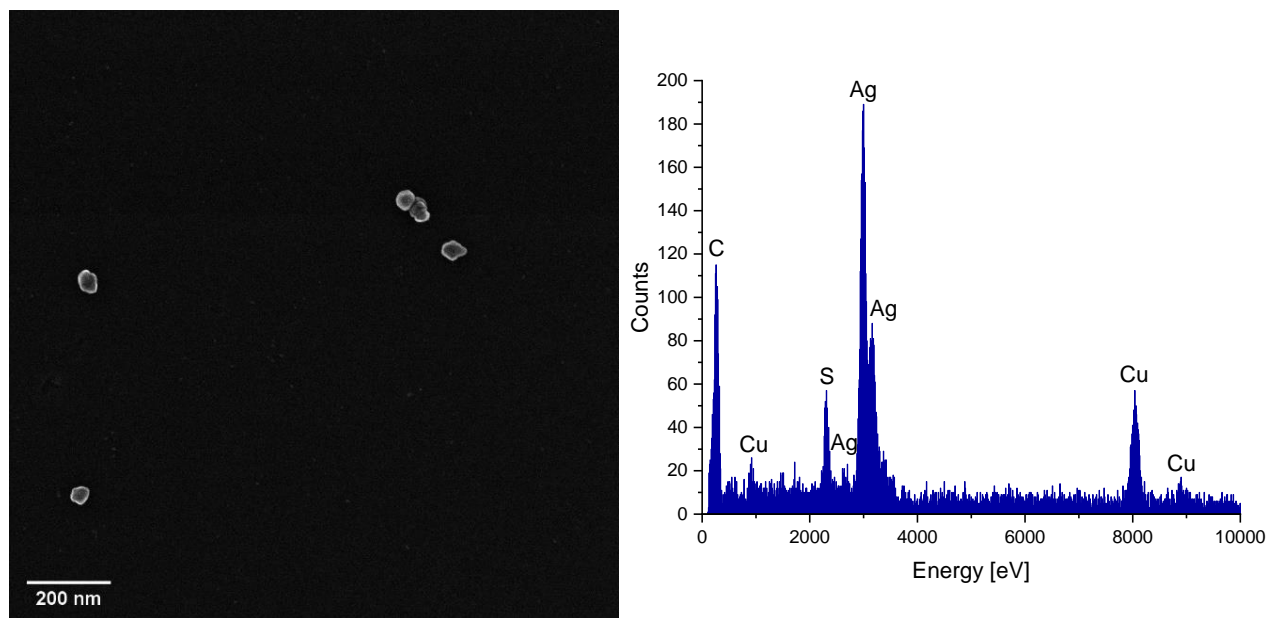
Figure S4. TEM-SE image of Ag$_2$S-NPs (type II) and EDX spectrum. Additional C- and Cu-signals in the spectrum result from the sample carrier (copper grid with carbon film) and carbohydrate contamination during TEM measurements.

33

34
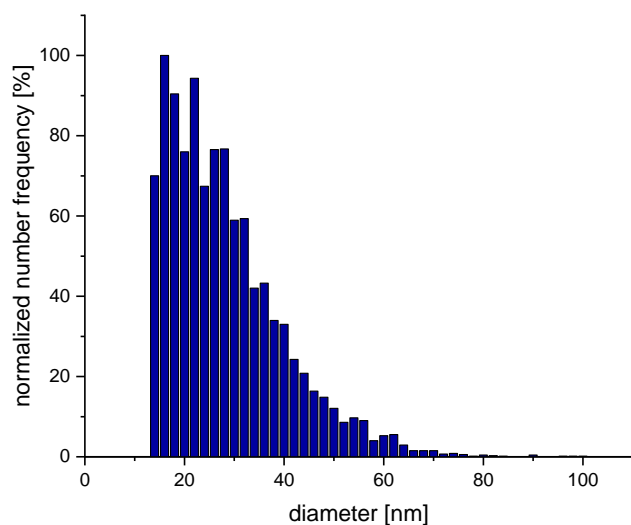
Figure S5. Particle size distribution of Ag₂S-NPs (type I) based on normalized particle
number frequency obtained by sp-ICP-MS measurement. The most frequent diameter was
18 nm, and the average diameter was 25 nm.

38
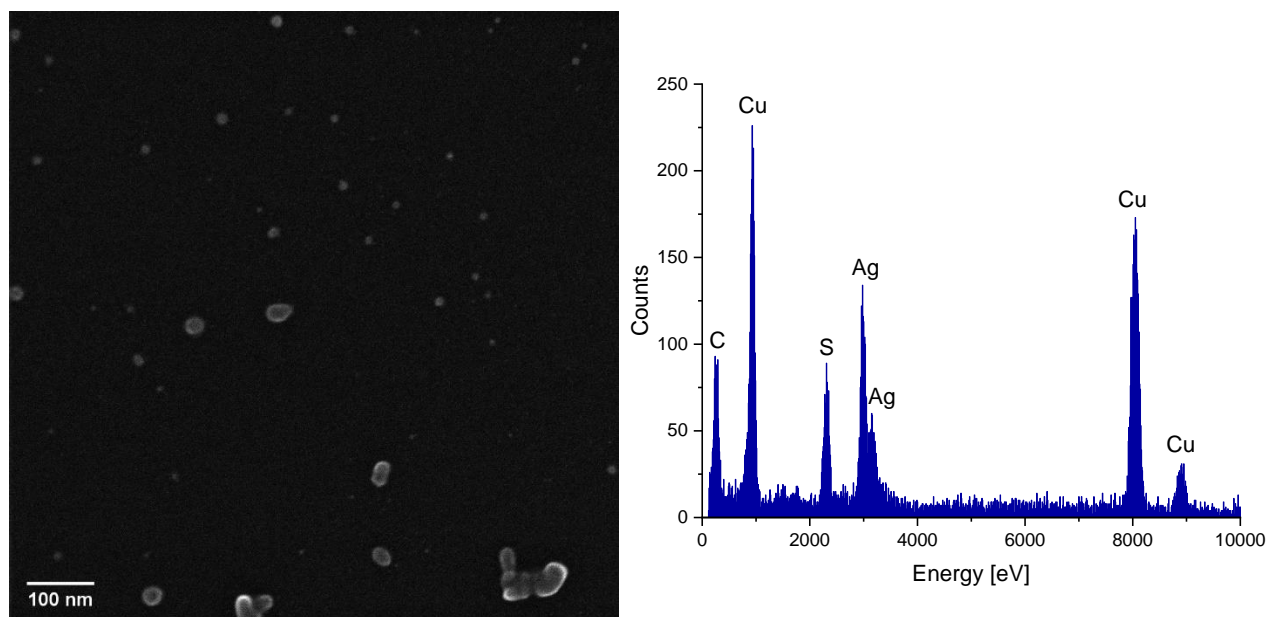
Figure S6. TEM-SE image of Ag2S-NPs (type I) and the corresponding EDX spectrum.
Additional C- and Cu-signals in the spectrum result from the sample carrier (copper grid
with carbon film) and carbohydrate contamination during TEM measurements.

42

43
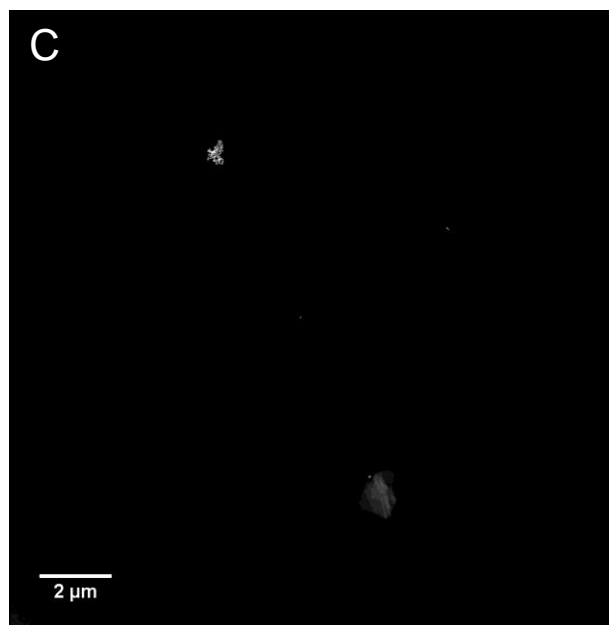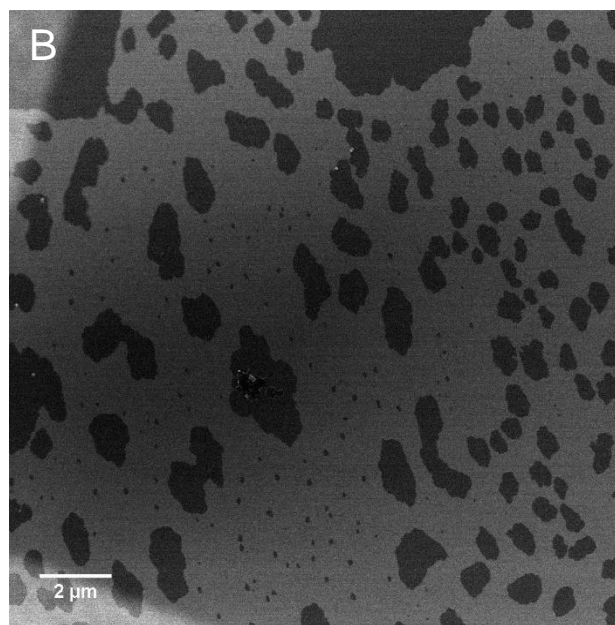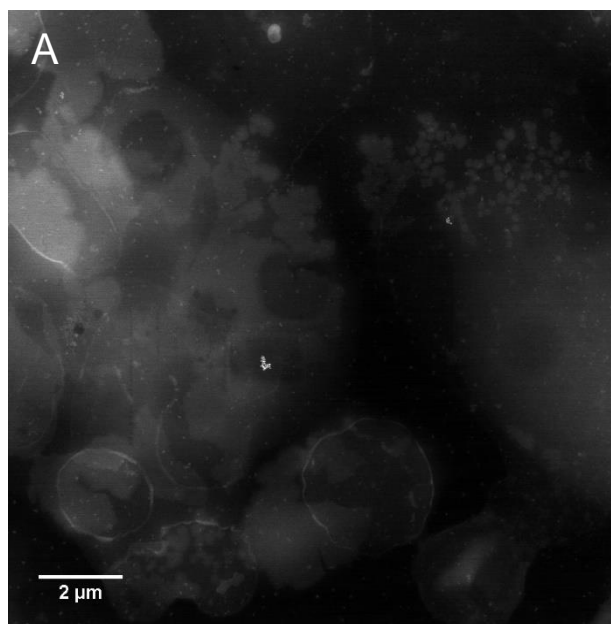
Figure S7: TEM-HAADF (A, C) and TEM-SE (B) images of samples containing CA@Ag-NPs in UPW. All samples were subjected to CPE, whereas the CPE extract was applied without added EtOH (A) and after mixing with EtOH (B, C) to the TEM grid. C represents the same sample as B but another image area and magnification. Particles visible in A and C represent Ag-b-NPs as confirmed by EDX measurements (not shown).

44
45
46
47
48

49

50
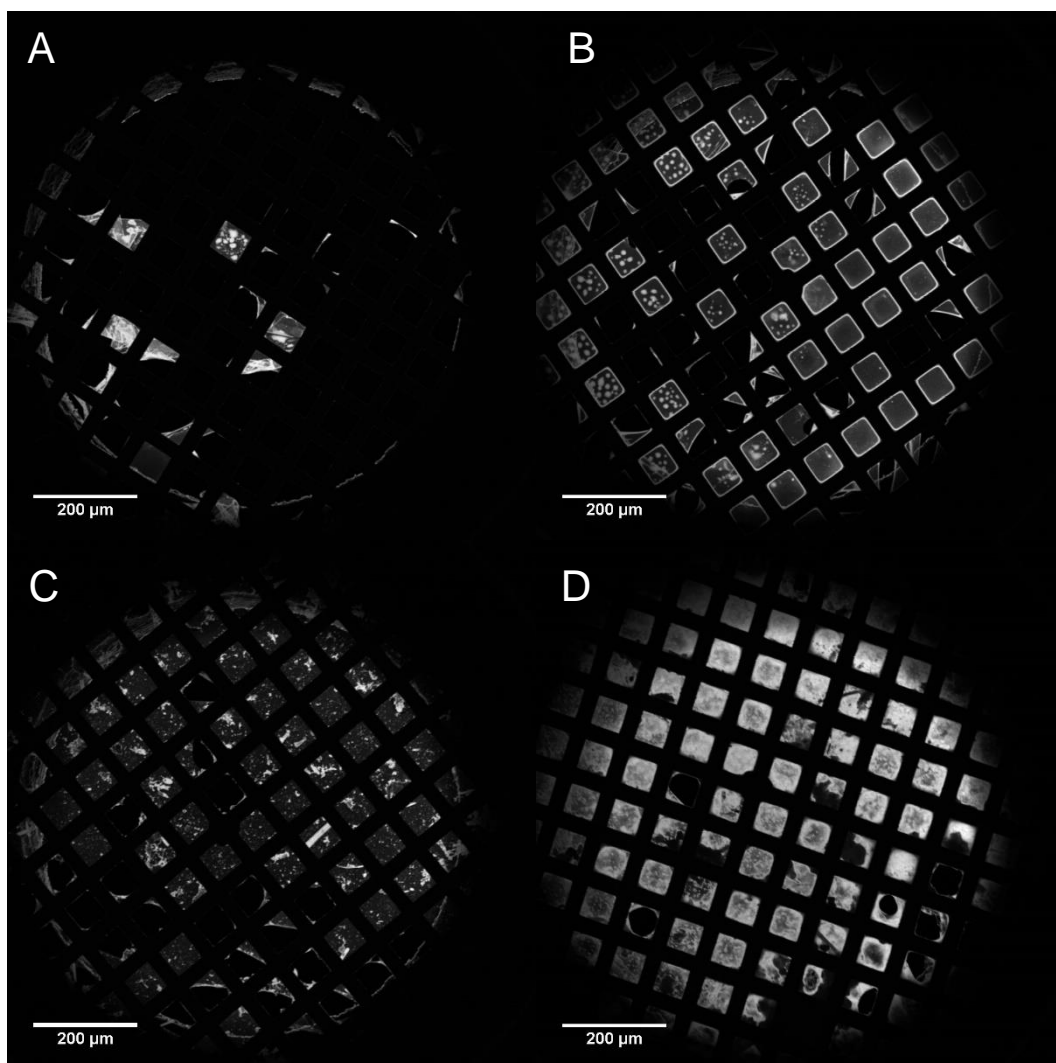
51
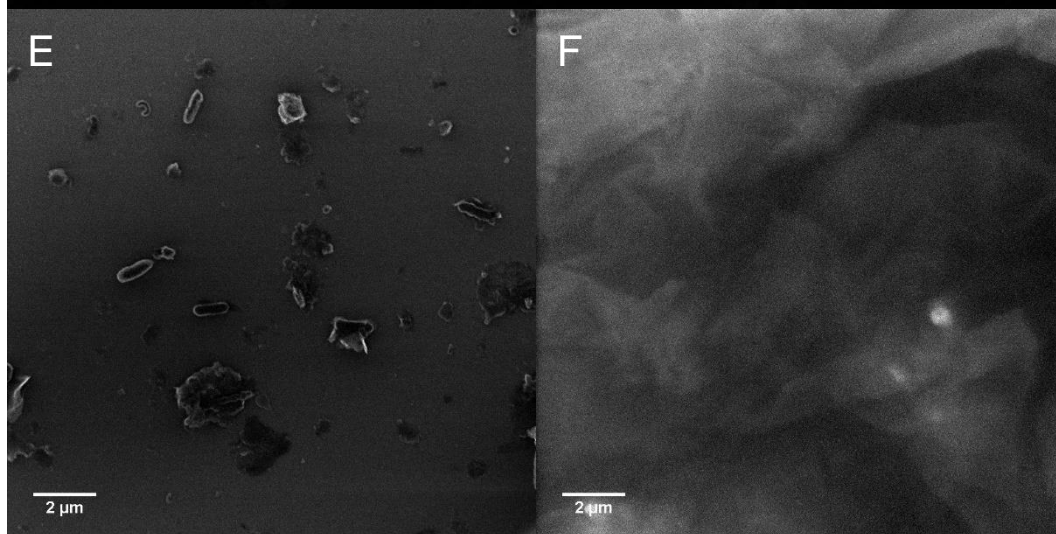
52
53 **Figure S8: TEM-HAADF (A-D) and TEM-SE (E, F) images of grids prepared from CPE**
54 **extracts of UPW (A, B) and river water samples (C-F). During grid preparation, washing**
55 **was performed with EtOH (A, C, E) or cyclohexane (B, D, F), respectively.**

56
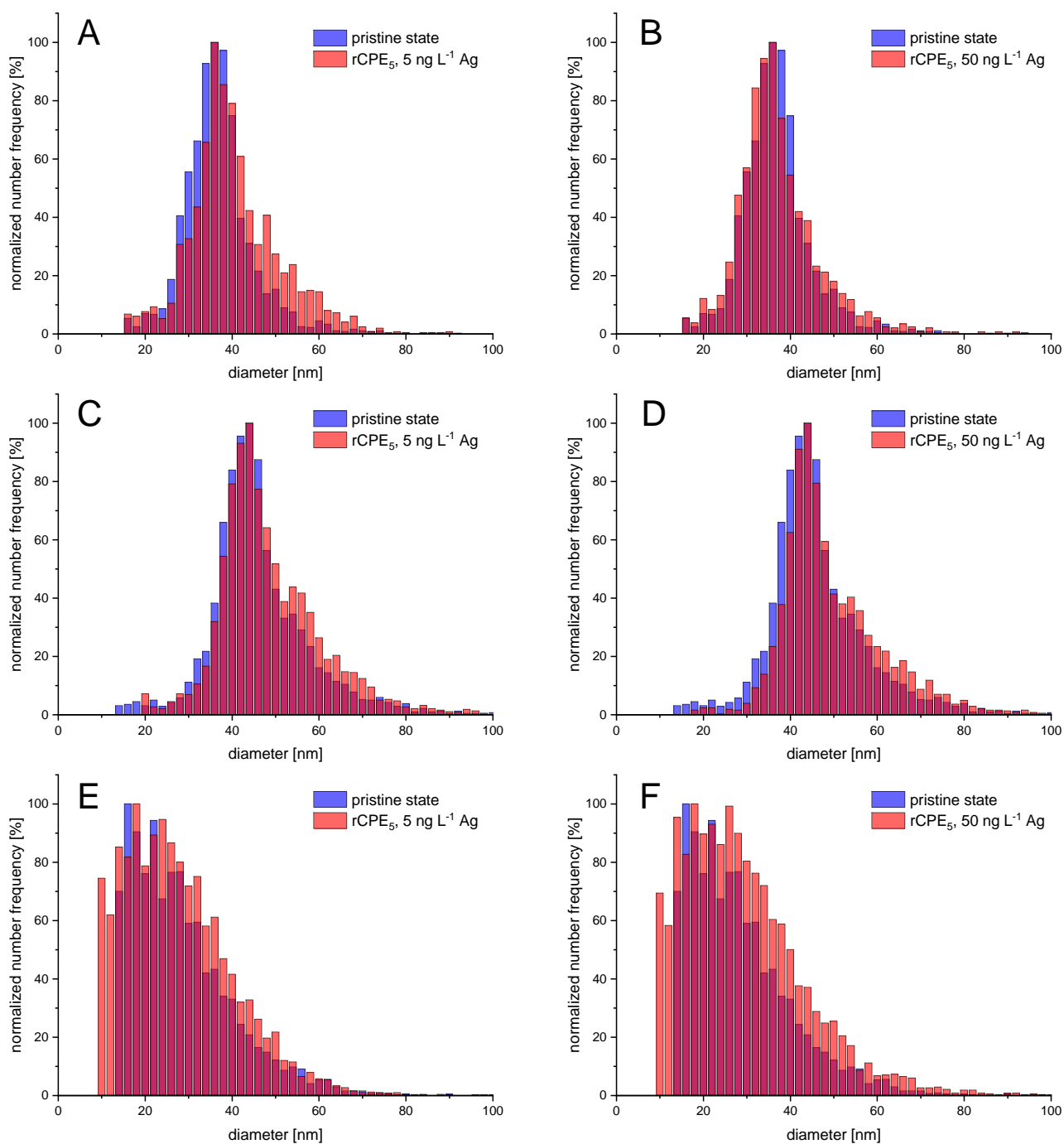
Figure S9. Comparison of particle size distributions of CA@Ag-NPs (A, B), Ag$_2$S-NPs (type II) (C, D), and Ag$_2$S-NPs (type I) (E, F) after rCPE$_5$ with concentrations of c(Ag) = 5 ng L^{-1} as well as c(Ag) = 50 ng L^{-1} and the Ag-b-NPs before rCPE$_5$ (pristine state). The size distributions presented are based on normalized particle number frequencies obtained by sp-ICP-MS measurements.

62 **Table S1. Characteristics of water samples collected from the Isarkanal river and TOC**
63 **content of a composite sample containing all samples to equal amounts.**

Sample number	pH	TOC [mg L^{-1}]	O$_2$ content [mg L^{-1}]
1	8.33		12.89
2	8.33		12.71
3	8.34		12.44
4	8.32		12.35
5	8.33		12.41
6	8.33		12.60
Composite sample		9.88 ± 0.38	

64

8.5   PUBLIKATION 5

Sampling and pre-treatment effects on the quantification of (nano)silver and selected trace elements in surface water – Application in a Dutch case study

Andreas Wimmer, Rob Ritsema, Michael Schuster, and Petra Krystek

Abdruck des Artikels mit allgemeiner Genehmigung (siehe Kapitel 7.5) aus Science of The Total Environment 2019, 663, 154-161.

Short Communication

Sampling and pre-treatment effects on the quantification of (nano)silver and selected trace elements in surface water - Application in a Dutch case study

Andreas Wimmer [a], Rob Ritsema [b], Michael Schuster [a], Petra Krystek [c,d,*]

[a] *Technical University of Munich, Division of Analytical Chemistry, Department of Chemistry, Lichtenbergstraße 4, Garching 85748, Germany*
[b] *Stichting Waterproef, Section Chemistry, Dijkgraaf Poschlaan 6, Edam 1135 GP, the Netherlands*
[c] *TNO, Department Environmental Modelling, Sensing and Analysis (EMSA), Princetonlaan 6, Utrecht 3584 CB, the Netherlands*
[d] *Vrije Universiteit Amsterdam, Department Environment and Health, De Boelelaan 1085, Amsterdam 1081 HV, the Netherlands*

HIGHLIGHTS

- This interlaboratory study investigated channel water with high comparability.
- Silver based nanoparticles were identified in a Dutch channel.
- Nanoparticle content declined with distance to a wastewater treatment plant.
- Evidences for particulate species of other elements in channel water became obvious.

GRAPHICAL ABSTRACT
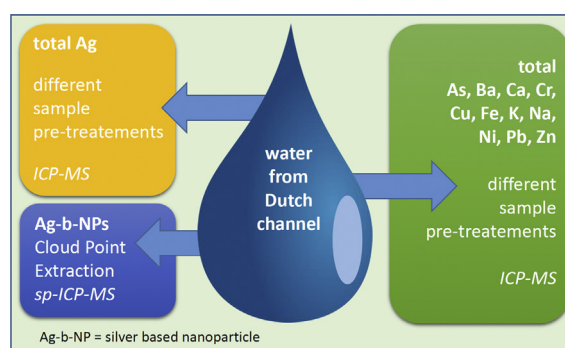
ABSTRACT

Detection and quantification of trace elements in aqueous samples is crucial in terms of environmental monitoring and risk assessment for (heavy) metals in the environment. Silver (Ag) in its nanoparticulate form is commonly used as antimicrobial additive in consumer products and pharmaceuticals. Since released dissolved Ag species act as the actual antimicrobial agent, Ag nanomaterials are supposed to pose risks to the environment by a release of dissolved species. Unfortunately, no standard protocols exist yet to gain reliable information about the presence and distribution of nanomaterials in the environment. Therefore, we present an interlaboratory collaboration involving three laboratories to quantify silver, silver based nanoparticles (Ag-b-NPs) and a wide range of relevant trace elements after different sample pre-treatments for profiling surface water of a Dutch channel. Besides quantification of the elements, different sample pretreatments like acidification, with or without filtration, and their effect on the measurable elemental content were studied. Total Ag and Ag-b-NPs were quantified at lower ng L^{-1} range in the channel water whereas reasonable differences depending on the pre-treatment were identified; Ba, As, Pb, Co, Cr, Cu, Ni and Zn were detected at μg L^{-1} range and Na, K, Mg, Ca and Fe at mg L^{-1} range. Significant sample pre-treatment effects were observed for the elements Cr, Cu, Fe, Pb and Zn, which is very likely due to the existence of particulate species. Measured concentrations were well comparable among the three laboratories underpinning method validity and correctness allowing for a comprehensive, reliable risk assessment for nanomaterials in the environment.

© 2019 Elsevier B.V. All rights reserved.

* Corresponding author.
E-mail address: petra.krystek@vu.nl (P. Krystek).

1. Introduction

Determining trace elements in natural water has always been a main aspect of aqueous analytical chemistry (Ahmad et al., 2010; Beauchemin et al., 1987; Demirak et al., 2006; Elci et al., 1992; Suthar et al., 2009). Although modern wastewater treatment plants (WWTPs) reduce the amount of environmentally emitted elements, especially remaining heavy metals in natural water bodies are alarming since they may pose risks to human and environmental health.

Owing to the highest (eco)toxicity after mercury, silver (Ag) has been focused in a lot of studies addressing sources and environmental fate of this contaminant in the environment so far (Krug, 2014). Especially particulate Ag species are of high concern since they are reported to be even more harmful to the environment than dissolved ones (Krug, 2014). As a special heavy metal, Ag in the form of nanoparticles (AgNPs) is used in a broad variety of pharmaceuticals and consumer products (Krystek et al., 2011), like personal care (Kessler, 2011), functional fabrics (Benn and Westerhoff, 2008; Geranio et al., 2009; Mitrano et al., 2016; Mitrano et al., 2014), house appliances (Jiang et al., 2014) or products used for food storage (Richter et al., 2015). AgNPs are supposed to be released during production, usage and, eventually, disposal of these products (Troester et al., 2016). Then, AgNPs are transported via wastewater streams to WWTPs retaining major proportions of the incoming AgNPs (about 95%) (Li et al., 2013; Li et al., 2016a). Nevertheless, traces of AgNPs enter the environment as anthropogenic contaminants (Sun et al., 2016; Troester et al., 2016). Supplementary to this source, AgNPs are also reported to exist naturally formed from dissolved silver species (Sharma et al., 2015; Wimmer et al., 2018). Once released into the environment, AgNPs undergo a confusing variety of surface modifications, like homo- and hetero-aggregation, adsorption to natural organic matter or formation of silver sulfide or silver chloride coatings (Laborda et al., 2016; Levard et al., 2012; Li et al., 2016b; McGillicuddy et al., 2017; Meier et al., 2016; Sun et al., 2016). Therefore, particulate Ag detected in natural water samples is henceforth named silver based nanoparticles (Ag-b-NPs). Detecting Ag-b-NPs in environmental samples has been a major challenge for analytical chemistry so far (Leopold et al., 2016). With nanoparticles being present at very low concentrations (few ng L^{-1}) in a complex environmental matrix, their quantitative detection is hardly feasible and very time consuming with current techniques (Krystek et al., 2015). Cloud point extraction (CPE) is a tool that may overcome these limitations. This method species selectively extracts Ag-b-NPs from aqueous, environmental samples and simultaneously enriches the particles to detectable concentrations for electrothermal atomic absorption spectrometry (ET-AAS) or inductively coupled plasma mass spectrometry (ICP-MS) (Duester et al., 2016; Hartmann et al., 2014; Hartmann et al., 2013). Single particle (sp) ICP-MS represents a new development in the sector of mass spectrometry able to gain information about nanoparticle size distributions besides their elemental concentration (Degueldre and Favarger, 2003; Degueldre et al., 2006; Lee et al., 2014). Highly resolved detection times record transient signals once particles are atomised and ionised in the ICP. The number of these signals refers to the particle concentration, whereas signal areas correspond to the particle sizes. A recent study revealed the concentration level of Ag-b-NPs in a river in southern Germany with 0.9–2.3 ng L^{-1} detected Ag-b-NPs (Li et al., 2013; Li et al., 2016a; Troester et al., 2016), which is totally in accordance with a study modelling the lower (Q$_{0.15}$) and upper (Q$_{0.85}$) concentration of Ag-b-NPs in surface water at the range of 0.4 to 2.78 ng L^{-1} (Sun et al., 2016).

In the presented study, CPE-sp-ICP-MS measurements for Ag-b-NPs are extended on a Dutch channel receiving the effluent of a WWTP shortly before its estuary into an inland sea. Moreover, total silver and a variety of further elements were measured in the water samples. In depth analysis of several elements in water samples, which were pretreated differently, indicates the existence of particulate species besides Ag-b-NPs. A valid and reliable data set for Ag-b-NPs and further

elements, which pose potential risks to human and environmental health, is scarce yet but essential for a comprehensive risk assessment.

This work was carried out as interlaboratory collaboration study involving three laboratories A, B and C. It aims (i) to compare different sample preparation and conservation techniques prior analysis and (ii) to quantify silver and selected trace elements within the reach of a Dutch channel, whereas (iii) especially Ag in dissolved and (nano)particulate form were focused and quantified, whereas particles were extracted by CPE.

2. Experimental

2.1. Instrumentation

For this interlaboratory collaboration study, ICP-MS instruments as available at the three laboratories were used. In total, five different ICP-MS instruments were used as summarised in Table 1.

For the sample digestion assisted by microwave radiation, a CEM type Mars6 oven from CEM corporation (Matthews, NC, USA) was used. Conditions applied were: 20 min (1200 W) ramp to 170 °C, which was maintained for 25 min before cooling down.

2.2. Materials, reagents and standards

For on-site filtration, disposable syringe filters (PES, 0.45 μm, prefilter PP, 34 mm, housing) from Dispolab (Someren, The Netherlands) were used. Standard disposable sampling bottles (HDPE, PET) from Eijkelkamp (Giesbeek, The Netherlands) and various disposable tubes were used, too. All disposable materials were checked batch wise for contamination (criterion concentration observed <0.5 × detection limit).

All chemicals were of analytical grade or of higher purity and ultrapure water (UPW) with a resistivity of 18.2 MΩ cm was used.

Concentrated hydrochloric acid (HCl) and/or concentrated nitric acid (HNO$_3$) (both of suprapur grade, Merck, Darmstadt, Germany) were used for solutions and/or sample digestion. For calibration in quantitative ICP-MS measurements as well as for internal standardization, traceable single element stock standards from accredited suppliers (Merck (Darmstadt, Germany) and Inorganic Ventures (Christiansburg, VG, USA)) were used.

For cloud point extraction (CPE), the surfactant TX-114 (AppliChem, Darmstadt, Germany), D-penicillamine (Sigma Aldrich, St. Louis, MO, USA) and disodium ethylenediaminetetraacetate (Na$_2$EDTA, Merck) as complexing agents for dissolved Ag(I)-species, and sodium acetate anhydrous (Merck) mixed with acetic acid (glacial, Merck) as pH-buffer were used. Ethanol (EtOH, emsure grade) was obtained by Merck.

To calibrate nebulization efficiency in sp-ICP-MS measurements, a gold (Au) NP dispersion (28 nm particle size, NIST reference material 8012) was received from the National Laboratory of Standards and Technology (NIST, Gaithersburg, MD, USA).

2.3. Water samples: Collection, on-site filtration and conservation

Surface water samples of a ~6 km section of the Dutch channel Goyersgracht were taken at three locations (see Fig. 1) on 2018-06-12. At L1, the sample was collected immediately after a WWTP (Blaricum) discharged its effluent into the channel, at L2, sampling at the channel was done from a bridge, and at L3, a sample was taken from the sluice to the inland sea Eemmeer. At each location (L1-L3), the samples were taken as follows: 100 mL HDPE bottle for trace elements (only acidified to pH 2, HNO$_3$, LX.1); 100 mL HDPE bottle for trace elements (filtrated and acidified to pH 2, HNO$_3$, LX.2); 500 mL PET bottle (not-filtrated and not-acidified) for nanoparticle analysis (LX.3).

Table 1
ICP-MS instrumentations as used for this interlaboratory collaboration study (x = measurement carried out; * = method under accreditation (ISO/IEC 17025); ** = software: Agilent's MassHunter (version C.01.04, build 544.3) with single-particle-tool).

Instrument	Type	Total quantification of Ag	Quantification of particulate Ag by sp-mode	Total quantification of trace elements*	Laboratory
Agilent 7700	CCT-ICP-MS			x	A
Thermo iCap Q	CCT-ICP-MS	x			A
Agilent 7500 CX	CCT-ICP-MS			x	B
Thermo ELEMENT XR	HR-ICP-MS	x			B
Agilent 7900	CCT-ICP-MS	x	x**		C

2.4. Analytical procedures

The studies were carried out in three laboratories A, B and C, whereas the used instruments as well as the methodological information are summarised in Tables 1 and 2.

2.5. Sample pre-treatments prior total quantification of silver and selected trace elements

For the quantification of Ag and other elements at laboratory A, samples were analysed directly for LX.1 and LX.2. In addition, for samples LX.2 also microwave assisted digestion with *aqua regia* (HNO_3:HCl; 1:3) was used. In this case, 25 mL of the water sample and 8 mL *aqua regia* were mixed before digestion and then brought to a final volume of 50 mL prior analysis using ICP-MS.

At laboratory B, 10 mL of received water samples (LX.1, LX.2) were additionally acidified with 0.2 mL a*qua regia* (HNO_3:HCl; 1:3) for the quantification of Ag; hereby, possibly formed colloid silver chloride (AgCl) was transformed into a soluble complex $[AgCl_2]^-$. For determination of the other trace elements, no further pre-treatment was applied and the samples were directly measured in the supplied acidified and filtered water samples.

Laboratory C measured total Ag in the solely acidified water samples LX.1 and in the acidified and filtrated samples LX.2. After shaking, each sample was divided into three individually treated 15 mL aliquots acidified with nitric acid to 1.625% (w/w) total acid content. After an incubation time of at least 3 h prior measurement, all samples were shaken again and forwarded to the ICP-MS measurement.

2.6. Total quantification of total silver and selected trace elements by ICP-MS

At laboratory A, trace elements except Ag were determined under ISO/IEC 17025 (NEN-EN-ISO/IEC 17025, 2005) accreditation in accordance with ISO 17294-2 (NEN-EN-ISO 17294-2, 2016) by using an Agilent 7700 ICPMS. Quantification of Ag, not under accreditation, was performed with a Thermo iCAP Q ICP-MS. More details are given in Table 2.

At laboratory B, the trace elements were measured by an Agilent 7500 CX ICP-MS following a routine series under ISO/IEC 17025 accreditation as in-house method. As long as the quantification of Ag is not under accreditation, a new method was set-up by using the high resolution (HR)-ICP-MS. All details are summarised in Table 2.

At laboratory C, no accreditation was available and the quantification of total silver in the samples LX.1 and LX.2 was performed using an
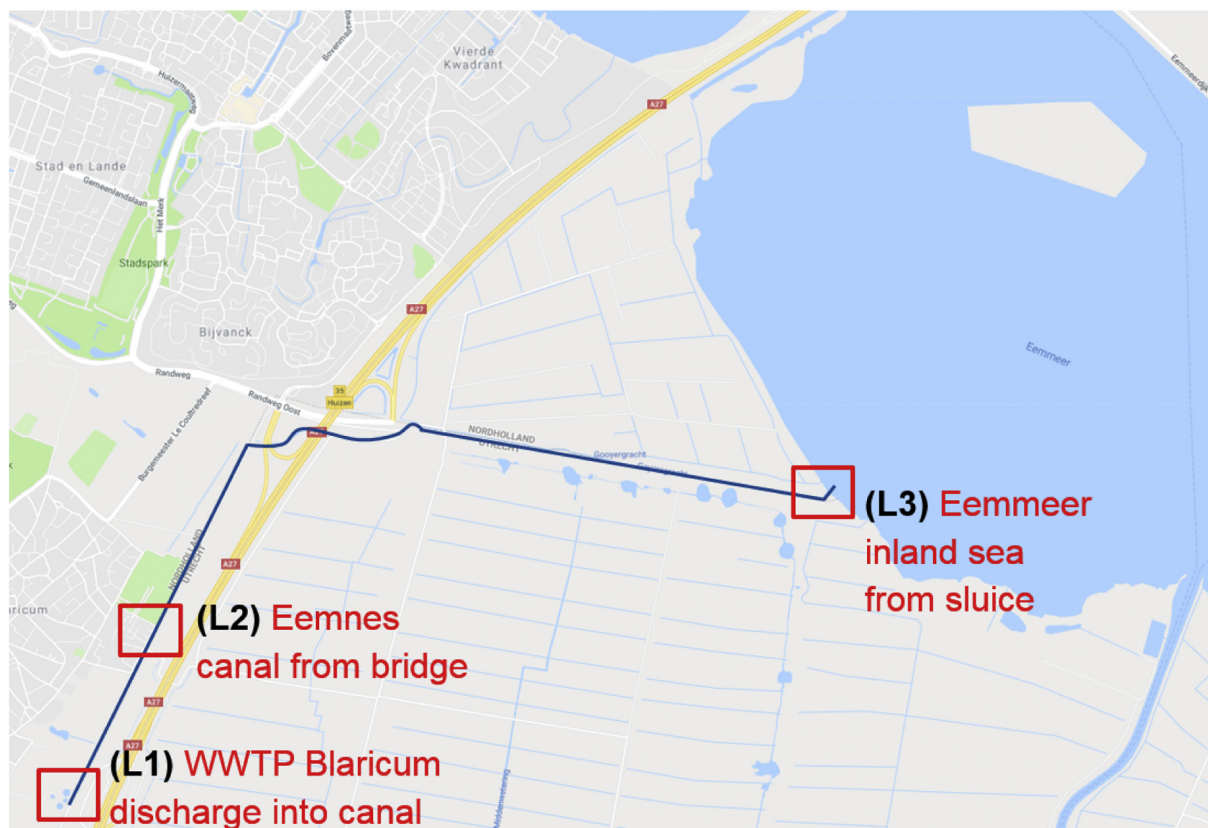
Fig. 1. Sampling locations along the channel Goyersgracht in the Netherlands. Map is based on Google Maps; 09-17-2018.

Table 2
Sample pre-treatment and ICP-MS measurement setting as used for the total quantification at three laboratories A, B and C (n.m. = not measured; LR = low resolution; CCT = collision cell technique).
Pre-treatments are abbreviated as follows: only on-site acidified by HNO_3 (PT1); on-site filtered and acidified by HNO_3 (PT2); additional acidification by HNO_3 (PT3); microwave digestion with aqua regia (PT4); additional acidification by aqua regia (PT5); no on-site sample pre-treatment but CPE for Ag-b-NP quantification (PT6).

	Laboratory	Na	K	Mg	Ca	Fe	Ba	As	Pb	Co	Cr	Cu	Ni	Zn	Ag
Sample pre-treatment	A							PT1 and PT2							PT1 and PT2 and PT1 + PT5
ICP-MS operation mode	A	CCT-He	CCT-He	CCT-He	CCT-He	CCT-He	no gas	CCT-He	No gas	CCT-He	CCT-He	CCT-He	CCT-He	CCT-He	no gas
Selected isotope	A	^{23}Na	^{39}K	^{24}Mg	^{44}Ca	^{56}Fe	^{137}Ba	^{75}As	^{206}Pb, ^{207}Pb, ^{208}Pb	^{59}Co	^{52}Cr	^{63}Cu	^{60}Ni	^{66}Zn	^{107}Ag
Internal standard	A	^{45}Sc	^{45}Sc	^{45}Sc	^{72}Ge	^{45}Sc	^{175}Lu	^{72}Ge	^{175}Lu	^{45}Sc	^{45}Sc	^{72}Ge	^{45}Sc	^{72}Ge	^{103}Rh
Sample pre-treatment	B							PT2							PT1 + PT3 and PT2 + PT3
ICP-MS operation mode	B	CCT-He	CCT-He	CCT-He	CCT-He	CCT-He	CCT-He	CCT-He	CCT-He	CCT-He	CCT-He	CCT-He	CCT-He	CCT-He	LR
Selected isotope	B	^{23}Na	^{39}K	^{26}Mg	^{44}Ca	^{56}Fe	^{137}Ba	^{75}As	^{208}Pb	^{59}Co	^{52}Cr	^{63}Cu	^{60}Ni	^{66}Zn	^{107}Ag
Internal standard	B	^{72}Ge	^{72}Ge	^{72}Ge	^{72}Ge	^{72}Ge	^{185}Re	^{72}Ge	^{209}Bi	^{72}Ge	^{45}Sc	^{103}Rh	^{103}Rh	^{103}Rh	^{103}Rh
Sample pre-treatment	C							–							PT1 + PT4 and PT2 + PT4 and PT6
ICP-MS operation mode	C	n.m.	n.m.	n.m.	n.m.	n.m.	n.m.	n.m.	n.m.	n.m.	n.m.	n.m.	n.m.	n.m.	CCT-He
Selected isotope	C	n.m.	n.m.	n.m.	n.m.	n.m.	n.m.	n.m.	n.m.	n.m.	n.m.	n.m.	n.m.	n.m.	^{107}Ag
Internal standard	C	n.m.	n.m.	n.m.	n.m.	n.m.	n.m.	n.m.	n.m.	n.m.	n.m.	n.m.	n.m.	n.m.	^{115}In

Agilent 7900 ICP-MS measuring the isotope ^{107}Ag in helium collision mode. ^{115}In was used as internal standard, by adding traces of a stock solution containing 400 µg L^{-1} In (in 1.625% HNO_3 (w/w) via a Y connecting tubing to the sample immediately before nebulization. For calibration, solutions containing dissolved Ag(I) in the range from 0.5 to 100 ng L^{-1} were prepared in 1.625% HNO_3 (w/w) from the 1000 mg L^{-1} Ag(I) sock solution and measured together with all samples. All details are given in Table 2.

2.7. Sample preparation for cloud point extraction of silver nanoparticles

To determine Ag-b-NPs in all samples, CPE was used to extract and enrich Ag-b-NPs from the aqueous, untreated samples LX.3, whereas simultaneously selectively particles were separated from dissolved Ag (I) species and matrix constituents. CPE followed the procedures already published in literature (Duester et al., 2016; Hartmann et al., 2014; Hartmann et al., 2013). All samples were shaken thoroughly and afterwards allowed to settle down for 5 h. The clear supernatant was divided into three 40 mL aliquots and filled into 50 mL falcon tubes, which were weighted prior use to enable handling precise volumes by weight. Each 40 mL aqueous sample was mixed with 100 µL acetic acid (1.25 M and 400 µL sodium acetate solution (1 M)) for pH buffering. Afterwards, 3 mL saturated EDTA solution and 1 mL D-penicillamine were added to chelate dissolved Ag(I) species. After adding 1 mL of the surfactant TX-114 (10% (w/w)), the mixture was shaken and incubated for exactly 30 min at 40 °C. Afterwards, phase separation between the surfactant rich phase and the aqueous phase was promoted by centrifugation (12 min, 4500g). All samples were cooled in an ice bath for 5 min to increase the surfactant's viscosity followed by phase separation by decanting the aqueous supernatant. This extraction procedure collects all Ag-b-NPs in a 500 µL surfactant rich droplet. 500 µL EtOH were added to each of these droplets and all samples were gravimetrically filled up to exactly 10 mL using UPW. This results in an enrichment factor of 4 for Ag-b-NPs in the samples. Dilution of the surfactant droplet with EtOH and UPW is necessary for nebulizing during the ICP-MS measurement. The diluted extracts were then split: 4 mL were mixed with 100 µL HNO_3 to dissolve Ag-b-NPs for a total silver measurement in the extracts by ICP-MS; the remaining 6 mL were measured by sp-ICP-MS without additional treatment to get information about the size distribution of Ag-b-NPs in the analysed channel water.

2.8. Analysis of extracted silver nanoparticles by (single particle) ICP-MS

Size distributions of the extracted particles were determined by sp-ICP-MS measurements of the diluted extracts. To calibrate elemental sensitivity, a 1 µg L^{-1} dissolved Ag(I) solution was prepared in the same matrix of the extracts, i.e. a certain amount of the Ag(I) stock solution was mixed with 2.5 mL TX-114 (10% (w/w)) and 2.5 mL EtOH and filled up to 50 mL with UPW. To determine nebulization efficiency, a 48 ng L^{-1} AuNP dispersion was prepared from NIST RM 8012 (28 nm, 48 mg L^{-1} stock concentration) in the same matrix of the extracts as described above. The pump rate was gravimetrically determined as 0.316 mL min^{-1}. For calibration, an already published protocol was followed (Peters et al., 2014). All calibration solutions were measured together with the diluted CPE extracts. Dwell time was set to 500 µs, resulting in 120,000 data points for an acquisition time of 1 min each sample. Data evaluation assumes spherical particles with a density of silver bulk material of 10.5 g cm^{-3}. Very small particles are not detectable in sp-ICP-MS measurements since their particle signal is overlapped by the background signal (Lee et al., 2014). CPE reduces this background signal to a minimum so that all particles ≥8 nm particle size are detectable. Concentration measured in this mode therefore refers only to particles ≥8 nm.

Besides particle sizes, total silver was measured in all CPE extracts. Calibration solutions were prepared from the dissolved Ag(I) stock

solution in the range from 0 to 20 ng L^{-1} in the same matrix of the extracts, i.e. certain amounts of Ag(I) standard were mixed with 1.25 mL HNO$_3$ (conc.), resulting eventually in 1.625% (w/w) HNO$_3$ in the diluted sample, 2.5 mL TX-114 (10% (w/w)), and 2.5 mL EtOH and filled up to 50 mL using UPW. All diluted CPE extracts were measured together with the prepared calibration solutions. Ag concentrations in CPE extracts measured by conventional ICP-MS measurements include all particulate Ag species extracted, thus not only particles ≥8 nm but also <8 nm.

2.9. Quality assurance/quality control (QA/QC) aspects

The total quantification of trace elements was carried out at two laboratories which are accredited according ISO/IEC 17025 (NEN-EN-ISO/IEC 17025, 2005) for these activities. This included various evaluation criteria; e.g. all calibration curves of trace elements were checked on the correlation coefficient R^2 > 0.999. A regular check on the recovery of a known standard at a medium calibration level was carried out after analysing 10 samples and its determined recovery had to be in the range of (92 to 108)%. Furthermore, chemical blanks as well as control samples were analysed within each sequence and the data were accordingly evaluated. Furthermore, the laboratories participate regularly into round robin studies.

3. Results and discussion

3.1. Quantification of total and particulate silver

Dissolved and particulate Ag was found in water of the channel at all three sampling locations; the results are summarised in Table 3. The results are presented in the flow order directly after a WWTP (L1), middle location of the channel (L2), and merging of the channel Goyersgracht into the inland sea (Eemmeer; L3). L1 contained the highest amounts of total Ag; the solely acidified sample L1.1 contained 27.7 (laboratory A), 27.4 (laboratory B) and 28.3 (laboratory C) ng L^{-1} total Ag. Additional filtration reduces the amount of Ag to 10.8 (A), 12.6 (B) and 7.9 (C) ng L^{-1}. Since 2.4 ng L^{-1} particulate Ag with 1.7 ng L^{-1} Ag-b-NPs ≥ 8 nm were detected by sp-ICP-MS, filtration reduces detectable Ag not only by the amounts of particulate species but most likely also by dissolved Ag species attached to suspended particulate matter retained by the 0.45 μm filter. However, all measured concentrations were very well comparable among the three laboratories measuring independently treated subsamples of the same sample. Total digestion with

Table 3
Measured concentration of total silver, particulate silver and particulate silver (≥8 nm) in all investigated water samples by the three laboratories A. B and C (n.m. = not measured).

	Laboratories		
	A	B	C
Location 1	c(Ag) [ng L^{-1}]		
Microwave digestion (L1.1)	153.0	n.m.	n.m.
Acidified (L1.1)	27.7	27.4	28.3
Acidified + filtrated (L1.2)	10.8	12.6	7.9
Particulate species (L1.3)	n.m.	n.m.	2.4
Particulate species (≥8 nm) (L1.3)	n.m.	n.m.	1.7
Location 2	c(Ag) [ng L^{-1}]		
Microwave digestion (L2.1)	103.0	n.m.	n.m.
Acidified (L2.1)	19.0	28.5	24.1
Acidified + filtrated (L2.2)	7.5	10.7	10.0
Particulate species (L2.3)	n.m.	n.m.	1.8
Particulate species (≥8 nm) (L2.3)	n.m.	n.m.	0.9
Location 3	c(Ag) [ng L^{-1}]		
Microwave digestion (L3.1)	45.0	n.m.	n.m.
Acidified (L3.1)	12.1	17.5	15.0
Acidified + filtrated (L3.2)	6.5	6.4	6.4
Particulate species (L3.3)	n.m.	n.m.	1.6
Particulate species (≥8 nm) (L3.3)	n.m.	n.m.	0.7

aqua regia of the unfiltered samples led to the highest concentration of 153 ng L^{-1} total Ag apparently due to a maximum of released and dissolved Ag species. Within the reach of the channel at L2, lower concentrations for total Ag in samples L2.1 were measured: 19.0 (A), 28.5 (B), 24.1 (C) ng L^{-1} total Ag. Filtration again reduced the measurable amount to 7.5 (A), 10.7 (B) and 10.0 (C) ng L^{-1} total Ag. The digested sample contained 103 ng L^{-1} total Ag. Moreover, the amount of particulate silver also decreased: in L2 only 1.8 ng L^{-1} total particulate silver and 0.9 ng L^{-1} Ag-b-NPs ≥ 8 nm were detected. The decrease in Ag concentration along the channel could also be observed for the final sample L3 after the channel's estuary into the inland sea Eemmeer. The acidified sample L3.1 contained 12.1 (A), 17.5 (B) and 15.0 (C) ng L^{-1} total Ag with a reduction after filtration to 6.5 (A), 6.4 (B) and 6.4 (C) ng L^{-1} total Ag. The digested sample contained 45 ng L^{-1} total Ag. In L3 also the lowest amount of particulate Ag of 1.6 ng L^{-1} with 0.7 ng L^{-1} Ag-b-NPs ≥ 8 nm was measured. Overall, the concentrations of total Ag and Ag-b-NPs was reduced from L1 to L3. L1 is located directly next to a WWTP discharge point, which is supposed to serve as an anthropogenic source for Ag-b-NPs in natural waters (Duester et al., 2014; Kaegi et al., 2013; Li et al., 2013; Li et al., 2016a). Ag-b-NPs are therefore emitted from the WWTP into the channel, whereby total and particulate Ag is diluted within the reach of the channel until lowest concentrations were measured in the inland sea at L3. This observation is totally in line with a recent study on Ag-b-NPs in water of a river in Southern Germany, where the anthropogenic influence of WWTP emitting Ag-b-NPs into the river water could be clearly discovered (Li et al., 2016a). For all samples, measured concentrations by the three laboratories A, B and C were very well comparable underpinning method validity of each laboratory's method. Nevertheless, it should be noted that concentrations measured by laboratory B exceeded the concentrations measured by laboratory A and C in most cases. B used *aqua regia* for acidification, whereas A and C used nitric acid. *Aqua regia* seems to mobilize more Ag species in the aqueous sample compared to nitric acid – most likely by dissolving AgCl species, which are not dissolved by nitric acid (Bianco et al., 2015).

The three laboratories, also determined total organic carbon (TOC) and dissolved organic carbon (DOC) in all samples in a range from 10 to 13 mg L^{-1} (remark: methods are not described in detail within this publication). These observations showed that there is no correlation between TOC (resp. DOC) and quantified amounts of Ag, and Ag-b-NPs.

sp-ICP-MS measurements revealed, that Ag-b-NPs in the channel are – regardless of the sampling location – of comparable particle size distributions of 8 to 20 nm particle size (see Fig. 2A). The maximum of the particle size distribution was located at 8 nm. Together with the fact that concentrations (see Table 3) measured by CPE-ICP-MS (all particulate Ag species) were steadily higher than measured by CPE-sp-ICP-MS (only Ag-b-NPs ≥ 8 nm), this proves that there was a distinct amount of Ag-b-NPs < 8 nm present in the water samples. Fig. 2B clearly shows the existence of Ag-b-NPs as transient signals in the single particle mass spectra. Found particle sizes equal sizes of naturally occurring Ag-b-NPs as presented in the literature (Li et al., 2016a; Wimmer et al., 2018).

3.2. Total quantification of selected trace elements

Besides Ag in dissolved and particulate form, selected trace elements were quantified in the solely acidified (LX.1) and simultaneously acidified and filtrated samples (LX.2) by laboratories A and B. These measurements should primarily address the effect of filtration on the measurable amount of several elements in the acidified samples and the overall comparability of results. All measured concentrations are given in Table 4.

Overall, all elements were quantified with good agreement by the two laboratories emphasising method validity, result reliability and quality control. Especially analyte homogeneity is given since concentrations measured independently by the two laboratories in the subsamples are totally consistent.
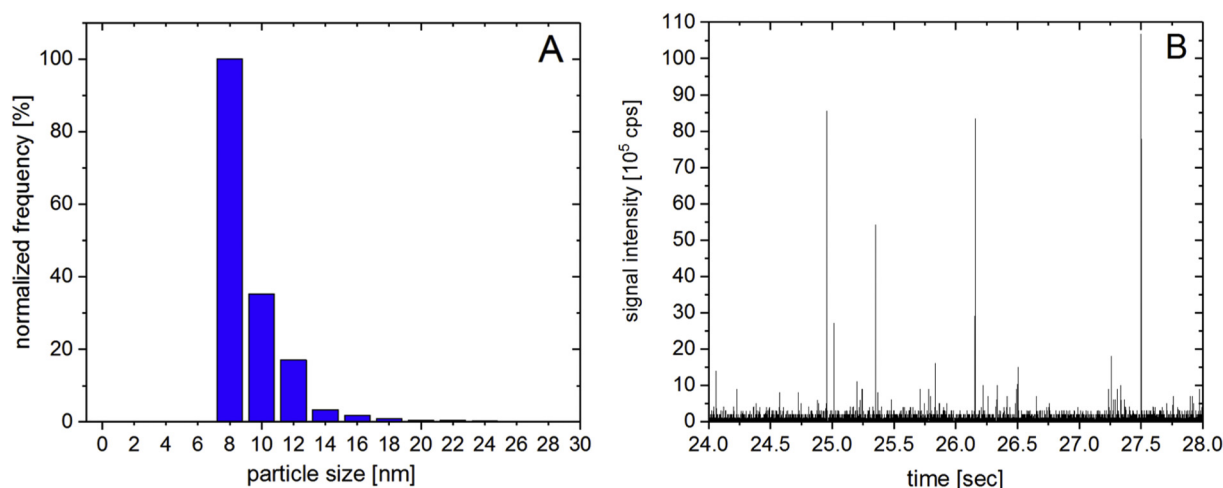
Fig. 2. A: exemplary particle size distribution of Ag-b-NPs extracted from the water sample at L3. Particles <7 nm aren't detectable anymore using sp-ICP-MS since particle signals are indistinguishable from the instrument's background signal in this case. B: exemplary time resolved spectra measured in single particle mode (dwell time 500 μs) for ^{107}Ag showing clearly the existence of Ag-b-NPs in the CPE extract of the water sample L3.

Regarding sample conservation and pre-treatment, two groups of elements became obvious. For some elements, there was no difference in concentrations for the solely acidified and acidified and filtrated samples detectable. Concentrations for all investigated alkali metals (Na, K) and alkaline earth metals (Mg, Ca, Ba) were not affected by filtration for sample pre-treatment and were all present in the mg L^{-1} range. Moreover, no filtration effect was observable for the measurement of As and the transition metals Co and Ni. This observation reveals, that all mentioned elements were present as totally dissolved species able to pass the filter without any retention. As was present in the samples from 0.5 to 1.4 μg L^{-1}, Co from 0.2 to 0.4 μg L^{-1} and Ni from 1.6 to 2.4 μg L^{-1}. In some cases, the concentration decreased from the WWTP effluent discharge point (L1) till the channel's estuary into the Eemmeer (L3) (Na, K, Mg, Ca, Co), stayed constant (Ba) or even increased (As, Ni). Therefore, no significant correlation between sampling location or distance within the channel from the WWTP discharge point and the measured concentration could be detected.

In contrast to the above cited elements, the measured concentrations of Pb and the transition metals Fe, Cr, Cu and Zn along the channel were heavily dependent of the sample conservation procedure. In all cases, filtration led to a notably decrease in concentration. Fe was present in the samples from 0.1 to 0.5 mg L^{-1}, whereas filtration reduced the measured 0.5 mg L^{-1} to 0.1–0.2 mg L^{-1}, for instance. Again, both laboratories quantified Fe and the following elements very well comparably underlining method validity and correctness. The comparable results for two laboratories and the described filtration effect was observed for Pb, Cr, Cu and Zn as well. These elements were present in the μg L^{-1} range. Fe content in channel water increased steadily with increasing distance from the WWTP discharge point from 0.1 to 0.5 mg L^{-1} from L1.1 to L3.1, which was also observed for especially Pb and slightly for Zn. However, no special industrial activities are identified between L1.1. and L3.1. This small increase in concentration can be explained by local input from the sediment, for instance. Furthermore, the channel is located nearby and parallel (between L1.1. and L2.1.) to the highway A27 in a high traffic area (see Fig. 1). Between L2.1. and L3.1., at least half of the way is still parallel to the highway. Between L1.1. and L2.1., there is also a gas station with a parking lot located. This might have an effect on the emission of common (heavy) metals from traffic and transport. On the opposite side of the channel, a small living area without industrial influence is located and the second half of the way, the channel solely passes through fields and meadows. However, this is only a possible assumption to explain the increasing concentration of some elements within the reach of the channel, which might be subject to a subsequent study. Contents of Cr and Cu stayed constant within the reach of the channel. Essentially, filtration affects measured concentrations only for Pb, Fe, Cr, Cu and Zn, whereby all other investigated elements were not influenced by filtration. Very likely, Pb, Fe, Cr, Cu and Zn were significantly abundant as particulate species or were bound as ionic or dissolved M^{n+} species to suspended particulate matter and therefore retained by the filtration process.

Table 4
Measured concentration of total silver, particulate silver and particulate silver (>7 nm) in all investigated water samples by the three laboratories A, B and C.

		Concentration [mg L^{-1}]					Concentration [μg L^{-1}]							
		Na	K	Mg	Ca	Fe	Ba	As	Pb	Co	Cr	Cu	Ni	Zn
L1	Laboratory													
Acidified (L1.1)	A	82	19	6.0	47	0.1	9.0	0.6	0.5	0.3	0.8	5.8	1.8	9.0
Acidified + filtrated (L1.2)	A	80	18	5.8	46	0.1	9.0	0.6	0.3	0.3	0.7	2.4	1.7	8.0
Acidified + filtrated (L1.2)	B	79	20	4.7	43	<0.1	9.1	0.5	0.3	0.3	0.8	2.1	1.6	7.9
L2	Laboratory													
Acidified (L2.1)	A	75	19	5.2	44	0.4	8.0	1.0	1.0	0.4	0.8	5.3	1.8	14
Acidified + filtrated (L2.2)	A	76	19	5.3	44	0.1	7.0	0.9	0.3	0.3	0.6	3.0	1.8	10
Acidified + filtrated (L2.2)	B	76	21	4.3	46	0.1	6.5	0.9	0.3	0.4	0.6	3.5	1.9	11
L3	Laboratory													
Acidified (L3.1)	A	69	18	4.7	42	0.5	8.0	1.4	0.9	0.3	0.8	6.5	2.4	12
Acidified + filtrated (L3.2)	A	68	17	4.6	41	0.2	7.0	1.4	0.3	0.2	0.6	3.4	2.3	8.0
Acidified + filtrated (L3.2)	B	81	19	3.8	49	0.1	8.1	1.4	0.3	0.3	0.6	3.1	2.4	6.9

Therefore, it can be stated that there was very likely a distinct amount of particulate species other than Ag-b-NPs present in the examined water samples.

4. Conclusion

This study addressed the quantification of Ag, Ag-b-NPs, and a variety of selected elements in surface water samples for profiling the Dutch channel Goyersgracht. Ag and other elements were quantified by ICP-MS. For Ag-b-NP determination, particles were extracted from the aqueous samples by CPE and measured via ICP-MS and sp-ICP-MS. Ag was present in the channel water in the ng L^{-1} range, whereas concentration decreased within the reach of the channel from a sampling location directly next to a WWTP discharge point till the channel's estuary into an inland sea, which underlines the anthropogenic origin of Ag in the channel. Approximately 10% of the measurable silver was present as particulate species with particle sizes ranging from 8 to 20 nm. Filtration of all samples led to lower total Ag concentrations indicating the loss of both Ag-b-NPs and dissolved Ag species bound to suspended particulate matter by the filtration process. Overall, CPE coupled to sp-ICP-MS combined with total Ag measurements via ICP-MS is a valuable tool for the examination of Ag-b-NPs and their fate in channel water and further. The easy applicable, thoroughly validated, and fast CPE is suitable to be implemented in operational analysis and routine environmental monitoring of surface water.

Furthermore, Ba, As, Pb, Co, Cr, Cu, Ni, and Zn were present in channel water in the μg L^{-1} range and Na, K, Mg, Ca and Fe in the mg L^{-1} range. Sample pre-treatment strongly influenced the measurable concentration of several elements. Only some element concentrations were reduced by filtration significantly; these were Cr, Cu, Fe, Pb, and Zn. Therefore, it can be assumed that one group of elements exists as particulate species and is thus retained by filtration, whereby the other group of elements is highly dissolved and able to pass filtration membranes. Concentrations were very well comparable among the three collaborating laboratories underlining method validity, correctness, and quality control. The proposed methods can be used for environmental monitoring of nanoparticles and further dissolved elements in river water. Only by a comprehensive dataset for nanoparticles in the environment, valid risk assessment is possible.

Acknowledgement

References

Ahmad, M.K., Islam, S., Rahman, M.S., Haque, M.R., Islam, M.M., 2010. Heavy metals in water, sediment and some fishes of Buriganga River, Bangladesh. Int. J. Environ. Res. 4, 321–332.

Beauchemin, D., McLaren, J.W., Mykytiuk, A.P., Berman, S.S., 1987. Determination of trace metals in a river water reference material by inductively coupled plasma mass spectrometry. Anal. Chem. 59, 778–783.

Benn, T.M., Westerhoff, P., 2008. Nanoparticle silver released into water from commercially available sock fabrics. Environ. Sci. Technol. 42, 4133–4139.

Bianco, C., Kezic, S., Visser, M.J., Pluut, O., Adami, G., Krystek, P., 2015. Pilot study on the identification of silver in skin layers and urine after dermal exposure to a functionalized textile. Talanta 136, 23–28.

Degueldre, C., Favarger, P.Y., 2003. Colloid analysis by single particle inductively coupled plasma-mass spectroscopy: a feasibility study. Colloids Surf. A Physicochem. Eng. Asp. 217, 137–142.

Degueldre, C., Favarger, P.Y., Wold, S., 2006. Gold colloid analysis by inductively coupled plasma-mass spectrometry in a single particle mode. Anal. Chim. Acta 555, 263–268.

Demirak, A., Yilmaz, F., Levent Tuna, A., Ozdemir, N., 2006. Heavy metals in water, sediment and tissues of Leuciscus cephalus from a stream in southwestern Turkey. Chemosphere 63, 1451–1458.

Duester, L., Burkhardt, M., Gutleb, A.C., Kaegi, R., Macken, A., Meermann, B., et al., 2014. Toward a comprehensive and realistic risk evaluation of engineered nanomaterials in the urban water system. Front. Chem. 2, 1–6.

Duester, L., Fabricius, A.-L., Jakobtorweihen, S., Philippe, A., Weigl, F., Wimmer, A., et al., 2016. Can cloud point-based enrichment, preservation, and detection methods help to bridge gaps in aquatic nanometrology? Anal. Bioanal. Chem. 1–7.

Elci, L., Soylak, M., Dogan, M., 1992. Preconcentration of trace metals in river waters by the application of chelate adsorption on Amberlite XAD-4. Fresenius J. Anal. Chem. 342, 175–178.

Geranio, L., Heuberger, M., Nowack, B., 2009. The behavior of silver Nanotextiles during washing. Environ. Sci. Technol. 43, 8113–8118.

Hartmann, G., Hutterer, C., Schuster, M., 2013. Ultra-trace determination of silver nanoparticles in water samples using cloud point extraction and ETAAS. J. Anal. At. Spectrom. 28, 567–572.

Hartmann, G., Baumgartner, T., Schuster, M., 2014. Influence of particle coating and matrix constituents on the cloud point extraction efficiency of silver nanoparticles (Ag-NPs) and application for monitoring the formation of Ag-NPs from Ag+. Anal. Chem. 86, 790–796.

Jiang, D., Chen, L., Xie, J., Chen, M., 2014. Ag2S/g-C3N4 composite photocatalysts for efficient Pt-free hydrogen production. The co-catalyst function of Ag/Ag2S formed by simultaneous photodeposition. Dalton Trans. 43, 4878–4885.

Kaegi, R., Voegelin, A., Ort, C., Sinnet, B., Thalmann, B., Krismer, J., et al., 2013. Fate and transformation of silver nanoparticles in urban wastewater systems. Water Res. 47, 3866–3877.

Kessler, R., 2011. Engineered nanoparticles in consumer products: understanding a new ingredient. Environ. Health Perspect. 119, A120–A125.

Krug, H.F., 2014. Nanosafety research—are we on the right track? Angew. Chem. Int. Ed. 53, 12304–12319.

Krystek, P., Ulrich, A., Garcia, C.C., Manohar, S., Ritsema, R., 2011. Application of plasma spectrometry for the analysis of engineered nanoparticles in suspensions and products. J. Anal. At. Spectrom. 26, 1701–1721.

Krystek, P., Bäuerlein, P.S., Kooij, P.J.F., 2015. Analytical assessment about the simultaneous quantification of releasable pharmaceutical relevant inorganic nanoparticles in tap water and domestic waste water. J. Pharm. Biomed. Anal. 106, 116–123.

Laborda, F., Bolea, E., Cepriá, G., Gómez, M.T., Jiménez, M.S., Pérez-Arantegui, J., et al., 2016. Detection, characterization and quantification of inorganic engineered nanomaterials: a review of techniques and methodological approaches for the analysis of complex samples. Anal. Chim. Acta 904, 10–32.

Lee, S., Bi, X., Reed, R.B., Ranville, J.F., Herckes, P., Westerhoff, P., 2014. Nanoparticle size detection limits by single particle ICP-MS for 40 elements. Environ. Sci. Technol. 48, 10291–10300.

Leopold, K., Philippe, A., Wörle, K., Schaumann, G.E., 2016. Analytical strategies to the determination of metal-containing nanoparticles in environmental waters. Trends Anal. Chem. 84 (Part A), 107–120.

Levard, C., Hotze, E.M., Lowry, G.V., Brown, G.E., 2012. Environmental transformations of silver nanoparticles: impact on stability and toxicity. Environ. Sci. Technol. 46, 6900–6914.

Li, L., Hartmann, G., Döblinger, M., Schuster, M., 2013. Quantification of nanoscale silver particles removal and release from municipal wastewater treatment plants in Germany. Environ. Sci. Technol. 47, 7317–7323.

Li, L., Stoiber, M., Wimmer, A., Xu, Z., Lindenblatt, C., Helmreich, B., et al., 2016a. To what extent can full-scale wastewater treatment plant effluent influence the occurrence of silver-based nanoparticles in surface waters? Environ. Sci. Technol. 50, 6327–6333.

Li, L., Zhou, Q., Geng, F., Wang, Y., Jiang, G., 2016b. Formation of nanosilver from silver sulfide nanoparticles in natural waters by Photoinduced Fe(II, III) redox cycling. Environ. Sci. Technol. 50, 13342–13350.

McGillicuddy, E., Murray, I., Kavanagh, S., Morrison, L., Fogarty, A., Cormican, M., et al., 2017. Silver nanoparticles in the environment: sources, detection and ecotoxicology. Sci. Total Environ. 575, 231–246.

Meier, C., Voegelin, A., Pradas del Real, A., Sarret, G., Mueller, C.R., Kaegi, R., 2016. Transformation of silver nanoparticles in sewage sludge during incineration. Environ. Sci. Technol. 50, 3503–3510.

Mitrano, D.M., Rimmele, E., Wichser, A., Erni, R., Height, M., Nowack, B., 2014. Presence of nanoparticles in wash water from conventional silver and nano-silver textiles. ACS Nano 8, 7208–7219.

Mitrano, D.M., Limpiteeprakan, P., Babel, S., Nowack, B., 2016. Durability of nano-enhanced textiles through the life cycle: releases from landfilling after washing. Environ. Sci.: Nano 3, 375–387.

NEN-EN-ISO 17294-2, 2016. Water Quality - Application of Inductively Coupled Plasma Mass Spectrometry (ICP-MS) - Part 2: Determination of Selected Elements Including Uranium Isotopes.

NEN-EN-ISO/IEC 17025, 2005. General Requirements for the Competence of Testing and Calibration Laboratories.

Peters, R.J.B., Rivera, Z.H., van Bemmel, G., Marvin, H.J.P., Weigel, S., Bouwmeester, H., 2014. Development and validation of single particle ICP-MS for sizing and quantitative determination of nano-silver in chicken meat. Anal. Bioanal. Chem. 406, 3875–3885.

Richter, A.P., Brown, J.S., Bharti, B., Wang, A., Gangwal, S., Houck, K., et al., 2015. An environmentally benign antimicrobial nanoparticle based on a silver-infused lignin core. Nat. Nanotechnol. 10, 817.

Sharma, V.K., Filip, J., Zboril, R., Varma, R.S., 2015. Natural inorganic nanoparticles - formation, fate, and toxicity in the environment. Chem. Soc. Rev. 44, 8410–8423.

Sun, T.Y., Bornhöft, N.A., Hungerbühler, K., Nowack, B., 2016. Dynamic probabilistic modeling of environmental emissions of engineered nanomaterials. Environ. Sci. Technol. 50, 4701–4711.

Suthar, S., Nema, A.K., Chabukdhara, M., Gupta, S.K., 2009. Assessment of metals in water and sediments of Hindon River, India: impact of industrial and urban discharges. J. Hazard. Mater. 171, 1088–1095.

Troester, M., Brauch, H.-J., Hofmann, T., 2016. Vulnerability of drinking water supplies to engineered nanoparticles. Water Res. 96, 255–279.

Wimmer, A., Kalinnik, A., Schuster, M., 2018. New insights into the formation of silver-based nanoparticles under natural and semi-natural conditions. Water Res. 141, 227–234.

8.6   PUBLIKATION 6

Silver Nanoparticle Levels in River Water: Real Environmental Measurements and Modeling Approaches – A comparative Study

Andreas Wimmer, Adriaan A. Markus, and Michael Schuster

Silver Nanoparticle Levels in River Water: Real Environmental Measurements and Modeling Approaches—A Comparative Study

Andreas Wimmer,[†,§] Adriaan A. Markus,[‡,§] and Michael Schuster*,[†]

[†]Division of Analytical Chemistry, Department of Chemistry, Technical University of Munich, Garching 85748, Germany
[‡]Deltares, P.O. Box 177, 2600 MH, Delft, The Netherlands

S *Supporting Information*

ABSTRACT: Due to severe analytical challenges, methods for quantification of silver-based nanoparticles (Ag-*b*-NPs) in environmental samples are scarce. Modeling approaches try to overcome these limitations, paving a way for valid concentration data of nanomaterials in the environment essential for comprehensive risk assessments. However, a comparison of both analytical and modeling approaches is essential to ensure validity and reliability of measurements and estimates. Here, we present analytical measurements of Ag-*b*-NPs in the River Isar in southern Germany, sampled from its source to the confluence with the river Danube. A stable level of approximately 1−2 ng L^{-1} of Ag-*b*-NPs was measured in the river, whereas concentration peaks near wastewater treatment plants (WWTPs) climbed to 2.47−69.08 ng L^{-1} of Ag-*b*-NPs but were quickly diluted to the stable level in the river's reach. Simultaneously, a one-dimensional model approach successfully reproduced measured Ag-*b*-NP concentrations and distribution. Predictions rested upon data about population size, flow velocities, and WWTP removal efficiencies. It was assumed that WWTPs can be modeled as point sources and that the wastewater is mixed quickly over the river's cross section. The model distinguished between unabsorbed and adsorbed Ag-*b*-NPs and total silver and revealed that the NPs adsorb quickly to the suspended sediment in the river.
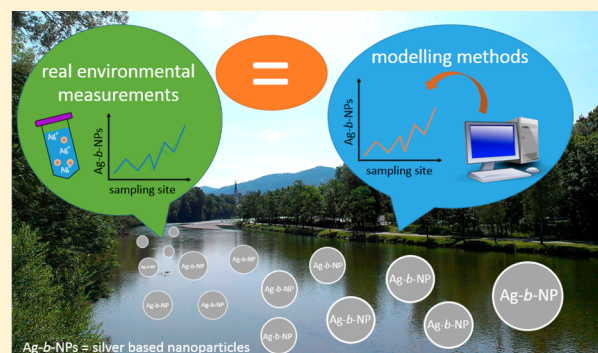
INTRODUCTION

Many current studies have focused on the sources, release, and distribution routes of silver-based nanoparticles (Ag-*b*-NPs) in the environment.[1−11] We use the term Ag-*b*-NPs to consider the fact that nanoparticles (NPs), once released into the environment, are likely present with a diversity of coatings and compositions.[9,10]

In most cases, Ag-*b*-NPs are attributed to anthropogenic sources,[1,5,12,13] being released from consumer products containing nanosilver. Moreover, Wimmer et al.[7] found evidence for geogenic Ag-*b*-NPs in lakes derived from naturally occurring dissolved Ag(I) traces after reduction by natural organic matter. Ag-*b*-NPs are expected to be present in surface waters at a range from 0.4 ng L^{-1} (15% quantile concentration) to 2.78 ng L^{-1} (85% quantile concentration) based on modeling systems[14] that are in line with an empirical environmental study by Li et al.[5]

The determination of Ag-*b*-NPs in real environmental samples is essential for a proper risk assessment. Unfortunately, due to a dearth of analytical techniques capable of measuring nanomaterials at the ng L^{-1} scale, in complex matrices, and in the presence of various interfering substances, environmental occurrence data of Ag-*b*-NPs are scarce. Cloud point extraction (CPE) can selectively extract and enrich Ag-*b*-NPs species from complex environmental matrices, allowing for a more comprehensive understanding of nanomaterials in the environ-

ment.[4,5,15−18] Ag-*b*-NPs have already been measured in environmental samples with a limit of detection as low as 0.2 ng L^{-1} applying CPE.[5]

Additionally, a variety of modeling approaches has been developed. For instance, in the Dutch reaches of the Rhine and Meuse Rivers, NP concentrations were estimated based on available data of NP content in consumer products and the total usage of these materials.[19] Moreover, mathematical models calibrated with existing laboratory data have helped to explain homo- and heteroaggregation, sedimentation, dissolution, or transformation of nanomaterials in the environment, showing that heteroaggregation is likely crucial for determining the environmental behavior of nanomaterials.[20] The concentration of nanomaterials in a typical river system, attributed mainly to wastewater emissions, was predicted via an existing modeling approach using the estimated usage of NPs in consumer products, their modeled fate and transport, and known removal efficiencies in wastewater treatment plants (WWTPs).[21] Models do not require sampling or analytical methods and quickly lead to results once the system is set up.

However, in most cases, calculations rely on basic estimates and manufacturer specifications, which are neither trustworthy nor available across all cases and ignore various influences and factors that cannot be identified clearly. Therefore, we present the extraction (by CPE) and measurement of total and particulate silver (Ag) in real environmental samples from the River Isar in southern Germany together with a model addressing initial data sets about wastewater conversion, hydrological, and geological circumstances. Good agreement between the measured and modeled concentrations would suggest that both methods are suitable to provide valid concentration data for nano risk assessment in the environment.

■ MATERIALS AND METHODS

Materials. A dissolved inductively coupled plasma (ICP) Ag(I) standard ($AgNO_3$ in 3% (v/v) HNO_3, βAg = 1000 mg L^{-1}) and ICP Rh(III) standard ($Rh(NO_3)_2$ in 2%–3% (v/v) HNO_3, βRh = 1000 mg L^{-1}), used as the internal standard, were obtained from Merck (Darmstadt, Germany). A silver nanoparticle (AgNP) dispersion (60 nm, βAg = 20 mg L^{-1}, citrate stabilized) was purchased from Sigma-Aldrich (St. Louis, MO, USA). HNO_3 (65%, suprapure) was obtained from Merck. The Supporting Information (SI) lists the chemicals applied during the CPE procedure. All the chemicals were at least of analytical grade and were checked for contamination by ICP-MS prior to usage.

Quality Assurance and Quality Control. Due to extremely low Ag concentrations in the samples (ng L^{-1}), strict quality assurance and control measures are vital. All dilutions were done using ultrapure water (UPW) with a resistivity of 18.2 MΩ cm^{-1}, provided by a Milli-Q-Gradient-System (Millipore GmbH, Billerica, MA, USA). Moreover, on each measurement day, a blank sample consisting of 40 mL of UPW was subjected to the whole CPE and measurement procedure. No Ag-b-NPs were found in the blank samples. Therefore, our quantitative results were not blank corrected. The analysis' robustness was evaluated investigating triplicate samples with a relative standard deviation less than 10%.

Instrumentation. The Ag content in corresponding organic extracts was quantified to calculate the Ag-b-NP concentration in aqueous samples, using a Zeeman-corrected electrothermal atomic absorption spectrometer (ET-AAS) AAnalyst 800 (PerkinElmer, Waltham, MA, USA). A 7900 ICP-MS (Agilent, Santa Clara, CA, USA) was used to perform total Ag measurements in the river water. The SI gives more details on the ET-AAS and ICP-MS instrumental setup.

Collection of Water Samples. Surface water samples were collected from the River Isar in July 2016, under dry weather conditions following a sunny period lasting at least one week (Figure S3). A similar sampling campaign in 2015 has been described in our previous work.[5] The River Isar is located in southern Germany, originating in the Alps; it passes through rural areas over a length of approximately 290 km, followed by the Munich metropolitan region, with 1.5 million inhabitants and about 6 million people in the catchment area. In the downstream regions, several cities (each having approximately 50,000 inhabitants) are located along the river, until it reaches the Danube River. Figure S1 and Table S1 show hydrological data of the River Isar. Several WWTPs (Figure S2, Table S2) are located along the River Isar, discharging their effluent directly into the river. Water samples were collected according to the German standard sampling

procedure DIN 38402 T15, 2012[22] from the river's source to its estuary and, in particular, exactly next to each WWTP discharge point and 1.5 km downstream to observe the dilution effects of Ag-b-NPs released into the water (see SI for further discussion). Figure S3 and Table S3 show all sampling sites. A telescope sampler was used to collect water samples from the river's middle water body, avoiding contamination from stirred up riparian sediments. All water samples were stored in unused, clean, and disposable PVC containers that were rinsed 3 times with the water sample prior to usage. Following laboratory transportation, all samples were stored in the dark at 6 °C, pretreated, and measured immediately. A subsample from each sample was stabilized on-site for total Ag quantification by adding 3% (v/v) subboiled nitric acid. Subsamples without acidification were used for Ag-b-NP determination. Common water quality parameters (i.e., pH, conductivity, temperature, dissolved oxygen, suspended particulate matter (SPM), total organic carbon (TOC)) were determined directly after sampling (SI).

Extraction and Enrichment Procedure of Ag-b-NPs in Water Samples. Cloud point extraction, a well-established and validated method for species-selective extraction and enrichment of metallic NPs, such as Ag-b-NPs, from aqueous samples, was used for sample preparation.[15−18] For more information on the extraction procedure, see the SI.

Quantification of Ag-b-NPs in CPE-Extracts of River Water. To understand the amount of Ag-b-NPs in the primary water sample, Ag was quantified in organic extracts after CPE by ET-AAS as presented by Li et al.[5] For calibration, dispersions of a known AgNP concentration were prepared from the AgNP stock dispersion and subjected to the same extraction procedure as the aqueous samples. The SI gives more details on instrument settings, calibration, and measurement.

Quantification of Total Ag in River Water. Total Ag in river water was measured in acidified samples, using an Agilent 7900 ICP-MS. For the calibration, solutions of known Ag concentration were prepared from the Ag(I) standard solution. The SI gives detailed information.

Modeling Method. The hydrology of the River Isar and its main tributaries was modeled using a one-dimensional network consisting of several branches—the Isar itself, the Isar channel in Munich, and the Loisach and Amper Rivers being the most important tributaries in terms of flow rate (Figure S1, Table S1). As no detailed information on the Isar's geometry or hydrology was available, a steady flow was assumed; cross sections and further geographical features were derived from data from the Bavarian Environmental Protection Agency (Table S1). Details on the modeling approach itself are given in the SI.

Seven WWTPs (for location and capacity data, see Figure S2 and Table S2) are located along the river, the largest by far being the one at Gut Marienhof (250,000 m^3 day^{-1}). These WWTPs are modeled as point sources with a discharge based on their capacity and a load of total Ag based on the measured environmental concentration (Table S3). For the load of Ag-b-NPs, both the measurements and the estimates by Markus et al.[19] were utilized. They estimated an average contribution of Ag-b-NPs to wastewater per person of 46 mg per year. The SI presents model calculation details.

Ag-b-NPs were assumed to enter the river system as unadsorbed nanoparticles and to be subjected to aggregation processes once released into the river.[20,21] Processes and

Table 1. Overview of WWTPs along the River Isar Including Their Sampling Site Number (see also Table S3)[a]

name (sampling site)	capacity (m^3 day^{-1})	concentration Ag-*b*-NPs (ng L^{-1})	concentration total Ag (ng L^{-1})	estimated influx Ag-*b*-NPs (kg year^{-1})	estimated efflux Ag-*b*-NPs (kg year^{-1})
Bad Tölz (3)	7000	20.88 ± 0.09	86.72 ± 0.02	1.6	0.05
Ismaning (7)	6500	2.47 ± 0.05	23.86 ± 0.15	1.5	0.006
Gut Marienhof (9)	250,000	18.53 ± 0.14	60.80 ± 0.01	58	1.7
Freising (12)	12,000	0.70 ± 0.39	73.01 ± 0.01	2.8	0.003
Moosburg (14)	10,000	4.72 ± 0.02	38.02 ± 0.13	2.3	0.017
Landshut (18)	15,500	32.40 ± 0.17	125.09 ± 0.04	3.6	0.18
Landau (21)	3500	69.08 ± 0.10	189.05 ± 0.01	0.8	0.09

[a]The influx was estimated using a waste load of 46 mg nanosilver per person per year.[19] The efflux was estimated from the measured Ag-*b*-NP concentration. Measured concentrations represent Ag-b-NP concentrations in samples from the river taken immediately next to WWTP effluent discharge areas.

process coefficients used to estimate Ag-*b*-NPs in the River Isar were previously described by Markus et al.[21] As net sedimentation is unlikely to occur due to the large flow velocity, except perhaps near the river banks, sedimentation has been ignored in this study. Consequently, total nanosilver, the sum of free Ag-*b*-NPs and Ag-*b*-NPs adsorbed to suspended solids, can be considered conservative. Adsorption and aggregation transform one fraction into another but do not cause a net change in the total amount of Ag. The assumption of the Ag-*b*-NPs entering as *unadsorbed* particles therefore only has consequences for the distribution over the various fractions, not for the total concentration.

The model results include the concentration of unadsorbed Ag-*b*-NPs, Ag-*b*-NPs adsorbed to suspended solids, and the total concentration of Ag along the River Isar and its tributaries. As the concentration of Ag-*b*-NPs is quite low, a process like homoaggregation plays almost no role. Furthermore, it is assumed that no dissolution occurs. As Kaegi et al. have observed, Ag-*b*-NPs are likely to form Ag$_2$S, which is quite insoluble.[10]

■ RESULTS AND DISCUSSION

Waste Loads from WWTPs. The determination of waste loads discharged by the WWTPs is a crucial base for the model. Table 1 contains the WWTP capacity and the measured concentrations of Ag-*b*-NPs and total Ag, as well as the estimated influx of Ag-*b*-NPs, which is based on an estimate of 46 mg nanosilver per year per person[7] and a per capita use of 200 L water per day. A large fraction of nanomaterial (90%−95% or more) remains in sewage sludge, so the net efflux will be much lower than the influx.[10] This leads to a ratio of 3%, or a retention of 97%, for the Gut Marienhof WWTP, which is well within previously reported ranges (SI).[5,10,23−25] For the other smaller WWTPs, the ratio of silver efflux to influx varies from less than 1% to 10%. Therefore, the model calculations were performed using a retention factor of 97%.

Concentration of Ag-*b*-NPs and Total Ag along River Isar: Measurement and Model. Past fieldwork in 2015 revealed a distinct effect of WWTP effluent on the occurrence of Ag-*b*-NPs in the River Isar.[5] The presented 2016 measurements clearly confirm these observations (Figure 1A, Table S3): In the upstream parts of the River Isar, Ag-*b*-NPs were hardly detectable. The first WWTP in Bad Tölz (sampling site 3) led to an Ag-*b*-NP load peak of 20.88 ng L^{-1}. Downstream, NPs were diluted very quickly in the reach of the river. Such high load peaks were observed at every other

WWTP discharge point. Remarkable decreases in Ag-*b*-NP concentration were observed 1.5 km downstream of these points. In these cases, Ag-*b*-NPs were diluted, and their concentrations remained nearly constant until the next WWTP discharge point. Between two WWTP discharge points, Ag-*b*-NPs reached a constant level of approximately 1 ng L^{-1}. Finally, the Ag-b-NP concentration remained at 1.40 ng L^{-1} after the Isar's estuary drained into the Danube River, which agrees well with our previous study and other published data.[5] Total Ag concentrations in river water behaved similarly to Ag-*b*-NPs, exhibiting similar load peaks and dilution in the river's reach. The concentration ranged from 4.86 ng L^{-1} (site 6) to 189.05 ng L^{-1} (site 21), whereas the highest total Ag concentrations measured exactly next to the WWTP discharge points ranged from 23.86 ng L^{-1} (WWTP Ismaning, site 7) to 189.05 ng L^{-1} (WWTP Landau, site 21). The Ag-*b*-NP proportion varied widely; however, the highest proportions were found at sampling sites with the highest total Ag concentrations. At the Bad Tölz WWTP (site 3), 24% of total Ag was particulate, and at the Landau WWTP (site 21), 37% of total Ag was particulate. Additional measurements showed a pH typical for river water, ranging from 7 to 8 (Table S3). Dissolved oxygen content was constant, approximately 10 mg L^{-1}, in all samples. SPM concentrations ranged from 0.31 to 2.14 g L^{-1}. The lowest TOC content, 0.46 mg L^{-1}, was measured at sampling site 1, and the highest TOC contents were present near WWTP effluent discharge points, for instance, 3.95 mg L^{-1} at the Freising WWTP (site 12).

The predicted concentrations of Ag-*b*-NPs, both the unadsorbed fraction and the fraction adsorbed to suspended solids, along with the sum, are shown in Figure S4, together with the measured concentrations of Ag-*b*-NPs. The inflow of the Loisach River at 102 km increases the fraction of adsorbed Ag-*b*-NPs according to the model; at the location of the Gut Marienhof WWTP (154 km), the unadsorbed fraction increases significantly, then decreases downstream as Ag-*b*-NPs become adsorbed to suspended solids. As the SPM concentration is rather high, the aggregation process is very fast. The clear peak at the Bad Tölz WWTP (78 km), upstream of the Loisach, that was seen in the measurements did not recur. A possible explanation is a discrepancy in the hydrology used in the model vis-à-vis the actual flow rate. If that was much smaller than assumed, it would lead to a more significant contribution from the Bad Tölz WWTP and thus to higher concentrations (see additional information on the transport modeling in the SI). Alternatively, it may be due to a much lower lateral mixing than expected. The measurements of total Ag, showing a similar peak, indicate that this is not due to
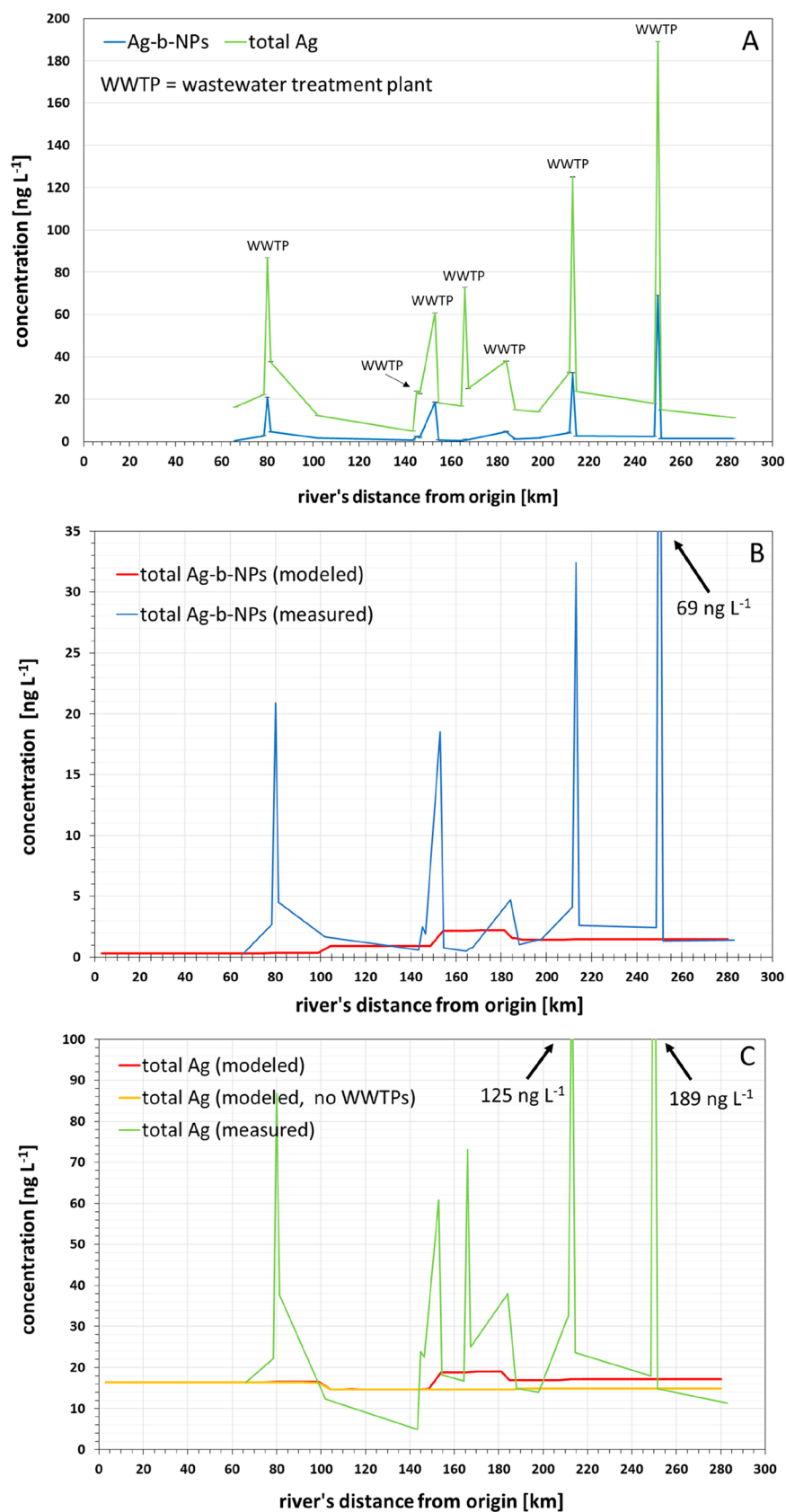
Figure 1. Measured concentrations of Ag-*b*-NPs (blue) and total Ag (green) along the reach of the River Isar; WWTP indication next to the measured values represent sampling river water directly next to a wastewater treatment plant (WWTP) effluent discharge point (A). The modeled (red) and total amount of Ag-*b*-NPs (red) compared with the empirical environmental measurement of Ag-*b*-NPs (blue) (B). Predicted concentrations of total Ag, with (red) and without (yellow) WWTP effluent loads taken into account for the calculation compared with empirical measurements (green) (C). Measurement uncertainties are listed in Table S3 in the SI.

anomalies in the measurements (Figure 1C). Due to relatively high flow velocities, there is no observable NP sedimentation in the model.

The measured increase in the Ag-*b*-NP concentration at the Gut Marienhof WWTP (154 km) is well represented in the model. The decrease downstream may indicate that Ag-*b*-NPs actually dissolve, a process omitted in the model. The total concentration of Ag is relatively constant in this reach of the river, and the model result agrees reasonably with the measurements.

This is not the case for the downstream reach from 180 to 250 km. The modeled concentrations for both Ag-*b*-NPs and total Ag are two to three times as high as measured. This does not appear to be attributable to the Landshut WWTP or the Amper River. However, further downstream, the model result is again comparable to the field measurements. The model is able to correctly predict the increasing Ag-*b*-NP level within the reach of the River Isar, except for the load peaks near WWTP discharge areas, which could not be represented (Figure 1, Table S4).

In terms of total Ag concentrations, both the measured and modeled results are fairly constant along the river (Figure 1C). The influence of WWTPs, as Ag sources, is limited; this can be seen by setting the Ag loads to zero in the model (yellow graph in Figure 1C). In addition, there are no defined processes for Ag, so that it acts as a conservative substance within the model. Similar to observations made for Ag-*b*-NPs, the total Ag load peaks near WWTP discharge points are not represented by the model (Figure 1C). Nevertheless, the modeled concentrations of total Ag between the WWTP spots, and especially in the downstream regions near the estuary, are again comparable to the measured values (Table S4). This indicates the model is able to estimate total Ag loads in the River Isar.

In this study, we demonstrate the distinct effect that WWTPs along a river can have on the occurrence of Ag, especially as NPs. The River Isar was sampled from its source to the estuary, north into the Danube River. Ag-*b*-NPs were only found downstream past Munich, whereby load peaks were detectable next to WWTP discharge points, which were quickly diluted downstream. Except for these load peaks, the applied model could reasonably accurately predict Ag-*b*-NP and total Ag concentrations in river water using a simplified hydrological network for the river, WWTPs as modeled point sources, and appropriate boundary conditions. To be more precise, the modeled concentrations for Ag-*b*-NPs lie for the most part in the range between 0.5 and 2.0 times the measured concentrations (10 out 17 sampling locations). For total Ag, almost all modeled concentrations lie in this range (15 out of 17 locations). Hence, this method was a complementary technique for Ag-*b*-NP quantification, providing a valid database of quantities of Ag-*b*-NPs in the environment allowing for a comprehensive risk assessment.

ASSOCIATED CONTENT

Ⓢ Supporting Information

The Supporting Information is available free of charge on the ACS Publications website at DOI: 10.1021/acs.es-tlett.9b00211.

Detailed information on instrumentation, extraction and enrichment procedure of Ag-*b*-NPs in water samples, quantification of Ag-*b*-NPs in CPE extracts of river water, and determination of further water quality parameters. Figure S1: Map of the River Isar and its tributaries. Table S1: Hydrological data of the River Isar and its tributaries. Figure S2: Location of all examined WWTPs along the River Isar. Table S2: Name, location, and capacity of all examined WWTPs along the River Isar, with detailed information on the modeling approach including transverse mixing, modeling the aggregation process, transport modeling, exemplary calculation, and boundary conditions. Figure S4: Location of all sampling sites along the River Isar. Table S3: Water quality data and total and particulate Ag concentrations for each sampling site along the River Isar. Table S4: Compilation of measured and modeled concentrations. Figure S5: Modeled unabsorbed and adsorbed fractions of Ag-b-NPs and modeled total amount of Ag-b-NPs in river water. (PDF)

AUTHOR INFORMATION

Corresponding Author
*Tel: +49 (0)89 289 13763. Fax: +49 (0)89 289 14513. E-mail: michael.schuster@ch.tum.de.

ORCID 🄲
Andreas Wimmer: 0000-0002-1746-8932

Author Contributions
§A. Wimmer and A. Markus contributed equally to the presented study.

Notes
The authors declare no competing financial interest.

REFERENCES

(1) Benn, T.; Cavanagh, B.; Hristovski, K.; Posner, J. D.; Westerhoff, P. The Release of nanosilver from consumer products used in the home. *J. Environ. Qual.* **2010**, *39* (6), 1875−1882.

(2) Colman, B. P.; Espinasse, B.; Richardson, C. J.; Matson, C. W.; Lowry, G. V.; Hunt, D. E.; Wiesner, M. R.; Bernhardt, E. S. Emerging Contaminant or an Old Toxin in Disguise? Silver Nanoparticle Impacts on Ecosystems. *Environ. Sci. Technol.* **2014**, *48* (9), 5229−5236.

(3) Kim, B.; Park, C.-S.; Murayama, M.; Hochella, M. F. Discovery and Characterization of Silver Sulfide Nanoparticles in Final Sewage Sludge Products. *Environ. Sci. Technol.* **2010**, *44* (19), 7509−7514.

(4) Li, L.; Hartmann, G.; Döblinger, M.; Schuster, M. Quantification of Nanoscale Silver Particles Removal and Release from Municipal Wastewater Treatment Plants in Germany. *Environ. Sci. Technol.* **2013**, *47* (13), 7317−7323.

(5) Li, L.; Stoiber, M.; Wimmer, A.; Xu, Z.; Lindenblatt, C.; Helmreich, B.; Schuster, M. To What Extent Can Full-Scale Wastewater Treatment Plant Effluent Influence the Occurrence of Silver-Based Nanoparticles in Surface Waters? *Environ. Sci. Technol.* **2016**, *50* (12), 6327−6333.

(6) Mittelman, A. M.; Lantagne, D. S.; Rayner, J.; Pennell, K. D. Silver Dissolution and Release from Ceramic Water Filters. *Environ. Sci. Technol.* **2015**, *49* (14), 8515−8522.

(7) Wimmer, A.; Kalinnik, A.; Schuster, M. New insights into the formation of silver-based nanoparticles under natural and semi-natural conditions. *Water Res.* **2018**, *141*, 227−234.

(8) Kaegi, R.; Voegelin, A.; Sinnet, B.; Zuleeg, S.; Siegrist, H.; Burkhardt, M. Transformation of AgCl nanoparticles in a sewer system-A field study. *Sci. Total Environ.* **2015**, *535*, 20−27.

(9) Kaegi, R.; Voegelin, A.; Ort, C.; Sinnet, B.; Thalmann, B.; Krismer, J.; Hagendorfer, H.; Elumelu, M.; Mueller, E. Fate and transformation of silver nanoparticles in urban wastewater systems. *Water Res.* **2013**, *47* (12), 3866−3877.

(10) Kaegi, R.; Voegelin, A.; Sinnet, B.; Zuleeg, S.; Hagendorfer, H.; Burkhardt, M.; Siegrist, H. Behavior of Metallic Silver Nanoparticles in a Pilot Wastewater Treatment Plant. *Environ. Sci. Technol.* **2011**, *45* (9), 3902−3908.

(11) Pradas del Real, A. E.; Castillo-Michel, H.; Kaegi, R.; Sinnet, B.; Magnin, V.; Findling, N.; Villanova, J.; Carrière, M.; Santaella, C.; Fernández-Martínez, A.; Levard, C.; Sarret, G. Fate of Ag-NPs in Sewage Sludge after Application on Agricultural Soils. *Environ. Sci. Technol.* **2016**, *50* (4), 1759−1768.

(12) Kessler, R. Engineered Nanoparticles in Consumer Products: Understanding a New Ingredient. *Environ. Health Perspect.* **2011**, *119* (3), A120−A125.

(13) Duester, L.; Burkhardt, M.; Gutleb, A. C.; Kaegi, R.; Macken, A.; Meermann, B.; von der Kammer, F. Toward a comprehensive and realistic risk evaluation of engineered nanomaterials in the urban water system. *Front. Chem.* **2014**, *2* (39), 1−6.

(14) Sun, T. Y.; Bornhöft, N. A.; Hungerbühler, K.; Nowack, B. Dynamic Probabilistic Modelling of Environmental Emissions of Engineered Nanomaterials. *Environ. Sci. Technol.* **2016**, *50* (9), 4701−4711.

(15) Hartmann, G.; Hutterer, C.; Schuster, M. Ultra-trace determination of silver nanoparticles in water samples using cloud point extraction and ETAAS. *J. Anal. At. Spectrom.* **2013**, *28* (4), 567−572.

(16) Hartmann, G.; Schuster, M. Species selective preconcentration and quantification of gold nanoparticles using cloud point extraction and electrothermal atomic absorption spectrometry. *Anal. Chim. Acta* **2013**, *761*, 27−33.

(17) Duester, L.; Fabricius, A.-L.; Jakobtorweihen, S.; Philippe, A.; Weigl, F.; Wimmer, A.; Schuster, M.; Nazar, M. F. Can cloud point-based enrichment, preservation, and detection methods help to bridge gaps in aquatic nanometrology? *Anal. Bioanal. Chem.* **2016**, *408*, 7551−7557.

(18) Hartmann, G.; Baumgartner, T.; Schuster, M. Influence of Particle Coating and Matrix Constituents on the Cloud Point Extraction Efficiency of Silver Nanoparticles (Ag-NPs) and Application for Monitoring the Formation of Ag-NPs from Ag+. *Anal. Chem.* **2014**, *86* (1), 790−796.

(19) Markus, A. A.; Parsons, J. R.; Roex, E. W. M.; Kenter, G. C. M.; Laane, R. W. P. M. Predicting the contribution of nanoparticles (Zn, Ti, Ag) to the annual metal load in the Dutch reaches of the Rhine and Meuse. *Sci. Total Environ.* **2013**, *456−457*, 154−160.

(20) Markus, A. A.; Parsons, J. R.; Roex, E. W. M.; de Voogt, P.; Laane, R. W. P. M. Modelling aggregation and sedimentation of nanoparticles in the aquatic environment. *Sci. Total Environ.* **2015**, *506−507*, 323−329.

(21) Markus, A. A.; Parsons, J. R.; Roex, E. W. M.; de Voogt, P.; Laane, R. W. P. M. Modelling the transport of engineered metallic nanoparticles in the river Rhine. *Water Res.* **2016**, *91*, 214−224.

(22) *Deutsche Einheitsverfahren zur Wasser-, Abwasser- and Schlammuntersuchung − Probenahme aus Fließgewässern*, German DIN 38402 T15, DIN Group, 2012.

(23) Ma, R.; Levard, C.; Judy, J. D.; Unrine, J. M.; Durenkamp, M.; Martin, B.; Jefferson, B.; Lowry, G. V. Fate of Zinc Oxide and Silver Nanoparticles in a Pilot Wastewater Treatment Plant and in Processed Biosolids. *Environ. Sci. Technol.* **2014**, *48* (1), 104−112.

(24) Kiser, M. A.; Ryu, H.; Jang, H.; Hristovski, K.; Westerhoff, P. Biosorption of nanoparticles to heterotrophic wastewater biomass. *Water Res.* **2010**, *44* (14), 4105−4114.

(25) Gómez-Rivera, F.; Field, J. A.; Brown, D.; Sierra-Alvarez, R. Fate of cerium dioxide (CeO2) nanoparticles in municipal wastewater during activated sludge treatment. *Bioresour. Technol.* **2012**, *108*, 300−304.

Supporting Information

Silver Nanoparticle Levels in River Water: Real Environmental Measurements and Modelling Approaches–a Comparative Study

Andreas Wimmer [a, #], Adriaan A. Markus [b, #], Michael Schuster [a, *]

[a] Division of Analytical Chemistry, Department of Chemistry, Technical University of Munich, Garching 85748, Germany

[b] Deltares, P.O.Box 177, 2600 MH Delft, The Netherlands

[*] Corresponding author. Tel: +49 (0)89 289 13763; fax: +49 (0)89 289 14513; E-mail address: michael.schuster@ch.tum.de

[#] A. Wimmer and A. Markus contributed equally to the presented study.

20 pages

5 Figures

4 Tables

Instrumentation

The quantification of silver (Ag) in organic extracts after cloud point extraction (CPE) of aqueous samples was conducted using a Zeeman corrected electrothermal atomic absorption spectrometer (ET-AAS) AAnalyst 800 (PerkinElmer, Waltham, MA, USA) equipped with a transversally heated THGA 800 graphite tube atomizer and an autosampler AS-72 (Perkin Elmer). High-purity Argon 4.8 (Westfalen, Münster, Germany) served as inert gas during the measurements. The Ag hollow cathode lamp (Photron, Victoria, Australia) was operated at the recommended current of 10 mA and Ag quantification was based on the absorption line at $\lambda = 328.1$ nm, with an integration time of 5 s.

The measurements of total Ag in river water was performed using a 7900 ICP-MS (Agilent, Santa Clara, CA, USA) equipped with an autosampler, SPS4 (Agilent). Argon 4.8 was used as the plasma gas. ^{107}Ag was chosen as the target mass for quantification and integration time was set to 0.5 s. ^{103}Rh was used as internal standard. To avoid polyatomic interferences, He collision mode was applied. Data evaluation was performed in Agilent's MassHunter Workstation 4.4 (Version C.01.04, build 544.3).

Extraction and Enrichment Procedure of Ag-*b*-NPs in Water Samples

Cloud point extraction, a well-established and validated method for species-selective extraction and enrichment of metallic NPs, such as Ag-*b*-NPs, from aqueous samples, was used for sample preparation.[1-4] This micellar mediated technique is able to separate Ag-*b*-NPs from dissolved Ag species with an enrichment factor of about 100. To the best knowledge of the authors, the lowest limit of detection, so far, for Ag-*b*-NPs in environmental samples of 0.2 ng L^{-1} can be achieved by applying this method.[5] For the extraction procedure, acetic acid (glacial), ethanol, ethylenediaminetetraacetate (EDTA) disodium salt, sodium acetate anhydrous, ethanol, and nitric acid (65%) were purchased from Merck and Triton X-114 was obtained from AppliChem (Darmstadt, Germany). The D-penicillamine was purchased from Sigma Aldrich. In brief, 40 mL of each aqueous sample was treated, without filtration, with a 3.0 mL saturated EDTA solution, 1.0 mL 0.1 M D-penicillamine solution, 100 µL 1.25 M acetic acid, 400 µL 1 M sodium acetate solution, and 1 mL of 10 % (w/w) TX-114 in a 50 mL tapered polypropylene falcon tube. After incubating the mixture at 40°C for 30 min, phase separation was enhanced by centrifugation at 4472 *g* for 12 min. After cooling the sample over ice, the aqueous supernatant was decanted and the remaining Ag-*b*-NP containing, surfactant rich phase

52 was forwarded for measurement.

53

Quantification of Ag-*b*-NPs in CPE-Extracts of River Water

55 Prior to measurement, the surfactant-rich phase was dissolved in 100 µL of EtOH. The ET-AAS was

56 used to perform the Ag quantification. For calibration, dispersions containing citrate-stabilized 60 nm

57 AgNPs of a known concentration were prepared and subjected to the same extraction procedure as

58 the samples. Thus, the calibration function compensated for all adverse effects during the extraction

59 process. Even commercially available NP dispersions can contain a certain amount of dissolved

60 species. Therefore, the 60 nm AgNP dispersion was pre-cleaned before usage through dialysis

61 overnight, using a 3.5 kDa cellulose dialysis membrane. The Ag mass concentration of the so

62 prepared 60 nm AgNP dispersion was determined using a 7900 ICP-MS and Ag(I) standard solutions

63 for calibration.

64

65

Determination of Further Water Quality Parameters

67 Six more parameters describing water quality were determined for each sample. The pH, conductivity,

68 and temperature were measured using a VWR pH 110 portable pH, mV, and temperature instrument

69 (VWR, Radnor, PA, USA). The VWR DO210 portable dissolved oxygen and temperature instrument

70 (VWR) was used to measure the dissolved oxygen of all samples. All measurements were carried out

71 on-site directly after sampling. To determine the suspended particulate matter (SPM) in all samples,

72 100 mL of the thoroughly shaken sample were filtered using a dried, weighted 0.45 µm

73 polyethersulfone syringe filter (VWR). Afterwards, each filter was dried to a constant mass in a

74 drying cabinet at 40°C. The SPM is calculated by dividing the mass increase of each filter by the

75 initially filtered sample volume. Total organic carbon (TOC) values were determined using a TOC-

76 L CPH/CPN system (Shimadzu, Nakagyo-ku, Kyōto, Japan) and a potassium hydrogen phthalate

77 solution (Naclai Tesque, Kyōto, Japan) of a known concentration was used for TOC calibration.

78
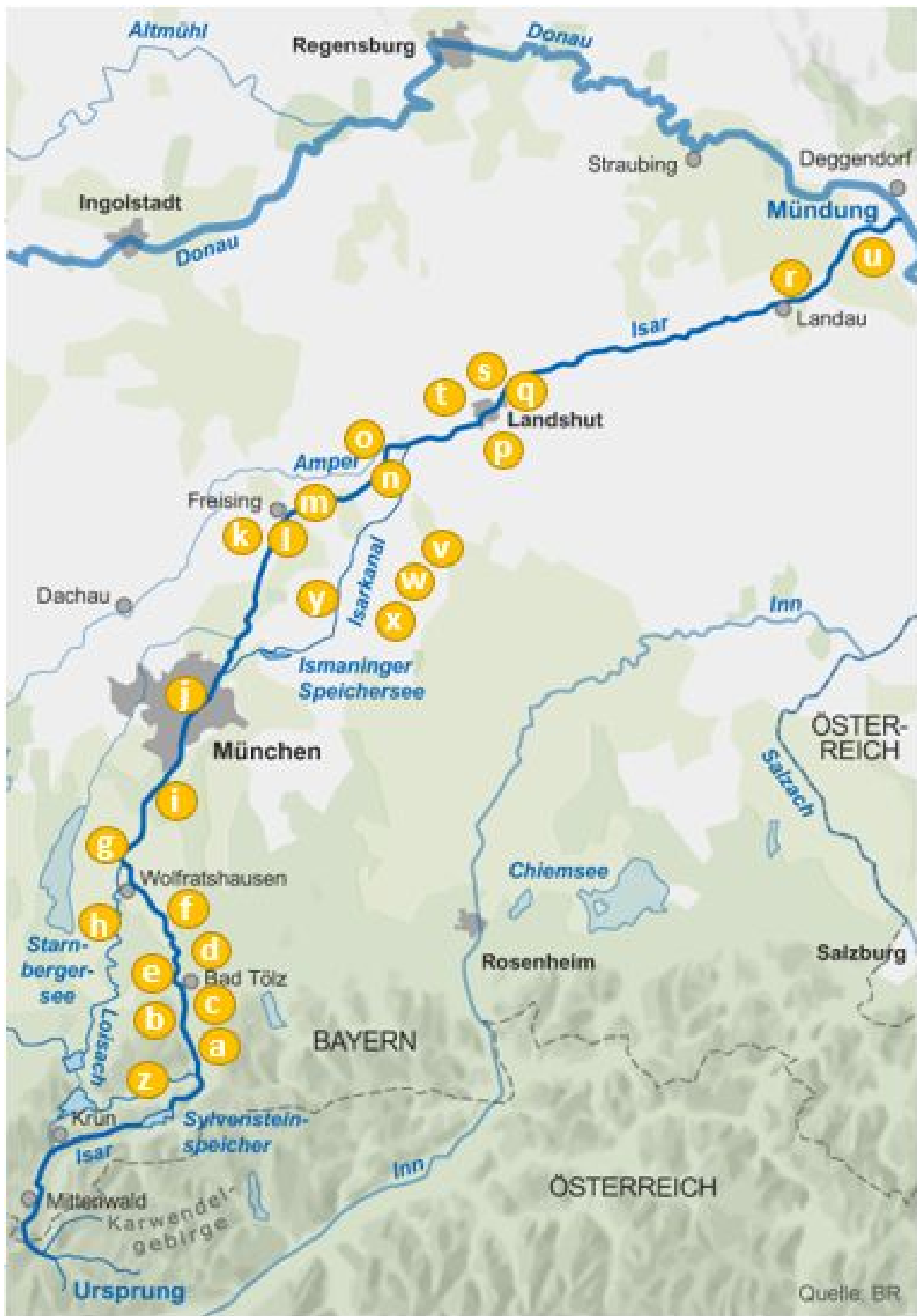
Figure S1. Map of the river Isar and its tributaries in southern Germany. Names of all tributaries are abbreviated. For full explanation, see Table S1. The map is sourced from Bayerischer Rundfunk (BR/Christian Sonnberger; http://www.br.de/themen/bayern/isar-dossier-karte104.html).

Table S1. Hydrological data from the river Isar and its tributaries during the sampling day in July 2016, used for setting up a simple hydrological network of the river Isar. Data obtained by the Bavarian Environmental Protection Agency and the Flood Information Center of Bavaria.

location	width [m]	depth [cm]	flow rate [m^3 s^{-1}]	coordinates
Isar				
Lengries (a)	38	114	21.2	47.684261171183614, 11.571889287851768
Bad Tölz (e)	61	101	26	47.76144372972256, 11.556476937636898
Puppling (g)	42	130	54.2	47.91616323236766, 11.44614690277267
Baierbrunn (i)	120	34	no data available	48.01428442261681, 11.488794212579693
München (j)	64.4	78	54.8	48.1453629477706, 11.596799809514579
Freising (k)	56	62	30	48.39816107051033, 11.752228993476255
Moosburg (n)	60	86	65	48.46547548299086, 11.9461642583811
Landshut (q)	71	119	152	48.5275960974435, 12.133436509828686
Landau (r)	67	113	173	48.67521066623552, 12.69267539688097
Plattling (u)	80	179	156	48.77092597275722, 12.883554673638109
tributaries				
Arzbach (b)	3.8	16	0.8	47.70781003341639, 11.551295526470437
Große Gaisach (c)	2	29	1.52	47.739545872814276, 11.57620963880828
Ellbach (d)	5	50	0.84	47.76153556029325, 11.571175707214998

5

Zeller Bach (f)	5.6	19	0.17	47.83610419298666, 11.536405096581028
Loisach (h)	40	315	37.1	47.83522581701558, 11.414963182937628
Moosach (l)	11.6	59	2.23	48.4081151951624, 11.77812795498983
Schleifermoosach (m)	9.5	38	0.23	48.40511584880104, 11.762270989470029
Amper (o)	32	73	16	48.481733744506556, 11.928129498103583
Tiefenbach (p)	2	8	0.02	48.50404118658549, 12.10080156590242
Flutmulde (s)	7	96	1.14	48.54591058508104, 12.136667463405924
Pfettrach (t)	5	26	0.5	48.5535820124605, 12.111032288340672
Strogen (v)	11	42	0.61	48.412995024840654, 11.982435821519225
Sempt (w)	7	69	1.57	48.3294613127844, 11.922949011498014
Saubach (x)	8	67	1.24	48.32931259384908, 11.91604422437746
Gfällach (y)	7	39	0.26	48.31828550773963, 11.820451194709786
Jachen (z)	13	154	0.99	47.6115166736595, 11.502866973659463

83

Figure S2. Location of all examined wastewater treatment plants(WWTPs) along the river Isar. The map is sourced from Bayerischer Rundfunk (BR/Christian Sonnberger; http://www.br.de/themen/bayern/isar-dossier-karte104.html).

Table S2. Name, location and capacity of all examined WWTPs along the river Isar. Information on the capacity was obtained from the WWTP managers.

symbol	name	capacity [$m^3\ d^{-1}$]
A	WWTP Bad Tölz	7000
B	WWTP Ismaning	6500
C	WWTP Gut Marienhof	250000
D	WWTP Freising	12000
E	WWTP Moosburg	10000
F	WWTP Landshut	15500
G	WWTP Landau	3500

88

Transverse mixing downstream of the WWTPs

As stated in the main text, sample points have been located 1.5 km downstream of the various WWTPs to measure the effect of the discharge mixed over the river section. The question arises whether this distance, advised in the sampling standard procedure DIN 38 402 T15, is large enough to ensure well-mixedness. To estimate this, the transverse dispersion coefficient is required. According to Baek and Seo[6] this coefficient can be estimated via various relationships, both empirical and theoretical, with more or less details regarding the geometry and other properties of the river in question. Numerically, the coefficient D (in $m^2 \, s^{-1}$) is roughly $(h \cdot u_*)/6$, where h is the depth (in the order of 1 m – Table S1) and u_* is the shear stress velocity.

To estimate the shear stress velocity:

$$u_* = U \cdot \sqrt{(g/C^2)}$$

where U the flow velocity, g the gravitational acceleration and C the Chézy coefficient (typically $C^2 \sim 3000 \, m^2 \, s^{-1}$). With a flow velocity of 1 m s^{-1} this gives $u_* = 0.06$ m s^{-1}, so that the dispersion coefficient becomes $D = 0.01 \, m^2 \, s^{-1}$.

A point source of effluent in the river will reach a width in the order of $\sqrt{Dt}$, with t being the travel time. Given the hydrological data (Table S1), the travel time for reaching 1.5 km downstream of the WWTP discharge point is in the order of 1.5 km / (1 m s^{-1}) = 1500 s.

The width of the river Isar is typically 70 m. To achieve a fully mixed cross-section in this time, a dispersion coefficient of 3 $m^2 \, s^{-1}$ is required. The dispersion coefficient, however, as estimated is 300 times smaller.

The above estimation holds for point sources with no momentum only, whereas discharges from a WWTP are not point sources and possess a certain momentum. The mixing will be more rapid and extend over a larger width. Nevertheless, the conclusion is that the effluent plumes from the various WWTPs may not quite have reached the full width of the river and therefore a variation in the concentration over the river cross-section is to be expected.

An alternative estimate is provided by Bleninger and Jirka[7] who provide a simple formula for the length L after which the plume is laterally mixed:

$L \approx 10 \, b^2/h$

117   where b is the river width and h the representative depth. With a typical width of 70 m and a depth of

118   1 m, this formula gives: L = 36 km.

119   Since the model that was applied is a *one-dimensional* network model of the river Isar and several of

120   its tributaries, it is not possible to represent the concentration peaks that were found around the

121   discharge points. To represent such peaks a two-dimensional or even three-dimensional model would

122   have been necessary.

Detailed Information on the modeling approach

Modeling the aggregation processes

In the water quality model as applied here, the following processes were distinguished:

- Free (unadsorbed and non-aggregated) nanoparticles can be adsorbed to suspended sediment particles (heteroaggregation) or cluster together into homogeneous aggregates (homoaggregation).
- The free nanoparticles, the homogeneous aggregates, and the nanoparticles adsorbed to suspended sediment can settle onto the bottom. This process is, however, of negligible influence, as the flow velocity in the river is too large to allow particles to actually settle on the bottom.

The mathematical formulation of these processes is shown below:[8]

$$\frac{dC_{free}}{dt} = -k_1 C_{free}^2 - k_2 C_{free} C_{agg} - k_3 C_{free} C_{sed}$$

$$\frac{dC_{agg}}{dt} = +k_1 C_{free}^2 + k_2 C_{free} C_{agg}$$

$$\frac{dC_{ads}}{dt} = +k_3 C_{free} C_{sed}$$

where:

- C_{free} is the concentration of "free" (unadsorbed and non-aggregated) nanoparticles,
- C_{agg} is the concentration of clustered nanoparticles, forming homogeneous aggregates,
- C_{ads} is the concentration of nanoparticles adsorbed to suspended sediment and
- C_{sed} is the concentration of suspended sediment.

The coefficients k_1, k_2 and k_3 are the rate coefficients for respectively the homoaggregation processes (formation of homogeneous aggregates and expansion thereof) and heteroaggregation.

145 **Transport modelling**

146 As the hydrological data on the river system are limited, we chose a simplified model set-up: each

147 tributary as well as the main river was represented by a one-dimensional branch, consisting of ten to

148 twenty grid cells. Within each branch, the flow rate is constant in time and space and the cross-section

149 was taken constant as well. Because the flow rates as reported in table S1 are not consistent (there is

150 no major contribution in the stretch between Munich and Landshut that can explain the increase in

151 flow rate of about 100 m^3 s^{-1}), the actual flow rates used were made consistent with the upstream

152 tributaries, resulting in a flow rate of 103 m^3 s^{-1} instead of 152 m^3 s^{-1}. The figure below illustrates the

153 division of the branches into grid cells.

154
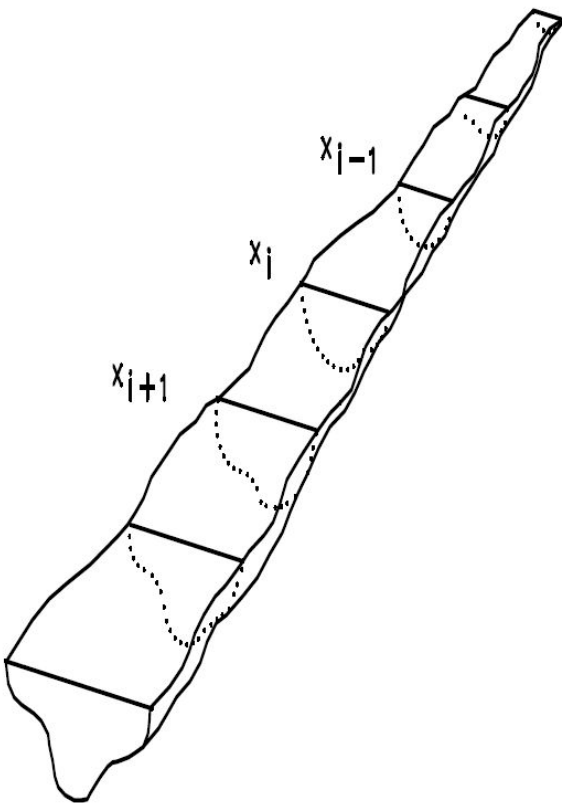
155

156 **Figure S3.** Schematic view of a river branch divided into several grid cells.

157

Exemplary calculation for representing a WWTP as a point source of Ag-*b*-NPs in the river Isar

Assuming a typical water consumption of 200 L per person per day, the capacity of WWTP C (Gut Marienhof, responsible for Munich) corresponds to 1.25 Mio. people, which is quite close to the population of Munich (1.45 Mio inhabitants). Given the estimate by Markus et al.[9] for a mean contribution of 46 mg Ag-*b*-NPs a year per person to wastewater in the catchment area of the WWTP, 1.25 Mio people would produce 58 kg Ag-*b*-NPs in waste per year, emitted into wastewater. Based on the measured 18.53 ng L^{-1} Ag-*b*-NPs next to WWTP C (Table S3) in the Isar, and the capacity of WWTP C, a resulting 1.7 kg Ag-*b*-NPs a year would be discharged by WWTP C. The ratio between the 58 kg Ag-*b*-NP of annual waste produced by humans and the release of 1.7 kg a year into the Isar for WWTP C corresponds to a 97% retention of Ag-*b*-NPs by WWTP C; this is in very good agreement to published data about the removal efficiency of nanoparticles in WWTPs.[5] Overall, the concentration of Ag-*b*-NPs in the Isar was estimated as 3% of the estimate by Markus et al.[9] For total Ag, the concentrations measured at the location of the WWTPs and tributaries were used as inputs of the model.

Boundary conditions

Running the model requires the input of initial and boundary conditions. Three upstream boundaries, one for each river (Isar and its two main tributaries, Amper and Loisach), were based on measured data from suspended particulate matter, Ag-*b*-NPs, and total Ag of the river Isar (Table S3, sampling location 1), the Amper River (Table S3, sampling location 11), and the Loisach River (Table S3, sampling location 5). The chosen monitoring points for the Amper and Loisach Rivers are those closest to the tributaries. Initial conditions do not matter much as the model has a residence time of approximately three days. By running the model for a period that is several times this residence time (e.g. 10 days), a steady state that is independent of the initial condition is reached.

185

Figure S4. Location of all sampling sites along the river Isar. The map is sourced from Bayerischer

Rundfunk (BR/Christian Sonnberger; http://www.br.de/themen/bayern/isar-dossier-karte104.html).

Table S3. Water quality data and total and particulate Ag concentrations for each sampling site of the river Isar.

	location	T [°C]	pH	conductivity [mS]	O2 [ppm]	SPM [g L^{-1}]	TOC [mg L^{-1}]	Ag concentration [ng L^{-1}]	AgNP concentration [ng L^{-1}]	AgNP proportion [%]
1	Isar Lenggrieß	12.7	7.9	0.36	10.2	0.43	0.46 ± 0.03	16.35 ± 0.02	0.33 ± 0.03	2.0
2	1.5 km before WWTP Bad Tölz	14.3	8.0	0.37	10.1	0.87	0.50 ± 0.02	22.21 ± 0.04	2.70 ± 0.06	12.2
3	WWTP Bad Tölz	16	7.9	0.38	9.9	0.40	0.64 ± 0.03	86.72 ± 0.02	20.88 ± 0.09	24.1
4	1.5 km after WWTP Bad Tölz	15	8.0	0.37	10.1	0.65	0.49 ± 0.07	37.56 ± 0.15	4.50 ± 0.07	12.0
5	Isar Wolfratshausen	18	8.2	0.34	10.4	1.43	1.00 ± 0.04	12.29 ± 0.05	1.65 ± 0.04	13.5
6	1.5 km before WWTP Ismaning	18.7	8.3	0.45	10.3	0.80	1.08 ± 0.06	4.87 ± 0.04	0.60 ± 0.31	12.3
7	WWTP Ismaning	16.7	7.7	0.63	10.0	0.52	0.64 ± 0.05	23.86 ± 0.15	2.47 ± 0.05	10.3
8	1.5 km after WWTP Ismaning	16.7	7.9	0.53	10.7	1.25	1.01 ± 0.06	22.55 ± 0.07	1.91 ± 0.15	8.5
9	WWTP Gut Marienhof	23	8.5	0.4	9.6	0.89	1.39 ± 0.03	60.80 ± 0.01	18.53 ± 0.14	30.5
10	1.5 km after WWTP Gut Marienhof	22.2	8.5	0.42	10.4	0.31	1.44 ± 0.07	18.26 ± 0.03	0.77 ± 0.07	4.2
11	1.5 km before WWTP Freising	22.7	8.8	0.43	9.7	0.84	1.61 ± 0.05	16.76 ± 0.05	0.53 ± 0.13	3.1
12	WWTP Freising	23.4	7.6	1.4	8.3	0.82	3.95 ± 0.08	73.01 ± 0.01	0.71 ± 0.39	1.0
13	1.5 km after WWTP Freising	21.1	8.7	0.4	11.7	0.68	1.53 ± 0.08	25.06 ± 0.09	0.80 ± 0.07	3.2
14	WWTP Moosburg	25.2	8.8	0.48	8.5	1.09	1.8 ± 0.03	38.02 ± 0.13	4.72 ± 0.02	12.4
15	Isar after estuary of Amper	23.7	8.5	0.53	10.3	1.22	2.73 ± 0.04	14.93 ± 0.021	1.04 ± 0.17	6.9
16	Isar Hofham	24.1	8.4	0.46	14.0	0.45	2.43 ± 0.02	14.00 ± 0.02	1.52 ± 0.12	10.9
17	1.5 km before WWTP Landshut	26.3	8.1	0.45	9.4	0.96	2.49 ± 0.07	32.71 ± 0.01	4.10 ± 0.16	12.5
18	WWTP Landshut	25.6	8.2	0.45	9.8	1.64	1.77 ± 0.06	125.09 ± 0.04	32.40 ± 0.17	25.9
19	1.5 km after WWTP Landshut	25.9	8.2	0.46	9.6	0.56	1.85 ± 0.07	23.62 ± 0.02	2.61 ± 0.11	11.1
20	1.5 km before WWTP Landau	23.7	8.3	0.45	9.4	0.78	1.61 ± 0.03	17.98 ± 0.02	2.44 ± 0.09	13.6
21	WWTP Landau	23.2	7.7	0.7	7.9	1.28	3.6 ± 0.03	189.05 ± 0.01	69.08 ± 0.1	36.5
22	1.5 km after WWTP Landau	23.5	8.1	0.47	9.5	1.32	1.57 ± 0.02	14.89 ± 0.02	1.31 ± 0.07	8.8
23	Danube near Deggendorf	24.4	8.1	0.47	8.7	2.14	2.17 ± 0.14	11.31 ± 0.01	1.40 ± 0.04	12.4

Table S4: Compilation of measured and modelled concentrations of Ag-*b*-NPs and total Ag as a function of the sampling location (see Table S3) and the ratio modelled/measured concentrations showing comparability of the results.

sampling location	concentration of Ag-*b*-NPs [ng L-1]		ratio	concentration of total Ag [ng L-1]		ratio
	measured	modelled		measured	modelled	
1	0.33	0.33	1.0	16.35	16	1.0
2	2.70	0.33	0.1	22.21	16	0.7
4	4.50	0.36	0.1	37.56	17	0.5
5	1.75	0.90	0.5	12.29	15	1.2
6	0.60	0.91	1.5	4.87	15	3.1
8	1.91	0.92	0.5	23.86	15	0.6
10	0.77	2.20	2.9	18.26	15	0.8
11	0.53	2.20	4.2	16.76	19	1.1
13	0.80	2.20	2.8	25.06	19	0.8
14	4.72	0.72	0.2	38.02	17	0.4
15	1.04	1.83	1.8	14.93	17	1.1
16	1.52	1.83	1.2	14.00	17	1.2
17	4.10	1.83	0.4	32.71	17	0.5
19	2.61	1.85	0.7	23.62	17	0.7
20	2.44	1.87	0.8	17.98	17	0.9
22	1.31	1.87	1.4	14.89	17	1.1
23	1.40	1.87	1.3	11.31	17	1.5
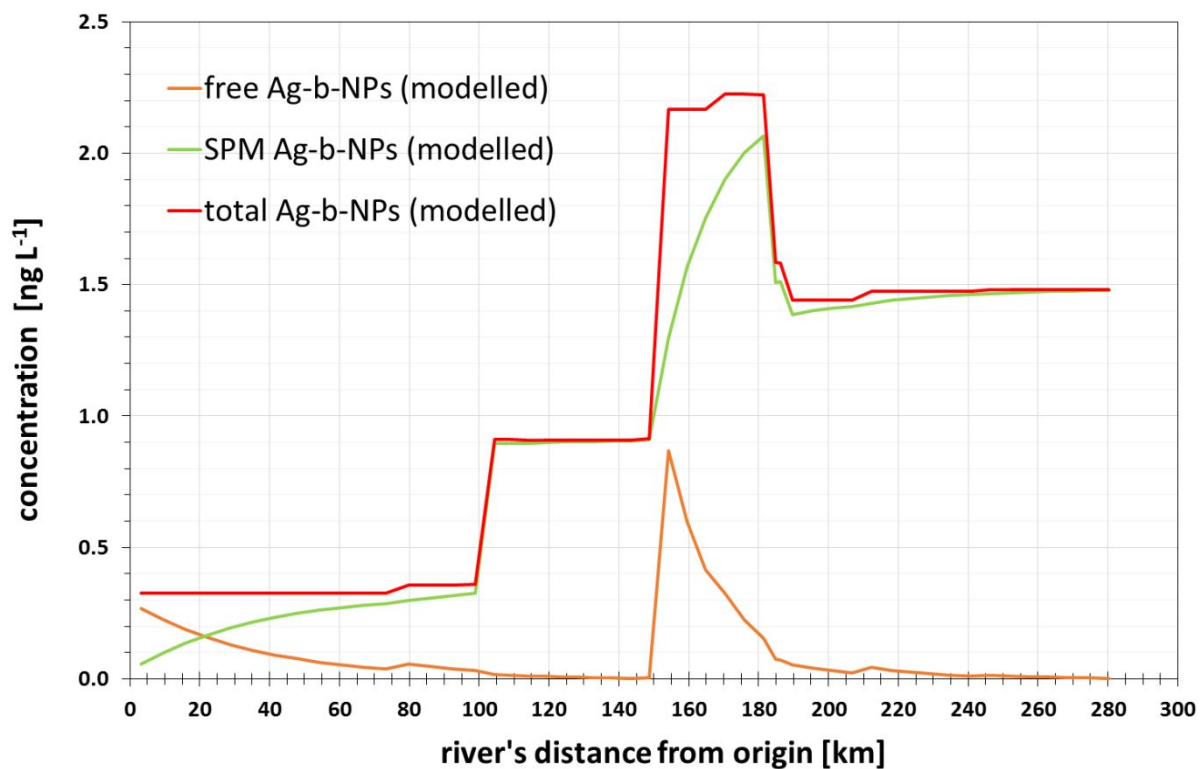
Figure S5: The modelled unadsorbed fraction (free Ag-*b*-NPs, orange), fraction adsorbed to suspended solids (SPM Ag-*b*-NPs, green), and total amount of Ag-*b*-NPs (red) in the river Isar with increasing distance from the river's origin.

References

1. Hartmann, G.; Baumgartner, T.; Schuster, M., Influence of Particle Coating and Matrix Constituents on the Cloud Point Extraction Efficiency of Silver Nanoparticles (Ag-NPs) and Application for Monitoring the Formation of Ag-NPs from Ag+. *Analytical Chemistry* **2014,** *86*, (1), 790-796.

2. Hartmann, G.; Hutterer, C.; Schuster, M., Ultra-trace determination of silver nanoparticles in water samples using cloud point extraction and ETAAS. *Journal of Analytical Atomic Spectrometry* **2013,** *28*, (4), 567-572.

3. Hartmann, G.; Schuster, M., Species selective preconcentration and quantification of gold nanoparticles using cloud point extraction and electrothermal atomic absorption spectrometry. *Analytica Chimica Acta* **2013,** *761*, 27-33.

4. Duester, L.; Fabricius, A.-L.; Jakobtorweihen, S.; Philippe, A.; Weigl, F.; Wimmer, A.; Schuster, M.; Nazar, M. F., Can cloud point-based enrichment, preservation, and detection methods help to bridge gaps in aquatic nanometrology? *Analytical and Bioanalytical Chemistry* **2016**, 1-7.

5. Li, L.; Stoiber, M.; Wimmer, A.; Xu, Z.; Lindenblatt, C.; Helmreich, B.; Schuster, M., To What Extent Can Full-Scale Wastewater Treatment Plant Effluent Influence the Occurrence of Silver-Based Nanoparticles in Surface Waters? *Environmental Science & Technology* **2016,** *50*, (12), 6327-6333.

6. Baek, K. O.; Seo, I. W., On the methods for determining the transverse dispersion coefficient in river mixing. *Advances in Water Resources* **2016,** *90*, 1-9.

7. Bleninger, T.; Jirka, G. H., How to deal with mixing zones for priority pollutant discharges? *Presentation Universität Karlsruhe* **sine annum**.

228 8.   Markus, A. A.; Parsons, J. R.; Roex, E. W. M.; de Voogt, P.; Laane, R. W. P. M.,

229   Modeling aggregation and sedimentation of nanoparticles in the aquatic environment.

230   *Science of The Total Environment* **2015,** *506-507*, 323-329.

231

232 9.   Markus, A. A.; Parsons, J. R.; Roex, E. W. M.; Kenter, G. C. M.; Laane, R. W. P. M.,

233   Predicting the contribution of nanoparticles (Zn, Ti, Ag) to the annual metal load in

234   the Dutch reaches of the Rhine and Meuse. *Sci Total Environ* **2013,** *456-457*, 154-160.

235

236

8.7 PUBLIKATION 7

Copper Drinking Water Pipes as a Previously Undocumented Source of Silver-Based Nanoparticles

Andreas Wimmer, Jessica Beyerl, and Michael Schuster

Copper Drinking Water Pipes as a Previously Undocumented Source of Silver-Based Nanoparticles

Andreas Wimmer, [ORCID] Jessica Beyerl, and Michael Schuster*

Division of Analytical Chemistry, Department of Chemistry, Technical University of Munich, Garching 85748, Germany

S *Supporting Information*

ABSTRACT: Wastewater streams are widely known to release silver-based nanoparticles (Ag-b-NPs) into the environment with a plethora of unknown consequences. Until recently, studies have commonly associated Ag-b-NP sources with products that contain these NPs for antimicrobial reasons, such as fabrics, cosmetics, and medical products. However, our study reveals that there is a thus far completely undocumented source of Ag-b-NPs: copper drinking water pipes. We applied cloud point extraction hyphenated to electrothermal atomic absorption spectrometry or single-particle inductively coupled plasma mass spectrometry to analyze the concentration and perform size-selective quantification of Ag-b-NPs in tap water passing through copper pipes. Up to 83 ng of total silver and 25 ng of Ag-b-NPs were present in tap water samples per liter, which resulted in an NP proportion of approximately 30% of total silver. In total, 96% of the measurable particle sizes ranged from 10 to 36 nm. Additionally, 53 μg of copper was released per liter tap water on average. The measurements included tap water from different sampling days and from four different buildings with varying ages, whereas Ag-b-NPs could be detected in the tap water of two buildings. Silver traces in the copper pipe material of 27.5 ± 4.4 μg g^{-1} were found to be responsible for the release of nanoparticulate silver into the tap water.
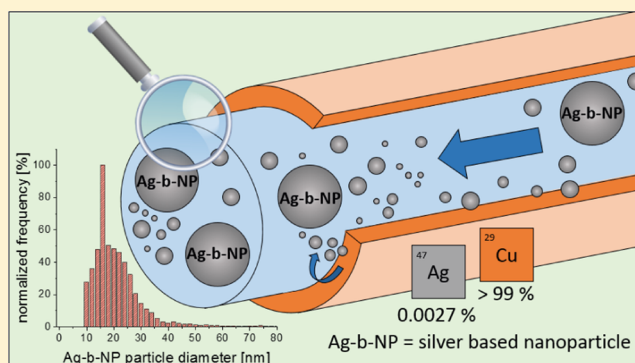
INTRODUCTION

Proper risk assessment of engineered nanoparticles (ENPs) in the environment requires knowledge of nano-(eco)toxicology[1] and simultaneous information about the environmental concentrations, chemical compositions, shapes, and surface modifications of all particles. To date, there are numerous studies available that deal with ENP sources and the possible mechanisms that release them into nature.[2−7] A number of industrial sectors, such as personal care,[8] functionalized fabrics,[9−11] house appliances,[12] and food storage[13] add silver-based nanoparticles (Ag-b-NPs) to a broad variety of products, where the release of particles should occur during any stage of their lifecycle, namely, production, usage, and disposal.[14] Solid and liquid water streams serve as the main pathways for nanomaterials in the environment, together with an unclear particle release mechanism from the use and abrasion of ENP-containing products.[15−19] The increasing research for ENP stabilization and functionalization techniques indicates a stronger probability that ENPs enter aquatic environments.[20]

On the basis of these exposure scenarios, dynamic probabilistic material flow analysis attempts to evaluate the environmentally relevant concentrations when ENPs enter streams.[21−24] In a recent study, concentrations of engineered Ag-b-NPs in surface water were estimated to range from 0.4 to 2.78 ng L^{-1}.[24] These values are in good agreement with our previous study,[6] which for the first time tracked natural Ag-b-NPs through representative municipal wastewater treatment plants (WWTPs). The effect of WWTP effluents on Ag-b-NP concentrations along a river was also investigated.[6] After passing through an urban area, a river receives effluent from several WWTPs, which contribute approximately 1.7 ng L^{-1} of WWTP-related Ag-b-NPs near the mouth of the river. Recently, experiments revealed that Ag-b-NPs can be formed naturally from geogenic traces of silver in the sub-ng L^{-1} range[25] and that, contrary to common interpretations in the literature,[26] Ag-b-NPs are preferably formed under dark conditions. Particle formation also does not require elevated temperatures.[26] At environmentally relevant concentrations, i.e., in the low ng L^{-1} range, Ag-b-NP formation can occur in the dark at low temperatures, e.g. in groundwater or at the bottom of lakes. Particle size increases gradually with the increase in reaction time, which suggests that Ostwald ripening occurs even at such low particle concentrations.[25] These Ag-b-NPs may also form and exhibit Ostwald ripening if drinking water contains traces of silver that derives from plumbing materials.

Due to recent progress in the development of analytical techniques,[4,6,27−30] it is now possible to identify thus far undocumented sources of Ag-b-NPs. Until recently, water supply pipework was thought to be the main source of ionic heavy metal species in tap water, such as cadmium (Cd), chromium (Cr), cobalt (Co), copper (Cu), iron (Fe), lead (Pb), manganese (Mn), nickel (Ni), selenium (Se), and zinc (Zn) due to the corrosion of the plumbing material.[31−33] Copper, a very common water pipe material, always contains traces of silver,[34] a natural impurity, which is capable of releasing silver ions as well as Ag-b-NPs in the ng L^{-1} range into tap water that passes through copper pipes. The main sources of copper in an urban environment are tap water and roof runoff.[35−37] For nanoparticles that migrate from the pipe material to tap water, previous studies have only discussed lead dioxide (PbO_2)-NPs,[38] Cu-NPs,[39] and Fe-NPs[40] to date. Given the fact that massive volumes of tap water significantly influence wastewater streams and, as we show in this study, that tap water can contain non-negligible amounts of Ag-b-NPs, tap water as a source of Ag-b-NPs in aquatic environments can no longer be ignored in risk assessment studies and flow analysis models.

In this study, we use the term silver-based nanoparticles (Ag-b-NPs) for all types of nanoparticles that consist mainly of silver as a cumulative concept since nanoparticulate silver can be characterized by a daunting variety of nanosized particles with different sizes, morphologies, elemental compositions, and surface modifications.[41−43]

■ MATERIALS AND METHODS

Materials. A dissolved Ag(I) standard ($AgNO_3$ in 3% HNO_3, $\beta_{Ag} = 1000$ mg L^{-1}) and an inductively coupled plasma (ICP) multielement standard (Merck IV, $\beta = 1000$ mg L^{-1}, 6% HNO_3) were obtained from Merck (Darmstadt, Germany). An AgNP dispersion (60 nm, $\beta_{Ag} = 20$ mg L^{-1}, citrate stabilized) was purchased from Sigma-Aldrich (St. Louis, MO). A gold nanoparticle (AuNP) dispersion (National Institute of Science and Technology (NIST) reference material RM 8013, 56 nm, $\beta_{Au} = 52$ mg L^{-1}, citrate stabilized) was supplied by the National Institute of Standards and Technology (Gaithersburg, MD). Acetic acid (glacial), ethanol, ethylenediaminetetraacetate disodium salt dihydrate, sodium acetate anhydrous, ethanol, and nitric acid (65%) were purchased from Merck. Triton X-114 was obtained from AppliChem (Darmstadt, Germany). D-Penicillamine was purchased from Sigma-Aldrich. All chemicals were at least of analytical grade and checked for contamination via ICP-mass spectrometry (ICP-MS) analysis prior to use. Therefore, all chemical solutions exhibiting the desired concentrations for subsequent experiments were prepared and silver and other observed elements were quantified according to the procedures described in the "Instrumentation" section. Ultrapure water (UPW, with a resistivity of 18.2 MΩ cm^{-1}) was obtained using a Milli-Q gradient system (Millipore GmbH, Schwalbach, Germany). All used glass vessels were rinsed thrice with nitric acid 6.5% (w/w), steamed with nitric acid vapor for at least 4 h, rinsed three times with UPW, and stored afterward in a particle-free environment until use.

Water Sample Collection and Determination of General Water Parameters. In this study, we analyzed tap water from four buildings in Southern Germany that were built in different years. On the basis of national regulations, copper tap water pipes had been installed in every building.[44] The buildings (B) were built in 1978 (B1), 1997 (B2), 2002 (B3), and 2011 (B4). In 2016, we performed sampling according to the German DIN 38402-15 regulation.[45] All water samples were collected in new, disposable 500 mL polyvinylchloride containers, which were rinsed thrice with UPW prior to analysis. In every building, one water tap system was sampled over a period of several days, whereas the tap was only used for sampling and afterward kept closed until the next day. The final sample volume ranged from approximately 0.5−2.0 L (more details on the final sample volume are given in the Supporting Information). For each building, the examined tap was not used for 13−14 days prior to the first sampling day. Each day, seven samples were collected from every tap over a period of approximately 15 min. As we intended to perform a realistic sampling, flow velocities were not artificially adjusted. Immediately after sampling, the pH, redox potential, oxygen content, and temperature of each water sample were determined using a portable pH, mV, and temperature instrument pH110 (VWR, Radnor, PA) and the portable DO201 instrument (VWR) was used to determine the amount of dissolved oxygen. Immediately after sampling, all samples were stored in a refrigerator at 7 °C and Ag-b-NPs and all other examined elements were quantified only hours after the sampling to ensure sample stability.

Samples were divided into two parts, whereas the part intended for elemental analysis was acidified immediately after sampling to 3.25% (w/w) with ultrapure nitric acid (obtained by sub-boiling distillation). The sample parts intended for particle size measurements were not acidified to prevent particle dissolution. All samples were handled and measured without filtration.

Instrumentation. The quantification of Ag-b-NPs in organic extracts and the determination of silver traces in dissolved copper water pipe material were conducted with a Zeeman-corrected electrothermal atomic absorption spectrometer (ET-AAS) (AAnalyst 800, PerkinElmer, Waltham, MA) equipped with a transversally heated THGA 800 graphite tube atomizer and an AS-72 autosampler. Highly pure Argon 4.8 (Westfalen, Münster, Germany) served as the inert gas during measurements. A silver hollow cathode lamp (Photron, Victoria, Australia) was operated at the recommended current of 10 mA and silver quantification was based on the absorption line at $\lambda = 328.1$ nm with an integration time of 5 s.

Multielement and single-particle ICP-MS (sp-ICP-MS) measurements were performed using an inductively coupled plasma mass spectrometer (7900 ICP-MS, Agilent, Santa Clara, CA) equipped with an SPS4 autosampler (Agilent) and a MicroMist nebulizer (Glass Expansion, Melbourne, Australia). Argon 4.8 was used as the plasma gas. Tap water multielemental analysis included the determination of the total concentrations of silver, copper, chromium, iron, lead, nickel, and zinc. A multielement standard containing all examined elements (Merck IV) was used for calibration. Isobaric spectral overlaps were avoided by proper isotope selection: ^{52}Cr, ^{56}Fe, ^{60}Ni, ^{63}Cu, ^{66}Zn, ^{107}Ag, and ^{208}Pb. Integration time was set to 0.5 s, and ^{103}Rh was used as an internal standard that was added online to all samples immediately before nebulization. Due to natural variations in Pb isotopic abundances, the ^{208}Pb signal was corrected using an equation that considers the sum of the ^{206}Pb, ^{207}Pb, and ^{208}Pb isotopes.[46] To avoid potential polyatomic interferences, all measurements were carried out in He collision mode (kinetic energy discrimination; He rate: 5 mL min^{-1}).[47]

Particle size distributions were measured in single-particle mode. The dwell time was set to 100 μs with an acquisition time of 90 s, which resulted in 900 000 data points for each measurement. The peristaltic pump rate was gravimetrically determined as 0.346 mL min^{-1} and ^{107}Ag was selected as a target mass. On the basis of previously published operational procedures,[48] the transport efficiency, which describes the ratio of the amount of analyte that passes the plasma and reaches the detector to the amount of analyte aspirated, was determined using the NIST RM 8013 reference material (AuNP, 56 nm, β_{Au} = 52 ng L^{-1}). Since signal intensity is element-specific, a second calibration, based on a dissolved silver standard (1 μg L^{-1} in 3.25% (w/w) HNO$_3$), was necessary to determine elemental sensitivity. Particle size distributions were evaluated using Agilent MassHunter Workstation 4.4 software (version C.01.04, build 544.3) equipped with the Single Nanoparticle Application Module.

Determination of Total Silver in the Copper Water Pipe Material. Three 1 g pieces of a copper water pipe previously installed and used in B1 for a period of several years were freed from varnish, cleaned, dried, and then dissolved in 5 mL of HNO$_3$ (65% (w/w)), which yielded a clear blue solution within minutes. Due to severe matrix effects caused by high excess of copper in the dissolved samples, we applied the standard addition technique for ET-AAS silver quantification. The corresponding furnace temperature program is listed in Table 1.

Table 1. ET-AAS Temperature Program for the Determination of Silver Traces in the Dissolved Water Pipe Material[a]

process	temperature [°C]	ramp time [s]	hold time [s]	internal argon flow [mL/min]
drying 1	110	1	30	250
drying 2	130	15	30	250
matrix elimination	800	10	20	250
atomization	1700	0	5	0
clean out	2450	1	3	250

[a]Atomic absorption was measured during the atomization step with an integration time of 5 s.

Determination of Ag-b-NPs in Tap Water. Cloud point extraction (CPE) was used for species-selective extraction and enrichment of Ag-b-NPs from the water samples.[27,28,30] This procedure provided efficient retention of the dissolved Ag(I) species and matrix components allowing the selective extraction of Ag-b-NPs followed by unobstructed and highly sensitive measurements via ET-AAS or sp-ICP-MS. Details, trueness, and robustness of the applied extraction technique have already been described by Hartmann et al.[27,28,30]

Briefly, 40 mL of each sample was mixed with an aqueous solution of an ethylenediaminetetraacetic acid disodium salt, D-penicillamine, sodium acetate, acetic acid, and the surfactant TX-114.[25,27,28] These mixtures were incubated at 40 °C for 30 min and centrifuged (12 min, 4500g) to enhance phase separation. After a cooling step (5 min, ice bath), the aqueous supernatant was removed by decanting. The remaining surfactant droplets were dissolved either in 100 μL of ethanol for ET-AAS measurements or in ethanol (500 μL) and UPW to a total volume of 10 mL for sp-ICP-MS measurements.

ET-AAS has a high silver sensitivity, requires a low sample volume (20 μL), and tolerates high concentrations of organic matrix constituents. Thus, ET-AAS analysis provides a high enrichment factor of 80 and a limit of detection (LOD) for silver as low as 0.2 ng L^{-1}.[28] Calibration is performed by subjecting 60 nm citrate-coated AgNP dispersions of known concentration to the entire CPE-ET-AAS procedure. Commercially available AgNPs can undergo dissolution processes during storage. Particle stock dispersions are freed from dissolved silver species impurities by dialysis (3.5 kDa membrane by ZelluTrans, Carl Roth, Karlsruhe, Germany) prior to use. The Ag concentration of purified AgNP dispersions is determined by ICP-MS.

sp-ICP-MS was used to perform Ag-b-NP size distribution measurements. Here, all calibration samples, AuNP dispersion, and the dissolved silver standard were prepared in a surfactant-containing matrix (2.5 mL of TX-114 and 2.5 mL of ethanol, filled to a total volume of 50 mL with UPW). This way it could be ensured that the calibration samples behave similarly to the analyte samples after CPE during the measurement approach. Previous studies have generally assumed that Ag-b-NPs smaller than 20 nm are unable to be measured using conventional sp-ICP-MS techniques.[49] A recently published study by our group suggests that this limit could be undercut by coupling CPE to sp-ICP-MS.[6] The strong complexing agents ethylenediamine-tetraacetic acid and D-penicillamine transform silver and other metal ions into negatively charged complex compounds, which are not extracted by the CPE procedure. The organic CPE extracts are therefore free from dissolved silver species and contain only Ag-b-NPs in an enriched form. The elimination of silver ion interference and the selective particle enrichment lead to an improved signal-to-noise ratio for sp-ICP-MS particle measurements, which in turn allows for an unparalleled limit of detection (LOD) of 0.25 ng L^{-1} for Ag-b-NPs and a corresponding size detection limit of 10 nm (see Figure S1). Interestingly, the extraction efficiency of CPE drops significantly for particles >100 nm, allowing for selective extraction of nanosized particles.[30]

sp-ICP-MS measurements are based on the conjecture that Ag-b-NPs are spherical and that the nanoparticles are composed entirely of silver. Measurements of ^{52}Cr, ^{56}Fe, ^{60}Ni, ^{63}Cu, ^{66}Zn, and ^{208}Pb in CPE extracts did not show any evidence for particulate species containing these elements, so we conclude that solely Ag was present in nanoparticulate form in the samples. Due to NP concentrations in the lower to sub-ng L^{-1} range, techniques such as electron microscopy or light scattering could not be applied for supplementary investigations. Using conventional sp-ICP-MS approaches, the exact composition of Ag-b-NPs cannot be determined. The measurements rely on the prerequisite that only Ag masses of Ag-b-NPs can be measured providing the basis for the determination of particle size distributions and concentrations. Therefore, the bulk density of silver is used for sp-ICP-MS data processing.

■ RESULTS AND DISCUSSION

Water Pipe Material as a Silver Source. Copper pipes and fittings are used in the plumbing systems of public and domestic buildings worldwide. The main reasons for their widespread use are high durability of copper pipes and fittings and the fact that they are easily installed and resist bacteria growth. A disadvantage, however, is that copper can dissolve into water as it migrates throughout the plumbing system,

especially at pH values <7. This disadvantage, along with its elevated cost, explains why other materials, to an increasing extent, are replacing copper in newer constructions. In Germany, for instance, copper as a construction material for water supply systems is still the most common (44%), followed by plastics (21%), and different types of steel (15%) (Figure 1). From a chemical point of view, it is very unlikely that
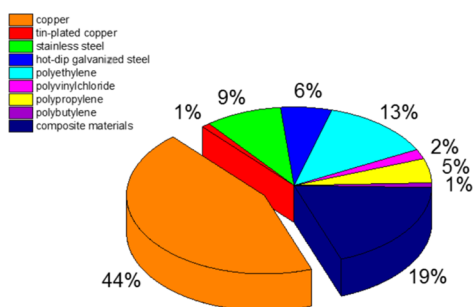
Figure 1. Compilation of all construction materials currently in use for tap water supply systems and their respective proportions in Germany.[52]

plastics as the second most common plumbing material contain silver and emit it to tap water. These organic polymer materials show no classical corrosion and silver is not used in the production of these materials. Stainless steel shows less corrosion than copper, and there are no hints in the literature that steel used for plumbing purposes contains silver. In the present work, we therefore focused on the release of silver in nonparticulate and particulate forms from copper-based plumbing systems. The Guideline Value for the copper concentration of tap water in Europe is 2 mg L^{-1},[44] which is identical to the value proposed by the World Health Organization.[50] According to the U.S. Environmental Protection Agency,[51] copper must not exceed a concentration of 1.3 mg L^{-1} in American drinking water.

The production of pipes for water supply systems uses highly pure copper that is refined to nearly 100% purity. Nevertheless, this highly pure copper always contains trace

impurities of silver,[34] typically in the lower mg kg^{-1} range. In this study, we analyzed a copper pipe, which was in use in building B1, with regard to its silver content. We found a silver content in copper pipe material of 27.5 ± 4.4 mg kg^{-1} with which we are able to show that, along with copper, silver traces can also be released into drinking water. Moreover, silver exists not only in a dissolved but also in a nanoparticulate form. This study is the first to show that silver traces, as impurities in copper pipes, are responsible for the existence of nano-particulate silver in tap water.

Quantification of Total Silver and Nanoparticulate Silver in Tap Water. To quantify the total and nano-particulate silver, tap water samples were taken from four buildings of different ages (built from 1978 to 2011). All buildings are located in the same city and each has an identical local water source (Table S1). Silver quantification and speciation began with samples from the oldest building (B1), followed by measurements of the tap water samples obtained from buildings B2 to B4 (see Table S4). Overall, no correlation between measured concentrations and pH, redox potential, O₂ content, temperature, and measured concentrations could be detected (see Table S2).

Dissolution of copper and silver is thought to be a slow process that occurs mainly in water, which is stored for days or even weeks in the pipe material. Therefore, in the first series of experiments, 400 mL of tap water from a water tap in B1, not used for 14 days, was analyzed in portions of approximately 60 mL (Table S2). Figure 2 shows the results from CPE-sp-ICP-MS measurements that were performed in the volume range from 67 to 122 mL. Ag-b-NPs were clearly detectable during CPE-sp-ICP-MS analysis (Figure 2A) and exhibited a rather broad particle size range from 10 to 80 nm (Figure 2B) with a distinct maximum at 16 nm. The particle size distribution also suggests that particles that are less than 10 nm, thus, not measurable via CPE-sp-ICP-MS, are also present in tap water. Most of the measurable particles (96%) fall into a size range between 10 and 36 nm with an average particle size of 19 nm.

Figure 3 summarizes the cumulative masses of total silver and measurable Ag-b-NPs with an increasing volume of tap water (see data in Table S2). Mass concentrations of total
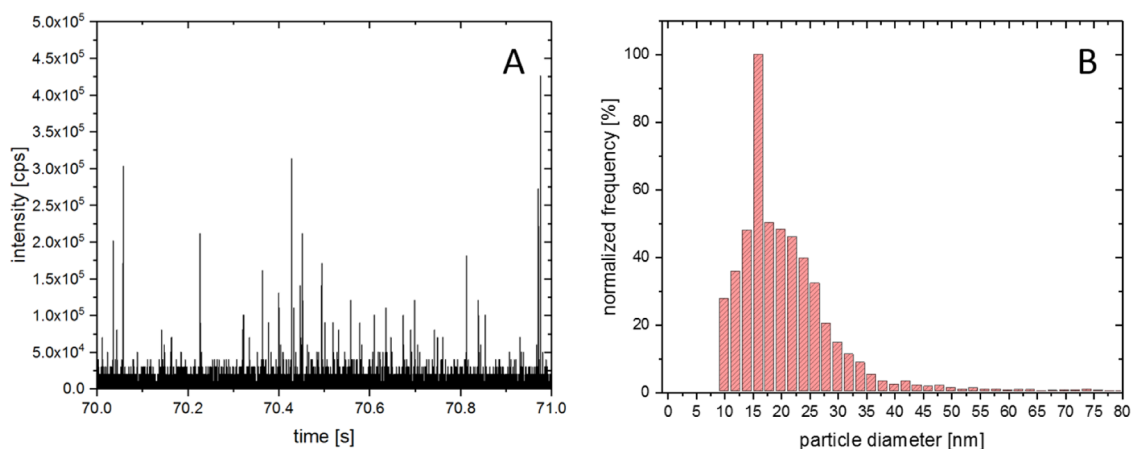
Figure 2. (A) [107]Ag mass spectra of the sp-ICP-MS measurement for tap water samples from building B1 taken on May 19, 2016 (after an accumulation period of 14 days), in the subsample from 67 to 122 mL (Table S2). Dwell time was set to 100 μs. (B) Particle size distribution with the normalized frequency found in the tap water sample described in (A). Particles <10 nm are not detectable using CPE-sp-ICP-MS. No reasonable NP amounts for particles >80 nm could be detected and are, thus, not depicted in the figure. For reasons of transparency, the mass spectra of the sp-ICP-MS measurement of the corresponding blank sample (UPW sample subjected to CPE as above-mentioned) is given in Figure S2.
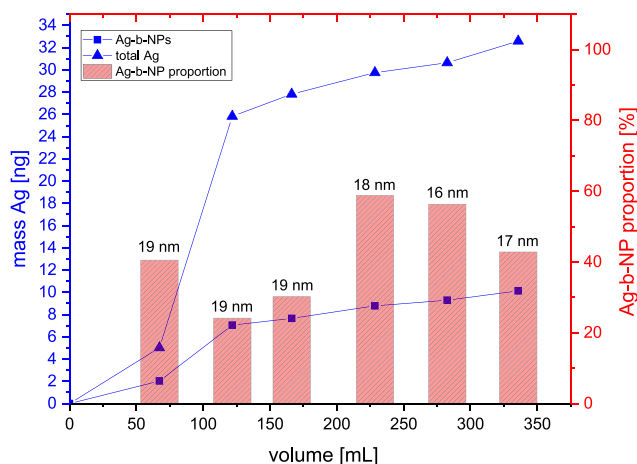
Figure 3. Cumulative masses of total silver (▲) and Ag-b-NPs (■) released into tap water from plumbing systems with an increasing tap water volume. Samples were taken from building B1 on May 19, 2016 (after an accumulation period of 14 days), with a tap water flux of 50 mL min⁻¹. The bars describe the Ag-b-NP proportion with respect to the mass of total silver. Numbers above the bars represent the average particle sizes found in each sample. Detailed data including error calculations are given in Table S2.

Figure 4. Cumulative masses of Ag-b-NP released from water pipe material into tap water with an increasing relative volume of tap water. The relative volume is calculated on the basis of the minimum tap water volume required to have no detectable total silver in the water runoff beyond the LOD of 0.2 ng L⁻¹. Samples were collected from building B1 on different days. Error bars indicate the uncertainty calculated via Gaussian error propagation based on pipetting uncertainties and the standard deviations of independently treated and measured subsamples ($n = 3$).

silver and Ag-b-NPs increased rapidly within the first 120 mL of tap water followed by a slower mass increase of both total silver and Ag-b-NPs toward the final volume of 400 mL. In total, 33.1 ± 0.7 ng of total silver and 10.2 ± 0.8 ng of Ag-b-NPs (approximately 30% of the total silver) were found in the 400 mL of tap water that we analyzed, which corresponds to 83 ng of total silver and 25 ng of Ag-b-NPs per liter tap water. Average particle sizes between 16 and 19 nm remained constant with tap water runoff. Unfortunately, it was not possible to observe whether silver was initially released in a particulate form or whether the Ag-b-NPs were formed later from released, dissolved silver, or both simultaneously.

To investigate Ag-b-NP accumulation in more detail, we examined tap water from building B1 throughout different time periods in which the water tap was not used. To establish a basis of comparison for all measurements, the water pipes were cleared until the total silver concentration was below the LOD of 0.2 ng L⁻¹ before we started a new accumulation period. As presented in Figure 4 and Table S3, Ag-b-NPs were detectable in tap water from all sampling days.

On May 19, 2016, after an accumulation period of 14 days, we observed a total Ag-b-NP quantity of 10.2 ± 0.8 ng in the tap water. After another period of 14 (May 19 to June 02, 2016) and 11 days (June 02 to June 13, 2016), high total Ag-b-NP masses, similar to the first period, were found in the tap water runoff: 10.4 ± 1.7 ng on June 02 and 8.6 ± 1.4 ng on June 13. Thus, a period of 11−14 days, during which the tap water stood idle in the pipes, led to reproducible Ag-b-NP accumulations between 8.6 and 10.4 ng L⁻¹. Surprisingly, the tap water samples collected on two consecutive days (June 14 and 15) were also characterized by significant Ag-b-NP accumulations of 5.4 ± 1.2 and 2.1 ± 1.2 ng, respectively. These results indicate that even short periods (such as 24 h) can lead to an accumulation of nanoparticulate silver if the water stands idle in the pipes.

The metallic plumbing systems in older buildings normally develop inner passive surface barrier layers, which reduce the release of heavy metal species into tap water. For copper

plumbing systems, malachite layers form inside the pipe.[53−55] Therefore, in addition to building B1, the newer buildings, i.e., B2−B4, were examined in an analogous manner. Unfortunately, it was not possible to determine the silver content and the trace element composition of the copper pipes installed in all of the field site buildings. A direct comparison of the age-related corrosion in the copper pipes was therefore not possible. Nevertheless, silver was released from the pipe material into the examined tap water from each building (Figure 5). In total, the amount of silver measured in tap water sampled on June 02, 2016, after an accumulation period of 14 days in each building is as follows: 42.6 ± 2.8 ng (B1), 0.7 ± 0.2 ng (B2), 21.5 ± 0.7 ng (B3), and 1.2 ± 0.2 ng of total silver (B4). Nanoparticulate silver was only found in tap water of B1 and B3, i.e., 10.4 ± 1.7 ng of Ag-b-NPs (B1) and 3.0 ± 0.3 ng of Ag-b-NPs (B3) in total, which corresponds to NP proportions of 24% (B1) and 14% (B3). A second sampling period over a period of 13 days (June 02−15) at B3 yielded results similar to the first measurement on June 02, underpinning reproducibility of the results (see size LOD and Table S5 for measured values).

Although the plumbing systems in all investigated buildings receive the same water with similar temperatures (10 °C as fed by the local water supplier;[56] ∼23 °C measured after sampling), silver release into the water was reproducible within single buildings but quite different between buildings B1 and B4. Silver release within a specific plumbing system is related to not only the age of a building but also other factors, such as the chemical composition of the pipes (e.g., the silver content).

Does Ag-b-NP Formation Correlate with the Presence of Copper and Other Heavy Metal Species in Tap Water? The fact that there are traces of silver in copper pipes suggests that Ag-b-NP occurrence in tap water that passes through such pipes is a consequence of copper corrosion. To investigate this in more detail, we also measured the tap water
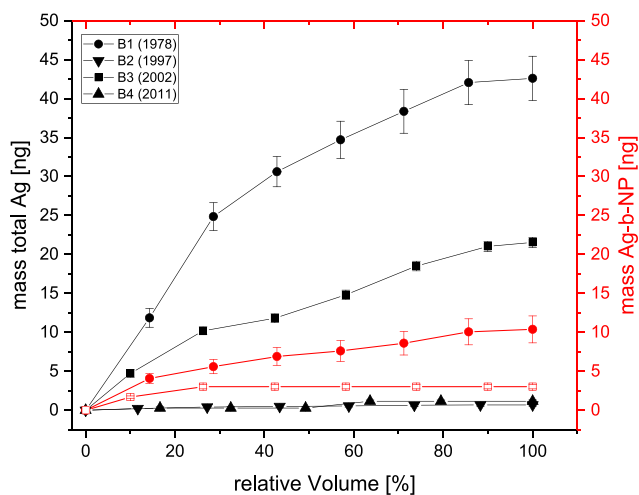
Figure 5. Cumulative masses of total released silver and Ag-b-NPs from the water pipe material into tap water sampled from different buildings (building construction dates from 1978 to 2011) on June 02, 2016 (after an accumulation period of 14 days). The relative volume in percentage is calculated by dividing the cumulative volume of the corresponding sample by the minimum tap water volume required to have no detectable additional silver in the water runoff beyond the LOD of 0.2 ng L^{-1}. Error bars indicate the uncertainty calculated via a Gaussian error propagation based on pipetting uncertainties and the standard deviations of independently treated and measured subsamples (n = 3).

from building B1 for copper and other heavy metals, i.e., iron, nickel, chromium, zinc, and lead, which are possibly contained in plumbing materials, such as fittings, connections, and soldering joints. If our hypothesis is true, we expect to observe a clear correlation between the copper concentration and the occurrence of silver or Ag-b-NPs.

Figure 6A,B shows the measured concentrations of each element and Ag-b-NPs with increasing water flow. The given concentrations represent the respective concentration in each 200 mL water sample portion. As presented in Figure 6A, total Ag, Ag-b-NP, and total copper concentrations behaved similarly with increasing tap water runoff: the first 200 mL sample contained 92.6 ± 0.5 μg L^{-1} total copper and 56.1 ± 0.7 ng L^{-1} total silver with a silver proportion based on the copper content of 0.60‰. In the second sample, concentrations even rose to 107.2 ± 0.3 μg L^{-1} total copper and 61.5 ± 1.3 ng L^{-1} total silver with a silver proportion of 0.57‰. This was followed by a rapid decrease to concentrations of approximately 20 μg L^{-1} total copper and 17 ng L^{-1} total silver (with a silver proportion of 0.85‰), which remained constant after a tap water runoff of 800 mL. On the basis of Table S6, total copper and silver concentrations never exceeded the upper limit values recommended by the WHO[50] or U.S. EPA[51] guidelines for water quality and European[44] tap water regulations. The Ag-b-NP concentration gradient behaved in a similar manner to the total silver concentration gradient, starting at 21.2 ± 1.0 ng L^{-1} in the first 200 mL sample, whereas the nanoparticulate fraction of the total silver was approximately 23−38%. The high correlation among total copper, total Ag, and Ag-b-NP release from the plumbing system into tap water is underpinned by their Pearson correlation coefficients (PCCs), which are listed in Table 2. A bivariate correlation between the concentrations of two elements (including nanoparticulate species) in each sub-
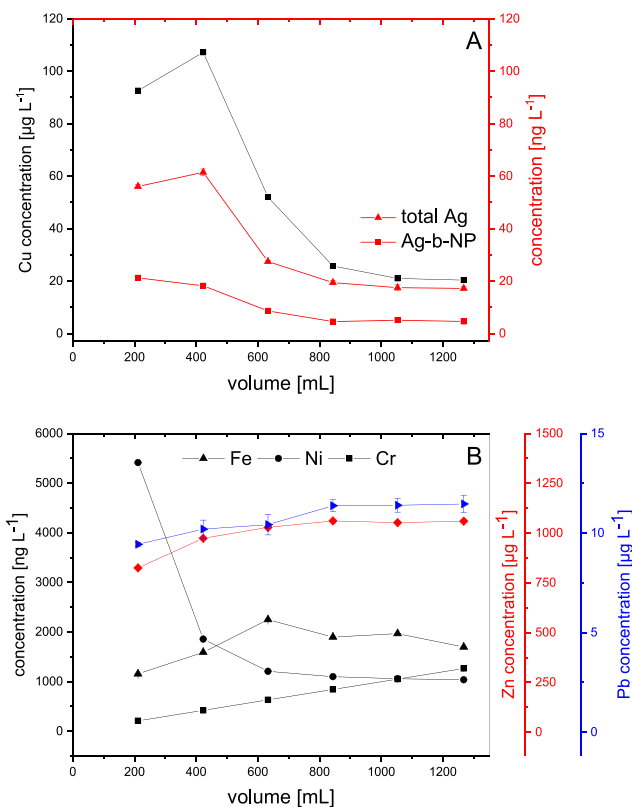
Figure 6. (A) Concentrations of total and particulate silver (red) and copper (black) and (B) concentrations of total iron, nickel, chromium, zinc, and lead in subsequent ~200 mL tap water samples with increasing total tap water runoff. Error bars indicate the uncertainty calculated via a Gaussian error propagation based on pipetting uncertainties and the standard deviations of independently treated and measured subsamples (n = 3).

sample is investigated as a measure of linearity via the PCCs. The PCC for the Ag/Ag-b-NP correlation is 0.98, 0.99 for the Ag/Cu correlation, and 0.99 for the Ag-b-NP/Cu correlation. These results indicate that there is a distinct correlation and confirms the assumption that both copper and silver (total and nanoparticulate) are simultaneously leached into tap water primarily via the pipe material itself, which is made of copper.

We observed no further correlations between the other examined elements and total copper, total silver, or Ag-b-NPs, respectively (Figure 6B and Table 2). Thus, silver cannot be released from components that contain zinc, such as brass fittings and taps, or components made from steel that contain iron, chromium, and nickel. Additionally, high PCC values for the Pb/Cr and Pb/Zn correlation reveal that there is a combined leaching process between lead and chromium or between lead and zinc, respectively, from the plumbing system into tap water.

For the sake of completeness, it has to be noted that reciprocal proportionalities were also observable, as indicated by a correlation factor ranging from −1.0 to −0.90. This is given for the correlation between concentrations of Ag-b-NPs or Ni and Cr, Pb, or Zn, respectively. This means that Ag-b-NP or Ni concentrations decrease with increasing tap water runoff, while the concentrations of Cr, Pb, and Zn increase with increasing runoff. Current literature and data of the investigated plumbing systems do neither give any reason for the increasing amounts of Cr, Pb, and Zn with increasing tap

Table 2. Pearson Correlation Coefficients between the Measured Concentration Gradients of All Examined Elements and the Ag-b-NPs[a]

	Ag	Ag-b-NP	Cr	Cu	Fe	Ni	Pb	Zn
Ag		0.98	−0.88	0.99	−0.68	0.69	−0.88	−0.81
Ag-b-NP	0.98		−0.91	0.99	−0.74	0.83	−0.94	−0.92
Cr	−0.88	−0.91		−0.90	0.50	−0.75	0.94	0.84
Cu	0.99	0.99	−0.90		−0.58	0.65	−0.90	−0.78
Fe	−0.68	−0.74	0.50	−0.58		−0.83	0.58	0.81
Ni	0.69	0.83	−0.75	0.65	−0.83		−0.84	−0.98
Pb	−0.88	−0.94	0.94	−0.90	0.58	−0.84		0.92
Zn	−0.81	−0.92	0.84	−0.78	0.81	−0.98	0.92	

[a]Elements and Ag-b-NPs released from the plumbing system via tap water runoff show distinct correlations when coefficients extend 0.90 (marked in green for proportionality and marked in orange for reciprocal proportionality).

water runoff nor reasons for an assumption that Ag-b-NP and Ni concentrations are related to concentrations of Cr, Pb, and Zn. Thus, there is no justified reason to believe that there is a distinct connection between decreasing Ag-b-NP and Ni concentrations and decreasing Cr, Pb, and Zn concentrations, which might be just a consequence of coincidence.

For currently installed water supply systems, the only way to determine the silver source was to observe potential correlations between the silver concentrations and the concentrations of other elements present in the tap water samples. We consciously discarded any experiments with model water supply systems since they do not represent realistic sampling scenarios. Moreover, they are hardly relevant when discussing realistic Ag-b-NP exposure and the conclusions important for risk assessment.

Environmental Impact. In this study, we discovered that widely used tap water pipes made from copper represent a hitherto undocumented source of Ag-b-NP release into tap water. A significant portion of these particles is deposited in wastewater streams where they contribute to the Ag-b-NP load that derives from other sources, such as Ag-b-NPs released from fabrics, cosmetics, or medical products.

Particulate silver species ranging in size from <10 to 80 nm (96% of the particles exhibit sizes from 10 to 36 nm) were found in tap water that passes through copper water pipes, whereas Ag-b-NPs represented an approximately 30% proportion of the total silver. Total silver and particulate silver concentrations were in the ng L^{-1} range (17−62 ng L^{-1} total silver and 5−21 ng L^{-1} Ag-b-NPs), which pose no risk to environmental or human health based on current (eco)-toxicological literature.[1,57] However, long-term monitoring of Ag-b-NPs released into the environment is a crucial step to perform comprehensive risk assessments of nanomaterials,

especially in the case of tap water that is consumed extensively throughout the world. Moreover, identifying the sources of Ag-b-NPs that are released into the environment is essential for proper risk assessments of nanoparticulate pollution.

The release of copper and, as a consequence, the release of silver and Ag-b-NPs from copper-based plumbing systems into tap water depend on a variety of factors. These factors include local water quality, silver and trace element content of the copper pipes, and the flow velocity resp. residence time, i.e. the time period, in which the water stands within the pipes. Correct predictions concerning the release of Ag-b-NPs into tap water are also not possible because it is, in many cases, not clear how many buildings in a specific country or region are equipped with copper-based plumbing systems.

On the basis of the data obtained in this study and data from the German Federal Statistical Office,[58] we can make a very rough estimate of the Ag-b-NP release into German drinking water: the population-related daily drinking water consumption in Germany is 9.8 × 10^9 L (81 Mio inhabitants × 121 L inhabitant^{-1}). If we assume that 44% of the plumbing systems in Germany are made of copper[52] with a silver content of 28 mg kg^{-1} and, in the worst-case scenario, that we reach the maximum tolerable copper concentration of 2 mg L^{-1}, this indicates that an Ag-b-NP mass of 30 kg (30% of the total silver released from the plumbing pipes) is released each year into drinking water in Germany. In reality, only one-tenth or less of copper may be released, which corresponds to an annual Ag-b-NP release of 3 kg in Germany, which represents a possibly more realistic value. Taking the population into account, this leads to a Ag-b-NP release of 100 ng per person per day. We might expect similar population-related values for other highly industrialized countries. The present results and estimations do not include the contribution of trade, commerce, and industry that may increase the release of Ag-b-NPs into drinking water. To put these findings into perspective, the release of 37 μg Ag-b-NPs per person per year is correlated to the minimum amount of Ag-b-NPs released from a commercially available antimicrobial sock, which is 19 μg Ag-b-NPs each washing cycle.[59] We can conclude that the Ag-b-NP amount derived from plumbing systems per person each year corresponds to approximately two washing cycles of functionalized socks.

Therefore, we can no longer ignore the fact that Ag-b-NPs originate, to a significant extent, from conventional copper water pipes when discussing possible exposure scenarios and the (eco)toxicological effects of nanomaterials. This observation could possibly change the prevailing opinion that consumer and medicinal products, which contain nanosilver for antimicrobial reasons, are the main contributors of Ag-b-NPs to environmental samples, such as wastewater, river, and lake water.

■ ASSOCIATED CONTENT

ⓢ Supporting Information

The Supporting Information is available free of charge on the ACS Publications website at DOI: 10.1021/acs.est.9b04271.

> Particle size distribution of 10 nm Ag-b-NPs (Figure S1); drinking water characteristics (Table S1); ^{107}Ag mass spectra of the sp-ICP-MS measurement of a blank and tap water sample (Figure S2); additional data on samples taken from building 1 (mass of Ag-b-NP and total Ag, Ag-b-NP proportions, pH, redox potential, O$_2$

content, and temperature) (Table S2); cumulative masses of Ag-b-NPs in tap water from building 1 sampled on different days (Table S3); cumulative summary of the Ag-b-NP mass in tap water from buildings 1−4 (Table S4); cumulative masses of Ag-b-NPs and total silver in tap water from building 3 (Figure S3); summary of cumulative Ag-b-NP masses and total silver in tap water from building 3 (Table S5); and concentrations of Cu, Ag, Cr, Fe, Ni, Zn, and Pb in tap water runoff from building 1 (Table S6) (PDF)

■ AUTHOR INFORMATION

Corresponding Author

*E-mail: michael.schuster@ch.tum.de. Tel: +49 (0)89 289 13763. Fax: +49 (0)89 289 14513.

ORCID ⬤

Andreas Wimmer: 0000-0002-1746-8932

Author Contributions

M.S. supervised the study. A.W. designed the study and its experimental setup. A.W. carried out sampling and all corresponding analytical measurements were assisted by J.B. A.W. and J.B. evaluated the acquired measurement data. A.W. and M.S. wrote the manuscript.

Notes

The authors declare no competing financial interest.

■ REFERENCES

(1) Krug, H. F. Nanosafety Research—Are We on the Right Track? *Angew. Chem., Int. Ed.* **2014**, *53*, 12304−12319.

(2) Kim, B.; Park, C.-S.; Murayama, M.; Hochella, M. F. Discovery and Characterization of Silver Sulfide Nanoparticles in Final Sewage Sludge Products. *Environ. Sci. Technol.* **2010**, *44*, 7509−7514.

(3) Mittelman, A. M.; Lantagne, D. S.; Rayner, J.; Pennell, K. D. Silver Dissolution and Release from Ceramic Water Filters. *Environ. Sci. Technol.* **2015**, *49*, 8515−8522.

(4) Li, L.; Hartmann, G.; Döblinger, M.; Schuster, M. Quantification of Nanoscale Silver Particles Removal and Release from Municipal Wastewater Treatment Plants in Germany. *Environ. Sci. Technol.* **2013**, *47*, 7317−7323.

(5) Benn, T.; Cavanagh, B.; Hristovski, K.; Posner, J. D.; Westerhoff, P. The Release of Nanosilver from Consumer Products Used in the Home. *J. Environ. Qual.* **2010**, *39*, 1875−1882.

(6) Li, L.; Stoiber, M.; Wimmer, A.; Xu, Z.; Lindenblatt, C.; Helmreich, B.; Schuster, M. To What Extent Can Full-Scale Wastewater Treatment Plant Effluent Influence the Occurrence of Silver-Based Nanoparticles in Surface Waters? *Environ. Sci. Technol.* **2016**, *50*, 6327−6333.

(7) Colman, B. P.; Espinasse, B.; Richardson, C. J.; Matson, C. W.; Lowry, G. V.; Hunt, D. E.; Wiesner, M. R.; Bernhardt, E. S. Emerging Contaminant or an Old Toxin in Disguise? Silver Nanoparticle Impacts on Ecosystems. *Environ. Sci. Technol.* **2014**, *48*, 5229−5236.

(8) Kessler, R. Engineered Nanoparticles in Consumer Products: Understanding a New Ingredient. *Environ. Health Perspect.* **2011**, *119*, A120−A125.

(9) Mitrano, D. M.; Limpiteeprakan, P.; Babel, S.; Nowack, B. Durability of nano-enhanced textiles through the life cycle: releases from landfilling after washing. *Environ. Sci.: Nano* **2016**, *3*, 375−387.

(10) Mitrano, D. M.; Rimmele, E.; Wichser, A.; Erni, R.; Height, M.; Nowack, B. Presence of Nanoparticles in Wash Water from Conventional Silver and Nano-silver Textiles. *ACS Nano* **2014**, *8*, 7208−7219.

(11) Geranio, L.; Heuberger, M.; Nowack, B. The Behavior of Silver Nanotextiles during Washing. *Environ. Sci. Technol.* **2009**, *43*, 8113−8118.

(12) Jiang, D.; Chen, L.; Xie, J.; Chen, M. Ag2S/g-C3N4 composite photocatalysts for efficient Pt-free hydrogen production. The co-catalyst function of Ag/Ag2S formed by simultaneous photo-deposition. *Dalton Trans.* **2014**, *43*, 4878−4885.

(13) Richter, A. P.; Brown, J. S.; Bharti, B.; Wang, A.; Gangwal, S.; Houck, K.; Cohen Hubal, E. A.; Paunov, V. N.; Stoyanov, S. D.; Velev, O. D. An environmentally benign antimicrobial nanoparticle based on a silver-infused lignin core. *Nat. Nanotechnol.* **2015**, *10*, 817.

(14) Troester, M.; Brauch, H.-J.; Hofmann, T. Vulnerability of drinking water supplies to engineered nanoparticles. *Water Res.* **2016**, *96*, 255−279.

(15) Duester, L.; Burkhardt, M.; Gutleb, A. C.; Kaegi, R.; Macken, A.; Meermann, B.; von der Kammer, F. Toward a comprehensive and realistic risk evaluation of engineered nanomaterials in the urban water system. *Front. Chem.* **2014**, *2*, No. 39.

(16) Sun, T. Y.; Gottschalk, F.; Hungerbühler, K.; Nowack, B. Comprehensive probabilistic modelling of environmental emissions of engineered nanomaterials. *Environ. Pollut.* **2014**, *185*, 69−76.

(17) Nowack, B.; Ranville, J. F.; Diamond, S.; Gallego-Urrea, J. A.; Metcalfe, C.; Rose, J.; Horne, N.; Koelmans, A. A.; Klaine, S. J. Potential scenarios for nanomaterial release and subsequent alteration in the environment. *Environ. Toxicol. Chem.* **2012**, *31*, 50−59.

(18) Keller, A. A.; McFerran, S.; Lazareva, A.; Suh, S. Global life cycle releases of engineered nanomaterials. *J. Nanopart. Res.* **2013**, *15*, No. 1692.

(19) Kaegi, R.; Ulrich, A.; Sinnet, B.; Vonbank, R.; Wichser, A.; Zuleeg, S.; Simmler, H.; Brunner, S.; Vonmont, H.; Burkhardt, M.; Boller, M. Synthetic TiO2 nanoparticle emission from exterior facades into the aquatic environment. *Environ. Pollut.* **2008**, *156*, 233−239.

(20) Kah, M.; Beulke, S.; Tiede, K.; Hofmann, T. Nanopesticides: State of Knowledge, Environmental Fate, and Exposure Modeling. *Crit. Rev. Environ. Sci. Technol.* **2013**, *43*, 1823−1867.

(21) Gottschalk, F.; Sonderer, T.; Scholz, R. W.; Nowack, B. Modeled Environmental Concentrations of Engineered Nanomaterials (TiO2, ZnO, Ag, CNT, Fullerenes) for Different Regions. *Environ. Sci. Technol.* **2009**, *43*, 9216−9222.

(22) Sun, T. Y.; Gottschalk, F.; Hungerbühler, K.; Nowack, B. Comprehensive probabilistic modelling of environmental emissions of engineered nanomaterials. *Environ. Pollut.* **2014**, *185*, 69−76.

(23) Gottschalk, F.; Sun, T.; Nowack, B. Environmental concentrations of engineered nanomaterials: Review of modeling and analytical studies. *Environ. Pollut.* **2013**, *181*, 287−300.

(24) Sun, T. Y.; Conroy, G.; Donner, E.; Hungerbuhler, K.; Lombi, E.; Nowack, B. Probabilistic modelling of engineered nanomaterial emissions to the environment: a spatio-temporal approach. *Environ. Sci.: Nano* **2015**, *2*, 340−351.

(25) Wimmer, A.; Kalinnik, A.; Schuster, M. New insights into the formation of silver-based nanoparticles under natural and semi-natural conditions. *Water Res.* **2018**, *141*, 227−234.

(26) Sharma, V. K.; Filip, J.; Zboril, R.; Varma, R. S. Natural inorganic nanoparticles - formation, fate, and toxicity in the environment. *Chem. Soc. Rev.* **2015**, *44*, 8410−8423.

(27) Hartmann, G.; Baumgartner, T.; Schuster, M. Influence of Particle Coating and Matrix Constituents on the Cloud Point Extraction Efficiency of Silver Nanoparticles (Ag-NPs) and Application for Monitoring the Formation of Ag-NPs from Ag. *Anal. Chem.* **2014**, *86*, 790−796.

(28) Hartmann, G.; Hutterer, C.; Schuster, M. Ultra-trace determination of silver nanoparticles in water samples using cloud point extraction and ETAAS. *J. Anal. At. Spectrom.* **2013**, *28*, 567−572.

(29) Duester, L.; Fabricius, A.-L.; Jakobtorweihen, S.; Philippe, A.; Weigl, F.; Wimmer, A.; Schuster, M.; Nazar, M. F. Can cloud point-based enrichment, preservation, and detection methods help to bridge

gaps in aquatic nanometrology? *Anal. Bioanal. Chem.* **2016**, *408*, 7551−7557.

(30) Hartmann, G.; Schuster, M. Species selective preconcentration and quantification of gold nanoparticles using cloud point extraction and electrothermal atomic absorption spectrometry. *Anal. Chim. Acta* **2013**, *761*, 27−33.

(31) Fuge, R.; Pearce, N. J. G.; Perkins, W. T. Unusual sources of aluminium and heavy metals in potable waters. *Environ. Geochem. Health* **1992**, *14*, 15−18.

(32) Pajonk, G. Elution of heavy metals from fitting- and pipe-materials - Part 1: Basics of standardisation. *Mater. Corros.-Werkstoffe Korros.* **2002**, *53*, 534−545.

(33) El Haraoui, N.; Tao, T.; Xin, K. L.; Wang, Q. H. Analysis of heavy metals and ions in tap water: a case of Shanghai P district. *Fresenius Environ. Bull.* **2014**, *23*, 395−399.

(34) Pauwels, J.; De Angelis, L.; Peetermans, F.; Ingelbrecht, C. Determination of traces of silver in copper by direct Zeeman graphite furnace atomic absorption spectrometry. *Fresenius' J. Anal. Chem.* **1990**, *337*, 290−293.

(35) Sorme, L.; Lagerkvist, R. Sources of heavy metals in urban wastewater in Stockholm. *Sci. Total Environ.* **2002**, *298*, 131−145.

(36) van Breemen, A. J. H.; Vermij, P. H. M. Instruments to reduce the leaching of heavy metals from building materials in the Netherlands. *Water Sci. Technol.* **2007**, *55*, 79−85.

(37) Houhou, J.; Lartiges, B. S.; Montarges-Pelletier, E.; Sieliechi, J.; Ghanbaja, J.; Kohler, A. Sources, nature, and fate of heavy metal-bearing particles in the sewer system. *Sci. Total Environ.* **2009**, *407*, 6052−6062.

(38) Liu, H. Z.; Kuznetsov, A. M.; Masliy, A. N.; Ferguson, J. F.; Korshin, G. V. Formation of Pb(III) Intermediates in the Electrochemically Controlled Pb(II)/PbO2 System. *Environ. Sci. Technol.* **2012**, *46*, 1430−1438.

(39) Olivares, T. E.; Cienfuegos, R.; Vargas, I. T.; Pizarro, G. E. Experimental evidence for enhanced copper release from domestic copper plumbing under hydrodynamic control. *Corros. Sci.* **2014**, *80*, 473−481.

(40) Trueman, B. F.; Gagnon, G. A. Understanding the Role of Particulate Iron in Lead Release to Drinking Water. *Environ. Sci. Technol.* **2016**, *50*, 9053−9060.

(41) Kaegi, R.; Voegelin, A.; Ort, C.; Sinnet, B.; Thalmann, B.; Krismer, J.; Hagendorfer, H.; Elumelu, M.; Mueller, E. Fate and transformation of silver nanoparticles in urban wastewater systems. *Water Res.* **2013**, *47*, 3866−3877.

(42) Kaegi, R.; Voegelin, A.; Sinnet, B.; Zuleeg, S.; Siegrist, H.; Burkhardt, M. Transformation of AgCl nanoparticles in a sewer system - A field study. *Sci. Total Environ.* **2015**, *535*, 20−27.

(43) Meier, C.; Voegelin, A.; Pradas del Real, A.; Sarret, G.; Mueller, C. R.; Kaegi, R. Transformation of Silver Nanoparticles in Sewage Sludge during Incineration. *Environ. Sci. Technol.* **2016**, *50*, 3503−3510.

(44) TrinkwV. Verordnung über die Qualität von Wasser für den menschlichen Gebrauch (*German drinking water regulation*) 2001.

(45) DIN 38402-15: German standard methods for the examination of water, waste water and sludge - General information (group A) - Part 15: Sampling from running waters (A 15), 2010.

(46) Wolf, R. E. Analysis of Lead (Pb) in Antacids and Calcium Compounds for Proposition 65 Compliance. *At. Spectrosc.* **1997**, *18*, 169−175.

(47) May, T. W.; Wiedmeyer, R. H. A table of polyatomic interferences in ICP-MS. *At. Spectrosc.* **1998**, *19*, 150−155.

(48) Peters, R. J. B.; Rivera, Z. H.; van Bemmel, G.; Marvin, H. J. P.; Weigel, S.; Bouwmeester, H. Development and validation of single particle ICP-MS for sizing and quantitative determination of nano-silver in chicken meat. *Anal. Bioanal. Chem.* **2014**, *406*, 3875−3885.

(49) Lee, S.; Bi, X.; Reed, R. B.; Ranville, J. F.; Herckes, P.; Westerhoff, P. Nanoparticle Size Detection Limits by Single Particle ICP-MS for 40 Elements. *Environ. Sci. Technol.* **2014**, *48*, 10291−10300.

(50) WHO. *Guidelines for Drinking-Water Quality*; WHO, 2011.

(51) US-EPA. US Environmental Protection Agency - National Primary Drinking Water Regulations, 2018.

(52) Umweltbundesamt, Trink was - Trinkwasser aus dem Hahn. *Gesundheitliche Aspekte der Trinkwasser-Installation*, 2007, 10.

(53) Vargas, I. T.; Fischer, D. A.; Alsina, M. A.; Pavissich, J. P.; Pastén, P. A.; Pizarro, G. E. Copper Corrosion and Biocorrosion Events in Premise Plumbing. *Materials* **2017**, *10*, No. 1036.

(54) Vargas, I. T.; Alsina, M. A.; Pastén, P. A.; Pizarro, G. E. Influence of solid corrosion by-products on the consumption of dissolved oxygen in copper pipes. *Corros. Sci.* **2009**, *51*, 1030−1037.

(55) Calle, G. R.; Vargas, I. T.; Alsina, M. A.; Pastén, P. A.; Pizarro, G. E. Enhanced Copper Release from Pipes by Alternating Stagnation and Flow Events. *Environ. Sci. Technol.* **2007**, *41*, 7430−7436.

(56) SWM, M. C. U.-. Münchner Trinkwasser-Analysewerte, 2018, 4.

(57) Westerhoff, P.; Atkinson, A.; Fortner, J.; Wong, M. S.; Zimmerman, J.; Gardea-Torresdey, J.; Ranville, J.; Herckes, P. Low risk posed by engineered and incidental nanoparticles in drinking water. *Nat. Nanotechnol.* **2018**, *13*, 661−669.

(58) Destatis, German Federal Statistical Office Pressemitteilung vom 21.01.2015 - 24/15, 2014.

(59) Benn, T. M.; Westerhoff, P. Nanoparticle Silver Released into Water from Commercially Available Sock Fabrics. *Environ. Sci. Technol.* **2008**, *42*, 4133−4139.

Copper drinking water pipes as a previously undocumented source of silver-based nanoparticles

Andreas Wimmer [a], Jessica Beyerl [a], Michael Schuster [a, *]

[a] Division of Analytical Chemistry, Department of Chemistry, Technical University of Munich,

D-Garching 85748, Germany

Corresponding Author:

[*] Prof. Dr. Michael Schuster

E-Mail: michael.schuster@tum.de

Tel: +49 (0) 89 289 13763

Fax: +49 (0) 89 289 14513

11 pages

6 Tables

3 Figure
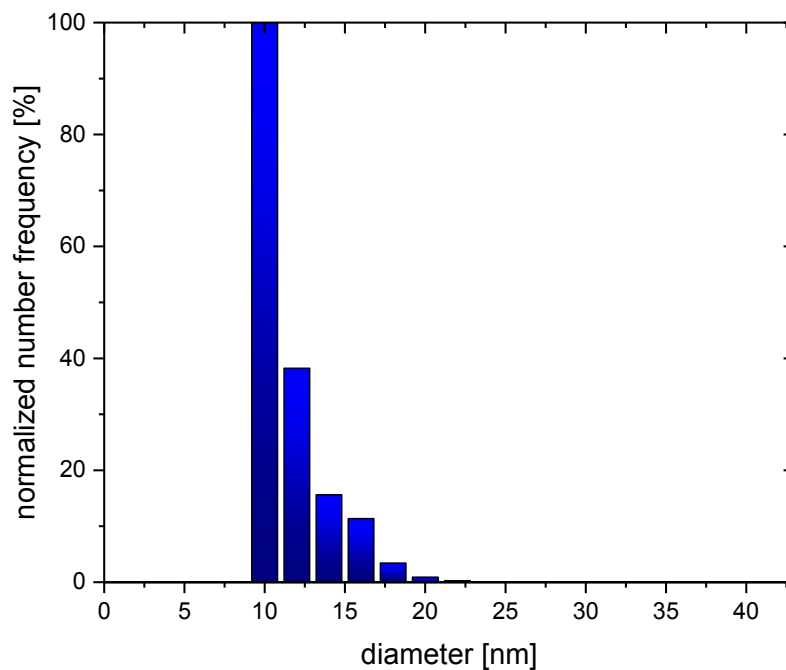
Figure S1. Particle size distribution of commercially available citrate stabilized 10 nm AgNPs (Sigma Aldrich). A AgNP dispersion containing 4.2 ng L^{-1} Ag was subjected to CPE and the extract was diluted with UPW and EtOH as described. The diluted extract was then forwarded to sp-ICP-MS applying a dwell time of 100 µs. Raw data was blank-corrected and transformed in the presented particle size distribution.

Table S1. Drinking water characteristics measured by the local water supplier.[3]

temperature [°C]	9.9
pH	7.54
conductivity [μS cm^{-1} at 25 °C]	544
dissolved organic content [mg L^{-1}]	<0.3
total organic content [mg L^{-1}]	0.3
total water hardness [°dH]	16.2
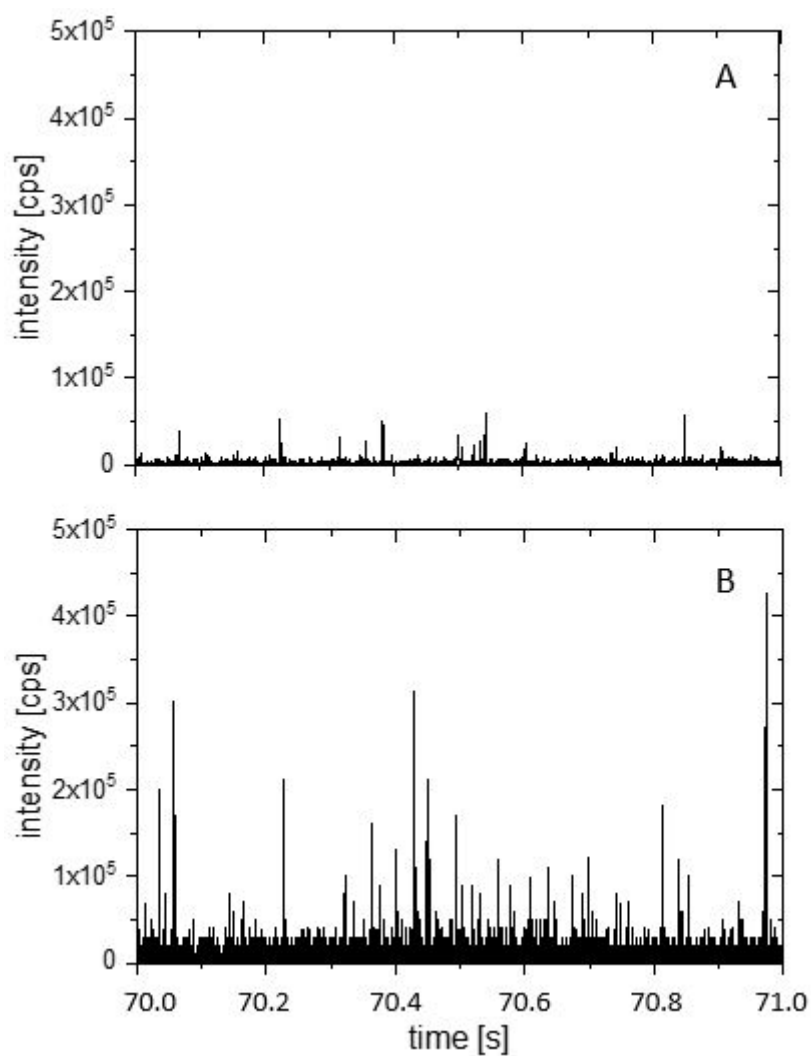
Figure S2. [107]Ag mass spectra of the sp-ICP-MS measurement for a blank sample (A) and tap water samples from building B1 (B) taken on May 19, 2016 (after an accumulation period of 14 days), in the subsample from 67 to 122 mL (Table S2). Dwell time was set to 100 μs.

Table S2. The cumulative masses of Ag-b-NP and total silver in tap water from building 1 sampled on May 19, 2016 (after an incubation period of 14 days) with a tap water flux of 50 mL min^{-1}. The Ag-b-NP proportion is calculated with respect to the mass of total silver. Furthermore, pH, redox potential, oxygen content and temperature from all examined samples are given. Errors indicate the uncertainty calculated via a Gaussian error propagation based on pipetting uncertainties and the standard deviations of independently treated and measured subsamples (n = 3).

volume [mL]	mass Ag-b-NP [ng]	mass total Ag [ng]	Ag-b-NP proportion [%]	pH	redox potential [mV]	O$_2$ [mg L^{-1}]	temperature [° C]
67	2.0 ± 0.3	5.0 ± 0.3	40.5	8.4	89	8.5	23
122	7.1 ± 0.6	25.8 ± 0.3	27.3	8.3	87	8.5	23
166	7.7 ± 0.6	27.8 ± 0.5	27.5	8.4	85	8.4	23
229	8.8 ± 0.7	29.7 ± 0.5	29.6	8.3	90	8.4	23
283	9.3 ± 0.8	30.6 ± 0.6	30.3	8.4	89	8.4	23
336	10.1 ± 0.8	32.6 ± 0.6	31.1	8.4	88	8.6	23
403	10.2 ± 0.8	33.1 ± 0.7	30.7	8.4	87	8.5	23

Table S3. The cumulative masses of Ag-b-NPs in tap water from building 1 sampled on different days (after an incubation period of 14 days prior to first sampling) with increasing relative volume of tap water. The relative volume is calculated on the basis of the minimum tap water volume required to have no detectable total silver in the water runoff beyond the LOD of 0.2 ng L^{-1}. The total sample volume until no additional silver release was observed is given in parentheses besides each sampling date. Errors indicate the uncertainty calculated via a Gaussian error propagation based on pipetting uncertainties and the standard deviations of independently treated and measured subsamples (n = 3).

May 19 (403 mL)		June 02 (1478 mL)	
relative volume [%]	mass Ag-b-NPs [ng]	relative volume [%]	mass Ag-b-NPs [ng]
0	0.00	0	0
16.7	2.0 ± 0.3	14.3	4.1 ± 0.6
30.2	7.1 ± 0.6	28.6	5.6 ± 0.9
41.2	7.7 ± 0.6	42.8	6.9 ± 1.1
56.7	8.8 ± 0.7	57.0	7.6 ± 1.3
70.1	9.3 ± 0.8	71.2	8.9 ± 1.5
83.3	10.1 ± 0.8	85.7	10.1 ± 1.7
100	10.2 ± 0.8	100	10.4 ± 1.7

June 13 (891 mL)		June 14 (1087 mL)		June 15 (1053 mL)	
relative volume [%]	mass Ag-b-NPs [ng]	relative volume [%]	mass Ag-b-NPs [ng]	relative volume [%]	mass Ag-b-NPs [ng]
0	0	0	0	0	0
14.0	2.4 ± 0.4	14.8	1.5 ± 0.5	13.8	0.3 ± 0.5
28.5	4.2 ± 0.6	28.5	2.6 ± 0.7	27.4	1.0 ± 0.6
42.8	5.2 ± 0.8	42.5	3.2 ± 0.8	41.1	1.3 ± 0.8
57.2	6.1 ± 1.0	56.7	4.3 ± 1.0	59.2	1.5 ± 1.0
71.6	7.1 ± 1.1	70.9	4.9 ± 1.1	72.7	1.7 ± 1.1
86.0	8.1 ± 1.3	85.2	5.4 ± 1.2	86.2	2.1 ± 1.2
100	8.6 ± 1.4	100	5.4 ± 1.2	100	2.1 ± 1.2

Table S4. The cumulative masses of Ag-b-NPs and total Ag in tap water from buildings 1-4 sampled on June 02, 2016 (after an incubation period of 14 days) with increasing relative volume of tap water. The relative volume is calculated on the basis of the minimum tap water volume required to have no detectable total silver in the water runoff beyond the LOD of 0.2 ng L^{-1}. The total sample volume, until no additional silver release was observed, is given in parentheses together with each buildings' construction year. Errors indicate the uncertainty calculated via a Gaussian error propagation based on pipetting uncertainties and the standard deviations of independently treated and measured subsamples (n = 3).

building 1 (1978, 908 mL)				building 2 (1997, 1195 mL)			
relative volume [%]	mass Ag-b-NP [ng]	mass total Ag [ng]	Ag-b-NP proportion [%]	relative volume [%]	mass Ag-b-NP [ng]	mass total Ag [ng]	Ag-b-NP proportion [%]
0	0	0	0	0	0	0	0
14	4.1 ± 0.6	11.9 ± 1.2	34	12	n.d.	0.2 ± 0.1	0
29	5.6 ± 0.9	24.9 ± 1.8	23	27	n.d.	0.4 ± 0.1	0
43	6.9 ± 1.1	30.6 ± 1.9	23	43	n.d.	0.5 ± 0.1	0
57	7.6 ± 1.3	34.7 ± 2.4	22	59	n.d.	0.5 ± 0.1	0
71	8.6 ± 1.5	38.4 ± 2.8	22	74	n.d.	0.6 ± 0.1	0
86	10.1 ± 1.7	42.1 ± 2.8	24	88	n.d.	0.7 ± 0.2	0
100	10.4 ± 1.7	42.6 ± 2.8	24	100	n.d.	0.7 ± 0.2	0
building 3 (2002, 776 mL)				building 4 (2011, 1834 mL)			
relative volume [%]	mass Ag-b-NP [ng]	mass total Ag [ng]	Ag-b-NP proportion [%]	relative volume [%]	mass Ag-b-NP [ng]	mass total Ag [ng]	Ag-b-NP proportion [%]
0	0	0	0	0	0	0	0
10	1.7 ± 0.1	4.7 ± 0.4	36	17	n.d.	0.3 ± 0.2	0
26	3.0 ± 0.3	10.2 ± 0.5	30	32	n.d.	0.3 ± 0.2	0
42	3.0 ± 0.3	11.8 ± 0.6	26	49	n.d.	0.3 ± 0.2	0
58	3.0 ± 0.3	14.8 ± 0.6	20	64	n.d.	1.2 ± 0.2	0
74	3.0 ± 0.3	18.5 ± 0.6	16	79	n.d.	1.2 ± 0.2	0
90	3.0 ± 0.3	21.0 ± 0.6	14	100	n.d.	1.2 ± 0.2	0
100	3.0 ± 0.3	21.5 ± 0.7	14				
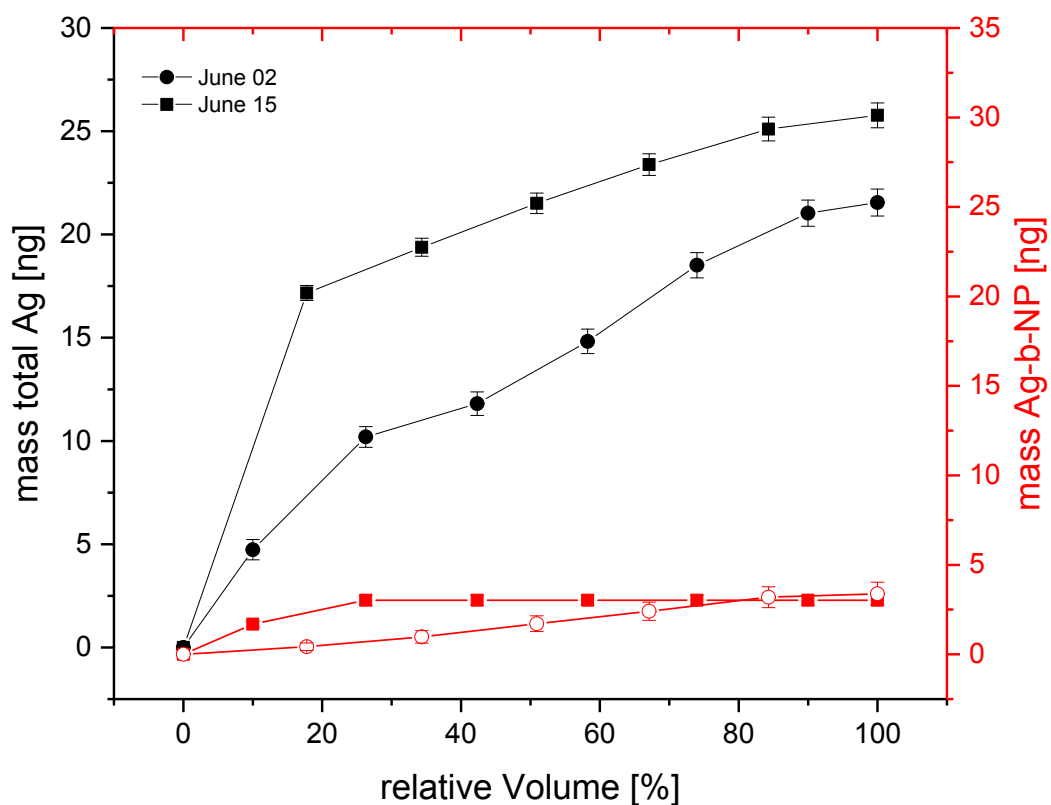
Figure S3. The cumulative masses of released total Ag and Ag-b-NPs from water pipe material into tap water from building 3 sampled on June 02 and June 15, 2016 (after an incubation period of 14 days prior to first sampling). The relative volume is calculated on the basis of the minimum tap water volume required to have no detectable total silver in the water runoff beyond the LOD of 0.2 ng L^{-1}. Errors indicate the uncertainty calculated via a Gaussian error propagation based on pipetting uncertainties and the standard deviations of independently treated and measured subsamples (n = 3).

Table S5. The cumulative masses of Ag-b-NPs and total Ag in tap water from building 3 sampled on June 02 and June 15, 2016 (after an incubation period of 14 days prior to first sampling) with increasing relative volume of sampled tap water. The relative volume is calculated on the basis of the minimum tap water volume required to have no detectable total silver in the water runoff beyond the LOD of 0.2 ng L^{-1}. Errors indicate the uncertainty calculated via a Gaussian error propagation based on pipetting uncertainties and the standard deviations of independently treated and measured subsamples (n = 3).

02.06.				15.06.			
relative volume [%]	mass Ag-b-NP [ng]	mass total Ag [ng]	Ag-b-NP proportion [%]	relative volume [%]	mass Ag-b-NP [ng]	mass total Ag [ng]	Ag-b-NP proportion [%]
0	0	0	0	0	0	0	0
10	1.7 ± 0.1	4.7 ± 0.4	36	18	0.4 ± 0.2	17.2 ± 0.4	2
26	3.0 ± 0.3	10.2 ± 0.5	30	34	1.0 ± 0.4	19.4 ± 0.4	5
42	3.0 ± 0.3	11.8 ± 0.6	26	51	1.7 ± 0.44	21.5 ± 0.5	8
58	3.0 ± 0.3	14.8 ± 0.6	20	67	2.4 ± 0.5	23.4 ± 0.5	10
74	3.0 ± 0.3	18.5 ± 0.6	16	84	3.2 ± 0.6	25.1 ± 0.6	13
90	3.0 ± 0.3	21.0 ± 0.6	14	100	3.4 ± 0.6	25.8 ± 0.6	13
100	3.0 ± 0.3	21.5 ± 0.7	14				

Table S6. Concentration of Cu, Ag, Ag-b-NPs, Cr, Fe, Ni, Zn and Pb with increasing volume of tap water runoff in each sample portion of approximately 200 mL supplemented by limits for all elements according to WHO guidelines for drinking water quality,[1] German drinking water regulations[2] and metal contents in drinking water according to the local water supplier. Errors indicate the uncertainty calculated via a Gaussian error propagation based on pipetting uncertainties and the standard deviations of independently treated and measured subsamples (n = 3).

volume [mL]	Cu concentration [μg L^{-1}]	Ag concentration [ng L^{-1}]	Ag-b-NP concentration [ng L^{-1}]	Cr concentration [ng L^{-1}]	Fe concentration [ng L^{-1}]	Ni concentration [ng L^{-1}]	Zn concentration [μg L^{-1}]	Pb concentration [μg L^{-1}]
211	92.6 ± 0.5	56.1 ± 0.7	21.2 ± 1.0	211.4 ± 3.5	1157.2 ± 1.3	5413.4 ± 1.3	825.0 ± 0.7	9.4 ± 0.1
423	107.2 ± 0.3	61.5 ± 1.3	18.2 ± 0.5	422.9 ± 7.7	1592.9 ± 1.9	1857.8 ± 1.1	974.0 ± 0.1	10.2 ± 0.5
633	52.0 ± 0.7	27.4 ± 0.6	8.7 ± 0.5	633.0 ± 3.3	2250.4 ± 1.4	1208.0 ± 1.3	1028.8 ± 1.6	10.4 ± 0.5
843	25.7 ± 0.1	19.4 ± 0.7	4.6 ± 0.5	843.5 ± 3.8	1898.4 ± 1.7	1101.5 ± 1.8	1061.1 ± 1.1	11.4 ± 0.3
1053	21.0 ± 0.4	17.5 ± 1.1	5.1 ± 0.6	1053.0 ± 5.7	1969.9 ± 1.7	1059.9 ± 2.0	1052.3 ± 0.8	11.4 ± 0.3
1267	20.4 ± 0.7	17.2 ± 0.7	4.6 ± 0.3	1267.4 ± 6.3	1698.2 ± 1.2	1037.4 ± 2.3	1060.1 ± 1.1	11.5 ± 0.4
limit according to WHO guidelines (German drinking water regulations)								
	2,000 (2,000)	10,000 (10,000)		50,000 (50,000)	--- (200,000)	70 000 (20,000)	3,000 (5,000)	10 (10)
metal contents according to local water supplier								
	<200	Not measured		<5,000	<20,000	<2,000	<200	<1

References

1. WHO, Guidelines for drinking-water quality - 4th ed. **2011**.
2. TrinkwV, Verordnung über die Qualität von Wasser für den menschlichen Gebrauch *(german drinking water regulation)* **2001**.
3. SWM, Munich City Utilities, Münchner Trinkwasser-Analysewerte **2018**.

8.8 PUBLIKATION 8

What happens to silver-based nanoparticles if they meet seawater?

Andreas Wimmer, Alexander Urstoeger, Nils Christoph Funck, Franziska Petra Adler, Leonhard Lenz, Markus Doeblinger, and Michael Schuster.
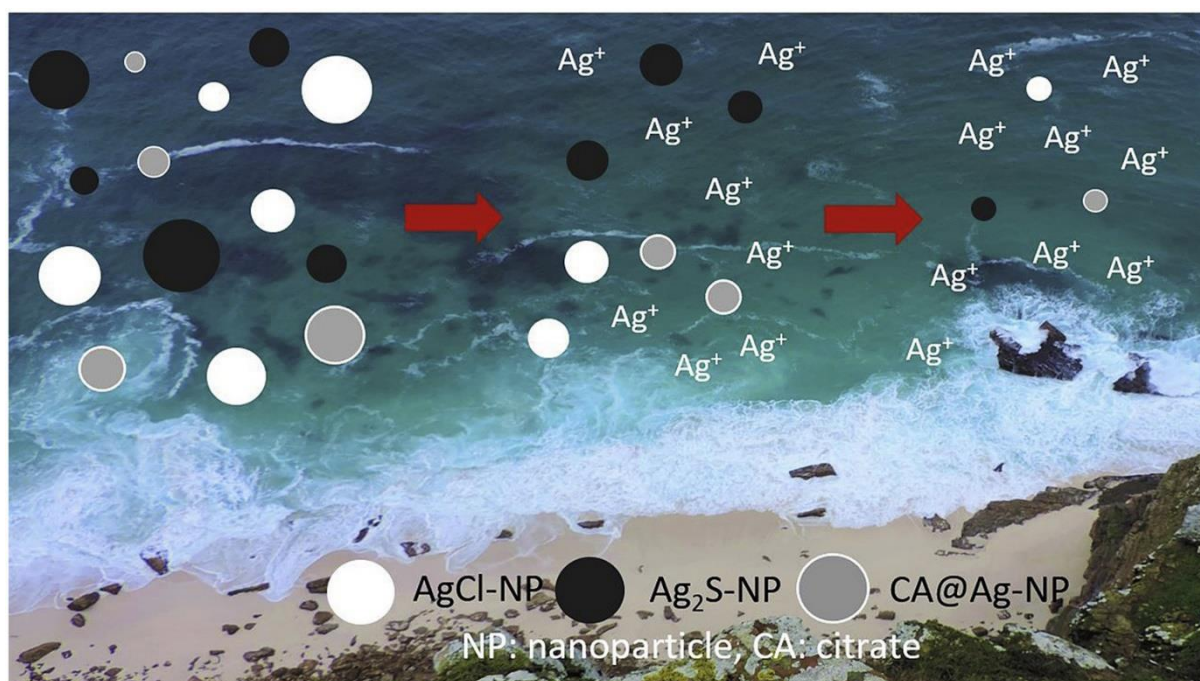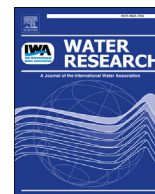
What happens to silver-based nanoparticles if they meet seawater?

Andreas Wimmer [a, 1], Alexander Urstoeger [a, 1], Nils Christoph Funck [a],
Franziska Petra Adler [a], Leonhard Lenz [a], Markus Doeblinger [b], Michael Schuster [a, *]

[a] Division of Analytical Chemistry, Department of Chemistry, Technical University of Munich, Lichtenbergstraße 4, Garching, 85748, Germany
[b] Department of Chemistry, Ludwig-Maximilians-Universität München, Butenandtstr. 5–13 (E), Munich, 81377, Germany

ABSTRACT

Silver based nanoparticles (Ag-b-NPs) in the environment are of current concern as they may pose risks to human and environmental health, even at low concentration levels. It is widely known that Ag-b-NPs, once released from products containing these particles for antimicrobial reasons, can pass through wastewater treatment plants to some extent. These particles are transported via running waterways and eventually reach the sea. However, the fate of environmentally relevant ng L^{-1} traces of Ag-b-NPs in seawater has not yet been sufficiently studied. Analytical techniques capable of determining these ultratraces of Ag-b-NPs in seawater are scarce and struggle furthermore with the high chloride content in highly saline matrices, such as seawater. In this study, we extracted Ag-b-NPs from matrices with varying salinity via cloud point extraction (CPE) and determined concentration and size of Ag-b-NPs in extracts with single particle inductively coupled plasma mass spectrometry (sp-ICP-MS). Applying this extraction and measurement technique, we were able to investigate the fate of Ag-b-NPs with different coatings (citrate and the predominant coatings in nature, silver sulfide and silver chloride) in matrices with increasing salinity and real seawater. All types of Ag-b-NPs were dissolved in all matrices almost independently of the chemical composition of the nanoparticles (NPs), whereas dissolution rates increased with increasing salinity due to the formation of soluble Ag(I) species and - in the presence of chloride - $AgCl_x^{1-x}$ (x > 1) complexes. After an incubation time of not more than 72 h, Ag-b-NPs were dissolved almost completely. During the dissolution process, NP shrinkage could be clearly observed by sp-ICP-MS. Supplementary electron microscopy measurements revealed that the sulfur content in silver sulfide nanoparticles (Ag_2S-NPs) increased during the dissolution process. Finally, we were able to investigate the dissolution process of real Ag-b-NPs in wastewater after increasing the salinity to seawater levels.

© 2019 Elsevier Ltd. All rights reserved.

1. Introduction

Due to the growing use of silver nanoparticles (Ag-NPs) in commercially available products and applications, such as food storage containers, sporting goods, fabrics, food additives in animal feed, cosmetics, medical devices and many others (Kim et al., 2010; Peters et al., 2014), these nanoparticles are increasingly released into the environment. This has intensified the discussion about concerns regarding environmental compatibility of Ag-NPs. Several studies have dealt with the toxicity of silver nanoparticles in organs (Ahamed et al., 2010; Krug, 2014; Kumar et al., 2017; Wiemann et al., 2017) and metabolic pathways (Foldbjerg et al., 2009;

Gopinath et al., 2010; Park et al., 2010; Ribeiro et al., 2015; Wise et al., 2010; Zhang et al., 2018). In addition to silver ions generated by dissolution of nanoparticles, Ag-NPs themselves are believed to negatively affect organisms (Asharani et al. 2008, 2009; Beer et al., 2012; Kim et al., 2009; Qian et al., 2013). Silver in this particulate form is believed to surpass even the ecotoxicological hazards of the corresponding bulk material (Hansen and Baun, 2012; Pettitt and Lead, 2013). Therefore, Ag-NPs should be monitored and analyzed in environmental samples in order to understand their fate and distribution in the environment, especially addressing the question of how environmental matrices influence particle dissolution and aggregation (Pasricha et al., 2012).

Once released into the environment, Ag-NPs interact readily with naturally occurring organic and inorganic substances and thus undergo a broad variety of surface modifications, which include adsorption of organic molecules present in the environment or

reactions with, e.g. dissolved species resulting in Ag$_2$S or AgCl coatings, whereas Ag$_2$S dominates environmentally relevant surface modifications (Kaegi et al. 2011, 2013, 2015). Therefore, Ag-NPs in the environment are described hereinafter as silver-based nanoparticles (Ag-b-NPs) so as to take every kind of surface modification into account.

Li et al. showed that over 94.6% of Ag-b-NPs were removed from wastewater treatment plant (WWTP) influent, but still resulted in an Ag-b-NP concentration ranging from 0.7 to 11.1 ng L^{-1} in the effluent released into the environment (Li et al., 2016).

These nanoparticles are transported in rivers and finally reach the sea, and the resulting fate of Ag-b-NPs can be characterized by two main processes: aggregation and dissolution. The Derjaguin–Landau–Verwey–Overbeak (DLVO) theory describes the stability of nanoparticle dispersions in aqueous matrices as an interplay of van der Waals interactions and electrostatic repulsion (Derjaguin and Landau, 1993; Lodeiro et al., 2016; Quik et al., 2014; Verwey, 1947). Once nanoparticles (NPs) are dispersed in matrices of high ionic strength, e.g. seawater, the net charge of the particles deriving from the corresponding electric double layer surrounding the particles is reduced. This results in an increase of remaining attractive forces encouraging attachment and thus aggregation of NPs (Lodeiro et al., 2016). Consequently, it is believed that Ag-b-NPs are not transported long distances in seawater. However, *Toncelli* et al. observed that the dissolution process dominates the fate of Ag-b-NPs in seawater at low concentrations (ng L^{-1} range) completely compensating for a DLVO-type aggregation effect (Toncelli et al., 2017). In general, the dissolution of Ag-b-NPs is best described by a widely accepted model established by Liu and Hurt, (2010). Ag-b-NPs in aqueous matrices undergo a cooperative oxidation process involving dissolved oxygen and protons forming peroxide intermediates and eventually water. Simultaneously, Ag(0) is readily oxidized to dissolved Ag(I), which is encouraged by a relatively low redox gap of −0.8 V (Liu and Hurt, 2010; Toncelli et al., 2017). Liu and Hart did not observe Ag-b-NP dissolution in deoxygenated seawater, and they were able to decrease it at a reduced pH due to an equilibrium shift (Liu and Hurt, 2010). Based on their observations and experiments, Liu and Hurt developed the following equation (Liu and Hurt, 2010):

$$2Ag_{(s)} + \frac{1}{2}O_{2(aq)} + 2H^+ \leftrightarrow 2Ag^+_{(aq)} + H_2O_{(l)} \qquad (1)$$
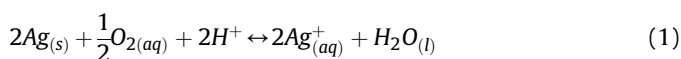
This dissolution process is furthermore influenced by the concentration of Ag-b-NPs and the constituents of natural water bodies like natural organic matter (NOM) and - in the case of seawater - high chloride contents. The dissolution rate is accelerated with decreasing Ag-b-NP concentration (Toncelli et al., 2017). NOM was reported to facilitate dissolution of Ag-b-NPs in aqueous matrices by complexation of Ag(I) and shifting of the equilibrium (Loza et al., 2014). Chloride present in aqueous matrices is able to eventually trap Ag(I) from the cooperative oxidation of Ag(0) to form soluble AgCl$_x^{1-x}$ (x > 1) complexes. According to the general rules of reaction equilibrium, this trapping process might accelerate the dissolution in seawater. However, *Liu* et al. reported that an incubation of Ag-b-NPs at mg L^{-1} range in seawater actually slowed down the dissolution process compared to an incubation in UPW. In reality, the higher pH of seawater in contrast to UPW inverts the equilibrium shift induced by the complexation of Ag(I) by Cl$^-$ (Liu and Hurt, 2010). However, especially for low Ag-b-NP concentrations in seawater, this may no longer be the case.

There have been several studies focusing on the fate of Ag-b-NPs in seawater. *Teo* et al. found that the Ag-b-NP dissolution at an initial Ag-b-NP concentration of 0.1 mg L^{-1} was much faster in seawater than in ultra-pure (UPW) water or lake water (Teo and Pumera, 2014). Additionally, for nanoparticle concentrations of 200 ng L^{-1} and 2000 ng L^{-1}, a decrease in size and concentration with increasing time was observed when dispersed in seawater, with the dissolution rate being influenced by the thickness of the particles' coatings (Toncelli et al., 2017). Furthermore, it has been reported that, albeit to a very little extent, Ag-b-NPs can be freshly formed from an interaction of dissolved Ag(I) with NOM (Toncelli et al., 2017). However, the Ag-b-NP concentrations used in those studies were in the sub µg L^{-1} to upper µg L^{-1} range (Lodeiro et al., 2017; Teo and Pumera, 2014; Toncelli et al., 2017), which by far exceeds concentrations found in natural samples, which are typically in the pg L^{-1} to lower ng L^{-1} range (Li et al., 2016; Sun et al., 2016; Wimmer et al., 2018). Furthermore, previous studies on the fate of Ag-b-NPs in seawater used >200 ng L^{-1} of polyethyleneimine and polyvinylpyrrilidone coated Ag-NPs for their experiments (Toncelli et al., 2017), which do not exist in nature. On the contrary, *Kaegi* et al. were able to show that Ag-NPs entering a WWTP are sulfidized to a variable degree independent of their original coating (Kaegi et al. 2011, 2013).

For our work, we used naturally relevant silver nanoparticle modifications, such as silver sulfide, silver chloride and core silver nanoparticles at an environmentally relevant concentration of 50 ng L^{-1}. Our goal was to study the fate and stability of the nanoparticles once they were released into a seawater matrix. The salinity of seawater, which is the mass fraction of dissolved material in seawater, is 35.17 g kg^{-1}. The majority of the salinity is represented by Cl$^-$ at a mass fraction of 19.35 g kg^{-1}, followed by Na$^+$ with a mass fraction of 10.78 g kg^{-1}, SO$_4^{2-}$ with a mass fraction of 2.71 g kg^{-1} and Mg^{2+} (1.28 g kg^{-1}), Ca^{2+} (0.41 g kg^{-1}), and K$^+$ (0.40 g kg^{-1}) (Millero et al., 2008). The contribution of NaCl to the total Cl$^-$ content calculated from this data is 85.9%. Such a high salt content causes instrumental problems in ICP-MS measurement, e.g. cone clogging and both spectral and non-spectral interferences. Dilution of the samples helps to avoid these problems, but it also leads to a significant loss of detection power.

We therefore used cloud point extraction (CPE), which is a highly selective separation and enrichment technique enabling Ag-b-NP extraction from complex aqueous solutions regardless of particle coating and without changing particle size and chemical composition (Hartmann et al. 2013, 2014). Dissolved silver, NOM and other particulate matter are tolerated in concentrations up to 100 µg L^{-1}, 100 mg L^{-1} and 0.1 mol L^{-1}, respectively. After CPE, the enriched and separated Ag-b-NPs can be forwarded to ICP-MS measurement for Ag concentration analysis and/or sp-ICP-MS for particle number and size determination.

Our experiments were furthermore supplemented by transmission electron microscopy (TEM) and energy-dispersive X-ray (EDX) spectroscopy to investigate the composition and possible transformation of the nanoparticles during incubation in seawater.

2. Materials and methods

2.1. Materials

Ag(I) ICP-standard (AgNO$_3$ in 3% HNO$_3$, β_{Ag} = 1000 mg L^{-1}), acetic acid (glacial), ethanol, ethylenediaminetetraacetate (EDTA) disodium salt, sodium chloride, sodium acetate anhydrous as well as ethanol and nitric acid (suprapure, 65%) were purchased from Merck (Darmstadt, Germany). Indium ICP-standard (In(NO$_3$)$_3$ in 2−3% HNO$_3$, β_{In} = 1000 mg L^{-1}), sulfur ICP-standard (H$_2$SO$_4$ in water, β_S = 1000 mg L^{-1}), dispersions of citrate stabilized silver nanoparticles (CA@Ag-NPs) (β_{Ag} = 20 mg L^{-1}), D-penicillamine, and sodium sulfide (Na$_2$S) were purchased from Sigma-Aldrich (St. Louis, MO, USA).

CA@Ag-NPs used in this study exhibited two different size

distributions, whereas sp-ICP-MS measurements (details are given in the Supporting Information (SI) Figs. S1 and S2) revealed maximum frequency particle sizes of 24 nm and 58 nm. It should be noted that throughout the entire study, particle sizes are given as maximum frequency sizes. We chose to use the maximum frequency sizes in order to enable comparison among widely varying particle types and size distributions. The maximum frequency size is the size that the most frequent particles comprising the entire distribution exhibit on the basis on number frequency. In all examined cases, this value was identical to the one determined on the basis of mass frequency. Therefore, particle size distributions themselves are usually presented as mass frequency unless otherwise specified.

Since CA@Ag-NP dispersions contain impurities of dissolved Ag, the stock dispersions were freed from dissolved Ag species by dialysis (3.5 kDa regenerated cellulose membrane by ZelluTrans, Carl Roth, Karlsruhe, Germany) prior to use. A citrate stabilized gold nanoparticle (CA@Au-NP) dispersion (NIST reference material RM 8013, 56 nm, $\beta_{Au} = 52$ mg L^{-1}, citrate stabilized) was purchased from the National Institute of Standards and Technology (Gaithersburg, MD, USA). Natural organic matter from the Suwannee River (SRNOM) - a reference material from the International Humic Substance Society (IHSS) - was used for all experiments investigating the influence of NOM on the stability of Ag-b-NPs in seawater. Triton X-114 was obtained from AppliChem (Darmstadt, Germany). All chemicals were at least of analytical grade and checked for silver contamination by ICP-MS prior to use. UPW (resistivity of 18.2 MΩcm) was obtained by a Milli-Q-Gradient-System (Millipore GmbH, Schwalbach, Germany). Solely filtrated natural sea water collected from the Gulf Stream in the Gulf of Mexico (S9148, 0.45 μm membrane-filtered, 3.5% salinity, 35 g L^{-1} salt including 89% NaCl (31 g L^{-1}) and 7% sulfate (2.4 g L^{-1})) was obtained from Sigma-Aldrich.

2.2. Instrumentation

A quadrupole mass spectrometer 7900 ICP-MS (Agilent, Santa Clara, CA, USA) equipped with an autosampler SPS4 (Agilent) and a MicroMist nebulizer (Glass Expansion, Melbourne, Australia) was used for Ag concentration and particle size determination. Argon 4.8 (Westfalen, Münster, Germany) was used as plasma gas (nebulizer gas pressure: $4.35 \cdot 10^2$ kPa). Ag quantification was carried out with the target masses ^{107}Ag (analyte) and ^{115}In (internal standard) in He CCT-mode (kinetic energy discrimination, He flow rate: 4.3 mL min^{-1}) to reduce isobaric and polyatomic interferences. Integration time for ^{107}Ag was set to 0.5 s. Data evaluation was performed using the Agilent MassHunter Workstation 4.4 software (version C.01.04, build 544.3).

In single particle mode, the dwell time was set to 500 μs, which results in 120,000 data points for an acquisition time of 60 s. ^{107}Ag was chosen as the target mass, and the pump rate was gravimetrically determined as 0.310 mL min^{-1}. Transport efficiency η describes the proportion of initial particles in the sample which finally reach the detector. The dispersion containing CA@Au-NP (RM 8103) at a Au concentration of $\beta = 52$ ng L^{-1} was used to determine η (~8%) according to a previously approved procedure (Montano et al., 2016; Peters et al., 2014). Before usage, the nanoparticle suspensions were ultrasonicated for 1 min in an ultrasonic bath of Ulsonix Proclean 3.0DSP (Ulsonix, Berlin, Germany) to prevent particle aggregation. Due to an element-specific signal intensity, elemental sensitivity was calibrated using an Ag(I) solution with a concentration of 1 μg L^{-1}. Particle size distributions were evaluated using the Agilent MassHunter Workstation 4.4 software (version C.01.04, build 544.3) equipped with the Single Nanoparticle Application Module.

(Scanning) transmission electron microscopy ((S)TEM) and energy-dispersive X-ray spectroscopy (EDX) measurements were conducted at 300 kV using a FEI Titan Themis electron microscope (Thermo Fischer Scientific, Waltham, MA, USA) equipped with a SuperX EDX detector. STEM was performed in annular dark field (ADF) mode. TEM samples were prepared on carbon film coated copper grids (S 162-6, Plano GmbH, Wetzlar, Germany). Before applying a small droplet of sample dispersion on the TEM grids, they were treated with a H_2/O_2 plasma for 5 s to make them hydrophilic. After an incubation period of 10 min, excess liquid was blotted away with filter paper. The samples were subsequently dried and inserted into the TEM.

TOC content of WWTP effluent samples was determined with a TOC-L-Analyzer (Shimadzu, Kyoto, Japan) following a standard protocol with potassium hydrogen phthalate as the calibrant. Therefore, aqueous solutions of potassium hydrogen phthalate containing 0.5–10 mg L^{-1} TOC were measured for calibration. Samples were measured without filtration and further acidified and thoroughly mixed shortly before the measurement started to ensure sample homogeneity and remove inorganic carbonates.

2.3. Nanoparticle synthesis and characterization

Silver sulfide nanoparticles (Ag$_2$S-NP) were synthesized according to a procedure published by Hartmann et al., (2014). For this purpose, 0.2 mL of a 10 mM Na$_2$S solution were added to 10 mL of a suspension containing 58 nm CA@Ag-NP ($\beta_{Ag} = 10$ mg L^{-1}). The mixture was stirred for 3 h in the dark at room temperature (RT). Silver chloride nanoparticles (AgCl-NPs) were prepared following a procedure proposed by Zhou et al., (2017). In this case, 8.5 mg AgNO$_3$ and 25 mg TX-114 were added to 50 mL of UPW. The solution was mixed dropwise with 1 mL of a 50 mM NaCl solution and was further stirred in the dark at RT for another 30 min. The synthesized Ag$_2$S and AgCl suspensions were dialyzed in the dark for three days, changing the water twice a day in order to separate the nanoparticles from the dissolved silver species and matrix constituents. The dialyzed NP suspensions were then stored in the dark at 5 °C and were stable for weeks. Particle size distribution, shape, and chemical composition of the synthesized Ag$_2$S-NPs and AgCl-NPs as well as CA@Ag-NPs were determined by (S)TEM-EDX.

2.4. Incubation and separation of Ag-b-NPs from highly saline matrices

Artificial seawater with 31 g L^{-1} NaCl and real seawater were mixed with aqueous dispersions of CA@Ag-NPs (24 nm, 58 nm maximum frequency size), synthesized AgCl-NPs and Ag$_2$S-NPs to gain dispersions with a volume of 40 mL and an Ag concentration of 50 ng L^{-1}. For reasons of comparability, similar NP dispersions were prepared in UPW. The influence of NOM on the stability of Ag-b-NPs in seawater was examined by adding 5 mg L^{-1} SRNOM to the aforementioned samples. WWTP effluent containing real Ag-b-NPs was collected from a plant in Southern Germany (WWTP Garching, capacity: 4'100 m^3 day^{-1}, building date: 1999) using disposable 500 mL PVC bottles, which were rinsed three times with the sample matrix prior to sampling. To obtain a final salt concentration of 31 g L^{-1}, NaCl was added in small portions while vigorously stirring to avoid localized salt overconcentration. All incubation experiments were prepared in triplicate, protected from light, shaken, and incubated for a certain period (1 h, 2 h, 3 h, 24 h, 48 h, 72 h).

During incubation, Ag-b-NPs may be partly or completely dissolved. CPE was used for selective enrichment of Ag-b-NPs from dissolved silver species and the highly saline matrix (Duester et al., 2016; Hartmann et al., 2013; Hartmann and Schuster, 2013). In brief, 40 mL of each sample were mixed with aqueous solutions of

ethylenediaminetetraacetic acid disodium salt, D-penicillamine, sodium acetate, acetic acid, and the surfactant TX-114 (Hartmann et al. 2013, 2014; Wimmer et al., 2018). After incubation at 40 °C for 30 min, separation of the surfactant phase was enhanced by centrifugation (12 min, 4500 g). The phase-separated mixtures were cooled (5 min, ice bath) and the aqueous supernatant was then removed by decanting. Details as well as the trueness and robustness of the CPE procedure are described by Hartmann et al. 2013, 2014. The remaining surfactant droplets containing the extracted and enriched Ag-b-NPs were diluted with ethanol (500 μL) and UPW to a total volume of 10 mL for the ICP-MS and sp-ICP-MS measurements. Samples are divided into further sub-samples. Those intended for sp-ICP-MS analysis are forwarded to measurement without further treatment. Sub-samples intended for conventional ICP-MS analysis are further mixed with HNO$_3$ yielding in a final acid concentration of 1.625% (v/v). HNO$_3$ is used to dissolve NPs in CPE extracts to increase sample homogeneity.

2.5. Determination of concentration and particle size of Ag-b-NPs in CPE extracts

Conventional ICP-MS was used to quantify total Ag concentration in the CPE extracts. In most cases, these measurements were supplemented by sp-ICP-MS measurements, which allow for the calculation of Ag-b-NP particle size in the CPE extracts by measuring the total mass of each single Ag-b-NP in the sample and, eventually, for the calculation of the total concentration of Ag-b-NPs by summation of each single Ag-b-NP mass. Calibration was performed with aqueous Ag(I) solutions of known concentration ranging from 5 to 200 ng L^{-1} (limit of detection, LOD = 0.2 ng L^{-1}; background equivalent concentration, BEC = 0.5 ng L^{-1}). Since these solutions underwent no CPE, they were prepared in a UPW matrix (acidified to 1.625% (v/v) HNO$_3$) including 5% (v/v) of TX-114 10% (w/w) and 5% (v/v) of ethanol (which is, e.g., 2.5 mL TX-114 10% (w/w) and 2.5 mL EtOH for a total volume of 50 mL) to mimic the matrix of the samples after CPE.

Quantitative sp-ICP-MS measurements were performed with non-acidified CPE extracts. Calibration samples (52 ng L^{-1} CA@AuNP dispersion and 1 μg L^{-1} Ag(I) solution) were prepared in a UPW matrix including 5% (v/v) of TX-114 10% (w/w) and 5% (v/v) of ethanol (which is, e.g., 2.5 mL TX-114 10% (w/w) and 2.5 mL EtOH for a total volume of 50 mL) to mimic the matrix of the samples after CPE. The calculations are subject to some uncertainties as they assume a spherical shape for all particles and require knowledge about the density ρ of the particulate materials (Peters et al., 2014), which is derived from the bulk materials Ag (ρ = 10.49 g cm^{-3}), AgCl (ρ = 7.23 g cm^{-3}) and Ag$_2$S (ρ = 5.56 g cm^{-3}) (according to the GESTIS Substance Database, Dec. 2018). In the case of Ag-b-NPs in real environmental samples (WWTP effluent), the NP modification is unknown but very likely Ag$_2$S (Kaegi et al., 2013). Despite its limitations, sp-ICP-MS is still the only method able to simultaneously determine concentration and particle size distribution of NPs at ng L^{-1} concentration levels, so it is the method of choice.

Size detection limit (SDL) for sp-ICP-MS measurement of Ag-b-NPs was determined to 8 nm. Transient signals deriving from nanoparticles being atomized in the plasma of the ICP-MS are registered during the measurement. The signal size corresponds to the size of the corresponding nanoparticle, i.e. small particles lead to only very little signals. Signals of smaller particles in the time resolved sp-mass spectra are not distinguishable anymore from signals derived from traces of dissolved Ag species or the instrument's background and are thus not applicable for data processing. Thus, concentrations measured by sp-ICP-MS represent the total Ag concentration of all particulate Ag species sized >8 nm.

2.6. Characterization of size, morphology and chemical composition of Ag-b-NPs incubated in real seawaters

Mass spectrometric analysis was supplemented by electron microscopy to investigate the fate of Ag-b-NPs in highly saline matrices. To meet limits of detection for TEM-EDX, Ag-b-NP dispersions were mixed 1:10 with real seawater, resulting in a total volume of 1.5 mL and incubated for 1 h. Afterwards, samples were filled in 3.5 kDa regenerated cellulose membranes surrounded by 1 L UPW to perform a dialysis for 24 h. UPW was replaced every 4 h. Dialysis can eliminate both Ag(I) deriving from potentially dissolved Ag-b-NPs and the high saline seawater matrix, which would otherwise cause incrustations on the TEM grid. A droplet of each prepared sample was examined by TEM-EDX as described in the "Instrumentation" section and compared to NPs which had not been in contact with seawater.

2.7. Error calculations

For all measurements, three independent subsamples were treated and measured individually. Each subsample was measured with three replicates n (U, n = 3). The uncertainty U was calculated via Gaussian error propagation based on pipetting uncertainties and standard deviations of the independently measured sub-samples. Blank samples were used to correct Ag concentrations in all incubation experiments.

3. Results and discussion

3.1. Nanoparticle characterization

The chemical composition, shape, and particle size of the commercially available and synthesized particles were analyzed to gain information about the pristine state of the particles prior to any incubation experiments. For this purpose, dispersions of the freshly synthesized and purified CA@Ag-NPs, AgCl-NPs and Ag$_2$S-NPs were prepared on copper grids and investigated with STEM and EDX.

STEM measurement of both types of CA@Ag-NPs showed spherical, sole particles with a particle size range of approximately 42–120 nm (SI, Fig. S1) and 14-100 nm (SI, Fig. S2). Maximum frequency particle sizes were determined by sp-ICP-MS as 24 nm and 58 nm, respectively. An examplary image of a particle sizing 53 nm and the corresponding EDX spectrum are given in Fig. 1. The particle related signals indicate that the core of the particle consists of pure silver.

The synthesized AgCl-NPs showed cubic non-aggregated particles with a broad size range of approximately 18–200 nm (SI, Fig. S3) with a maximum frequency particle size of 94 nm determined by sp-ICP-MS. Fig. 2 shows an example of a STEM-ADF image of a AgCl-NP cube with a side length of 100 nm and the corresponding EDX spectrum. The EDX spectrum reveals a Ag to Cl ratio of 1:1, which complies with the presence of AgCl particles.

Fig. 3 shows a TEM image of the synthesized Ag$_2$S-NPs and the corresponding EDX spectrum. In this case, some bridging between neighboring particles occurred and some particles show small cavities. A narrow particle size distribution was observed with a size range of 48–160 nm (SI, Fig. S4) and a maximum frequency particle size of 82 nm determined by sp-ICP-MS. EDX measurements revealed a Ag to S ratio of 2:1, which indicates the presence of Ag$_2$S-NPs. Obviously, the reaction of CA@Ag-NPs with sulfide resulted in the formation of fully sulfurized particles combined with an increase in the average size of the particles from 58 nm to 82 nm (SI, Fig. S4).

Fig. 1. STEM-ADF image and corresponding EDX spectrum of a citrate coated silver nanoparticle. Additional Cu-, O- and C-signals in the spectrum result from the sample support (carbon film on copper grid) and carbohydrate contamination during illumination.

3.2. Dissolution of differently coated and sized Ag-b-NPs incubated in UPW, artificial seawater, and real seawater

We examined the fate of differently coated and sized Ag-b-NPs in UPW, artificial seawater, and real seawater. Our preliminary tests prior to the incubation experiments confirmed the applicability of CPE to species selectively extract and enrich Ag-b-NPs from saline matrices. Extraction efficiency for Ag-b-NPs even increased from 88% in the UPW matrix to 94% in the highly saline matrix. Moreover, the co-extraction of soluble Ag(I) species from highly saline matrices into the organic phase amounted to less than one percent. Therefore, CPE is suitable to (i) quantitatively extract Ag-b-NPs from highly saline matrices into the organic phase and to (ii) perform this process species selectively. In other words, soluble Ag(I) species deriving from former Ag-b-NPs by means of dissolution in saline matrices are prevented from being transported into the organic phase.

We applied a dual approach for investigating the fate of Ag-b-NPs in UPW and highly saline matrices. First, we quantified the total concentration of Ag-b-NPs present after a certain incubation time, whereby these particles were thus able to resist an occurring NP dissolution process. Concentrations related to Ag for these remaining Ag-b-NPs in each incubation matrix (UPW, artificial, and real seawater) with increasing incubation time measured by CPE-ICP-MS are shown in Fig. 4 and Table S1 (see SI). Table S1 includes further concentration data measured for the same samples by CPE-sp-ICP-MS. These concentrations represent the concentration of particles ≥8 nm.

Second, we were able to display the change in sizes of Ag-b-NPs being incubated in the different matrices for increasing incubation time by CPE-sp-ICP-MS measurements (Fig. 5).

All experiments started with an initial Ag-b-NP concentration of ~50 ng L^{-1} (Fig. 4). As mentioned above, comparison of CPE-ICP-MS and CPE-sp-ICP-MS allowed differentiation between concentration of the total amount of particulate Ag species and those <8 nm (SI, Table S1). In most cases, CPE-sp-ICP-MS was not able to quantify all

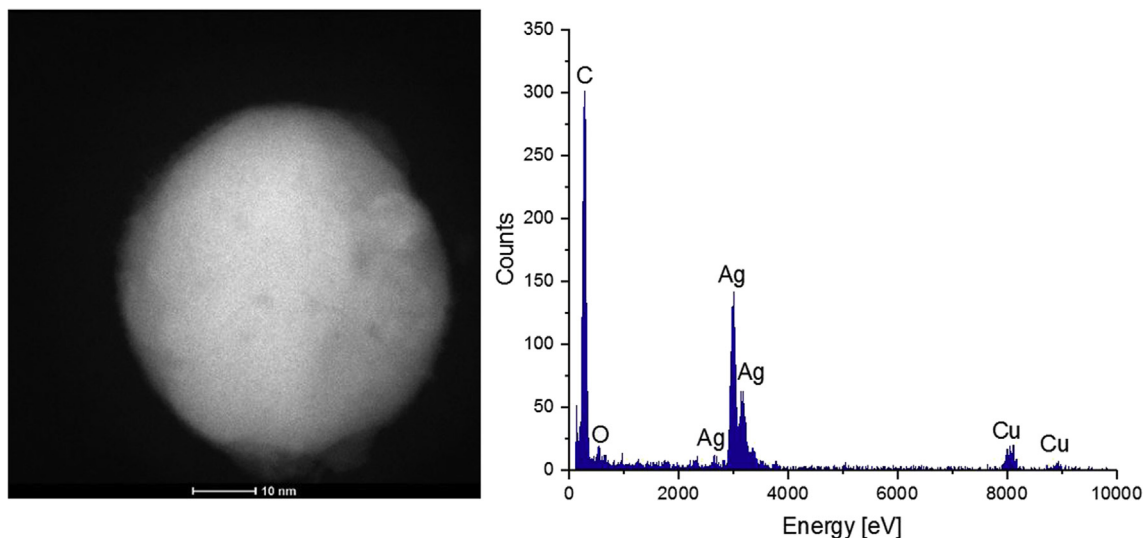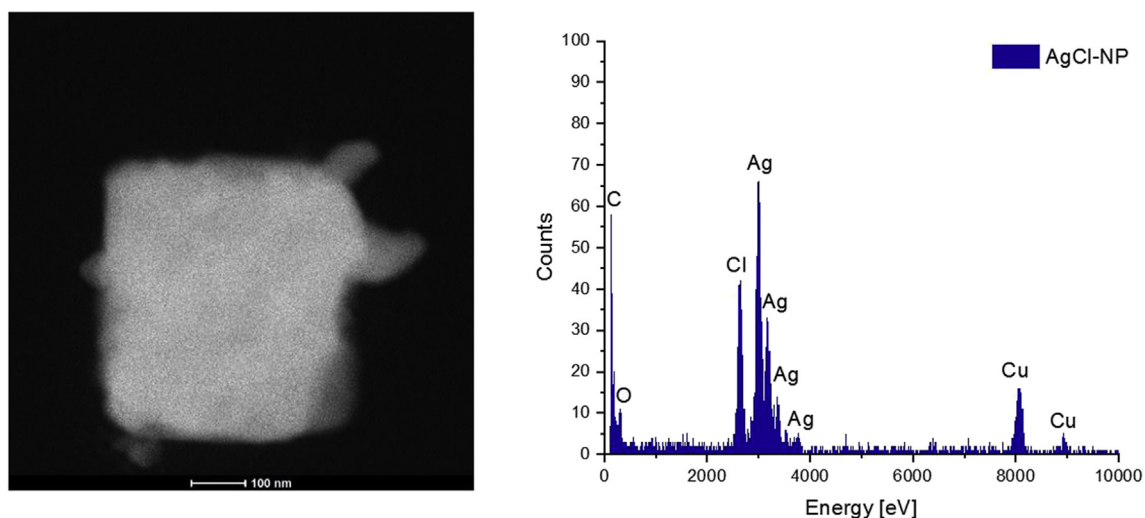**Fig. 2.** STEM-ADF image and corresponding EDX spectrum of a silver chloride nanoparticle. Additional Cu-, O- and C-signals in the spectrum result from the sample support (carbon film on copper grid) and carbohydrate contamination during illumination.
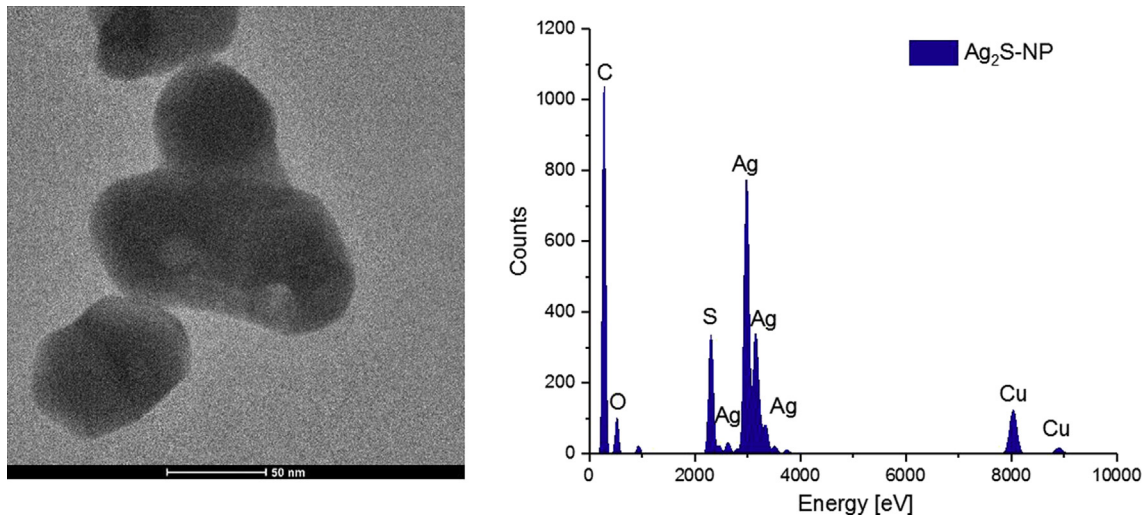
Fig. 3. TEM image and corresponding EDX spectrum of silver sulfide nanoparticles. Additional Cu-, O- and C-signals in the spectrum result from the sample support (carbon film on copper grid) and carbohydrate contamination during illumination.

particulate species since low concentrations of particles <8 nm were present. However, no correlation between the appearance of particles <8 nm and incubation time, matrix, and NP coating was detected.

As already described in the literature, cooperative oxidation processes transforming Ag(0) to soluble Ag(I) species followed by formation of soluble $AgCl_x^{1-x}$ (x > 1) in the presence of chloride (Levard et al., 2012; Liu and Hurt, 2010; Lodeiro et al., 2017) basically led to dissolution of all types of Ag-b-NPs in the three different matrices.

UPW establishes massive dilution pressure, readily transforming large parts of particulate Ag(0) into dissolved Ag(I) species by an equilibrium shift to dissolved Ag species (equation (1)), which is further promoted by the comparatively low pH of UPW (~5−6)

compared to non-purified or natural water (~7−8) (Liu and Hurt, 2010). After an incubation period of 3 h in the UPW matrix, only 87% of the initially applied CA@Ag-NPs (58 nm pristine maximum frequency size) remained as particles. It should be noted that the sizes in brackets represent the mean pristine particle size before incubation, which is enclosed for the sake of clarity. After the same incubation time, only 1% of the initially applied CA@Ag-NPs (24 nm pristine maximum frequency size) remained. Due to the extremely large intrinsic surface of these small particles, oxidation to dissolved Ag(I) is massively promoted for smaller particles (Zhang et al., 2011). After 3 h of incubation in UPW, 26% of AgCl-NPs (94 nm pristine maximum frequency size) remained particulate. Since the AgCl particles initially exhibited a maximum frequency particle size of 94 nm, we would suggest a slow dissolution process.

Fig. 4. Concentration of Ag present as nanoparticles for all four investigated Ag-b-NP types incubated in UPW, artificial seawater, and seawater with increasing incubation time. Measurements were performed by CPE-ICP-MS and, thus, concentrations correspond to the total amount of Ag-b-NPs (see SI, Table S1 for detailed measured values).
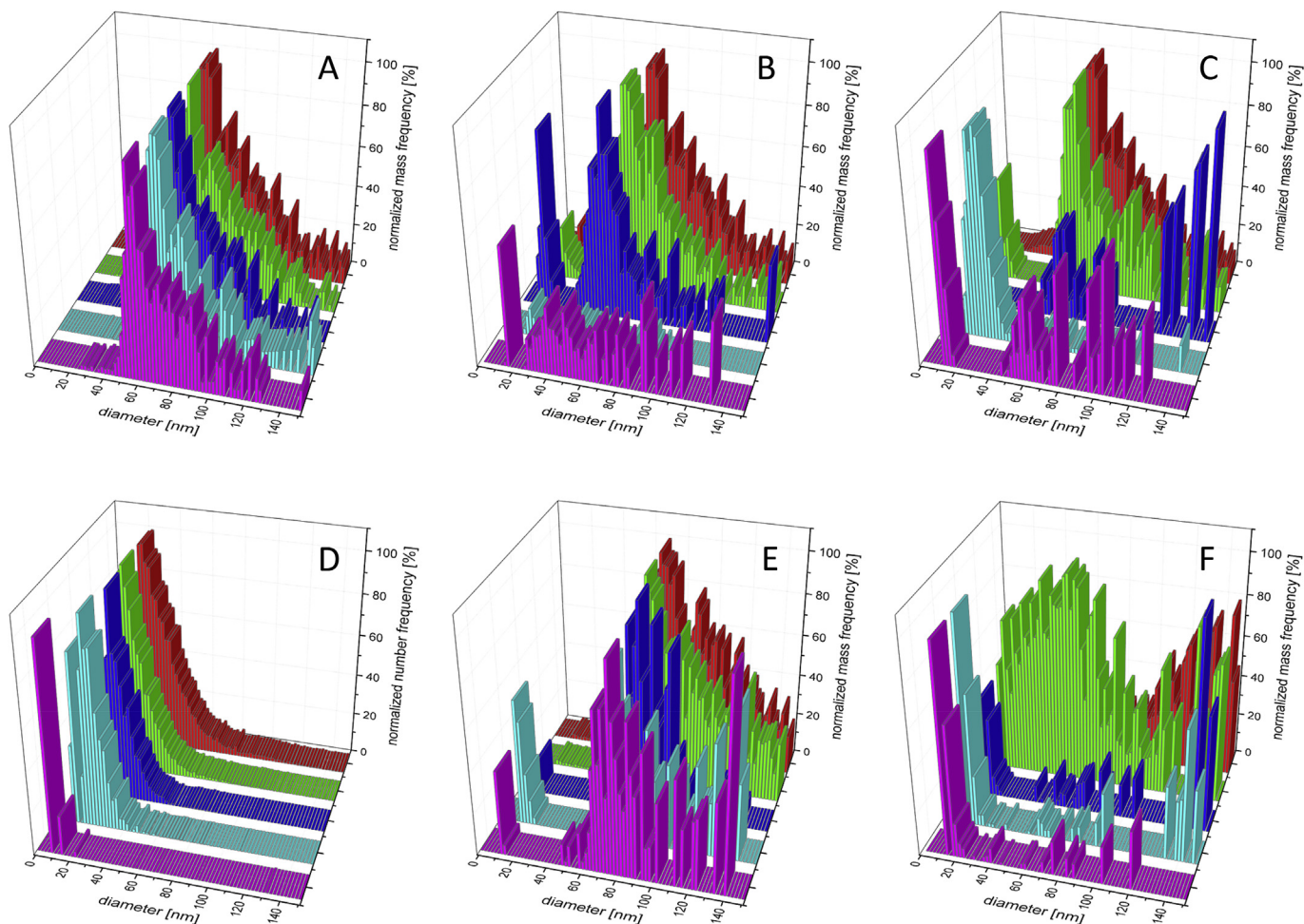
Fig. 5. Particle size distributions referred to normalized mass or number frequency of CA@Ag-NPs (58 nm pristine maximum frequency size) in UPW (A), CA@Ag-NPs (58 nm pristine maximum frequency size) in artificial seawater (B), CA@Ag-NPs (58 nm pristine maximum frequency size) in seawater (C), CA@Ag-NPs (24 nm pristine maximum frequency size) in seawater (D), Ag$_2$S-NPs (82 nm pristine maximum frequency size) in seawater (E), and AgCl-NPs (94 nm pristine maximum frequency size) in seawater (F). The four size distributions presented in each diagram are related to the pristine state (red), 1 h of incubation (green), 24 h of incubation (blue), 48 h of incubation (turquoise), and 72 h of incubation (purple). See also SI, Fig. S6 for another perspective of diagram F. Particles <8 nm were not detectable with sp-ICP-MS. Presented results are based on CPE-sp-ICP-MS measurements. (For interpretation of the references to color in this figure legend, the reader is referred to the Web version of this article.)

However, we observed quite high dissolution rates for AgCl-NPs, which can be explained by the fact that Ag in AgCl is already present in oxidation state I, accelerating the cooperative oxidation process responsible for the dissolution (Liu and Hurt, 2010). Since 69% of Ag$_2$S-NPs (82 nm pristine maximum frequency size) resisted dissolution after 3 h of incubation, the high insolubility of Ag$_2$S seems to compensate for the Ag oxidation state of I and thus prohibits these particles from fast dissolution. The general trend continued with increasing incubation time to 72 h, whereby 42% of the initially applied CA@Ag-NPs (58 nm pristi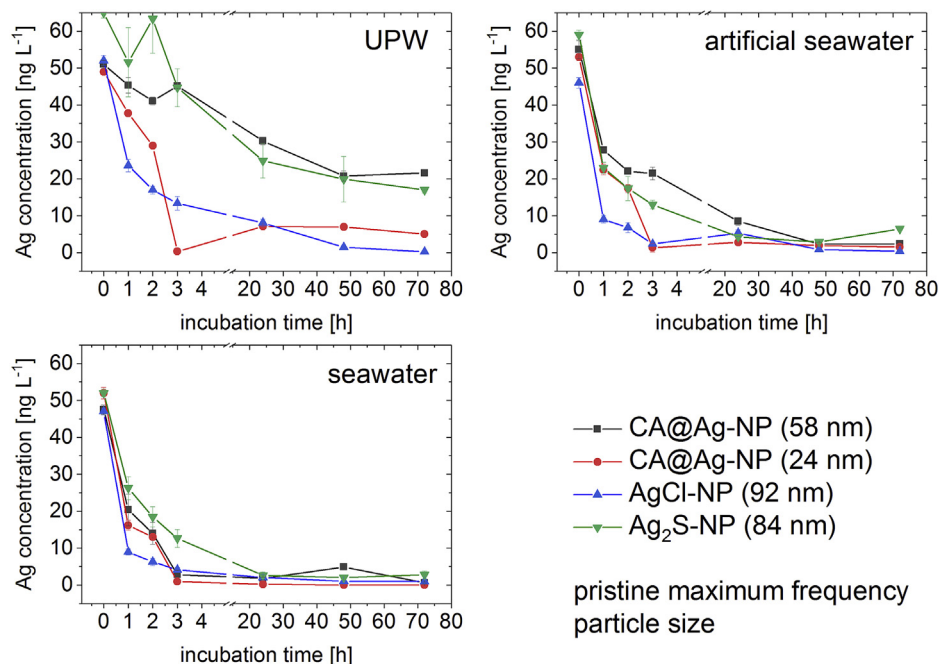ne maximum frequency size), 26% of Ag$_2$S-NPs (82 nm pristine maximum frequency size), 10% of CA@Ag-NPs (24 nm pristine maximum frequency size), and 1% of AgCl-NP (94 nm pristine maximum frequency size) resisted dissolution. Overall, CA@Ag-NPs (58 nm pristine maximum frequency size) seemed to be the most stable modification of Ag-b-NPs in UPW, followed by Ag$_2$S-NPs (82 nm pristine maximum frequency size), CA@Ag-NPs (24 nm pristine maximum frequency size), and AgCl-NPs (94 nm pristine maximum frequency size). This is somewhat surprising since silver sulfide is one of the most insoluble salts. However, CA@Ag-NPs (58 nm pristine maximum frequency size) exceeded this insolubility, likely due to the fact that the coating reagent can slow down the oxidative dissolution

process. Citrate coating has already been reported to be able to reduce Ag(I) to Ag(0), forming either new particles or being inserted into already existing particles (Kittler et al., 2010).

The presence of chloride, able to trap Ag(I) and thus shift the dissolution equilibrium (Liu and Hurt, 2010), leads to increasing dissolution rates for all types of Ag-b-NPs in artificial seawater. After an incubation of 3 h, only 3% of the initially applied CA@Ag-NPs (24 nm pristine maximum frequency size), 5% of AgCl-NPs (94 nm pristine maximum frequency size), 22% of Ag$_2$S-NPs (82 nm pristine maximum frequency size), and 39% of CA@Ag-NPs (58 nm pristine maximum frequency size) resisted dissolution and remained particulate. After 72 h, the dissolution process in seawater was almost finished, in contrast to incubation in UPW matrix, where 11% of Ag$_2$S-NPs (82 nm pristine maximum frequency size) and 1–4% of the other Ag-b-NPs were still present as particulate species. Again, small particle sizes encouraged dissolution, as CA@Ag-NPs (24 nm pristine maximum frequency size) were dissolved significantly faster than CA@Ag-NPs (58 nm maximum frequency size). Again, CA@Ag-NPs (58 nm pristine maximum frequency size) and Ag$_2$S-NPs (94 nm pristine maximum frequency size) were more stable than CA@Ag-NPs (24 nm pristine maximum frequency size) and AgCl-NPs (94 nm pristine maximum

frequency size).

Dissolution rates reached their maximum in experiments involving real seawater as the incubation matrix. This observation is only partially reflected in the current literature. Liu et al. described that dissolution rates for Ag-b-NPs in the mg L^{-1} range incubated in seawater even decreased to some extent because the comparatively high pH (~8) in seawater shifts the equilibrium of the dissolution process at the expense of dissolved Ag(I) species (Liu and Hurt, 2010). However, reducing the Ag-b-NP concentration to an environmentally relevant level of some ng L^{-1} was reported to accelerate the dissolution process (Toncelli et al., 2017). In our experiment, the latter case seems to prevail, and it controls the dissolution process in real seawater. In general, we observed a dramatic drop in the concentration of remaining NPs in seawater within the first 3 h, whereas only 24% of the initially applied Ag$_2$S-NPs (82 nm pristine maximum frequency size), 9% of AgCl-NPs (94 nm pristine maximum frequency size), 6% of CA@Ag-NPs (58 nm pristine maximum frequency size), and 2% of CA@Ag-NPs (24 nm maximum frequency size) were still present as NPs in seawater. After incubation for 72 h, only 1−9% of Ag-b-NPs resisted dissolution in seawater. It is remarkable that some particles of all types of Ag-b-NPs could still be detected, indicating a certain stability of particle traces in seawater. This partial dissolution of Ag-b-NPs in aqueous matrices even after incubating for several days has also been described by Loza et al., (2014). Again, CA@Ag-NPs (24 nm pristine maximum frequency size) and AgCl-NPs (94 nm pristine maximum frequency size) showed only low stability during the incubation experiment in seawater for the aforementioned reasons. CA@Ag-NPs (58 nm pristine maximum frequency size) and Ag$_2$S-NPs (82 nm pristine maximum frequency size) displayed slightly higher stability. Very interestingly, Ag$_2$S-NPs (94 nm pristine maximum frequency size) even surpassed the stability of CA@Ag-NPs (58 nm pristine maximum frequency size) marginally, which could not be observed in any of the incubation experiments described above. This observation probably goes along with high concentrations of sulfate present in real seawater, which was not the case for UPW and artificial seawater, indicating the stability of silver sulfide coatings. However, the presence of sulfide coatings requires the reduction of S(VI) in sulfate to S(-II) in sulfide, which might take place to a small extent by integrating sulfate into the aforementioned cooperative oxidation reactions (Liu and Hurt, 2010).

CPE-sp-ICP-MS provides an even more detailed insight into the NP dissolution process (Fig. 5), as it describes the evolution of particle size distributions over time. Particle size distributions for CA@Ag-NPs (58 nm pristine maximum frequency size), Ag$_2$S-NPs (82 nm pristine maximum frequency size), and AgCl-NPs (94 nm pristine maximum frequency size) are given as normalized mass frequency. We chose this kind of presentation because very small particles <8 nm are present to a varying extent in all samples, but contribute only very little to the total particle mass. However, particles <8 nm would misleadingly affect the particle size distributions if presented as normalized number frequency. For CA@Ag-NPs (24 nm pristine maximum frequency size), presenting normalized number frequencies was feasible due to the narrow range of small particle sizes. In depth analysis of sp-ICP-MS data revealed additional information regarding particle numbers and their variation after incubation in aqueous matrices (Table 1).

Fig. 5A shows blank corrected particle size distributions of CA@Ag-NPs (58 nm pristine maximum frequency size) incubated in UPW for 1 h, 24 h, 48 h, and 72 h. As seen in Fig. 4 (SI, Table S1), the NP concentration was reduced by dissolution to 42% within 72 h. However, the NP size distribution did not change during the observed incubation period, so the maximum frequency size (Table 1) stayed constant during the experiment, which is due to

Table 1
Compilation of the total number of NPs and numbers within a defined size range as well as the measured maximum frequency NP size; each measurement addresses a certain type of Ag-b-NP, incubation matrix and incubation time. Sizes in brackets represent the pristine maximum frequency size. Presented results are based on CPE-sp-ICP-MS measurements.

	0 h	1 h	24 h	48 h	72 h
CA@Ag-NPs (58 nm) in UPW					
total number	10899	3716	1858	1019	1513
NP ≤30 nm	8098	988	256	7	86
NP >30 nm	2801	2728	1602	1012	1427
maximum frequency size [nm]	58	62	62	61	59
CA@Ag-NPs (58 nm) in artificial seawater					
total number	10899	10374	8380	2433	1548
NP ≤30 nm	8098	8573	7692	2218	1291
NP >30 nm	2801	1801	688	215	257
maximum frequency size [nm]	58	57	46	10	10
CA@Ag-NPs (58 nm) in seawater					
total number	3269	10206	2382	1852	3446
NP ≤30 nm	608	8977	2333	1801	3390
NP >30 nm	2661	1229	50	50	56
maximum frequency size [nm]	58	59	12	17	10
CA@Ag-NPs (24 nm) in seawater					
total number	8695	9425	1879	288	1110
NP ≤16 nm	195	718	0	59	1077
NP >16 nm	8499	8708	1879	230	32
maximum frequency size [nm]	24	19	9	10	8
Ag$_2$S-NPs (82 nm) in seawater					
total number	4929	4936	771	546	1486
NP ≤30 nm	2341	2446	623	530	1356
NP >30 nm	2588	2490	147	17	130
maximum frequency size [nm]	73	73	69	11	11
AgCl-NPs (94 nm) in seawater					
total number	815	9240	2482	5170	4141
NP ≤30 nm	0	7593	2447	5145	4118
NP >30 nm	815	1647	35	25	23
maximum frequency size [nm]	70	15	12	12	12

the fact that primarily small particles were readily dissolved, thus not influencing the maximum frequency size of approximately 58 nm. We observed a rapid decrease of the total particle number within the first hour of incubation (Table 1), whereas particles ≤30 nm in particular were dissolved. Due to their high intrinsic surface, the small particle fraction was dissolved first. During the following days, almost all particles ≤30 nm were dissolved, whereas the number of particles >30 nm was reduced slightly, indicating their predominant stability.

Incubation of CA@Ag-NPs (58 nm pristine maximum frequency size) in artificial seawater (Fig. 5B) led to a reduction of the maximum frequency size of the particles from 58 nm to 46 nm within the first day of incubation, which goes along with a decrease in NP concentration (Figs. 4 and SI, Table S1). Table 1 shows that particles >30 nm in particular were dissolved, whereas the number of particles ≤30 nm stayed constant or increased. However, it is very likely that particles ≤30 nm were still dissolved, but the simultaneous dissolution of particles >30 nm also led to the formation of particles ≤30 nm. After 48 h of incubation, the maximum frequency particle size was reduced dramatically to 10 nm because a large proportion of particles was dissolved. In this case, the number of particles >30 nm and ≤30 nm was reduced equally.

In contrast to an incubation of CA@Ag-NPs (58 nm pristine maximum frequency size) in artificial seawater, the rapid concentration drop for an incubation in seawater occurred earlier after 24 h of incubation (Figs. 4 and SI, Table S1). This goes along with a
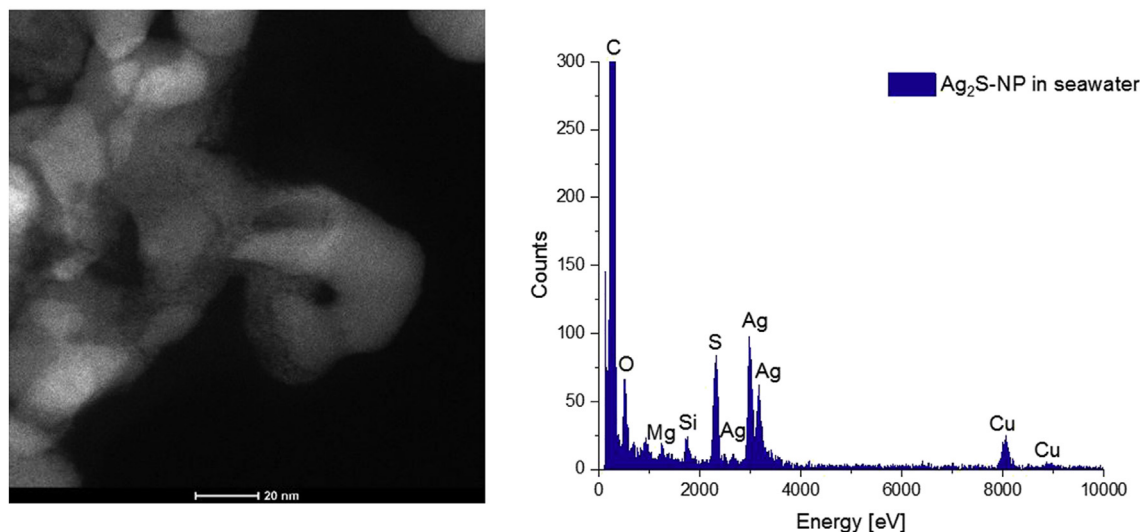
Fig. 6. STEM-ADF image of Ag$_2$S-NPs after incubation in seawater and corresponding EDX spectrum. Additional Cu-, O- and C-signals in the spectrum result from the sample support (carbon film on copper grid) and carbohydrate contamination during illumination.

strong decrease of the maximum NP frequency size from 58 nm to 12 nm after the same incubation period (Table 1, Fig. 5C). In Fig. 5C, particles exhibiting a maximum frequency particle size of 58 nm with a size range of approximately 14–100 nm were only observable until 1 h of incubation. Particles >30 nm were almost completely dissolved after 24 h of incubation (Table 1). Again, shrinking of particles >30 nm contributed to a constant number of particles ≤30 nm despite the accelerated dissolution of small particles taking place as well. This fast-shrinking process was enhanced at an increasing salinity of the incubation matrix.

For CA@Ag-NPs (24 nm pristine maximum frequency size), only traces of Ag-b-NPs were detectable after 24 h of incubation in seawater (Fig. 4, Table S1). The maximum frequency particle size was reduced from 24 nm to approximately 10 nm during the entire incubation period (Fig. 5D). Moreover, a fast drop in the NP number was observed after an incubation time of 24 h, whereas particles ≤16 nm accounted for the predominant particulate species (Table 1).

Particle size distributions of Ag$_2$S-NPs (82 nm pristine maximum frequency size) became narrower within the first 24 h of incubation (Fig. 5E), whereby maximum frequency particle sizes were hardly reduced from initially 73 nm to 69 nm. However, we observed a rapid drop in concentration (Fig. 4, Table S1) and particle number (Table 1), whereas NPs ≤30 nm and >30 nm were dissolved equally. As expected, smaller particles were dissolved faster due to their high intrinsic surface. Dramatically shrunk Ag$_2$S-NPs, formerly exhibiting sizes >30 nm, contributed as additional particles ≤30 nm. With decreasing proportion of particles >30 nm and the almost complete dissolution of initial 82 nm particles during the days of incubation, the concentration of smaller particles increased in Fig. 5E. Thus, particles of all sizes were affected by dissolution in seawater, whereas the dissolution of initial 82 nm particles resulted in a large number of remaining particles ≤30 nm.

After only 1 h of incubation, the mean particle size of AgCl-NPs (94 nm pristine maximum frequency size) incubated in seawater massively decreased from 94 nm to 15 nm, whereas the initial broad particle size distribution (approximately ranging from 60–150 nm) was completely reversed after 1 h (Fig. 5F; see also SI, Fig. S6 for another perspective). The experiment started with approximately 800 particles >30 nm (Table 1) and no measurable particles ≤30 nm. But, after only 1 h of incubation in seawater, the

number of particles ≤30 nm increased dramatically to approximately 7'000, and the number of particles >30 nm doubled. This indicates that AgCl-NPs >30 nm were dissolved or even broken up, forming thousands of smaller particles with a broad size range from 8–120 nm. With an increasing incubation time of 24 h or longer, the concentration of particles >30 nm as well as the total concentration of AgCl-NPs still present in seawater was reduced to marginal values. Thus, NPs >30 nm were dissolved quickly in seawater in favor of residual smaller particles, which contribute only very little to the total concentration of NPs present in seawater.

Overall, CPE-sp-ICP-MS allows for the determination of particle sizes of Ag-b-NPs incubated in aqueous matrices at environmentally relevant concentration levels. Particle sizes were reduced, while this process depended on the particle coating and was accelerated by increasing salinity of the incubation media. Regarding long-term incubation of >72 h, no relevant Ag-b-NP concentrations sustained the most extreme conditions seawater constitutes for all kinds of investigated particles. For a short-term observation, however, our results show that larger Ag-b-NPs of >30 nm freshly released into seawater are transformed within 72 h to small particles <30 nm. This may lead to a short-term increase in the environmental (eco)toxicity and bioavailability of these particles, which are believed to be more critical in this respect than larger particles (Kittler et al., 2010).

In addition to the concentration and particle size of Ag-b-NPs, their surface modification and chemical composition influence the (eco)toxicology of these contaminants in the aqueous environment. As a result, we supplemented our examination of Ag-b-NPs in saline matrices with STEM-EDX measurements. No changes in the chemical composition of CA@Ag-NPs and AgCl-NPs after incubation for 1 h in sea water were detected by STEM-EDX. Rather small (d<20 nm) Ag$_2$S-NPs were detected using STEM after incubation in seawater (Fig. 6). Furthermore, TEM images show that Ag$_2$S-NP aggregate and form Ag$_2$S bridges to neighboring particles when being incubated in seawater (SI, Fig. S5, which is not the case for freshly prepared nanoparticle suspensions. This is a fully expected result based on the DLVO theory (Derjaguin and Landau, 1993; Lodeiro et al., 2016; Quik et al., 2014; Verwey, 1947): Increasing ionic strength in sea water reduces particles' stability and thus promotes aggregation. Some of the particles also have cavities. EDX measurement showed that a ratio of Ag:S of 1:1
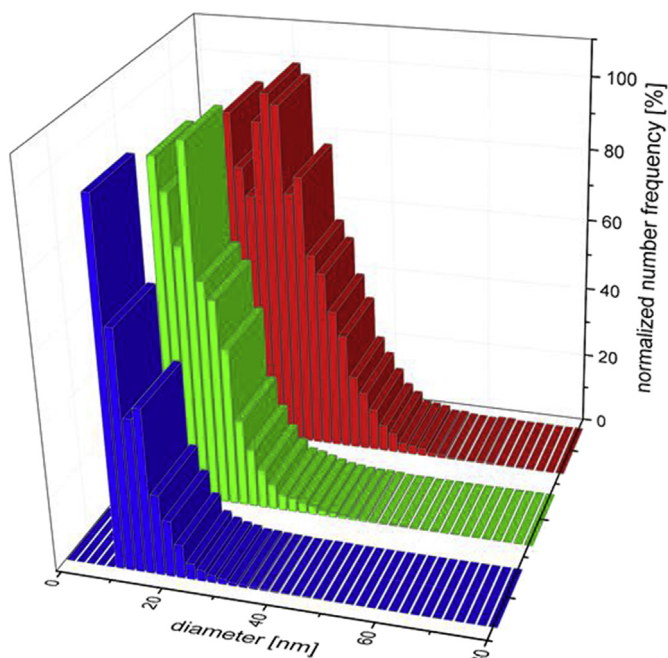
Fig. 7. Particle size distribution of Ag-b-NPs in WWT effluent before (red) and after incubation with (blue) and without (green) added NaCl. Incubation time was set to 72 h. Particles <8 nm were not detectable with sp-ICP-MS. Presented results are based on CPE-sp-ICP-MS measurements. (For interpretation of the references to color in this figure legend, the reader is referred to the Web version of this article.)

occurred in such particles. The signals arising from Mg, Si, among others, came either from the seawater matrix or TEM grids. The changing ratio of Ag:S from the initial 2:1 (Fig. 3) to 1:1 indicates that silver is dissolved while sulfur is accumulating around the particles when incubated in seawater.

3.3. Influence of incubation temperature and natural organic matter

Beyond the influence of nanoparticle coatings and matrix composition on the fate of Ag-b-NPs in seawater, we investigated the effect of increasing incubation temperature on the stability of Ag-b-NPs in real seawater (see SI, Table S2 for detailed measured values). Starting again with 50 ng L^{-1} CA@Ag-NPs (58 nm pristine maximum frequency size), we found that 55% of the initial NPs remained in the solutions after 1 h of incubation at a temperature of 23 °C and 61% at a temperature of 60 °C. After increasing the incubation time to 2 h, 49% of the initial NPs remained at a temperature of 23 °C, and 44% remained at a temperature of 60 °C. Comparable concentrations of remaining NPs independent of the applied incubation temperature indicates that there is no significant temperature effect on the dissolution of Ag-b-NPs in seawater. Similar observations were made for all other types of Ag–b-NPs.

NOM plays an important role in Ag-b-NP transformation processes in aqueous environments. On the one hand, NOM is able to decelerate Ag-b-NP dissolution effects in natural water bodies by blocking potential Ag oxidation sites of the NPs after adsorption, by serving as an oxidative sink in the cooperative redox system by NOM-oxidation, and, finally, by allowing a reversible reaction of formed Ag(I) to Ag(0) with NOM as the reductant (Liu and Hurt, 2010). The last point in particular is crucial for an environmentally relevant system containing dissolved Ag(I) species, since they are readily reduced to Ag(0) by NOM forming new Ag-b-NPs. *Wimmer* et al. have already reported on evidences that this

process takes place in nature and is responsible for the existence of naturally formed Ag-b-NPs in the aqueous environment (Wimmer et al., 2018). As a result, we compared dispersions of CA@Ag-NPs (58 nm pristine maximum frequency size) and Ag$_2$S-NPs (82 nm pristine maximum frequency size) incubated in seawater for 1 h and 72 h with NOM (5 mg L^{-1}) and without NOM (see SI; Table S3 for detailed measured values). For CA@Ag-NPs (58 nm pristine maximum frequency size) after 1 h incubation, we found 74% (83% with NOM) remaining particles, which were reduced to 16% (4%) after 72 h. In the case of Ag$_2$S-NPs (82 nm pristine maximum frequency size), 87% (91% with NOM) of initially inserted NPs remained as particles after 1 h of incubation, whereas only 13% (2%) were left after 72 h. As these values illustrate, NOM did not protect Ag-b-NPs from dissolution in seawater. Within the first hour of incubation, there is no distinct effect of NOM observable, but, after 72 h, NOM increased the dissolved number of NPs for both types of Ag-b-NPs dramatically. In contrast to common expectations, NOM did support Ag-b-NP dissolution. The most likely explanation for this suprising behavior is that NOM forms complexes with dissolved Ag(I) species, removes them from the Ag(0)-Ag(I) equilibrium, and therefore accelerates the dissolution process (Liu and Hurt, 2010).

3.4. Dissolution of Ag-b-NPs in WWTP effluent

The main contamination source, respectively the main entry phase for Ag-b-NPs into the aquatic environment is wastewater released, e.g., by WWTPs. Ag-b-NPs in waste water are usually sulfidized to a large degree and most likely consist of Ag$_2$S (Kaegi et al., 2013). In addition to experiments with synthesized particles of known composition, we also investigated the fate of real particles in freshly sampled WWTP effluent with and without the addition of sodium chloride, which was added to the solutions prior to incubation to obtain a final salt concentration of 31 g L^{-1} NaCl. The initial total Ag-b-NP concentration in the effluent was 17.45 ± 1.19 ng L^{-1} measured with CPE-ICP-MS and 9.19 ± 0.02 ng L^{-1} measured with CPE-sp-ICP-MS, indicating that the solutions contained significant quantities of small particles <8 nm. The mean particle size (based on number frequency) for particles ≥ 8 nm measured by CPE-sp-ICP-MS was 22 nm (pristine maximum frequency size; see Fig. 7). After incubation for 72 h, the solutions contained a total Ag-b-NP concentration of 4.60 ± 0.41 ng L^{-1} and 3.70 ± 0.27 ng L^{-1} for particles ≥8 nm, with a mean particle size of 14 nm (16 nm maximum frequency size). Obviously, Ag-b-NPs contained in the effluent solutions were not stable in this matrix even under dark conditions and the data reveal that mainly small particles were dissolved. The addition of sodium chloride prior to incubation increased particle dissolution dramatically. After an incubation time of 72 h, a total Ag-b-NP concentration of 2.86 ± 0.42 ng L^{-1} and 1.51 ± 0.06 ng L^{-1} for particles ≥8 nm with a mean particle size of 11 nm (10 nm maximum frequency size) was observed. Ag-b-NPs that are present in real environmental samples obviously share the fate of particles investigated in the model experiments described above: Ag-b-NPs dissolve within 72 h to a large extent, whereas the dissolution is accelerated in the presence of chloride. Particle dissolution goes along with the reduced particle sizes presented in Fig. 7. However, dissolution took place more slowly than in the model experiments. A complex interrelation between NOM present in the WWTP effluent (TOC = 2.3 mg L^{-1}) trapping Ag(I) and shifting the equilibrium towards enhanced dissolution (Loza et al., 2014) and the ability of NOM to protect Ag-b-NP from dissolution by reduction of Ag(I) to Ag(0) forming new particles (Toncelli et al., 2017) is, among other things, responsible for decreased dissolution rates. Nevertheless, Ag-b-NPs initially contained in WWTP effluent and

transported by rivers to the sea can be expected to be dissolved within a short period of time.

4. Conclusion

All types of Ag-b-NPs were largely dissolved within a reasonable amount of time, whereby dissolution rates increased with the salinity of the incubation matrix. CA@Ag-NPs (24 nm pristine maximum frequency size) were dissolved significantly faster than CA@Ag-NPs (58 nm pristine maximum frequency size) due to their higher intrinsic surface. Additionally, we particularly examined environmentally more relevant Ag-b-NPs, namely Ag_2S- and AgCl-NPs because these particles are believed to be the most predominant species in the environment (Kaegi et al., 2013; Ma et al., 2014; Nowack et al., 2012; Sharma et al., 2015). Ag_2S-NPs (82 nm pristine maximum frequency size) displayed higher stability compared to AgCl-NPs (94 nm pristine maximum frequency size). All four examined particle types were dissolved almost completely in real seawater within three days.

Ag-b-NPs as a potential threat to marine environmental health is extensively discussed in the literature. However, our results confirm that CA@Ag-NPs in environmentally relevant concentrations are not stable in seawater for more than three days. AgCl-NPs and even Ag_2S-NPs share this fate despite the low solubility of the corresponding salts. Locally arising increased concentrations of soluble Ag(I) species caused by the dissolution of Ag-b-NPs may affect the health of the environment, but only for a limited time, and it may be compensated by a massive dilution effect of Ag(I) in the oceans. Once Ag-b-NPs reach the sea, they are dissolved and no longer constitute a significant risk to environmental health.

Funding

Author contribution

M. Schuster supervised the study. A. Wimmer designed the study and its experimental setup. A. Wimmer carried out incubation experiments and all corresponding analytical measurements assisted by N. Funk, F. Adler, and L. Lenz. A. Wimmer evaluated acquired measurement data. A. Urstoeger synthesized and characterized all types of Ag-b-NPs. M. Doeblinger carried out TEM measurements. A. Urstoeger, assisted by A. Wimmer, and M. Doeblinger evaluated and discussed TEM measurements. A. Wimmer, A. Urstoeger and M. Schuster wrote the manuscript.

Declaration of competing interest

The authors declare that they have no known competing financial interests or personal relationships that could have appeared to influence the work reported in this paper.

Appendix A. Supplementary data

Supplementary data to this article can be found online at https://doi.org/10.1016/j.watres.2019.115399.

References

Ahamed, M., Alsalhi, M.S., Siddiqui, M.K., 2010. Silver nanoparticle applications and human health. Clin. Chim. Acta 411 (23–24), 1841–1848.

Asharani, P.V., Lian Wu, Y., Gong, Z., Valiyaveettil, S., 2008. Toxicity of silver nanoparticles in zebrafish models. Nanotechnology 19 (25), 255102.

Asharani, P.V., Low Kah Mun, G., Hande, M.P., Valiyaveettil, S., 2009. Cytotoxicity and genotoxicity of silver nanoparticles in human cells. ACS Nano 3 (2), 279–290.

Beer, C., Foldbjerg, R., Hayashi, Y., Sutherland, D.S., Autrup, H., 2012. Toxicity of silver nanoparticles—nanoparticle or silver ion? Toxicol. Lett. 208 (3), 286–292.

Derjaguin, B., Landau, L., 1993. Theory of the stability of strongly charged lyophobic sols and of the adhesion of strongly charged particles in solutions of electrolytes. Prog. Surf. Sci. 43 (1), 30–59.

Duester, L., Fabricius, A.-L., Jakobtorweihen, S., Philippe, A., Weigl, F., Wimmer, A., Schuster, M., Nazar, M.F., 2016. Can cloud point-based enrichment, preservation, and detection methods help to bridge gaps in aquatic nanometrology? Anal. Bioanal. Chem. 408 (27), 7551–7557.

Foldbjerg, R., Olesen, P., Hougaard, M., Dang, D.A., Hoffmann, H.J., Autrup, H., 2009. PVP-coated silver nanoparticles and silver ions induce reactive oxygen species, apoptosis and necrosis in THP-1 monocytes. Toxicol. Lett. 190 (2), 156–162.

Gopinath, P., Gogoi, S.K., Sanpui, P., Paul, A., Chattopadhyay, A., Ghosh, S.S., 2010. Signaling gene cascade in silver nanoparticle induced apoptosis. Colloids Surfaces B Biointerfaces 77 (2), 240–245.

Hansen, S.F., Baun, A., 2012. When enough is enough. Nat. Nanotechnol. 7, 409.

Hartmann, G., Baumgartner, T., Schuster, M., 2014. Influence of particle coating and matrix constituents on the cloud point extraction efficiency of silver nanoparticles (Ag-NPs) and application for monitoring the formation of Ag-NPs from Ag+. Anal. Chem. 86 (1), 790–796.

Hartmann, G., Hutterer, C., Schuster, M., 2013. Ultra-trace determination of silver nanoparticles in water samples using cloud point extraction and ETAAS. J. Anal. Atomic Spectrom. 28 (4), 567–572.

Hartmann, G., Schuster, M., 2013. Species selective preconcentration and quantification of gold nanoparticles using cloud point extraction and electrothermal atomic absorption spectrometry. Anal. Chim. Acta 761, 27–33.

Kaegi, R., Voegelin, A., Ort, C., Sinnet, B., Thalmann, B., Krismer, J., Hagendorfer, H., Elumelu, M., Mueller, E., 2013. Fate and transformation of silver nanoparticles in urban wastewater systems. Water Res. 47 (12), 3866–3877.

Kaegi, R., Voegelin, A., Sinnet, B., Zuleeg, S., Hagendorfer, H., Burkhardt, M., Siegrist, H., 2011. Behavior of metallic silver nanoparticles in a pilot wastewater treatment plant. Environ. Sci. Technol. 45 (9), 3902–3908.

Kaegi, R., Voegelin, A., Sinnet, B., Zuleeg, S., Siegrist, H., Burkhardt, M., 2015. Transformation of AgCl nanoparticles in a sewer system - a field study. Sci. Total Environ. 535, 20–27.

Kim, B., Park, C.-S., Murayama, M., Hochella, M.F., 2010. Discovery and characterization of silver sulfide nanoparticles in final sewage sludge products. Environ. Sci. Technol. 44 (19), 7509–7514.

Kim, S., Choi, J.E., Choi, J., Chung, K.H., Park, K., Yi, J., Ryu, D.Y., 2009. Oxidative stress-dependent toxicity of silver nanoparticles in human hepatoma cells. Toxicol. In Vitro 23 (6), 1076–1084.

Kittler, S., Greulich, C., Diendorf, J., Köller, M., Epple, M., 2010. Toxicity of silver nanoparticles increases during storage because of slow dissolution under release of silver ions. Chem. Mater. 22 (16), 4548–4554.

Krug, H.F., 2014. Nanosafety research—are we on the right track? Angew. Chem. Int. Ed. 53 (46), 12304–12319.

Kumar, V., Sharma, N., Maitra, S.S., 2017. In vitro and in vivo toxicity assessment of nanoparticles. Int. Nano Lett. 7 (4), 243–256.

Levard, C., Hotze, E.M., Lowry, G.V., Brown, G.E., 2012. Environmental transformations of silver nanoparticles: impact on stability and toxicity. Environ. Sci. Technol. 46 (13), 6900–6914.

Li, L., Stoiber, M., Wimmer, A., Xu, Z., Lindenblatt, C., Helmreich, B., Schuster, M., 2016. To what extent can full-scale wastewater treatment plant effluent influence the occurrence of silver-based nanoparticles in surface waters? Environ. Sci. Technol. 50 (12), 6327–6333.

Liu, J., Hurt, R.H., 2010. Ion release kinetics and particle persistence in aqueous nano-silver colloids. Environ. Sci. Technol. 44 (6), 2169–2175.

Lodeiro, P., Achterberg, E.P., El-Shahawi, M.S., 2017. Detection of silver nanoparticles in seawater at ppb levels using UV-visible spectrophotometry with long path cells. Talanta 164, 257–260.

Lodeiro, P., Achterberg, E.P., Pampín, J., Affatati, A., El-Shahawi, M.S., 2016. Silver nanoparticles coated with natural polysaccharides as models to study AgNP aggregation kinetics using UV-Visible spectrophotometry upon discharge in complex environments. Sci. Total Environ. 539, 7–16.

Loza, K., Diendorf, J., Sengstock, C., Ruiz-Gonzalez, L., Gonzalez-Calbet, J.M., Vallet-Regi, M., Köller, M., Epple, M., 2014. The dissolution and biological effects of silver nanoparticles in biological media. J. Mater. Chem. B 2 (12), 1634–1643.

Ma, R., Levard, C., Judy, J.D., Unrine, J.M., Durenkamp, M., Martin, B., Jefferson, B., Lowry, G.V., 2014. Fate of zinc oxide and silver nanoparticles in a pilot wastewater treatment plant and in processed biosolids. Environ. Sci. Technol. 48 (1), 104–112.

Millero, F.J., Feistel, R., Wright, D.G., McDougall, T.J., 2008. The composition of standard seawater and the definition of the reference-composition salinity scale. Deep Sea Res. Oceanogr. Res. Pap. 55 (1), 50–72.

Montano, M.D., Olesik, J.W., Barber, A.G., Challis, K., Ranville, J.F., 2016. Single Particle ICP-MS: advances toward routine analysis of nanomaterials. Anal. Bioanal. Chem. 408 (19), 5053–5074.

Nowack, B., Ranville, J.F., Diamond, S., Gallego-Urrea, J.A., Metcalfe, C., Rose, J., Horne, N., Koelmans, A.A., Klaine, S.J., 2012. Potential scenarios for nanomaterial release and subsequent alteration in the environment. Environ. Toxicol. Chem. 31 (1), 50–59.

Park, E.J., Yi, J., Kim, Y., Choi, K., Park, K., 2010. Silver nanoparticles induce

cytotoxicity by a Trojan-horse type mechanism. Toxicol. In Vitro 24 (3), 872—878.

Pasricha, A., Jangra, S.L., Singh, N., Dilbaghi, N., Sood, K.N., Arora, K., Pasricha, R., 2012. Comparative study of leaching of silver nanoparticles from fabric and effective effluent treatment. J. Environ. Sci. 24 (5), 852—859.

Peters, R.J.B., Rivera, Z.H., van Bemmel, G., Marvin, H.J.P., Weigel, S., Bouwmeester, H., 2014. Development and validation of single particle ICP-MS for sizing and quantitative determination of nano-silver in chicken meat. Anal. Bioanal. Chem. 406 (16), 3875—3885.

Pettitt, M.E., Lead, J.R., 2013. Minimum physicochemical characterisation requirements for nanomaterial regulation. Environ. Int. 52, 41—50.

Qian, H., Peng, X., Han, X., Ren, J., Sun, L., Fu, Z., 2013. Comparison of the toxicity of silver nanoparticles and silver ions on the growth of terrestrial plant model Arabidopsis thaliana. J. Environ. Sci. 25 (9), 1947—1956.

Quik, J.T.K., Velzeboer, I., Wouterse, M., Koelmans, A.A., van de Meent, D., 2014. Heteroaggregation and sedimentation rates for nanomaterials in natural waters. Water Res. 48, 269—279.

Ribeiro, M.J., Maria, V.L., Scott-Fordsmand, J.J., Amorim, M.J.B., 2015. Oxidative stress mechanisms caused by Ag nanoparticles (NM300K) are different from those of AgNO(3): effects in the soil invertebrate enchytraeus crypticus. Int. J. Environ. Res. Public Health 12 (8), 9589—9602.

Sharma, V.K., Filip, J., Zboril, R., Varma, R.S., 2015. Natural inorganic nanoparticles - formation, fate, and toxicity in the environment. Chem. Soc. Rev. 44 (23), 8410—8423.

Sun, T.Y., Bornhöft, N.A., Hungerbühler, K., Nowack, B., 2016. Dynamic probabilistic modeling of environmental emissions of engineered nanomaterials. Environ. Sci. Technol. 50 (9), 4701—4711.

Teo, W.Z., Pumera, M., 2014. Fate of silver nanoparticles in natural waters; integrative use of conventional and electrochemical analytical techniques. RSC Adv. 4 (10), 5006—5011.

Toncelli, C., Mylona, K., Kalantzi, I., Tsiola, A., Pitta, P., Tsapakis, M., Pergantis, S.A., 2017. Silver nanoparticles in seawater: a dynamic mass balance at part per trillion silver concentrations. Sci. Total Environ. 601—602, 15—21.

Verwey, E.J.W., 1947. Theory of the stability of lyophobic colloids. J. Phys. Colloid Chem. 51 (3), 631—636.

Wiemann, M., Vennemann, A., Blaske, F., Sperling, M., Karst, U., 2017. Silver nanoparticles in the lung: toxic effects and focal accumulation of silver in remote organs. Nanomaterials 7 (12), 441.

Wimmer, A., Kalinnik, A., Schuster, M., 2018. New insights into the formation of silver-based nanoparticles under natural and semi-natural conditions. Water Res. 141, 227—234.

Wise, J.P., Sr, Goodale, B.C., Wise, S.S., Craig, G.A., Pongan, A.F., Walter, R.B., Thompson, W.D., Ng, A.K., Aboueissa, A.M., Mitani, H., Spalding, M.J., Mason, M.D., 2010. Silver nanospheres are cytotoxic and genotoxic to fish cells. Aquat. Toxicol. 97 (1), 34—41.

Zhang, J.L., Zhou, Z.P., Pei, Y., Xiang, Q.Q., Chang, X.X., Ling, J., Shea, D., Chen, L.Q., 2018. Metabolic profiling of silver nanoparticle toxicity in Microcystis aeruginosa. Environ. Sci.: Nano 5 (11), 2519—2530.

Zhang, W., Yao, Y., Sullivan, N., Chen, Y., 2011. Modeling the primary size effects of citrate-coated silver nanoparticles on their ion release kinetics. Environ. Sci. Technol. 45 (10), 4422—4428.

Zhou, X.-x., Li, Y.-j., Liu, J.-f., 2017. Highly efficient removal of silver-containing nanoparticles in waters by aged iron oxide magnetic particles. ACS Sustain. Chem. Eng. 5 (6), 5468—5476.

Supplementary Information

What happens to silver-based nanoparticles if they meet seawater?

Andreas Wimmer[1,#], Alexander Urstoeger[1,#], Nils Christoph Funck[1], Franziska Petra Adler[1],

Leonhard Lenz[1], Markus Doeblinger[2], Michael Schuster[1,*]

[1] Division of Analytical Chemistry, Department of Chemistry, Technical University of Munich,

Garching 85748, Germany

[2] Department of Chemistry, Ludwig-Maximilians-Universität München, Butenandtstr. 5–13 (E),

81377 Munich, Germany

[#] These authors contributed equally to the presented study.

[*] Corresponding author. Tel: +49 (0)89 289 13763; fax: +49 (0)89 289 14513; E-mail address:

michael.schuster@ch.tum.de

10 pages

6 Figures

3 Tables
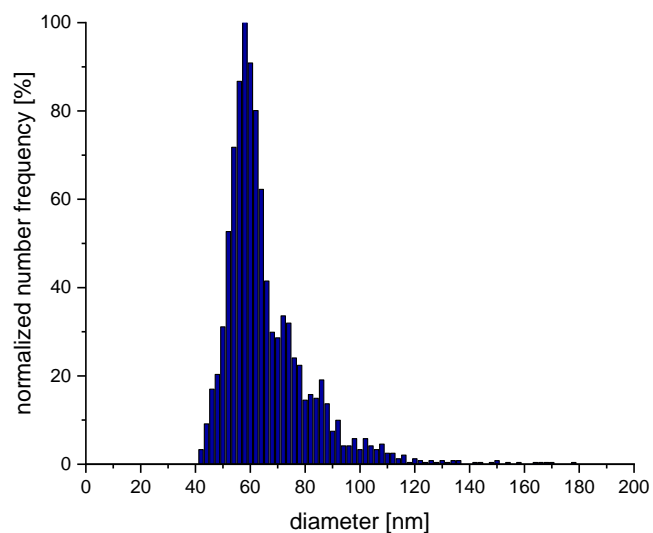
Figure S1: Particle size distribution based on particle number frequency of CA@Ag-NPs obtained from sp-ICP-MS measurement. The maximum frequency particle size is 58 nm.
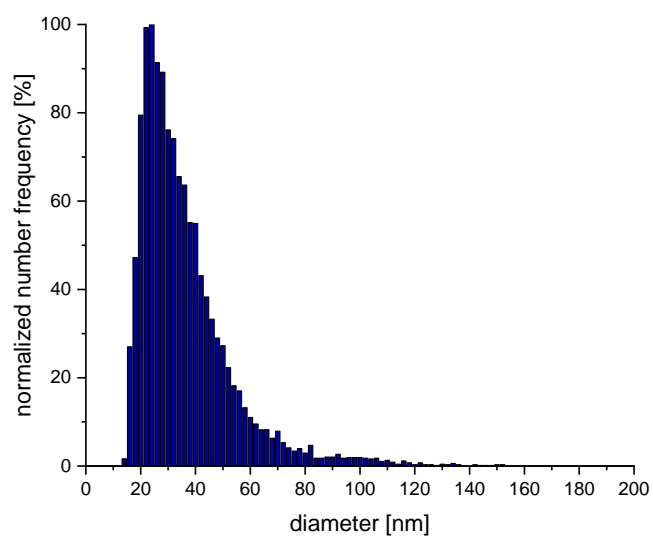
Figure S2: Particle size distribution based on particle number frequency of CA@Ag-NPs obtained from sp-ICP-MS measurement. The maximum frequency particle size is 24 nm.
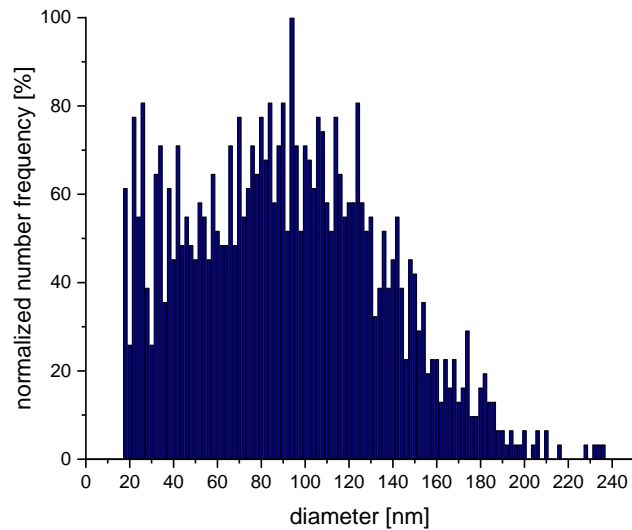
Figure S3: Particle size distribution based on particle number frequency of synthesized AgCl-NPs obtained from sp-ICP-MS measurement. The maximum frequency particle size is 94 nm.
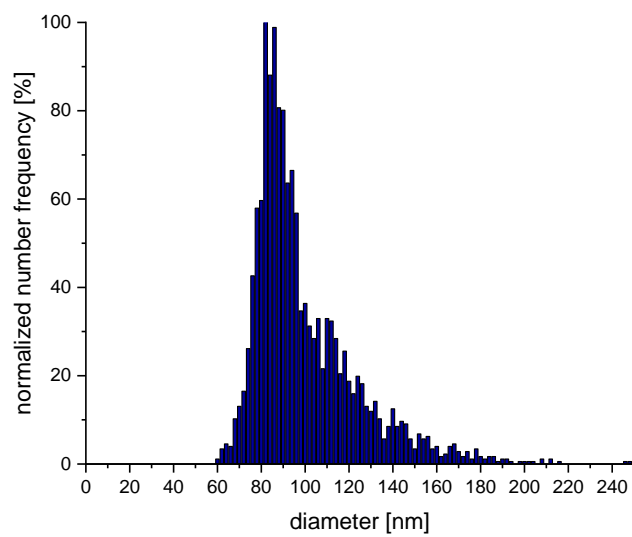
Figure S4: Particle size distribution based on particle number frequency of synthesized Ag$_2$S-NPs obtained from sp-ICP-MS measurement. The maximum frequency particle size is 82 nm.

Table S1: Compilation of measured Ag concentrations of total Ag-b-NPs (conventional ICP-MS) and Ag-b-NPs ≥ 8 nm (sp-ICP-MS) after incubation in ultra-pure water, artificial sea water and real sea water for a defined period of time supplemented by corresponding uncertainties U, the proportion of Ag-b-NPs < 8 nm in each sample and the proportion of remaining Ag-b-NPs in each incubation experiment. Given particle sizes represent the pristine maximum frequency particle sizes without incubation in the investigated media. "---" indicates measurements, in which no concentration beyond the limit of detection (LOD = 0.2 ng L^{-1}) could be detected.

incubation time [h]	Ag concentration of total Ag-b-NPs [ng L^{-1}]	U [ng L^{-1}]	Ag concentration of Ag-b-NPs ≥8nm [ng L^{-1}]	U [ng L^{-1}]	proportion Ag-b-NPs <8 nm [%]	proportion of remaining Ag-b-NPs [%]
CA@Ag 24 nm	ultra-pure water					
0	49.13	0.78	47.07	1.21	4.2	100
1	37.76	0.61	34.00	0.95	10.0	77
2	28.93	0.45	26.64	3.55	7.9	59
3	0.35	0.22	0.13	0.17	62.7	1
24	7.14	0.17	6.16	3.98	13.8	15
48	6.97	0.55	7.53	3.15	0.0	14
72	5.03	0.62	5.36	1.38	0.0	10
CA@Ag 58 nm	ultra pure water					
0	51.62	1.09	51.11	1.45	1.0	100
1	45.35	2.15	45.46	2.75	0.0	88
2	41.08	1.04	40.55	3.03	1.3	80
3	45.15	0.59	45.26	0.35	0.0	87
24	30.24	1.00	29.49	6.66	2.5	59
48	20.76	1.39	20.93	5.04	0.0	40
72	21.61	0.63	21.62	2.19	0.0	42
AgCl 94 nm	ultra pure water					
0	52.15	1.35	51.74	1.68	0.8	100
1	23.63	1.74	19.47	0.99	17.6	45
2	17.01	1.10	13.71	1.19	19.4	33
3	13.38	1.87	10.93	1.32	18.3	26
24	8.10	1.00	4.37	0.66	46.0	16
48	1.47	0.54	1.22	0.44	16.9	3
72	0.28	0.16	0.07	0.03	75.6	1
Ag$_2$S 82 nm	ultra pure water					
0	65.27	1.45	65.82	2.04	0.0	100
1	51.60	9.34	56.19	4.56	0.0	79
2	63.32	9.34	56.52	4.96	10.7	97
3	44.71	5.17	51.18	8.68	0.0	69
24	24.91	4.65	16.18	1.47	35.0	38
48	19.91	6.21	14.58	3.71	26.7	30
72	17.00	0.79	14.29	0.20	16.0	26

CA@Ag 24 nm	artificial sea water					
0	53.37	1.02	50.53	1.45	5.3	100
1	22.49	1.45	20.15	0.27	10.4	42
2	17.39	1.12	13.56	1.92	22.0	33
3	1.36	1.18	0.00	0.00	100.0	3
24	2.83	0.14	2.55	1.23	10.2	5
48	1.93	0.21	1.34	0.16	30.7	4
72	1.52	0.40	1.02	0.13	33.3	3

CA@Ag 58 nm	artificial sea water					
0	55.25	2.45	54.74	0.67	0.9	100
1	27.76	0.70	27.02	1.81	2.7	50
2	22.06	0.78	20.28	0.68	8.1	40
3	21.46	1.69	20.15	1.59	6.1	39
24	8.49	1.06	7.21	2.98	15.1	15
48	2.33	0.56	1.91	0.91	17.8	4
72	2.41	0.34	1.91	0.91	20.7	4

AgCl 94 nm	artificial sea water					
0	46.02	1.45	39.19	3.47	14.8	100
1	9.05	0.99	8.98	1.92	0.8	20
2	6.79	1.32	6.46	0.61	4.9	15
3	2.34	0.59	2.88	1.54	0.0	5
24	5.31	0.85	0.74	0.61	86.1	12
48	0.86	0.24	2.34	1.57	0.0	2
72	0.41	0.34	0.88	0.52	0.0	1

Ag₂S 82 nm	artificial sea water					
0	59.23	1.33	59.11	1.05	0.2	100
1	22.99	1.54	28.76	1.80	0.0	39
2	17.39	3.25	16.17	4.43	7.0	29
3	13.02	1.18	14.04	1.38	0.0	22
24	4.29	0.09	0.88	0.72	79.5	7
48	2.88	0.42	0.50	0.19	82.7	5
72	6.44	0.32	3.99	0.57	38.1	11

CA@Ag 24 nm	sea water					
0	52.04	1.56	50.23	1.23	3.5	100
1	16.21	0.34	13.12	0.64	19.1	31
2	12.98	0.24	10.54	1.34	18.8	25
3	0.98	0.12	0.42	0.52	56.9	2
24	---	---	0.14	0.06	---	0
48	---	---	0.25	0.07	---	0
72	---	---	0.17	0.07	---	0

CA@Ag 58 nm	sea water					
0	47.50	1.21	47.92	1.59	0.0	100
1	20.37	4.32	22.50	0.57	0.0	43
2	14.00	2.95	12.59	1.74	10.0	29
3	2.86	1.15	5.98	0.76	0.0	6
24	1.81	0.30	1.33	0.11	26.9	4

48	4.90	0.44	8.19	0.73	0.0	10
72	0.62	0.25	1.78	0.22	0.0	1
AgCl 94 nm	sea water					
0	47.98	0.92	47.34	1.34	1.3	100
1	8.99	0.82	5.60	0.62	37.7	19
2	6.29	0.99	0.29	0.22	95.4	13
3	4.14	0.73	0.11	0.08	97.3	9
24	2.09	0.79	0.43	0.19	79.5	4
48	1.01	0.18	0.26	0.07	74.2	11
72	0.96	0.50	0.26	0.07	72.8	2
Ag$_2$S 82 nm	sea water					
0	52.67	1.01	50.58	1.36	4.0	100
1	26.26	3.12	19.61	1.03	25.3	50
2	18.47	2.79	16.61	0.45	10.1	35
3	12.65	2.45	9.29	2.05	26.5	24
24	2.67	0.83	2.62	1.00	1.8	5
48	2.03	0.65	2.18	0.83	0.0	4
72	2.77	1.06	2.12	0.46	23.2	5
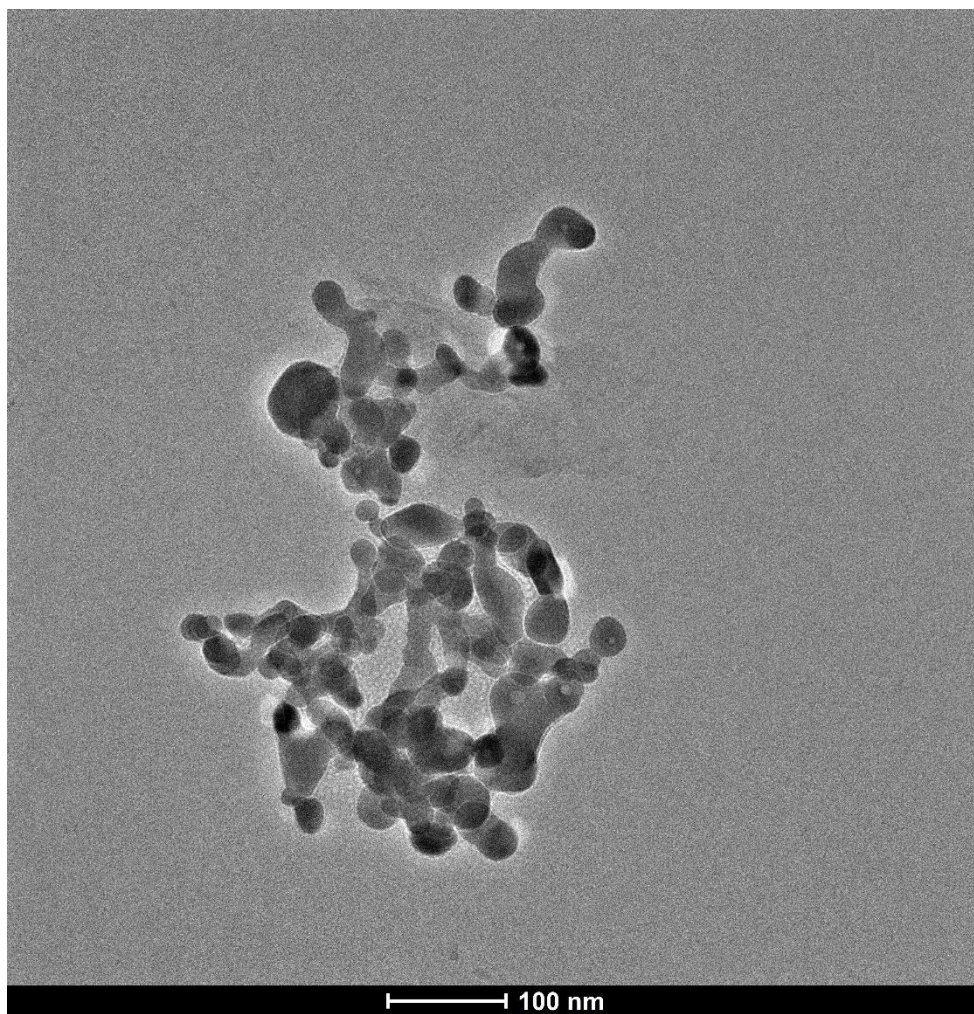
Figure S5: TEM image of an Ag$_2$S-NP aggregate after incubation in seawater for 1 h.
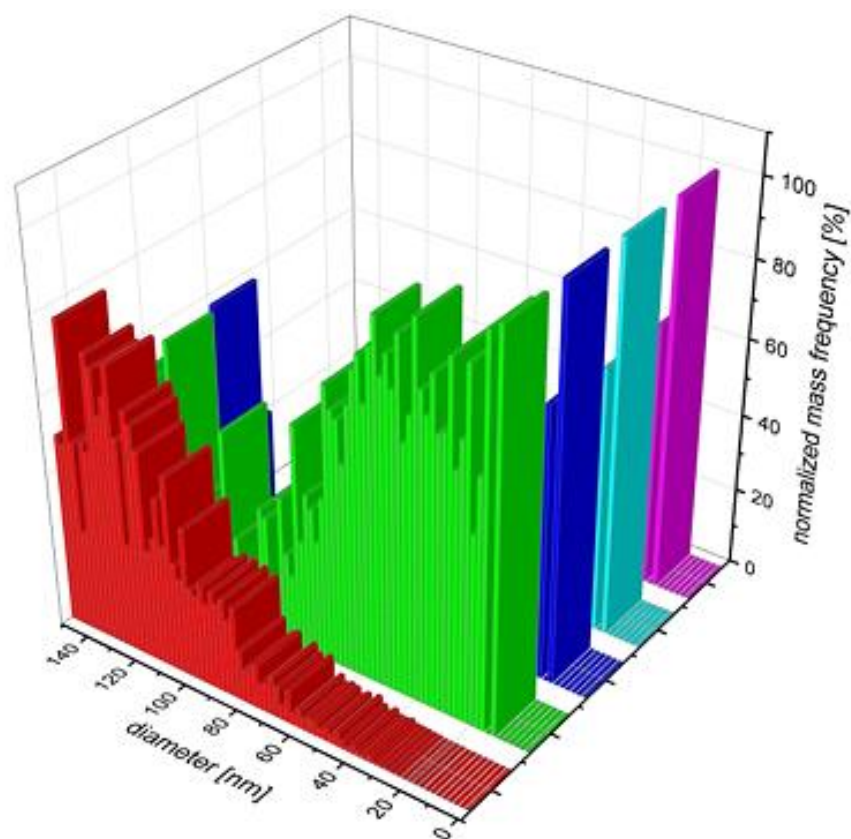
Figure S6: Particle size distributions of pristine (red) AgCl-NPs and incubated in seawater for 1 h of incubation (green), 1 day of incubation (blue), 2 days of incubation (turquiose), and 3 days of incubation (purple) presented as normalized mass frequency. Presented results are based on CPE-sp-ICP-MS measurements.

Table S2: Compilation of measured Ag concentrations of total Ag-b-NPs (conventional ICP-MS) after incubation in real sea water for a defined period of time at 23 °C and 60 °C supplemented by corresponding uncertainties U and the proportion of remaining Ag-b-NPs in each incubation experiment. Given particle sizes represent the pristine maximum frequency particle sizes without incubation in the investigated media.

incubation time [h]	Ag concentration of total Ag-b-NPs [ng L^{-1}]	U [ng L^{-1}]	proportion of remaining Ag-b-NPs [%]
CA@Ag 58 nm	**23 °C incubation temperature**		
0	48.45	0.33	100
1	26.59	0.44	55
2	23.64	0.21	49
CA@Ag 58 nm	**60 °C incubation temperature**		
0	49.62	0.82	100
1	30.19	1.05	61
2	22.05	0.45	44

Table S3: Compilation of measured Ag concentrations of total Ag-b-NPs (conventional ICP-MS) after incubation in aqueous solutions of NOM for an increasing incubation time supplemented by corresponding uncertainties U and the proportion of remaining Ag-b-NPs in each incubation experiment. Given particle sizes represent the pristine maximum frequency particle sizes without incubation in the investigated media.

incubation time [h]	Ag concentration of total Ag-b-NPs [ng L^{-1}]	U [ng L^{-1}]	proportion of remaining Ag-b-NPs [%]
CA@Ag 58 nm	**0 mg L^{-1} NOM**		
0	51.34	0.56	100
1	37.80	0.33	74
72	8.32	0.56	16
CA@Ag 58 nm	**5 mg L^{-1} NOM**		
0	49.88	0.41	100
1	41.54	0.65	83
72	1.98	0.09	4
Ag$_2$S 82 nm	**0 mg L^{-1} NOM**		
0	52.05	0.38	100
1	45.38	0.56	87
72	6.93	0.11	13
Ag$_2$S 82 nm	**5 mg L^{-1} NOM**		
0	47.79	0.36	100
1	43.65	0.26	91
72	1.08	0.08	2

8.9   PUBLIKATION 9

New Insights into the formation of silver-based nanoparticles under natural and semi-natural conditions
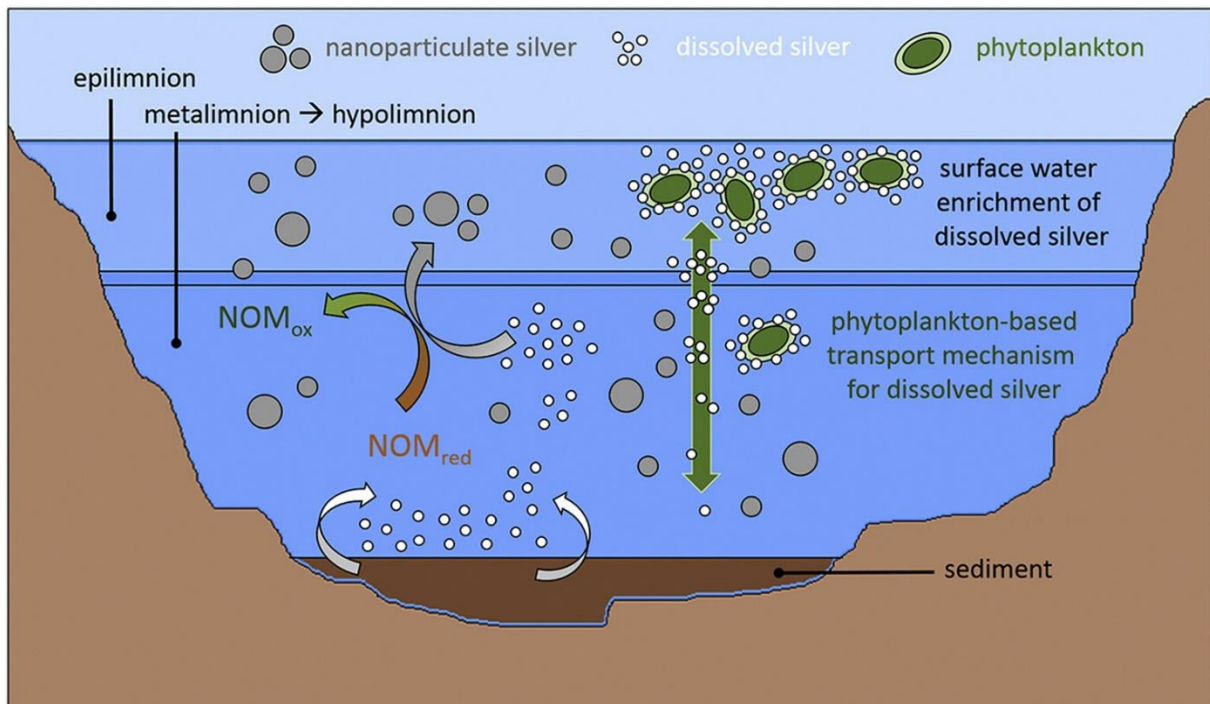
Andreas Wimmer, Anna Kalinnik, and Michael Schuster

New insights into the formation of silver-based nanoparticles under natural and semi-natural conditions

Andreas Wimmer, Anna Kalinnik, Michael Schuster[*]

Division of Analytical Chemistry, Department of Chemistry, Technical University of Munich, Garching, 85748, Germany

ABSTRACT

For the first time, the natural formation of silver-based nanoparticles (Ag-b-NPs) was studied in field investigations of two pre-alpine lakes in Germany that contain geogenic silver traces in the sub-ng L^{-1} range. Light-sensitive microorganisms most likely accumulate and transport these silver traces from deeper water layers to the surface. At the surface of the eutrophic lake, approximately 40% of total silver (5.7 ng L^{-1}) consisted of Ag-b-NPs, whereas in the oligotrophic lake with similar enrichment of silver species, no Ag-b-NPs were detected. Additional lab experiments with nature-related Ag(I) concentrations in the lower-ng L^{-1} range and natural o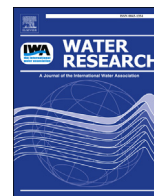rganic matter with total organic carbon values of ≤ 5 mg L^{-1} revealed that, contrary to common interpretation in the literature, Ag-b-NPs are also or even preferably formed in the dark. Particle size increases gradually with increasing reaction time, showing that Ostwald ripening occurs even at such low particle concentrations. When sulfide ions are present, smaller Ag-b-NPs with a narrower size distribution are formed.

© 2018 Elsevier Ltd. All rights reserved.

1. Introduction

Numerous studies on sources of engineered silver nanoparticles (EAgNPs) and their possible release and distribution in the environment have already been reported (Benn et al., 2010; Colman et al., 2014; Kim et al., 2010; Li et al. 2013, 2016; Mittelman et al., 2015). Because of a lack of analytical techniques with sufficient selectivity and detection power, most of these studies were performed by spiking natural or semi-natural samples with EAgNPs, typically in the mg L^{-1} and μg L^{-1} ranges, and by modeling based on dynamic probabilistic material flow analysis (Gottschalk et al. 2009, 2013; Sun et al. 2014, 2015; Tan et al., 2017). In a recent study, the lower ($Q_{0.15}$) and upper ($Q_{0.85}$) concentrations of EAgNPs present in surface waters were estimated to be 0.40 and 2.78 ng L^{-1} (Sun et al., 2016). These values are consistent with the findings of our previous study in which we described, for the first time, the distribution of real silver-based nanoparticles (Ag-b-NPs) in representative wastewater treatment plants (WWTPs) that use different input and treatment technologies.

Additionally, we clarified the extent to which the effluent of WWTPs influences the concentration of Ag-b-NPs along a river. A gradual progressive increase in the Ag-b-NP level of the river over a distance of 150 km with a final Ag-b-NP concentration of 1.7 ng L^{-1} was found (Li et al. 2013, 2016). More importantly, we further observed that surrounding lakes, which do not receive WWTP effluent, also showed measurable Ag-b-NP concentrations, with levels ranging from 0.5 to 1.3 ng L^{-1}, indicating that Ag-b-NPs might be formed naturally via the reduction of Ag(I) species by natural organic matter (NOM).

It has already been demonstrated that both humic and fulvic acids from different sources (river, sediment and soil) can reduce Ag(I) to Ag-b-NPs at elevated temperatures (e.g., at 90 °C) (Adegboyega et al., 2013; Akaighe et al., 2011). Also, irradiation with artificial sunlight was reported to be a key factor for reduction of Ag(I) to Ag-b-NPs by NOM in the aquatic environment (Hou et al., 2013; Lu et al., 2016; Yin et al. 2012, 2014). However, these laboratory studies were performed at NOM concentrations as high as 100 mg L^{-1} and Ag(I) concentrations as high as 200 mg L^{-1} (Adegboyega et al., 2013; Akaighe et al., 2011; Hou et al., 2013; Lu et al., 2016; Sharma et al., 2015; Yin et al. 2012, 2014), strongly exceeding the concentrations of silver (pg L^{-1} to ng L^{-1}) and NOM (typically < 10 mg L^{-1}) in natural waters (Silvestry-Rodriguez et al., 2008).

Robust and extensively validated analytical methods recently developed by our group (Duester et al., 2016; Hartmann et al. 2013, 2014; Li et al. 2013, 2016) enable the measurement of Ag-b-NPs even in complex matrices such as WWTP influents, ensuring high species selectivity and a limit of detection (LOD) as low as $0.2 \, ng \, L^{-1}$. In combination with single-particle inductively coupled plasma mass spectrometry (spICP-MS), size-selective measurements with a LOD of $0.25 \, ng \, L^{-1}$ for particles as small as 10 nm can also be performed, paving the way for a more comprehensive understanding of the formation of Ag-b-NPs under natural conditions.

For this purpose, we studied the natural formation of Ag-b-NPs in lakes with different eutrophication degrees, which do not receive silver from anthropogenic sources. These results are compared with the results of similar measurements performed in a lake located in the same area that is polluted with Ag-b-NPs from WWTP effluent.

The measurements in the natural environment are supplemented by laboratory experiments with nature-related silver and NOM concentrations. The effects of light irradiation, NOM content, incubation time as well as temperature and the presence of sulfide on the formation and size distribution of Ag-b-NPs are studied in detail.

In this study, we use the term Ag-b-NPs to reflect the fact that silver can form a confusing diversity of nanosized particles with different sizes, morphologies, compositions, and surface coatings, which usually cannot be fully characterized at environmentally relevant concentrations with current analytical techniques. Moreover, Ag-b-NPs exhibit very dynamic behavior, such as Ostwald ripening, even at very low naturally occurring particle concentrations.

2. Material and methods

2.1. Materials

All chemicals were at least of analytical grade and were used without further purification. Ultra-pure water (UPW) with a resistivity of $18.2 \, M\Omega \, cm^{-1}$ was obtained from a Direct-Q system (Millipore, Billerica, USA). NOM from the Suwannee River (SRNOM) — a reference material from the International Humic Substance Society (IHSS) — was used for all experiments involving NOM-induced Ag-b-NP formation. We prepared a NOM stock solution with a TOC concentration of $20 \, mg \, L^{-1}$ by dissolving the dry powder in UPW. ICP-MS measurements revealed trace impurities of $3 \, ng \, L^{-1}$ Ag in this NOM stock solution, which did not affect the experiments and conclusions. An AuNP dispersion (particle size: 56 nm; NIST reference material 8013) used for spICP-MS calibration was obtained from the National Institute of Standards and Technology (Gaithersburg, MD, USA). AgNP dispersions (particle size: 60 nm; $cAgNP = 20 \, mg \, L^{-1}$) used for ET-AAS calibration were obtained from Sigma-Aldrich (St. Louis, MO, USA). The used dissolved Ag(I) standard ($1000 \, mg \, L^{-1}$) was based on $AgNO_3$ in 3% HNO_3. Triton TX-114 was used as a surfactant for the nanoparticle extraction procedure, D-penicillamine and disodium ethylenediaminetetraacetate were used as complexing agents, and acetic acid (glacial) and sodium acetate (anhydrous) were used for pH buffering. All glassware was thoroughly cleaned by being rinsed with 6.5% HNO_3 solution, followed by steaming with HNO_3 vapor for 4 h and triplicate washing with UPW prior to use.

2.2. Lake water collection

We sampled lake water from two natural lakes in Bavaria, Germany. Sampling sites are shown in Fig. A1; Table A1 contains the corresponding coordinates (GPS data). The lakes were carefully chosen to represent a typical oligotrophic lake (Lake Königssee) and a eutrophic lake (Lake Waginger See). Table A1 gives more detailed information about the lakes. For each site, we collected samples at different depths (to at least 10 m depth) using a LIMNOS water sampler (Hydro-Bios, Kiel, Germany). Lake Waginger See was sampled to the ground (max. 23 m), which was not possible for Lake Königssee with a maximum depth of 190 m. All water samples were collected in new, one-way polyvinyl chloride (PVC) containers (500 mL), which were rinsed threefold with the sample before they were filled to volume. Immediately after collecting each sample, we measured its temperature and pH using a pH 110 handheld measurement system (VWR, Darmstadt, Germany).

2.3. Instrumentation

For ET-AAS measurements, we used an AAnalyst 800 instrument (Perkin Elmer, Waltham, MA, USA) equipped with a transversally heated graphite atomizer THGA 800 and an AS-72 autosampler. A silver hollow-cathode lamp (Maasen GmbH, Reutlingen, Germany) as the light source for AAS measurements was operated at the recommended current of 10 mA. We integrated the AAS signal over 5 s at the absorption line $\lambda = 328.1 \, nm$ to quantify the silver in the samples. High-purity argon (99.998%) was used as an inert gas during the measurements.

We measured the total silver concentration and AgNP size distribution in single-particle mode (target mass ^{107}Ag) with a 7900 ICP-MS instrument (Agilent Technologies, Santa Clara, CA, USA) equipped with an autosampler (ASX-520). The Agilent MassHunter Workstation 4.4 software (version C.01.04, build 544.3) was used for data evaluation. The dwell time was set to $100 \, \mu s$, resulting in 600,000 data points for an acquisition time of 1 min. The pump rate was gravimetrically determined as $0.316 \, mL \, min^{-1}$. For calibration, we followed the recently published protocol (Peters et al., 2014). In brief, we determined the transport efficiency, i.e., the part of all sample particles finally reaching the detector, for the spICP-MS measurement using AuNP NIST reference material 8013. The transport efficiency for Au and Ag are identical; however, AuNPs are more stable than AgNPs and are available as a certified reference material. We carried out a second calibration using a $1 \, \mu g \, L^{-1}$ dissolved silver standard solution ($AgNO_3$ in HNO_3) in single-particle mode to determine element sensitivity. All optimized system parameters for spICP-MS mode are given in Table A3.

We performed total silver concentration measurements by ICP-MS with ^{107}Ag as the target mass driven in helium collision mode. As internal standards, we chose ^{151}Eu and ^{115}In. The measured lake water samples were not filtered but were stabilized by the addition of 3.25% (w/w) HNO_3. For calibration, we applied a properly diluted Ag(I) stock solution ($1000 \, mg \, L^{-1}$ in HNO_3) to obtain calibration solutions in the upper $pg \, L^{-1}$ and lower $ng \, L^{-1}$ range.

We conducted TOC measurements of all real environmental samples, which were measured undiluted without filtration, using a TOC-L CSH/CSN analyzer (Shimadzu, Kyoto, Japan). All samples were mixed thoroughly seconds before the TOC analysis started. For calibration, we prepared standard solutions containing 10 and $100 \, mg \, L^{-1}$ TOC based on potassium hydrogen phthalate solutions in UPW.

2.4. Selective enrichment of Ag-b-NPs from water samples

We used cloud point extraction (CPE), a robust and thoroughly validated method developed by our group (Duester et al., 2016; Hartmann et al. 2013, 2014; Li et al., 2016), to separate and enrich Ag-b-NPs from environmental and artificial samples. Dissolved Ag(I) species and matrix components are efficiently retained by this procedure, paving a way to an undisturbed and highly sensitive measurement of Ag-b-NPs, e.g., by CPE-ET-AAS or CPE-spICP-MS.

For CPE, we mixed 40-mL samples containing Ag-b-NPs and Ag(I) species with 3.0 mL of saturated ethylendiaminetetraacetic acid disodium salt (EDTA) solution, 1.0 mL of saturated D-penicillamine solution, 400 μL of 1 M sodium acetate solution, 100 μL of 1.25 M acetic acid, and 1 mL of 10% (w/w) TX-114 in 50-mL tapered polypropylene sample tubes. The mixtures were incubated at 40 °C for 30 min. After centrifugation (12 min, 4500 g) the samples were cooled for 5 min in an ice bath; the aqueous supernatants were subsequently removed by decanting. The remaining viscous surfactant droplets containing the enriched and separated Ag-b-NPs were diluted either with ethanol for ET-AAS measurement or with ethanol and UPW for ICP-MS measurement.

2.5. Determination of Ag-b-NPs by ET-AAS

ET-AAS is very sensitive for silver and requires a sample volume of only 20 μL. Organic matrix constituents can be easily eliminated with an appropriate furnace temperature program, which has already been described in our previous publications (Hartmann et al. 2013, 2014; Hartmann and Schuster, 2013; Li et al., 2013). ET-AAS uses a high-precision pipetting system for sample application, which can handle small solvent volumes with higher viscosity. Therefore, we diluted the surfactant droplet obtained by CPE with only 100 μL of ethanol, allowing for a high enrichment factor of 80 and an LOD for silver as low as $0.2 \, \text{ng L}^{-1}$. We calibrated the system identically to the CPE procedure used for ET-AAS measurement. For this purpose, we applied particle stock solutions of 60 nm citrate-coated AgNPs, which were freed from impurities of dissolved silver species by dialysis prior to use.

2.6. Determination and size distribution of Ag-b-NPs by spICP-MS

ICP-MS uses nebulizers for sample introduction, which cannot handle highly concentrated surfactant solutions. Therefore, we diluted the surfactant droplet obtained by CPE with 400 μL of ethanol and UPW to a total volume of 10 mL. Additionally, we prepared all calibration solutions and dispersions in the same uniform manner. Because of the almost complete separation of particles from dissolved silver species by the CPE procedure, the limit of detection for particles measured by spICP-MS was improved substantially and the smallest detectable particle size was reduced, leading to a hitherto unequaled LOD of $0.25 \, \text{ng L}^{-1}$ for particles as small as 10 nm.

2.7. Sample preparation for NOM- and sulfide-induced formation of Ag-b-NPs under semi-natural conditions

To observe potential Ag-b-NP formation from dissolved Ag(I) species under the influence of NOM, we added a solution of dissolved Ag(I) ($AgNO_3$ in 3% HNO_3) to 40 mL of aqueous SRNOM solutions representing TOC concentrations of 0, 1, and $5 \, \text{mg L}^{-1}$, yielding in a final Ag(I) concentration of $50 \, \text{ng L}^{-1}$. One-way polypropylene vials were used as reaction vessels, which were wrapped with several layers of aluminum foil to prevent the incidence of light. Control experiments allowing the incidence of light were also performed. For these experiments, we used glass vessels, which allow better light transmission. In addition to reaction samples containing dissolved Ag(I), we prepared reference samples containing NOM but no Ag(I) to observe potential silver backgrounds related to the NOM material. Furthermore, we added 1 mL of HOAc/NaOAc pH buffer (8.203 g NaOAc in 3.29 mL of HOAc and 36.71 mL of UPW) to each reaction mixture. We prepared all NOM/Ag(I) combinations in triplicate to assess the reproducibility of NOM-induced formation experiments. The mixtures were incubated for 24 h at 7 and 23 °C. Afterwards, we added 50 μL of a 0.1 M NH_3

solution to adjust the pH of the sample and the mixtures were then subjected to Ag-b-NP concentration analysis by CPE-ET-AAS and CPE-spICP-MS for determination of their particle concentrations and size distributions, respectively. In a second experimental setup, we investigated the influence of dissolved sulfide. We prepared all NOM/Ag(I) model mixtures as previously described, whereas 160 μL of 4 mM Na_2S solution, which was obtained by dissolving 0.6632 g of Na_2S in 5 mL of UPW, was added to all samples. Sulfide was added ultimately to ensure identical reaction times for all samples.

3. Results and discussions

3.1. Formation of Ag-b-NPs in natural lakes

In this study, we investigated two dimictic, mainly groundwater-fed, natural lakes located within the pre-alpine area in southern Germany. The lakes with different eutrophication degrees (see Table A1) were investigated with respect to the proportion of Ag-b-NPs as a part of the total silver concentration at various water depths. Both lakes showed similar total silver concentrations of 0.84 ± 0.52 (lowest value) to $5.69 \pm 0.33 \, \text{ng L}^{-1}$ (highest value) within the upper water layers (see Table A2). The lakes as well as their small tributaries do not receive WWTP effluent, which might contain silver species from anthropogenic sources. The oligotrophic fjord-like Lake Königssee (volume: $5 \times 10^8 \, \text{m}^3$; max. depth: 190 m) exhibits a high water quality (total phosphorus (TP): $5 \, \mu\text{g L}^{-1}$; visibility depth: 10.5 m). Motor boats are not allowed, and there are no agricultural influences. The eutrophic Lake Waginger See (TP: $24 \, \mu\text{g L}^{-1}$; visibility depth: 2.8 m; volume: $9 \times 10^7 \, \text{m}^3$; max. depth: 27 m) is protected from WWTP effluent by a perimeter sewerage system, whereas the lake clearly shows agricultural influences. Nevertheless, fertilization with sewage sludge, a potential source for the introduction of Ag-b-NPs or other silver species into the lake, is not applied around the lake and tributaries.

Unfortunately, very little is known about natural silver concentrations in the hydrosphere. The estimated silver concentration in the oceans is $0.04 \, \text{ng L}^{-1}$ (Schutz and Turekian, 1965); other authors (Ranville and Flegal, 2005) have reported oceanic silver concentrations ranging from 0.02 to $10.5 \, \text{ng L}^{-1}$, depending on the location where the samples were collected. The silver concentrations measured in the pre-alpine lakes lie within this concentration range. We therefore anticipate that the measured silver concentrations are of geogenic origin.

Total organic carbon (TOC) as a measure of NOM concentration in the lakes is consistent with the eutrophication degree ranging from an average of $1.32 \, \text{mg L}^{-1}$ (Lake Königssee) to $5.10 \, \text{mg L}^{-1}$ (Lake Waginger See), whereby only negligible variations of the TOC values were observed with increasing water depth (see Table A2). This consistency also applies to the weakly basic pH values, which range from 7.7 to 8.3.

We examined Lake Waginger See in April 2017 during the beginning of thermal stratification. Lake Königssee was examined in September 2016 and showed a pronounced thermal stratification with a distinct thermocline between the epilimnion and the metalimnion. In the case of Lake Waginger See, we collected samples from the surface of the lake to its bottom. Lake Königssee is very deep (100 m–190 m); we therefore only collected samples to the upper metalimnion, which was identical with the visibility depth at this time.

In both lakes, the highest total silver concentrations were always observed near the water surface and the concentrations gradually decreased with increasing water depth. In Lake Königssee, we could not detect any silver ($<0.77 \, \text{ng L}^{-1}$) in the transition zone between

the epilimnion and the metalimnion or in the metalimnion to the visibility depth of approximately 10 m. This observation is interesting because it implies that there must be a mechanism that transports silver species from lower water layers to the surface of the lake. The most likely explanation for this unexpected observation is that light-sensitive microorganisms, e.g., cyanobacteria, which are omnipresent in the pre-alpine lakes, accumulate silver and transport it to the surface of the lake, where the light intensity for photosynthesis is highest.

In natural and in contaminated water bodies, microorganisms can serve as a major sink for heavy metals (Acharya and Apte, 2013; Anjana et al., 2007; Awasthi and Rai, 2004; Blanco et al., 1999; Cain et al., 2008; Markou et al., 2015). Cyanobacteria, for example, can bind heavy metal species via a metabolically mediated active uptake (bioaccumulation) and/or a passive biosorption process via their exopolysaccharide (EPS) coating (De Philippis et al., 2011). Bioaccumulation requires living cells and is a comparatively slow process. Biosorption, which does not necessarily require living cells, follows faster kinetics, reaching a sorption maximum within hours (De Philippis et al. 2003, 2011; Demirel et al., 2009; Kadukova, 2016; Vannela and Verma, 2006). Crystalline Au(0) nanoparticles (AuNPs) can be observed in cyanobacteria within the first minutes of incubation with dissolved Au(III) species present in high concentrations (mg L^{-1} range) (Rosken et al., 2014). Obviously, cyanobacteria can bind and immediately reduce Au(III) species to AuNPs, suggesting a biosorption more than a bioaccumulation process. Ag(I) also shows a strong tendency for reduction to Ag(0), so bioaccumulation and/or biosorption might be a pathway for the formation of Ag-b-NPs in natural waters from geogenic Ag(I) sources (Kang et al., 2014; Yin et al., 2016). This does not necessarily exclude that (dissolved) NOM also plays a major role in the natural formation of Ag-b-NPs. In our investigations Ag-b-NP formation was only observed in the samples collected from Lake Waginger See, which, compared with Lake Königssee, provides an approximately five times higher NOM concentration (see Table A2) but also approximately twice as much of chlorophyll a, which is a measure of the number of cyanobacteria and/or phototrophic eukaryotes (see Table A1) present in the lake. The data given in Fig. 2 and Table A2 indicate that the comparatively high NOM and local total silver concentrations are the most likely explanation for Ag-b-NP formation at the surface of Lake Waginger See. Approximately 40% (2.35 ± 0.08 ng L^{-1}) of the near-surface silver was transferred to Ag-b-NPs, as demonstrated by spICP-MS measurements showing that Ag-b-NPs in the surface sample from Lake Waginger See exhibited a particle size ranging from 10 to 30 nm, whereas 75% of all of the detected nanoparticles from Lake Waginger See were 10–15 nm in size (Fig. 1). With spICP-MS, an Ag-b-NP concentration of 0.98 ± 0.12 ng L^{-1} was determined. The discrepancy compared with the concentration measured by CPE-ET-AAS (2.35 ± 0.08 ng L^{-1}, Table A2) suggests that particles smaller than 10 nm, which cannot be detected by spICP-MS, were also formed. Thus, a substantial mass fraction of Ag-b-NPs smaller than 10 nm might exist.

Even though thermal stratification in Lake Waginger See was not in a fully developed state, we could observe a concentration gradient for total silver ranging from a depth of 10 m (1.76 ± 0.89 ng L^{-1}) to the surface of the lake with the highest observed total silver concentration of 5.69 ± 0.33 ng L^{-1} and a corresponding Ag-b-NP concentration of 2.35 ± 0.08 ng L^{-1} (Table A2, sampling site SS1). With increasing depth (1–23 m, SS1), the Ag-b-NP concentration decreased to a constant level of 0.7–0.8 ng L^{-1}. This uniform depth-independent distribution of Ag-b-NPs is most likely a remnant of the turnover cycles of the lake, and it shows that Ag-b-NPs, unlike dissolved silver species, are not accumulated by light-sensitive microorganisms and are therefore not transported
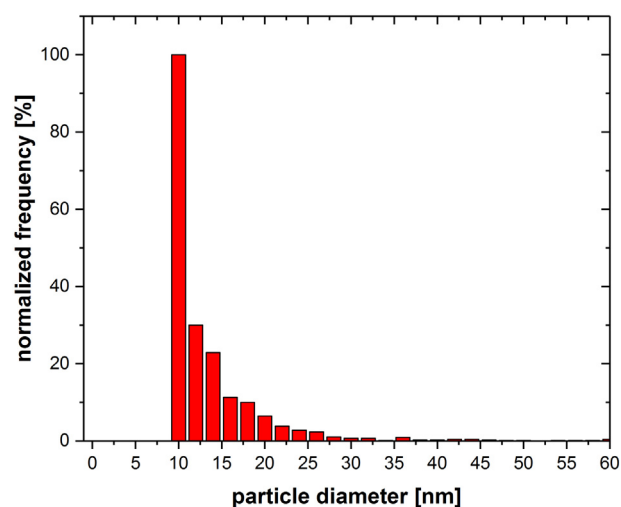
Fig. 1. Particle size distribution of naturally formed Ag-b-NPs (cAg-b-NP = 0.98 ± 0.12 ng L^{-1}) in surface water of Lake Waginger See, Germany, as measured using CPE-spICP-MS. Sampling site is SS1 (details see Table A1). Particles <10 nm are not detectable by CPE-spICP-MS.
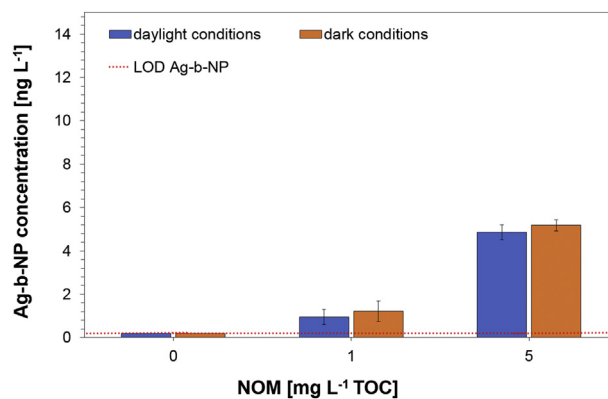
Fig. 2. Influence of daylight and dark conditions on the NOM-induced formation of Ag-b-NPs from 50 ng L^{-1} Ag(I). All samples were incubated for 24 h at 7 °C. Error bars indicate standard deviation of three independent replicates ($n = 3$). Limit of detection (LOD) for Ag-b-NPs is 0.2 ng L^{-1}.

to the surface of the lake.

The fact that Ag-b-NPs were also observed in deeper water layers, where daylight is scarce, is a strong indication that Ag-b-NP formation does not necessarily require light. We were able to clarify some of the aspects of NOM- and sulfide-mediated Ag-b-NP formation under dark conditions (see following sections).

An increase in the total silver concentration was also observed near the bottom of Lake Waginger See (Table A2, SS1). This increase in silver concentration is most likely caused by the release of silver species from the sediment/detritus of the lake.

Ag-b-NPs formed and concentrated at the surface of the lake during summer stratification can be reasonably assumed to be partly or completely dissolved during the turnover cycles of the lake. Because of the more uniform distribution of Ag-b-NPs within the lake during these cycles, the state of equilibrium between Ag-b-NP formation and Ag-b-NP dissolution (Sigg and Lindauer, 2015; Zook et al., 2011) shifts toward Ag-b-NP dissolution because of the comparatively low Ag-b-NP and total silver concentrations at these times. During summer stratification with accumulated silver concentrations at the surface of the lake, Ag-b-NPs are obviously rebuilt in higher concentrations.

A completely different behavior was observed in the mesotrophic Lake Chiemsee (TP: 8 µg L^{-1}; visibility depth: 5.1 m; volume 2×10^9 m^3; max. depth: 73 m), another dimictic pre-alpine lake, which was investigated in our previous work (Li et al., 2016). Lake Chiemsee receives effluent from several WWTPs along its main tributary, Tiroler Achen. Here, we observed a uniform distribution of Ag-b-NPs over the lake and negligible differences in Ag-b-NP levels (0.3–0.5 ng L^{-1}) within a depth of 0–10 m during summer stratification. In this lake, water exchange occurs within 1.26 years; thus, the lake is obviously a reservoir for WWTP-based Ag-b-NPs submitted by its tributaries.

3.2. Formation of Ag-b-NPs under semi-natural conditions

There is some evidence that NOM and sulfur play a key role in the formation of Ag-b-NPs from dissolved Ag(I) species in natural waters. Analytical techniques developed in our group enable not only the measurement of Ag-b-NP concentrations in the sub-ng L^{-1} range with high selectivity and accuracy but also the observation of particle formation via size-selective measurements of particles as small as 10 nm in the same concentration range. Therefore, the measurements in the natural environment were supplemented by laboratory experiments with nature-related silver concentrations in the ng L^{-1} range and with TOC concentrations ≤ 5 mg L^{-1} obtained by the preparation of appropriate NOM reference material solutions. Therefore, we studied the effects of daylight and dark conditions, NOM content, incubation time, temperature, and the presence of sulfide on the formation and size distribution of Ag-b-NPs in detail to achieve a more comprehensive understanding of the natural formation of Ag-b-NPs in the aquatic environment.

At ultra-trace levels in the ng L^{-1} range, reproducibility and accuracy of experiments is a major issue. Effects such as the loss of analyte by sorption, e.g., to vessel walls, or contamination of solvents and reagents become more dominant and can lead to serious errors. For this reason, all experiments involving NOM- and sulfur-induced formation of Ag-b-NPs from Ag(I) were performed under the strict rules of ultra-trace analysis to avoid systematical errors to the extent possible.

3.3. NOM-induced formation of Ag-b-NPs from Ag(I) under daylight and dark conditions

Because Ag(I) is a very photosensitive species, the effects of light irradiation on the formation of Ag-b-NPs from Ag(I) are assumed to play a key role. However, we observed only negligible differences in the NOM-induced formation of Ag-b-NPs from Ag(I) under daylight and under dark conditions (Fig. 2). The experiments were performed with an initial Ag(I) concentration of 50 ng L^{-1} and with NOM solutions with a TOC of 0, 1, or 5 mg L^{-1} over a time span of 24 h at a temperature of 7 °C. Substantial formation of Ag-b-NPs was only observed in solutions with a TOC of 5 mg L^{-1}. In this case, approximately 10% of the initial Ag(I) content was transferred to Ag-b-NPs with a slightly higher conversion rate under dark conditions. Apparently, light irradiation is not a key factor for NOM-induced formation of Ag-b-NPs at environmentally relevant concentrations. Numerous studies with non-natural Ag(I) and NOM concentrations have indicated that the reduction of Ag(I) to Ag-b-NPs is enabled through the formation of photo-induced radical species formed by NOM under the influence of light irradiation, preferably at elevated temperatures (Adegboyega et al., 2013; Akaighe et al., 2011; Hou et al., 2013; Lu et al., 2016; Yin et al., 2014). Our experiments indicate that other light-independent mechanisms that enable the formation of Ag-b-NPs at ultra-trace levels under dark conditions and at low temperatures must also exist. Low-molecular-weight quinones, which are usually contained in

NOM, are principally capable of reducing dissolved metallic species to form clusters and, finally, nanoparticles under dark conditions (Jiang et al., 2015; Yuan et al., 2016). However, there might also exist other unknown NOM-related mechanisms that trigger the formation of Ag-b-NPs from dissolved Ag(I) species under natural conditions.

3.4. Formation of Ag-b-NPs from Ag(I) in the presence of NOM and sulfide

Sulfur is omnipresent in the aquatic environment (Kaegi et al., 2013; Kent et al., 2014) and shows a strong binding affinity to silver if it is present in lower oxidation states. Sulfide ions, for example, immediately form Ag$_2$S in the presence of Ag(I), a very stable compound with a solubility product K_{Sp} as low as 5×10^{-51} mol^3 L^{-3} (Levard et al. 2011, 2012) (25 °C). Ag$_2$S formation can also occur in natural waters, e.g., in anaerobic zones of eutrophic lakes. Thus, the formation of Ag-b-NPs not only in the presence of NOM but also in the presence of sulfide, a final product of the anaerobic digestion of sulfur-containing compounds, warrants investigation. In one of our previous publications, we demonstrated that the applied CPE procedure is independent of the composition with respect to the coating of extracted Ag-b-NPs. For Ag$_2$S@AgNPs, an extraction efficiency of approximately 90% has been observed (Hartmann et al., 2014). Therefore, the coatings/chemical composition of extracted Ag-b-NPs cannot be extinguished using CPE. Nonetheless, substantial changes in the conversion rate of Ag(I) to Ag-b-NPs were observed in the presence of sulfide. Compared with the results obtained when NOM was used as reducing agent (see previous section), the conversion of Ag(I) to Ag-b-NPs (dark conditions, cAg(I) = 50 ng L^{-1}, TOC 5 mg L^{-1}, 7 °C, 24 h) was dramatically increased from 10% to 46% when sulfide (160 µM) was added to the solutions (Figs. 2 and 3). At 23 °C, the conversion rate of Ag(I) to Ag-b-NPs (TOC 5 mg L^{-1}) reached 70%. Even without the addition of NOM, 11% (7 °C) and 23% (23 °C) of the initial Ag(I) was transferred to Ag-b-NPs. Moreover, the conversion rate was linearly dependent ($R^2 = 0.84$ at 7 °C, $R^2 = 0.87$ at 23 °C) on the NOM concentration (TOC 0–5 mg L^{-1}).

The size of particles formed from Ag(I) (50 ng L^{-1}) in the presence of NOM (TOC 1 mg L^{-1} and 5 mg L^{-1}) and sulfide (160 µM) was also investigated. We observed a pronounced effect of incubation time on the particle size distribution under dark conditions. Fig. 4 shows that the increase of incubation time from 1 to 24 h led to a substantial shift of the particle size distribution from smaller to larger particles, especially in the size range from 15 to 25 nm.
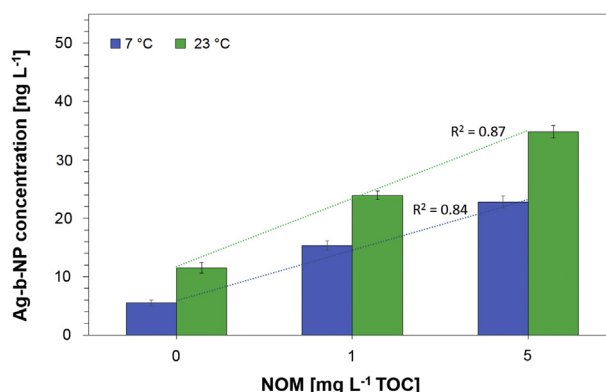

Fig. 3. Effects of NOM concentration and incubation temperature on the Ag-b-NP formation from 50 ng L^{-1} Ag(I) in the presence of 160 µM sulfide. The mixtures were incubated at 7 °C and 23 °C for 24 h. All experiments were conducted in the absence of light. Error bars indicate standard deviation of three independent replicates ($n = 3$).
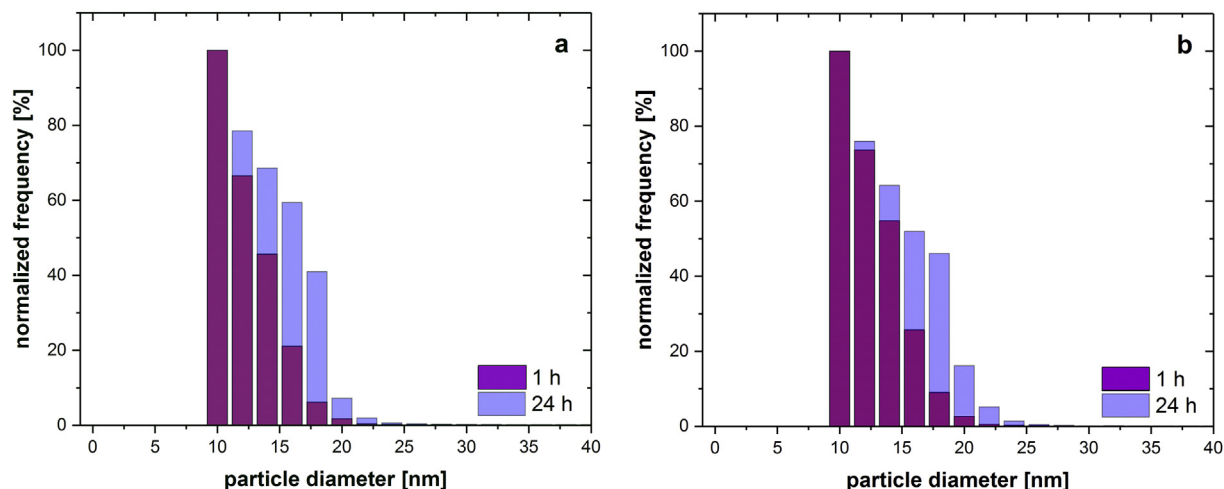
Fig. 4. Influence of incubation time and NOM concentration on the size distribution of Ag-b-NPs formed at 23 °C from 50 ng L^{-1} Ag(I) in the presence of 160 μM sulfide: (a) NOM: 1 mg L^{-1}; (b) NOM: 5 mg L^{-1}. All experiments were conducted in the absence of light. Particles <10 nm are not detectable using CPE-spICP-MS.

Apparently, Ostwald ripening occurs even at such low metal concentrations, leading to the growth of larger particles at the expense of smaller ones (Hansen et al., 2013). In this context, we also investigated the particle size distribution obtained in the presence of NOM (TOC 5 mg L^{-1}) with and without sulfide (160 and 0 μM). Obviously, incubation without sulfide led to a substantially broader particle size distribution (Fig. 5a) compared with the size distribution obtained after incubation with sulfide (Fig. 5b). The most likely explanation for this observation is that the extraordinarily low solubility product constant of Ag$_2$S, which is the species most likely formed in the solutions with added sulfide, hinders Ostwald ripening.

In the literature, a lower size limit of 20 nm has been reported for Ag-b-NPs whose size can be determined by spICP-MS (Lee et al., 2014). We lowered this size limit dramatically by application of the CPE procedure, which eliminates the background caused by dissolved silver species; thus, particles as small as 10 nm can be measured reliably via CPE-spICP-MS. Nevertheless, even smaller particles are reasonably assumed to be formed from Ag(I) in the presence of NOM and/or sulfide. The size of such small particles can currently not be determined at sub-ng L^{-1} levels with modern

analytical techniques, particularly if NOM, a colloidal suspension with a broad particle size distribution, is present in higher concentrations.

4. Conclusions

We discovered that Ag-b-NPs can be formed naturally from geogenic silver traces in water bodies if NOM and/or other ubiquitous reducing agents such as sulfide ions are present in sufficient concentrations. Moreover, light-sensitive microorganisms can collect dissolved silver species and transport them to the surface of natural water bodies, leading to a considerable local enrichment of silver. If some necessary but not fully known conditions are met, nanoparticle formation occurs in natural waters even at silver concentrations in the sub-ng L^{-1} range. Our lab experiments with nature-related silver and NOM concentrations revealed that particle formation is not necessarily photocontrolled. It can occur under dark conditions and at low temperatures, such as in deep water layers, in pores, or even in groundwaters. Because of the extraordinary chemical affinity between silver and sulfur, Ag-b-NP formation is enhanced in the presence of traces of sulfide. In addition,
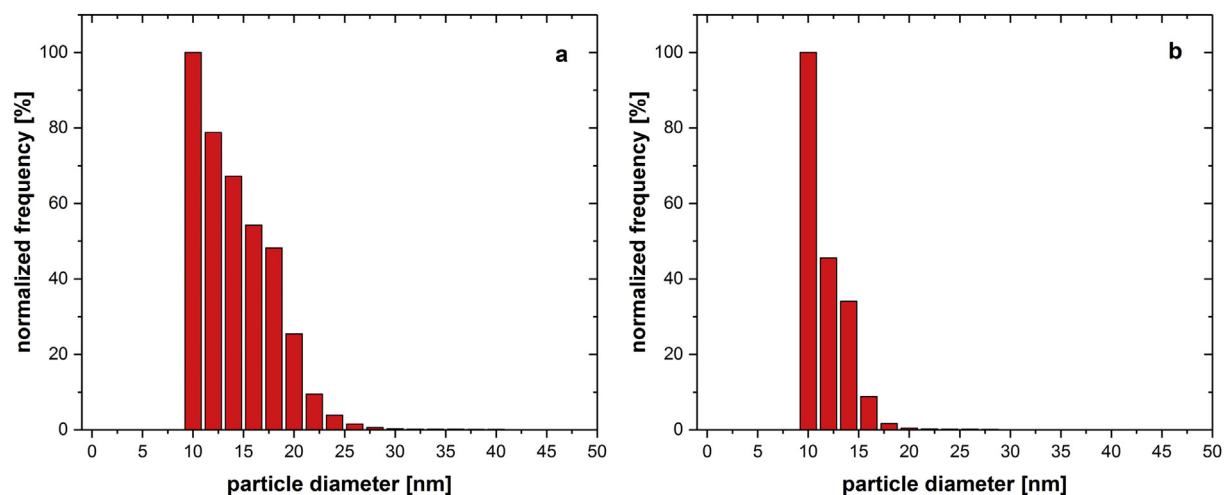

Fig. 5. Effect of sulfide addition on the particle size distribution of Ag-b-NPs formed from Ag(I) (50 ng L^{-1}) in the presence of NOM (5 mg L^{-1} TOC). All mixtures were incubated at 23 °C for 1 h: (a) 0 μM sulfide; (b) 160 μM sulfide. All experiments were conducted in the absence of light. Particles <10 nm are not detectable using CPE-spICP-MS.

this exceptional affinity leads to the formation of smaller particles that are obviously less prone to Ostwald ripening. Even though sulfide dominates particle formation, NOM concentration also plays a major role if present in substantial concentrations. The lab experiments as well as the observations in the natural lakes show that higher NOM concentrations with TOC values of approximately $5 \, mg \, L^{-1}$ substantially increase the formation of Ag-b-NPs from traces of dissolved silver species. Generally, the lab investigations reflect the observations made in the natural lakes remarkably well. Even the sizes of Ag-b-NPs measured in surface water of the eutrophic lake are very similar to particle sizes observed in the lab experiments.

A currently much debated question is whether and to what extend the increasing production of EAgNPs influences the concentration of Ag-b-NPs in surface waters. Moreover, the answer to this question is very important for estimating the influence of transformed engineered Ag-b-NPs released by, for example, WWTPs on the biological balance in natural water bodies. Our findings show that the concentration of naturally formed Ag-b-NPs at the surface of an eutrophic pre-alpine lake in southern Germany is similar to WWTP-based Ag-b-NP concentrations measured in a river originating in the same region (Li et al., 2016). The river Isar receives effluents from a series of WWTPs, including effluents from the city of Munich with 1.43 million inhabitants (Li et al., 2016). Final clarification of the influence that Ag-b-NPs of different origin might have on the biological balance in natural waters requires knowledge of the chemical composition of the particles rather than their concentration. We are currently working on techniques that will enable a highly efficient species-preserving enrichment of Ag-b-NPs from natural and contaminated waters. We are confident that these investigations will enable high-resolution transmission electron microscopy and energy-dispersive X-ray spectroscopy measurements, which will provide new insights into the composition and shape of natural and transformed engineered Ag-b-NPs in the aquatic environment.

Funding

Author contribution

M.S. supervised the study. M.S., A.W. and A.K. designed the study and its experimental setup. A.W. carried out real water sampling and the corresponding analytical measurements. In-house laboratory experiments were conducted by A.W. and A.K. M.S. wrote the manuscript, assisted by A.W.

Declaration of interests

None.

Acknowledgement

Appendix A. Supplementary data

Supplementary data related to this article can be found at https://doi.org/10.1016/j.watres.2018.05.015.

References

Acharya, C., Apte, S.K., 2013. Insights into the interactions of cyanobacteria with uranium. Photosynth. Res. 118 (1–2), 83–94.

Adegboyega, N.F., Sharma, V.K., Siskova, K., Zbořil, R., Sohn, M., Schultz, B.J., Banerjee, S., 2013. Interactions of aqueous Ag+ with fulvic acids: mechanisms of silver nanoparticle formation and investigation of stability. Environ. Sci. Technol. 47 (2), 757–764.

Akaighe, N., MacCuspie, R.I., Navarro, D.A., Aga, D.S., Banerjee, S., Sohn, M., Sharma, V.K., 2011. Humic acid-induced silver nanoparticle formation under environmentally relevant conditions. Environ. Sci. Technol. 45 (9), 3895–3901.

Anjana, K., Kaushik, A., Kiran, B., Nisha, R., 2007. Biosorption of Cr(VI) by immobilized biomass of two indigenous strains of cyanobacteria isolated from metal contaminated soil. J. Hazard Mater. 148 (1–2), 383–386.

Awasthi, M., Rai, L.C., 2004. Adsorption of nickel, zinc and cadmium by immobilized green algae and cyanobacteria: a comparative study. Ann. Microbiol. 54 (3), 257–267.

Benn, T., Cavanagh, B., Hristovski, K., Posner, J.D., Westerhoff, P., 2010. The release of nanosilver from consumer products used in the home. J. Environ. Qual. 39 (6), 1875–1882.

Blanco, A., Sanz, B., Llama, M.J., Serra, J.L., 1999. Biosorption of heavy metals to immobilised Phormidium laminosum biomass. J. Biotechnol. 69 (2–3), 227–240.

Cain, A., Vannela, R., Woo, L.K., 2008. Cyanobacteria as a biosorbent for mercuric ion. Bioresour. Technol. 99 (14), 6578–6586.

Colman, B.P., Espinasse, B., Richardson, C.J., Matson, C.W., Lowry, G.V., Hunt, D.E., Wiesner, M.R., Bernhardt, E.S., 2014. Emerging contaminant or an old toxin in Disguise? Silver nanoparticle impacts on ecosystems. Environ. Sci. Technol. 48 (9), 5229–5236.

De Philippis, R., Colica, G., Micheletti, E., 2011. Exopolysaccharide-producing cyanobacteria in heavy metal removal from water: molecular basis and practical applicability of the biosorption process. Appl. Microbiol. Biotechnol. 92 (4), 697–708.

De Philippis, R., Paperi, R., Sili, C., Vincenzini, M., 2003. Assessment of the metal removal capability of two capsulated cyanobacteria, Cyanospira capsulata and Nostoc PCC7936. J. Appl. Phycol. 15 (2–3), 155–160.

Demirel, S., Ustun, B., Aslim, B., Suludere, Z., 2009. Toxicity and uptake of iron ions by synechocystis sp E35 isolated from Kucukcekmece Lagoon, Istanbul. J. Hazard Mater. 171 (1–3), 710–716.

Duester, L., Fabricius, A.-L., Jakobtorweihen, S., Philippe, A., Weigl, F., Wimmer, A., Schuster, M., Nazar, M.F., 2016. Can cloud point-based enrichment, preservation, and detection methods help to bridge gaps in aquatic nanometrology? Anal. Bioanal. Chem. 1–7.

Gottschalk, F., Sonderer, T., Scholz, R.W., Nowack, B., 2009. Modeled environmental concentrations of engineered nanomaterials (TiO2, ZnO, Ag, CNT, Fullerenes) for different regions. Environ. Sci. Technol. 43 (24), 9216–9222.

Gottschalk, F., Sun, T., Nowack, B., 2013. Environmental concentrations of engineered nanomaterials: review of modeling and analytical studies. Environ. Pollut. 181, 287–300.

Hansen, T.W., Delariva, A.T., Challa, S.R., Datye, A.K., 2013. Sintering of catalytic nanoparticles: particle migration or Ostwald ripening? Acc. Chem. Res. 46 (8), 1720–1730.

Hartmann, G., Baumgartner, T., Schuster, M., 2014. Influence of particle coating and matrix constituents on the cloud point extraction efficiency of silver nanoparticles (Ag-NPs) and application for monitoring the formation of Ag-NPs from Ag+. Anal. Chem. 86 (1), 790–796.

Hartmann, G., Hutterer, C., Schuster, M., 2013. Ultra-trace determination of silver nanoparticles in water samples using cloud point extraction and ETAAS. J. Anal. At. Spectrom. 28 (4), 567–572.

Hartmann, G., Schuster, M., 2013. Species selective preconcentration and quantification of gold nanoparticles using cloud point extraction and electrothermal atomic absorption spectrometry. Anal. Chim. Acta 761, 27–33.

Hou, W.-C., Stuart, B., Howes, R., Zepp, R.G., 2013. Sunlight-driven reduction of silver ions by natural organic matter: formation and transformation of silver nanoparticles. Environ. Sci. Technol. 47 (14), 7713–7721.

Jiang, C., Garg, S., Waite, T.D., 2015. Hydroquinone-mediated redox cycling of iron and concomitant oxidation of hydroquinone in oxic waters under acidic conditions: comparison with iron–natural organic matter interactions. Environ. Sci. Technol. 49 (24), 14076–14084.

Kadukova, J., 2016. Surface sorption and nanoparticle production as a silver detoxification mechanism of the freshwater alga Parachlorella kessleri. Bioresour. Technol. 216, 406–413.

Kaegi, R., Voegelin, A., Ort, C., Sinnet, B., Thalmann, B., Krismer, J., Hagendorfer, H., Elumelu, M., Mueller, E., 2013. Fate and transformation of silver nanoparticles in urban wastewater systems. Water Res. 47 (12), 3866–3877.

Kang, F., Alvarez, P.J., Zhu, D., 2014. Microbial extracellular polymeric substances reduce Ag+ to silver nanoparticles and antagonize bactericidal activity. Environ. Sci. Technol. 48 (1), 316–322.

Kent, R.D., Oser, J.G., Vikesland, P.J., 2014. Controlled evaluation of silver nanoparticle sulfidation in a full-scale wastewater treatment plant. Environ. Sci. Technol. 48 (15), 8564–8572.

Kim, B., Park, C.-S., Murayama, M., Hochella, M.F., 2010. Discovery and characterization of silver sulfide nanoparticles in final sewage sludge products. Environ. Sci. Technol. 44 (19), 7509–7514.

Lee, S., Bi, X., Reed, R.B., Ranville, J.F., Herckes, P., Westerhoff, P., 2014. Nanoparticle size detection limits by single particle ICP-MS for 40 elements. Environ. Sci. Technol. 48 (17), 10291–10300.

Levard, C., Hotze, E.M., Lowry, G.V., Brown, G.E., 2012. Environmental transformations of silver nanoparticles: impact on stability and toxicity. Environ. Sci. Technol. 46 (13), 6900–6914.

Levard, C., Reinsch, B.C., Michel, F.M., Oumahi, C., Lowry, G.V., Brown, G.E., 2011. Sulfidation processes of PVP-coated silver nanoparticles in aqueous solution: impact on dissolution rate. Environ. Sci. Technol. 45 (12), 5260–5266.

Li, L., Hartmann, G., Döblinger, M., Schuster, M., 2013. Quantification of nanoscale silver particles removal and release from municipal wastewater treatment plants in Germany. Environ. Sci. Technol. 47 (13), 7317–7323.

Li, L., Stoiber, M., Wimmer, A., Xu, Z., Lindenblatt, C., Helmreich, B., Schuster, M., 2016. To what extent can full-scale wastewater treatment plant effluent influence the occurrence of silver-based nanoparticles in surface waters? Environ. Sci. Technol. 50 (12), 6327–6333.

Lu, D., Liu, Q., Zhang, T., Cai, Y., Yin, Y., Jiang, G., 2016. Stable silver isotope fractionation in the natural transformation process of silver nanoparticles. Nat. Nanotechnol. 11 (8), 682–686.

Markou, G., Mitrogiannis, D., Celekli, A., Bozkurt, H., Georgakakis, D., Chrysikopoulos, C.V., 2015. Biosorption of Cu2+ and Ni2+ by Arthrospira platensis with different biochemical compositions. Chem. Eng. J. 259, 806–813.

Mittelman, A.M., Lantagne, D.S., Rayner, J., Pennell, K.D., 2015. Silver dissolution and release from ceramic water filters. Environ. Sci. Technol. 49 (14), 8515–8522.

Peters, R.J.B., Rivera, Z.H., van Bemmel, G., Marvin, H.J.P., Weigel, S., Bouwmeester, H., 2014. Development and validation of single particle ICP-MS for sizing and quantitative determination of nano-silver in chicken meat. Anal. Bioanal. Chem. 406 (16), 3875–3885.

Ranville, M.A., Flegal, A.R., 2005. Silver in the North Pacific ocean. Geochem. Geophys. Geosyst. 6.

Rosken, L.M., Korsten, S., Fischer, C.B., Schonleber, A., van Smaalen, S., Geimer, S., Wehner, S., 2014. Time-dependent growth of crystalline Au-0-nanoparticles in cyanobacteria as self-reproducing bioreactors: 1. Anabaena sp. J. Nanoparticle Res. 16 (4).

Schutz, D.F., Turekian, K.K., 1965. The investigation of the geographical and vertical distribution of several trace elements in sea water using neutron activation analysis. Geochem. Cosmochim. Acta 29 (4), 259–313.

Sharma, V.K., Filip, J., Zboril, R., Varma, R.S., 2015. Natural inorganic nanoparticles - formation, fate, and toxicity in the environment. Chem. Soc. Rev. 44 (23), 8410–8423.

Sigg, L., Lindauer, U., 2015. Silver nanoparticle dissolution in the presence of ligands and of hydrogen peroxide. Environ. Pollut. 206 (Suppl. C), 582–587.

Silvestry-Rodriguez, N., Bright, K.R., Slack, D.C., Uhlmann, D.R., Gerba, C.P., 2008. Silver as a residual disinfectant to prevent biofilm formation in water distribution systems. Appl. Environ. Microbiol. 74 (5), 1639–1641.

Sun, T.Y., Bornhöft, N.A., Hungerbühler, K., Nowack, B., 2016. Dynamic probabilistic modeling of environmental emissions of engineered nanomaterials. Environ. Sci. Technol. 50 (9), 4701–4711.

Sun, T.Y., Conroy, G., Donner, E., Hungerbuhler, K., Lombi, E., Nowack, B., 2015. Probabilistic modelling of engineered nanomaterial emissions to the environment: a spatio-temporal approach. Environ. Sci.: Nano 2 (4), 340–351.

Sun, T.Y., Gottschalk, F., Hungerbühler, K., Nowack, B., 2014. Comprehensive probabilistic modelling of environmental emissions of engineered nanomaterials. Environ. Pollut. 185 (Suppl. C), 69–76.

Tan, Z.-Q., Yin, Y.-G., Guo, X.-R., Amde, M., Moon, M.H., Liu, J.-F., Jiang, G.-B., 2017. Tracking the transformation of nanoparticulate and ionic silver at environmentally relevant concentration levels by hollow fiber flow field-flow fractionation coupled to ICPMS. Environ. Sci. Technol. 51 (21), 12369–12376.

Vannela, R., Verma, S.K., 2006. Cu2+ Removal and recovery by SpiSORB: batch stirred and up-flow packed bed columnar reactor systems. Bioproc. Biosyst. Eng. 29 (1), 7–17.

Yin, Y., Liu, J., Jiang, G., 2012. Sunlight-induced reduction of ionic Ag and Au to metallic nanoparticles by dissolved organic matter. ACS Nano 6 (9), 7910–7919.

Yin, Y., Shen, M., Zhou, X., Yu, S., Chao, J., Liu, J., Jiang, G., 2014. Photoreduction and stabilization capability of molecular weight fractionated natural organic matter in transformation of silver ion to metallic nanoparticle. Environ. Sci. Technol. 48 (16), 9366–9373.

Yin, Y., Yang, X., Hu, L., Tan, Z., Zhao, L., Zhang, Z., Liu, J., Jiang, G., 2016. Superoxide-mediated extracellular biosynthesis of silver nanoparticles by the Fungus Fusarium oxysporum. Environ. Sci. Technol. Lett. 3 (4), 160–165.

Yuan, X., Davis, J.A., Nico, P.S., 2016. Iron-mediated oxidation of methoxyhydroquinone under dark conditions: kinetic and mechanistic insights. Environ. Sci. Technol. 50 (4), 1731–1740.

Zook, J.M., Long, S.E., Cleveland, D., Geronimo, C.L.A., MacCuspie, R.I., 2011. Measuring silver nanoparticle dissolution in complex biological and environmental matrices using UV–visible absorbance. Anal. Bioanal. Chem. 401 (6), 1993.

Appendix A. Supplementary data

New Insights into the Formation of Silver-Based Nanoparticles under Natural and Semi-Natural Conditions

Conditions

Andreas Wimmer[a], Anna Kalinnik[a], Michael Schuster[a,*]

[a]Division of Analytical Chemistry, Department of Chemistry, Technical University of Munich, Garching 85748, Germany

Corresponding Author:

[*] Prof. Dr. Michael Schuster

E-Mail: michael.schuster@tum.de

Tel: +49 (0) 89 289 13763

Fax: +49 (0) 89 289 14513

5 pages

1 Figure

3 Tables
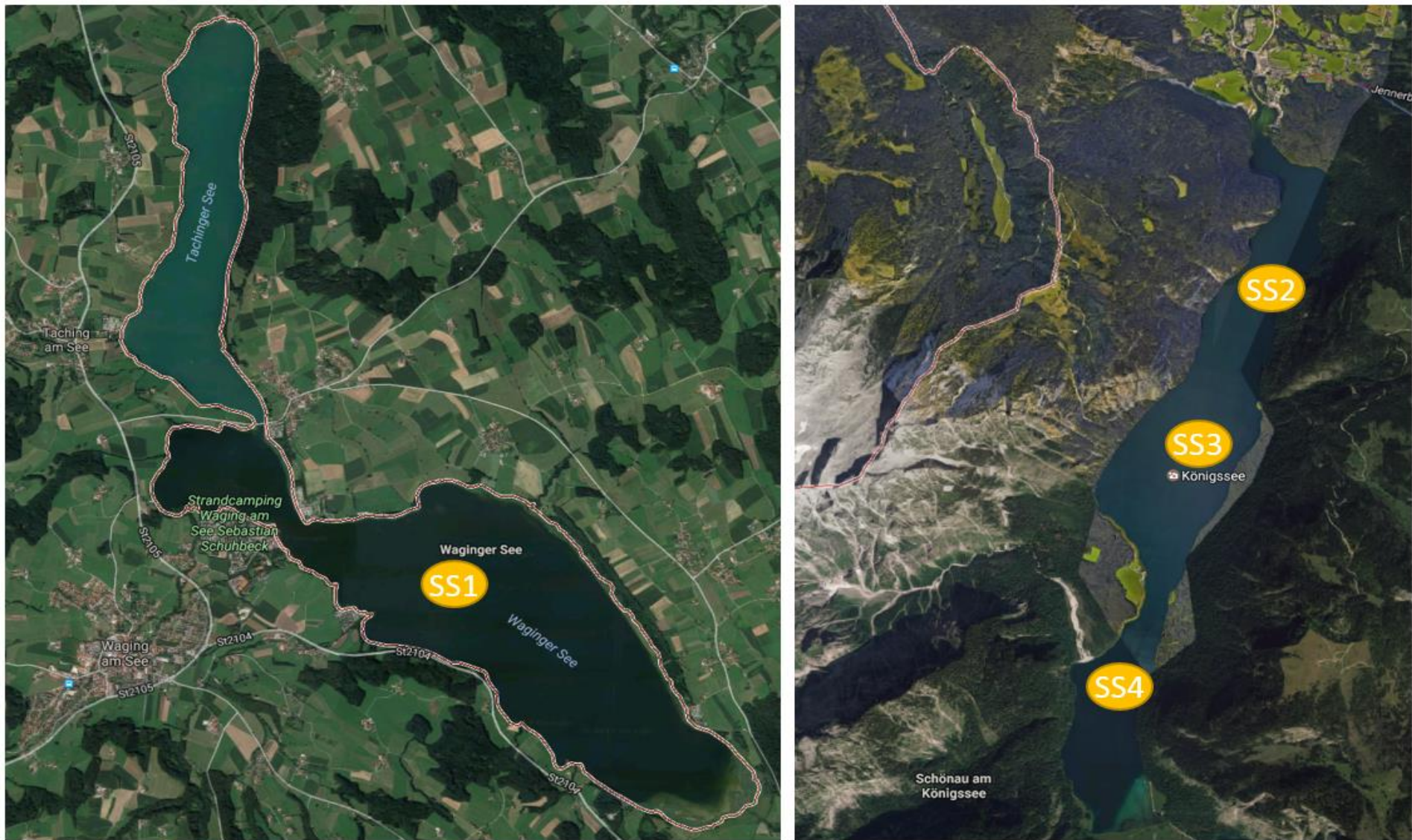
Fig. A1. Location of sampling sites (SS1 to SS4) in the investigated lakes (source: Google Maps).

Table A1

Characteristic data of the examined lakes.

Lake	Surface Area [km^2]	Max. Depth [m]	Volume [million m^3]	Total Phosphorus (TP, µg/L)	Chlorophyll-A [µg/L]	Visibility Depth [m]	Circulation Type	Eutrophication Status
Waginger See	6.6	27	90	24	7	2.8	dimictic	eutrophic
Königssee	5.2	190	512	5	3	10.5	dimictic	oligotrophic

Source : Protection and Management of Surface Waters, Water Protection of Lakes, Bavarian Environmental Protection Agency (LfU), 2006.

Table A2

Summary of all measured parameters of the examined lake water samples (LOD (limit of detection) Total Silver = 0.77 ng L^{-1}, LOD Ag-b-NP = 0.2 ng L^{-1}). Sampling was carried out on April 29, 2017 (SS1) and September 29, 2016 (SS2 – SS4). Standard deviation is based on three independent replicates (n = 3).

SS1 (Lake Waginger See, Coordinates: 47°56'29.2''N 12°46'24.4''E)					
Depth [m]	Temperature [°C]	pH	TOC [mg L^{-1}]	Total Silver Concentration [ng L^{-1}]	Ag-b-NP Concentration [ng L^{-1}]
0	10	8	4.78 ± 0.04	5.69 ± 0.33	2.35 ± 0.08
1	9.9	7.9	5.19 ± 0.08	4.61 ± 0.31	0.77 ± 0.12
3	9.8	7.8	5.56 ± 0.04	2.49 ± 0.36	0.75 ± 0.05
6	8.8	7.9	4.90 ± 0.04	1.68 ± 0.15	0.67 ± 0.03
10	8.3	8	5.04 ± 0.06	1.76 ± 0.89	0.71 ± 0.08
13	7.8	8.3	4.72 ± 0.02	< DL	0.75 ± 0.14
16	7.2	8.2	5.07 ± 0.07	< DL	0.83 ± 0.07
18	7	7.9	5.18 ± 0.08	< DL	0.78 ± 0.07
23	6.9	8.3	5.24 ± 0.01	3.29 ± 0.15	0.68 ± 0.09
SS2 (Lake Königssee, Coordinates: 47°34'34.8''N 12°59'31.9''E)					

Depth [m]	Temperature [°C]	pH	TOC [mg L^{-1}]	Total Silver Concentration [ng L^{-1}]	Ag-b-NP Concentration [ng L^{-1}]
0	16.1	8	1.26 ± 0.01	2.25 ± 0.53	< DL
3	15.3	7.8	1.20 ± 0.03	0.67 ± 0.25	< DL
6	12.1	8.3	1.33 ± 0.04	1.08 ± 0.26	< DL
10	8.6	7.9	1.42 ± 0.03	< DL	< DL

SS3 (Lake Königssee, Coordinates: 47°33'14.5''N 12°58'35.9''E)

Depth [m]	Temperature [°C]	pH	TOC [mg L^{-1}]	Total Silver Concentration [ng L^{-1}]	Ag-b-NP Concentration [ng L^{-1}]
0	18.2	7.7	1.25 ± 0.04	0.84 ± 0.52	< DL
3	16.2	7.9	1.35 ± 0.03	< DL	< DL
6	12.6	8.3	1.39 ± 0.01	< DL	< DL
10	9.6	7.9	1.33 ± 0.04	< DL	< DL

SS4 (Lake Königssee, Coordinates: 47°31'53.0''N 12°58'04.1''E)

Depth [m]	Temperature [°C]	pH	TOC [mg L^{-1}]	Total Silver Concentration [ng L^{-1}]	Ag-b-NP Concentration [ng L^{-1}]
0	16.5	8.2	1.25 ± 0.01	1.95 ± 0.49	< DL
3	15.8	8.1	1.36 ± 0.01	0.90 ± 0.37	< DL
6	12.4	7.9	1.36 ± 0.01	< DL	< DL
10	8.9	8	1.33 ± 0.03	< DL	< DL

Table A3

System parameters for sp-ICP-MS measurements.

Pump rate	0.346 mL min^{-1}
Dwell-time	100 µs
Helium mode	Off
Reference material	AuNPs (NIST Reference Material 8013), 56 nm
Reference element mass (Au)	197 u e^{-1}
Reference material concentration	52.0 ng/L
Reference material density	19.32 g/cm^3
Ionic standard concentration (Ag$^+$)	1.0 µg/L
Target element mass (Ag)	107 u e^{-1}
Target material density (AgNP)	10.5 g/cm^3
Analyte mass fraction	1.0
Sample and calibration matrix	5% (v/v) EtOH, 5% (v/v) TX-114 (10% (w/w))
Rinsing step 1	surfactant matrix (2.5 mL EtOH, 2.5 mL TX-114 (10% (w/w)), 38 mL UPW)
Rinsing step 2	HNO$_3$ (1%)
Rinsing step 3	UPW

9 Vollständige Publikationsliste

Originalarbeiten (begutachtet)

1. Li, L., Stoiber, M., **Wimmer, A.**, Xu, Z., Lindenblatt, C., Helmreich, B., Schuster, M., To What Extent Can Full-Scale Wastewater Treatment Plant Effluent Influence the Occurrence of Silver-Based Nanoparticles in Surface Waters? *Environmental Science & Technology* **2016**, 50 (12), 6327-6333, DOI: 10.1021/acs.est.6b00694.

2. Duester, L., Fabricius, A.-L., Jakobtorweihen, S., Philippe, A., Weigl, F., **Wimmer, A.**, Schuster, M., Nazar, M. F., Can cloud point-based enrichment, preservation, and detection methods help to bridge gaps in aquatic nanometrology? *Analytical and Bioanalytical Chemistry* **2016**, 408 (27), 7551–7557, DOI: 10.1007/s00216-016-9873-5.

3. **Wimmer, A.**, Kalinnik, A., Schuster, M., New insights into the formation of silver-based nanoparticles under natural and semi-natural conditions. *Water Research* **2018**, 141, 227-234, DOI: 10.1016/j.watres.2018.05.015.

4. **Wimmer, A.**, Ritsema, R., Schuster, M., Krystek, P., Sampling and pre-treatment effects on the quantification of (nano)silver and selected trace elements in surface water - Application in a Dutch case study. *Science of the Total Environment* **2019**, 663, 154-161, DOI: 10.1016/j.scitotenv.2019.01.244.

5. **Wimmer, A.**, Markus, A. A., Schuster, M., Silver Nanoparticle Levels in River Water: Real Environmental Measurements and Modeling Approaches—A Comparative Study. *Environmental Science & Technology Letters* **2019**, 6, 353-358, DOI: 10.1021/acs.estlett.9b00211.

6. **Wimmer, A.**, Beyerl, J., Schuster, M., Copper Drinking Water Pipes as a Previously Undocumented Source of Silver-Based Nanoparticles. *Environmental Science & Technology* **2019**, 53, 13293-13301, DOI: 10.1021/acs.est.9b04271.

7. **Wimmer, A.**, Urstoeger, A., Funck, N. C., Adler, F. P., Lenz, L., Doeblinger, M., Schuster, M, What happens to silver-based nanoparticles if they meet seawater? *Water Research* **2020**, 171, 115399, DOI: 10.1016/j.watres.2019.115399.

8. Urstoeger, A., **Wimmer, A.**, Kaegi, R., Reiter, S., Schuster, M., Looking at Silver-Based Nanoparticles in Environmental Water Samples: Repetitive Cloud Point Extraction Bridges Gaps in Electron Microscopy for Naturally Occurring Nanoparticles. *Environmental Science & Technology* **2020**, 54, 12063-12071, DOI: 10.1021/acs.est.0c02878.

9. **Wimmer, A.**, Urstoeger, A., Hinke, T., Aust, M., Altmann, P. J., Schuster, M. Separating dissolved silver from nanoparticulate silver is the key: Improved cloud-point-extraction hyphenated to single particle ICP-MS for comprehensive analysis of silver-based nanoparticles in real environmental samples down to single-digit nm particle sizes. *Analytica Chimica Acta* **2021**, 1150, 238198, DOI: 10.1016/j.aca.2021.01.001.

Populärwissenschaftliche Arbeiten

1. **Wimmer, A.**, M. Schuster, Den Silbernanopartikeln auf der Spur. *GIT Labor-Fachzeitschrift* **2016**, 11, 26-29, https://www.git-labor.de/forschung/umwelt/den-silbernanopartikeln-auf-der-spur.

2. **Wimmer, A.**, M. Schuster, Tracking Silver Nanoparticles. *G.I.T. Laboratory Journal* **2017**, 7/8, 19-21, https://www.laboratory-journal.com/science/environment/tracking-silver-nanoparticles.

3. **Wimmer, A.**; Silver Nanoparticles In Natural Waters: Is it Only Humans Who Are To Blame? *Science Trends* **2018**, https://sciencetrends.com/silver-nanoparticles-in-natural-waters-is-it-only-humans-who-are-to-blame/.

Konferenzbeiträge (begutachtet)

Posterpräsentationen

1. **Wimmer, A.**, Weigl, F., Schuster, M., Cloud Point Extraction Allows Insight into the Occurrence of Silver Nanoparticles in Natural Water Bodies. *NanoImpact* **2017**, Monte Verità, Schweiz.

2. **Wimmer, A.** Schuster, M., Größenselektive Bestimmung von Silbernanopartikeln in Umweltproben, *ANAKON* **2017**, Tübingen, Deutschland.

3. **Wimmer, A.**, Schuster, M., Silver nanoparticles in natural water bodies - is it only humans who are to blame? *European Winter Conference on Plasma Spectrochemistry* **2019**, Pau, Frankreich.

Vorträge

1. **Wimmer, A.**, To What Extent Can Full-Scale Wastewater Treatment Plant Effluent Influence the Occurrence of Silver Nanoparticles in Surface Waters? *Final Conference of COST Action ES 1205* **2017**, Departamento de Biologia & CESAM Universidade de Aveiro, Portugal.

2. **Wimmer, A.**, Cloud Point Extraction Hyphenated to Single Particle ICP-MS Allows Size-Selective Insights into Ultra-Traces of Silver Nanoparticles in Real Environmental Samples. *Winter Conference on Plasma Spectrochemistry* **2018**, Amelia Island, Florida, USA.

3. **Wimmer, A.**, Schuster, M., Cloud Point Extraction Hyphenated to Single Particle ICP-MS Allows Insights into Naturally Occurring Silvernanoparticles. *5. Interdisziplinäres Doktorandenseminar des Deutschen Arbeitskreises für Analytische Spektroskopie (DAAS)* **2018**, Geesthacht, Deutschland.

4. **Wimmer, A.**, Schuster, M., Silver nanoparticles in natural water bodies - is it only humans who are to blame? *Engineered Nanoparticles in Aquatic and Terrestrial Compartments: Fate, Effects and Analytics* **2018**, Landau, Deutschland.

Weitere Vorträge

1. **Wimmer, A.**, Schuster, M., Application of Cloud Point Extraction for the determination of silver nanoparticles in environmental samples. *Workshop on Cloud Point Extraction* **2016**, Bundesanstalt für Gewässerkunde, Koblenz, Deutschland.

2. **Wimmer, A.**, Schuster, M., Measurement of manufactured nanomaterials in environmental samples. *Scientific Stakeholder Meeting on Nanomaterials in the Environment* **2017**, Umweltbundesamt, Dessau, Deutschland.

3. **Wimmer, A.**, Nachweis von Nanopartikeln in der Umwelt. *Expertendialog Stoffpolitik* **2017**, Verband der chemischen Industrie, München, Deutschland.

4. **Wimmer, A.**, Schuster, M., Nanosilber in Oberflächengewässern: Ist der Mensch immer schuld? *Begleitforschung zur Nanotechnologie in Bayern* **2018**, Bayerisches Landesamt für Umwelt, Augsburg, Deutschland.

Preise und Auszeichnungen

2017 **Bayerischer Umweltpreis** der bayerischen Landesstiftung für die weltweit erste Messung von Silbernanopartikeln in Realproben

2018 **Elena Dodova and John Danku Memorial Award** Auszeichnung für herausragende studentische Präsentation auf der „2018 Winter Conference on Plasma Spectrochemistry" in Florida

2018 **Vortragspreis des Springer Verlags** für den besten Vortrag des Interdisziplinären Doktorandenseminars des Deutschen Arbeitskreises für Analytische Spektroskopie am Helmholtz Zentrum Geesthacht, Institut für Küstenforschung

10 Referenzen

1. https://web.pa.msu.edu/people/yang/RFeynman_plentySpace.pdf; aufgerufen am 07.02.**2021**.

2. http://www.deutsches-museum.de/fileadmin/Content/data/020_Dokumente/040_KuT_Artikel/2000/24-1-1.pdf; aufgerufen am 07.02.**2021**.

3. Bayda, S., M. Adeel, T. Tuccinardi, M. Cordani, and F. Rizzolio, *The History of Nanoscience and Nanotechnology: From Chemical-Physical Applications to Nanomedicine.* Molecules (Basel, Switzerland), **2019**. 25(1): p. 112.

4. Europäische Kommission; *Empfehlung der Kommission zur Definition von Nanomaterialien*, Amtsblatt der Europäischen Union, **2011**/696/EU.

5. Abschlussbericht: Fraunhofer Inst. f. Molekularbiologie u. Angewandte Oekologie: *Verbesserung der Luftqualität durch photokatalytisches Pflaster*, **2010**.

6. Bhushan, B., Jung, Y.C., Nosonovsky, M., *Springer Handbook of Nanotechnology*, Springer, Heidelberg, **2010**.

7. Cong, H. and J.A. Porco, *Chemical Synthesis of Complex Molecules Using Nanoparticle Catalysis.* ACS Catalysis, **2012**. 2(1): p. 65-70.

8. Serp, P., Philippot, K., *Nanomaterials in Catalysis,* Wiley-VCH, Weinheim, **2012**.

9. Khan, A., M. Qamar, and M. Muneer, *Synthesis of highly active visible-light-driven colloidal silver orthophosphate.* Chemical Physics Letters, **2012**. 519-520: p. 54-58.

10. Luo, X., A. Morrin, A.J. Killard, and M.R. Smyth, *Application of Nanoparticles in Electrochemical Sensors and Biosensors.* Electroanalysis, **2006**. 18(4): p. 319-326.

11. Davis, M.E., Z. Chen, and D.M. Shin, *Nanoparticle therapeutics: an emerging treatment modality for cancer.* Nature Reviews Drug Discovery, **2008**. 7(9): p. 771-782.

12. Freeman, R. and I. Willner, *Optical molecular sensing with semiconductor quantum dots (QDs).* Chemical Society Reviews, **2012**. 41(10): p. 4067-4085.

13. Hurnaus, T. and J. Plank, *Behavior of Titania Nanoparticles in Cross-linking Hydroxypropyl Guar Used in Hydraulic Fracturing Fluids For Oil Recovery.* Energy & Fuels, **2015**. 29(6): p. 3601-3608.

14. Haase, M. and H. Schäfer, *Upconverting Nanoparticles.* Angewandte Chemie International Edition, **2011**. 50(26): p. 5808-5829.

15. Pappert, G., M. Rieger, R. Niessner, and M. Seidel, *Immunomagnetic nanoparticle-based sandwich chemiluminescence-ELISA for the enrichment and quantification of E. coli.* Microchimica Acta, **2010**. 168(1): p. 1-8.

16. Kaur, A. and U. Gupta, *A review on applications of nanoparticles for the preconcentration of environmental pollutants.* Journal of Materials Chemistry, **2009**. 19(44): p. 8279-8289.

17. Urstoeger, A., L. Zacherl, M. Muhr, Y. Selic, M. Wenisch, M. Klotz, and M. Schuster, *Magnetic solid phase extraction of silver-based nanoparticles in aqueous samples: Influence of particle composition and matrix effects on its application to environmental samples and species-selective elution and determination of silver sulphide nanoparticles with sp-ICP-MS.* Talanta, **2021**. 225: p. 122028.

18. Song, H. and E.R. Carraway, *Reduction of Chlorinated Ethanes by Nanosized Zero-Valent Iron: Kinetics, Pathways, and Effects of Reaction Conditions.* Environmental Science & Technology, **2005**. 39(16): p. 6237-6245.

19.   O'Carroll, D., B. Sleep, M. Krol, H. Boparai, and C. Kocur, *Nanoscale zero valent iron and bimetallic particles for contaminated site remediation.* Advances in Water Resources, **2013**. 51: p. 104.

20.   Yaqoob, A.A., K. Umar, and M.N.M. Ibrahim, *Silver nanoparticles: various methods of synthesis, size affecting factors and their potential applications – a review.* Applied Nanoscience, **2020**. 10(5): p. 1369-1378.

21.   Li, L., G. Hartmann, M. Döblinger, and M. Schuster, *Quantification of Nanoscale Silver Particles Removal and Release from Municipal Wastewater Treatment Plants in Germany.* Environmental Science & Technology, **2013**. 47(13): p. 7317-7323.

22.   Cho, Y.-M., Y. Mizuta, J.-i. Akagi, T. Toyoda, M. Sone, and K. Ogawa, *Size-dependent acute toxicity of silver nanoparticles in mice.* Journal of Toxicologic Pathology, **2018**. 31(1): p. 73-80.

23.   Hartmann, G., T. Baumgartner, and M. Schuster, *Influence of Particle Coating and Matrix Constituents on the Cloud Point Extraction Efficiency of Silver Nanoparticles (Ag-NPs) and Application for Monitoring the Formation of Ag-NPs from Ag+.* Analytical Chemistry, **2014**. 86(1): p. 790-796.

24.   Hartmann, G., C. Hutterer, and M. Schuster, *Ultra-trace determination of silver nanoparticles in water samples using cloud point extraction and ETAAS.* Journal of Analytical Atomic Spectrometry, **2013**. 28(4): p. 567-572.

25.   Hartmann, G. and M. Schuster, *Species selective preconcentration and quantification of gold nanoparticles using cloud point extraction and electrothermal atomic absorption spectrometry.* Analytica Chimica Acta, **2013**. 761: p. 27-33.

26.   Sun, T.Y., N.A. Bornhöft, K. Hungerbühler, and B. Nowack, *Dynamic Probabilistic Modeling of Environmental Emissions of Engineered Nanomaterials.* Environmental Science & Technology, **2016**. 50(9): p. 4701-4711.

27.   Sun, T.Y., F. Gottschalk, K. Hungerbühler, and B. Nowack, *Comprehensive probabilistic modelling of environmental emissions of engineered nanomaterials.* Environ Pollut, **2014**. 185: p. 69-76.

28.   Nowack, B., H. Krug, and M. Height, *120 Years of Nanosilver History: Implications for Policy Makers.* Environmental Science & Technology, **2011**. 45(7): p. 3189-3189.

29.   http://nano.dguv.de/fileadmin/user_upload/documents/textfiles/Grundlagen/Nano Trust_Dossier_Kosmetika.pdf; aufgerufen am 12.11.**2020**.

30.   https://nanopartikel.info/wissen/materialien/titandioxid/; aufgerufen am 12.11.**2020**.

31.   https://www.nanopartikel.info/nanoinfo/materialien/zinkoxid/materialinfo-zinkoxid; aufgerufen am 08.11.**2020**.

32.   Schmid, G., *Nanoparticles*, Wiley-VCH, Weinheim, **2013**.

33.   Tolaymat, T.M., A.M. El Badawy, A. Genaidy, K.G. Scheckel, T.P. Luxton, and M. Suidan, *An evidence-based environmental perspective of manufactured silver nanoparticle in syntheses and applications: a systematic review and critical appraisal of peer-reviewed scientific papers.* Sci Total Environ, **2010**. 408(5): p. 999-1006.

34.   Xia, Y., Y. Xiong, B. Lim, and S.E. Skrabalak, *Shape-controlled synthesis of metal nanocrystals: simple chemistry meets complex physics?* Angew Chem Int Ed Engl, **2009**. 48(1): p. 60-103.

35.   Bärsch, N., J. Jakobi, S. Weiler, and S. Barcikowski, *Pure colloidal metal and ceramic nanoparticles from high-power picosecond laser ablation in water and acetone.* Nanotechnology, **2009**. 20(44): p. 445603.

36.   Yu, S.-j., Y.-g. Yin, and J.-f. Liu, *Silver nanoparticles in the environment.* Environmental Science: Processes & Impacts, **2013**. 15(1): p. 78-92.

37.   _https://www.bioni-living.de/optisolan-fassadenfarbe-gegen-algen-online-kaufen_;
        aufgerufen am 07.02.**2021**.

38.   Kaegi, R., B. Sinnet, S. Zuleeg, H. Hagendorfer, E. Mueller, R. Vonbank, M. Boller, and M.
        Burkhardt, _Release of silver nanoparticles from outdoor facades._ Environmental
        Pollution, **2010**. 158(9): p. 2900-2905.

39.   Mueller, N.C. and B. Nowack, _Exposure Modeling of Engineered Nanoparticles in the
        Environment._ Environmental Science & Technology, **2008**. 42(12): p. 4447-4453.

40.   _https://www.silverell.com/ueber-silverell/; aufgerufen am 07.02.**2021**_

41.   Mitrano, D.M., P. Limpiteeprakan, S. Babel, and B. Nowack, _Durability of nano-
        enhanced textiles through the life cycle: releases from landfilling after washing._
        Environmental Science: Nano, **2016**. 3(2): p. 375-387.

42.   Mitrano, D.M., E. Rimmele, A. Wichser, R. Erni, M. Height, and B. Nowack, _Presence of
        Nanoparticles in Wash Water from Conventional Silver and Nano-silver Textiles._ ACS
        Nano, **2014**. 8(7): p. 7208-7219.

43.   Geranio, L., M. Heuberger, and B. Nowack, _The Behavior of Silver Nanotextiles during
        Washing._ Environmental Science & Technology, **2009**. 43(21): p. 8113-8118.

44.   Benn, T.M. and P. Westerhoff, _Nanoparticle Silver Released into Water from
        Commercially Available Sock Fabrics._ Environmental Science & Technology, **2008**.
        42(11): p. 4133-4139.

45.   Benn, T., B. Cavanagh, K. Hristovski, J.D. Posner, and P. Westerhoff, _The Release of
        Nanosilver from Consumer Products Used in the Home._ Journal of Environmental
        Quality, **2010**. 39(6): p. 1875-1882.

46.   Balagna, C., S. Perero, E. Percivalle, E.V. Nepita, and M. Ferraris, _Virucidal effect against
        coronavirus SARS-CoV-2 of a silver nanocluster/silica composite sputtered coating._
        Open Ceramics, **2020**. 1: p. 100006.

47.   Jeremiah, S.S., K. Miyakawa, T. Morita, Y. Yamaoka, and A. Ryo, _Potent antiviral effect of
        silver nanoparticles on SARS-CoV-2._ Biochemical and biophysical research
        communications, **2020**. 533(1): p. 195-200.

48.   Jindal, S. and P. Gopinath, _Nanotechnology based approaches for combatting COVID-
        19 viral infection._ Nano Express, **2020**. 1(2): p. 022003.

49.   Medhi, R., P. Srinoi, N. Ngo, H.-V. Tran, and T.R. Lee, _Nanoparticle-Based Strategies to
        Combat COVID-19._ ACS Applied Nano Materials, **2020**. 3(9): p. 8557-8580.

50.   N. Kanani, _Galvanotechnik_, Hanser Verlag, München, **2009**.

51.   Schmidl, G., _Plasmonisch aktive Schichten und Nanostrukturen für die Material- und
        Sensorentwicklung._Dissertation, Technische Universität Ilmenau, **2019**.

52.   Das, R., S.S. Nath, D. Chakdar, G. Gope, and R. Bhattacharjee, _Synthesis of silver
        nanoparticles and their optical properties._ Journal of Experimental Nanoscience, **2010**.
        5(4): p. 357-362.

53.   Doria, G., J. Conde, B. Veigas, L. Giestas, C. Almeida, M. Assunção, J. Rosa, and P.V.
        Baptista, _Noble metal nanoparticles for biosensing applications._ Sensors (Basel), **2012**.
        12(2): p. 1657-87.

54.   Zhou, H., D. Yang, N.E. Mircescu, N.P. Ivleva, K. Schwarzmeier, A. Wieser, S. Schubert, R.
        Niessner, and C. Haisch, _Surface-enhanced Raman scattering detection of bacteria on
        microarrays at single cell levels using silver nanoparticles._ Microchimica Acta, **2015**.
        182(13): p. 2259-2266.

55.   Ye, Q., J.S. Zhao, F.F. Huo, J. Wang, S.Y. Cheng, T.F. Kang, and H.X. Dai, _Nanosized
        Ag/alpha-MnO2 catalysts highly active for the low-temperature oxidation of carbon
        monoxide and benzene._ Catalysis Today, **2011**. 175(1): p. 603-609.

56. Naik, B., S. Hazra, V.S. Prasad, and N.N. Ghosh, *Synthesis of Ag nanoparticles within the pores of SBA-15: An efficient catalyst for reduction of 4-nitrophenol.* Catalysis Communications, **2011**. 12(12): p. 1104-1108.

57. Kühling, W., *Nano-Silber – der Glanz täuscht*, Bund Freunde der Erde, **2009**.

58. Europäische Union, Verordnung (EG) Nr. 1907/2006 ("REACH-Verordnung"), **2006**.

59. Nair, P.M., S.Y. Park, and J. Choi, *Evaluation of the effect of silver nanoparticles and silver ions using stress responsive gene expression in Chironomus riparius.* Chemosphere, **2013**. 92(5): p. 592-9.

60. Kaveh, R., Y.-S. Li, S. Ranjbar, R. Tehrani, C.L. Brueck, and B. Van Aken, *Changes in Arabidopsis thaliana Gene Expression in Response to Silver Nanoparticles and Silver Ions.* Environmental Science & Technology, **2013**. 47(18): p. 10637-10644.

61. van Aerle, R., A. Lange, A. Moorhouse, K. Paszkiewicz, K. Ball, B.D. Johnston, E. de-Bastos, T. Booth, C.R. Tyler, and E.M. Santos, *Molecular mechanisms of toxicity of silver nanoparticles in zebrafish embryos.* Environmental Science & Technology, **2013**. 47(14): p. 8005-8014.

62. Krug, H.F., *Nanosafety Research—Are We on the Right Track?* Angewandte Chemie International Edition, **2014**. 53(46): p. 12304-12319.

63. Brunner, T.J., P. Wick, P. Manser, P. Spohn, R.N. Grass, L.K. Limbach, A. Bruinink, and W.J. Stark, *In vitro cytotoxicity of oxide nanoparticles: comparison to asbestos, silica, and the effect of particle solubility.* Environ Sci Technol, **2006**. 40(14): p. 4374-81.

64. Chernousova, S. and M. Epple, *Silver as Antibacterial Agent: Ion, Nanoparticle, and Metal.* Angewandte Chemie International Edition, **2013**. 52(6): p. 1636-1653.

65. Liu, W., Y. Wu, C. Wang, H.C. Li, T. Wang, C.Y. Liao, L. Cui, Q.F. Zhou, B. Yan, and G.B. Jiang, *Impact of silver nanoparticles on human cells: effect of particle size.* Nanotoxicology, **2010**. 4(3): p. 319-30.

66. Tiwari, D.K., T. Jin, and J. Behari, *Dose-dependent in-vivo toxicity assessment of silver nanoparticle in Wistar rats.* Toxicol Mech Methods, **2011**. 21(1): p. 13-24.

67. Valodkar, M., R.N. Jadeja, M.C. Thounaojam, R.V. Devkar, and S. Thakore, *In vitro toxicity study of plant latex capped silver nanoparticles in human lung carcinoma cells.* Materials Science and Engineering: C, **2011**. 31(8): p. 1723-1728.

68. World Health Organization, Guidlines for Drinking-water Quality, Genf, **2008**.

69. Verordnung über die Qualität von Wasser für den menschlichen Gebrauch, www.gesetze-im-internet.de/bundesrecht/trinkwv_2001/gesamt.pdf, aufgerufen am 07.02.**2021**.

70. Gaiser, B.K., T.F. Fernandes, M.A. Jepson, J.R. Lead, C.R. Tyler, M. Baalousha, A. Biswas, G.J. Britton, P.A. Cole, B.D. Johnston, Y. Ju-Nam, P. Rosenkranz, T.M. Scown, and V. Stone, *Interspecies comparisons on the uptake and toxicity of silver and cerium dioxide nanoparticles.* Environ Toxicol Chem, **2012**. 31(1): p. 144-54.

71. Griffitt, R.J., J. Luo, J. Gao, J.C. Bonzongo, and D.S. Barber, *Effects of particle composition and species on toxicity of metallic nanomaterials in aquatic organisms.* Environ Toxicol Chem, **2008**. 27(9): p. 1972-8.

72. Nowack, B., J.F. Ranville, S. Diamond, J.A. Gallego-Urrea, C. Metcalfe, J. Rose, N. Horne, A.A. Koelmans, and S.J. Klaine, *Potential scenarios for nanomaterial release and subsequent alteration in the environment.* Environ Toxicol Chem, **2012**. 31(1): p. 50-9.

73. Hund-Rinke, K., Marscheider-Weidemann, F., Kemper, M., *Beurteilung der Gesamtumweltexposition von Silberionen aus Biozid-Produkten*, im Auftrag des Umweltbundesamtes, UBA Texte 43-08, Dessau **2008**.

74.   Blaser, S.A., M. Scheringer, M. Macleod, and K. Hungerbühler, *Estimation of cumulative aquatic exposure and risk due to silver: contribution of nano-functionalized plastics and textiles.* Sci Total Environ, **2008**. 390(2-3): p. 396-409.

75.   Silver, S., *Bacterial silver resistance: molecular biology and uses and misuses of silver compounds.* FEMS Microbiol Rev, **2003**. 27(2-3): p. 341-53.

76.   Khan, S., A. Mukherjee, and N. Chandrasekaran, *Silver nanoparticles tolerant bacteria from sewage environment.* Journal of Environmental Sciences, **2011**. 23(2): p. 346-352.

77.   *Silver nanoparticles one of the fastest growing product categories in the nanotechnology industry,* Nanotechnology News, 19.04.**2006**.

78.   Lowry, G.V., K.B. Gregory, S.C. Apte, and J.R. Lead, *Transformations of Nanomaterials in the Environment.* Environmental Science & Technology, **2012**. 46(13): p. 6893-6899.

79.   Levard, C., E.M. Hotze, G.V. Lowry, and G.E. Brown, *Environmental Transformations of Silver Nanoparticles: Impact on Stability and Toxicity.* Environmental Science & Technology, **2012**. 46(13): p. 6900-6914.

80.   Thalmann, B., Kaegi, R., Voegelin, A., Morgenroth, E., *Präsentation auf der 8th International Conference on the Environmental Effects of Nanoparticles and Nanomaterials,* Aix-en-Provence, **2013**.

81.   Lombi, E., E. Donner, S. Taheri, E. Tavakkoli, K. Jämting Å, S. McClure, R. Naidu, B.W. Miller, K.G. Scheckel, and K. Vasilev, *Transformation of four silver/silver chloride nanoparticles during anaerobic treatment of wastewater and post-processing of sewage sludge.* Environ Pollut, **2013**. 176: p. 193-7.

82.   Muth-Köhne, E., L. Sonnack, K. Schlich, F. Hischen, W. Baumgartner, K. Hund-Rinke, C. Schäfers, and M. Fenske, *The toxicity of silver nanoparticles to zebrafish embryos increases through sewage treatment processes.* Ecotoxicology, **2013**. 22(8): p. 1264-1277.

83.   Burkhardt, M., S. Zuleeg, R. Kägi, B. Sinnet, J. Eugster, M. Boller, and H. Siegrist, *Verhalten von Nanosilber in Kläranlagen und dessen Einfluss auf die Nitrifikationsleistung in Belebtschlamm.* Umweltwissenschaften und Schadstoff-Forschung, **2010**. 22(5): p. 529-540.

84.   Kim, B., C.-S. Park, M. Murayama, and M.F. Hochella, *Discovery and Characterization of Silver Sulfide Nanoparticles in Final Sewage Sludge Products.* Environmental Science & Technology, **2010**. 44(19): p. 7509-7514.

85.   Nowack, B., *Nanosilver Revisited Downstream.* Science, **2010**. 330(6007): p. 1054-1055.

86.   Levard, C., B.C. Reinsch, F.M. Michel, C. Oumahi, G.V. Lowry, and G.E. Brown, *Sulfidation Processes of PVP-Coated Silver Nanoparticles in Aqueous Solution: Impact on Dissolution Rate.* Environmental Science & Technology, **2011**. 45(12): p. 5260-5266.

87.   Walczyk, D., F.B. Bombelli, M.P. Monopoli, I. Lynch, and K.A. Dawson, *What the cell "sees" in bionanoscience.* J Am Chem Soc, **2010**. 132(16): p. 5761-8.

88.   Stankus, D.P., S.E. Lohse, J.E. Hutchison, and J.A. Nason, *Interactions between natural organic matter and gold nanoparticles stabilized with different organic capping agents.* Environmental science & technology, **2011**. 45(8): p. 3238-3244.

89.   Williams, D.B., Carter, C.B., *High-Resolution TEM, Transmission Electron Microscopy,* Springer, Luxemburg, **2009**.

90.   Pyrz, W.D. and D.J. Buttrey, *Particle Size Determination Using TEM: A Discussion of Image Acquisition and Analysis for the Novice Microscopist.* Langmuir, **2008**. 24(20): p. 11350-11360.

91.   Brandt, A., B. Gómez-Nieto, J. Friedland, R. Güttel, and K. Leopold, *Determination of activation energies for atomization of gold nanoparticles in graphite furnace atomic absorption spectrometry.* Spectrochimica Acta Part B: Atomic Spectroscopy, **2020**. 173: p. 105976.

92.   Brandt, A., K. Kees, and K. Leopold, *Characterization of various metal nanoparticles by graphite furnace atomic absorption spectrometry: possibilities and limitations with regard to size and shape.* Journal of Analytical Atomic Spectrometry, **2020**. 35(11): p. 2536-2544.

93.   Brandt, A. and K. Leopold, *Investigation of the atomization mechanism of gold nanoparticles in graphite furnace atomic absorption spectrometry.* Spectrochimica Acta Part B: Atomic Spectroscopy, **2018**. 150: p. 26-32.

94.   Brucker, D. and K. Leopold, *Sizing silver nanoparticles in chicken meat using direct slurry sampling graphite furnace atomic absorption spectrometry.* Analytical and Bioanalytical Chemistry, **2019**. 411(19): p. 4551-4558.

95.   Mozhayeva, D. and C. Engelhard, *A critical review of single particle inductively coupled plasma mass spectrometry – A step towards an ideal method for nanomaterial characterization.* Journal of Analytical Atomic Spectrometry, **2020**. 35: p. 1740-1783.

96.   Borovinskaya, O., B. Hattendorf, M. Tanner, S. Gschwind, and D. Günther, *A prototype of a new inductively coupled plasma time-of-flight mass spectrometer providing temporally resolved, multi-element detection of short signals generated by single particles and droplets.* Journal of Analytical Atomic Spectrometry, **2013**. 28(2): p. 226-233.

97.   Hassellöv, M., J.W. Readman, J.F. Ranville, and K. Tiede, *Nanoparticle analysis and characterization methodologies in environmental risk assessment of engineered nanoparticles.* Ecotoxicology, **2008**. 17(5): p. 344-61.

98.   Radko, S.P. and A. Chrambach, *Separation and characterization of sub-µm- and µm-sized particles by capillary zone electrophoresis.* Electrophoresis, **2002**. 23(13): p. 1957-1972.

99.   Xu, X., K.K. Caswell, E. Tucker, S. Kabisatpathy, K.L. Brodhacker, and W.A. Scrivens, *Size and shape separation of gold nanoparticles with preparative gel electrophoresis.* Journal of Chromatography A, **2007**. 1167(1): p. 35-41.

100.   Surugau, N. and P.L. Urban, *Electrophoretic methods for separation of nanoparticles.* Journal of Separation Science, **2009**. 32(11): p. 1889-1906.

101.   Mozhayeva, D., I. Strenge, and C. Engelhard, *Implementation of Online Preconcentration and Microsecond Time Resolution to Capillary Electrophoresis Single Particle Inductively Coupled Plasma Mass Spectrometry (CE-SP-ICP-MS) and Its Application in Silver Nanoparticle Analysis.* Analytical Chemistry, **2017**. 89(13): p. 7152-7159.

102.   Tiede, K., A.B.A. Boxall, X. Wang, D. Gore, D. Tiede, M. Baxter, H. David, S.P. Tear, and J. Lewis, *Application of hydrodynamic chromatography-ICP-MS to investigate the fate of silver nanoparticles in activated sludge.* Journal of Analytical Atomic Spectrometry, **2010**. 25(7): p. 1149-1154.

103.   *M.E. Schimpf, K. Caldwell, J.C. Giddings, Field-flow fractionation handbook, John Wiley and Sons, New Jersey.* **2000**.

104.   Giddings, J.C., F.J. Yang, and M.N. Myers, *Theoretical and experimental characterization of flow field-flow fractionation.* Analytical Chemistry, **1976**. 48(8): p. 1126-1132.

105.   Müller, D., S. Cattaneo, F. Meier, R. Welz, and A. deMello, *Nanoparticle separation with a miniaturized asymmetrical flow field-flow fractionation cartridge.* Frontiers in Chemistry, **2015**. 3(45).

106.   Al-Ammar, A., A. Siripinyanond, and R. M. Barnes, *Simultaneous sample preconcentration and matrix removal using field-flow fractionation coupled to*

inductively coupled plasma mass spectrometry. Spectrochimica Acta Part B: Atomic Spectroscopy, **2001**. 56(10): p. 1951-1962.

107.   Ulrich, A., S. Losert, N. Bendixen, A. Al-Kattan, H. Hagendorfer, B. Nowack, C. Adlhart, J. Ebert, M. Lattuada, and K. Hungerbühler, *Critical aspects of sample handling for direct nanoparticle analysis and analytical challenges using asymmetric field flow fractionation in a multi-detector approach.* Journal of Analytical Atomic Spectrometry, **2012**. 27(7): p. 1120-1130.

108.   Gray, E.P., T.A. Bruton, C.P. Higgins, R.U. Halden, P. Westerhoff, and J.F. Ranville, *Analysis of gold nanoparticle mixtures: a comparison of hydrodynamic chromatography (HDC) and asymmetrical flow field-flow fractionation (AF4) coupled to ICP-MS.* Journal of Analytical Atomic Spectrometry, **2012**. 27(9): p. 1532-1539.

109.   Schwaferts, C., V. Sogne, R. Welz, F. Meier, T. Klein, R. Niessner, M. Elsner, and N.P. Ivleva, *Nanoplastic Analysis by Online Coupling of Raman Microscopy and Field-Flow Fractionation Enabled by Optical Tweezers.* Analytical Chemistry, **2020**. 92(8): p. 5813-5820.

110.   Li, L. and K. Leopold, *Ligand-Assisted Extraction for Separation and Preconcentration of Gold Nanoparticles from Waters.* Analytical Chemistry, **2012**. 84(10): p. 4340-4349.

111.   Li, L., K. Leopold, and M. Schuster, *Effective and selective extraction of noble metal nanoparticles from environmental water through a noncovalent reversible reaction on an ionic exchange resin.* Chemical Communications, **2012**. 48(73): p. 9165-9167.

112.   Njoki, P.N., I.I.S. Lim, D. Mott, H.-Y. Park, B. Khan, S. Mishra, R. Sujakumar, J. Luo, and C.-J. Zhong, *Size Correlation of Optical and Spectroscopic Properties for Gold Nanoparticles.* The Journal of Physical Chemistry C, **2007**. 111(40): p. 14664-14669.

113.   Traut, M., *Manual Malvern Zetasizer Nano ZS*, Malvern, **2013**.

114.   Xie, H., Y. Gu, and H.J. Ploehn, *Dendrimer-mediated synthesis of platinum nanoparticles: new insights from dialysis and atomic force microscopy measurements.* Nanotechnology, **2005**. 16(7): p. S492-501.

115.   Bordier, C., *Phase separation of integral membrane proteins in Triton X-114 solution.* Journal of Biological Chemistry, **1981**. 256(4): p. 1604-1607.

116.   Pryde, J.G., *Triton X-114: a detergent that has come in from the cold.* Trends in Biochemical Sciences, **1986**. 11(4): p. 160-163.

117.   Dörfler, H.D., *Grenzflächen und Kolloidchemie*, VCH, Weinheim, **1994**.

118.   Samaddar, P. and K. Sen, *Cloud point extraction: A sustainable method of elemental preconcentration and speciation.* Journal of Industrial and Engineering Chemistry, **2014**. 20(4): p. 1209-1219.

119.   Liu, J.-f., R. Liu, Y.-g. Yin, and G.-b. Jiang, *Triton X-114 based cloud point extraction: a thermoreversible approach for separation/concentration and dispersion of nanomaterials in the aqueous phase.* Chemical Communications, **2009**(12): p. 1514-1516.

120.   Wolszczak, M. and J. Miller, *Characterization of non-ionic surfactant aggregates by fluorometric techniques.* Journal of Photochemistry and Photobiology A: Chemistry, **2002**. 147(1): p. 45-54.

121.   Schmidt, H.H.-J., *Diagnostik und Therapie des Morbus Wilson.* Dtsch Arztebl, **2003**. 1000(1): p. 192-197.

122.   Walshe, J.M., *Wilson's disease; new oral therapy.* Lancet, **1956**. 270(6906): p. 25-6.

123.   Seignette, W.T., C.A. Haanen, A.P. Jansen, and C.L. Majoor, *The effects of penicillamine and versenate in the treatment of Wilson's disease and lead poisoning.* Folia Med Neerl, **1959**. 2: p. 65-78.

124. *G. Hartmann, Entwicklung und Validierung eines Verfahrens zur Quantifizierung von Edelmetall-Nanopartikeln in Wasserproben.* Dissertation, TU Münchnen, **2014**.

125. Harris, D.C., *Lehrbuch der quantitativen Analyse*, Vieweg, Braunschweig, **2014**.

126. Schwedt, G., *Analytische Chemie – Grundlagen, Methoden, Praxis,* Wiley-VCH-Verlag, Weinheim, **2008**.

127. Cammann, K., *Instrumentelle Anayltische Chemie – Verfahren, Anwendungen, Qualitätssicherung,* Spektrum Akademischer Verlag, Heidelberg, **2010**.

128. Welz, B., Sperling, M., *Atomabsorptionsspektrometrie,* Wiley-VCH-Verlag, Weinheim, **1997**.

129. Bodenseewerk Perkin-Elmer GmbH, *4100 ZL Atomabsorptions-Spektrometer Benutzerhandbuch*, Perkin-Elmer, **1991**.

130. Schuster, M., *Skriptum zur Vorlesung „Analytische Chemie",* TU München, **2011**.

131. https://commons.wikimedia.org/wiki/File:Photomultiplier_schema_de.png; aufgerufen am 12.11.**2020**.

132. Ferreira, S.L.C., M.A. Bezerra, A.S. Santos, W.N.L. dos Santos, C.G. Novaes, O.M.C. de Oliveira, M.L. Oliveira, and R.L. Garcia, *Atomic absorption spectrometry – A multi element technique.* TrAC Trends in Analytical Chemistry, **2018**. 100: p. 1-6.

133. Skoog, D., Holler, D.A., Crouch, S.R., Niessner, R. (Hrsg.), *Instrumentelle Anaylik*, Springer Spektrum, Heidelberg, **2013**.

134. Thomas, R., *A Beginner's Guide to ICP-MS Part I.* Spectroscopy, **2001**. 16(4): p. 38-42.

135. Thomas, R., *A Beginner's Guide to ICP-MS, Part II: The Sample-Introduction System.* Spectroscopy, **2001**. 16(5): p. 56-60.

136. Thomas, R., *A Beginner's Guide to ICP-MS, Part III: The Plasma Source.* Spectroscopy, **2001**. 16(6): p. 26-30.

137. Thomas, R., *A Beginner's Guide to ICP-MS, Part IV: The Interface Region.* Spectroscopy, **2001**. 16(7): p. 26-34.

138. Thomas, R., *A Beginner's Guide to ICP-MS, Part V: The Ion Focusing System.* Spectroscopy, **2001**. 16(9): p. 38-44.

139. Thomas, R., *A Beginner's Guide to ICP-MS, Part VI: The Mass Analyzer.* Spectroscopy, **2001**. 16(10): p. 44-48.

140. Thomas, R., *A Beginner's Guide to ICP-MS, Part X: Detectors.* Spectroscopy, **2002**. 17(4): p. 34-39.

141. Miller, P.E. and M.B. Denton, *The quadrupole mass filter: Basic operating concepts.* Journal of Chemical Education, **1986**. 63(7): p. 617.

142. Thomas, R., *A Beginner's Guide to ICP-MS, Part VII: Mass Separation Devices — Double-Focusing Magnetic-Sector Technology.* Spectroscopy, **2001**. 16(11): p. 22-27.

143. Thomas, R., *A Beginner's Guide to ICP-MS, Part VIII: Mass Analyzers: Time-of-Flight Technology.* Spectroscopy, **2002**. 17(1): p. 36-41.

144. Thomas, R., *A Beginner's Guide to ICP-MS, Part IX: Mass Analyzers: Collision/Reaction Cell Technology.* Spectroscopy, **2002**. 17(2): p. 42-48.

145. Thomas, R., *A Beginner's Guide to ICP-MS, Part XII: A Review of Interferences.* Spectroscopy, **2002**. 17(10): p. 24-31.

146. Evans, E.H. and J.J. Giglio, *Interferences in inductively coupled plasma mass spectrometry. A review.* Journal of Analytical Atomic Spectrometry, **1993**. 8(1): p. 1-18.

147. Li, G., Y. Duan, and G.M. Hieftje, *Space-charge effects and ion distribution in plasma source mass spectrometry.* Journal of Mass Spectrometry, **1995**. 30(6): p. 841-848.

148. Olivares, J.A. and R.S. Houk, *Suppression of analyte signal by various concomitant salts in inductively coupled plasma mass spectrometry.* Analytical Chemistry, **1986**. 58(1): p. 20-25.

149. Woods, G., *Lead isotope analysis: Removal of 204Hg isobaric interference from 204Pb using ICP-QQQ in MS/MS mode.* Application Note, Agilent Technologies, LDA UK Ltd., Stockport, UK, **2014**.

150. May, T.W. and R.H. Wiedmeyer, *A table of polyatomic interferences in ICP-MS.* Atomic Spectroscopy, **1998**. 19(5): p. 150-155.

151. Vaughan, M.A. and G. Horlick, *Correction Procedures for Rare Earth Element Analyses in Inductively Coupled Plasma-Mass Spectrometry.* Applied Spectroscopy, **1990**. 44(4): p. 587-593.

152. Hinds, M.W., D.C. GrÉGoire, and E. A. Ozaki, *Direct Determination of Volatile Elements in Nickel Alloys by Electrothermal Vaporization Inductively Coupled Plasma Mass Spectrometry.* Journal of Analytical Atomic Spectrometry, **1997**. 12(2): p. 131-135.

153. Voellkopf, U., M. Paul, and E.R. Denoyer, *Analysis of solid samples by ICP-mass spectrometry.* Fresenius' Journal of Analytical Chemistry, **1992**. 342(12): p. 917-923.

154. Rowan, J.T. and R.S. Houk, *Attenuation of Polyatomic Ion Interferences in Inductively Coupled Plasma Mass Spectrometry by Gas-Phase Collisions.* Applied Spectroscopy, **1989**. 43(6): p. 976-980.

155. Sakata, K.i. and K. Kawabata, *Reduction of fundamental polyatomic ions in inductively coupled plasma mass spectrometry.* Spectrochimica Acta Part B: Atomic Spectroscopy, **1994**. 49(10): p. 1027-1038.

156. Nakano, K., *Ultra-low level determination of phosphorus, sulfur, silicon and chlorine using the Agilent 8900 ICP-QQQ*, Application Note, Agilent Technologies, Japan, **2018**.

157. Thermo Fisher Scientific, Offenlegungsschrift der deutschen Patentanmeldung DE 10 2016 011 086 A1, **2017**.

158. C. Stephan, K.N., *Single Particle Inductively Coupled Plasma Mass Spectrometry: Understanding How and Why.* Single Particle ICP-MS Compendium, Perkin Elmer, **2014**: p. 7-11.

159. Degueldre, C. and P.Y. Favarger, *Colloid analysis by single particle inductively coupled plasma-mass spectroscopy: a feasibility study.* Colloids and Surfaces A: Physicochemical and Engineering Aspects, **2003**. 217(1–3): p. 137-142.

160. Laborda, F., E. Bolea, and J. Jiménez-Lamana, *Single Particle Inductively Coupled Plasma Mass Spectrometry: A Powerful Tool for Nanoanalysis.* Analytical Chemistry, **2014**. 86(5): p. 2270-2278.

161. Montano, M.D., H.R. Badiei, S. Bazargan, and J.F. Ranville, *Improvements in the detection and characterization of engineered nanoparticles using spICP-MS with microsecond dwell times.* Environmental Science: Nano, **2014**. 1(4): p. 338-346.

162. Montano, M.D., J.W. Olesik, A.G. Barber, K. Challis, and J.F. Ranville, *Single Particle ICP-MS: Advances toward routine analysis of nanomaterials.* Anal Bioanal Chem, **2016**. 408(19): p. 5053-74.

163. Peters, R.J.B., Z.H. Rivera, G. van Bemmel, H.J.P. Marvin, S. Weigel, and H. Bouwmeester, *Development and validation of single particle ICP-MS for sizing and quantitative determination of nano-silver in chicken meat.* Analytical and Bioanalytical Chemistry, **2014**. 406(16): p. 3875-3885.

164. Bisutti, I., I. Hilke, and M. Raessler, *Determination of total organic carbon – an overview of current methods.* TrAC Trends in Analytical Chemistry, **2004**. 23(10): p. 716-726.

165. Lee, S., X. Bi, R.B. Reed, J.F. Ranville, P. Herckes, and P. Westerhoff, *Nanoparticle Size Detection Limits by Single Particle ICP-MS for 40 Elements.* Environmental Science & Technology, **2014**. 48(17): p. 10291-10300.

166. Li, L., M. Stoiber, A. Wimmer, Z. Xu, C. Lindenblatt, B. Helmreich, and M. Schuster, *To What Extent Can Full-Scale Wastewater Treatment Plant Effluent Influence the*

Occurrence of Silver-Based Nanoparticles in Surface Waters? Environ Sci Technol, **2016**. 50(12): p. 6327-33.

167. Markus, A.A., J.R. Parsons, E.W.M. Roex, P. de Voogt, and R.W.P.M. Laane, *Modelling the transport of engineered metallic nanoparticles in the river Rhine.* Water Research, **2016**. 91: p. 214-224.

168. Derjaguin, B. and L. Landau, *Theory of the stability of strongly charged lyophobic sols and of the adhesion of strongly charged particles in solutions of electrolytes.* Progress in Surface Science, **1993**. 43(1): p. 30-59.

169. Lodeiro, P., E.P. Achterberg, J. Pampín, A. Affatati, and M.S. El-Shahawi, *Silver nanoparticles coated with natural polysaccharides as models to study AgNP aggregation kinetics using UV-Visible spectrophotometry upon discharge in complex environments.* Science of The Total Environment, **2016**. 539: p. 7-16.

170. Liu, J. and R.H. Hurt, *Ion Release Kinetics and Particle Persistence in Aqueous Nano-Silver Colloids.* Environmental Science & Technology, **2010**. 44(6): p. 2169-2175.

171. Lodeiro, P., E.P. Achterberg, and M.S. El-Shahawi, *Detection of silver nanoparticles in seawater at ppb levels using UV-visible spectrophotometry with long path cells.* Talanta, **2017**. 164: p. 257-260.

172. Teo, W.Z. and M. Pumera, *Fate of silver nanoparticles in natural waters; integrative use of conventional and electrochemical analytical techniques.* RSC Advances, **2014**. 4(10): p. 5006-5011.

173. Toncelli, C., K. Mylona, I. Kalantzi, A. Tsiola, P. Pitta, M. Tsapakis, and S.A. Pergantis, *Silver nanoparticles in seawater: A dynamic mass balance at part per trillion silver concentrations.* Sci Total Environ, **2017**. 601-602: p. 15-21.

174. Li, L., M. Stoiber, A. Wimmer, Z. Xu, C. Lindenblatt, B. Helmreich, and M. Schuster, *To What Extent Can Full-Scale Wastewater Treatment Plant Effluent Influence the Occurrence of Silver-Based Nanoparticles in Surface Waters?* Environmental Science & Technology, **2016**.

175. Li, L., M. Stoiber, A. Wimmer, Z. Xu, C. Lindenblatt, B. Helmreich, and M. Schuster, *To What Extent Can Full-Scale Wastewater Treatment Plant Effluent Influence the Occurrence of Silver-Based Nanoparticles in Surface Waters?* Environmental Science & Technology, **2016**. 50(12): p. 6327-6333.

176. https://de.wikipedia.org/wiki/Königssee; aufgerufen am 13.02.**2019**.